

**Effects of mitochondrial
dysfunction on neurofilament
turnover and distribution in
human neuroblastoma cells**

Adelheid Hanes

***PhD
October 2010***

**Effects of mitochondrial
dysfunction on neurofilament
turnover and distribution in
human neuroblastoma cells**

Adelheid Hanes

***A thesis submitted in partial
fulfilment of the requirements of
Nottingham Trent University for the
degree of Doctor of Philosophy***

October 2010

COPY RIGHT DECLARATION

This work is the intellectual property of the author. You may copy up to 5 % of this work for private study, or personal, non-commercial research. Any re-use of the information contained within this document should be fully referenced, quoting the author, title, university, degree level and pagination. Queries or requests for any other use, or if a more substantial copy is required, should be directed in the first instance to the author.

ABSTRACT

A common feature of neurodegenerative conditions including Parkinson's disease (PD) is the presence of intracytoplasmic proteinaceous inclusions. In PD these inclusions are called Lewy bodies (LBs) and contain a number of proteins including α -synuclein, ubiquitin and neurofilaments (NFs). NFs, the intermediate filaments expressed in neuronal cells are responsible for the maintenance of axonal structure. Although NFs were the first proteins identified in LBs their role in PD pathogenesis has not been fully explored. The work presented here attempts to address some of the gaps in the current knowledge concerning NF turnover and the role of NFs in PD using the human SH-SY5Y neuroblastoma cell line, commonly used as a cellular model of neurodegeneration. Mitochondrial dysfunction, dopamine (DA) mediated oxidative stress and impaired protein degradation have all been implicated in PD pathogenesis. The complex I inhibitor MPTP and its active metabolite (MPP⁺) induce Parkinsonism in humans and other primates and have been extensively used as PD mimetics in both cellular and animal models.

Addition of specific protease inhibitors in the presence of cycloheximide (an inhibitor of new protein synthesis) revealed that NF-heavy chains are degraded by macroautophagy and cathepsin D, possibly with some involvement of cysteine cathepsin, but not calpain or the ubiquitin proteasome system (UPS). This is in contrast to α -synuclein which was degraded by macroautophagy, the UPS and calpain. Treatment with MPP⁺ did not increase NF half-life despite a reduction in the activity of the 20S proteasome, cathepsin D and macroautophagy. However an activation of cysteine cathepsin activity was observed with MPP⁺ treatment, suggesting a role for these cathepsins in NF turnover following complex I inhibition. Inhibition of cysteine cathepsins in MPP⁺ treated cells resulted in increased cell death suggesting that activation of cysteine cathepsins is protective in this context. Following treatment with 100 μ M DA, NF turnover appeared to be reduced, accompanied by a reduction in 20S proteasome activity and macroautophagy but activation of calpain.

To allow analysis of the effects of mitochondrial dysfunction on the distribution of NFs in live cells, Green Fluorescent Protein (GFP) tagged NFs were produced. Live imaging of cells treated with a high dose of MPP⁺ displayed a retraction of axonal processes which occurred within the first 20 - 30 minutes of treatment. Analysis of the rate of retraction of GFP fluorescence and the remaining axonal structure indicated that NF retraction was not an early event in axonal retraction, at least with this concentration of MPP⁺.

The effect of mitochondrial dysfunction and/or proteasome inhibition on protein aggregation and inclusion formation was investigated in differentiated SH-SY5Y cells. Treatment with MPP⁺, epoxomicin (proteasome inhibitor, epoxo) or MPP⁺/epoxo resulted in an enrichment of NFs in a detergent insoluble fraction and accumulation of NF-H in a perinuclear location together with p62 and LC3, suggesting the attempted degradation of accumulated NF-H by macroautophagy. Further analysis of GFP-tagged NFs in MPP⁺ treated cells should assist in the elucidation of the role of NFs in the formation of inclusions and will allow analysis of protein partners during complex I dysfunction and other cellular states linked to neurodegeneration.

For Shaun and Megan

ACKNOWLEDGEMENTS

I would first like to thank my supervisory team; Professor Ellen Billett and Dr Luigi De Girolamo for giving me the opportunity to work for them and for all their time, support and guidance over the last few years. It has been quite a journey for me but I have been in good company. I would also like to thank Dr Alan Hargreaves who has acted as my internal assessor for all his advice.

I would like to give special thanks to Dr Christoph Ufer (Charité, Berlin) for all his help with molecular biology, the cloning of the GFP tagged neurofilaments and acting as tour guide during my visit to Berlin. I would also like to thank Professor Hartmut Kuhn (Charité, Berlin) for allowing me to spend a week in his laboratory doing qRT-PCR under the guidance of Dr Christoph Ufer. I would like to thank Dr Lyndsey Durose for all the MS analysis and her help with 2D-PAGE, silver-staining and in-gel trypsinization. Also, thank you Dr Susan Anderton, Dr Emma King and Marie Smith from the Advanced Microscopy Unit of the University of Nottingham (QMC) for their help with time-lapse imaging.

Thank you also, to all my friends and colleagues at NTU (both past and present); Asli, Flo, Julia, Ale, Debbie, Murali, Sara, Ricky, Katy, Wayne, David, Mel and Bego. They have always been there with advice and support, even putting up with the odd crisis here and there. Special thanks to Dr Cheryl Wells, she has not only taught me a great deal (for which I am grateful) but has also been a good friend, always there with help and support. Thanks also to all the technical staff at NTU, especially the biochemistry technicians for all their help.

I would like to also give special thanks to my close friends; Helena, Steph and Scott who were always there when I needed them. Special thanks also to Ronald and Martina who stepped up to help with baby-sitting when I needed them most. I would like to thank my parents for all they have taught me which has allowed me to become the person that I am. I would also like to thank my sister Carola for her support throughout the years. I would also like to thank my brother in law, Peter, for his support. It is great to have a visitor from SA every now and then.

Lastly, I would like to thank the most important people in my life - my husband, Sandy; my children, Shaun and Megan and my stepsons Liam and Tynan - who have had to put up with the all the long hours, the moods and without whose love and support I would not have been able to finish this work.

CONTENTS

CHAPTER 1: GENERAL INTRODUCTION

1.1. BACKGROUND TO PARKINSON'S DISEASE	1
1.2. LEWY BODIES (LBS)	4
<i>1.2.1. Background</i>	<i>4</i>
<i>1.2.2. Aggresomes and Lewy bodies</i>	<i>8</i>
1.3. OXIDATIVE STRESS AND MITOCHONDRIAL DYSFUNCTION	10
<i>1.3.1. Oxidative stress</i>	<i>10</i>
<i>1.3.1.1. Oxidative stress in neurodegeneration and ageing</i>	<i>10</i>
<i>1.3.1.2. Dopamine and the susceptibility of dopaminergic neurons</i>	<i>10</i>
<i>1.3.2. Mitochondrial dysfunction in neurodegeneration and ageing</i>	<i>12</i>
1.4. THE ROLE OF PROTEIN DEGRADATIVE PATHWAYS	13
<i>1.4.1. Ubiquitin Proteasome System (UPS)</i>	<i>14</i>
<i>1.4.1.1. Structure and function</i>	<i>14</i>
<i>1.4.1.2. Proteasomal deficiency during ageing and neurodegeneration</i>	<i>17</i>
<i>1.4.1.2.1. Overview</i>	<i>17</i>
<i>1.4.1.2.2. The effects of mitochondrial dysfunction on proteasome activity</i>	<i>18</i>
<i>1.4.1.2.3. The use of proteasome inhibitors as models for neurodegeneration</i>	<i>19</i>
<i>1.4.2. Autophagy-Lysosome Pathway</i>	<i>20</i>
<i>1.4.2.1. Background</i>	<i>20</i>
<i>1.4.2.2. Macroautophagy</i>	<i>22</i>
<i>1.4.2.2.1. Autophagosome membrane formation</i>	<i>22</i>
<i>1.4.2.2.2. Lysosomes</i>	<i>24</i>
<i>1.4.2.2.2.1. The role of cathepsins in ageing and neurodegeneration</i>	<i>24</i>
<i>1.4.2.2.3. The selectivity of macroautophagy depends on p62/SQSTM1</i>	<i>25</i>
<i>1.4.2.2.4. The role of macroautophagy in neurodegeneration</i>	<i>26</i>
<i>1.4.2.2.5. The role of mitophagy in neurodegeneration</i>	<i>28</i>
<i>1.4.3. Calpain</i>	<i>29</i>
<i>1.4.3.1. Background</i>	<i>29</i>
<i>1.4.3.2. Calpain in ageing and neurodegeneration</i>	<i>29</i>
1.5. NEUROFILAMENTS	30
<i>1.5.1. Function of neurofilaments</i>	<i>30</i>
<i>1.5.2. Composition and assembly of neurofilaments</i>	<i>30</i>
<i>1.5.2. Control of neurofilament gene expression</i>	<i>32</i>
<i>1.5.3. Phosphorylation of neurofilament proteins</i>	<i>33</i>
<i>1.5.4. Axonal transport</i>	<i>35</i>
<i>1.5.5. Neurofilaments in ageing and neurodegeneration</i>	<i>36</i>
1.6. SH-SY5Y CELLS	37
1.7. AIMS	38

CHAPTER 2: MATERIALS AND METHODS

2.1. MATERIALS	40
<i>2.1.1. Cell culture</i>	<i>40</i>
<i>2.1.1.1. Reagents</i>	<i>40</i>
<i>2.1.1.2. Plastic ware</i>	<i>40</i>
<i>2.1.2. Laboratory reagents</i>	<i>40</i>
<i>2.1.3. Specialist laboratory consumables</i>	<i>49</i>
<i>2.1.4. Specialist equipment</i>	<i>49</i>
2.2. METHODS	50
<i>2.2.1. Cell culture</i>	<i>50</i>

2.2.1.1. Maintenance of SH-SY5Y neuroblastoma cells	50
2.2.1.2. Subculture of SH-SY5Y neuroblastoma cells	50
2.2.1.3. Determination of cell number	50
2.2.1.4. Cryopreservation and resuscitation of SH-SY5Y neuroblastoma cells	51
2.2.1.5. Differentiation of SH-SY5Y cells	51
2.2.1.6. Quantification of axon outgrowth	52
2.2.1.7. Transfection of SH-SY5Y neuroblastoma cells with GFP tagged neurofilament proteins using LipofectAMINE™	52
2.2.1.8. Assessment of cell viability using the MTT reduction assay	52
2.2.2. Preparation of cell lysates	53
2.2.2.1. Preparation of total cell extracts	53
2.2.2.2. Preparation of cell lysates for proteasome activity determination	53
2.2.2.3. Preparation of cell lysates for cathepsin activity determination	54
2.2.2.4. Preparation of cell lysates for immunoprecipitation	54
2.2.3. Assessment of proteasome activity using a fluorogenic peptide assay	54
2.2.4. Assessment of cathepsin activity using a fluorogenic peptide assay	55
2.2.4.1. Cathepsin D activity assay	55
2.2.4.2. Cysteine cathepsin activity assay	56
2.2.5. Co-immunoprecipitation of GFP tagged fusion proteins and their associated proteins using the μMACS™ Epitope Tag Protein Isolation Kit	56
2.2.6. Determination of protein content	57
2.2.6.1. BC Assay	57
2.2.6.2. Bio-Rad protein assay	57
2.2.7. Denaturing Sodium-dodecyl-sulphate Polyacrylamide Gel Electrophoresis (SDS-PAGE)	58
2.2.8. Western blotting and immunoprobng	59
2.2.8.1. Western blotting	59
2.2.8.1.1. Wet-blotting	59
2.2.8.1.2. Semi-dry electroblotting	59
2.2.8.2. Immunoprobng	60
2.2.8.3. Secondary antibody detection of Western blots	60
2.2.8.3.1. Enhanced Chemiluminescence (ECL) detection	60
2.2.8.3.2. Alkaline phosphatase (AP) detection	60
2.2.9. Peptide mass fingerprinting of proteins co-immunoprecipitated with GFP tagged NF subunits	61
2.2.9.1. 2-dimensional polyacrylamide gel electrophoresis (2D-PAGE)	61
2.2.9.2. Silver staining of gels for mass spectrometry	62
2.2.9.3. In-gel trypsin digestion of excised protein bands or spots	62
2.2.10. Immunofluorescence imaging	63
2.2.10.1. Methanol fixation	63
2.2.10.2. Immunofluorescence staining	63
2.2.11. Live cell imaging	63
2.2.12. General molecular biology techniques	64
2.2.12.1. Amplification of neurofilament subunits by Polymerase Chain Reaction (PCR)	64
2.2.12.2. Agarose gel electrophoresis of DNA	65
2.2.12.3. Purification of DNA from agarose gels	65
2.2.12.4. Cloning of DNA fragments into pCR-2.1 TOPO and pCR-XL TOPO and transformation of E.coli competent cells	65
2.2.12.5. Purification of plasmid DNA from bacterial cells	66
2.2.12.5.1. Mini-Prep	66
2.2.12.5.2. Midi-Prep	66
2.2.12.6. Determination of DNA and RNA concentration	66
2.2.12.7. Restriction endonuclease digestion	67
2.2.12.7.1. Limited digests	67

2.2.12.7.2. Quantitative digests	67
2.2.12.8. Site-directed mutagenesis	67
2.2.12.9. Bacterial cell culture	68
2.2.12.9.1. Subculture of bacterial clones	68
2.2.12.9.2. Cryopreservation and resuscitation of bacterial cells	68
2.2.13. Quantitative Real-Time Polymerase Chain Reaction (qRT-PCR)	69
2.2.13.1. Preparation of standard DNA for qRT-PCR	69
2.2.13.1.1. Amplification and cloning of standard DNA	69
2.2.13.1.2. Preparation of standard solutions	69
2.2.13.1.2.1. Linearization of plasmid midi-prep DNA	69
2.2.13.1.2.2. Purification of linearized plasmid DNA	70
2.2.13.1.2.3. Preparation of standard DNA solutions for qRT-PCR	70
2.2.13.2. Preparation of sample cDNA preparations	71
2.2.13.2.1. RNA preparation	71
2.2.13.2.2. Reverse transcription PCR	72
2.2.13.3. Quantitative Real-Time PCR	72
2.2.14. Statistical analysis	74

CHAPTER 3: DEGRADATIVE PATHWAYS INVOLVED IN NEUROFILAMENT TURNOVER

3.1. INTRODUCTION	75
3.1.1. Neurofilament degradation	75
3.1.1.1. Background	75
3.1.1.2. Determination of half-life of proteins	76
3.1.2. Degradative pathways involved in cytoskeletal protein turnover	79
3.1.2.1. The Ubiquitin Proteasome System	79
3.1.2.2. Calpain	80
3.1.2.3. Autophagy-Lysosome Pathway	81
3.1.2.3.1. Macroautophagy	81
3.1.2.3.2. Lysosomal Proteases	84
3.1.2. Aims	85
3.2. RESULTS	86
3.2.1. Optimal cycloheximide concentration of assessment for the determination of cytoskeletal protein half-life	86
3.2.2. Degradative pathways involved in neurofilament turnover	90
3.2.3. Does inhibition of one pathway activate another?	92
3.2.3.1. Effect of inhibiting various proteolytic pathways on proteasome activity	93
3.2.3.2. Effect of inhibiting proteolytic pathways on the cleavage of α II-spectrin	94
3.2.3.3. Effect of inhibiting proteolytic pathways on macroautophagy	96
3.2.3.4. Effect of inhibiting proteolytic pathways on the activity of aspartyl and cysteine cathepsins	97
3.2.4. Effects of MPP ⁺ and dopamine on neurofilament turnover and degradative pathways	98
3.2.4.1. Effect of MPP ⁺ and DA on the half-life of neurofilament proteins, α -tubulin and vimentin	98
3.2.4.2. Effect of MPP ⁺ and DA on the activity of proteolytic pathways	99
3.2.4.2.1. Effect of MPP ⁺ and DA on proteasome activity	99
3.2.4.2.2. Effect of MPP ⁺ and DA on calpain and caspase 3 specific cleavage of α II-spectrin	101
3.2.4.2.3. Effect of MPP ⁺ and DA on macroautophagy	103
3.2.4.2.4. Effect of MPP ⁺ and DA on cathepsin activity	104
3.2. DISCUSSION	108

3.2.1. The establishment of an experimental model for the determination of the half-life of proteins	108
3.2.2. Degradative pathways involved in neurofilaments turnover	108
3.3.2.1. Estimations of half-life	108
3.3.2.2. Pathways involved in turnover of cytoskeletal proteins	109
3.3.2.2.1. The role of the proteasome	109
3.3.2.2.2. The role of calpain	110
3.3.2.2.3. The role of macroautophagy	111
3.3.2.2.4. The role of cathepsins	112
3.3.2.2.5. Conclusion	113
3.2.3. Effect of mitochondrial dysfunction and increased oxidative stress on neurofilament degradation	113
3.3.3.1. Effects of mitochondrial dysfunction	113
3.3.3.2. Effects of increased oxidative stress induced by dopamine	116
3.3.3.3. Conclusion	118

CHAPTER 4: INHIBITION OF COMPLEX I AND THE PROTEASOME IN RA/BDNF DIFFERENTIATED CELLS

4.1. INTRODUCTION	120
4.1.1. Differentiation of SH-SY5Y cells	120
4.1.2. The role of complex I and the proteasome in protein conformation diseases	124
4.1.3. Aims of this Chapter	126
4.2. RESULTS	127
4.2.1. Differentiation of SH-SY5Y cells with Retinoic acid and Brain Derived Neurotrophic Factor	127
4.2.1.1. Cellular morphology of RA/BDNF differentiated cells	127
4.2.1.2. The effect of RA/BDNF-induced differentiation on mRNA copy number and protein levels	130
4.2.1.2.1. The Validation of the use of GAPDH as a house-keeping gene for Quantitative Real-Time PCR results	130
4.2.1.2.2. Effect of RA/BDNF-induced differentiation on the expression of NTrkB, TG2 and Bcl-2	131
4.2.1.2.3. Effect of RA/BDNF-induced differentiation on the expression of Cytoskeletal Proteins	133
4.2.1.2.4. Effect of RA/BDNF-induced differentiation on Kinesin 5C, Dynein Light Intermediate Chain and the Proteasome ATPase PSMC1	137
4.2.2. Inhibition of Complex I and the Proteasome in RA/BDNF differentiated SH-SY5Y cells	139
4.2.2.1. Effect of complex I inhibition on the viability of RA/BDNF differentiated SH-SY5Y cells	139
4.2.2.2. Effect of Complex I Inhibition and Inhibition of Proteasome on Protein Expression	141
4.2.2.3. Effect of Inhibition of Complex I and the Proteasome on the Distribution of Cytoskeletal proteins	148
4.2.2.4. Effect of Inhibition of Complex I and the Proteasome on Macroautophagy	154
4.3 DISCUSSION	161
4.3.1. The Differentiation of SH-SY5Y neuroblastoma cells	161
4.3.1.1. Morphological Characteristics of RA and RA/BDNF differentiated SH-SY5Y neuroblastoma cells	161
4.3.1.2. The Effect of RA and RA/BDNF induced differentiation of SH-SY5Y neuroblastoma cells on mRNA and protein expression	161

4.3.1.3. Conclusion	165
4.3.2. Effect of Inhibition of Complex I and the Proteasome	167
4.3.2.1. Effects on proteins	167
4.3.2.2. Conclusion	172

CHAPTER 5: DEVELOPMENT AND CHARACTERISATION OF GFP-TAGGED NEUROFILAMENTS

5.1. INTRODUCTION	174
5.1.1. Green Fluorescent Protein	174
5.1.2. GFP-tagged Neurofilaments	174
5.1.3. Aims	176
5.2. RESULTS	177
5.2.1. Development and characterisation of GFP-tagged neurofilament medium chain	177
5.2.1.1. Cloning of human NF-M into pEGFP-C3	177
5.2.1.2. Characterisation of GFP/NF-M expression in SH-SY5Y cells	179
5.2.2. Development and characterisation of GFP-tagged neurofilament light chain	184
5.2.2.1. Cloning of human NF-L into pEGFP-C3	184
5.2.2.2. Characterisation of GFP/NF-L expression in SH-SY5Y cells	186
5.2.3. Development and characterisation of GFP-tagged neurofilament heavy chain	188
5.2.3.1. Cloning of human NF-H into pEGFP-C3	188
5.2.3.2. Characterisation of GFP/NF-H expression in SH-SY5Y cells	198
5.2.4. Immunoprecipitation of GFP tagged neurofilaments	203
5.2.4.1. Assessment of the solubility of GFP tagged neurofilaments in the immunoprecipitation lysis buffer	203
5.2.4.2. Identification of neurofilament-associating proteins by co-immunoprecipitation with GFP tagged neurofilaments	209
5.2.4.2.1. Determination of associated proteins by electrophoresis plus PMF	209
5.2.4.2.2. Determination of associated proteins using a targeted approach	211
5.2.5. The effect of an acute dose of MPP+ treatment on neurofilament dynamics in SH-SY5Y cells	213
5.3. DISCUSSION	217
5.3.1 GFP tagged neurofilaments	217
5.3.1.1. Development and characterisation of GFP/NF-M	217
5.3.1.2. Development and characterisation of GFP/NF-L	217
5.3.1.3. Development and characterisation of GF/NF-H	218
5.3.1.4. Conclusion	219
5.3.2. Neurofilament associating proteins identified by co-immunoprecipitation	220
5.3.2. Acute MPP+ treatment results in axonal retraction	221
5.3.4. Conclusion	222

CHAPTER 6: CONCLUSIONS AND FUTURE DIRECTIONS

6.1. DEGRADATIVE PATHWAYS INVOLVED IN THE TURNOVER OF CYTOSKELETAL PROTEINS	223
6.1.1. The half-lives and degradative pathways involved in the turnover of cytoskeletal proteins in SH-SY5Y cells	223

6.1.2. <i>Effects of complex I inhibition on cytoskeletal protein turnover</i>	224
6.1.3. <i>DA-mediated oxidative stress and cytoskeletal protein turnover</i>	226
6.2. ASSESSMENT OF PROTEIN AGGREGATION IN RA/BDNF DIFFERENTIATED SH-SY5Y CELLS FOLLOWING MITOCHONDRIAL DYSFUNCTION AND PROTEASOME INHIBITION	227
6.2.1. <i>Effects of mitochondrial dysfunction</i>	227
6.2.2. <i>Effects of proteasome inhibition</i>	229
6.2.3. <i>Effects of a combination of mitochondrial dysfunction and proteasome inhibition</i>	231
6.3. FUTURE DIRECTIONS	233
6.4. THE USE OF GFP TAGGED NFS TO MONITOR NF DYNAMICS	235
6.4.1. <i>Development and characterisation of GFP/NFs</i>	235
6.4.2. <i>Assessment of GFP/NF co-immunoprecipitation</i>	235
6.4.3. <i>Further recommendations for the use of GFP/NF subunits</i>	236
6.5. SUMMARY	237

CHAPTER 7: REFERENCE LIST

REFERENCES	238
-------------------	-----

APPENDICES

I. DETERMINATION OF THE MOLECULAR WEIGHTS OF αII-SPECTRIN BREAKDOWN PRODUCTS (SBDP)	i
II. OPTIMIZATION OF TRANSFECTION WITH LIPOFECTAMINE™2000	iii
III. RESTRICTION MAP AND MULTIPLE CLONING SITE OF pEGFP-C3	vi
IV. DETERMINATION OF THE MOLECULAR WEIGHT OF GFP AND GFP-TAGGED NEUROFILAMENTS	vi
V. PEPTIDE MASS FINGERPRINTS	xii
VI. PROPOSED EFFECTS OF COMPLEX I INHIBITION AND DA-MEDIATED OXIDATIVE STRESS ON DEGRADATIVE PATHWAYS AND TURNOVER OF CYTOSKELETAL PROTEINS	xvi

LIST OF FIGURES

CHAPTER 1: GENERAL INTRODUCTION

Figure 1.1 Images of Lewy bodies (LBs) in the substantia nigra (SNc) dopaminergic neurons from post-mortem samples of patients with sporadic PD.	4
Figure 1.2 A diagrammatic representation of the formation of aggresomes.	9
Figure 1.3 The Oxidation of Dopamine (DA).	11
Figure 1.4 Scheme describing the ubiquitination and degradation of proteins by the ubiquitin proteasome system.	16
Figure 1.5 Diagrammatic representations of the three main types of autophagy.	21
Figure 1.6 Autophagosome formation is controlled by ubiquitin-like reactions.	23
Figure 1.7 A scheme illustrating the proposed role of macroautophagy in the clearance of inclusions and protein aggregates.	26
Figure 1.8 A schematic of the assembly of neurofilament subunits into neurofilaments.	31
Figure 1.9 A cartoon drawing illustrating the position of various phosphorylation sites on the three neurofilament subunits.	34

CHAPTER 2: MATERIALS AND METHODS

Figure 2.1 A Typical plot of fluorescence units versus time (minutes) from which proteasome activity was determined.	55
Figure 2.2 Standard calibration curve for BSA (0 - 20 μ g) obtained using the BC Assay kit and measured at 570 nm.	57

CHAPTER 3: DEGRADATIVE PATHWAYS INVOLVED IN NEUROFILAMENT TURNOVER

Figure 3.1 Schematic diagram illustrating the inhibition of translational elongation by cycloheximide (CHX).	77
Figure 3.2 A diagrammatic representation of the role of LC3-II in autophagic vesicle formation.	83
Figure 3.3 A cartoon illustrating three theoretical scenarios in which a compound of interest may result in a change in the levels of LC3-II.	84
Figure 3.4 Assessment of the effect of cycloheximide (CHX) treatment of the viability of SH-SY5Y neuroblastoma cells.	87
Figure 3.5 Example of Western blots and plots from which the half-life of proteins were calculated.	89
Figure 3.6 Effect of the activation of macroautophagy by Rapamycin on the levels of NF-H compared to levels in total cells extracts of cycloheximide treated control cells.	92
Figure 3.7 The effects of treatment with various protease inhibitors on chymotrypsin-like activity (CLA) in SH-SY5Y cells	93
Figure 3.8 The activation of caspase 3 and calpain after 48 h treatment of SH-SY5Y cells with μ g/ml cycloheximide was assessed indirectly by monitoring the levels of α II-spectrin 145 kD and 120 kD cleavage products.	94
Figure 3.9 Effect of inhibition of proteolytic pathways on the cleavage of α II-spectrin in SH-SY5Y neuroblastoma cells.	95
Figure 3.10 Effect of inhibition of proteolytic pathways in SH-SY5Y neuroblastoma cells on the levels of LC3-II to monitor the inhibition or activation of macroautophagy.	96

Figure 3.11 Effect of inhibition of proteolytic pathways in SH-SY5Y cells on cathepsin activity.	97
Figure 3.12 Effect of MPP ⁺ and DA treatment on proteasome activity in SH-SY5Y cells.	100
Figure 3.13 Assessment of the morphology of SH-SY5Y neuroblastoma cells treated with 500 μ M Dopamine (DA) and 10 μ g/ml cycloheximide (CHX).	101
Figure 3.14 The Effect of MPP ⁺ and Dopamine (DA) treatment of SH-SY5Y cells on calpain and caspase 3 activity was investigated indirectly by monitoring the cleavage of α II-spectrin.	102
Figure 3.15 Effect of treatment of SH-SY5Y cells with 2 mM MPP ⁺ or 100 or 500 μ M Dopamine (DA) on the levels of LC3-II as a measure of macroautophagy.	103
Figure 3.16 Effect of treatment of SH-SY5Y cells with 2 mM MPP ⁺ or 100 μ M Dopamine (DA) was assessed using a fluorogenic peptide assay for cathepsin D activity.	105
Figure 3.17 Effect of co-treatment of SH-SY5Y neuroblastoma cells with MPP ⁺ or DA and a cysteine cathepsin inhibitor.	106
Figure 3.18 Determination of the effect of treatment with 2 mM MPP ⁺ and 100 μ M Dopamine (DA) on the activity of the cysteine cathepsins in SH-SY5Y neuroblastoma cells.	107
Figure 3.19 Schematic summarising the effect of 48 h treatment of SH-SY5Y neuroblastoma cells with MPP ⁺ (2 mM) with/without cycloheximide (CHX, 10 μ g/ml) or Dopamine (DA, 100 μ M or 500 μ M) with CHX on proteolytic pathways and the degradation of neurofilaments and cytoskeletal proteins.	119

CHAPTER 4: INHIBITION OF COMPLEX I AND THE PROTEASOME IN RA/BDNF DIFFERENTIATED CELLS

Figure 4.1 Schematic representation summarising the effect of RA and RA/BDNF induced differentiation of SH-SY5Y neuroblastoma cells on intracellular signalling cascades promoting cell survival and neuritogenesis.	123
Figure 4.2 Phase contrast images of SH-SY5Y cells differentiated using retinoic acid (RA) or RA followed by Brain Derived Neurotrophic Factor (BDNF).	127
Figure 4.3 The effect of RA and RA/BDNF-induced differentiation of the expression of GAPDH in SH-SY5Y cells.	130
Figure 4.4. A comparison of the mRNA copy number of GAPDH, β -actin and L32.	131
Figure 4.5 The expression of Neurotrophic Tyrosine Kinase Receptor B (NTrkB), tissue transglutaminase (TG2) and Bcl-2 in SH-SY5Y cells following differentiation with 10 μ M Retinoic acid (RA) or 10 μ M RA and 50 ng/ml Brain Derived Neurotrophic Factor (BDNF).	132
Figure 4.6 The expression of the neurofilament (NF) subunits in SH-SY5Y cells following differentiation with 10 μ M Retinoic Acid (RA) or 10 μ M RA and 50 ng/ml Brain Derived Neurotrophic Factor (BDNF).	134
Figure 4.7 Assessment of the effect of differentiation with 10 μ M retinoic acid (RA) or 10 μ M RA and 50 ng/ml Brain Derived Neurotrophic Factor (BDNF) on the phosphorylation of neurofilament (NF) heavy (H) and medium (M) subunits.	135
Figure 4.8 The expression of α -tubulin, vimentin and actin in SH-SY5Y neuroblastoma cells differentiated with 10 μ M retinoic acid (RA) or 10 μ M RA and 50 ng/ml Brain Derived Neurotrophic Factor (BDNF).	136

Figure 4.9 The expression of Kinesin 5C, Kinesin 5A and Dynein Light Intermediate Chain in SH-SY5Y cells differentiated with 10 μ M retinoic acid (RA) or 10 μ M RA and 50 ng/ml BDNF.	138
Figure 4.10 The expression of the Proteasome ATPase subunit, PSMC1, in SH-SY5Y cells following differentiation with 10 μ M retinoic acid (RA) or 10 μ M RA and 50 ng/ml Brain Derived Neurotrophic Factor (BDNF).	139
Figure 4.11 The effect of a range of MPP ⁺ concentrations on the viability of cells differentiated with 10 μ M Retinoic Acid (RA) and 50 ng/ml Brain Derived Neurotrophic Factor (BDNF) assessed by MTT reduction assay.	140
Figure 4.12 Effect of 24 h treatment with 500 μ M MPP ⁺ , 10 nM epoxomicin (epoxo) or 500 μ M MPP ⁺ and 10 nM epoxo on the expression of the three neurofilament subunits in RA/BDNF differentiated SH-SY5Y neuroblastoma cells.	142
Figure 4.13 Effect of treatment of RA/BDNF differentiated SH-SY5Y neuroblastoma cells with 500 μ M MPP ⁺ , 10 nM epoxomicin (epoxo) or 500 μ M MPP ⁺ /10 nM epoxo for 24 h on the phosphorylation status of NF-H and NF-M.	143
Figure 4.14 Assessment of the expression of α -tubulin, actin, vimentin and γ -tubulin following treatment of RA/BDNF differentiated SH-SY5Y cells with 500 μ M MPP ⁺ , 10 nM epoxomicin (epoxo) or 500 μ M MPP ⁺ /10 nM Epoxo for 24 h.	144
Figure 4.15 Assessment of the expression of kinesin 5C and 5A dynein light intermediate chain in RA/BDNF differentiated SH-SY5Y cells treated with 500 μ M MPP ⁺ , 10 nM epoxomicin (epoxo) or 500 μ M MPP ⁺ /10 nM epoxo for 24 h.	145
Figure 4.16 Effect of 500 μ M MPP ⁺ , 10 nM epoxomicin (epoxo) or 500 μ M MPP ⁺ /10 nM epoxo treatment of RA/BDNF differentiated SH-SY5Y neuroblastoma cells on the expression of PSMC1	146
Figure 4.17 Expression of tissue transglutaminase (TG2) in RA/BDNF differentiated cells treated with 500 μ M MPP ⁺ , 10 nM epoxomicin (epoxo) or 500 μ M MPP ⁺ /10 nM epoxo for 24 h.	146
Figure 4.18 Expression of Bcl-2 in RA/BDNF differentiated SH-SY5Y cells treated with 500 μ M MPP ⁺ , 10 nM epoxomicin (epoxo) or 500 μ M MPP ⁺ /10 nM epoxo for 24 h.	147
Figure 4.19 Effect of 24 h treatment of RA/BDNF differentiated SH-SY5Y cells with 500 μ M MPP ⁺ , 10 nM epoxomicin (epoxo) or 500 μ M MPP ⁺ /10 nM epoxo on the expression of α -synuclein.	147
Figure 4.20 The Levels of NF-M and phosphorylated NF-M in Igepal soluble and insoluble cell fractions of RA/BDNF differentiated SH-SY5Y cells treated with 500 μ M MPP ⁺ , 10 nM epoxomicin (epoxo) or 500 μ M MPP ⁺ /10 nM epoxo for 24 h.	149
Figure 4.21 Effect of 24 h treatment of RA/BDNF differentiated SH-SY5Y cells with 500 μ M MPP ⁺ , 10 nM epoxomicin (epoxo) or 500 μ M MPP ⁺ /10 nM epoxo on the levels NF-H and NF-L in igepal soluble and insoluble cell fractions.	150
Figure 4.22 Effect of 24 h treatment of RA/BDNF differentiated cells with 500 μ M MPP ⁺ , 10 nM epoxomicin (epoxo) or 500 μ M MPP ⁺ /10 nM epoxo on the levels of α -tubulin, vimentin and actin in the igepal soluble and igepal insoluble cell fractions.	151
Figure 4.23 The distribution of NF-H in RA/BDNF differentiated SH-SY5Y cells treated with 500 μ M MPP ⁺ , 10 nM epoxomicin (epoxo) or 500 μ M MPP ⁺ /10 nM epoxo for 24 h.	152

Figure 4.24 The distribution of vimentin in RA/BDNF differentiated SH-SY5Y cells treated with 500 μ M MPP+, 10 nM epoxomicin (epoxo) or 500 μ M MPP+/10 nM epoxo for 24 h.	153
Figure 4.25 Indirect measurement of macroautophagy by monitoring the levels of the autophagic vesicle marker, LC3-II, in RA/BDNF differentiated SH-SY5Y cells treated for 24 h with 500 μ M MPP+, 10 nM epoxomicin (epoxo) or 500 μ M MPP+/10 nM epoxo with or without 10 nM Bafilomycin A1 (BafA1).	154
Figure 4.26 The levels of p62 in RA/BDNF differentiated cells treated for 24 h with 500 μ M MPP+, 10 nM epoxomicin (epoxo) or 500 μ M MPP+/10 nM epoxo with or without Bafilomycin A1 (BafA1).	155
Figure 4.27 Effect of 24 h treatment of RA/BDNF differentiated cells treated with 500 μ M MPP+, 10 nM epoxomicin (epoxo) or 500 μ M MPP+/10 nM epoxo on the solubility of p62/SQSTM1 in igeal-containing cell lysis buffer.	156
Figure 4.28 Immunofluorescence staining of α -tubulin and p62/SQSTM1 in RA/BDNF differentiated SH-SY5Y cells treated for 24 h with 500 μ M MPP+, 10 nM epoxomicin (epoxo) or 500 μ M MPP+/10 nM epoxo.	157
Figure 4.29 Immunofluorescence staining of NF-H and p62/SQSTM1 in RA/BDNF differentiated SH-SY5Y cells either treated for 24 h with 500 μ M MPP+, 10 nM epoxomicin (epoxo) or 500 μ M MPP+/10 nM epoxo.	158
Figure 4.30 Effect of 24 h treatment of RA/BDNF differentiated SH-SY5Y cells with 500 μ M MPP+, 10 nM epoxomicin (epoxo) or 500 μ M MPP+/10 nM epoxo with or without 10 nM Bafilomycin A1 (BafA1) on the levels and activity of Cathepsin D.	159
Figure 4.31 Immunofluorescence staining of LC3 and NF-H in RA/BDNF differentiated SH-SY5Y cells treated with MPP+, epoxomicin (epoxo) or MPP+/epoxo.	160
Figure 4.32 Diagrammatic representation summarising of the effect of RA and RA/BDNF induced differentiation on protein expression in SH-SY5Y neuroblastoma cells.	166
Figure 4.33 Diagrammatic representation of the effects of 24 h treatment of RA/BDNF differentiated SH-SY5Y neuroblastoma cells with 500 μ M MPP+, 10 nM epoxomicin (epoxo) and 500 μ M MPP+/10 nM epoxo on protein levels and distribution.	173

CHAPTER 5: DEVELOPMENT AND CHARACTERISATION OF GFP-TAGGED NEUROFILAMENTS

Figure 5.1 The structure of GFP and its chromophore.	175
Figure 5.2 A schematic of the cloning procedure used to clone NF-M into pEGFP-C3.	179
Figure 5.3 The Characterisation of GFP/NF-M expression in SH-SY5Y cells.	180
Figure 5.4 Assessment of GFP/NF-M co-localisation with endogenous neurofilaments (NFs).	181
Figure 5.5 Assessment of the half-life of GFP/NF-M using Western blots of total cell extracts from SH-SY5Y neuroblastoma cells expressing GFP/NF-M and treated with 10 μ g/ml cycloheximide over a 72 hour time-course.	183
Figure 5.6 A schematic of the cloning procedure used to clone NF-L into pEGFP-C3.	186

Figure 5.7 Characterisation of GFP/NF-L expression in SH-SY5Y neuroblastoma cells.	187
Figure 5.8 GFP/NF-L aggregates were found in SH-SY5Y cells with high GFP/NF-L expression.	187
Figure 5.9 CpG plot showing GC content of NF-H cDNA and scheme depicting the cloning strategy adopted to clone the GC-rich N-terminus and the C-terminus of NF-H separately.	189
Figure 5.10 A schematic of the cloning procedure used to clone NF-H in two parts.	191
Figure 5.11 A Schematic describing the process by which N- and C-terminal parts of NF-H were ligated into the cloning vector (pCR-XL-TOPO).	193
Figure 5.12 The cloning strategy adopted to clone NF-H into the pEGFP-C3 expression vector using an EcoRI recognition sequence cloned into pEGFP-C3.	194
Figure 5.13 A schematic describing the subcloning of NF-H into pEGFP-C3.	195
Figure 5.14 Characterisation of truncated GFP/NF-H in SH-SY5Y neuroblastoma cells.	196
Figure 5.15 Sequence analysis of GFP/NF-H plasmid DNA revealed a single base deletion that resulted in a premature stop codon.	197
Figure 5.16 A Schematic describing the insertion of the base missing from the XmnI recognition sequence.	198
Figure 5.17 Characterisation of GFP/NF-H expression in SH-SY5Y neuroblastoma cells.	199
Figure 5.18 Co-localisation of GFP/NF-H with NF-M, NF-H and phosphorylated NF-M and NF-H in SH-SY5Y neuroblastoma cells.	200
Figure 5.19 Determination of the half-life of GFP/NF-H.	202
Figure 5.20 An illustration of the protocol used for the immunoprecipitation of GFP-tagged neurofilaments from cell lysates of SH-SY5Y cells.	203
Figure 5.21 Copperstained Western blot of Lysate supernatant (LS), excluded supernatant (ES) and cell debris pellet (P).	204
Figure 5.22 Analysis of the levels of GFP or GFP/NF in the lysate supernatant (LS), excluded supernatant (ES) and cell debris pellet (P) from untransfected cells (mock) or cells expressing either GFP, GFP/NF-M or GFP/NF-H.	205
Figure 5.23 The distribution of neurofilaments (NFs) in the lysate supernatant (LS), excluded supernatant (ES) and cell debris pellet (P) from SH-SY5Y neuroblastoma cells.	207
Figure 5.24 The Distribution of vimentin, α -tubulin and actin in the lysate supernatant (LS), excluded supernatant (ES) and pellet (P) from SH-SY5Y neuroblastoma cells.	208
Figure 5.25 SDS-PAGE and silver-staining of immunoprecipitated eluates from cell lysates of mock transfected cells and cells expressing GFP, GFP/NF-M or GFP/NF-H.	209
Figure 5.26 Two-dimensional SDS-PAGE of immunoprecipitates from cells expressing GFP or GFP/NF-M.	210
Figure 5.27 Co-immunoprecipitation of GFP/NF-M and GFP/NF-H with all three neurofilament subunits, phosphorylated NF-M and NF-H and vimentin.	211
Figure 5.28 Assessment of the presence/absence of a number of target proteins in immunoprecipitates from GFP/NF-M and GFP/NF-H expressing cells.	212
Figure 5.29 Analysis of the mean change in the length of axonal processes in GFP/NF-M expressing cells over time.	214
Figure 5.30 Mean change in the length of axonal processes of GFP/NF-H expressing cells during the first 45 minutes treatment with 5 mM MPP+.	215

Figure 5.31 Assessment of whether neurofilaments retract at a faster rate than the rest of the axonal process in GFP/NF-M expressing cells treated with 5 mM MPP+ for a period of 1 h.	216
---	-----

CHAPTER 6: CONCLUSIONS AND FUTURE DIRECTIONS

Figure 6.1 Flow diagram illustrating the effects of complex I inhibition on the activity of proteolytic pathways.	225
Figure 6.2 Flow diagram illustrating the effects of dopamine (DA)-mediated oxidative stress on the activity of proteolytic pathways.	227
Figure 6.3 Scheme representing the effects of 24 h treatment of RA/BDNF differentiated SH-SY5Y neuroblastoma cells with 500 μ M MPP+.	228
Figure 6.4 Scheme representing the effects of 24 h treatment of RA/BDNF differentiated SH-SY5Y neuroblastoma cells with 10 nM epoxomicin (epoxo).	230
Figure 6.5 Scheme representing the effects of 24 h treatment of RA/BDNF differentiated SH-SY5Y neuroblastoma cells with 500 μ M MPP+ and 10 nM Epoxomicin.	232

APPENDICES

Figure i The calculation of the apparent molecular weights of α II-spectrin breakdown products (SBDPs).	ii
Figure ii Determination of the optimum cell density required for transfection of SH-SY5Y neuroblastoma cells with LipofectAMINE™2000.	iv
Figure iii Determination of the optimum ratio of LipofectAMINE™2000 to DNA that resulted in the highest transfection efficiency while maintaining cell viability.	v
Figure iv Restriction Map and Multiple Cloning Site (MCS) of pEGFP-C3	vi
Figure v Determination of the molecular weights of GFP and GFP tagged neurofilaments of total cell extracts of SH-SY5Y cells expressing GFP, GFP/NF-M, GFP/NF-L or GFP/NF-H (truncated).	vii
Figure vi Determination of the molecular weight of GFP/NF-M and endogenous NF-M	viii
Figure vii Determination of the molecular weight of GFP/NF-L and endogenous NF-L	ix
Figure viii Determination of the molecular weight of GFP and GFP/NF-H	x
Figure ix Determination of the molecular weight of endogenous NF-H and GFP/NF-H	xi
Figure x Identification of GFP by mass spectrometry.	xii
Figure xi Identification of GFP/NF-H by mass spectrometry.	xii
Figure xii Identification of (A) GFP/NF-M and (B) NF-M in by mass spectrometry.	xiii
Figure xiii Identification of vimentin by mass spectrometry.	xiv
Figure xiv Identification of Hsc70 by mass spectrometry.	xv
Figure xv Summary of the proposed mechanisms of mitochondrial dysfunction and DA-mediated oxidative stress presented in this thesis integrated with current literature reviewed in chapter 1.	xvi

LIST OF TABLES

CHAPTER 1: GENERAL INTRODUCTION

Table 1.1 Genes identified in familial Parkinson's disease. _____	3
Table 1.2 List of proteins described as being components of Lewy bodies (LBs) _____	5

CHAPTER 2: MATERIALS AND METHODS

Table 2.1 List of Toxins and inhibitors used _____	44
Table 2.2 List of antibodies detailing their use, characteristics, the applications for which and concentration at which they were used and company they were purchased from _____	45
Table 2.3 Recipes for the preparation of resolving gel mix at various concentrations _____	58
Table 2.4 Stacking Gel Mix _____	58
Table 2.5 List of primers used for the amplification of neurofilament subunits _____	65
Table 2.6 List of primers used for the amplification of neurofilament subunits _____	68
Table 2.7 The linearization of standard plasmid DNA for each gene to relax the supercoiled DNA structure. _____	70
Table 2.8 Primers used to target sequences for amplification by Quantitative real-time PCR _____	74

CHAPTER 3: DEGRADATIVE PATHWAYS INVOLVED IN NEUROFILAMENT TURNOVER

Table 3.1 Summary of half-life data of cytoskeletal proteins determined in vivo from animal models or in vitro using cultured cells. _____	78
Table 3.2 Table summarizing the estimates of half-life for the neurofilament subunits, vimentin and α -tubulin using a range of cycloheximide concentrations. _____	88
Table 3.3 Estimates of half-life (T(1/2), h) and the effect of inhibition of the proteasome, macroautophagy, calpain and cathepsin D on the half-life of α -tubulin, α -synuclein, vimentin, NF-H, NF-M and NF-L. _____	91
Table 3.4 Estimates of half-life (T(1/2), h) and the effect MPP ⁺ and dopamine (DA) treatment on the half-life of α -tubulin, vimentin, NF-H, NF-M and NF-L. _____	99

CHAPTER 4: INHIBITION OF COMPLEX I AND THE PROTEASOME IN RA/BDNF DIFFERENTIATED CELLS

Table 4.1 Assessment of morphological characteristics to compare the efficiency of differentiation using 10 μ M Retinoic Acid (RA) or 50 ng/ml Brain Derived Neurotrophic Factor (BDNF) after 10 μ M RA pre-treatment. _____	129
Table 4.2 Effect of differentiation of SH-SY5Y cells with 10 μ M retinoic acid (RA) or 10 μ M RA and 50 ng/ml Brain Derived Neurotrophic Factor (BDNF) on protein and mRNA expression. _____	163
Table 4.3 Table summarising the effects of 24 h treatment of RA/BDNF differentiated SH-SY5Y cells with 500 μ M MPP ⁺ , 10 nM epoxomicin (epoxo) or MPP ⁺ /epoxo on protein and mRNA expression and the distribution of protein _____	168

CHAPTER 5: DEVELOPMENT AND CHARACTERISATION OF GFP-TAGGED NEUROFILAMENTS

Table 5.1 The transfection efficiency of GFP/NF-M in Human SH-SY5Y neuroblastoma cells using LipofectAMINE™2000.	182
Table 5.2 The transfection efficiency of GFP/NF-H in Human SH-SY5Y neuroblastoma cells using LipofectAMINE™2000.	201
Table 5.3 Summary of the results of immunoprobed Western blots of GFP/NF-M and GFP/NF-H immunoprecipitates used to identify NF-associating proteins.	221

LIST OF ABBREVIATIONS

ACN: acetonitrile
AD: Alzheimer's disease
ADP: adenosine diphosphate
ALS: amyotrophic lateral sclerosis
Atg: autophagy-related genes
ATP: adenosine triphosphate
BafA1: Bafilomycin A1
BCA: Bicinchoninic acid
BDNF: Brain derived neurotrophic factor
BSA: bovine serum albumin
CHX: cycloheximide
CK1: casein kinase I
CKII: casein kinase II
CLA: chymotrypsin-like activity
CMA: chaperone mediated autophagy
CMT: Charcot-Marie Tooth
COX6B: Cytochrome C oxidase subunit
CREB: cAMP-response element binding protein
DA: dopamine
DAT: dopamine transporter
DLB: dementia with Lewy bodies
DMEM: Dulbecco's modified eagles medium
DMSO: dimethyl sulfoxide
DMV: dorsal motor nucleus of the vagus
DNA: deoxyribose nucleic acid
DPBS: Dulbecco's phosphate buffered saline
DTT: dithiothreitol
DUB: deubiquitinating enzyme
E1: ubiquitin activating enzyme
E2: ubiquitin conjugating enzyme
E3: ubiquitin ligase
epoxo: epoxomicin
Erk: extracellular signal regulated kinase
HD: Huntington's disease
HEK293: human embryonic kidney 293
HSP: heat shock protein
GAP-43: growth associated protein-43
GFP: green fluorescent protein
IF: Intermediate filament
JNK: c-Jun-NH₂-terminal kinase
LB: Lewy body
LC3: light chain 3
LIR: LC3-II interacting region
LRRK2: Leucine rich repeat kinase 2
MAO: monoamine oxidase
MAP: microtubule associating protein
MAPK: mitogen-activated protein kinase
MF: microfilament
MPP+: 1-methyl-4-phenyl pyridinium
MPTP: 1-methyl-4-phenyl-1,2,3,6-tetrahydropyridine
MT: microtubule
MTOC: microtubule organising centre

MTT: 3-(4,5-dimethylthiazol-2-yl)-2,5-diphenyltetrazolium bromide
NeuN: neuronal nuclei
NGF: nerve growth factor
NIFID : Neuronal intermediate filament inclusion disease
NF: Neurofilament
NF-H: Neurofilament Heavy Chain
NF-M: Neurofilament Medium Chain
NF-L: Neurofilament Light Chain
NSE: neuron specific enolase
NT: neurotrophin
NTrkB: neurotrophic tyrosine kinase receptor B
6-OHDA: 6-hydroxy-dopamine
OPIDN: organophosphate induced delayed neuropathy
PAS: phagophore assembly site
PBS: phosphate buffered saline
PBI: N-terminal Phox and Bemlp
PCR: polymerase chain reaction
PD: Parkinson's disease
PepA: Pepstatin A
PI3K: phosphatidyl inositol 3-kinase
PKA: protein kinase A
PKC: protein kinase C
PKN: protein kinase N
PLA: caspase-like activity
PNS: peripheral nervous system
PP2A: protein phosphatase 2A
RA: retinoic acid
ROS: reactive oxygen species
RT-PCR: reverse transcription PCR
qRT-PCR: quantitative real-time PCR
SAP97: post-synaptic associated protein-97
SAPK: stress activated kinase
SBDP: spectrin breakdown products
SD: standard deviation
SDS-PAGE: sodium dodecyl sulphate polyacrylamide gel electrophoresis
SDS-PAG: sodium dodecyl sulphate polyacrylamide gel
SEM: standard error of the mean
SNpc: substantia nigra pars compacta
SOD1: superoxide dismutase 1
SQSTM1: sequestome 1
TBS: Tris buffered saline
TEA: triethylamine
TFA: trifluoroacetic acid
TG2: tissue transglutaminase
TH: tyrosine hydroxylase
TLA: trypsin-like activity
UBA: ubiquitin association
UCH-L1: ubiquitin C-terminal hydrolase L1
UPS: Ubiquitin Proteasome System
VDAC1: voltage-dependent anion channel 1
VMAT-2: vesicular monoamine transporter 2
WT: wild-type

CHAPTER 1

GENERAL INTRODUCTION

1.1. Background to Parkinson's disease

Parkinson's disease (PD) is a progressive neurodegenerative motor disorder first described by James Parkinson in 1817. It mainly affects the elderly and manifests in bradykinesia, rigidity, resting tremour, gait dysfunction and postural instability (reviewed by Olanow et al, 2001). Pathologically it is characterised by a selective degeneration of the dopaminergic neurons of the substantia nigra pars compacta (SNpc) but is only apparent once approximately 70 % of the nigral neurons have already been lost. A proportion of the remaining neurons contain intracytoplasmic inclusions called Lewy bodies (LBs, named after Fritz Heinrich Lewy) or Pale bodies (early forms of Lewy bodies) or may contain Lewy neuritis which are inclusions found in neuronal processes (Braak et al, 2003, reviewed by Olanow et al, 2004, and Robinson, 2008). Although most PD cases are idiopathic, genetic cases (Table 1.1) have provided insight into the pathways that may be involved in PD pathogenesis or disease progression (reviewed by Mouradian, 2002, and Robinson, 2008).

There is evidence for the involvement of defective cellular respiration in post-mortem PD brain (Parker et al, 1989) corroborated by the effects of the complex I inhibitor, 1-methyl-4-phenyl-1,2,3,6-tetrahydropyridine (MPTP) (Ballard et al, 1985, Ramsay et al, 1986) and the presence of oxidatively damaged mitochondrial complex I subunits in PD brain (Keeney et al, 2006). Furthermore, loss of function mutations (detailed in Table 1.1) in genes that play a role in the maintenance of mitochondrial homeostasis have been implicated in familial forms of PD (reviewed by Burbulla et al, 2010, and Schapira, 2009). The ability of toxins such as MPTP (Ballard et al, 1985, Langston et al, 1984, Langston, 1985) and rotenone (Betarbet et al, 2000, Panov et al, 2005, Sherer et al, 2002) to mimic aspects of parkinsonism has led to the suggestion that environmental factors such as exposure to herbicides or pesticides may be involved in PD, but to date no epidemiological evidence has identified a single causative agent (reviewed by Di Monte, 2001, Jenner, 2001, and Malkus et al, 2009). The lack of the discovery of a single cause has led to the suggestion that PD pathogenesis is multifactoral, involving both genetic (which could affect individual susceptibility) and environmental factors (reviewed by Di Monte, 2001, Jenner, 2001, and Sulzer, 2007). Interestingly cigarette smoking, coffee drinking (in men particularly) and high uric acid levels are associated with reduced risk of PD whereas significant head injury is associated with increased risk (Di Monte, 2001, Schapira, 2009). The protective effect of cigarette smoking may be due to inhibition of monoamine oxidase (MAO) by MAO inhibitors in smoke (Fowler et al, 1996) whereas the protective effect of coffee drinking may be due to the activation of the

phosphatidyl inositol 3 kinase (PI3K)/Akt pathway by caffeine which prevents apoptosis (Nakaso et al, 2008).

Increased oxidative stress (possibly resulting from mitochondrial dysfunction) has also been implicated in PD pathogenesis, evidence of which is in the form of oxidatively modified proteins, lipids and DNA in the substantia nigra of PD patients (Alam et al, 1997, Castellani et al, 1996, Lyras et al, 1998) and reduced levels of glutathione in PD brain (Riederer et al, 1989). The vulnerability of dopaminergic neurons may be a product of their structure and function, their high energy requirements and their predisposition to oxidative stress resulting from the auto-oxidation of dopamine (Hirsch et al, 1988, Sulzer, 2007, Sulzer et al, 2000).

PD is also characterised by the presence of aggregated proteins in LBs which suggests an accumulation of abnormal proteins modified by oxidative damage (Castellani et al, 1996, Dalfó & Ferrer, 2008) or aberrant phosphorylation (Chen & Feany, 2005, Forno et al, 1986, Hasegawa et al, 2002, Schmidt et al, 1996) and defective clearance by protein degradation pathways (McNaught et al, 2002, Schlossmacher et al, 2002). Since the discovery of mutations in *UCH-L1* (deubiquitinating enzyme) and *parkin* (an ubiquitin ligase) resulting in loss of function (Table 1.1), defects in the ubiquitin proteasome system (UPS) have been proposed to contribute to PD pathogenesis (Kitada et al, 1998, Leroy et al, 1998, Liu et al, 2002, Sriram et al, 2005). The bulk degradation of proteins may also occur via the autophagosome-lysosome pathway and since this pathway does not rely on the unfolding of proteins it may be a more efficient process than the UPS for the degradation of aggregated proteins (reviewed by Rubinsztein, 2006). Although previously thought of as a nonselective process, it is now known that protein complexes, aggregates and organelles can be targeted for degradation by macroautophagy by the interaction of p62/SQSTM1 and LC3-II in an ubiquitin-like reaction (discussed in more detail below, Pankiv et al, 2007). Due to the presence of p62 in proteinacious inclusions of numerous neurodegenerative conditions (Zatloukal et al, 2002) and the role of macroautophagy in the clearance of defective organelles including mitochondria (Geisler et al, 2010a) and protein aggregates (Lee et al, 2004, Rideout et al, 2004) more attention has recently been given to the role of the autophagosome-lysosome pathway in PD pathogenesis.

Table 1.1 Genes identified in familial Parkinson's disease.

Summary of the genetic causes of Parkinson's disease (PD) (reviewed by Burbulla et al, 2010, and Schapira, 2009).

<i>Gene</i>	<i>Function</i>	<i>Mutation</i>	<i>Clinical Features</i>	<i>References</i>
<i>Parkin</i> (<i>PARK2</i>)	Ubiquitin ligase and role in mitophagy	Several different types that result mainly in loss of function	Autosomal recessive juvenile onset (<40 y), symptoms can present as early as 7 y. No LBs.	(Kitada et al, 1998, Sriram et al, 2005)
<i>PINK1</i> (<i>PARK6</i>)	Mitochondrial kinase and role in mitophagy	Loss of function, mutations usually in kinase domain	Early onset parkinsonism (<40 y), early motor complications.	(Valente et al, 2004)
<i>DJ-1</i> (<i>PARK7</i>)	Transcription factor, chaperone, modulation of basal autophagy and mitochondrial homeostasis	Loss of function	Young onset and slow progression (rare).	(Bonifati et al, 2003)
<i>α-synuclein</i> (<i>PARK1</i> + <i>PARK4</i>)	Unknown function. May play a role in vesicular DA uptake.	Multiplication of WT; A53T; E46K; A30P	Duplications in late-onset, triplications in early onset. A53T and A30P - early onset with dementia. E46K - early dementia.	(Kruger et al, 1998, Polymeropoulos et al, 1997, Ross et al, 2008, Singleton et al, 2003)
<i>LRRK2</i> (<i>PARK8</i>)	Structure suggests numerous functions; protein-protein interaction, ubiquitin-binding, kinase and GTPase activity	several mutations, most common is G2019S in the kinase domain (increases autophosphorylation)	Numerous mutations linked to autosomal-dominant PD. Exhibit characteristics of several neurodegenerative diseases.	(Hernandez et al, 2005, reviewed in Mata et al, 2006, Zimprich et al, 2004)
<i>UCHL1</i> (<i>PARK5</i>)	ubiquitin carboxylhydrolase L1, deubiquitinating enzyme (DUB)	I93M missense mutation; reduced enzyme activity	Symptoms typical for PD	(Leroy et al, 1998)
<i>NF-M</i>	Neuronal intermediate filament	G336S mutation in the rod domain that results in abnormal assembly of NFs	Early onset PD, early but temporary response to levodopa.	(Lavedan et al, 2002)
<i>ATP13A2</i>	Lysosomal ATPase	Loss of function	Early onset PD with dementia	(Ramirez et al, 2006)

1.2. Lewy Bodies (LBs)

1.2.1. Background

LBs, classically described as having a dense core of granular material surrounded by fibrillar components that radiate at the periphery, may occur in isolation or in multiples, they may be spherical or elongated and range in size between 8-30 μm in diameter (Braak et al, 2003, Katsuse et al, 2003, reviewed by Shults, 2006). Images of LBs in the SNc from post-mortem samples from PD patients are shown in Figure 1.1.

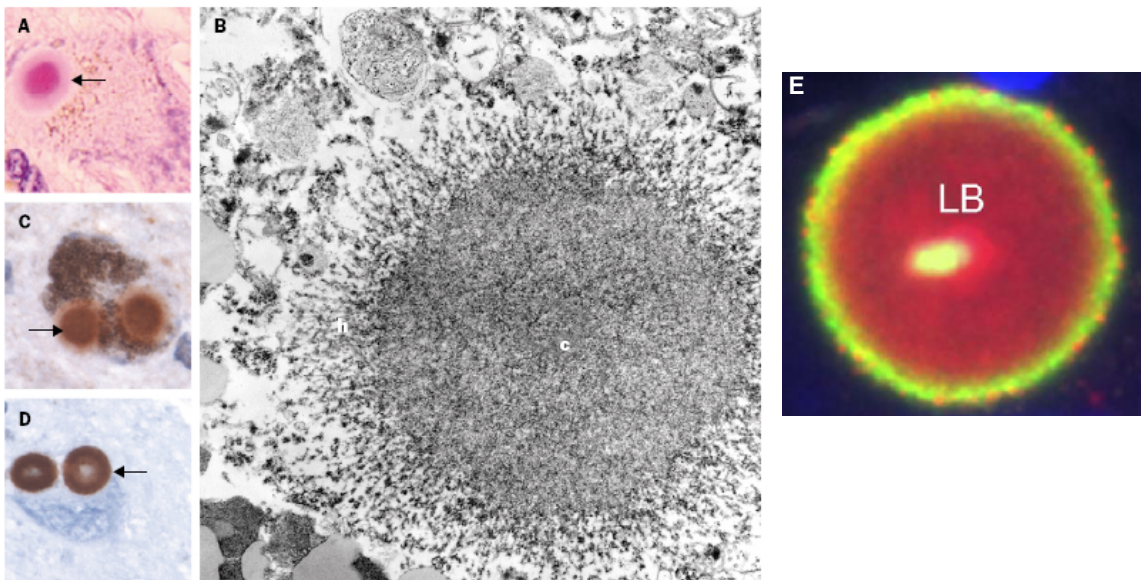


Figure 1.1 Images of Lewy bodies (LBs) in the substantia nigra (SNc) dopaminergic neurons from post-mortem samples of patients with sporadic PD.

(A) Eosin staining of spherical LBs with a distinct core and peripheral halo. (B) Electron micrograph of a LB reveals a dense core (c) and a peripheral halo of filamentous material (h). (C) LB stained with anti-ubiquitin, showing ubiquitin staining concentrated in the core. (D) LB stained with anti- α -synuclein revealed that α -synuclein staining is concentrated in the halo. (E) Immunofluorescence staining of LB for ubiquitin (red) and α -synuclein (green) revealed that ubiquitin staining was concentrated in the core and α -synuclein staining was concentrated in the halo. (A-D) Images obtained from Olanow et al (2004) and (E) image obtained from (McNaught & Olanow (2006).

LBs have been found to contain numerous proteins (some of which are listed in Table 1.2), the most abundant of which are α -synuclein, ubiquitin and the neurofilament (NF) subunits (Forno et al, 1986, Galloway et al, 1988, Galloway et al, 1992, Olanow et al, 2004, Schmidt et al, 1991).

Table 1.2 List of proteins described as being components of Lewy bodies (LBs)

Some known components of LBs discovered by immunohistochemical staining or analysis of protein components in isolated LBs

<i>Protein</i>	<i>Function</i>	<i>Reference(s)</i>
<i>α-synuclein</i>	Unknown	Presence in halo confirmed by immunohistochemistry (Katsuse et al, 2003, McNaught et al, 2002, Schlossmacher et al, 2002) and immuno-EM (Katsuse et al, 2003)
<i>ubiquitin</i>	Targets proteins for degradation by the proteasome	Core localisation established with immunohistochemistry (Galloway et al, 1988, Iwatsubo et al, 1996, McNaught et al, 2002, Schlossmacher et al, 2002, Schmidt et al, 1996, Schmidt et al, 1991) and immuno-EM (Galloway et al, 1992)
<i>Neurofilaments</i>	Neuronal intermediate filaments, cytoskeletal components	Presence in core and halo confirmed by Immunohistochemistry (Forno et al, 1986, Galloway et al, 1988, Hill et al, 1991, Iwatsubo et al, 1996, Schmidt et al, 1996, Schmidt et al, 1991) and immuno-EM (Galloway et al, 1992, Hill et al, 1991) , Western blotting (Pollanen et al, 1992)
<i>Parkin</i>	E3 ubiquitin ligase, involved in mitophagy	Presence in core established by immunohistochemistry (Schlossmacher et al, 2002). Western blotting of purified LBs immunoprecipitated the anti- α -synuclein (Schlossmacher et al, 2002)
<i>p62/SQSTM1</i>	p62 binds ubiquitinated proteins and LC3-II on autophagosomes	Presence in LBs confirmed by immunohistochemistry (Zatloukal et al, 2002)
<i>p35</i>	Cdk5 activator	Presence in LBs confirmed by immunohistochemistry (Nakamura et al, 1997)
<i>Cdk5</i>	Ser/Thr Kinase	Presence in halo and core established by immunohistochemistry (Brion & Couke, 1995, Nakamura et al, 1997, Takahashi et al, 2000) and immuno-EM (Takahashi et al, 2000)

Table 1.2 (continued)

<i>Protein</i>	<i>Function</i>	<i>Reference(s)</i>
<i>Tubulin</i>	Cytoskeletal component	Presence of tubulin confirmed by immunohistochemistry (Galloway et al, 1988, Katsuse et al, 2003). β -tubulin identified by an anti-Lewy body monoclonal antibody (Iwatsubo et al 1996)
<i>MAPI</i>	Microtubule associated protein 1	Immunohistochemistry (Galloway et al, 1988)
<i>MAP2</i>	Microtubule associated protein 2	Halo staining observed with immunohistochemistry (Galloway et al, 1988, Iwatsubo et al, 1996) but immunohistochemistry confirmed halo and core staining (Galloway et al, 1992)
<i>γ-Tubulin</i>	Cytoskeletal protein, component of centrosome	Presence in LBs confirmed by immunohistochemistry (McNaught et al, 2002)
<i>Pericentrin</i>	Component of centrosome	Presence in LB (more intense halo staining than core) confirmed by immunohistochemistry (McNaught et al, 2002)
<i>Components of the UPS (PA28, PA700)</i>	Degradation of proteins	Presence in core of LBs confirmed by immunohistochemistry (McNaught et al, 2002)
<i>Heat Shock Proteins (HSP70)</i>	Chaperones, protein folding and targeting of proteins for degradation	Presence in LBs confirmed by immunohistochemistry (McNaught et al, 2002)
<i>Tissue Transglutaminase (TG2)</i>	Cross-linking enzyme	Evidence of TG2 catalysed isodipeptide bonds in the halo of LBs that co-localises with α -synuclein (Junn et al, 2003)

It is noteworthy that unlike neurofibrillary tangles in AD, LBs do not stain with antibodies to tau (Brion & Couke, 1995, Galloway et al, 1988, Galloway et al, 1992, Pollanen et al, 1992), in addition other proteins that are abundantly expressed in neurons such as synaptophysin, β -synuclein and γ -synuclein are not found in LBs (reviewed by Olanow et al, 2004). LBs are not limited to the SNpc or to PD but are also found in the brains of patients suffering from dementia with LBs (DLB) and Alzheimer's disease (AD) in the cortical and brainstem regions and in some cases patients are diagnosed with both PD and AD (Brion & Couke, 1995, Iwatsubo et al, 1996, Schmidt et al, 1996, Schmidt et al, 1991, Takahashi et al, 2000).

As PD progresses LB pathology develops with it. During the earlier stages LBs are weakly stained with antibodies to α -synuclein and are less defined than at later stages when α -synuclein staining is more intense and LBs are well-defined (Braak et al, 2003, Katsuse et al, 2003). Pale bodies, often found in the SNpc and locus ceruleus and poorly stained with eosin have been hypothesized to be early forms of LBs (Braak et al, 2003, reviewed by Olanow et al, 2004, and Wakabayashi et al, 2006) and are usually larger in size than LBs and contain mitochondria (Bedford et al, 2008).

NFs (the first discovered protein components of LBs) are traditionally described as being localised to the filamentous halo of SNpc LBs (Forno et al, 1986, Galloway et al, 1988) however their presence in the core of detergent-treated SNc LBs was revealed by immunogold labelling and electron microscopy (Galloway et al, 1992). Cortical (Schmidt et al, 1991) and amygdala LBs (Schmidt et al, 1996) which stain poorly with eosin readily revealed NF staining in the core and halo. Since poor eosin staining is associated with earlier forms of LBs such as pale bodies (Braak et al, 2003, reviewed by Shults, 2006), the lack of core NF staining in immunohistochemistry of LBs may be an artefact resulting from the masking of NF epitopes in the densely compacted structure of the core. In fact work by Hill et al (1991) suggested that antibodies directed to the tail domain of NFs preferentially labelled NFs in the halo whereas antibodies directed to the rod and head domains labelled NFs in the LB core, an effect that may have been due the masking of epitopes in the core. Interestingly, although all three NF subunits (both phosphorylated and nonphosphorylated) have been found to be present in cortical LBs, phosphorylated NF-M (medium) appears to be the most prevalent subunit (Iwatsubo et al, 1996, Schmidt et al, 1991).

Many other neurodegenerative diseases such as amyotrophic lateral sclerosis (ALS), DLB and AD are also associated with abnormal accumulations of NFs in the brain (reviewed by Julien, 1999, and Petzold, 2005). Increased levels of NF-L have also been reported in the cerebrospinal fluid in patients with ALS and AD (Rosengren et al, 1996).

1.2.2. Aggresomes and Lewy bodies

Aggresomes were first described by Johnston, Ward and Kopito (1998) when they characterised the cellular and molecular response to the aggregation of misfolded proteins. They suggested that when the capacity of the proteasome is exceeded by either increased production of a misfolded protein or the impairment of the proteasome itself, aggregated proteins are sequestered into an ubiquitin-rich structure at the microtubule-organising centre (MTOC) and surrounded by a cage of vimentin filaments. They called this structure an aggresome. In addition to the aggregated proteins, mitochondria and vesicular bodies were also described trapped in the filamentous component of aggresomes. The authors suggested that the formation of aggresomes is a cellular response to remove abnormal aggregated proteins and promote cell survival (Figure 1.2, Johnston et al, 1998). Indeed work with huntingtin suggested that the formation of intranuclear inclusions of mutant huntingtin may be a cellular response to protect against cell death (Saudou et al, 1998).

Since the description of aggresomes a myriad of papers have been published describing the formation of aggresomes in numerous disease states and experimental models (Burnett & Pittman, 2005, Fu et al, 2005, Hasegawa et al, 2004, Kawaguchi et al, 2003, McNaught et al, 2002, Rajan et al, 2001). It is now accepted that aggresomes are formed in response to the accumulation of misfolded or damaged proteins which may be toxic to the cell as soluble oligomeric forms. These oligomeric forms are actively transported to the MTOC where they are accumulated into an aggresome and then degraded. Aggresomes are regions of enhanced proteolysis due to the recruitment of mitochondria, UPS components and autophagosomes and lysosomes (Fu et al, 2005, Kawaguchi et al, 2003, reviewed in Kopito, 2000).

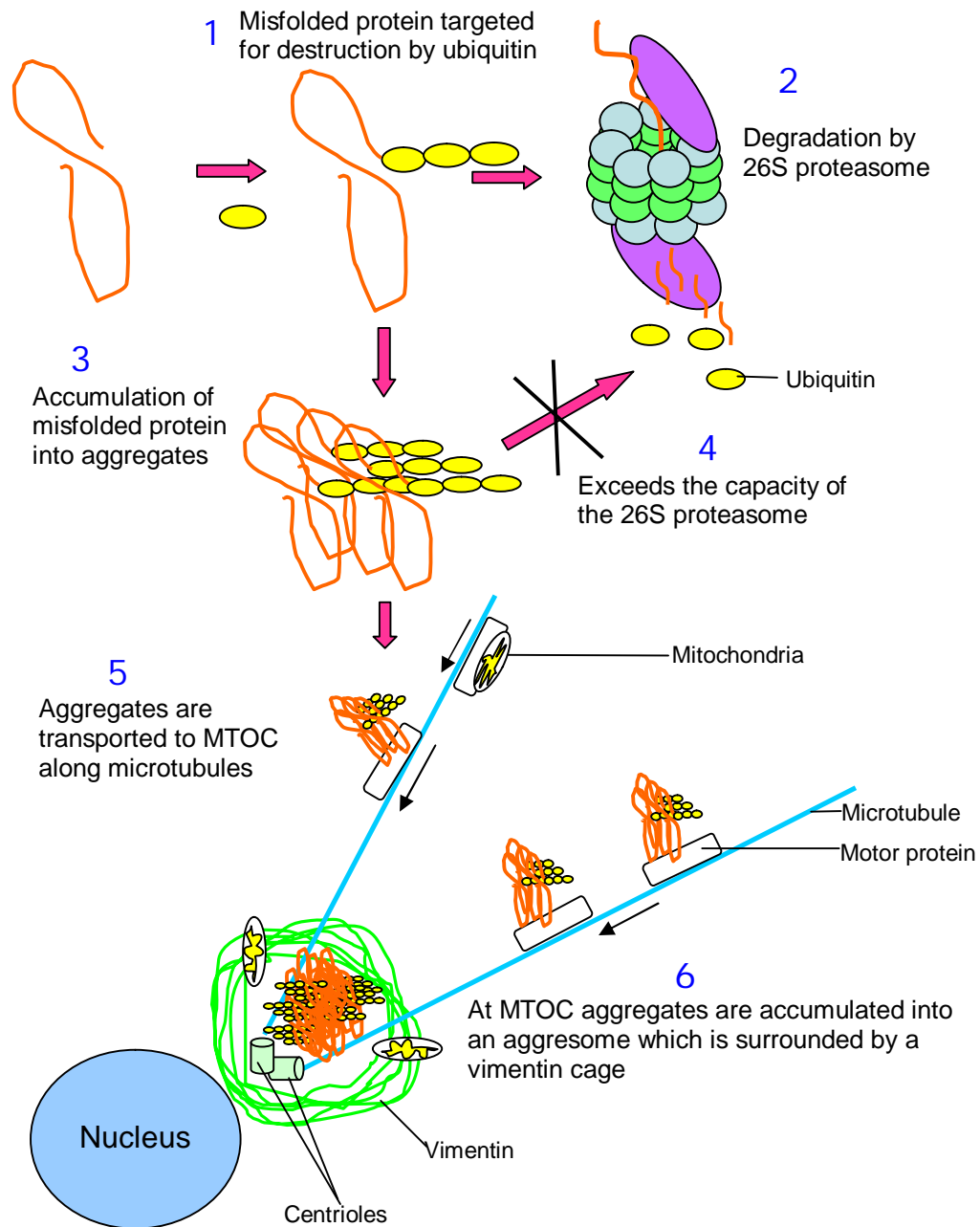


Figure 1.2 A diagrammatic representation of the formation of aggresomes.

Misfolded proteins are targeted for destruction by the Ubiquitin proteasome system (UPS) by the attachment of ubiquitin. If the capacity of the UPS is exceeded either via the overproduction of misfolded proteins or the impairment of the 26S proteasome, misfolded proteins are accumulated into aggregates. These aggregates are then transported along the microtubules to the microtubule organising centre (MTOC) where they are accumulated into a structure called an aggresome and surrounded by a 'cage' of vimentin filaments. In addition mitochondria and other vesicular structures are often found embedded in the filamentous component suggesting transport of mitochondria towards the aggresome (adapted from Johnston et al, 1998)

The centrosome is a natural choice as a 'hub' for protein degradation due to the close proximity of the endoplasmic reticulum (Wigley et al, 1999), lysosomes, chaperones such as Hsp70 and Hsp90 and the concentration in the centrosome of active proteasomal machinery

(Fabunmi et al, 2000, Wigley et al, 1999). Furthermore it is the MTOC from which microtubules, the tracks along which motor proteins move, originate. It is therefore the natural 'end-of-the-line' to which a retrograde motor would take its cargo. Interestingly, the presence of proteasomal elements in the centrosome is not dependent on an intact microtubule network suggesting that the UPS is not transported to the centrosome along the microtubule network (Fabunmi et al, 2000).

How and why LBs form remains unexplained despite extensive work in this area. The most promising hypothesis of LB formation suggests that LBs are originally formed as aggresomes for the removal of abnormal proteins that are potentially cytotoxic. However due to the over-production of abnormal proteins and the general failure of degradative pathways charged with their clearance, aggresomes are not cleared and form insoluble inclusions and LBs. Therefore LBs may be failed aggresomes (reviewed by McNaught et al, 2002, and Olanow et al, 2004). The lack of LBs in autosomal recessive juvenile parkinsonism resulting from loss of function mutations in the gene for parkin suggests that the ubiquitination of aggregated proteins is a requirement for their transport to the MTOC and aggresome formation (reviewed by Olanow et al, 2004).

1.3. Oxidative stress and mitochondrial dysfunction

1.3.1. Oxidative stress

1.3.1.1. Oxidative stress in neurodegeneration and ageing

Increased oxidative stress has been implicated in age-related neurodegenerative conditions due to the observed increase in oxidatively damaged proteins and lipids in post-mortem samples from patients with AD (Korolainen et al, 2006, Lyras et al, 1997, Smith et al, 1998), PD and DLB (Alam et al, 1997, Castellani et al, 1996, Lyras et al, 1998). Indeed the degree of lipid peroxidation and the levels of superoxide dismutase are increased in blood plasma from PD patients and accompanied by a decrease in the levels of glutathione (Sharma et al, 2008). This result is supported by another study of anti-oxidant levels in the blood of PD patients which showed an increase in the levels of superoxide dismutase and a decrease in the levels of antioxidants such as vitamin C and E compared to age-matched controls (Nikam et al, 2009).

1.3.1.2. Dopamine and the susceptibility of dopaminergic neurons

Dopamine (DA) is a neurotransmitter of dopaminergic neuronal cells which are responsible for the initiation of motor tasks and feedback (reviewed by Sulzer, 2007), a function which is evident when looking at the effects of dopaminergic neuronal loss on movement and the initiation of movement in patients with PD. DA is usually produced at neuronal terminals by the hydroxylation of tyrosine which is catalysed by tyrosine hydroxylase (TH, which is often used as a marker to stain dopaminergic neurons). Dopaminergic neurons are thought to be particularly susceptible to oxidative damage due to DA auto-oxidation in the presence of transition metal ions or deamination by MAO (Figure 1.3). The higher levels of MAO and iron in the SNpc increases the susceptibility of this region of the brain to oxidative stress compared to the rest of the brain (reviewed by Caudle et al, 2008, and Hom et al, 1997).

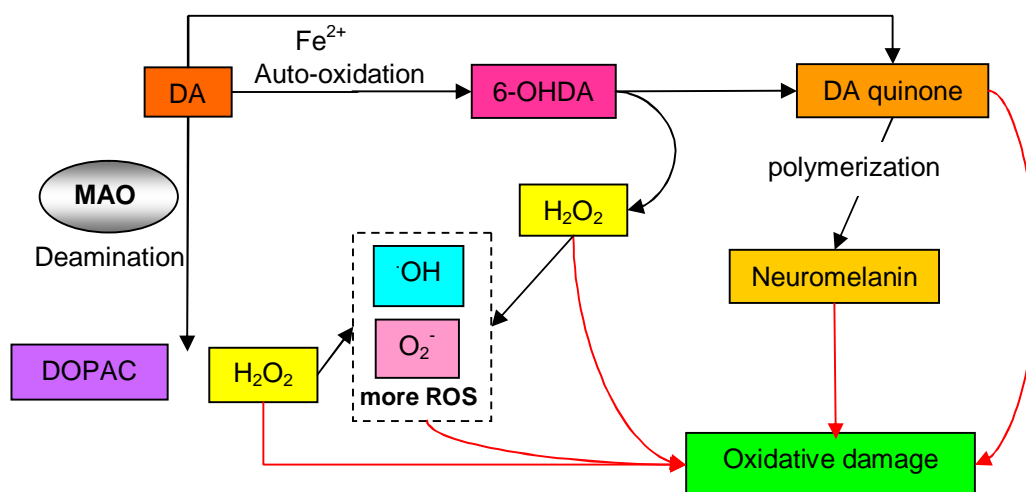


Figure 1.3 The Oxidation of Dopamine (DA).

Catalytic oxidation of DA by MAO results in the production of H_2O_2 and 3,4-dihydroxyphenylalanine which is rapidly oxidized to DOPAC by aldehyde dehydrogenase. Auto-oxidation of DA results in production of 6-hydroxy dopamine (6-OHDA) and H_2O_2 . Further oxidation of H_2O_2 produces additional reactive oxygen species (ROS), $\cdot\text{OH}$ and O_2^- . A more common DA auto-oxidation reaction is the production of DA quinone which polymerizes to form neuromelanin. All these products of DA oxidation can go on to cause oxidative damage to proteins, lipids and DNA (reviewed by Blum et al, 2001, Caudle et al, 2008, Luo et al, 1998, and Sulzer, 2007).

Dopaminergic neurons contain a number of feedback mechanisms to prevent DA toxicity including the inhibition of tyrosine hydroxylase, the uptake of DA into vesicles via the vesicular monoamine transporter-2 (VMAT-2), metabolism of DA by MAO and the reduction of DA quinone by glutathione. The maintenance of DA in synaptic vesicles against the concentration gradient is maintained by a vesicular H^+ -ATPase, the functioning of which can be undermined by a reduction in mitochondrial ATP production resulting in the release

of vesicular DA into the cytosol where it can contribute to neuronal toxicity (reviewed by Sulzer, 2007). The presence of DA enhanced the neurotoxicity and inclusion formation induced by neostriatal infusion of proteasome inhibitors in rats and in PC12 cells treated with proteasome inhibitors (Fornai et al, 2003).

Due to the preferential loss of dopaminergic neurons in PD, experimental models of PD have employed the use of DA, preferentially in cellular models (Hirrlinger et al, 2002, Stokes et al, 2002, Stokes et al, 2000), or 6-hydroxy-dopamine (6-OHDA) in both cellular (Cheung et al, 2009, Nakamura et al, 2006, Smith & Cass, 2007, Tirmenstein et al, 2005) and animal (Dabbeni-Sala et al, 2001, De Iuliis et al, 2005, Glinka et al, 1996) models. Due to the inability of 6-OHDA to cross the blood-brain barrier, the use of 6-OHDA in animal models of PD requires the direct injection of 6-OHDA into the striatum, SNpc or the ascending medial forebrain bundle (reviewed by Blum et al, 2001)

1.3.2. Mitochondrial dysfunction in neurodegeneration and ageing

Although the source of the increased ROS (reactive oxygen species) is uncertain, mitochondrial dysfunction has been implicated (reviewed by Butterfield & Kanski, 2001, Cassarino et al, 1997, Navarro et al, 2008), corroborated by the altered activity of complex I of the electron transport chain observed in the SNpc (Keeny et al, 2006) and in platelet mitochondria (Parker et al, 1989) of PD patients. Energy metabolism with ageing was also shown to be reduced by the accumulation of oxidatively damaged mitochondrial aconitase (an enzyme involved in the citric acid cycle) in ageing flies (Yan et al, 1997) and decreased mitochondrial energy production is observed in rat brain, particularly the hippocampus (associated with memory and cognitive abilities), with ageing (Navarro et al, 2008).

Support for the role of altered complex I activity in PD came from the accidental production of 1-methyl 4-phenyl 1,2,3,6-tetrahydropyridine (MPTP) as a contaminating by-product of synthetic heroine in Northern California in the 1980's. Drug users who injected MPTP quickly developed an accelerated form of Parkinsonism (Ballard et al, 1985, Langston et al, 1984, Langston, 1985, Snow et al, 2000). MPTP (capable of crossing the blood-brain barrier) is converted to its active metabolite, 1-methyl-4-phenyl pyridinium (MPP⁺), by monoamine oxidase B in astrocytes (Glover et al, 1986, Ransom et al, 1987). Once MPTP is converted to MPP⁺ it is concentrated in the brain due to the inability of MPP⁺ to cross the blood-brain barrier (reviewed by Tetrad & Langston, 1989). MPP⁺ is then selectively taken up by dopaminergic neurons via the DA transporter due to its structural similarity to DA

(Gessner et al, 1985, Javitch et al, 1985, Stephans et al, 2002) where it accumulates in mitochondria and inhibits complex I (Ramsay et al, 1986, Stephans et al, 2002).

As such MPTP treatment has been extensively used to establish experimental models of PD (Ahn et al, 2009, Bezard et al, 1997, Caneda-Ferron et al, 2008, Gupta et al, 1986, Langston et al, 1984, Shimoji et al, 2005, Stephans et al, 2002, Yazdani et al, 2006). The animal model that most closely resembles human PD is the MPTP treated primate model (Langston, 1985). It is noteworthy that the effects of MPTP were greater and more permanent in older primates and primates treated with small doses of MPTP over longer periods. Similarly aged mice were also shown to be more sensitive to MPTP treatment (Gupta et al, 1986).

Extensive evidence for the production of reactive oxygen species (ROS) as a result of MPTP/MPP⁺ treatment in animal (Blanchet et al, 1998, Cassarino et al, 1997, Fallon et al, 1997) and cellular models is available (Cassarino et al, 1997, Hom et al, 1997, Lotharius & O'Malley, 2000), however the toxic effects of MPTP/MPP⁺ are at least partly independent of ROS formation (Blanchet et al, 1998, Caneda-Ferron et al, 2008, Fonck & Baudry, 2001, Hom et al, 1997) and instead increase the vulnerability to oxidative stress (Lee et al, 2000). Cells capable of increasing energy production via glycolysis to compensate for decreased mitochondrial oxidative phosphorylation show some resistance to MPTP/MPP⁺ (Denton & Howard, 1987). Not only does MPTP result in increased ROS via complex I inhibition but also as a consequence of the release and intracellular accumulation of vesicular DA induced by the binding of acetylcholine receptors by MPTP (Lotharius & O'Malley, 2000, Song & Ehrich, 1997) and extracellularly as a result of DA efflux via the DAT transporter (Lotharius & O'Malley, 2000) and reduced DA re-uptake (Fonck & Baudry, 2001, reviewed in Obata, 2002, and Toshio et al, 2002). Indeed the presence of DA and its auto-oxidation increases the vulnerability of dopaminergic neurons to the effects MPTP/MPP⁺ (Boada et al, 2000, Lotharius & O'Malley, 2000).

1.4. The role of protein degradative pathways

A number of neurodegenerative diseases including PD are characterised by an abnormal accumulation of proteins into inclusion bodies (reviewed by Ross & Poirier, 2004). Under normal conditions the cytotoxic accumulation of proteins is prevented by their rapid clearance, so that equilibrium exists between the production of abnormal proteins and their degradation. Most protein degradation in the cell is mediated by the ubiquitin proteasome system (UPS) and the autophagy-lysosome pathway (reviewed by Goldberg, 2003, Martinez-Vicente & Cuervo, 2007, and Rubinsztein, 2006). However due to an age-related decline in proteolytic activity (Cuervo & Dice, 2000, Kapphahn et al, 2007, Keller et al, 2000, Kiffin et al, 2007, Sitte et al, 2000, Yu et al, 2009), the ability of cells to maintain this equilibrium is compromised during ageing.

1.4.1. Ubiquitin Proteasome System (UPS)

1.4.1.1. Structure and function

The UPS is not only responsible for the degradation of short-lived nuclear and cytosolic proteins and abnormal (misfolded or oxidatively damaged) proteins but also plays a role in the regulation of many cellular processes. It regulates the turnover of many regulatory proteins such as transcription factors and cell cycle regulators (reviewed by Coux et al, 1996) such as cyclin B and p27^{Kip1}, the degradation of which regulates the progression of cells through anaphase and triggers the G1/S transition respectively (Hattori et al, 2003, Machiels et al, 1997, Tsvetkov et al, 1999).

The 26S proteasome is an ATP-dependent multicatalytic proteolytic complex consisting of a 20S catalytic core and two 19S regulatory caps (PA700 or PA28, Figure 1.4), assembly of which requires the assistance of at least nine dedicated chaperones to ensure that the numerous proteins that make up the 26S proteasome are assembled correctly (reviewed by Bedford et al, 2010). The 20S catalytic core is a hollow barrel composed of two outer 7-membered rings of α -subunits and two inner 7-membered rings of β -subunits (Groll et al, 1997). Located on the β -rings and projecting into the inside of the barrel two of each of the three main types of catalytic active sites (trypsin-like, chymotrypsin-like and caspase-like) can be found (Heinemeyer et al, 1997).

In eukaryotes many different proteasomal subunits exist but based on their similarities all subunits can be classified as either α - or β -subunits. The core particle is composed of two identical halves in which the 7-membered α/β -rings are composed of 7 different α/β -subunits. The sequences of α -subunits are characterized by a high degree of conservation with all subunits containing a conserved motif at their N-terminus essential for the assembly of the proteasome (Coux et al, 1996, Yao et al, 1999). The sequences of the β -subunits on the other hand are not so conserved but all contain an N-terminal pro-sequence that is cleaved to reveal (on most β -subunits) an N-terminal threonine (Thr) residue (Coux et al, 1996) responsible for proteolytic activity (Jäger et al, 1999, Kisselev et al, 2000).

The N-termini of the α -subunits also control access to the proteolytic active sites confined within the core particle by forming a gated channel (Groll et al, 2000). This channel is opened by the 19S regulatory subunit which is responsible for interacting with proteins targeted for degradation by the UPS via a process called ubiquitination (the covalent binding of ubiquitin to the target protein). Ubiquitin is a 76 amino acid polypeptide (reviewed in Glickman & Ciechanover, 2002) which covalently binds to target proteins via one of its seven lysine residues.

The number of ubiquitin residues and the particular lysine residue linked to the target proteins acts as a signal targeting the proteins either for destruction (which requires at least four ubiquitin moieties linked via their *Lys48* residues) or for any of the non-proteolytic signalling functions of ubiquitin. Although *Lys63* chains are usually associated with non-proteolytic functions, the 26S proteasome binds both *Lys48* and *Lys63* polyubiquitinated proteins and both are degraded by the 26S proteasome (Bedford et al, 2010). The conjugation of ubiquitin to a target protein as illustrated in Figure 1.4 is accomplished by three different enzymes; E1 (ubiquitin-activating enzyme), E2 (ubiquitin-conjugating enzyme) and E3 (ubiquitin ligase; Glickman & Ciechanover, 2002).

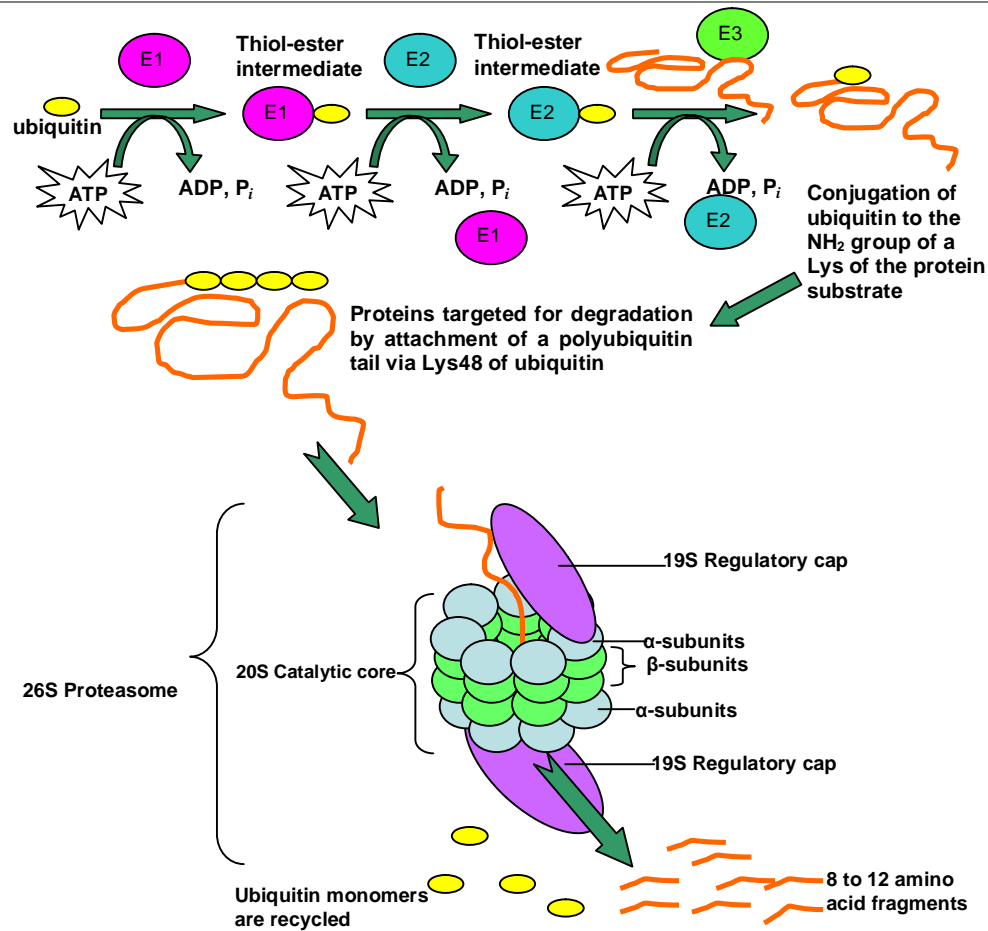


Figure 1.4 Scheme describing the ubiquitination and degradation of proteins by the ubiquitin proteasome system. E1 (ubiquitin-activating enzyme) activates ubiquitin via the hydrolysis of ATP to produce a high-energy thiol ester intermediate (E1-S~ubiquitin). Ubiquitin is then transferred to E2 (ubiquitin conjugating enzyme) via ATP hydrolysis to produce of another high-energy thiol ester intermediate (E2-S~ubiquitin). Ubiquitin is then transferred from E2 to a cysteine residue in the active site of E3 (ubiquitin ligase) which is bound to the protein substrate and catalyses the conjugation of ubiquitin to the ϵ -NH₂ group of a lysine residue of the protein substrate. Once the protein is ubiquitinated, further ubiquitin monomers are linked via their Lys48 residues to produce a polyubiquitin chain of at least 4 ubiquitin moieties which targets it to the 19S regulatory subunit of the 26S proteasome. The 26S Proteasome consists of 2 seven-membered rings each of α - and β -subunits, stacked one on top of the other to form the barrel-shaped 20S catalytic core. Two regulator 19S caps can be found at the entrance and exit. Proteins to be degraded (represented here in orange) are unfolded and pass through the inside of the 20S catalytic core where they are broken down (Ardley et al, 2005, Glickman & Ciechanover, 2002, ves-Rodrigues et al, 1998), resulting in fragments of 8-12 amino acids in length (Kisselev et al, 1999). Ubiquitin carboxy-terminal hydrolases or deubiquitinating enzymes (DUBs) which have the ability to break isopeptide bonds are responsible for the depolymerisation and recycling of ubiquitin chains (Coux et al, 1996, Glickman & Ciechanover, 2002).

1.4.1.2. Proteasomal deficiency during ageing and neurodegeneration

1.4.1.2.1. Overview

An age-related decline in proteasome activity has been reported in a number of tissues including the brain, retina and spinal cord (Kapphahn et al, 2007, Keller et al, 2000). In a recent proteomic analysis of oxidatively modified proteins with ageing, the deubiquitinating enzyme UCH-L1 was identified providing further support for the decline in UPS-directed protein degradation with ageing (Toda et al, 2010).

As mentioned earlier (section 1.3.1.1) oxidatively damaged proteins are increased with age and in PD and DLB, suggesting increased oxidative stress. One of the functions of the proteasome is the degradation of oxidatively modified proteins, which can be degraded in an ATP and ubiquitin independent manner directly by the 20S proteasome (Shringarpure et al, 2003). However, there is evidence that the proteasome itself is sensitive to oxidative damage, as seen in the spinal cord of aged rats (Keller et al, 2000) and in SH-SY5Y cells treated with dopamine (Caneda-Ferron et al, 2008). Lipofuscin/ceroid (a biological marker of ageing) accumulating in ageing post-mitotic fibroblasts has also been shown to directly inhibit proteasome activity (Sitte et al, 2000). The loss of proteasome function and increased oxidative damage with age has a cumulative effect resulting in increased vulnerability of cells to oxidative damage and the accumulation of oxidatively damaged proteins that are not cleared. Indeed inhibition of the proteasome with lactacystin in SH-SY5Y neuroblastoma cells increases the vulnerability of these cells to oxidative damage (Lev et al, 2006).

It has been reported that all three proteolytic activities [chymotrypsin-like (CLA), trypsin-like (TLA) and caspase-like (PLA)] of the proteasome are reduced in PD nigral tissues compared to age-matched controls (McNaught & Jenner, 2001, McNaught et al, 2003), a result supported in a further study by Tofaris et al (2003) who compared chymotrypsin-like activity in various brain regions of PD patients. The reduction in proteasome activity may be the result of an observed selective loss of the 20S α -subunits in the SNpc, the loss of which would prevent the normal assembly of proteasomes (McNaught et al, 2002, McNaught et al, 2003). Furthermore, a reduction in the levels PA700 and PA28 regulatory subunits was also observed in PD SNpc (McNaught et al, 2003). Support for the role of proteasome dysfunction in PD comes from early onset forms of the disease which arise due to mutations in components of the UPS; parkin (an ubiquitin ligase) and ubiquitin C-terminal hydrolase L1 (UCH-L1) (reviewed by Betarbet et al, 2005, Kitada et al, 1998, Leroy et al, 1998) and the

reduced expression of UCH-L1 mRNA and protein in the medulla oblongata and SNpc of PD patients with LB pathology (Barrachina et al, 2006).

Lys63 polyubiquitinated proteins are accumulated in characteristic inclusions of neurodegenerative conditions such as Huntington's disease (HD), AD and PD (reviewed by Bedford et al, 2010). In addition, immunohistochemical studies of LBs have revealed the presence of UPS components such as the ubiquitin activating enzyme E1, the regulatory subunits PA700 and PA28, the chaperone HSP70 (McNaught et al, 2002, reviewed in Olanow et al, 2004), 26S proteasome ATPase, ubiquitin conjugating enzyme UbcH7 (E2) and UCH-L1 (reviewed by Licker et al, 2009).

1.4.1.2. The effects of mitochondrial dysfunction on proteasome activity

The treatment of human SH-SY5Y neuroblastoma cells with the PD mimetic MPP⁺ also resulted in decreased activity of CLA and PLA of the proteasome, however since anti-oxidants were not protective in these cells, the effect of MPP⁺ on the proteasome in this case was reported not to be dependent on oxidative damage but rather through limited ATP availability (Caneda-Ferron et al, 2008). Furthermore, treatment of marmosets with MPTP resulted in a reduction in the activity of all three proteolytic activities of the 20S proteasome (CLA, TLA and PLA) and in the expression of the regulatory and structural subunits of the 26S proteasome (Zeng et al, 2006). Continuous infusion of rats with MPTP was also reported to result in a reduction proteasome activity (Fornai et al, 2005).

A role for the UPS in the clearance of aggregated proteins induced by chronic MPP⁺ treatment of rat mesencephalic neuronal cells was suggested by Sawada et al (2004) due to the increase in protein aggregation and inclusion formation following proteasome inhibition. In this case proteasome inhibition and aggregate formation was also accompanied by neuroprotection. Similarly, intranigral injection of rats with MPP⁺ and proteasome inhibitors revealed dopaminergic neuronal loss with MPP⁺ treatment which was blocked by proteasome inhibition (Sawada et al, 2004), suggesting again that the proteasome is involved in MPP⁺ induced cell death and that inclusions are protective. A role for the proteasome in cell death was also shown in HT22 cells and rat primary neuron cultures as a result of oxidative glutamate toxicity (van Leyen et al, 2005). However in rat cortical neurons proteasome inhibition induced apoptotic cell death (Rideout & Stefanis, 2002), suggesting that the role of the proteasome in cell survival and cell death is more complex. Increased levels of ubiquitinated proteins were also observed in human SK-N-MC neuroblastoma cells treated chronically with a rotenone (Sherer et al, 2002).

There is evidence of the involvement of other proteolytic pathways in the clearance of aggregated proteins. The clearance of aggregated proteins during washout and recovery of rotenone treated cells was only partially blocked by proteasome inhibition suggesting that other pathways are also involved in the clearance of aggregated proteins and aggresomes (Lee et al, 2002). One of the other pathways may be macroautophagy which is discussed in more detail in section 1.4.2.

1.4.1.2.3. The use of proteasome inhibitors as models for neurodegeneration

Since the suggestion of a role for defects in proteasome activity in neurodegenerative conditions characterized by protein aggregates, proteasome inhibition has been extensively used to induce inclusion formation in experimental models (Ardley et al, 2003, Bedford et al, 2008, Fornai et al, 2003, Ito et al, 2002, Junn et al, 2002, Rideout et al, 2001, Rideout & Stefanis, 2002, Sullivan et al, 2004). Evidence that inclusion formation is an active process is the requirement of transcription, which verifies that inclusions are not simply formed due to the passive build-up of ubiquitinated proteins that are not degraded. In addition ubiquitination is a requirement for the formation of inclusions (Rideout et al, 2005, Rideout & Stefanis, 2002). In HEK293 cells, proteasome inhibition and/or expression of a mutant aggregate-prone protein resulted in the expansion of the centrosome and recruitment of proteasomal elements from the cytosol (Wigley et al, 1999).

In cellular models, proteasome inhibition resulted in the formation of protein aggregates and inclusions (Fornai et al, 2003, Ito et al, 2002, Rideout et al, 2005, Rideout et al, 2001, Rideout & Stefanis, 2002) that preceded apoptotic cell death at later time-points (Rideout et al, 2005, Rideout & Stefanis, 2002). These aggregates contained proteins such as α -synuclein, ubiquitin (Fornai et al, 2003, Rideout et al, 2001, Rideout & Stefanis, 2002), chaperones such as Hsp70 and Hsp27, proteasomal subunits (Ito et al, 2002, Rideout & Stefanis, 2002), parkin, the ubiquitin-activating enzyme E1 (Fornai et al, 2003), and intermediate filaments such as α -internexin (Rideout & Stefanis, 2002) and vimentin (Ito et al, 2002). Similar inclusions were formed following proteasome inhibition in cellular models overexpressing parkin (Ardley et al, 2003, Junn et al, 2002).

Chronic low level proteasome inhibition in SH-SY5Y cells resulted in increased mitochondrial oxidative stress, reduced oxygen consumption at maximum respiration, reduced mitochondrial protein synthesis and increased association of mitochondria with lysosomal structures indicating increased mitochondrial turnover. In addition these cells also

contained the products of partial mitochondrial degradation and high concentrations of Lipofuscin indicating reduced macroautophagy (Sullivan et al, 2004). Therefore deficiencies in proteasome activity as observed during ageing and in age-related neurodegenerative conditions are likely to have an effect on the maintenance of mitochondrial homeostasis.

Intragastric injection of proteasome inhibitors in rats resulted in the formation of α -synuclein-positive inclusions in the dorsal motor nucleus of the vagus (DMV) but this was not accompanied by degeneration and no effect on the dopaminergic neurons of the substantia nigra was observed, the lack of which was attributed by the authors to the short treatment regime used (Miwa et al, 2006). Another study which employed microinfusion of proteasome inhibitors into the neostriatum of rats, revealed selective loss of dopaminergic neurons of the SNpc and the formation of inclusions immunoreactive for α -synuclein, ubiquitin, parkin and the ubiquitin activating enzyme E1 (Fornai et al, 2003).

Further evidence for the role of the proteasome in aberrant protein aggregation was obtained from a transgenic mouse model of 26S proteasome depletion resulting from the targeted conditional knockout of *PSMC1* (a proteasome ATPase which is an essential subunit of the 19S regulator cap). In these mice, *PSMC1* knockout was targeted to the catecholaminergic neurons and resulted in neurodegeneration and LB-like inclusions resembling pale bodies that contained proteins such as ubiquitin, α -synuclein, p62, γ -tubulin, NF, α B crystallin and numerous mitochondria and spherical structures (Bedford et al, 2008).

1.4.2. Autophagy-Lysosome Pathway

1.4.2.1. Background

Autophagy is traditionally described as a cellular adaptation to starvation (particularly in single cell organisms) which allows cells to provide for their energy and amino acid needs by self-digestion or catabolism until the situation improves. In humans autophagy can be upregulated in cells of organs such as the liver between meal times. Basal levels of autophagy are essential for the maintenance of cellular homeostasis allowing for the turnover of long-lived proteins and it is the only pathway available for the turnover of organelles and large protein complexes (reviewed by Ichimura et al, 2008b, and Nixon, 2006).

Autophagy can be divided into three main categories, represented in Figure 1.5:

- 1) *Macroautophagy*: a portion of the cytoplasm is engulfed by a newly formed autophagosome or phagophore. The outer membrane of the mature

autophagosome fuses with a lysosome which is followed by the degradation of its inner membrane and contents by the lysosomal proteases (reviewed by Bandhyopadhyay & Cuervo, 2007, Ichimura et al, 2008a, Luzio et al, 2007, Martinez-Vicente & Cuervo, 2007, and Mizushima et al, 2008).

- 2) *Microautophagy*: the lysosomal membrane invaginates and engulfs a small portion of the cytoplasm (Martinez-Vicente & Cuervo, 2007, Mizushima et al, 2008).
- 3) *Chaperone mediated autophagy (CMA)*: CMA is a more selective form of autophagy in which proteins are targeted for degradation by chaperone proteins such as Hsc70 which interacts with the lysosomal membrane receptor LAMP-2A (Bandhyopadhyay & Cuervo, 2007, Martinez-Vicente & Cuervo, 2007, Mizushima et al, 2008).

After degradation of proteins and lipids the resultant macromolecules are released into the cytosol via lysosomal permeases for recycling (reviewed by Xie & Klionsky, 2007).

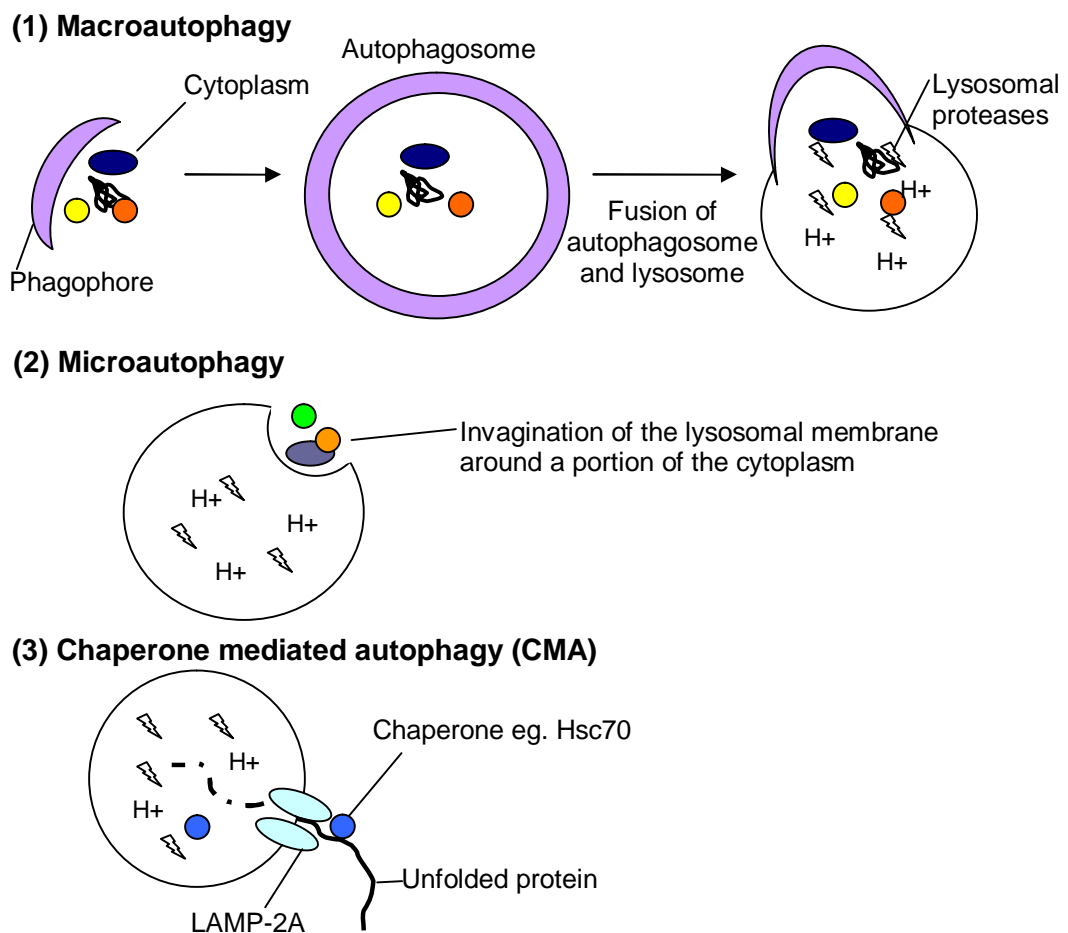


Figure 1.5 Diagrammatic representations of the three main types of autophagy.

(1) Macroautophagy, in which a phagophore forms and engulfs a portion of the cytoplasm, the autophagosome matures and then fuses with a lysosome; (2) Microautophagy, involves the invagination of the lysosomal membrane around a portion of the cytoplasm; and (3) Chaperone mediated autophagy (CMA), in which proteins are targeted for degradation by the lysosome by the binding of chaperone proteins such as Hsc70 which in turn binds to lysosomal membrane receptor, LAMP-2A (adapted from Martinez-Vicente & Cuervo, 2007, and Mizushima et al, 2008).

1.4.2.2. Macroautophagy

1.4.2.2.1. Autophagosome membrane formation

The process of autophagosome synthesis has been extensively studied in yeast and as such many of the components are called *Atg* (Autophagy-related genes) proteins based on their nomenclature in yeast models. Autophagosome synthesis in mammalian cells can apparently initiate anywhere in the cytoplasm (reviewed by Simonsen & Tooze, 2009) unlike yeast in which all autophagosomes arise from a single phagophore assembly site (PAS) containing *Atg* components required for autophagosome synthesis (Mari et al, 2010). However the source of the initiating phagophore membrane in mammalian cells is still elusive (Simonsen & Tooze, 2009). Recently Axe et al (2008) identified phosphatidylinositol 3-phosphate (PI-3P) rich structures called omegasomes near the endoplasmic reticulum in response to nutrient starvation in mammalian cells. These structures also contained *Atg8* (LC3, microtubule associated protein 1 light chain 3) and *Atg5*, proteins involved in autophagosome synthesis (Axe et al, 2008). The initiation of the autophagophore membrane requires the presence of assembly components such as beclin 1, *Atg14* and the class III phosphatidylinositol 3-kinase complex (*Vps34*; Itakura et al, 2008, Juhász et al, 2008).

Autophagosome synthesis is controlled by an ubiquitin-like conjugation system (Figure 1.6), involving two ubiquitin-like proteins, *Atg12* and LC3, both of which have a ubiquitin fold at their C-terminus. The recruitment of the ubiquitin-like conjugation system to the PAS is controlled by a self-assembling protein called *Atg9* (*ATG9L1*) which is normally found in punctate structures and is transported to the PAS by the *Atg9* transporting factors *Atg23* and *Atg27* (reviewed by Nixon, 2006, and Xie & Klionsky, 2007). In a recent report LC3 was shown to be phosphorylated by protein kinase A (PKA) at *Ser12* and that the induction of macroautophagy was dependent on LC3 dephosphorylation (Cherra et al, 2010).

The fusion of autophagosome and lysosome is dependent upon the presence of an intact microtubule network suggesting a role for microtubule motor proteins in the transport of autophagosomes to lysosomes (Webb et al, 2004). In fact disruption of dynein activity by the expression of dynein with ALS-associated mutations in PC12 cells expressing either mutant huntingtin or A53T α -synuclein impaired the autophagic clearance of protein aggregates (Ravikumar et al, 2005).

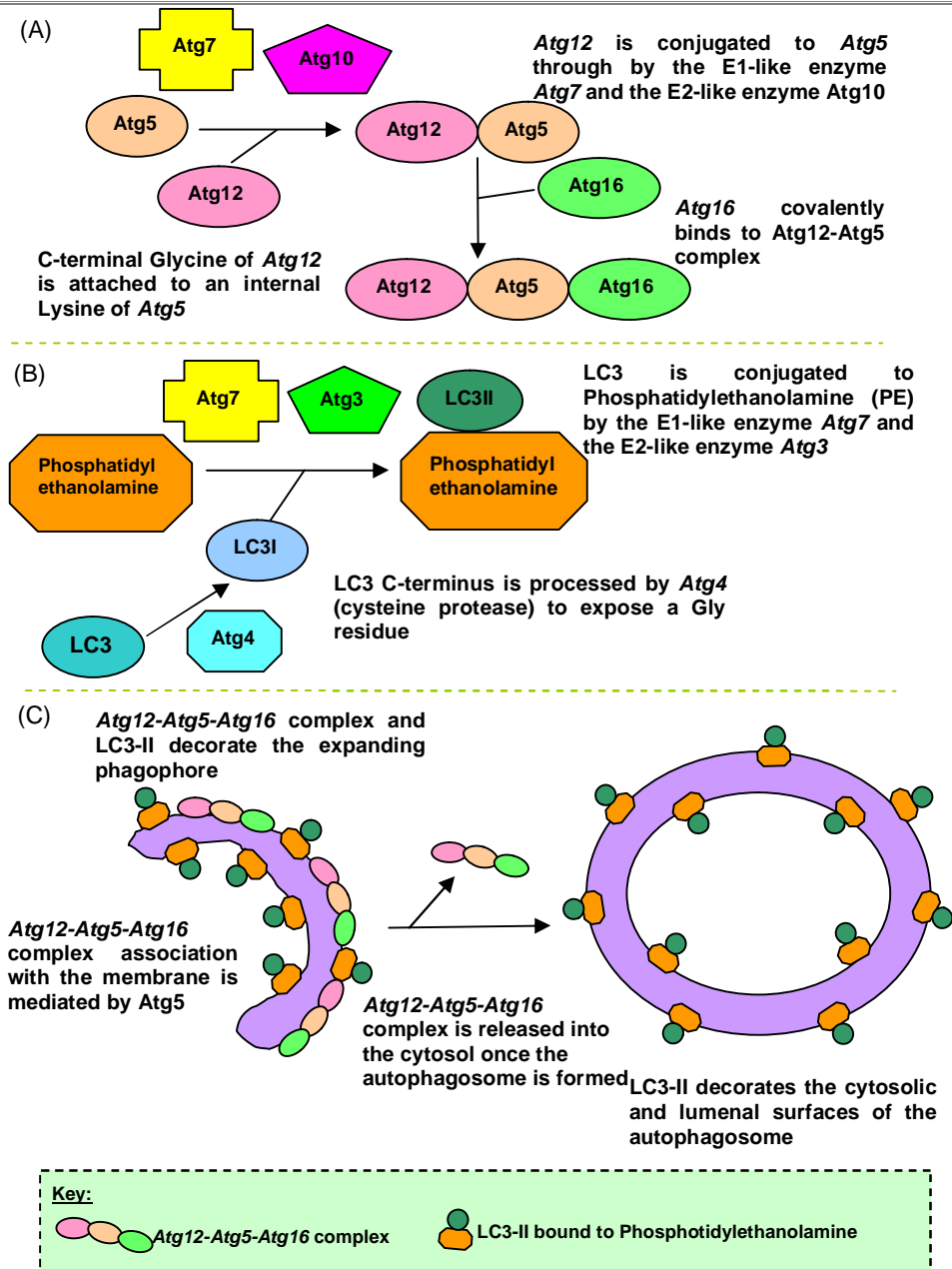


Figure 1.6 Autophagosome formation is controlled by an ubiquitin-like reactions.

(A) Formation of the *Atg12-Atg5-Atg16* complex is a ubiquitin-like conjugation event in which the binding of the C-terminal Glycine residue of *Atg12* to an internal Lysine residue of *Atg5* is facilitated by the E1-like activating enzyme *Atg7* and the E2-like conjugating enzyme *Atg10*. *Atg16* then covalently binds to the *Atg5* of the *Atg12-Atg5* complex on the side opposite to *Atg12*. The association of the *Atg12-Atg5-Atg16* complex with the expanding phagophore membrane is mediated by *Atg5*. (B) The conjugation of LC3 to phosphatidylethanolamine (PE) is another ubiquitin-like conjugation event. LC3 is cleaved by *Atg4* to reveal a Glycine residue. This processed form of LC3 (LC3-I) is conjugated to PE by *Atg7* (E1-like activating enzyme) and *Atg3* (E2-like conjugating enzyme). (C) The *Atg12-Atg5-Atg16* complex and PE bound LC3-II decorate the expanding phagophore or developing autophagosome. *Atg12-Atg5-Atg16* is preferentially found associated with the cytosolic surface of the phagophore whereas LC3-II is found on the luminal and cytosolic surfaces. Once the autophagosome is formed, *Atg12-Atg5-Atg16* is released but LC3-II remains associated. Following fusion with the lysosome, the cytosolic pool of LC3-II is cleaved from PE by *Atg4* and recycled whereas the luminal pool is degraded by lysosomal proteases together with the inner autophagosome membrane (reviewed by Xie & Klionsky, 2007).

1.4.2.2.2. Lysosomes

Lysosomes are membrane bound acidic organelles with a luminal pH of 4.6-5.0 maintained by H⁺-pumping vacuolar ATPases (reviewed by Luzio et al, 2007). They contain a wide spectrum of hydrolytic enzymes, which after synthesis and tagging with mannose-6-phosphate are delivered to endosomes which either fuse with lysosomes or mature into lysosomes themselves (Luzio et al, 2007). The most abundant lysosomal proteases are the cathepsins of which there are several types: B, L, S, V, C, F, K and X are cysteine proteases, whereas D is an aspartic protease and G is a serine protease (Stoka et al, 2001, reviewed by Turk & Stoka, 2007).

1.4.2.2.2.1. The role of cathepsins in ageing and neurodegeneration

The cysteine cathepsins have been suggested to also participate in both apoptosis and necrotic cell death depending on the degree of cysteine cathepsin leakage from lysosomes. If leakage from lysosomes is limited leading to the more selective release of cysteine cathepsins, apoptosis is triggered. Whereas if conditions are such that leakage is more pronounced necrotic cell death is triggered (Droga-Mazovec et al, 2008, Stoka et al, 2001, Turk & Stoka, 2007, reviewed by Vasiljeva & Turk, 2008, Wang et al, 2006a). Exposure of SH-SY5Y neuroblastoma to H₂O₂ resulted in oxidative damage, lysosomal membrane leakage followed by mitochondrial damage and the initiation of apoptotic cell death. However in this case it was cathepsin D and not cathepsin B activation that preceded caspase activation (Castino et al, 2007).

However cysteine cathepsins are also associated with cell survival, especially in cancer cells (Gocheva et al, 2006, Stoka et al, 2001, reviewed by Vasiljeva & Turk, 2008). Indeed inhibition of cysteine cathepsins such as cathepsin B and L results in apoptotic cell death in cancer cell lines (Colella et al, 2010, Gocheva et al, 2006, Zhu & Uckun, 2000). In osteosarcoma cells with mutations in mitochondrial DNA, the expression and activity of cathepsin B is elevated (Hamer et al, 2009).

Cathepsins have also been implicated in neurodegenerative conditions. A comparison of cathepsin activities in the frontal cortex grey and white matter of normal, AD, DLB and PD brain and the caudate nucleus of HD brain did not reveal changes in activities of any of the cathepsins other than cathepsin H in HD which was elevated. However the activity of

dipeptidyl aminopeptidase II (a serine protease with optimum pH of 4.5-5.5, Hui, 1988) was reduced in DLB and PD and elevated in HD (Mantle et al, 1995).

Mice with targeted neuronal deficiency in cathepsin D displayed extensive apoptotic and necrotic neuronal cell death as well as the presence of accumulated α -synuclein despite a compensatory upregulation of the expression of cathepsin B, L, F and H. In addition these mice also exhibited reduced proteasome activity and defective macroautophagy (Qiao et al, 2008). Similarly over-expression of GFP tagged human α -synuclein in *C.elegans* resulted in dopaminergic cell death and α -synuclein accumulation which was alleviated by the co-expression of human cathepsin D. The role of cathepsin D in preventing α -synuclein toxicity was also shown by the co-expression of cathepsin D in SH-SY5Y cells over-expressing α -synuclein (Qiao et al, 2008). Cathepsin D (Hamazaki, 1996) and cathepsin B may be involved in the degradation of β -amyloid. Decreasing the levels of the endogenous cathepsin B inhibitor (cystatin C) in mice expressing human amyloid precursor protein and β -amyloid lowers the levels of soluble β -amyloid, protecting them against early mortality and improving cognitive functioning (Sun et al, 2008).

1.4.2.2.3. The selectivity of macroautophagy depends on p62/SQSTM1

The traditional view that macroautophagy is a largely non-selective process has been replaced with the idea that proteins or organelles can be targeted for degradation through the interaction of macroautophagy targeting proteins. One such protein is p62/SQSTM1, which in humans has been suggested to act as a linking protein between ubiquitinated protein aggregates and LC3, thereby facilitating the removal of aggregates by autophagy (Bjorkoy et al, 2005, Pankiv et al, 2007).

p62 is a 440 amino acid protein containing an N-terminal Phox and Bemlp (PBI) domain, followed by a ZZ-type zinc-finger domain, a PEST region containing phosphorylation sites and a C-terminal ubiquitin association (UBA) domain (reviewed by Geetha & Wooten, 2002, and Ichimura et al, 2008a). The UBA domain (for interaction with ubiquitin) and PBI domain (for self-oligomerization) are both required for the formation of cytoplasmic p62 bodies containing ubiquitinated proteins which can then be degraded by autophagy (Bjorkoy et al, 2005). Its ability to interact with LC3-II is due to the presence of a LC3-II interacting region (LIR) which was mapped to a 22 amino acid stretch between the N-terminal PBI domain and the C-terminal UBA domain and shown to be essential for the autophagic degradation of ubiquitinated protein aggregates, providing evidence linking p62 to the clearance of

ubiquitinated protein aggregates by macroautophagy (Pankiv et al, 2007). A scheme illustrating the possible targeted degradation of inclusions and protein aggregates by p62 is given in Figure 1.7 (reviewed in Mizushima et al, 2008).

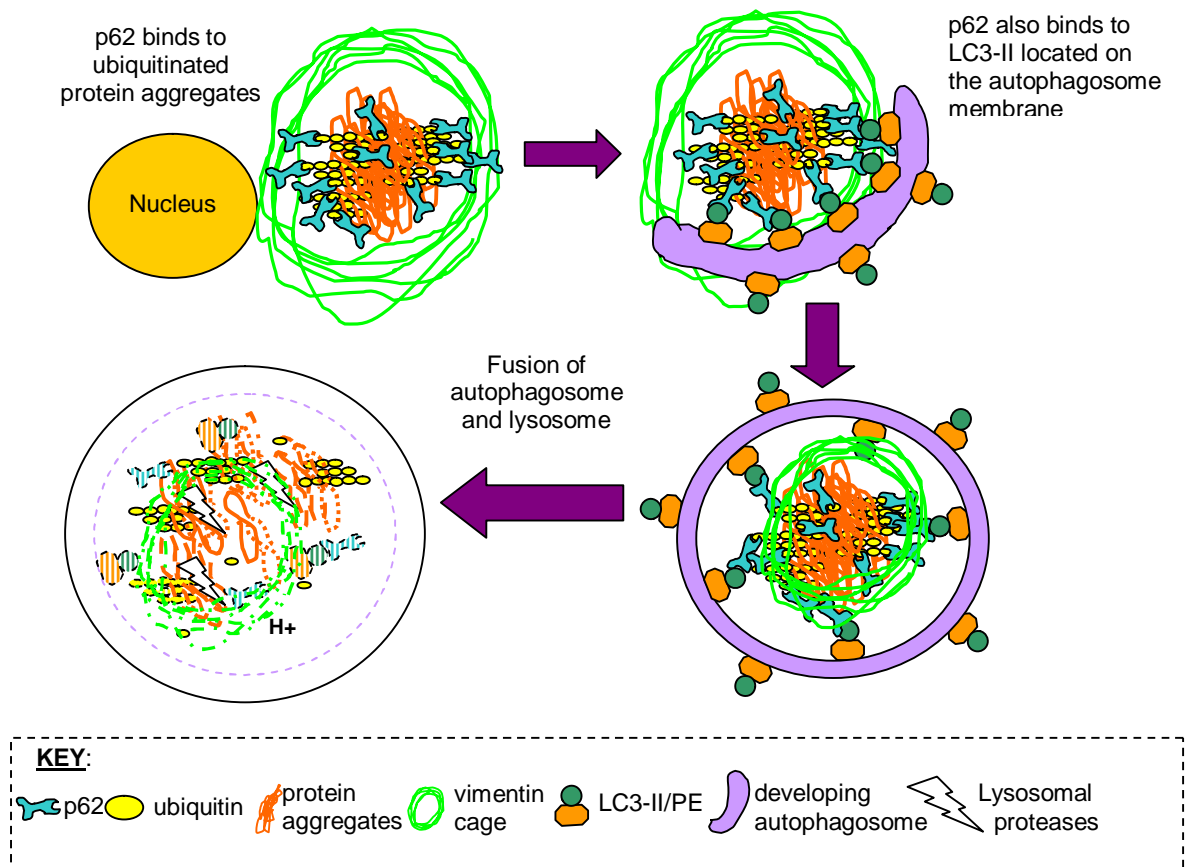


Figure 1.7 A scheme illustrating the proposed role of macroautophagy in the clearance of inclusions and protein aggregates.

Ubiquitinated protein aggregates bind p62/SQSTM1 which also interacts with LC3-II on the membrane of the developing autophagosome. The autophagosome engulfs the protein aggregate or inclusion. The autophagosome then fuses with a lysosome and aggregates and the inner autophagosome membrane are degraded by the lysosomal proteases.

1.4.2.2.4. The role of macroautophagy in neurodegeneration

During ageing there is a general decline in both macroautophagy and CMA. In studies with mice longevity is improved by caloric restriction which induces autophagy (reviewed by Mizushima et al, 2008). In mice, the targeted disruption of the expression of *Atg5* (involved in the formation of the autophagosome membrane) resulted in neurodegeneration, motor defects and an accumulation of inclusion bodies, highlighting the importance of basal autophagy in neuronal cells (Hara et al, 2006). The effect of the accumulation of toxic proteins or protein aggregates is largely dependent on the cell type affected; mitotic cells are

able to divide and distribute aggregates between daughter cells, effectively diluting the toxic products. Whereas terminally differentiated cells such as neurons do not have that option and need to be able to clear toxic proteins or aggregates. As cells age, their protein degradative pathways lose efficacy and the continued build-up of toxic products eventually leads to cell death (Martinez-Vicente & Cuervo, 2007).

A role for autophagy in PD is suggested by evidence that α -synuclein, a well known marker of LBs, is degraded by both chaperone-mediated autophagy and the UPS (Webb et al., 2003, Ghee et al., 2000, Cuervo et al., 2004) and by the reported induction of autophagy in SH-SY5Y cells by MPP⁺ (Zhu et al., 2007). PD-associated mutant forms of α -synuclein bind LAMP-2 with greater affinity than wild-type α -synuclein but are not internalized, thereby inhibiting CMA by blocking LAMP-2 (Cuervo et al, 2004). A recent report also showed that overexpression of α -synuclein in SK-H-SH, HeLa and HEK293 cells and transgenic mice impaired macroautophagy (Winslow et al, 2010). Protein aggregates formed in rotenone treated COS-7 cells expressing wild-type and PD-associated mutant forms of α -synuclein were cleared by macroautophagy but the efficiency of this clearance system decreased with longer treatment periods (Lee et al, 2004). In rat cortical neurons protein aggregates resulting from proteasome inhibition were also cleared by macroautophagy (Rideout et al, 2004).

This suggests that in response to protein aggregation as a result of cellular stress, cells may upregulate macroautophagy to clear these aggregates. In fact inhibition of macroautophagy in SH-SY5Y cells overexpressing α -synuclein results in cell death (Lee et al, 2004). Continued stress however eventually results in decreased efficiency of clearance systems and ultimately cell death. The presence of p62 in LBs and inclusions of other neurodegenerative conditions characterized by protein aggregation (Nakaso et al, 2004, Zatloukal et al, 2002) supports the hypothesis that these inclusion bodies are the result of the failed clearance of aggregates.

In a transgenic mouse model expressing superoxide dismutase 1 (SOD1) with a familial amyotrophic lateral sclerosis (ALS) mutation, the levels of p62 accumulated. p62 was shown to directly interact with polyubiquitinated mutant SOD1 in aggregates which did not appear to have a negative effect on cell viability and did not form in the absence of p62 (Gal et al, 2007). Proteasome inhibition of PC12 cells resulted in the accumulation of α -synuclein, p62 and ubiquitin in inclusion bodies that co-localized with γ -tubulin suggesting the formation of an aggresome-like structure. The accumulation of p62 was accompanied by the induction of p62 expression which shown to be essential for aggregate formation (Nakaso et al, 2004). An induction of p62 expression with proteasome inhibition was also observed in HeLa cells (Bjorkoy et al, 2005).

Evidence for the role of lysosomal degradation in PD pathogenesis was supplied by the identification of loss of function mutations in a lysosomal ATPase (*ATP13A2*) in a Chilean family with early-onset hereditary PD and an elevation *ATP13A2* mRNA in dopaminergic neurons of the SNpc of sporadic PD patients (Ramirez et al, 2006). In addition, the levels of LAMP1, Cathepsin L and Hsp73 are reduced in PD brain compared to age-matched controls (Chu et al, 2009). Lysosomal malfunction was suggested in a PD-mouse model resulting from chronic treatment with MPTP/probenecid. This model was characterised by dopaminergic neuron loss and the production of LB-like inclusions associated with numerous lipid filled vacuoles and large amounts of lipofuscin (Meredith et al, 2002). MPP⁺ treatment in SH-SY5Y neuroblastoma cells resulted in a dose-dependent increase in the levels of LC3-II (used as a marker of autophagosomes) which the authors attributed to an induction of autophagosome synthesis (Zhu et al, 2007). An upregulation of LC3-II levels following MPP⁺ treatment was also found in rat PC12 cells expressing A30P α -synuclein but in this work the authors also found that MPP⁺ impaired dynein activity and decreased dynein proteins levels. Thus preventing the autophagic clearance of α -synuclein by preventing autophagosome-lysosome fusion (Cai et al, 2009), which is dependent upon the activity of dynein (Ravikumar et al, 2005).

1.4.2.2.5. The role of mitophagy in neurodegeneration

Proteins involved in mitochondrial homeostasis have been identified in loss of function mutations observed in familial forms of PD. Parkin (an E3 ligase) and PINK1 (a mitochondrial Ser/Thr kinase) are involved in the targeting of dysfunctional mitochondria for removal by mitophagy (reviewed by Burbulla et al, 2010, Geisler et al, 2010a). PINK1 has a cytosolic and mitochondrial distribution and its translocation to mitochondria is dependent on its kinase activity. In functional mitochondria, PINK1-undergoes voltage dependent cleavage but in dysfunctional mitochondria PINK1 is not cleaved and full-length PINK1 accumulates. Accumulated PINK1 results in the recruitment and activation of parkin, which in turn catalyses the autoubiquitination of parkin at *Lys63* and the ubiquitination of VDAC1 (voltage-dependent anion channel 1) at *Lys27* which in turn recruits the adaptor p62 which targets the mitochondria for degradation by mitophagy. Knockdown of p62 and VDAC1 completely prevents autophagic mitochondrial clearance and recruitment of parkin to dysfunctional mitochondria respectively (reviewed by Burbulla et al, 2010, Geisler et al, 2010a).

In SH-SY5Y cells expressing either wild-type or PD associated PINK1 mutants together with wild-type GFP tagged parkin the importance of the interaction between functional PINK1 and parkin for the clearance of damaged mitochondria was demonstrated. In fact the kinase activity of PINK1 (often affected in PD mutants) was shown to be essential for the physical interaction of PINK1 and parkin (Geisler et al, 2010b). Similarly parkin with PD-associated mutations did not translocate to dysfunctional mitochondria in HeLa cells expressing either wild-type or mutant HA-tagged parkin and treated with a mitochondrial uncoupler. The importance of parkin and PINK1 in mitophagy was also demonstrated in SH-SY5Y cells expressing either wild-type or PD associated mutant parkin and PINK1. Therefore functional parkin and PINK1 are required for the clearance of defective mitochondria by mitophagy (Geisler et al, 2010a).

1.4.3. Calpain

1.4.3.1. Background

Calpain is a ubiquitously expressed calcium dependent cysteine proteases composed of an 80 kD catalytic subunit and a 30 kD regulatory subunit which are activated following autolytic cleavage of N-terminal fragments of both subunits when intracellular calcium levels are increased. Calpain is classified into two types according to the concentration of calcium required for activity: m-calpain (calpain II) which requires concentrations of 200-800 μM calcium and μ -calpain (calpain I) which requires concentrations of 2-75 μM calcium (reviewed by Goll et al, 2003, and Mehdi, 1991). The binding of calcium induces conformational changes in calpain that leads to the correct alignment of the catalytic active sites (Moldoveanu et al, 2002).

1.4.3.2. Calpain in ageing and neurodegeneration

In PD it has been reported that calpain-II expression is increased in nigral dopaminergic neurons (Mouatt-Prigent et al, 1996). In MPTP mouse models of PD calpain expression is increased (Chera et al, 2004) and calpain inhibition attenuates MPTP toxicity (Crocker et al, 2003). Interestingly, under conditions of stress, such as anoxia and reoxygenation and periods of chronic inflammation, calpains have been implicated in NF-M, NF-H (Stys & Jiang, 2002) and NF-L degradation (Kunz et al, 2004, Shields et al, 1997).

1.5. Neurofilaments

1.5.1. Function of neurofilaments

Neurofilaments are members of the intermediate filament (IF) family that are specifically expressed in neuronal cells. IFs are divided into five types, four found in the cytoplasm and one (the lamins) found in the nucleus, with a diameter of 10-12 nm. Together with the microtubules (MTs, 23-25 nm) and microfilaments (MFs, 5-8 nm), IFs make up the cytoskeleton of eukaryotic cells (reviewed by Janmey et al, 2003, and Perrot et al, 2008, Petzold, 2005).

Some recognised functions of NFs include the maintenance of axonal structure and the optimization of nerve impulse conduction velocity in myelinated neurons. The latter depends of myelin thickness and internodal length, which are proportional to axonal calibre, the thickness of which is thought to be dependent on the expression of NFs (Hoffman et al, 1987, Perrot et al, 2008, Zhu et al, 1997). NFs have also been proposed to act as docking sites for organelles in the axon (Hirokawa, 1982, Perrot et al, 2008); active mitochondria for example have been shown to interact with the side-arms of phosphorylated NFs (Hirokawa, 1982, Wagner et al, 2003), which may allow mitochondria to be spaced at intervals in long axons to provide energy for metabolic processes.

Another function of NFs is in the determination of dendritic architecture which is generally more dynamic in both developing and mature neurons and reflects the role of dendrites in neuronal plasticity (Kong et al, 1998). Neurofilaments have also been proposed to play a role in the regeneration of myelinated axons after peripheral nerve injury which is delayed in the absence of NFs (Zhu et al, 1997).

1.5.2. Composition and assembly of neurofilaments

Neurofilaments are composed of three separate protein subunits; NF-L (light, 68 kDa), NF-M (medium, 145-160 kDa) and NF-H (heavy, 190-210 kDa) which all have the same basic structure: an N-terminal head domain, a conserved alpha-helical rod domain of 310 amino acids and a variable length C-terminal domain (Perrot et al, 2008, Petzold, 2005). NFs are considered to be obligate heteropolymers because although NF-L can form homopolymers *in vitro*, these homopolymers are less mechanically stable and rely the inclusion of NF-M or NF-H to provide NFs with mechanical stability (Brown et al, 1998, Kim et al, 2007). NF-H

and NF-M are not capable of self-assembly and rely on the presence of NF-L (Chen et al, 2000). Some redundancy in the functioning of NF-H and NF-M is suggested by the compensatory upregulation of NF-M and α -tubulin expression in mice lacking NF-H (Rao et al, 1998).

The assembly of NFs occurs in five stages (figure 1.8): the central core domains of NF-L and either NF-H or NF-M are wound around each other to form heterodimers, which are then sorted in an anti-parallel fashion to form heterotetramers, two heterotetramers then come together to form protofibrils which are finally arranged in staggered, overlapping fashion to form the neurofilament (Janmey et al, 2003, Petzold, 2005).

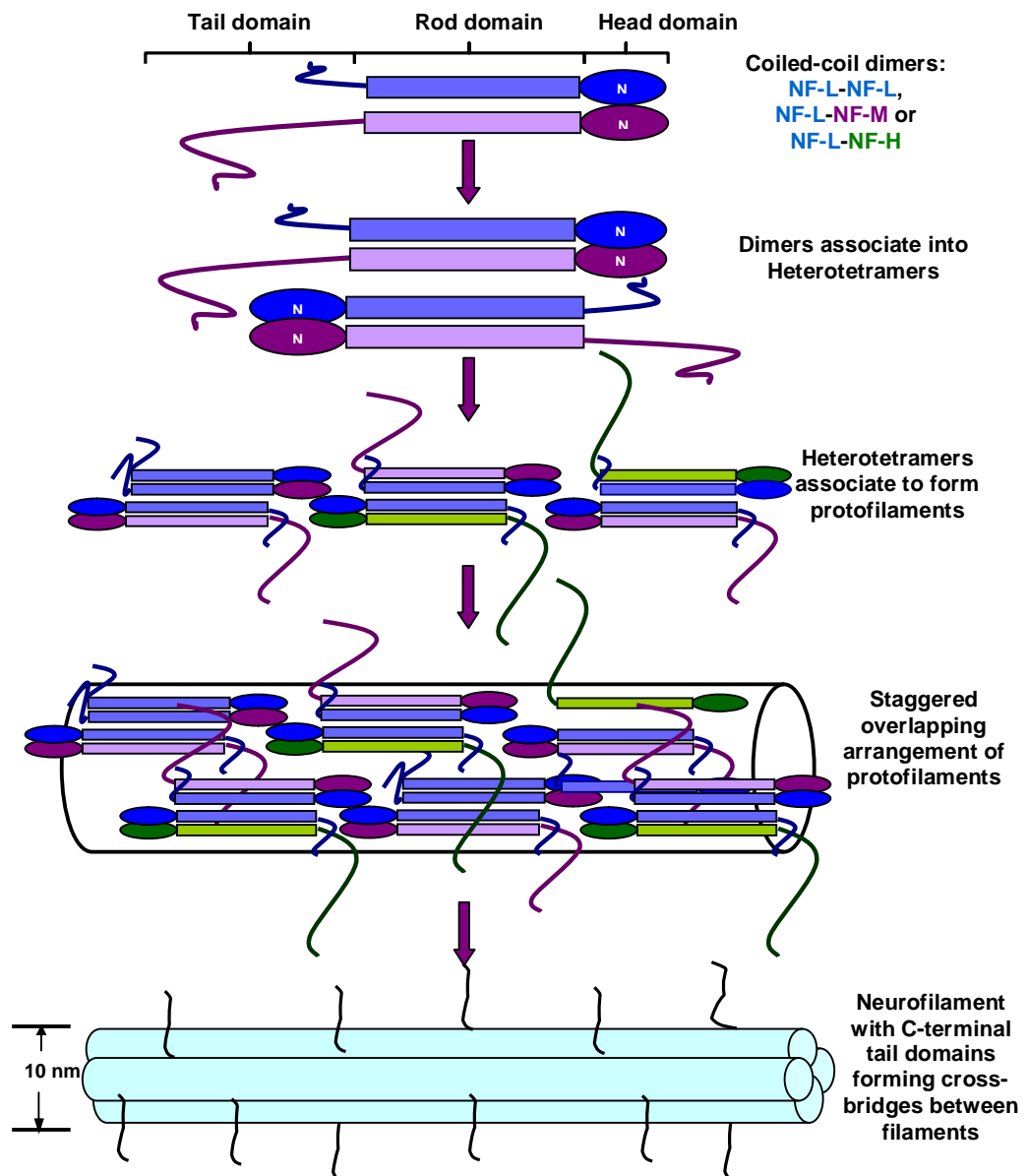


Figure 1.8 A schematic of the assembly of neurofilament subunits into neurofilaments.

The NF subunits come together as Heterodimers. Heterodimers then associate with each other in an anti-parallel fashion as heterotetramers. Heterotetramers associate to form protofibrils and then 4 protofibrils come together as neurofilaments. Figure adapted from Petzold et al (2005) and Janmey et al (2003).

Each NF is composed of four protofilaments which are intertwined helically to form the four-stranded structure (Wen & Wisniewski, 1984). The C-terminal tails of NF-H and NF-M form side-arm projections that project from the core filament and form interconnections with other NFs (resulting in a parallel arrangement of NF filaments in the axon), MTs and organelles (Bocquet et al, 2009, Chen et al, 2000, Hirokawa, 1982, Nakagawa et al, 1995), the length of which increases with phosphorylation (Janmey et al, 2003).

In mature neurons the stoichiometric ratio of NF-L:NF-M:NF-H is 7:3:2, suggesting that there are on average three NF-M/NF-L dimers to two NF-H/NF-L dimers and one NF-L/NF-L dimer in a fully differentiated NF (reviewed by Janmey et al, 2003, and Perrot et al, 2008). The importance of subunit stoichiometry for the maintenance of the NF network is highlighted by the decrease in NF-M and NF-H protein levels following the targeted disruption of NF-L gene expression (Zhu et al, 1997) and by the reduction in axonal calibre following the over-expression of each of the NF subunits individually, or co-expression NF-M and NF-H, in transgenic mice, which was only prevented by co-expression of either NF-M or NF-H with NF-L (Xu et al, 1996). It is now accepted that other intermediate filaments such as α -internexin and peripherin co-assemble with NFs (Yan et al, 2007, Yuan et al, 2006), although which intermediate filaments associate often depends on the developmental stage (Yan et al, 2007).

1.5.2. Control of neurofilament gene expression

During neuronal development it has been established that neurofilament expression is preceded by and replaces the expression of vimentin in neuronal progenitor cells in the central and peripheral nervous systems (Bignami et al, 1982). However, for a time NFs and vimentin have been shown to coexist in radially orientated filaments of early bipolar neuroblasts in the mouse embryo (Cochard & Paulin, 1984) and for a limited period in the rat embryo (Bignami et al, 1982). In addition vimentin and NFs have also been shown to exist in both separate filaments and the same filament in differentiated PC12 cells and N2a cells (Yabe et al, 2003).

NF-L is the first NF subunit expressed during neuronal development and is usually expressed with peripherin and α -internexin (Perrot et al, 2008). Peripherin does not polymerize with NF-M and NF-H and is usually downregulated in the CNS, although in the PNS it continues to be expressed (reviewed by Grant & Pant, 2000). Initially in developing neurons NF-L and NF-M are expressed whereas the expression of NF-H is delayed and associated with a more

mature phenotype (Carden et al, 1987, Grant & Pant, 2000). In cortical neurons the expression of NF-H was preceded by the expression of NF-L, NF-M and α -internexin providing further evidence for the delayed expression of NF-H during development (Yuan et al, 2009).

The genes coding for NF-M and NF-L are closely linked on chromosome 8 whereas the NF-H gene is found on chromosome 22. Several studies have suggested that the expression of NF-L and NF-M is mutually regulated and independent of NF-H (Grant & Pant, 2000, Perrot et al, 2008) providing a mechanism for the two-stage expression of NFs during development.

1.5.3. Phosphorylation of neurofilament proteins

The three NF subunits all contain multiple phosphorylation sites (Julien & Mushynski, 1982, Wong et al, 1984); up to 51 phosphorylation sites can be found on the C-terminus of NF-H. The head domains of NF-M and NF-L also contain protein kinase A (PKA), protein kinase C (PKC) and protein kinase N (PKN) phosphorylation sites (Ser44 for NF-M and Ser55 for NF-L) which become phosphorylated in the cell body soon after synthesis (Perrot et al, 2008, Sihag & Nixon, 1990) and are thought to regulate NF assembly by preventing the premature assembly of NFs (Manser et al, 2008).

The C-terminal domains of NF-H and NF-M form side-arm projections which project from the filament and contain numerous KSP phosphorylation sites (repeats of Lysine-Serine-Proline motifs) which become extensively phosphorylated in the axon (Nixon et al, 1987, Soussan et al, 1994). The kinases responsible for the phosphorylation of KSP sites in NF-M and NF-H are the proline directed kinases such as Cdk5 which is activated following the cleavage of p35 to p25 (Pant et al, 1997, Shea et al, 2004, Sun et al, 1996) and mitogen-activated protein kinases (MAPK) such as Erk1/2 (extracellular signal related kinase), SAPK (stress activated protein kinase), GSK β and p38 (Perrot et al, 2008). Erk1/2 and Cdk5 each preferentially phosphorylate NFs at different KSP motifs; the motif for which Erk1/2 has a higher affinity is KSPXXXK whereas Cdk5 has a higher affinity for KSPXK (Veeranna et al, 1998). There are some species differences in the type of KSP motifs which predominate in NFs, for example in rat NF-H contains 41 KSPXXXK motifs which are preferentially phosphorylated by Erk1/2 (Veeranna et al 1998) whereas human NF-H which contains 34 KSPXK motifs which are preferentially phosphorylated by Cdk5 (Pant et al 1997).

The Ser-Thr residues of the glutamic acid region of the three NF subunits are phosphorylated by casein kinase I (CKI) and the Ser473 on the tail of NF-L is phosphorylated by casein

kinase II (CKII, reviewed by Perrot et al, 2008). Figure 1.9 is a cartoon diagram illustrating the general structure of the three NFs and position of phosphorylation sites and kinases responsible for phosphorylation.

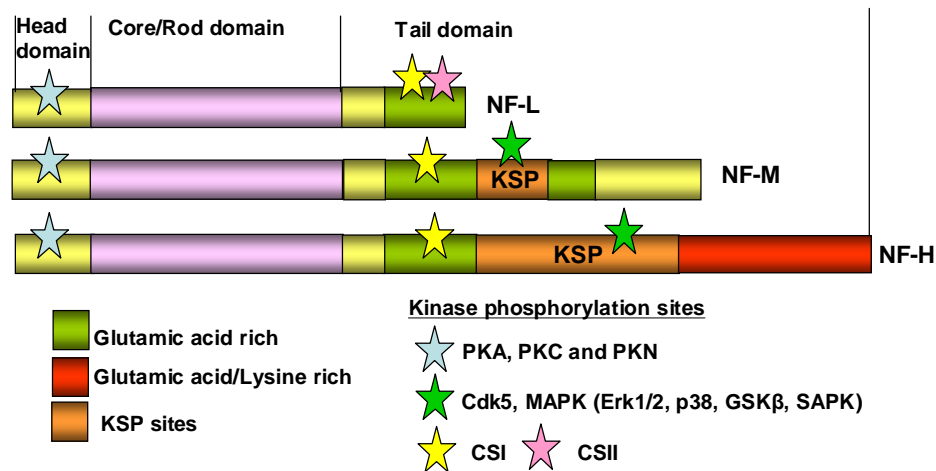


Figure 1.9 A cartoon drawing illustrating the position of various phosphorylation sites on the three neurofilament subunits.

The general structure of the three human neurofilament (NF) subunits with N-terminal head domain, conserved central core or rod domain and the variable length C-terminal tail domain. The glutamic acid rich regions are in green and the glutamic acid and lysine rich region in NF-H is indicated in red. The KSP sites are in orange and the various kinases responsible for the phosphorylation of NFs at various sites are indicated by the stars (Grant & Pant, 2000, Perrot et al, 2008).

It has been suggested that the resulting repulsive forces of phosphorylated side-arm projections increases NF spacing and axon diameter (Sanchez et al, 2000). Work with mice lacking the tail domain of NF-H revealed that the C-terminus of NF-H is not essential for axonal growth, NF transport or the maintenance of axonal calibre (Rao et al, 2002, Yuan et al, 2006) suggesting some redundancy in the functioning of NF-H and NF-M. Redundancy in the functioning of NF-M and NF-H in radial growth was also suggested in mice lacking NF-H in which increased NF-M phosphorylation compensated for the lack of NF-H (Sanchez et al, 2000).

It is noteworthy that the NF population is not homogeneously phosphorylated, instead a mixture of phosphorylation states from non-phosphorylated NFs to extensively phosphorylated NFs can be found in axonal structures (Brown, 1998). The phosphorylation of NFs is a dynamic process that involves both phosphorylation and dephosphorylation events that affect the associations and functioning of NFs as they progress along the axon (Nixon & Lewis, 1987, Nixon & Lewis, 1986).

1.5.4. Axonal transport

Neurofilaments are synthesized in cell bodies and assembled into hetero-oligomers, which are then transported along the axon by a process called axonal transport (Nixon & Lewis, 1986, Yabe et al, 1999, Yan et al, 2007, Yan & Brown, 2005, Yuan et al, 2003). Historically NFs have been described as being transported by slow axonal transport (1 mm/d) (reviewed in Chou & Goldman, 2000), but the current concensus is that NFs are transported rapidly (0.6 $\mu\text{m/s}$) but intermittently, accounting for an overall transport rate consistent with slow axonal transport (Brown et al, 2005, Lasek et al, 1993, Roy et al, 2000, Trivedi et al, 2007, Yuan et al, 2003). The vast majority of NF subunits are associated with the stationary NF network with only a small proportion (as little as 8 %) of NFs at any one time being associated with the more motile NF population (Brown et al, 2005, Nixon & Logvinenko, 1986). Ultrastructural studies of mouse N2a cells revealed a core of triton-insoluble NFs that are more closely bundled together than peripheral populations and exhibited increased reactivity to RT97 (which recognises developmentally delayed pNF-H). Newly synthesized and motile NFs were associated with the peripheral populations which were not as closely bundled (Yabe et al, 2001).

Several studies have provided evidence for the involvement of motor proteins in the axonal transport of NFs. The actin-based motor protein myosin (Jung et al, 2004) and the microtubule motor protein kinesin (most likely kinesin 5a) have been implicated in the anterograde transport of NFs (Jung et al, 2005, Theiss et al, 2005, Xia et al, 2003, Yabe et al, 1999). The motor protein dynein has been implicated in the retrograde transport of NFs within the axon and the initial anterograde transport of NFs just as they enter the axon from the cell body (He et al, 2005, Motil et al, 2006, Motil et al, 2007, Theiss et al, 2005, Wagner et al, 2004).

Work with GFP tagged NFs has also shown that when NFs enter the growth cone they immediately change direction and quickly move back in the retrograde direction into the axon often at rates faster than their entry into the growth cone (Uchida & Brown, 2004) and that NFs entering the growth cone are more dynamic, soluble and less phosphorylated and participate in the remodelling of the cytoskeleton during axonal elongation (Chan et al, 2003).

Phosphorylation plays an important role in this transport process although the exact mechanism is still not fully resolved. The phosphorylation status of the C-terminal domain of

NF-H and NF-M appears to affect NF transport rate. This is most likely due to the dissociation of phosphorylated NFs from the anterograde motor protein (Jung et al, 2005, Yabe et al, 2000), resulting in a greater association with the stationary axonal cytoskeleton (Ackerley et al, 2003). The kinase implicated in the regulation of axonal transport is Cdk5 since inhibition of Cdk5 in cortical neurons increased the transport rate of NFs (Ackerley et al, 2003, Moran et al, 2005, Shea et al, 2004). Further evidence of the effect of phosphorylation on NF transport is the decrease in NF-H transport in retinas following *in situ* phosphatase inhibition (Shea et al, 2003).

1.5.5. Neurofilaments in ageing and neurodegeneration

Age-related biochemical changes in NFs include the increased appearance of hyperphosphorylated NFs with ageing (Gou et al, 1995), which may be due to a decline in the activity of protein phosphatase 2A (PP2A; Veeranna et al, article in press). Furthermore NFs from aged rats were shown to contain more NF-H/NF-L than NF-M/NF-L and ultrastructural studies of NFs revealed that in the sciatic nerves and spinal cord of aged rats, NFs are more densely packed than in young rats (Uchida et al, 1999).

Abnormal accumulations of NFs have been reported in other neurodegenerative conditions and as a result of toxin treatment. As mentioned earlier NFs are major components of LBs (Forno et al, 1986) and aberrant NF phosphorylation and accumulation has been reported in AD (Anderton et al, 1982, Sternberger et al, 1985, Su et al, 1996). Most familial AD cases are the result of mutations in presenilin-1 which when expressed in N2a cells prevented the formation of a filamentous NF network and instead resulted in accumulations of NFs in the cell body (Dowjat et al, 2001).

Charcot-Marie-Tooth disease is characterised by mutations in NF-L which have been shown to result not only in the defective axonal transport of NFs and their accumulation in inclusions in the cell body but also in the accumulation of mitochondria in the cell body co-localizing with the mutant NF-L inclusions (Brownlees et al, 2002, Pérez-Ollé et al, 2005). In mouse primary cultured motor neurons the expression of CMT-associated mutant NF-L resulted in a reduction in cell viability and an aggregation of NF-L in the cell body (Zhai et al, 2007).

Abnormal accumulations of NFs are also a prominent pathological feature of amyotrophic lateral sclerosis (ALS or motor neuron disease). Disease progression in transgenic mice expressing an ALS-associated mutation in Cu²⁺/Zn²⁺ superoxide dismutase (SOD1) was

slower in mice also lacking NF-L suggesting a role for NFs in the pathogenesis of ALS (Williamson et al, 1998). Aberrant phosphorylation of neurofilaments in ALS may be induced by the stress activated protein kinase p38 α , the active form of which closely associates with NF accumulations in ALS (Ackerley et al, 2004). In addition, a role for Cdk5 in the aberrant phosphorylation of NFs in ALS was also suggested by immunostaining which revealed higher levels of Cdk5 in the spinal motor neurons of SOD1 mutant mice than in wild-type mice, accompanied by elevated levels of p25 compared to p35 (suggesting Cdk5 activation) and NF hyperphosphorylation (Nguyen et al, 2001).

In Neuronal Intermediate Filament Inclusion disease (NIFID), a fairly newly described condition with frontotemporal dementia and gliosis. Neuronal loss is characterised pathologically by severe anterior lobe and caudate atrophy and the presence of inclusion bodies containing NFs and α -internexin (Josephs et al, 2003, Molina-Porcel et al, 2008).

Exposure to environmental toxins has also been implicated in neurodegenerative conditions associated with NF abnormal phosphorylation and aggregation. NF accumulations induced by arsenic treatment may be due to its inhibitory effect on NF transport and activation of Cdk5 and JNK-1 (DeFuria & Shea, 2007). The accumulation of NFs has also been reported in rabbit spinal motor neurons (Kimura et al, 2007) and N2a cells following treatment with aluminium (Shea et al, 1997) and in SH-SY5Y cells treated with 2,5-hexadione (a neurotoxic metabolite of hexane) and acrylamide (Hartley et al, 1997). Aberrant activation of Cdk5 (Wang et al, 2006b) and an accumulation of NFs (Gupta et al, 2000) were observed in organophosphate-induced delayed neuropathy (OPIDN) in hens. In differentiating mouse N2a cells, subcytotoxic MPTP treatment resulted in an inhibition of axonal outgrowth and an increase in NF-H phosphorylation mediated by c-Jun-NH₂-terminal kinase (JNK) activation which when inhibited attenuated the MPTP-induced reduction in axonal outgrowth (De Girolamo & Billett, 2006).

1.6. SH-SY5Y cells

SH-SY5Y neuroblastoma cells are the thrice cloned derivative of the SK-N-SH cell line (Biedler et al, 1978), originally established in 1970 from a bone marrow biopsy of a 4 year old female patient with neuroblastoma (Biedler et al, 1973). The SK-N-SH parental cell line is composed of at least two distinct subclones that differ morphologically and biochemically from each other. One is a neuroblastic cell type (N-type) with a small amount of cytoplasm and delicate cell processes of variable length while the other is a larger epithelioid cell type

(S-type) (Biedler et al, 1973). The relative composition of the N and S cell types in the SK-N-SH cell line is largely dependent on culture conditions which favour one cell type over another (Sadée et al, 1987). Three subclones of the original parental cell line have been established; the SH-SY5Y cell line composed predominantly of the N-type cells, the SH-EP cell line composed predominantly of S-type cells and the SH-IP cell line composed of an intermediate cell type (Biedler et al, 1978).

The SH-SY5Y neuroblastoma cell line expresses the muscarinic cholinergic receptor, the μ and δ opioid receptors, dopamine- β -hydroxylase, tyrosine hydroxylase (Biedler et al, 1973, Biedler et al, 1978, Sadée et al, 1987) and MAOA (Fitzgerald et al, 2007) and are able to take up and produce DA (Sadée et al, 1987). These attributes have contributed to the use of both differentiated and undifferentiated SH-SY5Y neuroblastoma cells as models for dopaminergic neurons.

Differentiation of SH-SY5Y cells (discussed in more detail in chapter 5) is most often accomplished by either treating cells with retinoic acid (RA) alone or treating cells sequentially with RA and brain derived neurotrophic factor (BDNF). Arguments supporting the use of differentiated cells as a PD model include (a) the more mature homogeneous phenotype exhibited by the cells, (b) higher levels of DAT, TH and dopamine- β -hydroxylase (Xie et al, 2010) and (c) the inability of cells to divide prevents cells from diluting out protein aggregates between daughter cells (Hasegawa et al, 2004). The validity of the use of undifferentiated cells as a PD model is argued by the observed increased tolerance of RA differentiated cells to PD mimetics due to the upregulation of survival signalling (Cheung et al, 2009).

1.7. Aims

Although NFs were the first protein components identified in LBs (Forno et al, 1986, Galloway et al, 1988, Galloway et al, 1992), their role in PD pathogenesis and LB formation is still not fully understood. Altered NF expression was dismissed as a contributory factor in LB formation by Bergeron et al (1996) due to a lack of changes in NF-L mRNA levels in patients with PD or DLB compared to controls. However, this work did not look at changes in protein levels which may be affected by decreased or increased proteolysis or at post-translational modifications which may alter NF functioning and distribution. Since the discovery of mutations in α -synuclein in familial PD (Kruger et al, 1998, Polymeropoulos et al, 1997) and the presence of α -synuclein in LBs of idiopathic PD (McNaught et al, 2002) focus in PD research switched from NFs to α -synuclein.

Since then research has also concentrated on mitochondrial dysfunction and oxidative stress (reviewed by Schapira, 2009), protein aggregation and defects in protein degradative pathways (reviewed in Bedford et al, 2008, Robinson, 2008, and Schneider & Zhang, 2010) and axonal transport (Ittner et al, 2008, Morfini et al, 2007, Saha et al, 2004) and how all these pathways interact in disease pathogenesis (reviewed in Keller et al, 2004, Malkus et al, 2009). The identification of a rare mutation in the rod domain of NF-M in familial PD in a French/Canadian family which resulted in abnormal NF assembly (Lavedan et al, 2002) renewed interest in NFs in PD. However since three relatives heterozygous for the same mutation failed to develop PD, the mutation in NF-M may increase disease susceptibility rather than being a primary cause. Aberrant accumulations of NFs have been reported in several other neurodegenerative conditions including ALS, CMT disease, AD, NIFID and OPIDN. Several unanswered questions remain concerning the role of NFs in PD and LB pathology and the aims of this project were to address some of these questions.

Very little is known about the degradative pathways involved in NF turnover in healthy cells and whether defects in these pathways could contribute to the accumulation of NFs in LBs. To address this question, the effects of PD mimetics (MPP⁺ and DA) on degradative pathways and their involvement in NF degradation was investigated in proliferating SH-SY5Y neuroblastoma cells.

Secondly, to establish a model in which the effects of PD mimetics on NF distribution could be investigated in live cultures in real-time, green fluorescent protein (GFP) tagged human NF subunits were produced. Preliminary work using this model concentrated on investigating the effects of acute MPP⁺ toxicity on NF distribution. In addition, the feasibility of using the GFP tag in co-immunoprecipitation experiments to identify NF associating proteins was investigated.

Thirdly, to investigate the role of NFs in aggresome and inclusion formation it was necessary to develop a cellular model of inclusion formation. Since differentiated SH-SY5Y neuroblastoma cells develop inclusions more readily than undifferentiated cells (Hasegawa et al, 2004, reviewed in Robinson, 2008), SH-SY5Y cells were differentiated with retinoic acid (RA) and brain derived neurotrophic factor (BDNF). To induce inclusion formation, RA/BDNF differentiated cells were treated with MPP⁺, epoxomicin (proteasome inhibitor) or MPP⁺/epoxomicin and the effects of these treatments on the levels and distribution of NFs and the ability to produce inclusions was compared.

CHAPTER 2

MATERIALS AND METHODS

2.1. Materials

2.1.1. Cell culture

2.1.1.1. Reagents

Dulbecco's Modified Eagles Medium/F12 Ham, DMEM/F12 (12-719F); Penicillin-Streptomycin (17-603E); Foetal bovine serum (14-801F); L-glutamine (17-605E), Trypsin-EDTA (02-007E) purchased from Lonza, Berkshire, UK

DMEM/F12 (D6421); DMEM/F12 without phenol red (D6434); MEM non-essential amino acid solution (M7145); Hybri-max sterile filtered dimethyl sulfoxide, DMSO (D2650); trypan blue solution (0.4 %, T8154) purchased from Sigma-Aldrich, Poole, UK

Gibco Opti-MEM® I Reduced Serum Medium without phenol red purchased from Invitrogen Ltd (11058-021)

Dulbecco's Phosphate Buffered Saline (DPBS) from PAA Laboratories Ltd (H15-002)

2.1.1.2. Plastic ware

Cell culture flasks (T25, T75 and T125), 6 well plates and 96 well plates were supplied by Sarstedt, Leicester, UK

ibidi μ -dish ibiTreat tissue culture treated, sterile, 35 mm from Thistle Scientific Ltd, Glasgow, UK (806136)

BD Biocoat™ Poly-D-Lysine 8-well culture slides purchased from SLS Ltd, Nottingham UK (354632)

Nunc Lab-Tek 8 well sterile permanox chamber slide purchased from SLS Ltd, Nottingham UK (177445)

BD tissue culture dish (100 x 200 mm) purchases from SLS Ltd, Nottingham UK

IWAKI 35 mm glass base dish, 27 mm diameter purchased from SLS Ltd, Nottingham UK (TIS5450)

2.1.2. Laboratory reagents

Adenosine 5'-triphosphate, ATP from Sigma-Aldrich (A3377)

Bicinchoninic Acid (BCA) Kit from Sigma-Aldrich (BCA1-1KT)

Bio-Rad protein assay dye reagent concentrate from BioRad Laboratories Ltd, Hertfordshire, UK (500-0006)

BC Assay from Cheshire Sciences UK (UP40840A)

Bovine serum albumin, lyophilized powder, BSA from Sigma-Aldrich (A2153)

Igepal CA-630 from Sigma-Aldrich (I3021)

Dimethyl sulfoxide, DMSO from Sigma-Aldrich (472301)

Triethylamine, TEA from Sigma-Aldrich (471283)

3-(4,5-dimethylthiazol-2-yl)-2,5-diphenyltetrazolium bromide, MTT from Sigma-Aldrich (M2128)

All-trans retinoic acid from Sigma-Aldrich (R2625)

μMACS™ Epitope Tag (GFP) Protein Isolation Kits from Miltenyi Biotec Ltd (130-091-125)

Recombinant Human Brain Derived Neurotrophic Factor (BDNF) from Miltenyi Biotec Ltd (130-093-811)

HALT™ protease inhibitor cocktail - used at 1:100 from ThermoFisher Scientific (78430)

HALT phosphatase inhibitor cocktail - used at 1:100 from ThermoFisher Scientific (78428)

SDS-PAGE and Western blotting reagents

Biotinylated Protein Ladder, 9-200 kD from Cell Signaling Technology (#7727)

Dual colour Prestained Precision Plus Protein™ Standards, 10-250 kD from BioRad Laboratories Ltd, Hertfordshire, UK (#161-0374)

Pierce ECL Western blotting substrate from ThermoFisher Scientific (32106)

Uptima Uptilight™ High sensitivity WB Chemiluminescent Substrate from Cheshire Sciences (UK) Ltd (98490B)

Restore Plus Western blot stripping buffer from ThermoFisher Scientific (46430)

Copper phthalocyanine 3, 4', 4'', 4''' tetrasulphonic acid tetrasodium salt from Sigma-Aldrich (245356)

Acrogel-3-solution (40 % solution) acrylamide from BDH, Poole UK (443735T)

Accugel 29:1 (40 % solution) acrylamide from GeneFlow Ltd UK (A20068)

Dithiothreitol (DTT) from Melford Laboratories Ltd (MB1015)

2D-PAGE and mass spectrometry reagents

ReadyStrip™ IPG strips, pH 3 - 10, 7 cm from BioRad Laboratories Ltd, Hertfordshire, UK (163-2000)

Unstained Protein Ladder, 10-250 kD from New England Biolabs Inc (P7703S)

Silver staining kit from Fisher Scientific (GZ17115001)

LC-MS Grade Acetonitrile (ACN) from Fisher Scientific (A/0600/15)

LC-MS Grade water from Fisher Scientific (W/0112/15)

Trifluoroacetic acid (TFA) from Fisher Scientific (T/3258/04)

Mineral Oil, Biotechnology Grade from BioRad Laboratories Ltd, Hertfordshire, UK (163-2129)

Fluorogenic peptide substrates

N-Succinyl-Leu-Leu-Val-Tyr-AMC (7-amino-4-methylcoumarin) – CLA substrate used at 50 μM - stored as 40 mM in DMSO at -20°C which are diluted to 1 mM in assay buffer before use purchased from Enzo Life Sciences, Exeter, UK (BML-P802).

Z-Phe-Arg-AMC (7-amino-4-methylcoumarin) - OmniCathepsin™ fluorogenic substrate cleaved by cysteine cathepsins B, C/DPP-I, F, L2/V, L, O, S, X/Z used at 200 µM - stored at -20°C as 50 mM stocks in DMSO which are diluted to 10 mM in assay buffer before use purchased from Enzo Life Sciences, Exter, UK (BML-P139).

Cathepsin L activity assay kit (fluorometric) purchased from abcam, Cambridge UK (ab65306)

Cathepsin D activity assay kit (fluorometric) purchased from abcam, Cambridge UK (ab65302)

Horse radish peroxidase (HRP) and alkaline phosphatase (AP) conjugated Secondary Antibodies

Polyclonal goat anti-mouse IgG HRP conjugated antibody from DakoCytomation, Cambridgeshire, UK (PO447)

Polyclonal goat anti-rabbit IgG HRP conjugated antibody from DakoCytomation, Cambridgeshire, UK (PO448)

Polyclonal rabbit anti-goat IgG HRP conjugated antibody from DakoCytomation, Cambridgeshire, UK (PO449)

Polyclonal bovine anti-goat IgG (H + L) HRP conjugated antibody from Stratech Scientific Ltd, Suffolk UK (805-035-180)

Polyclonal horse anti-mouse IgG, AP conjugated antibody from Cell Signalling Technology (#7056)

Polyclonal goat anti-rabbit IgG, AP conjugated antibody from Cell Signalling Technology (#7054)

Polyclonal goat anti-mouse IgG AP conjugated antibody from DakoCytomation, Cambridgeshire, UK (DO486)

Immunofluorescence secondary antibodies and nuclear and organelle stains

VECTASHIELD anti-fade mountant containing Propidium Iodide from Vector Laboratories Ltd (H-1300)

VECTASHIELD anti-fade mountant from Vector Laboratories Ltd (H-1000)

Prolong Gold antifade with Dapi from Invitrogen Ltd (P36935)

Alexa fluor 568 donkey anti-sheep IgG from Invitrogen Ltd (A21099)

Alexa fluor 488 donkey anti-sheep IgG from Invitrogen Ltd (A11015)

Alexa fluor 568 donkey anti-rabbit IgG from Invitrogen Ltd (A10042)

Alexa fluor 488 donkey anti-mouse IgG from Invitrogen Ltd (A21202)

Alexa fluor 568 donkey anti-goat IgG from Invitrogen Ltd (A11057)

Alexa fluor 488 goat anti-mouse IgG from Invitrogen Ltd (A11001)

Alexa fluor 568 Goat anti-mouse IgG from Invitrogen Ltd (A11004)

Alexa fluor 488 goat anti-rabbit IgG from Invitrogen Ltd (A11008)

Molecular biology reagents

SensiMix™*Plus* SYBR Kit from Quantace (QT605)
QuikChange® XL Site-Directed Mutagenesis Kit from Stratagene
QIAprep® Spin Miniprep Kit from QIAGEN HOUSE (27106)
QIAquick® Plasmid Midi Kit from QIAGEN HOUSE (12143)
QIAquick® Gel Extraction Kit from QIAGEN HOUSE (28704)
RNAeasy mini-kit from QIAGEN HOUSE (74104)
E.coli TOP10 competent bacteria from Invitrogen Ltd
Kanamycin sulphate from *Streptomyces kanamyceticus* (K4000) from Sigma-Aldrich
TOPO TA Cloning Kit with pCR-2.1 TOPO vector and *E.coli* TOP10 competent cells from Invitrogen Ltd (K4500-01)
FastDigest™ EcoRI from Fermentas UK (FD0274)
FastDigest™ KpnI from Fermentas UK (FD0524)
FastDigest™ HindIII from Fermentas UK (FD0504)
6 x DNA loading dye from Fermentas UK (R0611)
PrimeSTAR™ HS DNA Polymerase
TopVision™ LE GQ Agarose from Fermentas UK (R0491)
AcuPrime™ *Taq* DNA Polymerase System from Invitrogen Ltd (12339016)
LipofectAMINE™2000 transfection reagent from Invitrogen (11668-019)
Superscript II reverse transcriptase from Invitrogen Ltd (18064014)
Advantage®-GC Genomic PCR kit (Clontech, TAKARA)
Platinum PCR SuperMix (Invitrogen)

Table 2.1 List of Toxins and inhibitors used

Compound	Function	Working Concentration	Purchased from
1-methyl-4-phenylpyridinium (MPP ⁺) iodide (solid), 100mM stock solution in DMEM/F12 stored at -20°C	Inhibitor of complex I of electron transport chain in oxidative phosphorylation	10 µM – 5 mM	Sigma-Aldrich (D048)
Epoxomicin (solid), 1 mM stock solution solubilised in DMSO and stored at -20°C	Irreversible specific inhibitor of 20S proteasome	5 – 10 nM	Enzo (PI-127)
Calpain Inhibitor III, Carbobenzoxy-valinyl-phenylalinal, MDL28170; 10 mM stock solution solubilised in DMSO and stored at -20 °C	Cell permeable inhibitor of calpain I and II (K _i = 8 nM). Sequence Z-Val-Phe-CHO	10 µM	Merck Chemicals Ltd (208722)
Bafilomycin A1 from <i>Streptomyces griseus</i> (solid), 10 µM stock solution, solubilised with DMSO and stored at -20 °C	Inhibitor of autophagy, inhibits fusion of autophagosome and lysosome	5 – 10 nM	Sigma-Aldrich (B1793)
3-methyl adenine, 3-MA (solid), stock solution of 50 mM, prepared in SFM by heating to 55 °C to solubilise	Inhibitor of autophagy	5 mM	Sigma-Aldrich (M9281)
Rapamycin from <i>Streptomyces hygroscopicus</i> (2.5 mg/ml in DMSO)	Inhibits mTOR, thereby activating macroautophagy	0.2 µg/ml	Sigma-Aldrich (R8781)
InSolution™ Cycloheximide (100 mg/ml in DMSO)	Inhibitor of new protein synthesis	10 µg/ml	Merck Chemicals Ltd (239765)
Pepstatin A, synthetic (solid), 1 mM stock solution solubilised with DMSO and stored at -20 °C	Reversible inhibitor of aspartic proteases. Inhibits cathepsin D, pepsin and rennin.	1 µM	Merck Chemicals Ltd (516481)
Cathepsin Inhibitor II (Z-Phe-Gly-NHO-Bz-pMe) (solid), 10 mM stock solution solubilised in DMSO and stored at -20 °C	Cysteine protease inhibitor. Selectively inhibits cathepsin B, L, S and papain	10 µM	Merck Chemicals Ltd (219417)

Table 2.2 List of antibodies detailing their use, characteristics, the applications for which and concentration at which they were used and company they were purchased from

Name	Specificity (immunogen)	Host species	Concentration used in each application			Purchased from
			WB	IF	IP	
Anti-γ-tubulin	γ-tubulin, 48 kDa; reacts with human and mouse (synthetic peptide EEFATEGTDKDVFFY-K, corresponding to amino acids 38-53 of human γ -tubulin)	Rabbit, polyclonal antiserum	1:2000		ND	Sigma (T3559)
B512	α-tubulin, 50 kDa; reacts with a variety of organisms including human, mouse and rat; recognises an epitope at C-terminal end (sarkosyl-resistant filaments from sea urchin)	Mouse, monoclonal	1:2000	1:200	ND	Sigma (T6074)
Anti-actin	Actin, 42 kDa; reacts with a variety of organisms including human (C-terminal actin fragment with sequence SGPSIVHRKCF)	Rabbit, affinity isolated antigen specific	1:1000	1:100	ND	Sigma (A2066)
RV202	Vimentin, 57 kDa; reacts with human, mouse, rat, chicken, dog, goat, hamster, monkey and cow (vimentin extract of calf lens)	mouse, monoclonal	1:5000	1:500	ND	abcam (ab8978)
N52	NF-H, phosphorylated and non-phosphorylated, 200 kDa; reacts with human, mouse; recognises an epitope at the carboxyterminal tail segment	Mouse, monoclonal	1:2000	1:200	ND	Sigma (N0142)
smi32	non-phosphorylated NF-H, 200 kDa; reacts with mouse and rat, (hypothalamus from Fischer 344 rats)	Mouse, monoclonal	1:1000	1:200	ND	abcam (ab28029)
RMO270	NF-M, phosphorylated and non-phosphorylated, 160 kDa; reacts with phosphate independent epitope in C-terminal domain. Reacts with human; (Rat neurofilaments)	Mouse, monoclonal (ascites)	1:500	1:50	ND	Invitrogen (13-0700)

Table 2.2. (continued)

Name	Specificity (immunogen)	Host species	Concentration used in each application			Purchased from
			WB	IF	IP	
smi31	pNF-H and pNF-M, 200 kDa and 160 kDa ; reacts with mammalian, <i>Xenopus</i> , chicken (homogenized hypothalami from Fischer 344 rats)	Mouse, monoclonal, ascites	1:1000	1:200	ND	abcam (ab24573)
RT97	pNF-H, 200 kDa, developmentally delayed ; reacts with human and rat (Triton X-100 insoluble rat brain protein)	Mouse, monoclonal	1:50	ND	ND	abcam (ab17126)
RNF403	pNF-M, 160 kDa ; reacts with human and rat, reacts exclusively with pNF-M (NF preparation from calf brain tissue)	Mouse, monoclonal	1:500	1:50	ND	abcam (ab9271)
DA2	NF-L, 68 kDa ; reacts with human NF-L (purified and dephosphorylated pig NF-L)	Mouse, monoclonal, ascites	1:2000	1:200	ND	Invitrogen (13-0400)
Anti-Kinesin 5A	Kinesin 5A, 110 kDa ; reacts with human, mouse, rat, cow (the synthetic peptide CGYEAEDQAKLFPLHQETAAS corresponding to amino acids 1007-1027 of mouse Kinesin 5A)	Rabbit, polyclonal	1:1000	1:100	ND	abcam (ab5628)
Anti-Kinesin 5C	Kinesin 5C, 110 kDa ; reacts human and rat (Synthetic peptide AVHAIRGGGGSSSNSTHYQK corresponding to amino acids 938-957 of human kinesin 5C)	Rabbit, polyclonal	1:1000	1:100	ND	abcam (ab5630)
Dynein 70.1	Dynein, 70 kDa ; reacts with a variety of species including human and rat, (cytoplasmic full length native protein purified from chick brain)	Mouse, monoclonal	1:2000	1:200	ND	abcam (ab6304)
anti-GFP	GFP, 27-30 kD ; reactive against all variants of <i>Aequorea victoria</i> GFP (highly purified recombinant GFP)	Rabbit, polyclonal	1:5000 - 1:10 000	ND	ND	Abcam (ab6556)

Table 2.2. (continued)

Name	Specificity (immunogen)	Host species	Concentration used in each application			Purchased from
			WB	IF	IP	
anti-α-synuclein (C-20)	α-synuclein, 19 kDa ; reacts with human	Rabbit, polyclonal	1:1000	1:100	ND	Santa Cruz (sc-7011-R)
anti-Cdk5 (C-8)	Cdk5, 30 kDa ; reacts with mouse, rat and human (recombinant peptide found in C-terminus of human Cdk5)	Rabbit, polyclonal	1:100	ND	ND	Santa Cruz (sc-173)
Bcl-2-100	Human Bcl-2, 26 kDa (synthetic peptide corresponding to amino acids 41-54 of Bcl-2 conjugated to thyroglobulin)	Mouse, monoclonal ascites fluid	1:1000	ND	ND	Sigma (B 3170)
anti-pAkt	Phosphorylated Akt (Ser473), 60 kDa ; reacts with human, mouse and rat (synthetic phosphopeptide corresponding to residues around Ser473 of mouse Akt)	Rabbit, monoclonal	1:1000	ND	ND	Cell Signalling Technology (193H12)
Anti-NTRK2	NTrk2/NTrkB, 90-100 kDa ; reacts with human	Rabbit, affinity isolated	1:200	ND	ND	Sigma Prestige Antibodies (HPA007637)
CTD19	Cathepsin D, 52 and 34 kDa ; reacts with human (native protein purified from human liver)	Mouse, monoclonal	1:1000	1:200	ND	abcam (ab6313)
Anti-LC3B	LC3B, 16-18 kDa ; reacts with human, rat and mouse (synthetic peptide corresponding to amino acids 2-15 of human LC3B)	Rabbit, affinity isolated	1:1000	1:100	ND	Sigma (L7543)

Table 2.2. (continued)

Name	Specificity (immunogen)	Host species	Concentration used in each application			Purchased from
			WB	IF	IP	
Anti-PSMC1	PSMC1, 50 kDa; 26S protease regulatory subunit 4, reacts with human	Rabbit, affinity isolated	1:2000	1:100	ND	Sigma Prestige Antibodies (HPA000872)
anti-p62 SQSTM1	p62 (SQSTM1), 62 kDa, recognises human p62, (peptide derived from residues 387-436 in the UBA domain)	Rabbit, polyclonal	1:1000	1:100	ND	Enzo (BML-PW9860)
anti-Hsc70 (HSP70), clone BRM-22	Hsp70, 70 kD; bovine, human, rat, rabbit, chicken, guinea pig, drosophila, nematode and plant (bovine brain Hsp70)	Mouse monoclonal, ascites	1:5000	ND	ND	Sigma (H5147)
anti- α -Fodrin (clone AA6)	α -Fodrin or α II-spectrin, 240 - 280 kDa and cleavage products 120 – 145 kDa; reacts with a variety of species including human (chicken blood cell membranes following hypotonic lysis and mechanical enucleation)	Mouse, monoclonal	1:5000	ND	ND	BIOMOL (FG 6090)
CUB 7402	Transglutaminase 2 (TG2), 77-85 kDa, reacts with guinea pig, dog, rabbit and human (purified guinea pig TG2)	Mouse, monoclonal	1:1000	1:100	ND	abcam (ab2386)

2.1.3. Specialist laboratory consumables

Black 96 well microplates purchased from Greiner Bio-One Ltd UK (655076)
μ Columns for μMACs protein isolation kits from Miltenyi Biotec Ltd (130-042-701)
Chromatography paper (3 mm) purchased from Fisher Scientific (CJF240090)
Sterilin inoculation loops (10 μl) purchased from Fisher Scientific (DIS-101-026V)
Fisherbrand immersion oil purchased from Fisher Scientific (FB69193)
0.22 μm pore nitro-pure nitrocellulose purchased from Genetic Research Instrumentation (WP2HY00010)
Sterilin sero 96 well microtitre plates purchased from SLS (MIC9008)

2.1.4. Specialist equipment

Aida image Analyser v 4.03 software (Raytek Scientific Ltd, Germany)
ATTO HorizBlot semi-dry blotter (ATTO corporation, Japan)
Beckman Coulter DU 530 Life Science UV/VIS Spectrophotometer (Beckman, UK)
Bio-Rad Spectrophotometer – Model 680 Microtitre plate reader
CBS Isothermal liquid nitrogen storage system 2300 series (Sanyo Biomedical Division, UK)
Consort mini power supply (GeneFlow, UK)
Power Pac mini power supply (Bio-Rad Laboratories Ltd, UK)
Mini-wet blotter (GeneFlow, UK)
FLUOstar OPTIMA (BMG LABTECH, UK)
FujiFilm FLA-5100 gel scanner (FujiFilm Life Sciences Products, UK)
FujiFilm Intellegent dark box (FujiFilm Life Sciences Products, UK)
Mini-Protean III (Bio-Rad Laboratories, UK)
Mini-Protean tetra (Bio-Rad Laboratories, UK)
Ohaus Scout Pro Balance (Fisher Scientific UK)
MIKRO 22R microfuge (Hettich, Germany)
Ultraflex III TOF/TOF (Brucker Daltonics Ltd UK)
iBlot (Invitrogen)
Sanyo CO₂ incubator MCO-17AIC (Sanyo Gallencamp PLC, UK)
Stuart orbital incubator S150
Leica CLSM Laser Confocal Scanning Microscope (Leica, Germany)
Leica Inverted CLSM laser confocal microscope (Leica, Germany)
Leica IRE2 time-lapse fluorescence microscope with full-stage incubation (Leica, Germany)
Olympus BX51 Fluorescence Microscope (Olympus, Japan)

Olympus Mercury lamp U-RFL-T (Olympus, Japan)
Nikon Digital Net camera DN100 (Nikon, Japan)
Nikon Eclipse TS 100 inverted microscope (Nikon, Japan)
Rotor-gene 3000 Thermal cycler (Corbett Research, Germany)
Soniprep 150 (MSE scientific instruments, UK)
Walker class II microbiological safety cabinet (Walker safety cabinets, UK)
Quartz Cuvette, ultra micro absorption cell, path length 10 mm, 50 µl volume purchased from Hellma (105.202-QS)
Philips pH meter - PW9409 (Pye-Unicam, UK)
Olympus CK2 ULWCD light microscope (Olympus, Japan)
MACS multistand from Miltenyi Biotec, Germany (016708)
µMACS™ Separator from Miltenyi Biotec, Germany (130-042-602)

2.2. Methods

2.2.1. Cell culture

2.2.1.1. Maintenance of SH-SY5Y neuroblastoma cells

Cells were maintained at 37°C in a humidified atmosphere of 95 % air, 5 % CO₂. Proliferating Human SH-SY5Y neuroblastoma cells were maintained in normal growth medium containing 10 % (v/v) heat inactivated foetal bovine serum, DMEM/F12, 1 % (v/v) MEM non-essential amino acids, 2 mM L-glutamine, 200 units/ml penicillin and 200 µg/ml streptomycin. Cells were maintained until they reached 85-90 % confluency before subculture. For maintenance and expansion, cells were grown in either T75 or T175 flasks.

2.2.1.2. Subculture of SH-SY5Y neuroblastoma cells

Once cells reached around 85-90 % confluency they were detached by trypsinization using 1 x Trypsin in Dulbecco's Phosphate Buffered Saline (DPBS). The cell monolayer was washed twice with DPBS to remove all traces of serum and detached with 1 x Trypsin/DPBS solution at 37°C for 3-5 minutes. Trypsin was quenched by the addition of growth medium. Cells were harvested by centrifugation at 300 x g for 5 minutes. Cell was determined number as described in section 2.2.1.3 and seeded at the required cell densities for different experiments.

2.2.1.3. Determination of cell number

Viable cell number was determined using a hemacytometer slide. The cell pellet was resuspended in 1 ml of growth medium by pipetting up and down at least 30 times to ensure

that the cells are not clumped together. Typically, a small aliquot of the cell suspension was then diluted 1 in 10 with growth medium in a 0.5 ml eppendorf tube. An equal volume of trypan blue solution (0.4 % (v/v)) was then added to the diluted cell suspension. Non-viable cells take up the dye and are stained while viable cells remain unstained. Cells were counted on the hemocytometer slide and an average number per square was determined. To calculate the number of cells per ml equation 1 was used. To calculate the percentage viable cells equation 2 was used. The number of cells per ml was used to determine the volume of cell suspension required to seed cells at the required cell density for experiments.

$$\text{Cells/ml} = \text{Average cells per square} \times \text{dilution factor} \times 10^4 \text{ ————— (1)}$$

Where the dilution factor = dilution factor for cell suspension x dilution factor for trypan blue (typically 10 x 2)

Each square is 0.25 mm x 0.25 mm

$$\% \text{ Viable cells} = [(\text{Number of stained cells}) / (\text{total number of cells})] \times 100 \text{ ——— (2)}$$

2.2.1.4. Cryopreservation and resuscitation of SH-SY5Y neuroblastoma cells

Cell pellets were resuspended in freezing mix (25 % (v/v) Heat inactivated foetal bovine serum, 10 % (v/v) DMSO, 200 units/ml Penicillin and 200 µg/ml streptomycin, 2 mM L-glutamine in DMEM/F12) at a cell density of 2×10^6 cells/ml. Cryovials were frozen at -80°C overnight and then transferred to liquid nitrogen storage.

2.2.1.5. Differentiation of SH-SY5Y cells

Cells were seeded at a density of 500 000 cells/flask in T25 flasks or at a density of 8000 cells/well in 8-well chamber slides. Cells were incubated overnight at 37°C in a humidified atmosphere of 5 % CO₂, 95 % air in full growth medium. Following overnight recovery the medium was replaced with differentiation medium (1 % (v/v) heat inactivated foetal bovine serum, DMEM/F12, 1 % (v/v) MEM non-essential amino acids, 2 mM L-glutamine, 200 units/ml penicillin and 200 µg/ml streptomycin) containing 10 µM all-trans retinoic acid (RA, Sigma). RA differentiation medium was replaced with fresh RA differentiation medium every three days. For cells differentiated using RA alone, cells were treated with RA for a period of eight days. For cells differentiated using a combination of RA and brain derived neurotrophic factor (BDNF), treatment with RA lasted for a period of five days. Cells were then washed twice with serum free medium (SFM; DMEM/F12, 2 mM L-glutamine, 200 units/ml penicillin and 200 µg/ml streptomycin, MEM non-essential amino acids) to remove all traces of serum and treated with 50 ng/ml BDNF in SFM. After three

days treatment with BDNF, cells were ready to be used in experiments. SFM containing BDNF was replaced every three to four days with fresh SFM containing BDNF.

2.2.1.6. Quantification of axon outgrowth

To quantify axon outgrowth to assess the differentiation of SH-SY5Y neuroblastoma cells with Retinoic acid (RA) or RA followed by BDNF, mitotic and RA or RA/BDNF differentiated SH-SY5Y cells cultured in T25 flasks and viewed by phase contrast microscopy using the 10 x objective. Images were analysed using Leica QWin software, in which axon length were measured and the number of cells with axon-like processes that are greater than 2.5 x the width of the cell body were counted and expressed as a percentage of the total number of cells.

2.2.1.7. Transfection of SH-SY5Y neuroblastoma cells with GFP tagged neurofilament proteins using LipofectAMINE™

SH-SY5Y cells were seeded at a cell density of 250 000 cells per 35mm diameter dishes (ibidi μ dish or Iwaki) or at a density of 1.5×10^6 cells in 100 mm culture dishes (BD) depending on the application. A LipofectAMINE™ 2000 to DNA ratio of 1 μ g DNA to 2 μ l LipofectAMINE™ 2000 was used. Following overnight recovery, the medium was removed, the monolayer rinsed twice with DPBS, and incubated with 1 x Gibco Opti-MEM® I Reduced Serum Medium. For transfection of cells in 35 mm dishes, 1 μ l of LipofectAMINE™ 2000 was added directly to 99 μ l of Opti-MEM® I in sterile 1.5 ml tubes. For transfection of cells in 100 mm dishes, 5 μ l of LipofectAMINE™ 2000 was added directly to 495 μ l of Opti-MEM® I in 1.5 ml tubes. After adding LipofectAMINE™ 2000, tubes were vortexed gently, briefly centrifuged and then incubated at room temperature for 5 minutes. Plasmid DNA (1 μ g for transfections in 35 mm dishes and 5 μ g for transfections in 100 mm dishes) was added to the Opti-MEM® I/LipofectAMINE™ 2000 mix, tubes were vortexed gently, briefly centrifuged and incubated for 30 minutes at room temperature. After the 30 minute incubation, the Opti-MEM® I/LipofectAMINE™2000/DNA mix was added directly the cells in a drop-wise fashion and plates were swirled to ensure equal dispersion. Cells were returned to the incubator for 4 h before media was replaced with growth medium without antibiotics. Following overnight recovery, the growth medium was replaced again with growth medium containing antibiotics.

2.2.1.8. Assessment of cell viability using the MTT reduction assay

Cell viability was assessed by MTT (3-(4,5-dimethylthiazol-2-yl)-2,5-diphenyltetrazolium bromide) reduction which in anchorage dependent cells is based on the principle that viable

cells will accumulate MTT intracellularly. The MTT is then reduced by mitochondrial enzymes and enzymes of the endoplasmic reticulum to produce a formazan product which is membrane impermeable and therefore accumulates in viable cells. The product can be solubilised in DMSO and detected using a spectrophotometer.

Undifferentiated cells were seeded at a density of 5000 cells/well while RA/BDNF differentiated cells were seeded at a density of 10 000 cells/wells in 96 well plates. Following overnight recovery cells were treated with a variety of different compounds in 100 µl of medium (see Table 2.1 for a comprehensive list) for a specified time course. 1 hour before the end of the time-point, MTT was added to each well to give a final concentration of 0.5 mg/ml and plates were re-incubated at 37°C in a humidified atmosphere of 95 % air, 5 % CO₂ for 1 hour. The medium was then aspirated from the wells and the formazan product was solubilised with 100 µl DMSO per well. Plates were agitated for 2 minutes on a plate shaker before measured using a microplate reader at 570 nm.

2.2.2. Preparation of cell lysates

2.2.2.1. Preparation of total cell extracts

To prepare total cell extracts following treatment spent media was transferred to a 15 ml tube. The monolayer was then washed twice with Dulbecco's PBS and the washes were added to the spent media. Floating cells were harvested by centrifugation at 300 x g for 5 minutes and washed twice with Dulbecco's PBS to remove any serum. In the meantime 300 µl of ice-cold total extraction buffer (50 mM Tris, pH 6.8; 5 mM EDTA; 1 % (w/v) SDS; 1 mM Sodium orthovanadate; 1 % (v/v) Halt Protease Inhibitor Cocktail; 1 % (v/v) Halt Phosphatase Inhibitor Cocktail) was added directly to the monolayer. The monolayer of cells in the flask was extracted into the total extraction buffer using a cell scraper and then transferred into a 1.5 ml tube on ice. Harvested and washed floating cells were combined to produce the total cell extract. Samples were then placed in a heating block at 100 °C for 5 minutes. Samples were sonicated on ice (3 x 3 sec bursts on 6-10 power setting) and then stored at -80 °C until required. The protein concentration of samples was determined using the BC Assay (see section 2.2.6.1.) and total cell extracts were analysed by SDS-PAGE as described in section 2.2.7.

2.2.2.2. Preparation of cell lysates for proteasome activity determination

Cells were seeded at a density of 250,000 cells per well in 6-well tissue culture plates. Following treatment, cells were detached using a cell scraper and transferred to 2 ml tubes and placed on ice. Cells were harvested by centrifugation at 300 x g for 7 minutes at 4 °C. To prepare cell lysates 100 µl ice-cold homogenisation buffer (20mM Tris/HCl, pH 7.0,

0.1mM EDTA, 1nM 2-mercaptoethanol, 5mM ATP, 20% (v/v) glycerol, 0.4% (v/v) Igepal CA-630) was added to the harvested cell pellets, samples were then vortex mixed vigorously for 1 minute followed by centrifugation at 17380 x g at 4 °C for 2 min. The resultant supernatant was transferred to a 0.5 ml microfuge tube and kept on ice to be used in the fluorogenic peptide assay for proteasome activity described in section 2.2.4.

2.2.2.3. Preparation of cell lysates for cathepsin activity determination

Cells were seeded at a density of 250 000 cells/well in 6-well tissue culture plates. Following treatment, cells were detached by mechanical detachment using a cell scraper and the cell suspension was transferred to 2 ml tubes and placed on ice. Cells were harvested by centrifugation at 300 x g for 7 minutes at 4 °C. Cells were lysed in 150 µl of ice-cold cell lysis buffer (provided with cathepsin L and cathepsin D assay kits, abcam) and incubated on ice for 10 min. The lysate was then centrifuged for 5 min at 20160 x g and the cleared supernatant was transferred to a 0.5 ml tube and kept on ice to be used in the fluorogenic peptide assays described in section 2.2.5.

2.2.2.4. Preparation of cell lysates for immunoprecipitation

Cells were seeded in 100 mm culture dishes (BD) at a cell density of 1.5×10^6 cells/dish. Cells were transfected with 5 µg of plasmid DNA using LipofectAMINE™2000 as described in section 2.2.1.6. Cells were allowed to recover for 48 hours before being extracted into a Low Salt Lysis Buffer (1% (v/v) Igepal CA-630, 50 mM Tris HCl, pH 8.0). Spent media was discarded and the monolayer was washed twice with DPBS to remove all traces of serum. 1 ml of ice-cold Low Salt Lysis Buffer was added directly to the monolayer and the lysate was collected using a cell scraper. The cell lysate was immediately mixed, placed on ice and incubated on ice for 30 minutes with occasional mixing. The cell lysate was then centrifuged for 10 minutes at 10,000 x g at 4°C. The supernatant was harvested and transferred to a fresh 1.5 ml tube and either kept on ice for immediate immunoprecipitation as described in section 2.2.5 or stored at -80°C until required. The cell debris pellet was dissolved in 1 ml of total extraction buffer (see section 2.2.2.1.), boiled for 5 min and stored at -80°C.

2.2.3. Assessment of proteasome activity using a fluorogenic peptide assay

20-30 µl of lysates (prepared as described in section 2.2.2.2.) were incubated at 37 °C with 10 µl of 1 mM *N-Succinyl-Leu-Leu-Val-Tyr-AMC* (the fluorogenic substrate for chymotryosin-like activity, CLA of the 20S proteasome) in assay buffer (50nM HEPES pH 8.0, 0.5mM EGTA) in a total reaction volume of 200 µl in black microtitre plates to give a

final working concentration of 50 μM for the CLA substrate. Using a FLUORstar OPTIMA fluorometer (BMG LABTECH), readings were taken every 5 minutes at excitation and emission wavelengths of 355 nm and 460 nm respectively for 1 hour. The rate of substrate cleavage is directly proportional to proteasome CLA activity. Protein estimation on each sample was carried out using the BioRad protein assay as described in section 2.2.6.2. Results were expressed as change in fluorescence units/min/ μg protein. An example of a typical plot showing change in fluorescence over time is given in Figure 2.1.

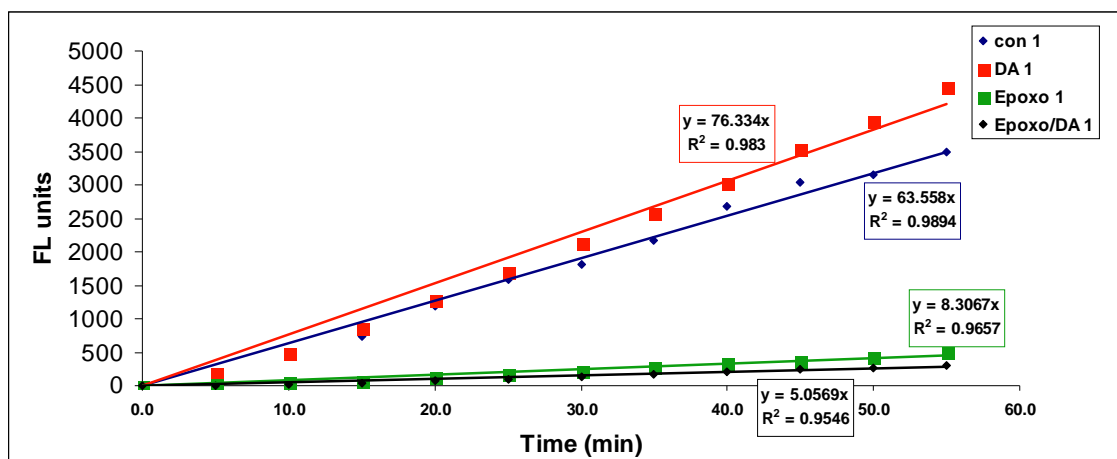


Figure 2.1 A Typical plot of fluorescence units versus time (minutes) from which proteasome activity was determined.

The rate of the reaction (protease activity) was determined from the slope of the 'line of best fit' on the linear portion of the curve for the fluorescence recordings taken every 5 minutes over a 1 hour period. The rate of the reaction was expressed as change in fluorescence over time per μg protein determined separately using the BioRad protein assay kit (section 2.2.6.2).

2.2.4. Assessment of cathepsin activity using a fluorogenic peptide assay

2.2.4.1. Cathepsin D activity assay

20 μl of cell lysates (prepared as described in section 2.2.2.3.) were incubated at 37°C with 20 μM (final concentration) cathepsin D substrate - (7-methoxycoumarin-4-yl)acetyl (Mca)-Gly-Lys-Pro-Ile-Leu-Phe-Phe-Arg-Leu-Lys(Dnp)-D-Arg-NH₂, provided with the cathepsin D assay kit (abcam) - in cathepsin assay buffer (1 M NaOAc pH 5.5, 1.2 M NaCl, 100 mM DTT) in a total reaction volume of 100 μl in black 96 well microtitre plates. Using a FLUORstar OPTIMA fluorometer (BMG LABTECH), readings were taken every 5 minutes at excitation and emission wavelengths of 355 nm and 460 nm respectively over an hour. The resultant fluorescence is a measure of the hydrolysis of the peptide substrate and by inference the protease activity. Protein estimation on each sample was carried out using the

BioRad protein assay as described in section 2.2.6.2. Results were expressed as change in fluorescence units/min/ μg protein.

2.2.4.2. Cysteine cathepsin activity assay

20 μl of cell lysates (prepared as described in section 2.2.2.3.), were incubated at 37°C with 200 μM (final concentration) OmniCathepsin™ substrate [*Z-Phe-Arg-AMC (7-amino-4-methylcoumarin)*] in cathepsin assay buffer (1 M NaOAc pH 5.5, 1.2 M NaCl, 100 mM DTT) in a total reaction volume of 100 μl in black 96 well microtitre plates. Using a FLUORstar OPTIMA fluorometer (BMG LABTECH), readings were taken every 5 minutes at excitation and emission wavelengths of 355 nm and 460 nm respectively over an hour. The resultant fluorescence is a measure of the hydrolysis of the peptide substrate and by inference the protease activity. Protein estimation on each sample was carried out using the BioRad protein assay as described in section 2.2.6.2. Results were expressed as change in fluorescence units/min/ μg protein.

2.2.5. Co-immunoprecipitation of GFP tagged fusion proteins and their associated proteins using the $\mu\text{MACS}^{\text{TM}}$ Epitope Tag Protein Isolation Kit

GFP tagged neurofilament proteins and their associated proteins were co-immunoprecipitated using the $\mu\text{MACS}^{\text{TM}}$ GFP Tag Protein Isolation Kit (Miltenyi) from lysates prepared in section 2.2.2.4. To magnetically label the GFP-tagged neurofilament subunits, 50 μl of anti-GFP MicroBeads were added to the lysate. After mixing the labelling reaction was incubated on ice for 30 minutes. The μ column was placed in the magnetic field of the μMACS separator and equilibrated by applying 200 μl of lysis buffer (1% (v/v) Igepal CA-630, 50 mM Tris HCl, pH 8.0). After the labelling reaction, the lysate was applied to the column and the excluded supernatant was collected. The column was then washed four times with Wash Buffer 1 (150 mM NaCl, 1 % (v/v) Igepal CA-630, 0.5 % sodium deoxycholate, 0.1 % (w/v) SDS, 50 mM Tris-HCl, pH 8.0). The column was then rinsed with 100 μl Wash Buffer 2 (20 mM Tris-HCl, pH 7.5) to remove residual salt and detergent from the immune complex before elution. 20 μl of Triethylamine (TEA) elution buffer (0.1 M Triethylamine pH 11.8, 0.1 % (v/v) Triton X-100) was applied to the column and incubated for 5 minutes at room temperature. The bound antigen was eluted from the column (E1, eluate 1) by the application of 50 μl of Triethylamine (TEA) elution buffer and collected in a 1.5 ml tube containing 3 μl 1 M MES, pH 3 for neutralisation. Eluate 2 (E2) was collected in a fresh 1.5 ml tube containing 3 μl 1 M MES, pH 3 by applying another 50 μl Triethylamine elution buffer. Eluates and excluded supernatants were stored at -80°C until required.

2.2.6. Determination of protein content

2.2.6.1. BC Assay

A microtitre plate version of the BC Assay was used to assay the protein content in all samples that are in buffers compatible with this assay. A standard curve was prepared by diluting 2-20 μg of 1 mg/ml BSA in a total volume of 20 μl directly into the microtitre plate. 5 μl of sample buffer was added to each standard whilst samples were diluted appropriately, typically 5 μl of sample was diluted in 20 μl water. 200 μl of BC reagent (Bicinchoninic Acid solution containing 0.08 % (w/v) copper (II) sulphate) was then added to each well. Plates were incubated at 37 °C for 30 minutes to allow for colour development. Absorbance was measured at 570 nm. Protein content of each sample was determined from the equation of the 'line of best fit' for the standard curve, an example of which is given in Figure 2.2.

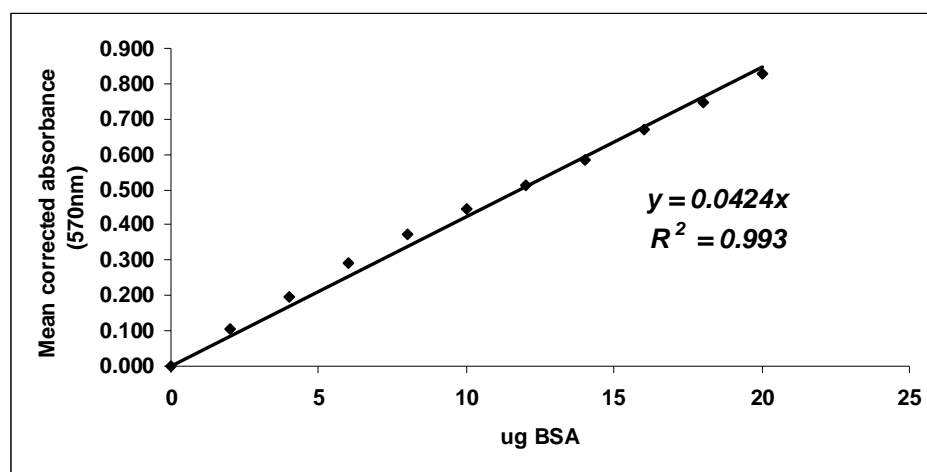


Figure 2.2 Standard calibration curve for BSA (0 - 20 μg) obtained using the BC Assay kit and measured at 570 nm.

Protein content of samples (unknowns) was determined using the equation of the 'line of best fit'.

2.2.6.2. Bio-Rad protein assay

The Bio-Rad microassay procedure was used as per manufacturer's instructions to assay the protein content of cell lysates used to assay proteasome activity. A standard curve was prepared using several dilutions of 1 mg/ml BSA from 5 to 50 $\mu\text{g}/\text{ml}$ in a volume of 800 μl . For the samples (unknowns), 10 μl of each sample was prepared in a volume of 800 μl . 200 μl of Bio-Rad dye reagent concentrate (Coomassie Brilliant Blue G-250, phosphoric acid, methanol) was added to each tube and mixed by vortex mixing. 200 μl of each sample and standard solution was transferred to a 96 well microtitre plate. Absorbance was measured at 570 nm. Protein content of each sample was determined from the equation of the 'line of best fit'.

2.2.7. Sodium Dodecyl Sulphate Polyacrylamide Gel Electrophoresis (SDS-PAGE)

For SDS-PAGE, the resolving gel mix was prepared as described in Table 2.3 depending on which concentration of resolving gel was required. After the addition of the required quantity of APS and TEMED, the resolving gel mix was poured between glass plates with 1.5 mm spacers that were assembled in the gel mould apparatus for the Bio-Rad Protean III or Tetra gel kit (Bio-Rad) as per manufacturer's instructions. The resolving gel mix was overlaid with 1 ml of water and allowed to set for at least 45 minutes at room temperature.

Table 2.3 Recipes for the preparation of resolving gel mix at various concentrations

Resolving Gel Concentration	7.5% (v/v)	10% (v/v)	12% (v/v)	15% (v/v)
40 % (v/v) acrylamide	1.9 ml	2.5 ml	3.0 ml	3.75 ml
1.5 M Tris buffer, pH 8.8	2.5 ml	2.5 ml	2.5 ml	2.5 ml
10 % (w/v) SDS	100 μ l	100 μ l	100 μ l	100 μ l
water	5.5 ml	4.9 ml	4.4 ml	3.65 ml
TEMED	5 μ l	5 μ l	5 μ l	5 μ l
APS	50 μ l	50 μ l	50 μ l	50 μ l

Once the resolving gel was set, the overlaying water was removed and the required volume of stacking gel (3-5 ml per gel) was transferred from the working stock solution (Table 2.4) and polymerised with the required volume of APS and TEMED.

Table 2.4 Stacking Gel Mix (working stock kept at 4°C and used as required):

Stacking gel concentration	4 % (v/v)
40 % (v/v) acrylamide	10 ml
0.5 M Tris buffer, pH 6.8	25 ml
10 % (w/v) SDS	1 ml
water	64 ml

To polymerize 10 ml stacking gel:

TEMED	20 μ l
10 % (w/v) APS	50 μ l

The stacking gel was allowed to polymerise in the presence of 10 or 15 well combs for at least 30 minutes after which the comb was removed.

The gels were then fixed into the gel tank according to manufacturer's instructions and the inner and outer reservoirs were then filled with Tris-glycine SDS-PAGE running buffer (0.0256 M Tris base, 0.192 M Glycine, 0.1 % (w/v) SDS, pH 8.3).

Samples were mixed with an equal volume of 2 x reducing sample buffer (40 ml of 10 % (w/v) SDS; 20 ml glycerol; 20 ml 0.5 M Tris-HCl, pH 6.8; 1.54 g DTT, 0.01 g Bromophenol blue). Samples and molecular weight standards were then incubated at 100 °C for 5 minutes in a heating block, followed by centrifugation at high speed for 10 seconds. Samples and standards were then applied into the wells and separated at 200 V until the dye-front approached the bottom of the gel (45 minutes to 1 hour).

2.2.8. Western blotting and immunoprobng

2.2.8.1. Western blotting

2.2.8.1.1. Wet-blotting

A wet blotting apparatus from GeneFlow was used for wet blotting. Following electrophoresis, gels were rinsed in Tris-glycine electroblotting buffer (39 mM Glycine, 48 mM Tris base, 0.0375 % (w/v) SDS, 20 % (v/v) methanol) to partially remove electrophoresis buffer salts. The nitrocellulose membranes and filter papers (4 pieces per gel) were cut to the gel dimensions (6 cm x 9 cm) and soaked with Tris-glycine electroblotting buffer. The immunoblot sandwich was prepared as follows: a sponge was placed on the red panel, followed by two pieces of filter paper and then the nitrocellulose membrane. The electrophoresis gel was then carefully placed onto the nitrocellulose taking care to avoid trapping air bubbles. The sandwich was then completed by placing the remaining two pieces of filter paper on top of the gel, followed by a sponge. The cassette was then closed and returned to the tank of the wet-blotting apparatus so that the red panel faced the anode and run at a constant 30 V overnight (16 h). Protein transfer was assessed by reversibly staining the nitrocellulose membranes with 0.05 % (w/v) Copper phthalocyanine 3, 4', 4'', 4''' tetrasulphonic acid tetrasodium salt in 12 mM HCl. The copperstained nitrocellulose membranes were then photographed with a FujiFilm CCD camera after which they were destained in 12 mM NaOH.

2.2.8.2. Semi-dry electroblotting

For lower molecular weight proteins such as α -synuclein and LC3B Proteins separated by electrophoresis were transferred to nitrocellulose membranes using either a semi-dry blotting technique using an iBlot (Invitrogen). Following electrophoresis, gels were rinsed in deionised water to partially remove electrophoresis buffer salts. The piece of filter paper provided with the iBlot transfer stacks was soaked in deionised water. The lower stack

containing the nitrocellulose membrane was placed into position on the iBlot apparatus, followed by the electrophoresis gel that was rinsed in water to remove electrophoresis buffer salts, taking care not to trap air bubbles. The piece of filter paper was then placed on top of the gel, followed by the upper stack. The provided sponge was put into position in the lid of the apparatus which was secured into place and proteins were transferred for 7 minutes. Protein transfer was assessed by reversibly staining the nitrocellulose membranes with 0.05 % (w/v) Copper phthalocyanine 3, 4', 4'', 4''' tetrasulphonic acid tetrasodium salt in 12 mM HCl. The copperstained nitrocellulose membranes were then photographed with a FujiFilm CCD camera after which they destained in 12 mM NaOH.

2.2.8.2. Immunoprobng

Nitrocellulose membranes were blocked with 3 % (w/v) marvel/TBS-Tween for 1 hour at room temperature. Membranes were probed with primary antibodies at the concentrations listed in Table 2.2 overnight at 4 °C diluted in 3 % (w/v) marvel/TBS-Tween. Following overnight incubation in primary antibody, nitrocellulose membranes were washed three times with TBS - 0.1 % (v/v) Tween. Membranes were then incubated in appropriate HRP (Horse Radish Peroxidase) conjugated secondary antibodies (1:1000) or in some cases AP (Alkaline Phosphatase) conjugated secondary antibodies (1:1000) for 1 ½ hours at room temperature diluted in 3 % (w/v) BSA/TBS-Tween. Membranes were then washed again three times with TBS- 0.1 % (v/v) Tween.

2.2.8.3. Secondary antibody detection of Western blots

2.2.8.3.1. Enhanced Chemiluminescence (ECL) detection

Membranes probed with HRP conjugated secondary antibodies were developed by Enhanced Chemiluminescence (ECL) using a FujiFilm CCD camera imaging device. Briefly, a 1:1 solution of detection reagent 1 and detection reagent 2 was pipetted directly onto the membrane. After 1 minute incubation, excess substrate was removed and the membrane transferred to the dark box of the FujiFilm CCD camera in which it was developed.

2.2.8.3.2. Alkaline phosphatase (AP) detection

Membranes probed with AP conjugated secondary antibodies were developed by a colorometric method using 0.75 M Tris, pH 9.5 buffer containing 0.08 mg/ml BCIP (5-Bromo-4-Chloro-3 Indolyl Phosphate, 33 µl of 50 mg/ml stock in 20 ml of substrate buffer) and 0.165 mg/ml NBT (Nitro Blue Tetrazolium, 44 µl of 75 mg/ml stock in 20 ml of

substrate buffer). Membranes were developed in the dark until bands are visible, whereupon development was stopped by extensive washing in deionised water.

2.2.9. Peptide mass fingerprinting of proteins co-immunoprecipitated with GFP tagged NF subunits

For 1-dimensional and 2-dimensional SDS-PAGE all solutions were prepared in ultra-pure water. For 1-dimensional SDS-PAGE (described in section 2.2.7) samples prepared in section 2.2.5 from 100 mm culture dishes were mixed with 5 x sample buffer so that a maximum volume of the sample could be loaded. Proteins were separated by SDS-PAGE as described in section 2.2.7.

2.2.9.1. 2-dimensional polyacrylamide gel electrophoresis (2D-PAGE)

For 2D-PAGE, the cell lysates were prepared from 5 x 100 mm culture dishes to increase protein concentration in eluates (see section 2.2.5.). 50 µl of the eluate was acetone precipitated by the addition of 4 volumes of ice-cold acetone overnight at -20 °C. Precipitated protein was harvested by centrifugation at full speed for 10 minutes at 4 °C. Protein pellets were dried at room temperature for 30 minutes, resuspended in 130 µl of sample rehydration buffer (8 M urea, 4 % (v/v) CHAPS, 0.2 % carrier ampholytes, 0.0002 % (w/v) bromophenol blue, 50 mM DTT) and 125 µl was applied to one of the IEF tray channels. A 7 cm pH 3-10 IPG strip was laid on the sample and passively hydrated for 1 hour at room temperature. The strip was covered with 700 µl mineral oil and focused using a Protean IEF cell programmed with the following focusing protocol: active hydration for 13 h and 40 min at 20 °C at 50 µA/strip, 250 V for 20 min (linear), 4000 V for 2 h and 30 min (linear) and 4000 V, rapid for 10000 Vhours.

The resolving gel was prepared with ultra-pure water as described in section 2.2.7 and allowed to set. The resolving gel was then topped with a layer of 4 % (v/v) polyacrylamide stacking gel prepared as described in section 2.2.7 using ultra-pure water. Strips were removed from the IEF tray and placed into a rehydration tray. Strips were equilibrated with DTT rehydration buffer (20 mg/ml DTT, 6 M urea, 2 % (w/v) SDS, 20 % (v/v) glycerol, 50 mM Tris-HCl, pH 8.8) for 15 minutes with gentle agitation to reduce sulphhydryl groups. The DTT rehydration buffer was then replaced with Iodoacetamide equilibration buffer (25 mg/ml iodoacetamide, 6 M urea, 2 % (w/v) SDS, 20 % (v/v) glycerol, 50 mM Tris-HCl, pH 8.8) and strips were incubated for 15 minutes with gentle agitation to alkylate the sulphhydryl groups to prevent sulphhydryl cross-bridges from reforming. The stacking gel was overlaid with 0.5 % (w/v) agarose in Tris-glycine SDS-PAGE running buffer containing 0.1 % (w/v) bromophenol blue and the IPG strip was slid in place between the two glass plates so that it rested on the top of the stacking gel. A piece of filter onto which 1 µl of protein standards

was applied was inserted at the acidic end of the IPG strip. Gels were assembled in the gel tank apparatus as described in section 2.2.7 and run at 200 V.

2.2.9.2. Silver staining of gels for mass spectrometry

All solutions used for silver staining were prepared using ultra-pure water. After SDS-PAGE, polyacrylamide gels were fixed for 1 hour with two changes of fixation solution (50 % (v/v) ethanol, 12 % (v/v) acetic acid). Gels were then washed three times for 20 minutes with 20 % (v/v) ethanol. Gels were sensitized by incubating for 2 minutes in 0.02 % (v/v) sodium thiosulphate and washed three times for 5 minutes ultra-pure water. Incubated gels with silver stain solution (0.2 % (w/v) silver nitrate, 0.076 % (v/v) formalin) for 20 minutes. Gels were washed twice with ultra-pure water for 20 seconds each and developed by adding developing solution (6 % (w/v) sodium carbonate, 0.0004 % sodium thiosulphate, 0.05 % (v/v) formalin). Development was stopped by adding a stop solution (12 % (v/v) acetic acid). Gels were kept in the fridge in ultra-pure water.

2.2.9.3. In-gel trypsin digestion of excised protein bands or spots

Silver stained polyacrylamide gels from which spots/bands were excised and trypsinized the day after they were silver stained. The excised spots/bands were dehydrated with the addition of 50 μ l of 2:1 acetonitrile (ACN): 25 mM NH_4HCO_3 for 15 minutes. The supernatant was removed and spots/bands were rehydrated with the addition of 50 μ l 25 mM NH_4HCO_3 for 10 minutes. The supernatant was removed and the dehydration/rehydration cycle was repeated. The spots/bands were then dehydrated with 50 μ l 2:1 ACN: 25 mM NH_4HCO_3 for 15 minutes and allowed to air-dry for 15 minutes. Dried spots/bands were resuspended in 12.5 ng/ μ l Promega sequencing grade trypsin (V5113) in 25 mM NH_4HCO_3 on ice (10 μ l of trypsin for bands and 4 μ l of trypsin for gel spots) and allowed to hydrate for 20-30 minutes. Excess trypsin was removed and spots were covered with 10-30 μ l 25 mM NH_4HCO_3 (enough to cover the gel) and incubated at 37°C for 4 hours prior to shaking for 20 minutes. The supernatant was removed and transferred to 0.5 ml tubes. An additional 20 μ l 80/20 ACN/water was added to the trypsinized gel spots/bands for a further 15 minutes, supernatant was removed and combined with the previous supernatant. Samples were stored at -80°C.

To perform mass spectrometry, 1 μ l of 1 % (v/v) Trifluoroacetic acid (TFA) was added, mixed and 1 μ l of samples were spotted directly onto the MALDI target plate with 1 μ l of 10 mg/ml CHCA matrix in 50:50 ACN:water containing 0.1 % TFA. Peptide mass spectra were processed using an Ultraflex III TOF/TOF Brucker Daltonik Ltd).

2.2.10. Immunofluorescence imaging

2.2.10.1. Methanol fixation

Cells in 8-well chamber slides were fixed with ice-cold 90 % (v/v) methanol/TBS for 20 minutes at -20 °C. For cytoskeletal staining, cells were then permeabilized for 10 minutes using 1 % (v/v) Triton X-100 in TBS at room temperature. In an alternative method when staining for smaller soluble proteins, cells were permeabilized using 0.2 % (v/v) Triton X-100. Wells were rinsed with PBS before staining.

2.2.10.2. Immunofluorescence staining

Fixed and permeabilised slides were blocked for 1 hour with 3 % (w/v) BSA/TBS-Tween (0.1%) at room temperature before incubating with primary antibodies (see Table 2.2 for a list of antibodies used and the dilutions at which they were used) diluted in 3 % (w/v) BSA/TBS-Tween (0.1 %) overnight at 4 °C in a humidified chamber. Cells were washed extensively with TBS/ 0.1 % (v/v) Tween 20. Cells were incubated with anti-IgG alexa-fluor conjugated secondary antibodies (1:200) for 2 hours at room temperature. Cells were then washed extensively with TBS/ 0.1 % (v/v) Tween 20 to remove all unbound secondary antibody. The chambers were removed and slides were mounted with anti-fade mountant and a glass coverslip (thickness size 0). The coverslip was sealed in place with clear nail varnish.

Slides were viewed by laser confocal microscopy using a Leica CLSM Laser confocal microscope. Cells were viewed using the 40 x and 63 x objective. AlexaFluor 488 and GFP were excited with the Argon laser (emission wavelength of 488 nm) and the AlexaFluor 568 and propidium iodide nuclear stain was excited with the Krypton laser (emission wavelength of 568 nm). Gain and offset were set against the control and kept constant for all treatments so that the fluorescence intensity between control and treatments were comparable.

Slides were also visualised using an Olympus Fluorescence microscope, AlexaFluor 488 was visualised using a blue filter for FITC visualisation, AlexaFluor 568 and Propidium Iodide were visualised using a green filter for TRITC visualization and DAPI was visualised using the UV filter. In addition cells were also visualized by phase contrast which allowed the overlaying of fluorescence signals on phase contrast images.

2.2.11. Live cell imaging

Cells were seeded at a density of 250 000 cells in 35 mm glass bottomed dishes (ibidi µdish or Iwaki) and transfected with GFP/NFs as described in section 2.2.1.7. Cells were imaged

live using a Leica inverted confocal microscope. GFP fluorescence was excited with the Argon laser (emission wavelength of 488 nm).

For time-lapse imaging cells expressing GFP-tagged NF-M or NF-H were viewed live using a Leica IRE2 time-lapse fluorescence microscope with full-stage incubation. The fluorescence from GFP-tagged neurofilaments was excited using the filter for FITC/GFP image acquisition. Fluorescence and DiC images were taken concurrently every 5 minutes over the course of an hour with shutters closing after each acquisition. Images were saved using Openlab image acquisition software and processed using ImageJ imaging software to produce overlaid images, time-lapse movies and to measure axonal process length.

2.2.12. General molecular biology techniques

2.2.12.1. Amplification of neurofilament subunits by Polymerase Chain Reaction (PCR)

Neurofilament subunit DNA was amplified cDNA preparations from SH-SY5Y neuroblastoma cells (kindly donated by Dr Julia Fitzgerald). A list of the primers used to amplify NF cDNA is given in Table 2.5. NF-M and NF-L cDNA were amplified by Advantage® 2 PCR in a 25 µl total reaction volume containing 1 µl of template DNA according to manufacturer's instructions. Initial attempts to amplify the entire sequence of NF-H using Advantage 2 PCR or PrimeSTAR™ HS DNA Polymerase, did not yield a full-length NF-H cDNA sequence. Due to the high GC content of the first 1000 bp of NF-H it was decided to clone NF-H in two separate parts; the so-called N-terminal part containing this GC-rich region and the C-terminal part. The N-terminal part was amplified using the Advantage®-GC Genomic PCR according to manufacturer's instructions with reactions containing 0, 2.5, 5.0 and 7.5 µl of 5 M GC melt to optimize the amount of GC melt in the reaction in a 25 µl reaction volume. The C-terminus part of NF-H was amplified using Platinum PCR SuperMix according to manufacturer's instructions.

Table 2.5 List of primers used for the amplification of neurofilament subunits

Name	Sequence
<i>hNF-M_fwd</i>	5'-GAATTCAGATGAGCTACACGTTGGACTC-3' (blue, EcoRI site; green, start codon; underlined, homologous to hNF-M cDNA)
<i>hNF-M_rev</i>	5'-TTTCCTTCAGTGGGTCTCACTGATTCAGCTG-3' (yellow, SalI site; red, stop codon; underlined, homologous to hNF-M cDNA)
<i>hNF-L_fwd</i>	5'-GAATTCCTCAGATTCCTTCAGCTACGAG-3' (blue, EcoRI site; green, start codon; underlined, homologous to hNF-L cDNA)
<i>hNF-L_rev</i>	5'-CGATTCTTCTTTCTAATCTGGGGGCAGCTG-3' (yellow, SalI site; red, stop codon; underlined, homologous to hNF-L cDNA)
<i>hNF-H_fwd</i>	5'-GAATTCCTCAGATGAGCTTCGGCGGCG-3' (blue, EcoRI site; green, start codon; underlined, homologous to hNF-H cDNA)
<i>hNF-H_rev</i>	5'-TGTTCCGGCGGTTCCCCTTCATTCAGCTG-3' (yellow, SalI site; red, stop codon; underlined, homologous to hNF-H cDNA)
<i>hNF-H_N_fwd</i>	5'-TGCTCAGGCCATGATGAGCTTCG-3' green, translational start; underlined, homologous to hNF-H cDNA
<i>hNF-H_N_rev</i>	5'-TGGTCCCTTCGGTAAGTCGTCGAC-3' pink, XmnI recognition site; underlined, homologous to hNF-H cDNA
<i>hNF-H_C_fwd</i>	5'-ACCAGGAAGCCATTCAGCAGCTG-3' pink, XmnI recognition site; underlined, homologous to hNF-H cDNA
<i>hNF-H_C_rev</i>	5'-TGTTCCGGCGGTTCCCCTTCAT-3' red, translational stop; underlined, homologous to hNF-H cDNA

2.2.12.2. Agarose gel electrophoresis of DNA

The products of PCR reactions or DNA fragments produced by restriction endonuclease digestion were evaluated by agarose gel electrophoresis. 0.8-1.5 % (w/v) agarose in 1 x TAE buffer (40 mM Tris, 2 mM EDTA, pH 8.5) and containing 0.0002 mg/ml Ethidium Bromide was prepared. DNA samples were mixed with 10 x DNA loading dye (0.025 % (w/v) bromophenol blue, 20 % ficoll, 1 % (w/v) SDS, 0.1 M EDTA, pH 8.0) or 5 x DNA loading dye (Fermentas) and applied to the wells. A DNA ladder (either the 1 kbp or the 100 bp) was also applied. Gels were electrophoresed in 1 x TAE buffer and run at 80 mA.

2.2.12.3. Purification of DNA from agarose gels

The desired band was cut out of the gel by viewing the gel on a UV light box. DNA was purified from the agarose gel using the QIAquick® gel extraction kit (QIAGEN) according to manufacturer's instructions. DNA was eluted by applying 25 µl sterile water to the QIAquick® spin column and incubating for 10 minutes at room temperature before centrifuging at 10,000 x g for 1 minute. Purified DNA was vortex mixed and centrifuge shortly. DNA concentration was determined using the method described in section 2.2.12.6.

2.2.12.4. Cloning of DNA fragments into pCR-2.1 TOPO and pCR-XL TOPO and transformation of *E.coli* competent cells

4 µl of purified DNA was transferred to a sterile 0.5 ml tube to which 1 µl of salt solution (provided with the cloning kit) and 1 µl of the pCR TOPO vector (Clontech, TAKARA) was added. The cloning reaction was incubated for 30 minutes at room temperature and then transferred to ice.

E. coli TOP10 competent bacteria (Invitrogen) were thawed quickly on ice. The cloning reaction was added to cells which were mixed gently by tapping. The cells were incubated on ice for 30 minutes and then subjected to heat shock treatment at 42°C for 30 seconds and placed on ice for 2 minutes. 250 µl of S.O.C. medium was added to the transformed cells which were incubated with shaking at 37°C for 1 hour. The bacteria were spread on pre-warmed LB agar plates containing 50 µg/ml kanamycin. Cells were incubated overnight at 37°C.

2.2.12.5. Purification of plasmid DNA from bacterial cells

2.2.12.5.1. Mini-Prep

To prepare mini-prep plasmid DNA, 2.5 ml LB broth containing 50 µg/ml kanamycin was inoculated with bacterial clones. Inoculated media were incubated overnight at 220 rpm at 37°C. Overnight cultures were poured into sterile 2 ml tubes and centrifuged for 5 minutes at 6,800 x g at room temperature to harvest the bacterial cell pellet. DNA was prepared using the QIAGEN® Plasmid Mini Kit (QIAGEN) as per manufacturer's instructions. To elute plasmid DNA from the QIAprep spin column, 30 to 50 µl of sterile water was applied directly onto the matrix of the column and incubated for 5 minutes at room temperature. The solution of plasmid DNA was collected by centrifugation at 17,900 x g for 1 minute in a fresh sterile 1.5 ml tube. The DNA solution was vortex mixed and centrifuged shortly. DNA concentration was determined using the method described in section 2.2.12.6

2.2.12.5.2. Midi-Prep

To prepare midi-prep plasmid DNA bacterial clones containing the desired plasmid were cultured over-night in 200 ml of LB broth containing 50 µg/ml kanamycin or 100 µg/ml ampicillin depending on the antibiotics resistance genes on the plasmid being purified. Following overnight culture, bacterial cells were harvested by centrifugation at 2500 x g for 15 minutes at 4°C. Plasmid DNA was prepared using the QIAGEN® Plasmid Midi Kit (QIAGEN) according to manufacturer's instructions. DNA pellets were air-dried at room temperature and resuspended in a total of 100 µl water. The average DNA midi-prep produced around 200 µg of plasmid DNA. DNA concentration was determined using the method described in section 2.2.12.6

2.2.12.6. Determination of DNA and RNA concentration

For Mini-Prep DNA preparations, the plasmid DNA solution was diluted 70 fold in 70 µl water. For midi-prep plasmid DNA solutions two dilutions of the plasmid DNA solutions

were prepared (1:100 and 1:200). Absorbance at 260 and 280 nm was measured using a UV spectrometer. DNA concentration was calculated using the equation below:

$$\text{OD}_{260} \times 50 \times \text{dilution factor} = [\text{DNA}; \text{ng}/\mu\text{l}].$$

For RNA preparations, RNA preparations were diluted 25 fold in 75 μl water. Absorbance at 260 and 280 nm was measured using a UV spectrometer. DNA concentration was calculated using the following equation:

$$\text{OD}_{260} \times 40 \times 25 = [\text{RNA}; \text{ng}/\mu\text{l}]$$

2.2.12.7. Restriction endonuclease digestion

2.2.12.7.1. Limited digests

To confirm the insertion of cloned DNA fragments into plasmid vectors, limited digests of Mini-prep DNA using restriction endonuclease were prepared. For limited digests 2.5 units of restriction endonuclease were used per reaction which consists of 2 μl of mini-prep DNA (approximately 0.1 μg) in a total reaction volume of 10 μl according to manufacturers instructions for the restriction endonuclease used. The reactions were then incubated at 37 $^{\circ}\text{C}$ for 1-2 hours and analysed by agarose gel electrophoresis.

2.2.12.7.2. Quantitative digests

To clone the neurofilaments into pEGFP-C3, quantitative digests were performed to cut the neurofilament DNA out of the cloning vector and to clone it into pEGFP-C3. The pEGFP-C3 used in this work contained rNF-M, so to replace the rNF-M with the human neurofilament DNA a quantitative digest of this plasmid was also performed. Typically 3 μg of plasmid DNA was digested with 30 units of restriction endonuclease in a total reaction volume of 100 μl . The reactions were incubated in a thermal cycler at 37 $^{\circ}\text{C}$ for 8-12 hours; enzymes were then deactivated at 65 $^{\circ}\text{C}$ for 20 minutes and held at 10 $^{\circ}\text{C}$.

2.2.12.8. Site-directed mutagenesis

PCR-derived mutations were corrected using the QuikChange® XL Site-Directed Mutagenesis Kit from Stratagene according to manufacturer's instructions. Mutagenic primers (listed in Table 2.6) were designed to be between 25 and 45 bases in length with the correction in the middle of the sequence and have a minimum GC content of 40% and a melting temperature (T_m) of $\geq 78^{\circ}\text{C}$ calculated using the equation for T_m below:

$$T_m = 81.5 + 0.45(\% \text{GC}) - 675/N - \% \text{ mismatch}$$

Where N is the primer length in bases

To insert a base into a sequence the following equation for the calculation of T_m was used:

$$T_m = 81.5 + 0.41(\% \text{GC}) - 675/N$$

Where N does not include the base being inserted

The mutagenesis reaction uses *PfuTurbo*® DNA Polymerase which replicates both plasmid strands with high fidelity and without displacing the mutant oligonucleotide primers. The set of mutagenesis primers bind to the complementary strands of the plasmid and each of these strands is extended during temperature cycling by *PfuTurbo*® DNA Polymerase resulting in a mutated plasmid with staggered nicks. Following temperature cycling the PCR product was treated with the endonuclease *Dpn* I which digests methylated and hemimethylated DNA and is used to digest the parental DNA template. The nicked plasmid DNA was transformed into *E.coli* XL10-Gold ultracompetent cells as per manufacturer's instructions. 500 µl of pre-warmed SOC medium (Invitrogen) was added to the transformed cells and they were incubated for 1 hour at 37°C with shaking at 220 rpm. The transformation reaction was then plated onto LB agar containing 50 µg/ml kanamycin and incubated overnight at 37°C. The following day, colonies were picked and plasmid DNA was purified using the mini-prep procedure described above. The sequences were confirmed to contain the corrections by sequencing.

Table 2.6 List of primers used for the amplification of neurofilament subunits

<i>Name</i>	<i>Sequence</i>
hNF-M_ Lys_Glu-fwd	5'-GAGAAGGTGCACTACCTG CAGCAGCAGAATAAG-3' Purple, base change to correct mutation (T _m 75.3°C)
hNF-M_ Lys_Glu-rev	5'-CTTATTCTGCTGCT CAGGTAGTGCACCTTCTC-3' Purple, base change to correct mutation(T _m 75.3°C)
hNF-L_ Lys_Arg-fwd	5'-GAGTCTGAAGAAGCAAAAC AAGAAGAAGAAGGAGGTG-3' Purple, base change to correct mutation (T _m 74.7°C)
hNF-L_ Lys_Arg-rev	5'-CACCTCCTTCTTCTTCTT CTTTGCTTCTTCAGACTC-3' Purple, base change to correct mutation (T _m 74.7°C)
hNF-H_N_ Phe_Ser-fwd	5'- GCTGGCTCCT CAGCGGCTTCCACT -3' Purple, base change to correct mutation (T _m 79.7°C)
hNF-H_N_ Phe_Ser-rev	5'- AGTGAAGCCGCTG CAGGAGCCAGC -3' Purple, base change to correct mutation (T _m 79.7°C)

2.2.12.9. Bacterial cell culture

2.2.12.9.1. Subculture of bacterial clones

Bacterial colonies were picked from existing LB-agar plates containing either 50 µg/ml kanamycin or 100 µg/ml ampicillin plates onto fresh LB-agar containing either 50 µg/ml kanamycin or 100 µg/ml ampicillin. Plates were incubated overnight at 37 °C.

2.2.12.9.2. Cryopreservation and resuscitation of bacterial cells

To prepare glycerol stocks of bacterial cultures, cultures were picked into a bibby sterilin with 1 ml of LB broth containing 50 µg/ml kanamycin and incubated overnight at 37°C at 220 rpm. An equal volume of glycerol freezing mix was added to the bacterial culture. Glycerol stocks were aliquoted into cryovials and stored at -80°C.

To resuscitate glycerol stocks of bacterial cells, a small amount of bacterial cells were picked from the surface of the tube using a sterile toothpick and cultured overnight in a bibby sterilin with 2 ml of LB broth containing 50 µg/ml kanamycin at 37°C at 220 rpm. To obtain single cultures a loop full of bacteria from the overnight culture was streaked on an LB agar plate containing 50 µg/ml kanamycin. Plates were incubated overnight at 37°C.

2.2.13. Quantitative Real-Time Polymerase Chain Reaction (qRT-PCR)

2.2.13.1. Preparation of standard DNA for qRT-PCR

2.2.13.1.1. Amplification and cloning of standard DNA

Primers (Table 2.8) designed for quantitative real-time PCR were used to amplify the TG2, dynein light intermediate chain, kinesin 5C, NTrkB, PSMC1, α 1-tubulin, GAPDH and Bcl-2 for standard DNA using the AcuPrime™ *Taq* DNA Polymerase System according to manufacturer's instructions (Invitrogen). Typically the total reaction volume was 25 µl; containing 1 µl of template DNA, 0.5 µl AcuPrime™ *Taq* DNA polymerase, 10 µM each of the forward and reverse primers and 2.5 µl 10 x AcuPrime™ PCR Buffer I. The PCR products were analysed by agarose gel electrophoresis using 1.5 % (w/v) agarose gels as described in section 2.2.12.2. The PCR products were excised from the gel and purified as described in section 2.2.12.3.

DNA segments were cloned into pCR-2.1 TOPO (Invitrogen) according to manufacturer's instructions and transformed into *E.coli* TOP10 competent bacteria (Invitrogen) as described in section 2.2.12.4. Six to 10 colonies were picked for sequencing. Plasmid DNA from selected clones was purified using the Qiagen Mini-Prep procedure as described in section 2.2.12.5.1. Plasmid DNA from the selected clones was analysed by restriction enzyme digestion using EcoRI as described in section 2.2.12.7. Clones for sequencing were then selected and 3000ng/20 µl DNA was sent to MWG for sequencing. Plasmid DNA midi-preps from selected clones were prepared as described in section 2.2.12.5.2.

2.2.13.1.2. Preparation of standard solutions

2.2.13.1.2.1. Linearization of plasmid midi-prep DNA

To relax the super-coiled DNA structure of the plasmid enough to allow DNA polymerase to gain access to the molecule, the plasmid midi-preps of standard DNA were linearized by restriction endonuclease digestion. The restriction endonuclease chosen for this task depended on the presence of its recognition sequence in the multiple cloning of the plasmid vector and the absence of this sequence from the DNA insert. Plasmid DNA was linearized using a FastDigest™ system (Fermentas). Briefly in a total volume of 100 µl, 10 µg of

DNA was digested by 10 µl Restriction Endonuclease in the presence of 10 µl 10 x FastDigest™ Buffer for 5 minutes at 37°C. The Restriction endonucleases used for the linearization of standard DNA are listed in Table 2.7.

Table 2.7 The linearization of standard plasmid DNA for each gene to relax the supercoiled DNA structure.

The linearization was accomplished by restriction endonuclease digestion using restriction endonucleases for which the recognition sequence is found in the multiple cloning site of the plasmid vector but is absent from the DNA insert.

<i>Gene</i>	<i>Plasmid</i>	<i>Restriction Endonuclease</i>
<i>NF-H</i>	pEGFP-C3	HindIII
<i>NF-M</i>	pEGFP-C3	KpnI
<i>NF-L</i>	pEGFP-C3	HindIII
<i>α-tubulin</i>	pCR-2.1 TOPO	HindIII
<i>PSMC1</i>	pCR-2.1 TOPO	HindIII
<i>NTrkB</i>	pCR-2.1 TOPO	HindIII
<i>Bcl-2</i>	pCR-2.1 TOPO	HindIII
<i>TG2</i>	pCR-2.1 TOPO	HindIII
<i>Dynein Light Intermediate Chain</i>	pCR-2.1 TOPO	HindIII
<i>KIF5C</i>	pCR-2.1 TOPO	HindIII
<i>GAPDH</i>	pC-2.1 TOPO	HindIII

95 µl of the linearized plasmid DNA was transferred to a fresh 1.5 ml tube for purification using the QIAquick PCR Purification Kit (QIAGEN). The remaining 5 µl of linearized plasmid DNA was run on an agarose gel to check that the DNA was linearized.

2.2.13.1.2.2. Purification of linearized plasmid DNA

Linearized plasmid DNA was purified using the QIAquick® PCR Purification Kit from QIAGEN according to manufacturer's instructions. DNA was eluted from the QIAprep column with 30 µl of water. The DNA concentration of the purified linearized plasmid DNA was measured using a nanodrop UV spectrometer and was between 100-300 ng/µl.

2.2.13.1.2.3. Preparation of standard DNA solutions for qRT-PCR

The number of double-stranded DNA molecules/µl in the original solution (purified linearized plasmid DNA prepared in section 2.2.13.1.2.2) was calculated using equation 1.

$$\frac{c(\text{DNA}[\text{ng}/\mu\text{l}]) / 1 \times 10^9}{\text{vector length} [\text{bp}] \times 660} \times 6.022 \times 10^{23} = \text{dsDNA molecules}/\mu\text{l} \dots \dots (1)$$

The volume of the original solution required to prepare 100 μl of standard solution 1 (SL1) in RT Buffer (10 mM Tris, pH 8, 15 mM KCl, 0.6 mM $\text{MgCl}_2 \cdot 6\text{H}_2\text{O}$) containing 1×10^{10} single-stranded DNA molecules was calculated using equation 2.

$$\frac{\left(\frac{100 \mu\text{l} \times 1 \times 10^{10} \text{ dsDNA molecules}/\mu\text{l}}{c(\text{dsDNA molecules}/\mu\text{l in original solution})} \right)}{2} = \mu\text{l original solution required} \dots (2)$$

Standard solution 2 (SL2) containing 1×10^8 ssDNA molecules/ μl was prepared by diluting 10 μl of SL1 in 990 μl RT Buffer. Standard solution 3 (SL3) containing 1×10^7 ssDNA molecules was prepared by making a ten-fold dilution of SL2.

2.2.13.2. Preparation of sample cDNA preparations

2.2.13.2.1. RNA preparation

To ensure that all surfaces and equipment used during the RNA extraction procedure were ribonuclease-free, all surfaces and equipment were cleaned with water, RNaseZap spray and 70 % (v/v) ethanol. Cells were seeded at a density of 500 000 cells per flask in T25 flasks and either maintained as proliferating cells or differentiated with RA or RA/BDNF as described in section 2.2.1.5. Toxin treated cells (MPP+ and/or epoxomicin) were predifferentiated with RA/BDNF before being treated.

Cells were detached by trypsinization and cell pellets were harvested as described in section 2.2.1.2. For the differentiation experiments, spent media was discarded and only attached cells were harvested. For experiments involving toxin treatment, spent media also was collected. Cell pellets were washed with DPBS and transferred to 1.5 ml tubes and collected by centrifugation at $300 \times g$ for 5 min. The supernatant was discarded and cell pellets were resuspended in freshly prepared RLT buffer (300 μl RLT + 3 μl β -mercaptoethanol) and applied to Qia-Shredder columns and centrifuged for 2 minutes at $10000 \times g$ for efficient cell lysis. The columns were discarded and RNA in the flow-through was precipitated by adding 300 μl of 70 % (v/v) ethanol. After mixing by pipetting, the flow-through/ethanol mix was applied to the RNeasy columns and centrifuged at $10000 \times g$ for 15 sec allowing the RNA to bind to the matrix of the RNeasy column. Contaminating proteins were washed off by adding 700 μl RW1 wash buffer and centrifuging at $10000 \times g$ for 15 sec. Salts and other contaminants were washed off by washing columns twice with 500 μl RPE wash buffer and centrifuging at $10000 \times g$ for 15 sec between each wash. To dry the matrix and remove all traces of ethanol columns were centrifuged again at $10000 \times g$ for 2 min.

Columns were then transferred to fresh tubes and 30 μ l of water was added to each column and incubated for a further 5 min. To collect RNA, columns were then centrifuged for 2 min at 10000 x g. RNA concentration was determined as described in section 2.2.12.6.

2.2.13.2.2. Reverse transcription PCR

All the different temperature steps in this reaction were performed in a thermal cycler. 1-3 μ g RNA was diluted to a maximum volume of 10 μ l with sterile deionized water. Two master mix solutions were prepared: Master Mix 1 contained 1 μ l oligodT₁₈ and 1 μ l dNTPs per reaction; Master Mix 2 contained 4 μ l 5 x first-strand buffer, 2 μ l 0.1 M DTT and 1 μ l water per reaction. Master Mix 1 was added to the RNA dilution and incubated at 65 °C for 5 min. The reaction was then transferred immediately to ice and Master Mix 2 was added, followed by incubation at 42 °C for 2 min. After which 1 μ l of SuperScript II reverse transcriptase (Invitrogen) was added to each reactions and reactions were incubated at 42 °C for 70 minutes, followed by 70 °C for 15 min and reactions were then held at 4 °C until storage at -20 °C.

2.2.13.3. Quantitative Real-Time PCR

Quantitative Real-Time PCR (qRT-PCR) reactions for each gene were run with a set of standards in which the numbers of DNA molecules are known. Standards used were; SL3 (10^7) \rightarrow 10^6 \rightarrow 10^5 \rightarrow 10^4 \rightarrow 10^3 \rightarrow 10^2 \rightarrow 10 \rightarrow 1 molecules/ μ l. Briefly, seven 1.5 ml tubes for the standard curve, one for the PCR master mix (MM) and one tube for the primer dilution were placed into a rack. 90 μ l of RT Buffer (10 mM Tris, pH 8, 15 mM KCl, 0.6 mM MgCl₂·6H₂O) was pipetted into the seven tubes for the standard curve. 90 μ l of water was added to the tube for the primer dilution and the required amount of water (depending on the number of reactions) was added to the tube for the PCR master mix. The primer mix containing 5 μ M of each primer (forward and reverse) was prepared by adding 5 μ l of each primer (100 μ M stock) to the 90 μ l of water in the primer mix tube. According to the suggested protocol for the SensiMixTMPlus SYBR Kit each 10 μ l reaction requires 5 μ l of SensiMixTMPlus SYBR, 0.4 μ l 5 μ M forward primer (200nM), 0.4 μ l 5 μ M reverse primer (200nM), 1 μ l DNA template and water to 10 μ l. A PCR master mix containing all the components except the template DNA (namely the 5 μ l SensiMixTMPlus SYBR, 0.4 μ l primer mix and 3.5 μ l water per reaction) was prepared. Standards were prepared by serial dilution; each dilution was mixed thoroughly by pipetting up and down 20 times. 9 μ l of the PCR master mix was pipetted into the PCR tubes for the rotorgene added 1 μ l of template DNA.

The reaction profile was as follows:

Enzyme Activation Step 95°C 10 minutes

45 cycles — { 95°C 15 sec not acquiring
 65°C 30 sec not acquiring
 72°C 30 sec acquiring on SYBR

Melting curve 60-99°C ramp up, rising by 0.5°C for each step

Wait 60 sec on 1st step, then 5 sec for each step afterwards

Acquired melt on SYBR

Data was analysed with the Rotor-gene 6000 series software. When samples and standards were selected an automatic threshold was calculated. The cycle number at which a reaction reaches the threshold is called the C_t value. The C_t values of the standards were used to produce a standard calibration curve from which the RNA copy number in the samples could be determined.

Table 2.8 Primers used to target sequences for amplification by Quantitative real-time PCR, melting temperature (T_m) was calculated using the formula: $T_m = 2(A+T) + 4(G + C)$

<i>Gene</i>	<i>Primers</i>	<i>T_m, °C</i>	<i>Size of amplified sequence</i>
<i>NF-H</i>	fwd: 5'-TCCTACCAGGAAGCCATTTCAG-3' rev: 5'-CCTTCTGGAAGCGAGAAAGGAA-3'	66 °C 66 °C	201 bp
<i>NF-M</i>	fwd: 5'-CAGCTACCAGGACACCATCCA-3' rev: 5'-GGAGCTTCCACCTTGGGTTTC-3'	66 °C 66 °C	265 bp
<i>NF-L</i>	fwd: 5'-GCAGCTTACAGGAAACTCTTGG-3' rev: 5'-GTTTCCTCCACTTCGATCTGCT-3'	66 °C 66 °C	214 bp
<i>α-tubulin 1b</i>	fwd: 5'-CTAATCCCTAGCCACTATGCGT-3' rev: 5'-GCGAACTTCATCAATGACTGTGG-3'	66 °C 66 °C	263 bp
<i>PSMC1</i>	fwd: 5'-TTGAGAGTGGTTGGCTCTGAAC-3' rev: 5'-TCAATGCGGCCTGGTCTGATAA-3'	66 °C 66 °C	306 bp
<i>NTrkB</i>	fwd: 5'-TGGCAGTGAAGACCCTGAAGG-3' rev: 5'-TTGCCCTCAGCCATCAGCAC-3'	66 °C	223 bp
<i>Bcl-2</i>	fwd: 5'-TAACGGAGGCTGGGATGCCTT-3' rev: 5'-AGCCTGCAGCTTTGTTTCATGG-3'	66 °C 66 °C	248 bp
<i>TG2</i>	fwd: 5'-GTCGTGACCAACTACAAC-3' rev: 5'-AGCAGTACGTCCCTTCGCTCT-3'	66 °C 66 °C	223 bp
<i>Dynein Light Intermediate Chain</i>	fwd: 5'-CGGTACCTCTGGTCATAATTGG-3' rev: 5'-AGGAGGAGATCCTATTTGACCG-3'	66 °C 66 °C	281 bp
<i>KIF5C</i>	fwd: 5'-GAGCAGCTCACCAAAGTTCACA-3' rev: 5'-CTTGGCGATCTGGGCTGAATG-3'	66 °C 66 °C	253 bp
<i>GAPDH</i>	fwd: 5'-CCATCACCATCTTCCAGGAGCGA-3' rev: 5'-GGATGACCTTGCCACAGCCTTG-3'	66 °C 66 °C	447 bp

2.2.14. Statistical analysis

Statistical analyses were performed using minitab15 and GraphPad Prism5. A variety of statistical tests for significance were used depending on the application. Tests used include the one- and two-tailed T-Tests and one-way and two-way ANOVA with Bonferroni's post-hoc tests.

CHAPTER 3

***DEGRADATIVE PATHWAYS INVOLVED IN
NEUROFILAMENT TURNOVER***

3.1. Introduction

3.1.1. Neurofilament degradation

3.1.1.1. Background

The major protein degradative pathways in the cell are the ubiquitin proteasome system, the autophagy-lysosome system (which includes the cathepsins) and the calpain system. A role for calpain in NF degradation has been extensively documented. All three NF subunits have been shown to be degraded by both μ - and m-calpain in *in vitro* experiments (Heijink et al, 2000, Kamakura et al, 1985, Shields et al, 1997), with NF-M being the most susceptible, followed by NF-L and NF-H respectively. Additionally *in vitro* experiments revealed that NFs were also degraded by cathepsin B but the order of susceptibility to degradation was altered to NF-M > NF-H > NF-L (Kamakura et al 1985). The cleavage of NF-L in protein homogenates from rat optic nerves incubated with calcium was inhibited by E-64 (Shields et al 1997), a cysteine protease inhibitor which in the past was frequently used to inhibit calpain (Iwasaki et al, 1987). However E-64 is a general cysteine protease inhibitor that also inhibits cathepsins B, H and L and is therefore not a specific calpain inhibitor (Barrett et al, 1982, Gour-Salin et al, 1994, reviewed by Rubinsztein et al, 2009).

Calpain has also been implicated in neurofilament degradation following cellular stress. NF degradation during anoxia and reoxygenation of transected rat optic nerves was abolished following calcium removal and reduced in the presence of two different calpain inhibitors (Stys & Jiang, 2002). In an animal model of spinal cord injury, NF degradation was prevented by leupeptin and E-64 suggesting a role for calcium activated neutral proteases in spinal cord injury (Iwasaki et al, 1987). In zymosan-induced model of inflammation calpain activation and the breakdown of NF-L was prevented by the calpain inhibitor MDL28170, suggesting that calpain is involved in NF-L degradation (Kunz et al, 2004). Further support of the role of calpain in neurofilament degradation comes from the similarity of the breakdown products in rat transected nerves with the products resulting from an experimental model of calpain-induced proteolysis by Western blotting (Schlaepfer et al, 1985).

Fasani et al (2004) investigated the role of trypsin and α -chymotrypsin in neurofilament degradation because in their hands the proteolysis of isolated neurofilaments by calpain and other cysteine activated proteases was very low. They found that trypsin and α -chymotrypsin could degrade all three neurofilament subunits but that NF-M exhibited the most resistance to proteolysis.

Another candidate protease for neurofilament turnover is the lysosomal enzyme cathepsin D. Its role in neurofilament degradation has previously been investigated using an *in vitro* approach in which neurofilament proteins prepared from post-mortem human brain were incubated with cathepsin D (also purified from post-mortem human brain). All three neurofilament subunits were degraded by cathepsin D but the higher molecular weight subunits exhibited a greater degree of proteolysis than NF-L (Nixon & Marotta, 1984). A role for cathepsin D was also suggested by Suzuki et al (1988) who showed that purified bovine brain cathepsin D degraded neurofilaments in a crude neurofilament fraction from bovine brain.

3.1.1.2. Determination of half-life of proteins

Pulse chase analysis, which involves the pre-incubation of cells with radiolabelled amino acid precursors such as ^{35}S -labelled methionine or cysteine to label proteins, is among the most widely used methods to determine protein half-lives because of the minimum impact this method has on cellular metabolism. During the chase period an excess of non-radiolabelled precursor molecules is added to prevent cells from incorporating any more radiolabel into proteins. During the chase period cell extracts are prepared at a number of time-points and the protein of interest is isolated by immunoprecipitation and the eluate is then analysed by SDS-PAGE (Zhou, 2004).

Pulse chase analysis is technically demanding and requires immunoprecipitation of the target protein out of the mix of radio-labelled proteins. Immunoprecipitation is best suited to work with soluble proteins and may not be appropriate for the isolation of neurofilaments (which are mainly insoluble) for half-life determination experiments. To avoid immunoprecipitation, the radio-labelled target protein could be added directly to cells but this requires microinjection which is itself technically demanding. Due to health and safety concerns there is also a move to move away from techniques requiring radioactive labelling when an alternative technique is available.

Another method often used to determine protein half-life is the interruption of new protein synthesis by compounds such as cycloheximide (CHX), combined with inhibition of different proteolytic pathways. Cycloheximide (CHX) is an antibiotic produced by *Streptomyces griseus* which inhibits protein synthesis in eukaryotes, by interrupting peptide chain elongation (Baliga et al, 1969) via binding to the 60S ribosomal subunit of the 80S

ribosome (Figure 3.1, Stocklein & Piepersberg, 1980). CHX has been used in SH-SY5Y cells over-expressing α -synuclein to assess the effect of proteasome inhibition on the levels of α -synuclein (Tofaris et al, 2001). Ren et al (2003) used puromycin (another protein synthesis inhibitor) to investigate the role of the proteasome in the degradation of α -tubulin in HEK293 cells.

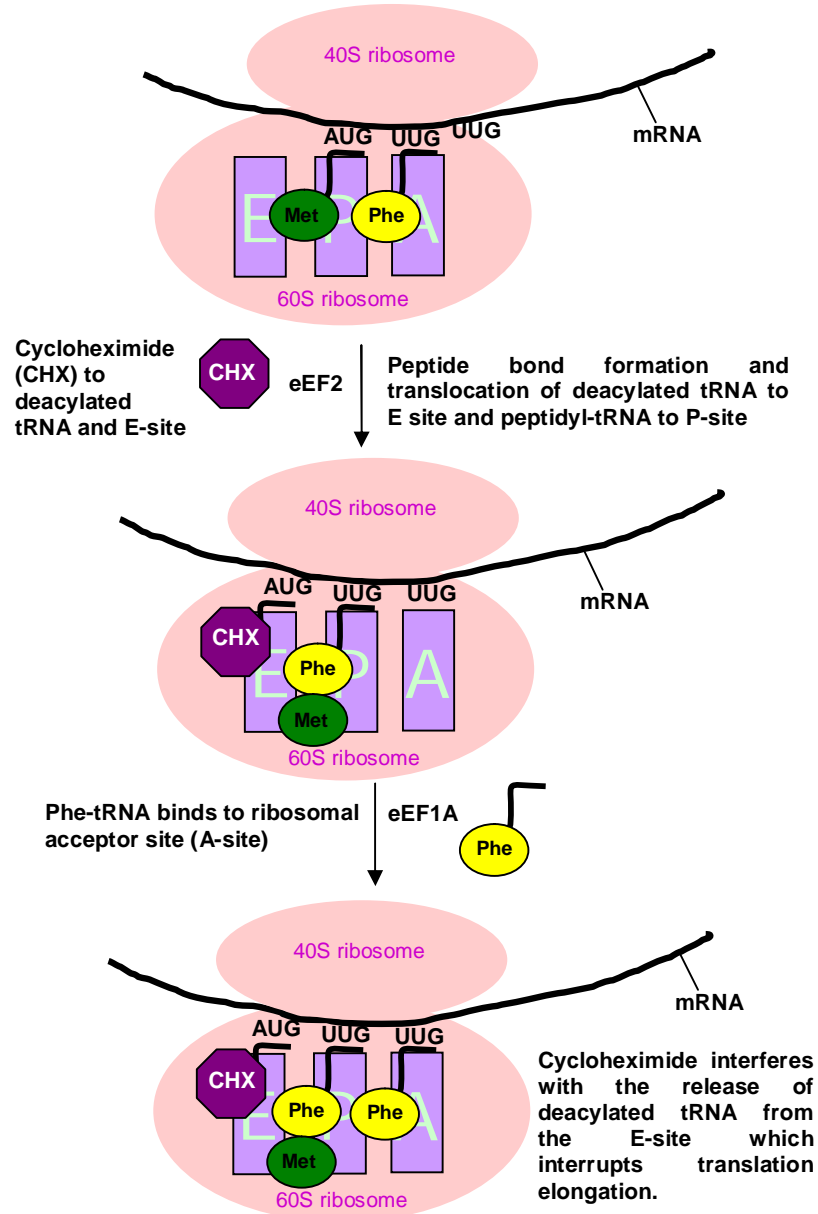


Figure 3.1 Schematic diagram illustrating the inhibition of translational elongation by cycloheximide (CHX).

During translational elongation eEF2 facilitates the translocation of deacylated-tRNA from the P-site on the 60S ribosome to the E-site after peptide bond formation and the translocation of the peptidyl-tRNA from the A-site to the P-site. The A-site is now free to accept the next aminoacyl-tRNA, the binding of which requires the action of eEF1A. Cycloheximide binds to the E-site on the 60S ribosomal subunit. The binding of cycloheximide interferes with the release of the deacylated-tRNA which stalls the ribosome and blocks translational elongation. The ability of Cycloheximide to bind to the E-site even when occupied by deacylated tRNA allows cycloheximide to interrupt translational elongation at any time (Schneider-Poetsch et al, 2010).

A comparison of different approaches to the determination of cytoskeletal protein half-life can be found in Table 3.1. Neurofilament turnover in mice using pulse-chase analysis has been reported to be biphasic, with a fast turnover rate and a slow turnover rate. The different turnover rates have been attributed to two different NF populations, the fast rate belonging to the more motile element while the slow turnover rate belonged to the more stationary element, which was most likely incorporated into the axonal cytoskeleton (Nixon & Logvinenko, 1986). The biphasic turnover of cytoskeletal proteins has also been reported by Safaei and Fischer (1990) in rats in which slower turnover rates were observed in the Triton X-100 insoluble fractions. Neither of these studies employed immunoprecipitation techniques to isolate NFs and other cytoskeletal proteins from the protein fractions analysed. Instead they used Coomassie blue staining of SDS-polyacrylamide gels (SDS-PAG) and immunoblotting to identify the bands corresponding to the NF subunits and the other cytoskeletal proteins investigated.

Table 3.1 Summary of half-life data of cytoskeletal proteins determined *in vivo* from animal models or *in vitro* using cultured cells.

<i>Cytoskeletal Element</i>	<i>in vivo or in vitro</i>	<i>Method</i>	<i>T(1/2)</i>	<i>Reference</i>
<i>NF-H, NF-L and NF-M</i>	<i>in vivo</i> , mice	Pulse-chase [³ H]-proline injected intracranially	20 d and 55 d	Nixon and Logvinenko (1986)
<i>NF-H, NF-L and NF-M</i>	<i>in vivo</i> , rats	Pulse-chase [³⁵ S]-methionine injected intracranially	18 d	Safaei and Fischer (1990)
<i>NF-L</i>	<i>in vivo</i> , mouse	Inducible expression of hNF-L. Turned off the expression of hNF-L then analysed samples by Immunoblotting	21 d	Millecamps et al (2007)
<i>α-tubulin</i>	<i>in vivo</i> , rats	Pulse-chase [³⁵ S]-methionine injected intracranially	4.8 d and 15 d	Safaei and Fischer (1990)
<i>α-tubulin</i>	<i>in vitro</i> , HEK293 cells	Inhibition of protein synthesis by puramycin. Monitored NF by immunoblotting	22.5 h	Ren et al (2003)

In the transgenic mouse model (mNF-L^{-/-}) with inducible human NF-L expression, NF-L expression was controlled using a Tet-off tetracycline-regulated system. Half-life was determined by switching-off hNF-L expression with doxycycline treatment and cerebellum extracts from animals treated over an 8 week time-course were analysed by SDS-PAGE and Western blotting with an anti-NF-L antibody (Millecamps et al, 2007).

There is a difference in the estimation of half-lives of proteins in cultured cells compared to half-life estimates in animal models. An example of this is the estimate of half-life of α -tubulin: in rats it was in the order of 5-15 days (Safaei and Fisher 1990) whereas in HEK293 cells, half-life was estimated at 22.5 h (Ren et al 2003). Therefore, estimates of half-life for neurofilament proteins in proliferating SH-SY5Y neuroblastoma cells can be expected to be considerably less than 18-22 days.

3.1.2. Degradative pathways involved in cytoskeletal protein turnover

All three degradative pathways (UPS, the autophagy-lysosome systems and the calpain system) have been suggested to play a role in the turnover of cytoskeletal proteins (Kamakura et al, 1985, Nixon & Marotta, 1984, Ren et al, 2003, Stys & Jiang, 2002, Suzuki et al, 1988). The following section will consider the use of specific inhibitors in an analysis of the roles of various proteases in protein degradation, together with a limited review of different approaches used to monitor protease activities.

3.1.2.1. The Ubiquitin Proteasome System

The discovery and development of proteasome inhibitors has enabled researchers to investigate the role of this multi-enzyme complex, containing trypsin-like, chymotrypsin-like and caspase-like activities, in many cellular processes. There are a number proteasome inhibitors available that differ in their specificity to the proteasome among the most frequently used are MG132, lactacystin and epoxomicin (reviewed in Groll & Huber, 2004). Epoxomicin is the most specific proteasome inhibitor available at this time which even at concentrations as high as 50 μ M does not inhibit papain, chymotrypsin, trypsin, cathepsin B or calpain (Sin et al, 1999).

Epoxomicin was originally identified for its anti-tumour and anti-inflammatory properties which were discovered to be due to its ability to irreversibly inhibit the chymotrypsin-like, trypsin-like and caspase-like activities of the 20S proteasome by binding to the 20S catalytic subunits LMP2, LMP7, Z and MECL1 (Sin et al 1999). The unique specificity of Epoxomicin for the proteasome was explained when the crystal structure of the epoxomicin:20S proteasome complex was revealed. The binding of epoxomicin to the 20S proteasome results in the formation of a morpholino ring (6-atom ring) between the nucleophilic amino terminal threonine (Thr1) of the β 5 (chymotrypsin-like activity) subunit

and the pharmacophore of Epoxomicin (Figure 3.2). A requirement for the formation of the morpholino ring is the presence of a nucleophilic amino terminal residue which is absent in most other proteases with the exception of other members of the Ntn (N-terminal nucleophile) family of hydrolases (Groll et al, 2000, reviewed in Groll & Huber, 2004). Epoxomicin most potently inhibits chymotrypsin-like activity, followed by trypsin-like activity and caspase-like activity (Kim et al, 1999). Proteasomes belong to the family of Ntn hydrolases since it is the hydroxyl group on the amino-terminal threonine which acts as a catalytic nucleophile which hydrolyses peptide bonds (Kisselev et al, 2000).

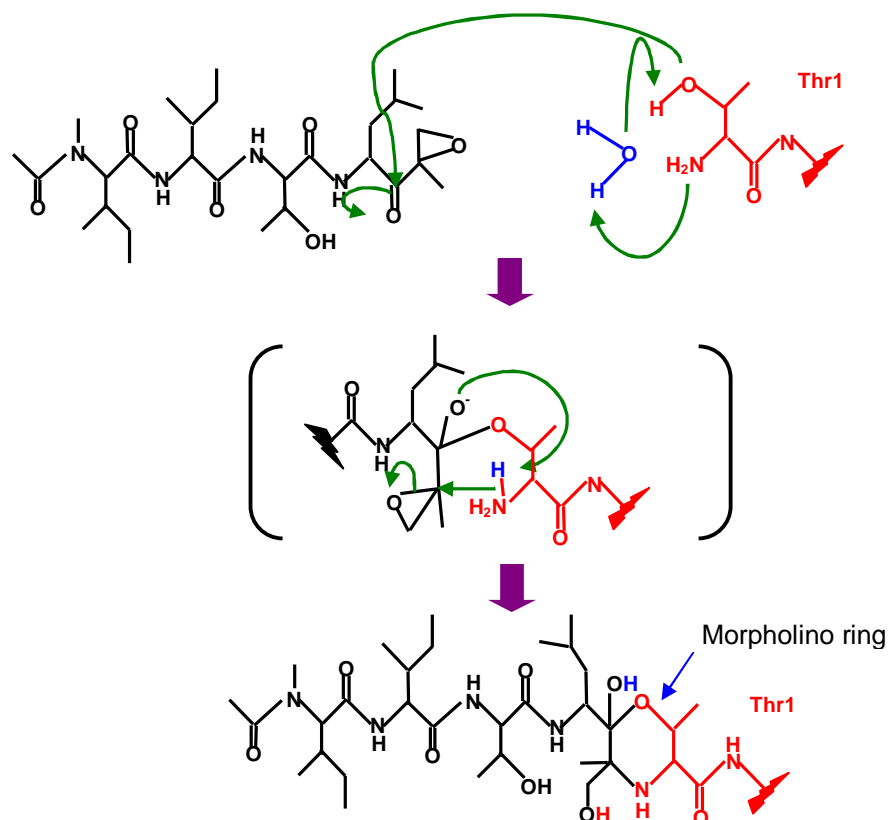


Figure 3.2 A scheme describing the possible mechanism for the formation of the morpholino ring structure between the pharmacophore of Epoxomicin and the amino terminal threonine residue of the $\beta 5$ subunit of the 20S proteasome (adapted from Groll et al, 2000).

3.1.2.1. Calpain

E-64 and leupeptin have frequently been used in the past as inhibitors for calpain; however these inhibitors are not specific for calpain since they also inhibit other cysteine proteases such as papain and cathepsin B. Another limitation to their use is that they are not membrane permeable making them unsuitable for the inhibition of calpain in situations where cell penetration is required. MDL28170 is a cell permeable calpain inhibitor which also inhibits cathepsin B and α -chymotrypsin to a small degree (reviewed by Mehdi, 1991),

and is now more frequently used. The most specific inhibitor for calpain is the endogenous calpain inhibitor calpastatin which is thought to play a role in the regulation of calpain activity *in vivo*. Interestingly the binding of calpastatin to calpain requires calcium but at a lower concentration than that required for calpain activation (reviewed by Goll et al, 2003).

Synthetic peptides used to assay calpain activity are usually poorly soluble in aqueous solutions and need to be used at concentrations of 1-2 mM but calpain activity is not optimal under these conditions. Calpain cleaves proteins at a limited number of sites specified by the structural conformation of the polypeptide chain rather than amino acid sequence, resulting in large proteolytic fragments. Another difficulty is that calpain rapidly loses proteolytic activity when assayed at temperatures above 25 °C (Goll et al 2003). Numerous proteins have been identified that can be cleaved by calpain, including α -tropomyosin, EGF receptor kinase, p35, desmin, MAP1, MAP2, tubulin, vimentin, neurofilament proteins, tau, myosin and α II-spectrin among others (Goll et al 2003).

A frequently used assay to monitor calpain activity involves the detection of calpain specific cleavage products of the cytoskeletal protein α II-spectrin. Cleavage of α II-spectrin by calpain results in 150 kD and 145 kD spectrin breakdown products (SBDPs) which can be detected by immunoprobining Western blots with an anti- α -spectrin antibody. α II-spectrin can also be cleaved by the caspase 3, a cysteinyl protease usually activated in apoptosis as part of the cell death cascade (reviewed in Wang, 2000), but cleavage by caspase 3 results in 150 kD and 120 kD SBDPs (Alvira et al, 2008, Chen et al, 2006, Dutta et al, 2002, Lewis et al, 2007, Nath et al, 1996, Tamada et al, 2005, Veeranna et al, 2004, Wang et al, 1996). Therefore it is possible by SDS-PAGE and Western blotting to distinguish between calpain and caspase 3 specific cleavage of α II-spectrin by monitoring the levels of the 145 kD and 120 kD SBDPs relative to full-length α II-spectrin (reviewed by Wang, 2000).

3.1.2.2. Autophagy-Lysosome Pathway

3.1.2.3.1. Macroautophagy

There are several compounds available that can either inhibit or activate macroautophagy. Rapamycin activates autophagy by inhibiting mTOR (mammalian target of rapamycin), a natural inhibitor of macroautophagy (Cuervo et al, 2004, reviewed by Martinez-Vicente & Cuervo, 2007). A widely used inhibitor of macroautophagy is Bafilomycin A1 (an antibiotic isolated from *Streptomyces*) which inhibits vacuolar-type H⁺ ATPase by binding to its membrane spanning pore domain (reviewed by Yamamoto et al, 1998, Yoshimori et al,

1991). Vacuolar H⁺ ATPase is found in organelles of the central vacuolar system such as lysosomes and endosomes where it plays an important role in maintaining the acidic environment of these compartments. To facilitate the fusion of autophagosomes and lysosomes, vacuolar H⁺ ATPase acidifies the luminal space of autophagosomes or lysosomes. So by inhibiting vacuolar ATPase, Bafilomycin A1 inhibits the fusion of autophagosome and lysosome (reviewed by Yamamoto et al, 1998). Another inhibitor of autophagy is 3-methyl adenine (3-MA) which inhibits autophagy by inhibiting autophagic vesicle formation (Seglen & Gordon, 1982).

Several methods can be used to monitor the number of autophagosomes in cells as a result of a treatment with a compound of interest and include electron microscopy, fluorescence microscopy using GFP-LC3 or anti-LC3 or monitoring LC3-II levels on immunoprobed Western blots. Electron microscopy is a widely used method to monitor macroautophagy but is prone to misinterpretation and requires expert analysis. The quantification of autophagy by counting GFP-LC3 or anti-LC3 puncta needs to be on a per cell basis, which may be difficult especially when dealing with a large number of cells. Whichever method is used, it is essential to remember that the accumulation of autophagosomes may be due to either increased autophagosome synthesis or reduced macroautophagy in which the fusion of autophagosomes with lysosomes is reduced or lysosomal proteolysis is affected (reviewed by Klionsky et al, 2008).

As shown in Figure 3.2, LC3-II is found on the luminal and cytosolic surfaces of the autophagosome. When the autophagosome fuses with the lysosome, the luminal pool of LC3-II is degraded by lysosomal proteases and the cytosolic pool of LC3-II is cleaved by Atg4B and recycled (reviewed by Ichimura et al, 2008, and Rubinsztein et al, 2007).

In higher eukaryotes, the levels of LC3-II (when using a loading control such as actin rather than LC3-I levels) are said to be a measure of the number of autophagic vesicles in a cell at a particular time. Since increased levels of LC3-II can result from increased autophagic vesicle synthesis or a reduction in autophagy, it is essential when trying to determine the effect of a treatment on autophagy to also look at LC3-II levels in the presence of inhibitors of autophagy. Since lysosomal protease inhibitors are not very specific, Bafilomycin A1 is often used in such instances (reviewed by Rubinsztein et al, 2009).

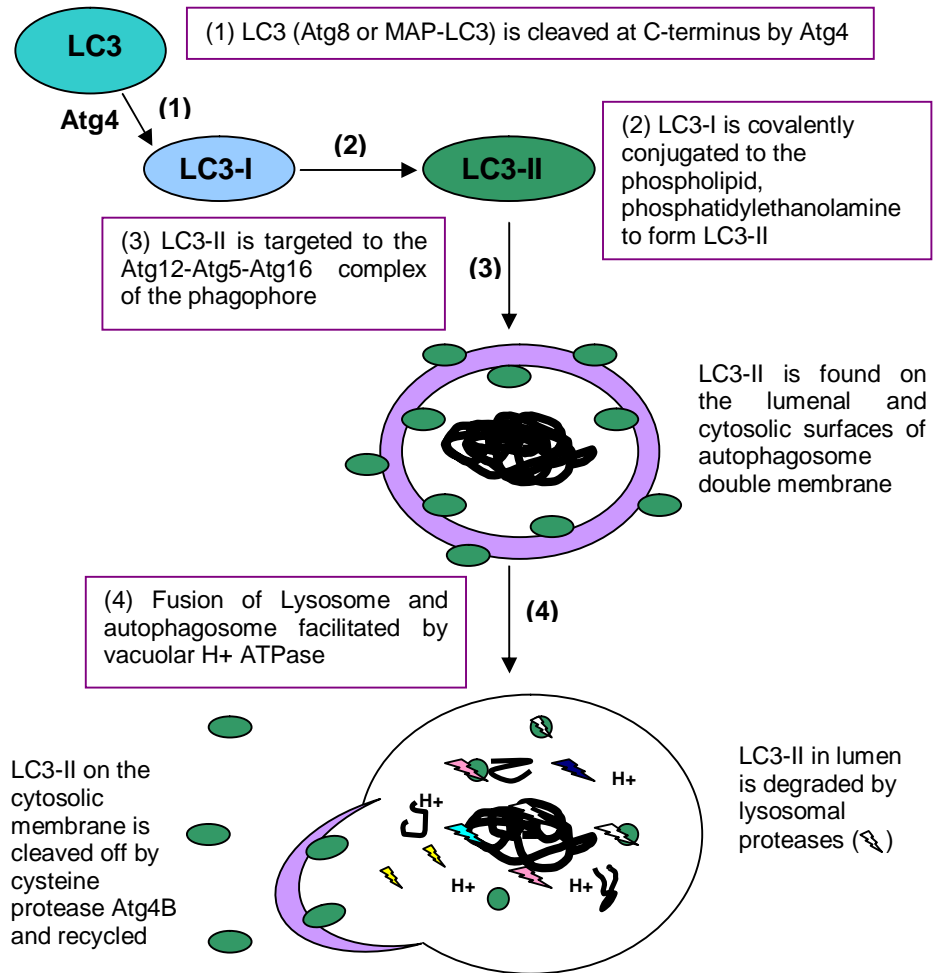
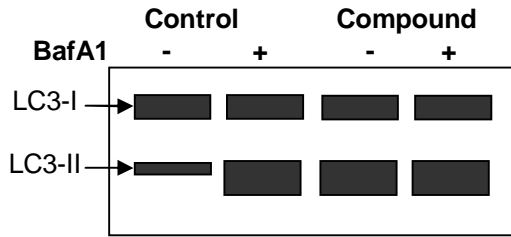


Figure 3.2 A diagrammatic representation of the role of LC3-II in autophagic vesicle formation.

The levels of LC3-II can be used as a reporter to monitor the number of autophagosomes at a particular time. The microtubule associated protein 1 light chain 3 (MAP-LC3/Atg8/LC3) is cleaved at its C-terminus to form LC3-I which becomes covalently conjugated to phosphatidylethanolamine to form LC3-II. LC3-II is targeted to the Atg12-Atg5-Atg16 complex of the phagophore and remains associated with the expanding membrane of the autophagosome as it matures. LC3-II can be found on the luminal and cytosolic surfaces of the autophagic membrane. When the lysosome and autophagosome fuse the luminal population of LC3-II is degraded by lysosomal proteases while the cytosolic population is recycled. An inhibitor of macroautophagy, Bafilomycin A1 inhibits the fusion of autophagosome and lysosome (adapted from Rubinsztein et al, 2009).

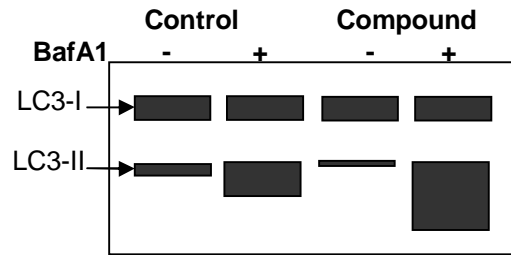
According to Rubinsztein et al (2009), LC3-II levels in Bafilomycin treated cells expressed as a ratio of the levels in untreated cells gives an indication of the effect of a particular compound on autophagy. In their review of the use of LC3-II levels to measure autophagy, they describe three different scenarios in which treatments with compounds affect LC3-II levels either by increasing/decreasing autophagosome degradation or by increasing autophagosome synthesis. The three scenarios are represented in the cartoon in Figure 3.3.

Scenario 1



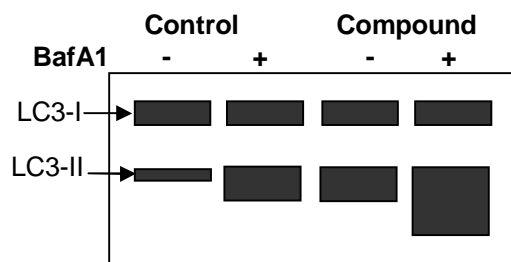
BafA1 increases LC3-II levels 3-fold
 Compound of interest increases LC3-II levels 3-fold
 Treatment with BafA1 + compound of interest increased LC3-II levels 3-fold
 → Compound results in a decrease in autophagosome formation.

Scenario 2



BafA1 increases LC3-II levels 3-fold
 Compound of interest decreases LC3-II levels 2-fold
 Treatment with BafA1 and compound of interest increases LC3-II levels 6-fold
 → Compound results in increased autophagosome degradation and synthesis

Scenario 3



BafA1 increases LC3-II levels 3-fold
 Compound of interest increases LC3-II levels 3-fold
 Treatment with BafA1 and compound of interest increases LC3-II levels 6-fold
 → Compound results in increased autophagosome synthesis

Figure 3.3 A cartoon illustrating three theoretical scenarios in which a compound of interest may result in a change in the levels of LC3-II.

To discern the effect of the compound on autophagy, samples are either untreated, treated with Bafilomycin A1 (BafA1), treated with the compound or treated with the compound and Bafilomycin A1. The levels of LC3-II (corrected for protein loading with actin, tubulin, etc) are compared to the levels of LC3-II in untreated samples (Rubinsztein et al, 2009).

3.1.2.3.2. Lysosomal Proteases

The most abundant lysosomal proteases are the cathepsins which include the aspartyl cathepsins (D and E), the cysteine cathepsins (B, C, F, H, K, L, O, S, V, W, X) and the serine cathepsin G (reviewed by Pillay et al, 2002). Surprisingly, some cysteine cathepsin splice variants are apparently found outside the lysosome in other cellular compartments or extracellularly (reviewed by Vasiljeva & Turk, 2008). Pepstatin A is a potent inhibitor of the aspartyl cathepsins, D and E as well as pepsin and rennin but has no effect on the activity of neutral and alkaline proteases (Marciniszyn et al, 1976). Cathepsin inhibitor II

(Z-FG-NHO-BzMe) is a serine and cysteine protease inhibitor that inhibits the cysteine cathepsins B, L, S and papain (Demuth et al, 1996).

3.1.2. Aims

Despite the large volume of literature available on neurofilaments not much is known about the degradative pathways involved in their turnover in unstressed conditions. Cellular stress can lead to the activation of degradative pathways and the subsequent degradation of proteins (Iwasaki et al, 1987, Kunz et al, 2004, Schlaepfer et al, 1985, Stys & Jiang, 2002) which may or may not normally be degraded by these proteases when cells are not stressed. Exposure to some compounds may even lead to the inhibition of the activity of a particular pathway (Caneda-Ferron et al, 2008, Zeng et al, 2006), which will prevent the degradation of its particular protein substrates. This chapter aims to provide further insight to the degradative pathways involved in neurofilament turnover in Human SH-SY5Y neuroblastoma cells in unstressed conditions. The second aim of this chapter is to investigate the effect of mitochondrial dysfunction (as a consequence of MPP⁺ treatment) and dopamine induced oxidative stress on the modulation of degradative pathways in general and on neurofilament turnover in particular.

3.2. Results

3.2.1. Optimal cycloheximide concentration of assessment for the determination of cytoskeletal protein half-life

To estimate the half-lives of various cytoskeletal proteins, including NFs, in proliferating SH-SY5Y cells, cells were treated with cycloheximide (CHX) over a period of 72 hours. The concentration of CHX that gave the most consistent estimates of half-life was determined by comparing a range of CHX concentrations.

The levels of NFs, α -tubulin and vimentin were monitored by probing Western blots of total cell extracts harvested every 24 hours over the 72 hour time-course, and time points compared by densitometric analysis. The arbitrary densitometry units (ADU) or signal at each time-point was expressed as a percentage of the signal or ADU at 0 hours. The natural logarithm of the percentage of the original signal [$\text{Ln}(\% \text{ original signal})$] was plotted against time. Half-lives were calculated from the gradient (k or decay rate constant) of the 'line of best fit' obtained from these plots.

The equation (equation 2) used to calculate half-life which was derived from equation 1 as illustrated below:

		C_t = level at time t
		C_o = original level
		k = decay rate constant
		t = time
(1)	$C_t = C_o e^{-kt}$	
(2)	$\rightarrow T(1/2) = \text{Ln}(2)/k$	

CHX treated cells (2 – 20 $\mu\text{g/ml}$) had a shrunken morphology and with the exception of cells treated with 2 $\mu\text{g/ml}$ cycloheximide, fewer cells were visible after 48 and 72 hours treatment (Figure 3.4 A). To monitor the effect of CHX on cell viability, the number of viable cells was determined by trypan blue exclusion and expressed as a percentage of the total number of cells (Figure 3.4 B). Data suggested that with 10 $\mu\text{g/ml}$ and 20 $\mu\text{g/ml}$ CHX there was slight toxicity at 48 hours and that by 72 hours only around half the cells survived compared to the control; 5 $\mu\text{g/ml}$ CHX only became toxic at 96 hours

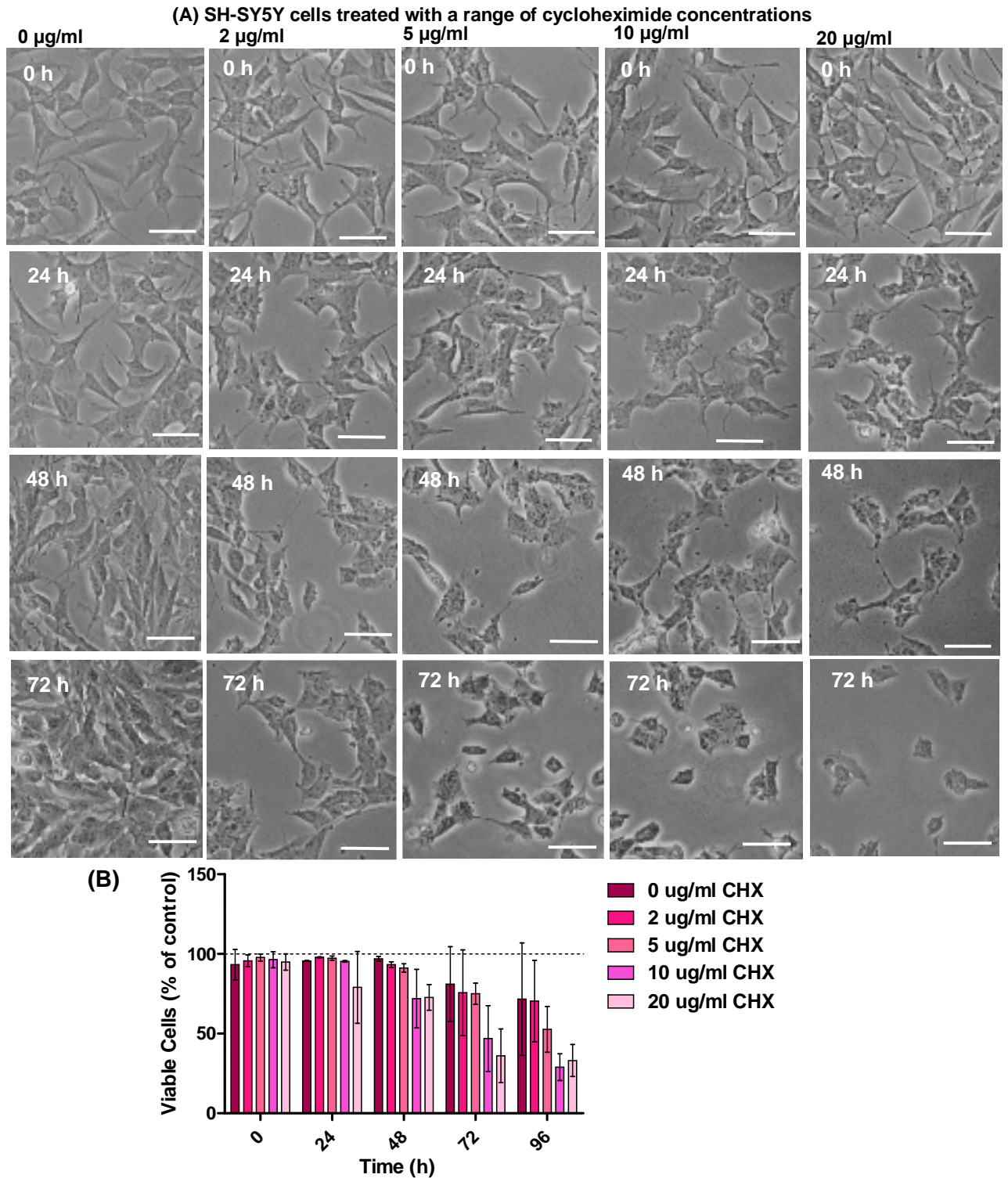


Figure 3.4 Assessment of the effect of cycloheximide (CHX) treatment of the viability of SH-SY5Y neuroblastoma cells.

(A) Phase contrast images of human SH-SY5Y neuroblastoma cells treated with 2 to 20 µg/ml cycloheximide over a 72 hour time-course. Cells were viewed at 100 x magnification, scale bar represents 40 µm and n = 4. (B) The percentage of viable cells treated with 2 to 20 µg/ml cycloheximide was determined by trypan blue exclusion and expressed as a percentage of the total number of cells. Error bars represent range, n = 2.

The estimates of half-life for the three NF subunits, α -tubulin, vimentin and α -synuclein obtained from their decay rate constants, using concentrations of CHX ranging from 2 to 20 $\mu\text{g/ml}$, are given in Table 3.2. An example of a typical Western blot and the resultant plots from which decay rate constants were determined is depicted in Figure 3.5 which details the half-life determination of NF-L. To reliably estimate half-life from the decay rate constant, only estimates from ‘lines of best fit’ with high R^2 values (0.8 and above) were considered. In general cells treated with 2 or 5 $\mu\text{g/ml}$ CHX yielded fewer reliable estimates than cells treated with 10 and 20 $\mu\text{g/ml}$ CHX. Due to the likely increased toxicity of 20 $\mu\text{g/ml}$ CHX, a concentration of 10 $\mu\text{g/ml}$ was selected for use in subsequent experiments.

Table 3.2 Table summarizing the estimates of half-life for the neurofilament subunits, vimentin and α -tubulin using a range of cycloheximide concentrations.

Estimates of half-life were obtained when plotting the natural logarithm of the percentage original signal [$\text{Ln}(\% \text{ original signal})$] against time (h). The number of experiments with R^2 values high enough (0.8 and above) to be included in the estimate of half-life are indicated in brackets. Half-life is expressed in hours \pm range (if only two experiments were included) or standard deviation (if three or more experiments were included).

<i>Protein</i>	<i>T(1/2), h</i>			
	<i>Concentration of Cycloheximide ($\mu\text{g/ml}$)</i>			
	<i>2 $\mu\text{g/ml}$</i>	<i>5 $\mu\text{g/ml}$</i>	<i>10 $\mu\text{g/ml}$</i>	<i>20 $\mu\text{g/ml}$</i>
<i>NF-H</i>	No estimate	58 \pm 47 (2)	53.2 \pm 28.3 (3)	40.2 \pm 23.5 (2)
<i>NF-M</i>	No estimate	40.5 (1)	66.6 \pm 7.8 (3)	40.5 \pm 9.1 (3)
<i>NF-L</i>	51.1 \pm 11.4 (3)	37.6 \pm 13.9 (3)	40 \pm 8.8 (3)	34.1 \pm 10.4 (4)
<i>Vimentin</i>	28.9 (1)	44.2 \pm 13 (3)	46.4 \pm 26.6 (4)	27.3 \pm 14.4 (4)
<i>α-Tubulin</i>	29.8 \pm 12.1 (3)	42.3 \pm 18.3 (3)	31.1 \pm 10.1 (3)	16.4 \pm 13.1 (2)
<i>α-Synuclein</i>	40.3 (1)	38.7 (1)	21.8 \pm 9.1 (2)	23.3 (1)

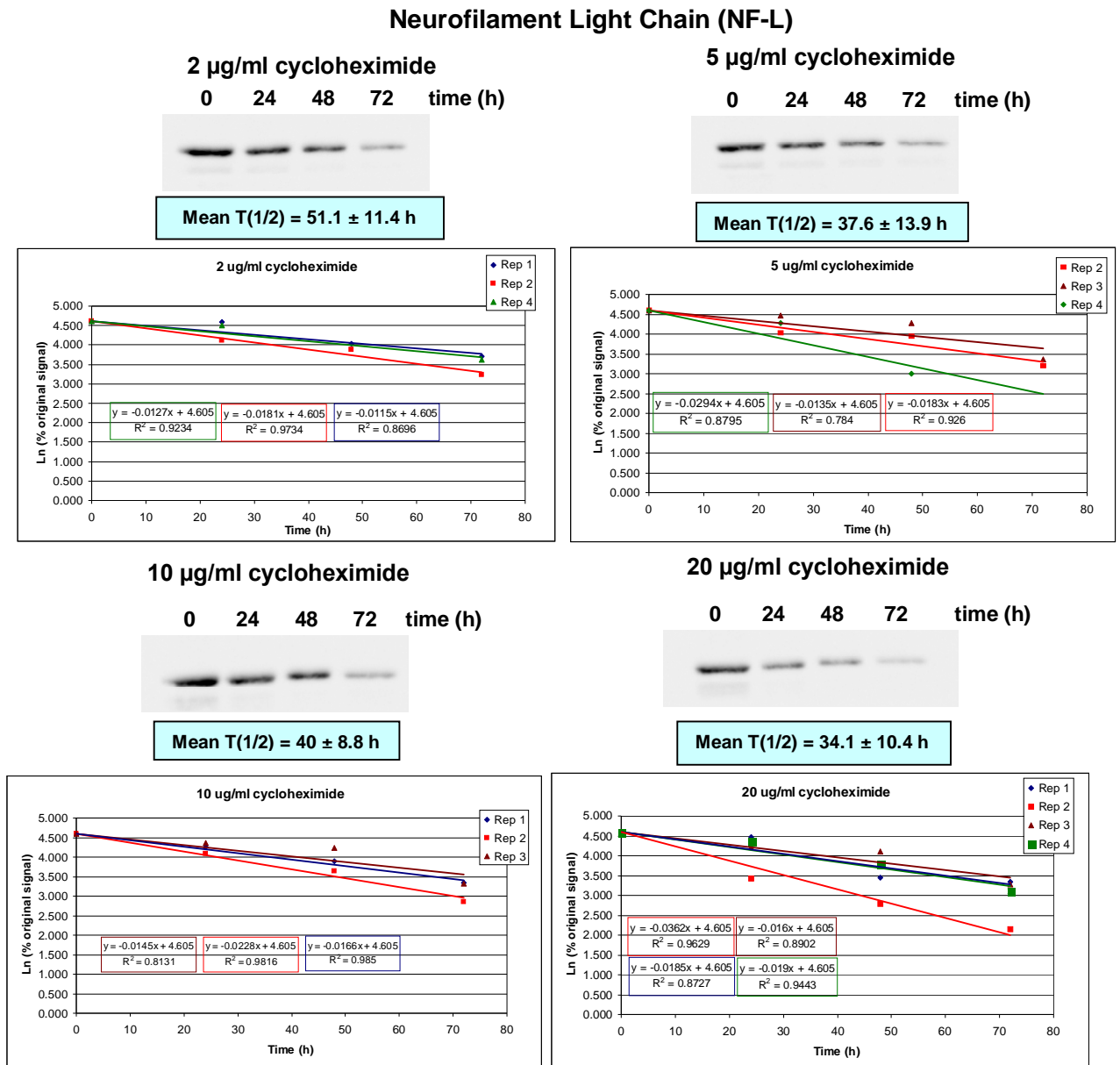


Figure 3.5 Example of Western blots and plots from which the half-life of proteins were calculated.

Representative blots of total cell extracts of SH-SY5Y cells treated with 2 -20 µg/ml cycloheximide over 72 hours, probed with anti-NF-L (DA2, from Zymed). Plots show estimates of NF-L half-life using 2 -20 µg/ml cycloheximide from Western blots from three or four (in the case of 20 µg/ml cycloheximide) individual experiments. Briefly, immunoprobed blots were analysed using AIDA densitometry software and the signal for the NF-L band at each time-point was expressed as a percentage of the original signal at t = 0 h. The natural logarithm of the percentage original signal [Ln(% original signal)] was plotted against time and the gradient of the line of best fit (decay rate constant - k) was used to calculate half-life using the equation: $T(1/2) = \text{Ln}(2)/k$. The mean half-life [T(1/2)] ± standard deviation calculated from the decay rate constants from each experiment is quoted above each plot.

3.2.2. Degradative pathways involved in neurofilament turnover

To establish which degradative pathways are involved in neurofilament turnover, proliferating SH-SY5Y cells were treated with 10 µg/ml CHX in the presence of Epoxomicin (proteasome inhibitor), Bafilomycin A1 (inhibitor of autophagy), MDL28170 (calpain inhibitor) or Pepstatin A (Cathepsin D inhibitor, aspartyl cathepsins) over a 72 hour period. The half-lives estimated for the three NF subunits in the presence or absence of each of the inhibitors listed above are summarized in Table 3.3.

The half-life of NF-H (Table 3.3) was estimated to be 48.6 ± 4.4 h (n =25). The half-life of NF-H was not significantly altered by epoxo or MDL28170 but inhibition of macroautophagy with BafA1 resulted in an increase in NF-H half-life to 134 ± 17.1 h, this increase in half-life was also observed in cells treated with PepA which inhibits cathepsin D [$T(1/2) > 169.1$ h] and in cells treated with epoxo, MDL28170 and BafA1 in combination (117 ± 11.7 h). The half-life of NF-H in the presence of Pepstatin A is quoted as greater than 169.1 h since levels of NF-H in two experiments did not drop, and the value is based on one experiment in which levels did decrease slightly over the 72 h time-course; it is clear however that pepstatin inhibited NF-H degradation.

The half-life of NF-M (Table 3.3) was estimated to be 53.5 ± 3.6 h (n = 21). Inhibition of the proteasome (epoxo), calpain (MDL28170) and macroautophagy (BafA1) had no effect on this half-life.

Compared to the half-life of the two larger NF subunits, the half-life of NF-L was significantly shorter ($p < 0.05$) at 37.2 ± 2.6 h (n = 27). As for NF-M, inhibition of the proteasome, macroautophagy, calpain and cathepsin D had no effect on the half-life of NF-L. The half-life of NF-L in cells treated with epoxo, BafA1 and MDL28170 in combination was similar to that in control cells.

The effects of inhibition of the proteasome, macroautophagy, calpain and cathepsin D on the half-lives of α -tubulin (a component of the microtubule network) and vimentin (an intermediate filament protein) were also determined (Table 3.3). The half-life of α -tubulin and vimentin were respectively estimated as 41.2 ± 4 h (n = 18) and 41.8 ± 4.1 h (n = 21), both significantly shorter than that of NF-M ($p < 0.05$). Inhibition of the proteasome, macroautophagy, calpain and cathepsin D had no significant effect on the half-lives of α -tubulin and vimentin.

Table 3.3 Estimates of half-life (T(1/2), h) and the effect of inhibition of the proteasome, macroautophagy, calpain and cathepsin D on the half-life of α -tubulin, α -synuclein, vimentin, NF-H, NF-M and NF-L.

Half-life is quoted as T(1/2) \pm SEM. In experiments for which T(1/2) could not be calculated because the slope of the line of best fit (k, rate constant) was positive, half-lives were quoted as greater than a value for that protein that could be calculated. The half-life of NF-L is significantly shorter than that of NF-H and NF-M (*Two-tailed T-Test, p < 0.05). The half-lives of α -tubulin, α -synuclein and vimentin are significantly shorter than that of NF-M (†Two-tailed T-Test, p < 0.05). The half-life of NF-H was increased following inhibition of macroautophagy and cathepsin D (§Two-tailed T-Test, p < 0.05).

Treatment	T(1/2) \pm SEM, h					
	NF-H	NF-M	NF-L	α -tubulin	vimentin	α -synuclein
Untreated (Cycloheximide)	48.6 \pm 4.4 (n = 25)	53.5 \pm 3.6 (n = 21)	37.2 \pm 2.6* (n = 27)	41.2 \pm 4† (n = 18)	39.4 \pm 3.7† (n = 24)	31.4 \pm 6.7† (n = 4)
Inhibition of proteasome (Epoxomicin)	37 \pm 11.4 (n = 4)	36.6 \pm 8.7 (n = 3)	29.9 \pm 7.3 (n = 4)	39.8 \pm 8.7 (n = 4)	34.0 \pm 1.0 (n = 4)	346.6
Inhibition of macroautophagy (Bafilomycin A1)	134 \pm 17.1§ (n = 4)	57.9 \pm 13.4 (n = 4)	40.9 \pm 7.6 (n = 4)	38.7 \pm 4.6 (n = 3)	44.7 \pm 17.3 (n = 4)	>346.6
Inhibition of calpain (MDL28170)	25.9 \pm 3.0 (n = 4)	50.3 \pm 10.6 (n = 4)	31.7 \pm 3.2 (n = 4)	21.0 \pm 4.3 (n = 4)	43.3 \pm 12.9 (n = 4)	>346.6
Inhibition of cathepsin D (Pepstatin A)	> 169.1§ (n = 3)	ND	38.4 \pm 2.6 (n = 3)	63.7 \pm 29.0 (n = 4)	25.2 \pm 2.6 (n = 4)	24.7
Epoxomicin, Bafilomycin A1 and MDL28170	117 \pm 11.7§ (n = 3)	53.8 \pm 11.5 (n = 3)	30.4 \pm 3.5 (n = 2)	ND	32.2 \pm 7.2 (n = 3)	ND

To confirm that the inhibition of degradative pathways in the presence of CHX could elucidate pathways involved in the turnover of proteins of interest the effect of inhibition of the proteasome, macroautophagy, calpain and cathepsin D on the half-life of α -synuclein was investigated (Table 3.3). The half-life of α -synuclein was estimated to be 31.4 \pm 6.7 h (n = 4) which is significantly shorter than that of NF-M (p < 0.05). Inhibition of cathepsin D with PepA had no effect on α -synuclein half-life but inhibition of the proteasome, macroautophagy and calpain all resulted in a large increase in α -synuclein half-life. In the case of Bafilomycin A1 and MDL28170, half-lives were quoted as greater than 346.6 h

because the levels of α -synuclein did not decrease over the 72 h time-course and as a result half-life could not be estimated using the decay rate constant and the equation for half-life.

To confirm that NF-H is degraded by macroautophagy, cells were treated with 0.2 μ g/ml Rapamycin (an inducer of autophagy) in the presence of 10 μ g/ml CHX for 48 h. Cells were also treated with 10 nM BafA1 and 5 mM 3-methyl adenine (3-MA, another inhibitor of autophagy), both in the presence of CHX for 48 h. Western blots probed with anti-NF-H (n52) showed that an induction of autophagy by rapamycin resulted in a decrease in NF-H levels compared to levels in CHX treated controls (Figure 3.6). The levels of NF-H were maintained in cells treated with BafA1 and 3-MA.

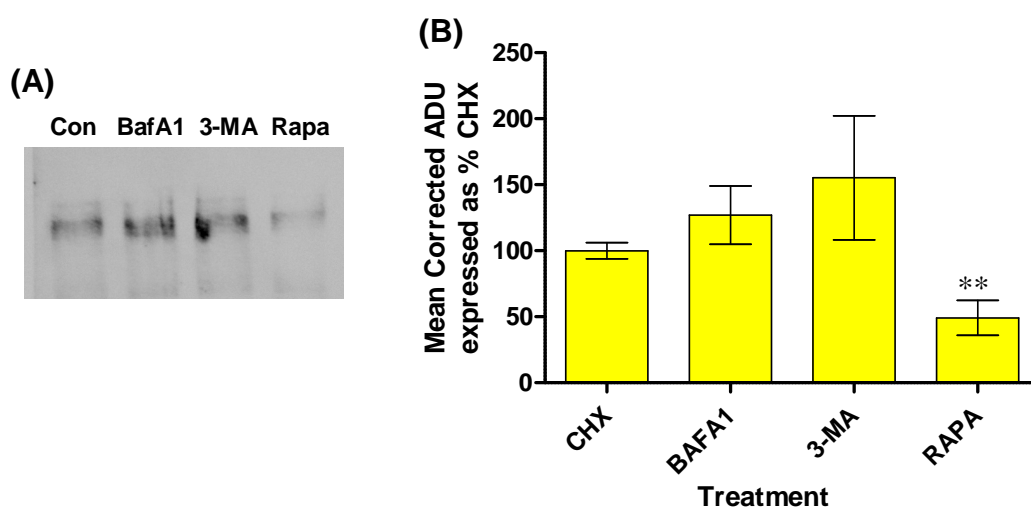


Figure 3.6 Effect of the activation of macroautophagy by Rapamycin on the levels of NF-H compared to levels in total cells extracts of cycloheximide treated control cells.

(A) A representative Western blot of total cell extracts of SH-SY5Y cells treated with either 0.2 μ g/ml Rapamycin (Rapa), 10 nM Bafilomycin A1 (BafA1) or 5 mM 3-methyl adenine (3-MA) in the presence of cycloheximide (CHX) probed with anti-NF-H (n52; 1:2000, Sigma). (B) Plot summarising the results of densitometric analysis of Western blots. The levels of NF-H were significantly lower in cells treated with Rapamycin than in CHX treated control cells ($p < 0.05$, One-way ANOVA, $n = 5$).

3.2.3. Does inhibition of one pathway activate another?

Since it has not been possible in most cases to clearly assign a pathway(s) involved in the turnover of all three NF subunits, the possibility that the inhibition of one proteolytic pathway resulted in a compensatory activation of one of the other pathways was investigated.

3.2.3.1. Effect of inhibiting various proteolytic pathways on proteasome activity

Chymotrypsin-like activity (CLA), chosen to represent proteasome activity, was assessed for cells treated with CHX in the presence or absence of epoxo, BafA1 and MDL28170 using a fluorogenic peptide assay as described in section 2.2.4. Interestingly, CLA was significantly reduced in cells treated with 10 $\mu\text{g/ml}$ CHX for 72 hours compared to untreated cells (Figure 3.7 A). This decrease in CLA is likely to be due to decreased proteasome levels since new protein synthesis is inhibited rather than a direct effect on the proteasome. CLA was significantly reduced by epoxomicin (by up to 60% with 5 nM and 75% by 10 nM epoxo), but the other inhibitors had no significant effect on CLA.

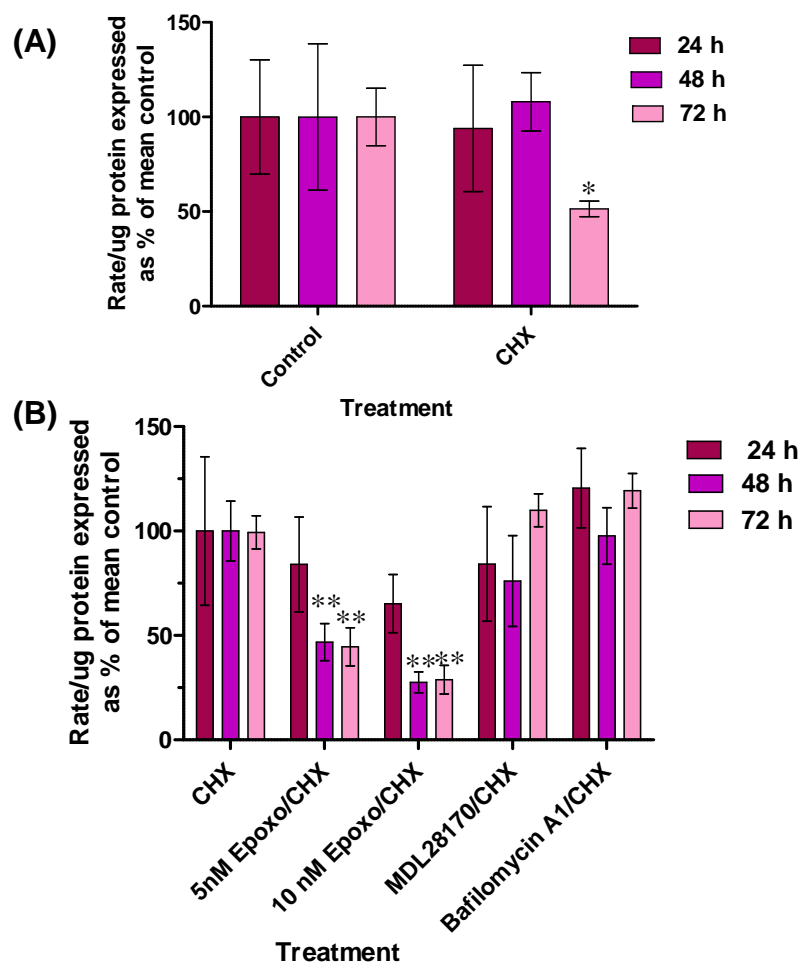


Figure 3.7 The effects of treatment with various protease inhibitors on chymotrypsin-like activity (CLA) in SH-SY5Y cells

(A) CLA was determined in extracts from untreated control cells compared to cells treated with 10 $\mu\text{g/ml}$ cycloheximide (CHX) over a 72 h time-course. CLA was significantly reduced in CHX treated cells after 72 h ($p < 0.05$, $n = 3$, Paired T-Test). (B) CLA in cells treated with either epoxomicin (5 nM or 10 nM), 5 nM Bafilomycin A1 or 10 μM MDL28170 in the presence or absence of CHX. CLA was significantly reduced in cells treated with 5 and 10 nM epoxomicin after 48 and 72 hours (** $p < 0.005$; Two-way ANOVA, $n = 3$). Error bars represent standard deviation.

3.2.3.2. Effect of inhibiting proteolytic pathways on the cleavage of α II-spectrin

To determine whether cycloheximide treatment results in the activation of calpain and/or caspase 3, the levels of the 145 kD calpain-specific spectrin breakdown product (SBDP) and the 120 kD caspase 3-specific SBDP relative to the full-length α II-spectrin were compared in cells treated with CHX for 48 h and untreated controls. The determination of the apparent molecular weights of the SBDPs by comparing their electrophoretic mobility to that of a set of molecular weight standards run on the same SDS-PAG is described in appendix I. Initial results suggest that after 48 h treatment with CHX no significant increase in the levels of the calpain and caspase 3 specific SBDPs of α II-spectrin was observed (Figure 3.8).

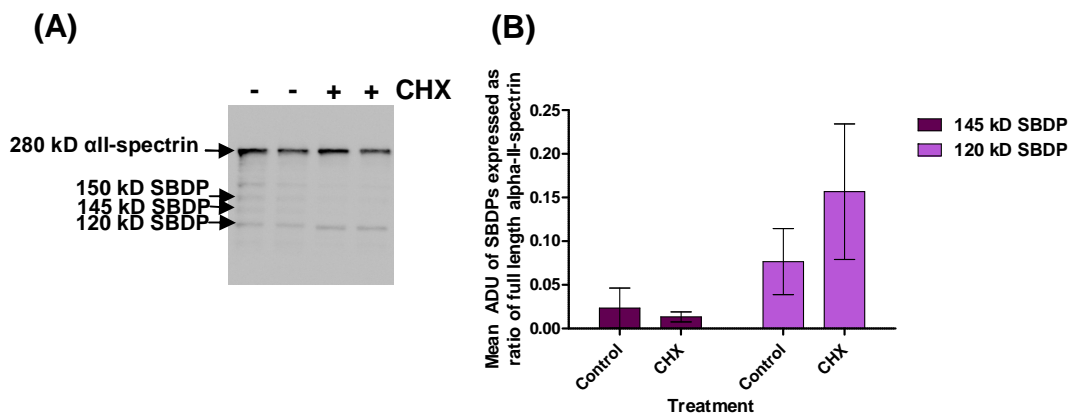


Figure 3.8 The activation of caspase 3 and calpain after 48 h treatment of SH-SY5Y cells with μ g/ml cycloheximide was assessed indirectly by monitoring the levels of α II-spectrin 145 kD and 120 kD cleavage products.

(A) Representative Western blot of total cell extracts of SH-SY5Y neuroblastoma cells either untreated or treated with 10 μ g/ml Cycloheximide for 48 h, probed with anti- α II-spectrin (Sigma, 1:1000). (B) Plot summarising the results of densitometric analysis of the Western blot. The arbitrary densitometry units (ADU) of the 145 kD and 120 kD spectrin breakdown products (SBDP) were expressed as a ratio of the full-length α II-spectrin for each sample. Error bars represent standard deviation (n = 3).

Inhibition of macroautophagy by BafA1 resulted in an increase in the production of the 145 kD and 120 kD SBDPs after 24 h compared to the control at the same time-point (Two-way ANOVA, Figure 3.9). However after 48 and 72 h, results were very variable making it difficult to come to any conclusion about the activation of calpain and/or caspase 3. No effect of the inhibition of calpain (with MDL28170), the proteasome (epoxo) or cathepsin D (PepA) was observed compared to the control at each time-point. When comparing the levels of the 145 kD and 120 kD SBDPs for each treatment with time by one-way ANOVA,

an increase in the 145 kD SBDP was observed after 72 h in controls and with proteasome inhibition and an increase in the 120 kD SBDP was observed in controls (after 48 and 72 h) and with proteasome and calpain inhibition for 72 h.

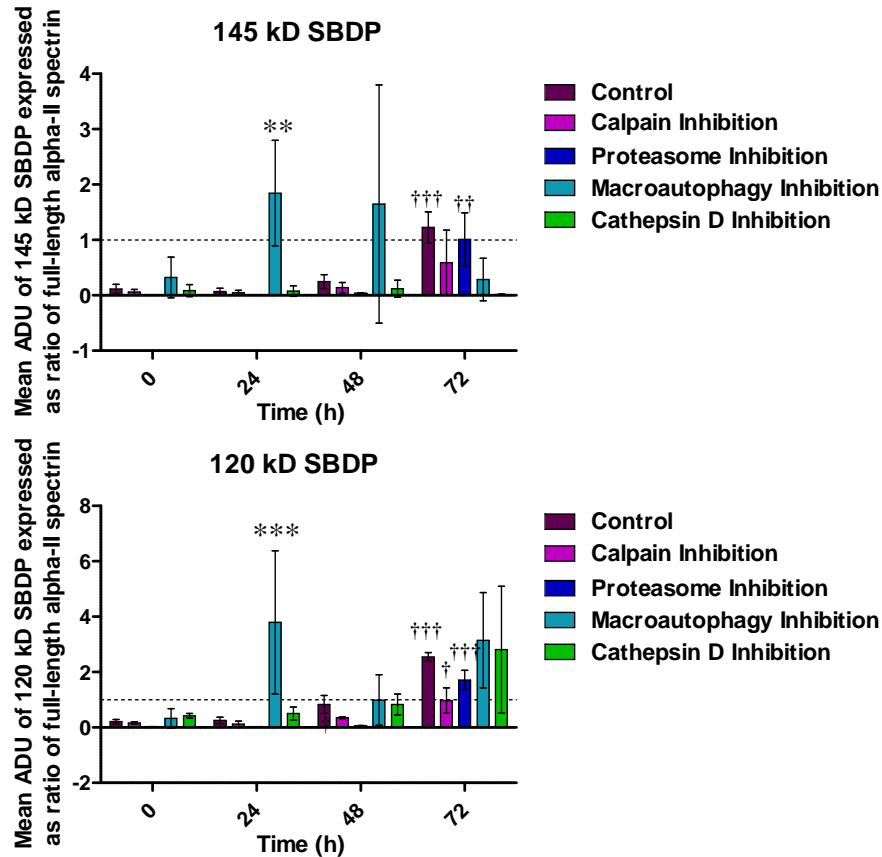


Figure 3.9 Effect of inhibition of proteolytic pathways on the cleavage of α II-spectrin in SH-SY5Y neuroblastoma cells.

Effect of the inhibition of calpain, the proteasome, macroautophagy and cathepsin D on the activation of caspase 3 and/or calpain was assessed indirectly by monitoring the levels of (A) 145 kD and (B) 120 kD α II-spectrin breakdown products (SBDPs). Plots summarise the results of densitometric analyses of Western blots of total cell extracts probed with anti- α II-spectrin (Sigma, 1:1000). The arbitrary densitometry units (ADU) of the 145 kD and 120 kD spectrin breakdown products (SBDP) were expressed as a ratio of the full-length α II-spectrin for each sample. The effect of each treatment on the levels of SBDPs was assessed over time (†One-way ANOVA, Bonferroni posthoc test). There was a significant increase in the cleavage of α II-spectrin after 48 and 72 h treatment with CHX. The effect of treatment with proteolytic inhibitors on the levels of SBDPs over time was compared to the levels of SBDPs in the CHX treated control over time (*Two-way ANOVA, Bonferroni posthoc test). Error bars represent standard deviation (n = 3).

3.2.3.3. Effect of inhibiting proteolytic pathways on macroautophagy

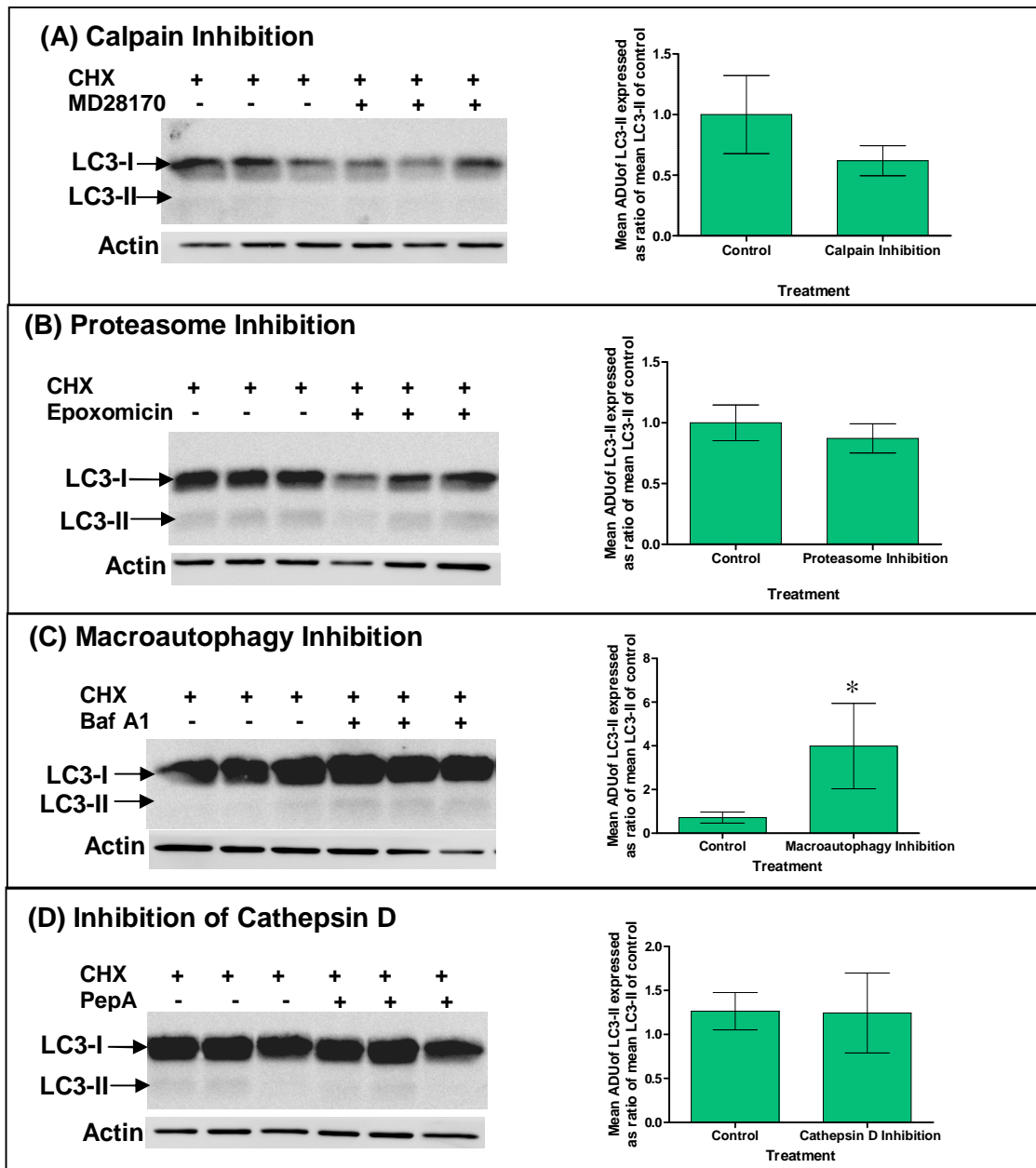


Figure 3.10 Effect of inhibition of proteolytic pathways in SH-SY5Y neuroblastoma cells on the levels of LC3-II to monitor the inhibition or activation of macroautophagy.

Western blots of total cell extracts from cells treated with 10 µg/ml Cycloheximide (CHX) with/without (A) 10 µM MDL28170 inhibiting calpain, (B) 5 nM Epoxomicin inhibiting the proteasome, (C) 10 nM Bafilomycin A1 inhibiting macroautophagy or (D) 1 µM Pepstatin A inhibiting cathepsin D, immunoprobed with anti-LC3 (1:1000) and anti-actin (1:1000). Plots summarise the results of densitometric analyses of LC3-II levels (corrected for total protein with actin) expressed as a ratio of LC3-II levels in CHX treated controls. In cells treated with Bafilomycin A1, levels of LC3-II were increased compared to CHX treated controls (Two-tailed T-Test, $p < 0.05$). Error bars represent standard deviation ($n = 3$).

The levels of LC3-II in total cell extracts of cells treated with MDL28170, epoxomicin (epoxo), Bafilomycin A1 (BafA1) or Pepstatin A (PepA) in the presence of CHX were monitored (Figure 3.10). Inhibition of macroautophagy with BafA1 resulted in an increase in LC3-II levels (around four-fold) compared to the levels in CHX treated control cells but there was no effect on LC3-II levels with inhibition of calpain, the proteasome or cathepsin D.

3.2.3.4. Effect of inhibiting proteolytic pathways on the activity of aspartyl and cysteine cathepsins

The effect of the inhibition of calpain with MDL28170, the proteasome with Epoxomicin, macroautophagy with Bafilomycin A1 (BafA1), cathepsin D (aspartyl cathepsin) with Pepstatin A (PepA) or the cysteine cathepsins (L, B, C, F, H, K, O, S, V, W, X) with Cathepsin Inhibitor III on the activity of the aspartyl and cysteine cathepsins was investigated using fluorogenic peptide assays. Since all the half-life data were obtained in cells treated with CHX, the effects were investigated in the presence of CHX (Figure 3.11).

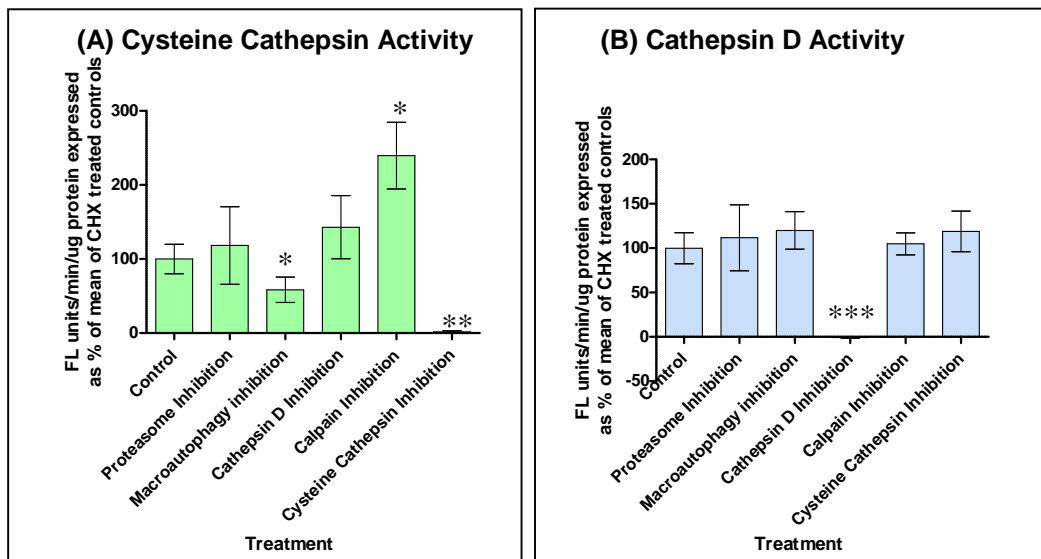


Figure 3.11 Effect of inhibition of proteolytic pathways in SH-SY5Y cells on cathepsin activity.

The influence of the inhibition of calpain (with MDL28170), the proteasome (with Epoxomicin), macroautophagy (with Bafilomycin A1), cathepsin D (with Pepstatin A) or the cysteine cathepsins (with Cathepsin inhibitor III) in the presence of cycloheximide (CHX) on the activity of (A) cysteine cathepsins and (B) cathepsin D was assessed using fluorogenic peptide assays. Activity (FL units/min/ μ g protein) was expressed as a percentage if the activity in CHX treated controls. Cysteine cathepsin activity was reduced with inhibition of macroautophagy and cysteine cathepsins but increased with calpain inhibition (two-tailed T-Test, $p < 0.05$). Cathepsin D activity was reduced following inhibition of cathepsin D but was unaffected by inhibition of proteolytic pathways (two-tailed T-Test, $p < 0.05$). Error bars represent standard deviation ($n = 3$).

The inhibition of macroautophagy with BafA1 and calpain with MDL28170 altered cysteine cathepsin activity. BafA1 reduced cysteine cathepsin activity to 58.5 ± 17 % of the activity in CHX treated control cells whilst MDL28170 increased cysteine cathepsin activity to 239.7 ± 45 % of activity in CHX treated control cells. Treatment with cathepsin inhibitor III resulted in complete inhibition of cysteine cathepsin, confirming that the activity measured is that of the cysteine cathepsins (Figure 3.11 A). However, with the exception of Pepstatin A (which resulted in complete inhibition of cathepsin D activity) treatment with the other inhibitors had no effect on cathepsin D activity (Figure 3.11 B).

3.2.4. Effects of MPP⁺ and dopamine on neurofilament turnover and degradative pathways

3.2.4.1. Effect of MPP⁺ and DA on the half-life of neurofilament proteins, α -tubulin and vimentin

To investigate whether MPP⁺ and/or dopamine has an effect on the half-life of neurofilament proteins, cells were treated with either 2 mM MPP⁺ or Dopamine (DA; 100 μ M or 500 μ M) in the presence of 10 μ g/ml CHX over a 72 hour time-course (Table 3.4). Significance tests were performed using a paired T-Test in which half-life estimates from total cell extracts of MPP⁺/CHX and DA/CHX treated cells were compared to estimates of half-life obtained from the CHX treated controls for each experiment. The values for half-life quoted in Table 3.4 were calculated using the percentage change in half-life in cells treated with MPP⁺/CHX or DA/CHX compared to their own CHX controls, multiplied by the mean half-life estimated from all the experiments in which cells were treated with CHX alone.

The half-life of NF-L in cells treated with 2 mM MPP⁺ in the presence of CHX was estimated to be shorter at 24.4 ± 2.1 h than that estimated in cells treated solely with CHX. 2 mM MPP⁺ treatment reduced the estimated half-lives of NF-H, NF-M, α -tubulin and vimentin but the effect was not statistically significant.

Treatment of cells with 100 μ M DA had no significant effect on the half-lives of the five cytoskeletal elements but in all cases the mean values for half-life tended to be greater than half-lives estimated in cells treated only with CHX. In cells treated with 500 μ M DA however the half-lives of all five cytoskeletal elements were significantly lower than in cells treated only with CHX.

Table 3.4 Estimates of half-life (T(1/2), h) and the effect MPP+ and dopamine (DA) treatment on the half-life of α -tubulin, vimentin, NF-H, NF-M and NF-L.

Half-life is quoted as $T(1/2) \pm SEM$ and was calculated by multiplying the percentage change in half-life for MPP+/CHX and DA/CHX compared to CHX treated controls with the mean half-life estimated for all CHX treated control experiments ($n \geq 18$). To test for significance, the half-life estimated in the presence of MPP+ or DA was compared to the half-life estimated for the cycloheximide treated controls for each experiment using a paired T-Test*. The half-life of NF-L was shorter than that of NF-H and NF-M under unstressed conditions (§ Two-tailed T-Test, $p < 0.05$). The half-lives of α -tubulin and vimentin were shorter than the half-life of NF-M († Two-tailed T-Test, $p < 0.05$). The half-life of NF-L was shorter in cells treated with MPP+/CHX than in CHX treated controls and in cells treated with 500 μ M DA/CHX, the half-lives of NF-H, NF-L and α -tubulin were shorter than in CHX treated controls (paired T-Test, * $p < 0.05$, ** $p < 0.005$).

Treatment	T(1/2) \pm SEM, h				
	NF-H	NF-M	NF-L	α -tubulin	vimentin
Untreated (cycloheximide)	48.6 \pm 4.4 (n = 25)	53.5 \pm 3.6 (n = 21)	37.2 \pm 2.6 [§] (n = 27)	41.2 \pm 4 [†] (n = 18)	39.4 \pm 3.7 [†] (n = 24)
2 mM MPP+	40.5 \pm 17.6 (n = 4)	43.7 \pm 6.7 (n = 3)	24.4 \pm 2.1** (n = 4)	35.4 \pm 10.3 (n = 3)	28.1 \pm 8.4 (n = 4)
100 μ M DA	307.7 \pm 125.7 (n = 3)	87.3 \pm 50.7 (n=3)	71.1 \pm 22.0 (n = 4)	105.1 \pm 52.0 (n = 3)	56.3 \pm 27.6 (n = 3)
500 μ M DA	21.4 \pm 1.9* (n = 3)	ND	17.6 \pm 2.4* (n = 3)	17.6 \pm 2.1* (n = 3)	ND

3.2.4.2. Effect of MPP+ and DA on the activity of proteolytic pathways

Cells were treated with 2 mM MPP+ or DA (100 μ M or 500 μ M) in the presence or absence of 10 μ g/ml cycloheximide and proteolytic activities estimated as described earlier (section 3.2.3) in order to assess the effect of complex 1 inhibition and oxidative stress on these activities.

3.2.4.2.1. Effect of MPP+ and DA on proteasome activity

CLA was significantly reduced in cells treated with 2 mM MPP+ alone for 48 h to around 40 % of the activity in untreated control cells (Figure 3.12 A). Since all the half-life data was acquired in cells co-treated with CHX, the effect MPP+ on CLA in the presence of CHX was also assessed (Figure 3.12 B). In cells co-treated with 2 mM MPP+ and CHX for 48 h, the effect of MPP+ was lost, ie there was no significant difference in CLA in MPP+/CHX treated cells compared to that in CHX treated control cells.

Treatment with 100 μ M DA for 48 h had no significant effect on CLA compared to CLA in untreated control cells (Figure 3.12 A), but in the presence of CHX 100 μ M DA resulted in a small decrease in CLA to around 78 % of CLA in CHX treated control cells. In cells treated with 100 μ M DA, CHX and 25 nM epoxo; CLA was reduced to 7 % of CLA in CHX treated control cells, indicating that the activity measured in CHX treated and CHX/100 μ M DA treated cells was proteasomal. Treatment of SH-SY5Y cells with CHX/500 μ M DA virtually abolished CLA.

Co-treatment with 25 nM epoxo resulted in virtual abolishment of CLA ($p < 0.001$) for all treatments indicating that the activity measured was proteasomal (Figure 3.12 B).

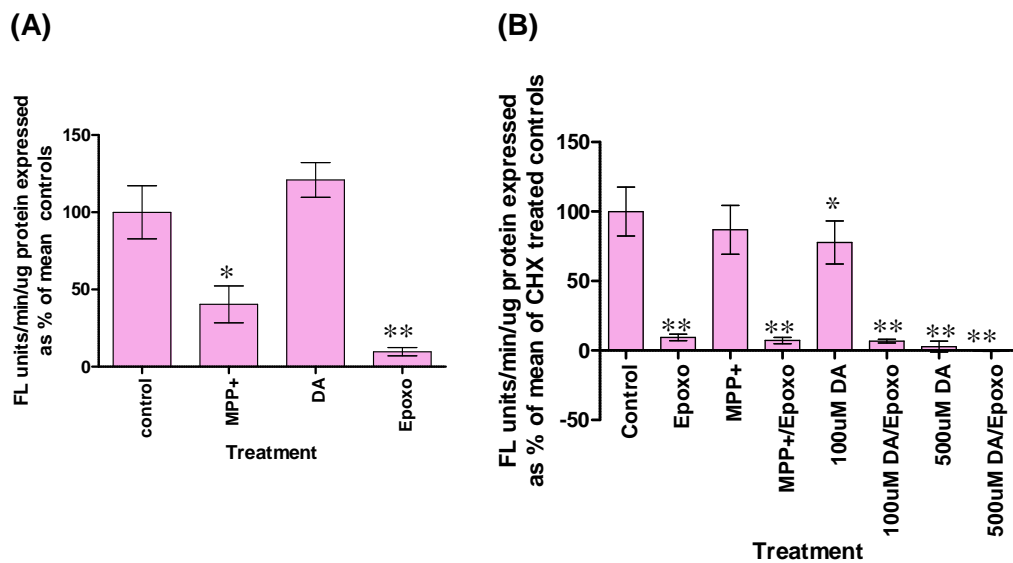


Figure 3.12 Effect of MPP+ and DA treatment on proteasome activity in SH-SY5Y cells.

Chymotrypsin-like Activity (CLA) of the 20S proteasome in cell lysates of cells (A) treated for 48 hours with either 2 mM MPP+; 25 nM Epoxomicin (Epoxo) or 100 μ M Dopamine (DA) expressed as a percentage of CLA in untreated control cells or (B) cells treated with 2 mM MPP+, 25 nM epoxo, 100 μ M DA or 500 μ M DA in the presence of 10 μ g/ml cycloheximide (CHX) for 48 h. There was a significant reduction in CLA in cells treated with 2 mM MPP+ (One-way ANOVA, * $p < 0.05$, $n = 5$) and cells treated with 25 nM Epoxomicin (One-way ANOVA, ** $p < 0.005$, $n = 6$) compared to CLA in untreated control cells. In the presence of CHX the effect of MPP+ on CLA was lost and treatment with 100 μ M DA resulted in a small reduction in CLA (One-way ANOVA, $p < 0.05$, $n = 6$), while treatment with 500 μ M DA resulted in a drastic reduction in CLA (One-way, ANOVA, ** $p < 0.005$, $n = 3$) compared to CHX treated controls. The addition of 25 nM Epoxomicin to all treatments resulted in a reduction in proteasome activity (One-way ANOVA, $p < 0.001$,) indicating that the measured activity was proteasomal.

3.2.4.2.2. Effect of MPP+ and DA on calpain and caspase 3 specific cleavage of α II-spectrin

A comparison of the morphology of cells treated with 500 μ M DA, 100 μ M DA or 2 mM MPP+ in the presence of 10 μ g/ml CHX for 48 h suggests that treatment with 500 μ M DA/CHX resulted in extensive cell death whereas cells treated with 100 μ M DA/CHX and 2 mM MPP+/CHX had a similar appearance to CHX treated controls (Figure 3.13).

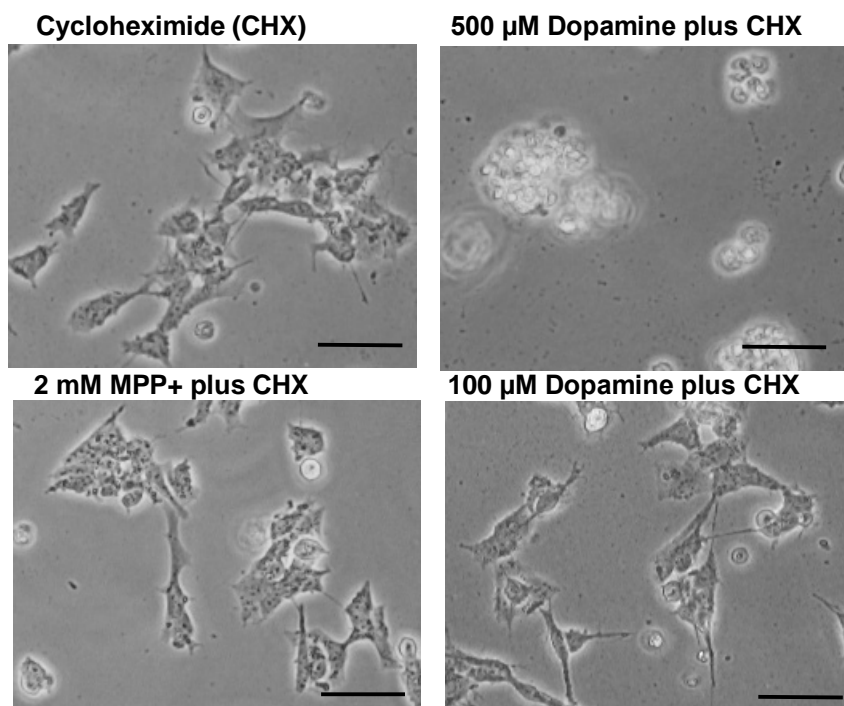


Figure 3.13 Assessment of the morphology of SH-SY5Y neuroblastoma cells treated with 500 μ M Dopamine (DA) and 10 μ g/ml cycloheximide (CHX).

Phase contrast images of either treated with 10 μ g/ml CHX or 500 μ M or 100 μ M DA plus CHX or 2 mM MPP+ plus CHX for 48 h. Treatment with 500 μ M DA plus CHX resulted in extensive cell death. Scale bar represents 40 μ m.

Treatment with 2 mM MPP+ and CHX for 48 h had no effect on cleavage of α II-spectrin compared to CHX treated controls (Figure 3.14 A-C). However, the inclusion of the calpain inhibitor (MDL28170) resulted in an increase in the production of the 120 kD caspase 3 specific SBDPs compared to CHX treated control (Figure 3.14 A and B).

Compared to CHX treated controls, 100 μ M DA/CHX treatment for 48 h (Figure 3.14 A and C) had no effect on the production of the 120 kD caspase 3 specific cleavage product, but increased the production of the 145 kD calpain-specific cleavage product (Figure 3.14 A and B). Surprisingly, the inclusion of the calpain inhibitor with 100 μ M DA/CHX, increased the cleavage of α II-spectrin and the production of both the 145 and 120 kD SBDPs (Figure 3.14 B and C). In cells treated with 500 μ M DA (Figure 3.14 A-C) there was a significant increase in the cleavage of α II-spectrin and the appearance of both the 145 kD (calpain) and 120 kD (caspase 3) specific SBDPs.

3.2.4.2.3. Effect of MPP+ and DA on macroautophagy

The levels of LC3-II increased three-fold following treatment with either 2 mM MPP+ or 10 nM Bafilomycin A1 and 2-fold following treatment with 100 μ M DA compared to CHX treated control cells. Co-treatment of cells treated with 2 mM MPP+ or 100 μ M DA with 10 nM Bafilomycin A1 resulted in a >4-fold increase in LC3-II levels compared to levels in CHX treated controls. However 500 μ M DA (+/- Bafilomycin A1) had no effect on LC3-II levels (Figure 3.15).

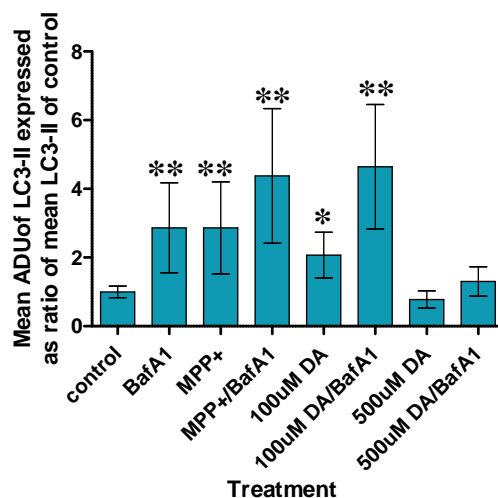


Figure 3.15 Effect of treatment of SH-SY5Y cells with 2 mM MPP+ or 100 or 500 μ M Dopamine (DA) on the levels of LC3-II as a measure of macroautophagy.

The plot represents the results of the densitometric analysis of the LC3-II band which was represented as a ratio of the LC3-II band in cycloheximide treated control cells. The levels of LC3-II increased 3-fold in total cell extracts of cells treated with BafA1 (T-Test, $p < 0.005$; $n = 6$) and MPP+ (T-Test, $p < 0.005$; $n = 6$) and 2-fold in cells treated with 100 μ M DA (T-Test, $p < 0.05$; $n = 3$). In cells treated with MPP+ or 100 μ M DA with BafA1, LC3-II levels increased 4 and 4.5-fold respectively (T-Test, $p < 0.005$, $n = 3$). In cells treated with 500 μ M DA with/without BafA1 the levels of LC3-II were similar to levels in CHX treated control cells. Error bars represent standard deviation.

3.2.4.2.4. Effect of MPP+ and DA on cathepsin activity

Treatment with 2 mM MPP+ resulted in a 30% reduction in cathepsin D activity whilst 100 μ M DA had no effect. Culture of cells with pepstatin A virtually abolished cathepsin D activity (Figure 3.16 A). A comparison of cathepsin D activity in CHX treated cells with activity in untreated controls revealed that CHX resulted in a 50 % reduction in cathepsin D activity (Figure 3.16 B). In cells incubated with CHX, addition of 2 mM MPP+ or 100 μ M DA had no effect on cathepsin D activity (Figure 3.16 C). In all cases cathepsin D activity was sensitive to Pepstatin A.

Co-treatment of SH-SY5Y cells with an inhibitor of cysteine cathepsins (Cathepsin Inhibitor III, calbiochem) and 2 mM MPP+ resulted in cell death compared to treatment with either MPP+ or the cathepsin inhibitor on their own (Figure 3.17). This effect was not seen in cells treated with 100 μ M DA and cathepsin inhibitor III.

The effect of 2 mM MPP+ and 100 μ M DA on the activity of the cysteine cathepsins was also investigated (Figure 3.18). Treatment with 2 mM MPP+ alone resulted in a marked increase (85%, Figure 3.18 A) in cysteine cathepsin activity, which exhibited a further increase when CHX was present (603.8 % of activity in CHX treated controls, Figure 3.18 B). Treatment of cells with the Cathepsin Inhibitor III was included as a control and in all cases resulted in a marked decrease in measured activity, indicating that the activity measured was that of the cysteine cathepsins. In cells treated with 100 μ M DA either in the presence or absence of CHX, no significant change in cysteine cathepsin activity was observed (Figure 3.18 A/B). Treatment with CHX resulted in a marked decrease in cysteine cathepsin activity which was similar to the activity observed in cells treated with Cathepsin Inhibitor III either in the absence or presence of CHX (Figure 3.18 C).

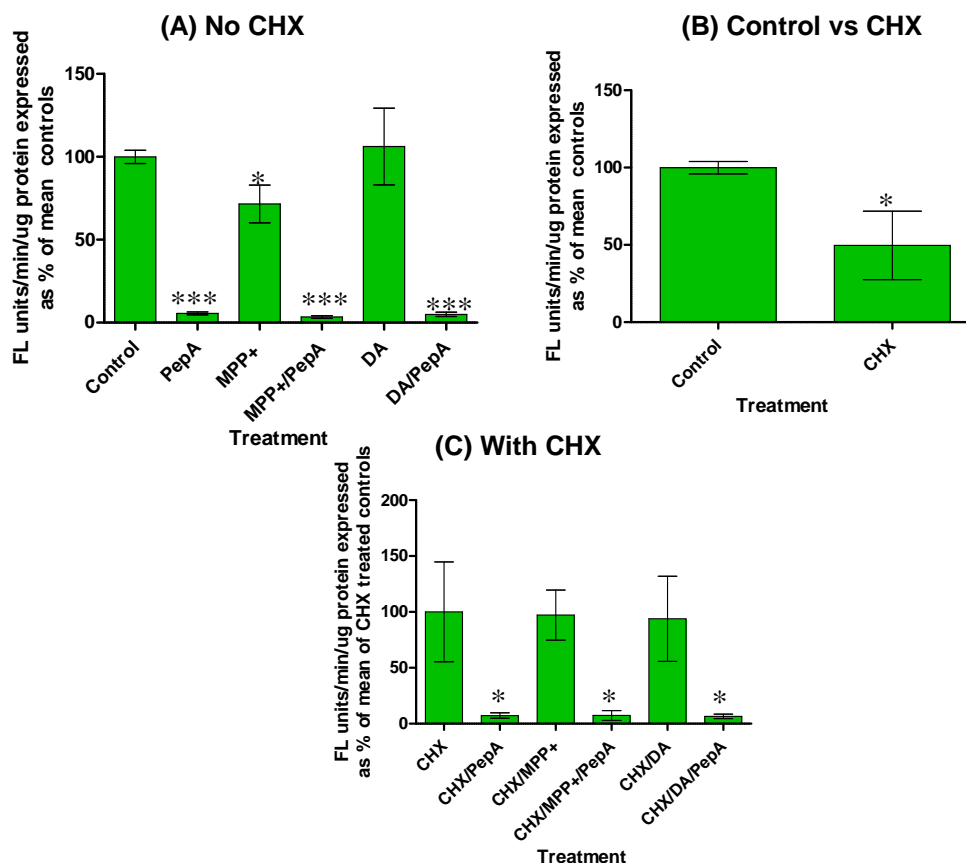


Figure 3.16 Effect of treatment of SH-SY5Y cells with 2 mM MPP+ or 100 μ M Dopamine (DA) was assessed using a fluorogenic peptide assay for cathepsin D activity.

(A) The activity of cathepsin D in cell lysates of SH-SY5Y cells treated with either 2 mM MPP+; or 100 μ M DA; or 1 μ M Pepstatin A; or 2 mM MPP+ and 1 μ M Pepstatin A; or 100 μ M DA and 1 μ M Pepstatin A. Activity was expressed as a percentage of the activity in untreated control cells. Treatment with MPP+ reduced cathepsin D activity to 71 % of the activity in untreated control cells ($p < 0.05$; T-Test, $n = 3$). Treatment with Pepstatin A either with or without MPP+ or DA reduced cathepsin D activity indicating that the activity measured is that of cathepsin D ($p < 0.001$; T-Test, $n = 3$). (B) The activity of cathepsin D in cell lysates of SH-SY5Y cells treated with 10 μ g/ml cycloheximide (CHX) with either 2 mM MPP+; or 100 μ M DA; or 1 μ M Pepstatin A; or 2 mM MPP+ and Pepstatin A; or 100 μ M DA and Pepstatin A. The activity of cathepsin D in cells treated with MPP+ and DA in the presence of CHX was similar to that in CHX treated control cells. Co-treatment with Pepstatin A resulted in a drastic reduction in cathepsin D activity indicating that the measured activity is that of cathepsin D. (C) The activity of cathepsin D in CHX treated controls expressed as a percentage of the activity in untreated controls. Treatment with CHX results in a significant reduction in measured cathepsin D activity ($p < 0.05$; T-Test, $n = 3$). Error bars represent standard deviation.

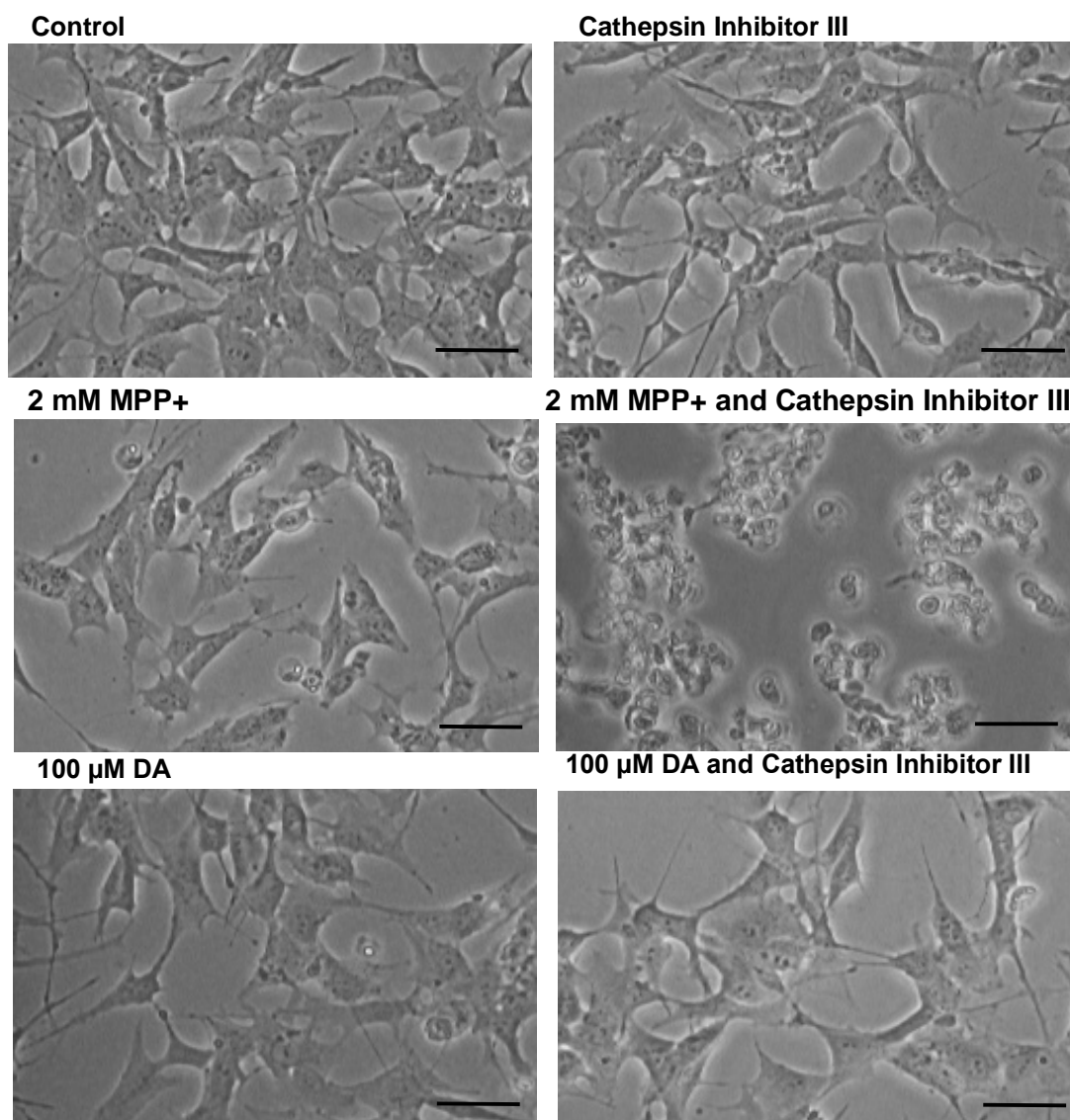


Figure 3.17 Effect of co-treatment of SH-SY5Y neuroblastoma cells with MPP+ or DA and a cysteine cathepsin inhibitor.

Phase contrast images of cells either untreated or treated with either 2 mM MPP+, 10 μM Cathepsin Inhibitor III (Calbiochem), 2 mM MPP+ and 10 μM Cathepsin Inhibitor III, 100 μM Dopamine (DA) or 100 μM DA and 10 μM Cathepsin Inhibitor for 48 hours. Treatment of SH-SY5Y cells with both MPP+ and Cathepsin Inhibitor III resulted in increased cell death compared to cells that were either untreated or treated with MPP+ or Cathepsin Inhibitor III alone. In cells treated with 100 μM DA and Cathepsin Inhibitor III, there was no visible additional effect on cell viability. Scale bar represents 40 μm

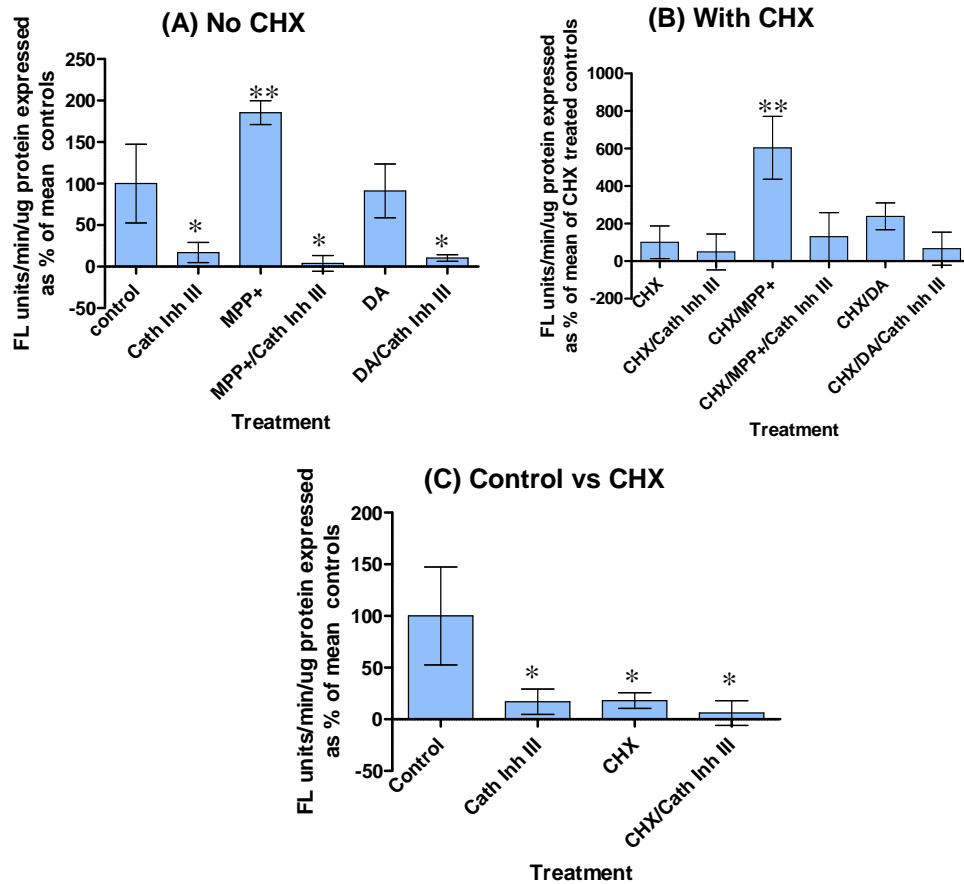


Figure 3.18 Determination of the effect of treatment with 2 mM MPP+ and 100 μ M Dopamine (DA) on the activity of the cysteine cathepsins in SH-SY5Y neuroblastoma cells.

Cysteine cathepsin activity measured using a fluorogenic peptide assay in (A) untreated cells or cells treated with either 10 μ M Cathepsin Inhibitor III (Cath Inh III), 2 mM MPP+, 2mM MPP/Cath Inh III, 100 μ M DA or 100 μ M DA/10 μ M Cath Inh III expressed as a percentage of the mean activity in controls. (B) Cysteine cathepsin activity in cells treated with 10 μ g/ml Cycloheximide (CHX) with either 10 μ M Cath Inh III, 2 mM MPP+, 2 mM MPP+/Cath Inh III, 100 μ M DA or 100 μ M DA/Cath Inh III expressed as a percentage of the mean activity in CHX treated control cells. An increase in the activity of cysteine cathepsins following treatment with 2 mM MPP+, either in the presence or absence of CHX and a reduction in cysteine cathepsin activity with treatments involving Cath Inh III was observed (* $p < 0.05$, ** $p < 0.005$; T-Test, $n = 3$). (C) The cysteine cathepsin activity in CHX treated control cells expressed as a percentage of the mean activity in untreated control cells. Treatment with CHX results in a significant decrease in cysteine cathepsin activity (* $p < 0.05$; T-Test, $n = 3$). Error bars represent standard deviation.

3.2. Discussion

3.2.1. The establishment of an experimental model for the determination of the half-life of proteins

To establish the optimum CHX concentration for treating SH-SY5Y neuroblastoma cells that would give the most reliable estimates of NF half-life whilst not causing extensive cell death, the effects of a range of concentrations of CHX on cell viability and estimates of half-life were examined. The most toxic concentrations of CHX (10 and 20 $\mu\text{g/ml}$) yielded most consistent estimates for NF half-life than the less toxic concentrations (2 and 5 $\mu\text{g/ml}$), suggesting that with 2 and 5 $\mu\text{g/ml}$ some protein synthesis was still occurring. Due to the dose dependent effects on cell viability, 10 $\mu\text{g/ml}$ was selected for subsequent experiments.

3.2.2. Degradative pathways involved in neurofilaments turnover

3.3.2.1. Estimations of half-life

The half-life of NF-L was found to be significantly shorter than that of the two larger subunits (NF-M and NF-H). This may be the result of the presence of extensive phosphorylation sites on the C-termini of NF-M and NF-H which when phosphorylated are known to increase the resistance of neurofilaments to degradation (Greenwood et al, 1993). The half-life of NF-L (37.2 ± 2.6 h) in this system was similar to that of the cytoskeletal proteins vimentin (39.4 ± 3.7) and α -tubulin (41.2 ± 4 h), and also that of α -synuclein (31.4 ± 6.7 h). The estimated α -synuclein half-life is similar to a previously reported 33.1 ± 6.3 h estimate in PC12 cells (Cuervo et al, 2004). An earlier estimate of the half-life of α -synuclein suggested a half-life of 2.76 ± 0.24 h but in this case the α -synuclein was His-tagged which may have increased its rate of degradation (Bennett et al, 1999).

The estimates of the half-life of cytoskeletal proteins in SH-SY5Y cells are considerably shorter than estimates of the half-life of cytoskeletal proteins *in vivo* which are usually quoted in days or even weeks. In brain tissue from rats labelled intracranially with [^{35}S]methionine for 10 days, cytoskeletal proteins were shown to exhibit biphasic decay rates. In total protein fractions; the fast-turnover rate for α -tubulin was around 5 days and the slow-turnover rate was around 15 days which was similar to that in a triton X-100 insoluble fraction. For NF-H, the half-life in the triton X-100 insoluble fraction was around 18 days (Safaei & Fischer, 1990). This estimate is similar to the half life of 21 days reported for NF-L in mice expressing human NF-L under doxycycline control (Millecamps et al,

2007). Nixon and Logvinenko (Nixon & Logvinenko, 1986) also reported a biphasic loss of radiolabelled NFs in mice for which fast-turnover rate was estimated as 20-22 days and the slow-turnover rate was estimated as 55 days.

The discrepancy in half-life determination in cultured cells compared to *in vivo* has been attributed to the shorter duration of experiments involving cultured cells (Safaei & Fischer, 1990), but may reflect the fact that cultured cells are usually mitotic. In fact, in HEK293 cells treated with the protein synthesis inhibitor puromycin, the half-life of α -tubulin was reported to be around 22.5 h (Ren et al, 2003) which is considerably less than the 5 to 15 day estimate *in vivo* (Safaei & Fischer, 1990) but is more in the range of the estimates reported herein. The half-life of vimentin has also previously been reported to be 32 h in mouse fibroblasts (Coleman & Lazarides, 1992). The shorter half-life of cytoskeletal proteins in cultured cells suggests that in these cells, cytoskeletal proteins are more labile.

3.3.2.2. Pathways involved in turnover of cytoskeletal proteins

An attempt to reveal the proteolytic pathways involved in the turnover of NF proteins was made by estimating half-life in cells treated with cycloheximide in the presence or absence of inhibitors to the major proteolytic pathways.

3.3.2.2.1. *The role of the proteasome*

In the case of α -synuclein, proteasome inhibition increased the half-life from 31.4 ± 6.7 h to 346.6 h. Since a role for the proteasome in the degradation of α -synuclein has been extensively documented (Bennett et al, 1999, Kim et al, 2006, Tofaris et al, 2001, Webb et al, 2003), these results confirm that treatment of SH-SY5Y cells with 5 nM Epoxomicin in the presence of CHX is sufficient to inhibit the proteasome. However in the present work there was no evidence for the involvement of the proteasome in the degradation of NF proteins, α -tubulin or vimentin in unstressed conditions.

Proteasome inhibition did not result in the activation of any of the other proteolytic pathways investigated. Therefore, the lack of evidence for proteasomal involvement in the degradation of NFs, α -tubulin or vimentin in this system is not due to the compensatory activation of any of other proteolytic pathways investigated. The only effect that was observed was a reduction the production of the 145 kD and 120 kD calpain and caspase 3 specific SBDPs after 72 h epoxomicin treatment. This conflicts with the results reported by

Hamano et al (2009) in which proteasome inhibition resulted in increased cleavage of α -spectrin and activation of caspase 3.

An alternative explanation for the lack of evidence for proteasomal involvement in NF, vimentin and α -tubulin degradation may be the incomplete inhibition of the proteasome with the concentration of epoxomicin used in this work. Although the concentration used was sufficient to prevent α -synuclein degradation, it may not be sufficient to prevent NF, α -tubulin or vimentin degradation. CLA was used as a measure of proteasomal activity but the proteasome also contains TLA and PLA protease activities which are not affected by epoxomicin to the same degree as CLA. TLA and PLA may be more important in the degradation of some proteins than CLA (Kisselev et al, 2006), therefore lack of evidence for proteasomal involvement in NF degradation may be limited to that of CLA.

The interaction of α -tubulin and parkin (an E3 which ubiquitinates tubulin) reported in literature, has led to the proposal of the involvement of the UPS in the degradation of α -tubulin (Ren et al, 2003). However a reported accumulation of polyubiquitinated α -tubulin following proteasome inhibition with lactacystin was only evident in cells overexpressing parkin (Ren et al, 2003), suggesting that the role of parkin may not be limited to targeting α -tubulin for degradation by the proteasome.

Owing to the high affinity binding of parkin to microtubules, parkin has also been suggested to stabilize microtubules and to play a role in the transport of misfolded proteins along microtubules to the aggresome, which is apart from its E3 ligase activity. In fact the binding of parkin to microtubules is not mediated via its ubiquitin-like domain but instead via the Linker, RING1 and RING2 tubulin-binding domains. The microtubule destabilizing effect of colchicine was attenuated in cells overexpressing parkin, providing evidence for the role of parkin in microtubule stabilization (Yang et al, 2005). Therefore, the targeting of α -tubulin for degradation by the proteasome via parkin-mediated polyubiquitination may be secondary to its function as a microtubule stabilizing agent.

3.3.2.2.2. The role of calpain

The inhibition of calpain by the inhibitor MDL28170 had no effect on the half-life of NF-M, NF-L or vimentin but slightly reduced the half-lives of NF-H and α -tubulin (but not significantly, $p = 0.08$). The half-life of α -synuclein was increased when calpain was inhibited, which is not unexpected since calpain has also been implicated in the degradation of α -synuclein (Kim et al, 2006, Kim et al, 2003).

The possible decrease in the half-lives of α -tubulin and NF-H would suggest that there is some compensatory activation of proteolytic pathways in cells treated with MDL28170. There was a slight decrease in the levels of LC3-II (but again not statistically significant) suggesting increased autophagic vesicle degradation. The slight decrease in LC3-II levels may be explained by the compensatory activation of cysteine cathepsins (cathepsin B, C, F, H, K, L, O, S, V, W and X) in cells treated with MDL28170 and CHX, the activity of which was increased significantly to 240 % of activity in CHX treated controls. This suggests that the cysteine cathepsins may play a role in the degradation of NF-H and α -tubulin. Indeed, leupeptin – a serine and cysteine protease inhibitor which inhibits trypsin, plasmin, kallikrein, papain, thrombin and cathepsins A and B - has been reported to suppress the degradation of neurofilaments in an experimental model of spinal cord injury (Iwasaki et al, 1987).

As indicated in the introduction to this chapter, there is an extensive volume of literature that implicates calpain in neurofilament degradation (Kunz et al, 2004, Schlaepfer et al, 1985, Shields et al, 1997, Stys & Jiang, 2002). In the study by Kunz et al (2004) calpain was activated following zymosan-induced inflammation leading to NF-L degradation. Stys and Jiang (2002) implicated calpain in NF-H and NF-M degradation following anoxia and reoxygenation of rat optic nerves. Other studies that implicated a role for calpain in NF degradation were *in vitro* based, in which isolated neurofilament proteins were either added directly to calcium-activated calpain or calcium was added to whole cell homogenates (Greenwood et al, 1993, Kamakura et al, 1985, Schlaepfer et al, 1985, Shields et al, 1997). However, in this SH-SY5Y cell model there is no evidence for the role of calpain in basal neurofilament turnover.

3.3.2.2.3. The role of macroautophagy

Inhibition of macroautophagy in SH-SY5Y cells had no effect on the half-life of NF-M, NF-L, α -tubulin and vimentin. It did however result in an increase in the half-life of NF-H (increased to 117 ± 11.7 h from 48.6 ± 4.4 h) and α -synuclein, implicating macroautophagy in the degradation of both these proteins. Evidence of the role of macroautophagy in the degradation of α -synuclein has already been reported in PC12 cells in which inhibition of macroautophagy by Bafilomycin A1 and 3-methyl adenine (3-MA) resulted in increased α -synuclein levels and activation of macroautophagy by Rapamycin resulted in increased clearance of α -synuclein (Webb et al, 2003). The induction of macroautophagy by Rapamycin is via the inhibition of mTOR (reviewed in Klionsky et al, 2008). To further

confirm the role macroautophagy in NF-H degradation, SH-SY5Y cells were treated with Bafilomycin A1, 3-MA or Rapamycin in the presence of CHX for 48 hours. SDS-PAGE and Western blotting of total cell extracts revealed that the levels of NF-H protein were significantly decreased following treatment with Rapamycin.

Since long-term inhibition of autophagy may cause nonspecific effects (reviewed in Rubinsztein et al, 2009), the effect of the inhibition of autophagy in the presence of CHX on the activities of the proteasome, calpain, cathepsin D and the cysteine cathepsins was also investigated. Inhibition of macroautophagy for 72 h resulted in a 10 % increase in proteasomal activity compared to CHX treated controls. After 24 hours treatment with Bafilomycin A1 and CHX, levels of the 145 kD calpain-specific and the 120 kD caspase-3-specific SBDPs were increased compared to CHX treated controls suggesting that treatment with Bafilomycin A1 resulted in calpain and caspase 3 activation. However, after 48 and 72 hours treatment with Bafilomycin A1 α II-spectrin cleavage was similar to CHX treated controls. Treatment with Bafilomycin A1 and CHX for 48 hours also resulted in a significant reduction in the activity of the cysteine cathepsins to 58.5 % of the activity in CHX treated control cells.

3.3.2.2.4. *The role of cathepsins*

Inhibition of cathepsin D with Pepstatin A had no effect on the half-life of NF-L, α -tubulin, vimentin or α -synuclein but resulted in a significantly increased NF-H half life indicating that cathepsin D plays a role in NF-H turnover. This is supported by early *in vitro* experiments using purified cathepsin D (Nixon & Marotta, 1984, Suzuki et al, 1988). Suzuki et al (1988) reported that NF-L was the most susceptible subunit to degradation by cathepsin D and that the incorporation of NF-M and NF-H into the assembled neurofilament protected NF-L from degradation. Their conclusion about the greater susceptibility of NF-L contradicts Nixon and Marotta (1984) who reported that NF-M and NF-H were more susceptible than NF-L to cathepsin D but Suzuki et al (1988) argued that the degradation of NF-M resulted in a 68 kD cleavage product which could not be distinguished from NF-L by SDS-PAGE, thus artificially increasing levels of the 68 kD NF protein. In this work however, there was no evidence to support the *in vivo* role of cathepsin D in the degradation of NF-M and NF-L.

Treatment with Pepstatin A plus CHX had no effect on the production of the 145 kD (calpain) and 120 kD (caspase-3) α II-spectrin products compared to CHX treated controls, suggesting that the inhibition of cathepsin D did not result in the activation of either calpain

or caspase 3. Furthermore treatment with Pepstatin A and CHX for 48 hours had no effect on the levels of LC3-II compared to CHX treated controls, suggesting that cathepsin D inhibition had no measurable effect on macroautophagy. When investigating the effect of Pepstatin A on the activity of cathepsin D and the cysteine cathepsins, the inhibition of cathepsin D by Pepstatin A was confirmed. Additionally, Pepstatin A was shown to have no effect on the activity of the cysteine cathepsins.

3.3.2.2.5. Conclusion

In conclusion; NF-H is degraded via macroautophagy and cathepsin D. Degradative pathways involved in the turnover of NF-M, NF-L vimentin and α -tubulin under basal conditions still remain elusive. However, there is some indication that the cysteine cathepsins may be involved in the degradation of α -tubulin and NF-H, due to the decrease in the half-lives of these proteins when cells are treated with MDL28170 and CHX, shown to result in an increase in the activity of the cysteine cathepsins.

3.2.3. Effect of mitochondrial dysfunction and increased oxidative stress on neurofilament degradation

3.3.3.1. Effects of mitochondrial dysfunction

The half-life of NF-L in cells treated with 2 mM MPP⁺ and CHX decreased significantly compared to CHX treated controls, suggesting that complex 1 inhibition via MPP⁺ activated a degradative pathway(s) involved in NF-L degradation. 2 mM MPP⁺ treatment had no significant effect on the half-lives of NF-M, NF-H, α -tubulin and vimentin. However in all cases, the half-lives were slightly shorter than the half-lives in CHX treated controls.

Previous work in this laboratory showed that 2 mM MPP⁺ treatment resulted in a decrease in proteasome activity (Caneda-Ferron et al, 2008); this was confirmed in the present study with 2 mM MPP⁺ treatment resulting in a 60% decrease in proteasome activity. However, in cells treated with MPP⁺ plus CHX, MPP⁺ did not reduce proteasomal activity, suggests that the effect of MPP⁺ on the proteasome may require new protein synthesis. However CHX itself resulted in a 50% reduction in proteasomal activity, possibly making additional effects more difficult to detect. The reduction in proteasome activity with CHX may be the result of the turnover of proteasomal subunits.

The effect of MPP⁺ on the activity of calpain and caspase 3 was monitored indirectly via the cleavage of α II-spectrin. Calpain specific cleavage of α II-spectrin results in 145 kD and 150 kD spectrin breakdown products (SBDPs) while caspase 3 specific cleavage results in 120 kD and 150 kD SBDPs. Treatment with MPP⁺ did not result in the appearance of additional 145 kD and 120 kD SBDPs compared to CHX treated controls, suggesting that MPP⁺ does not activate either calpain or caspase 3 after 48 h treatment.

The addition of the calpain inhibitor (MDL28170) however unexpectedly resulted in an increase in the production of the 120 kD caspase 3 specific cleavage product of α II-spectrin compared to CHX treated controls, suggesting an activation of caspase 3. In cells treated with MDL28170/CHX and also in cells treated with MPP⁺ (with or without CHX) an activation of the cysteine cathepsins was observed. Cysteine cathepsins have previously been shown to lead to caspase-mediated cell death in a number of cell lines including SH-SY5Y cells (Droga-Mazovec et al, 2008) and could be responsible for the cleavage of α II-spectrin detected in the present study. Cysteine proteases often all cleave the same substrates but at slightly different positions resulting in protease specific cleavage patterns (reviewed in Wang, 2000), it is not inconceivable that the cysteine cathepsins can also cleave α II-spectrin.

LC3-II levels in cells treated with 10 nM Bafilomycin A1 or 2 mM MPP⁺ in the presence of CHX increased about three-fold compared to levels in CHX treated controls. In cells treated with CHX, 2 mM MPP⁺ and 10 nM Bafilomycin A1 in combination there was a slight increase (four-fold of CHX treated controls) in LC3-II levels compared to levels in CHX/Bafilomycin A1 and CHX/MPP⁺ treated cells but this increase was not significant. According to the scenarios described by Rubinsztein et al (2009), an induction of autophagosome vesicle synthesis is indicated by an increase in LC3-II levels during BafA1 and compound of interest (MPP⁺ in this case) co-treatment above that seen when cells are treated with BafA1 alone. In the present work however the additional increase in LC3-II upon co-treatment with BafA1 is not significant, suggesting a reduction in macroautophagy.

Treatment with MPP⁺ in SH-SY5Y cells has previously been reported to result in increased levels of LC3-II as well as an increase in the number of autophagic vesicles (Zhu et al, 2007). The authors suggested that MPP⁺ induced autophagy by increasing autophagic vesicle formation - since co-treatment with Bafilomycin A1 and MPP⁺ treatment resulted in an additional increase in LC3-II levels to that seen in cells treated with MPP⁺ or Bafilomycin A1 alone; this was confirmed by electron microscopy. The difference between the work by Zhu et al (2007) and the work presented here is the inclusion of CHX to inhibit

new protein synthesis. The inclusion of CHX therefore may be preventing cells from increasing the number of autophagic vesicles. However if MPP⁺ inhibits autophagic degradation, an increase in autophagic vesicle production may be a compensatory effect by the cell to increase the degradation of the substrates of autophagy.

A reduction in the degradation of LC3-II can result from either a defect in the transport of autophagosomes to lysosomes, an inhibition of the fusion of autophagosome and lysosome or impaired lysosomal proteolytic activity (reviewed in Rubinsztein et al, 2009). Interference with dynein function has been shown to inhibit macroautophagy (Cai et al, 2009, Ravikumar et al, 2005). MPP⁺ has been shown to alter the transport of membranous organelles in squid axoplasm by increasing the rate of retrograde transport by dynein and decreasing the rate of anterograde transport by kinesin (Morfini et al, 2007). One would therefore expect that MPP⁺ would result in increased transport of autophagosomes to lysosomes, thus decreasing the levels of LC3-II. In another study MPP⁺ treatment of PC12 cells impaired the clearance of α -synuclein by macroautophagy by impairing the function of dynein (Cai et al, 2009).

Treatment of SH-SY5Y cells with MPP⁺ resulted in a significant decrease in cathepsin D activity (71.6 % of control). However in the presence of CHX, the effect of MPP⁺ on Cathepsin D activity was lost. When comparing cathepsin D activity in cells treated with CHX, it was revealed that CHX treatment alone reduced cathepsin D activity by half. Therefore, the effect of MPP⁺ on cathepsin D activity may be masked by the much greater effect of CHX, which may be due to the turnover of cathepsin D itself which can not be replenished in the presence of CHX.

What was more interesting was the effect of MPP⁺ on the activity of the cysteine cathepsins, here 2 mM MPP⁺ treatment resulted in a marked increase in cysteine cathepsin activity which was unaffected by the inclusion of CHX. In addition CHX treatment itself resulted in a massive reduction in cysteine cathepsin activity, suggesting that the cysteine cathepsins are turned over rapidly. Another interesting feature was that cells treated with both the cathepsin inhibitor and MPP⁺ exhibited extensive cell death. This suggests that cysteine cathepsin activity may be protective in SH-SY5Y cells treated with 2 mM MPP⁺. Microarray data has shown that the expression of cysteine cathepsins is elevated in response to MPP⁺ treatment in (Xu et al, 2005), however since the activity of the cysteine cathepsins remains elevated even in the presence of CHX, the effect of MPP⁺ in this case may not only be a result of increased expression.

There are a number of conflicting reports dealing with the role of the cysteine cathepsins in cell death. As mentioned earlier the cysteine cathepsins have been shown to induce caspase-dependent cell death in a number of cell lines (including in SH-SY5Y cells) by the cleavage of Bcl-2, Bcl-xL, Mcl-1 and Bid (Droga-Mazovec et al, 2008). However in human cancer cell lines; the inhibition of cysteine cathepsins leads to the induction of apoptosis (Zhu & Uckun, 2000) suggesting that the induction of the cysteine cathepsins is protective. In a highly invasive mitochondrial DNA depleted osteosarcoma cell line (with impaired mitochondrial respiration) cathepsin B expression is elevated (Hamer et al, 2009) and in human endocrine tumours increased cathepsin B and L expression is associated with invasion and metastasis (Gocheva et al, 2006). Zheng et al (2008) demonstrated that cathepsin L is able to degrade caspase 3 and cathepsin D but is itself not degraded by either cathepsin D or caspase 3.

3.3.3.2. Effects of increased oxidative stress induced by dopamine

The half-life of neurofilament proteins and α -tubulin in cells treated with 500 μ M DA and CHX was significantly reduced compared to CHX treated control cells. The half-lives of NF-H, NF-L and α -tubulin were reduced to 21.4 ± 1.9 , 17.6 ± 2.4 and 17.6 ± 2.1 h respectively. However in cells treated with the lower concentration of 100 μ M, DA did not result in an increase in NF, vimentin or α -tubulin proteolysis. Instead, half-lives tended to be greater.

Treatment with 100 μ M DA had no significant effect on proteasome activity compared to the activity in untreated controls. However, in cells treated with 100 μ M DA and CHX for 48 h, there was a significant reduction (around 22 %) in proteasome activity compared to the activity in CHX treated controls. 500 μ M DA treatment had a greater effect on proteasome activity, reducing proteasome activity to 3 % of the activity in CHX treated controls. 100 and 500 μ M DA has previously been shown to reduce proteasome activity after 72 and 48 h respectively, the effect of which was due to DA-mediated oxidative damage (Caneda-Ferron et al, 2008), and it is likely that some of the effects in the present work are due to oxidative stress caused by dopamine.

Exposure to 100 μ M DA for 48 h resulted in an increase in the production of the 145 kD calpain specific SBDP compared to CHX treated controls, suggestive of calpain activation. The half-lives of the neurofilament in cells treated with 100 μ M DA tended to be longer than in CHX treated controls. The activation of calpain has previously been shown to increase the phosphorylation of neurofilaments by the activation of Erk1,2 in rat primary

neuronal cultures treated with ionomycin resulting in calcium influx (Veeranna et al, 2004). In addition hypoxia treatment of rats results in calpain activation which leads to the cleavage of p35 to p25 and prolonged activation of cdk5 (Tamada et al, 2005) which has been implicated in the phosphorylation of neurofilaments (Pant et al, 1997, Sun et al, 1996). Calpain-induced activation of Cdk5 via p35 cleavage has also been reported in the brains of PD patients (Alvira et al, 2008). Increased phosphorylation of neurofilaments is associated with increased resistance to proteolysis (Greenwood et al, 1993).

The cleavage of α II-spectrin, resulting in the appearance of the 145 kD and 120 kD SBDPs was elevated in cells treated with 500 μ M DA for 48 h compared to CHX treated controls. This suggests that in these cells calpain and caspase 3 are activated. Phase contrast images indicated that 500 μ M DA resulted in extensive cell death which suggests the activation of cell death proteases. The inclusion of MDL28170 did not decrease the levels of the 145 and 120 kD SBDPs or 'rescue' the cells, most likely due to the high level of oxidative damage resulting from 500 μ M DA treatment.

In cells treated with 500 μ M DA, the half-lives of NFs and α -tubulin were half that in CHX treated controls. Calpain has previously been implicated in the degradation of NFs following stress which induces calcium activated cysteine proteases such as calpain (Kunz et al 2004, Schlaepfer et al 1985, Stys and Jiang 2002) and caspase 3 and calpain also often share substrates, though usually they cleave at slightly different sites (reviewed in Wang, 2000). It is therefore likely that in cells treated with 500 μ M DA, caspase 3 is activated and cleaves NFs and α -tubulin.

The effect of 100 and 500 μ M DA on macroautophagy was assessed by monitoring the levels of LC3-II in DA/CHX treated cells compared to Bafilomycin A1/CHX and CHX treated controls. In cells treated with 500 μ M DA/CHX, there was no change in the levels of LC3-II compared to CHX treated controls. However treatment with 500 μ M DA/CHX and Bafilomycin A1 did not result in an increase in LC3-II levels compared to CHX treated controls. This suggests that inhibition of macroautophagy by Bafilomycin A1 in this case was not able to prevent LC3-II degradation. This may be due to the activation of cell death proteases evident with this toxic concentration of DA.

In cells treated with 100 μ M DA/CHX, LC3-II levels were increased two-fold compared to levels in CHX treated controls. The addition of Bafilomycin A1 to 100 μ M DA/CHX resulted in a 4.5-fold increase in LC3-II compared to CHX treated controls, which was only slightly higher than the three-fold increase in Bafilomycin A1/CHX treated cells but not

significantly different. These results suggest that treatment with 100 μ M DA/CHX reduces macroautophagy. Treatment with 100 μ M DA had no effect on the activity of cathepsin D or the cysteine cathepsins in either the presence or absence of CHX.

3.3.3.3. Conclusion

The effects of MPP⁺ and DA treatment on protein degradative pathways and the half-life of cytoskeletal proteins is summarised in Figure 3.19. Briefly, MPP⁺ resulted in the activation of cysteine cathepsins and a reduction in the activity of cathepsin D and possibly macroautophagy (indicated by increased levels of LC3-II). The reduction in NF-L half-life and the overall decrease (although not significant) in half-life of the other NF proteins, α -tubulin and vimentin in cells treated with MPP⁺, suggests an involvement of cysteine cathepsins in their turnover. Further investigation should concentrate on clarifying the effects of MPP⁺ on cysteine cathepsins and macroautophagy.

500 μ M DA resulted in calpain and caspase 3 activation leading to extensive cell death. Calpain and most likely caspase 3 (since calpain and caspase 3 often cleave the same substrates) are candidates for the degradation of the neurofilament proteins and α -tubulin in cells treated with 500 μ M DA. 500 μ M DA also greatly reduced proteasomal activity, possibly as a result of DA-mediated oxidative damage (Caneda-Ferron et al, 2008).

In cells treated with 100 μ M DA, the half-life of neurofilament proteins tended to be longer than in CHX treated controls (albeit not statistically significant). This apparent increase in half-life could be due to decreased proteasome activity and/or decreased macroautophagy. However there is some evidence that the activation of calpain which could lead to the phosphorylation of neurofilaments thus increasing their resistance to proteolysis.

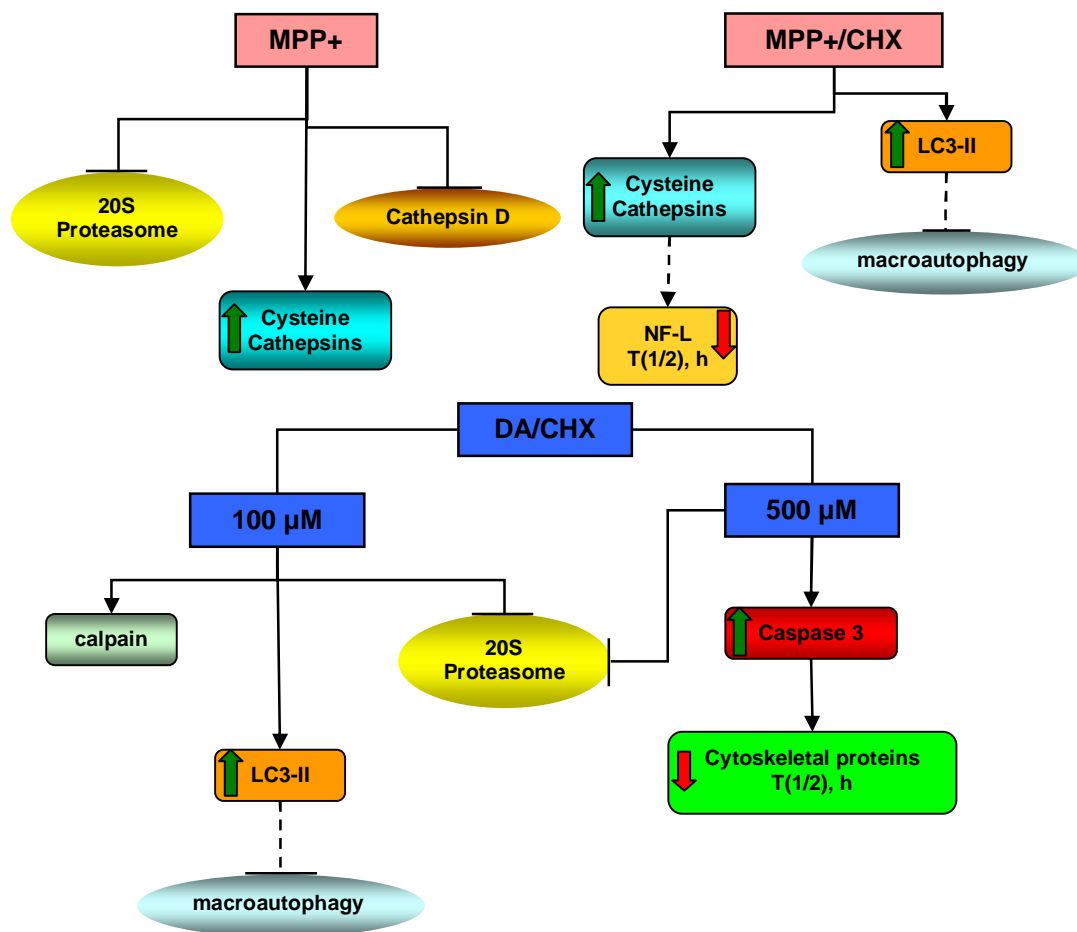


Figure 3.19 Schematic summarising the effect of 48 h treatment of SH-SY5Y neuroblastoma cells with MPP+ (2 mM) with/without cycloheximide (CHX, 10 μg/ml) or Dopamine (DA, 100 μM or 500 μM) with CHX on proteolytic pathways and the degradation of neurofilaments and cytoskeletal proteins.

MPP+ treatment resulted in an activation of cysteine cathepsins which may be responsible for the decrease in NF-L half-life suggesting a role for cysteine cathepsins in NF degradations that warrants further investigation. The activity of the 20S proteasome is reduced following treatment with MPP+ and DA. The levels of LC3-II were increased with 100 μM DA and MPP+ treatment suggesting an effect on macroautophagy, possibly inhibition of macroautophagy by preventing the fusion of autophagosome and lysosome but this effect needs further investigation. There is some indication of increased calpain activity with 100 μM DA and increased caspase 3 activity with 500 μM DA (by monitoring αII-spectrin cleavage products). The half-lives of all cytoskeletal proteins looked at were decreased with 500 μM DA suggesting cleavage by caspase 3. Green arrows refer to increased protein levels and red arrows represent a decrease.

CHAPTER 4

***INHIBITION OF COMPLEX I AND THE
PROTEASOME IN DIFFERENTIATED
SH-SY5Y CELLS***

4.1. Introduction

4.1.1. Differentiation of SH-SY5Y cells

Retinoic acid (RA), traditionally used to differentiate SH-SY5Y neuroblastoma cells, is a metabolic derivative of vitamin A that has a crucial role in development and differentiation of the nervous system. Retinoid deficiency in the adult CNS has been observed in neurodegenerative conditions and RA and other neurotrophins play a role in neuronal repair following injury (reviewed by Malik et al, 2000). The differentiation of SH-SY5Y cells with RA was first described by Pahlman et al (1984) with optimal differentiation at concentrations ranging from 100 nM to 10 μ M RA resulting in 40-50 % of cells exhibiting a differentiated morphology with processes longer than 50 μ m.

Changes in mRNA expression within the first 6 h of RA treatment detected using cDNA Microarrays included a number of genes either up or down regulated; many of which were cytoskeletal, transcription factors, receptors or proteins involved in cell signalling and cell cycle control. Upregulated mRNAs included amongst others; *HSPA8* (heat shock protein 70), Dynein Light chain, Kinesin 2, the proteasome non-ATPase subunit PSMD4, ubiquitin carbonyl-terminal esterase L1 (UCHL1), the ribosomal proteins L28 and L27, vimentin, Mitogen-activated protein kinase 4 (MAPK4), protein kinase inhibitor, Cytochrome C oxidase subunit (*COX6B*) and caspase 9. The most down-regulated mRNAs included profilin 1 and serine/threonine protein-kinase (Truckenmiller et al, 2001).

The activity and protein expression of tissue transglutaminase (TG2) protein is increased following RA-induced differentiation (Singh et al, 2003, Zhang et al, 1998). TG2 is a multifunctional enzyme with three separate enzymatic activities; ATPase, GTPase and Ca^{2+} -dependent transamidating activity which cross-links proteins or incorporates polyamines into protein substrates. It is this transamidating activity of TG2 that has been suggested to play a role in differentiation (Tucholski et al, 2001). Singh et al (2003) reported that TG2 catalyses the activation of the small G-protein RhoA via transamidation which in turn results in increased stress fibre and focal adhesion complex formation and the activation of p38 γ MAP kinase, which induces NF upregulation and neuritogenesis. In addition, TG2 was also shown to activate Erk1/2 and JNK via its transamidation activity as well as JNK-induced expression of growth associated protein-43 (GAP-43; Singh et al, 2003).

Recently Cheung et al (2009) re-evaluated the effect of RA-induced differentiation on neuronal markers in SH-SY5Y cells. They reported an increase in protein expression of

neuron specific enolase (NSE) - which was also previously reported by Pahlman et al (1984) - synaptophysin, post-synaptic associated protein-97 (SAP97) and neuronal nuclei (NeuN) after 7 days treatment. RA treatment however did not have a significant effect on protein expression of NF-H, dopamine transporter (DAT) and tyrosine hydroxylase (TH) (Cheung et al 2009). This lack of an effect on DAT and TH protein expression was previously reported by Presgraves et al (2004). In addition Encinas et al (2000) reported an increase in NF-M protein expression but no change in NF-L protein following RA treatment. An increase in the activation of Akt, Erk1/2, JNK and c-jun and a decrease in phospho-PKC levels with RA treatment was also reported (Cheung et al, 2009). However no increase in JNK phosphorylation was observed by Jämsä et al (2004). Bcl-2 protein is also reportedly upregulated following RA treatment, facilitated by NF- κ B activation (Feng & Porter, 1999) as is tau, p35 and CDK5 (Jämsä et al, 2004).

Combining RA with 12-0-tetradecanoyl-phorbol-13-acetate (TPA) - previously shown to induce differentiation of SH-SY5Y cells (Pahlman et al, 1983) - resulted in a greater number of cells exhibiting a differentiated morphology and longer processes (Pahlman et al, 1984). Study of protein expression in RA/TPA differentiated cells revealed that protein expression of TH and DAT was upregulated (Presgraves et al, 2004). Insulin and insulin-like growth factors have also been used to differentiate SH-SY5Y cells and reportedly result in increased expression of NF-L, NF-M and α -tubulin mRNA (Wang et al, 1992).

An additional method used to differentiate SH-SY5Y cells exploits the induced expression of the Neurotrophic Tyrosine kinase receptor B (NTrkB) during RA-induced differentiation, which enables the cells to be responsive to Brain Derived Neurotrophic Factor (BDNF) (Encinas et al, 1999, Fernandes et al, 2007, Kaplan et al, 1993, Ruiz-León & Pascual, 2001, Ruiz-León & Pascual, 2003). NTrkB belongs to a family of receptors which are responsive to neurotrophins such as Nerve Growth Factor (NGF), neurotrophin 3 (NT-3), NT-4/5, NT-6 and BDNF. Four different types of neurotrophin receptors have been identified and are classified according to their binding preferences; p75^{NTR} (which does not show a preference), NTrkA (binds NGF), NTrkB (binds BDNF or NT-4/5) and NTrkC (binds NT-3, reviewed by Kaplan & Miller, 1997). BDNF binding to NTrkB promotes cell survival during neuronal development and modulates synaptic plasticity in the adult brain (reviewed by Hu & Russek, 2008). BDNF is a neurotrophin which on binding NTrkB activates signal transduction pathways promoting cell survival and differentiation (Kaplan & Miller, 1997). In some neuroblastoma cell lines, RA treatment induces the expression of *BDNF* mRNA but in SH-SY5Y cells, levels of *BDNF* mRNA are too low for the cells to be self-sufficient making it necessary to supplement them with recombinant human BDNF (Kaplan et al, 1993).

The binding of BDNF to TrkB results in receptor dimerisation and activation by autophosphorylation. In the central and peripheral nervous systems, BDNF promotes survival by inducing the expression of Bcl-2 via the activation of the transcription factor cAMP-response element binding protein (CREB, Hu & Russek, 2008). Encinas et al (1999) reported that the BDNF induced the activation of the Ras/MAPK and phosphatidylinositol-3 kinase (PI 3-K)/Akt pathways (Kaplan & Miller, 1997) in SH-SY5Y cells facilitated neuritogenesis and cell survival respectively. BDNF treatment also induced the expression of GAP-43 mRNA which depended on the activation of the Ras/MAPK pathway but protein levels were only transiently elevated (Encinas et al 1999, 2000).

Encinas et al (2000) have described a protocol of RA/BDNF differentiation that yielded a nearly pure population of cells arrested in G1 with rounded cell bodies and an extensive network of interconnecting axon-like processes that exhibited strong NF-H staining in neuritic processes and the cell body. However Western blot analysis suggested a decrease in the levels of NF-L and NF-M during RA/BDNF induced differentiation (Encinas et al, 2000). RA/BDNF treatment also results in increased protein levels and phosphorylation of tau as well as increased levels of p35 and Cdk5 however no increase in JNK phosphorylation was observed (Jämsä et al, 2004). A diagrammatic representation summarising the effects of RA and RA/BDNF induced differentiation on signalling cascades in SH-SY5Y cells reviewed in this introduction can be found in Figure 4.1.

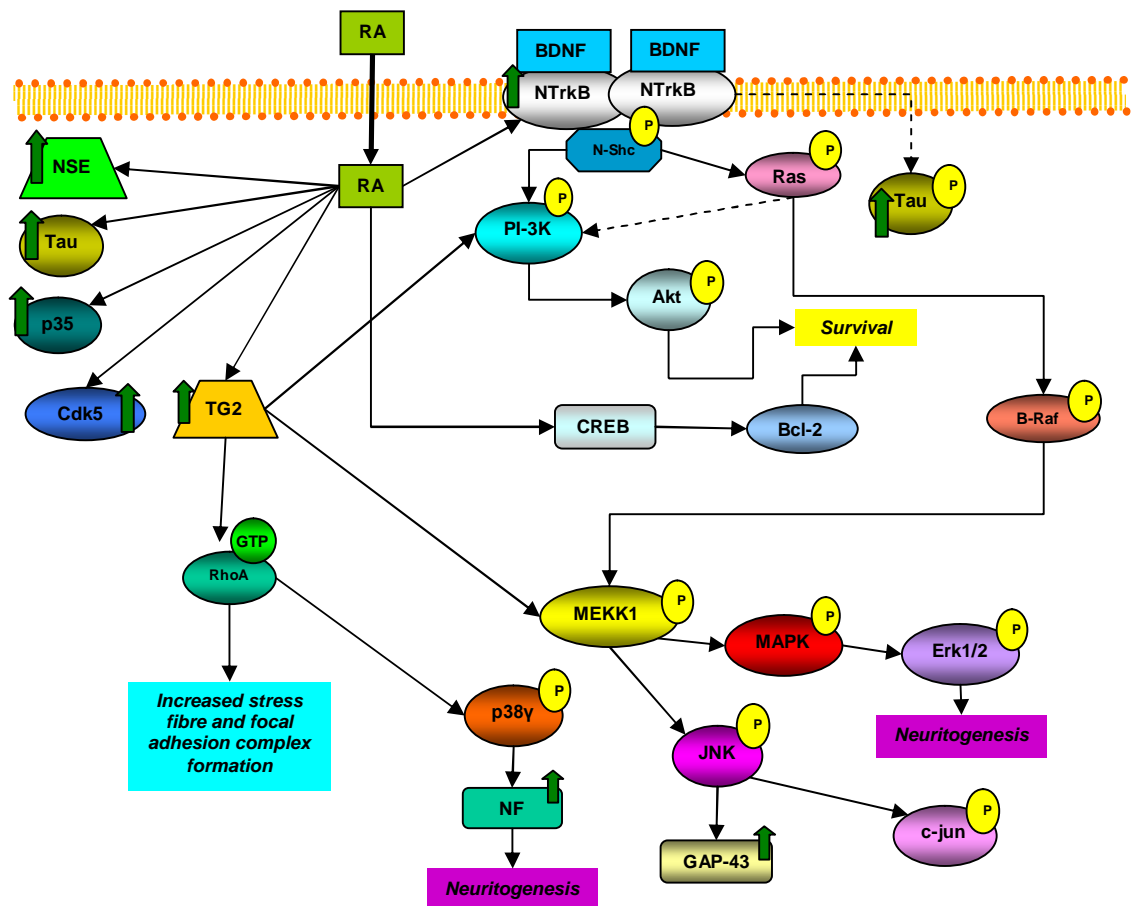


Figure 4.1 Schematic representation summarising the effect of RA and RA/BDNF induced differentiation of SH-SY5Y neuroblastoma cells on intracellular signalling cascades promoting cell survival and neuritogenesis. Arrows indicate protein upregulation. RA treatment results in the upregulation of protein expression and activity of tissue transglutaminase (TG2), which activates RhoA by transamidation which in turn results in increased stress fibre and focal adhesion complex formation, and the activation of p38 γ MAP kinase resulting in increased neurofilament (NF) protein expression and neuritogenesis (Singh et al, 2003). TG2 also activates Erk1/2 and JNK, resulting in JNK-induced c-jun phosphorylation and GAP-43 protein expression (Cheung et al, 2009, Singh et al, 2003). TG2 also activates MEK1 and MAPK, resulting in MEK1-induced MAPK phosphorylation and Erk1/2 protein expression (Cheung et al, 2009, Singh et al, 2003). Additional proteins upregulated by RA treatment include Neuron Specific Enolase (NSE) (Cheung et al, 2009, Pahlman et al, 1984), Bcl-2 (Feng & Porter, 1999), Tau, p35, Cdk5 (Jämsä et al 2004) and Neurotrophic Tyrosine Kinase Receptor B (NTrkB; Encinas et al 1999, 2000). Binding of BDNF to NTrkB facilitates receptor dimerization and activation by autophosphorylation (reviewed by Hu et al 2008) which in turn activates signalling cascades including Ras-MAPK pathway and the phosphatidylinositol-3-OH kinase (PI3-K)-Akt pathway responsible for neuritogenesis and cell survival respectively (Encinas et al 1999, reviewed in Hu et al 2008). RA/BDNF treatment also results in increased levels and phosphorylation of Tau protein (Jämsä et al, 2004).

4.1.2. The role of complex I and the proteasome in protein conformation diseases

Many neurodegenerative diseases are characterised by the presence of intra- and extra-cellular proteinaceous inclusions. Due to a general decline in the activity of protein degradative pathways, energy production and a build-up of oxidatively damaged proteins and organelles, ageing neurons may be particularly susceptible to problems with protein processing (reviewed by Robinson, 2008).

Numerous studies have suggested that inclusions or aggresomes in neuronal cells may be a protective mechanism since the inhibition of aggresome or inclusion formation often leads to increased apoptotic cell death (Bjorkoy et al, 2005, Hasegawa et al, 2004, Rideout et al, 2005, Tanaka et al, 2004). Aggresomes were first described by Johnston et al (1998) in human embryonic kidney 293 (HEK293) cells expressing mutant forms of integral membrane proteins that do not fold correctly, aggregates of which accumulate following either proteasome inhibition or over-expression. Aggregates of misfolded proteins were transported to the MTOC where they were surrounded by a “cage” of vimentin filaments. Ultra-structural analysis of aggresomes revealed that they contained a region of electron-dense particles surrounded by a fibrous region containing individual filaments of 8-10 nm in diameter. Frequently mitochondria and vesicular bodies appeared to be trapped in the filamentous region (Johnston et al, 1998). This description of aggresomes is reminiscent of LBs and has led to the hypothesis that LBs and proteinaceous inclusions in other neurodegenerative diseases may be formed in an aggresome-like process (McNaught et al, 2002, reviewed by Olanow et al, 2004).

Proteasome inhibition has previously been shown to result in the production of ubiquitinated protein aggregates in differentiated PC12 cells, some of which are also immunoreactive for α -synuclein. It is noteworthy that despite an increase in α -synuclein aggregation with proteasome inhibition, the actual levels of α -synuclein detected by Western blotting were similar to those in untreated cells (Rideout et al, 2001). A number of other studies have also employed the use of proteasome inhibitors to induce inclusion formation providing evidence for a role of defects in the UPS in protein aggregation (Fornai et al, 2003, Ito et al, 2002, Rideout et al, 2005, Rideout & Stefanis, 2002).

Mitochondrial Complex I inhibition by MPTP/MPP⁺ has been extensively used in experimental models of PD (Bezard et al, 1997, Caneda-Ferron et al, 2008, De Girolamo &

Billett, 2005, Gupta et al, 1986, Zeng et al, 2006). Continuous infusion of MPTP and MPP⁺ in mouse and rat models respectively was able to produce proteinaceous inclusions that resemble Lewy bodies (Fornai et al, 2005, Yazdani et al, 2006). Inclusions were also produced in a mouse model in which mice were treated chronically with MPTP and probenecid - which inhibits the clearance of MPTP (Meredith et al, 2002). Chronic exposure of rat mesencephalic cultures to MPP⁺ resulted in the occurrence of fine α -synuclein granules which when combined with lactacystin caused the formation of α -synuclein positive inclusions (Sawada et al, 2004).

p62/SQSTM1 has been identified in the cytoplasmic inclusions of a number of human diseases in both the liver and brain including Lewy bodies in PD and neurofibrillary tangles in AD (Nakaso et al, 2004, Zatloukal et al, 2002). Inclusions containing p62 and ubiquitin were also produced in a mouse model of amyotrophic lateral sclerosis (Gal et al, 2007) and a cell model expressing mutant huntingtin (Bjorkoy et al, 2005).

In NGF differentiated PC12 cells, proteasome inhibition lead to the formation of an aggresome-like structure located in the perinuclear region that was immunoreactive for p62, ubiquitin and γ -tubulin. Aggregate formation was dependent on the expression of p62 since downregulation of p62 expression with anti-sense oligonucleotides decreased the number of cells with p62-positive aggregates (Nakaso et al, 2004). Several studies have shown that proteasome inhibition leads to an upregulation in the expression of p62 at both the protein and mRNA level and as such in the number and size of p62 bodies (Bjorkoy et al, 2005, Nakaso et al, 2004).

Recently it has been suggested that aggregate-containing cells may induce macroautophagy to clear aggregates (Rideout et al, 2004). The structure of p62 supports the hypothesis that it plays a role in targeting polyubiquitinated protein aggregates for degradation by macroautophagy as it contains an N-terminal LC3 binding domain and a C-terminal ubiquitin binding domain (Bjorkoy et al, 2005, Pankiv et al, 2007). Using a double tag strategy that enabled them to follow labelled LC3 and p62 through the acidification process during autophagosome and lysosome fusion in live cells, Pankiv et al (2007) were able to show that even large p62 bodies were degraded by autophagy and that this degradation was inhibited by treatment with Bafilomycin A1. Knockdown of p62 expression using siRNA reduced the amount of ubiquitinated proteins within autolysosomes suggesting that p62 is required for the degradation of ubiquitinated aggregates by autophagy (Pankiv et al, 2007).

4.1.3. Aims of this Chapter

In this work the effects of RA and RA/BDNF induced differentiation of SH-SY5Y cells on the expression of cytoskeletal elements will be evaluated in more detail. Despite the large volume of literature available, some aspects of RA and RA/BDNF induced differentiation are still controversial, such as the effect of differentiation on the expression of NFs. Some studies suggest increased NF expression (Singh et al 2003) while others report either no change (Cheung et al, 2009, Encinas et al, 2000) or decreased expression (Encinas et al, 2000). In addition the effects of differentiation on the expression of markers of differentiation such as TG2, NTrkB and Bcl-2 will be revisited.

The main aim of this chapter is to establish whether the inhibition of complex I and/or the proteasome could result in the formation of inclusions resembling aggresomes in SH-SY5Y neuroblastoma cells. The inclusion-producing cell model could then be used to clarify whether neurofilaments play a role in aggresome or inclusion formation. Inclusions are produced more readily in differentiated SH-SY5Y cells than in proliferating cells (Hasegawa et al, 2004, Lee et al, 2004, reviewed by Robinson, 2008), since differentiated cells are not able to minimize inclusions by distributing protein aggregates between daughter cells. Terminally differentiated cells are also more prone to the accumulation of oxidatively damaged proteins and as such, protein degradation pathways such as the UPS play an essential role in the clearance of damaged proteins. Therefore, to establish an inclusion-producing cell model, SH-SY5Y neuroblastoma cells were differentiated using a modified differentiation protocol derived from the protocol described by Encinas et al (2000).

4.2. Results

4.2.1. Differentiation of SH-SY5Y cells with Retinoic acid and Brain Derived Neurotrophic Factor

4.2.1.1. Cellular morphology of RA/BDNF differentiated cells

Phase contrast images of SH-SY5Y cells induced to differentiate with RA or BDNF following RA pre-treatment are shown in Figure 4.2. Proliferating cells have a flattened appearance with few cellular processes. On treatment with 10 μ M RA, cells become more elongated with a greater number of cellular processes. There does not seem to be much difference in the appearance of cells treated with RA for 5 days or for 8 days. Cells treated with BDNF following RA pre-treatment have more compact cell bodies with longer cellular processes. For RA/BDNF differentiated cells, cellular processes are more numerous and appear to form an interconnecting network.

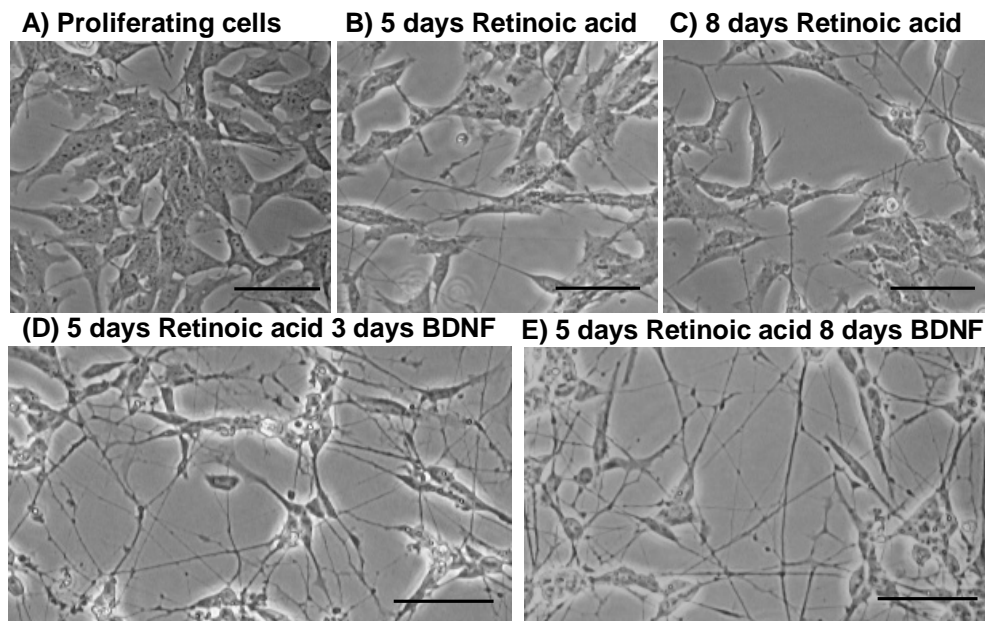


Figure 4.2 Phase contrast images of SH-SY5Y cells differentiated using retinoic acid (RA) or RA followed by Brain Derived Neurotrophic Factor (BDNF). Cells were either (A) proliferating, (B) differentiated for 5 days with 10 μ M RA, (C) differentiated for 8 days with 10 μ M RA, (D) differentiated for 5 days with 10 μ M RA followed by 3 days with 50 ng/ml BDNF or (E) differentiated for 5 days with 10 μ M RA followed by 8 days with 50 ng/ml BDNF. Scale bar represents 100 μ m.

Morphological characteristics were quantified by measuring the length of axonal processes and the diameter of cell bodies and by counting the number of cells with axon-like processes (summarized in Table 4.1). Axon-like processes were defined as being at least 2.5 times longer than the diameter of the cell body. The figures were obtained from phase contrast images of SH-SY5Y cells grown in T25 flasks and taken on an inverted microscope coupled to a digital camera. Cells were viewed at 100 x magnification using the 10 x objective. Images were analysed using QWin software from Leica to measure axon and cell body length. From the same images the percentage of cells with axon-like processes was determined by counting the number of cells in the field of view and then counting the number of cells with processes that have a length of at least 2.5 times the diameter of the cell body.

The cell body of cells differentiated with 10 μ M RA for 8 days ($38.8 \pm 2.2 \mu\text{m}$) is significantly larger ($p < 0.012$, T-Test) than that in proliferating SH-SY5Y cells ($30.3 \pm 2.6 \mu\text{m}$). In cells that are differentiated with RA followed by BDNF the cell bodies are significantly smaller (around 20 μm) than the cell bodies of proliferating cells (Table 6.1). The mean length of processes does not differ significantly between proliferating cells and cells induced to differentiate using RA. For cells induced to differentiate using BDNF following 5 days RA pre-treatment, the length of cell processes is significantly greater than in proliferating cells ($58.9 \pm 6.9 \mu\text{m}$). For cells treated with BDNF for 3 days the mean length of processes was $106.1 \pm 13.8 \mu\text{m}$ ($p < 0.006$, T-Test) and for cells treated with BDNF for 8 days it was $108.4 \pm 22.6 \mu\text{m}$ ($p < 0.022$, T-Test).

In proliferating cells, the percentage of cells with processes long enough to be 'axonal-like' (Table 6.1) is $9.0 \pm 3.2 \%$ of cells. This percentage increased with cells induced to differentiate with RA but the increase was only significant in cells treated for 5 days with RA ($20.1 \pm 5 \%$; $p < 0.031$, T-Test). In cells treated with BDNF following RA pre-treatment the percentage of cells with axon-like processes increased dramatically; for cells treated with BDNF for 3 days, $62.5 \pm 1.4 \%$ of cells had axons ($p < 0.0001$, T-Test) and for cells treated for 8 days with BDNF, $56.8 \pm 12.8 \%$ of cells had axons ($p < 0.003$, T-Test).

Table 4.1 Assessment of morphological characteristics to compare the efficiency of differentiation using 10 μ M Retinoic Acid (RA) or 50 ng/ml Brain Derived Neurotrophic Factor (BDNF) after 10 μ M RA pre-treatment. Morphological characteristics compared include mean cell body diameter, mean length of cellular processes and the percentage of cells with processes long enough to be defined as axons¹ (n = 3).

	<i>Diameter of the Cell body (μm)</i>	<i>SD</i>	<i>P (T-test, compared to mitotic)</i>	<i>Mean length of processes (μm)</i>	<i>SD</i>	<i>P (T-test, compared to mitotic)</i>	<i>Number of cells</i>	<i>Number of cells with axons¹</i>	<i>Percentage of cells with axons¹ (%)</i>	<i>SD</i>	<i>P (T-test, compared to mitotic)</i>
<i>Proliferating cells</i>	30.3	2.6		58.9	6.9		178 \pm 32	16 \pm 6.1	9.0	3.2	
<i>5 days RA</i>	29.7	0.6	0.698	75.7	9.3	0.066	147.7 \pm 22.3	30 \pm 10.5	20.1*	5	0.031
<i>8 days RA</i>	38.8*	2.2	0.012	71.2	16.3	0.295	84.3 \pm 12.7	12 \pm 6.6	14.1	6.9	0.308
<i>5 days RA/ 3 days BDNF</i>	22.1**	0.9	0.006	106.1**	13.8	0.006	143.7 \pm 49.7	89.3 \pm 21	62.5***	1.4	0.0001
<i>5 days RA/ 8 days BDNF</i>	19.5***	1.3	0.003	108.4*	22.6	0.022	138.7 \pm 75.7	72.3 \pm 27.1	56.8***	12.8	0.003

¹Axons are defined as processes that are at least 2.5 times longer than the diameter of the cell body

Two-sample T-test, compared to mitotic *p < 0.05, **p < 0.01, ***p < 0.005 (n = 3)

4.2.1.2. The effect of RA/BDNF-induced differentiation on mRNA copy number and protein levels

4.2.1.2.1. The Validation of the use of GAPDH as a house-keeping gene for Quantitative Real-Time PCR results

GAPDH was used as a loading control for quantitative real-time PCR experiments determining the effect of RA-induced and RA/BDNF-induced differentiation on the mRNA copy number of several genes including the neurofilament subunits, α -1 tubulin, the motor proteins (*dynein light intermediate chain* and *kinesin 5C*), tissue transglutaminase (*TG2*), *Bcl-2* and a proteasome ATPase subunit (*PSMC1*) knocked-down in a PD mouse model (Bedford et al, 2008).

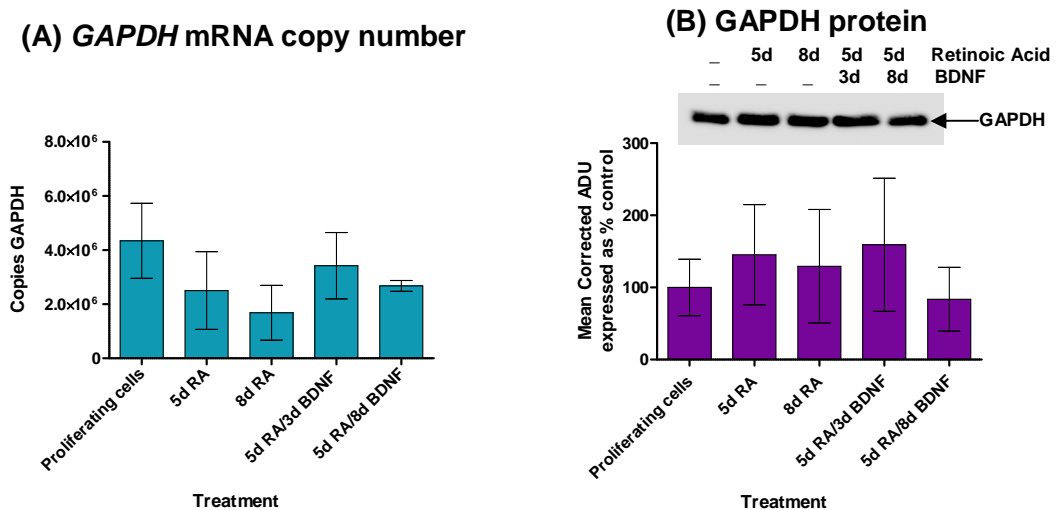


Figure 4.3 The effect of RA and RA/BDNF-induced differentiation of the expression of GAPDH in SH-SY5Y cells.

(A) The copy number of *GAPDH* mRNA per reaction as determined by quantitative real-time PCR. There is no significant change in the levels of *GAPDH* mRNA ($n = 3$). (B) Representative Western blot of total cell extracts of SH-SY5Y cells, either proliferating or differentiated with RA or RA/BDNF probed with anti-GAPDH (1:1000) and plot summarising the results of densitometric analysis of Western blots normalised for protein loading against total protein. There was no significant change in the levels of GAPDH in total cell extracts of RA and RA/BDNF differentiated cells compared to levels in total cell extracts from proliferating cells. Error bars represent standard deviation ($n = 3$).

The copy number of *GAPDH* mRNA (Figure 4.3 A) decreased slightly after RA treatment (but this decrease is not significant) and was similar in RA/BDNF differentiated cells to that in proliferating cells. The levels of GAPDH protein (Figure 4.3 B and C) in total cell extracts of proliferating cells and cells differentiated with either RA or RA/BDNF, investigated by

Western blotting with anti-GAPDH (1:1000), remained relatively similar in proliferating, RA differentiated and RA/BDNF differentiated cells.

To validate the use of *GAPDH* as a loading control, the copy number of *GAPDH* mRNA was compared to mRNA copy number of two other house-keeping genes, β -actin and ribosomal *L32* (Figure 4.4). All three show a similar pattern of expression with a lower copy number in cells treated with RA for 5 d but for *L32* the decrease was statistically significant ($p < 0.05$).

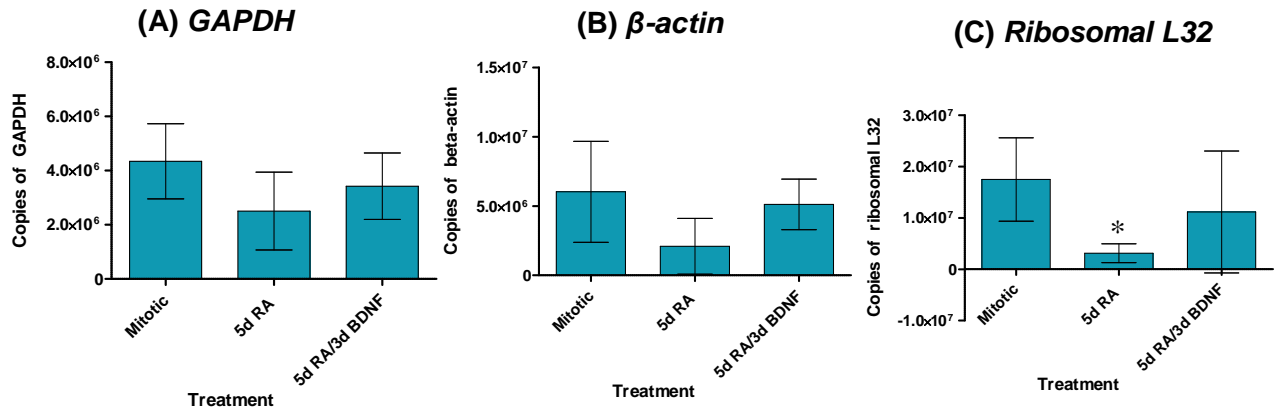


Figure 4.4. A comparison of the mRNA copy number of *GAPDH*, β -actin and *L32*.

Plots displaying the results of qRT-PCR of (A) *GAPDH*, (B) β -actin and (C) ribosomal *L32* from cDNA preparations from SH-SY5Y cells either proliferating or induced to treated the 10 μ M retinoic acid (RA) for 5 days or 50 ng/ml Brain Derived Neurotrophic Factor (BDNF) for 3 days following 5 days pre-treatment with 10 μ M RA (RA/BDNF). There was a significant decrease in mRNA copy number of *L32* compared to copy number in mitotic cells following 5 days RA treatment. Error bars represent standard deviation (* $p < 0.05$, T-Test; $n = 3$).

4.2.1.2.2. Effect of RA/BDNF-induced differentiation on the expression of *NTrkB*, *TG2* and *Bcl-2*

Both *NTrkB* and *TG2* mRNA expression was increased following RA and RA/BDNF induced differentiation but *Bcl-2* mRNA copy number remained unchanged after differentiation (Figure 4.5 A-C).

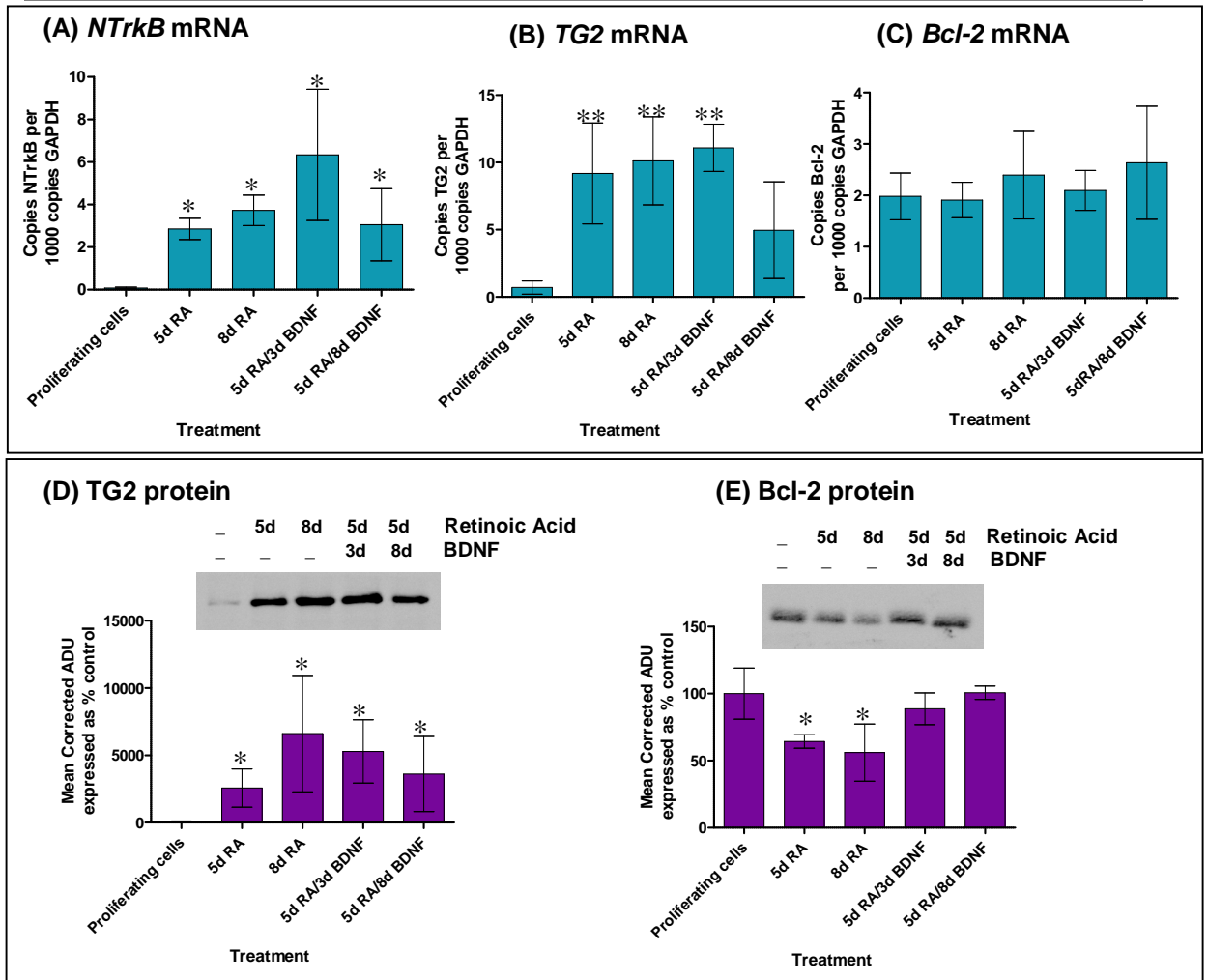


Figure 4.5 The expression of Neurotrophic Tyrosine Kinase Receptor B (*NTrkB*), tissue transglutaminase (*TG2*) and *Bcl-2* in SH-SY5Y cells following differentiation with 10 μ M Retinoic acid (RA) or 10 μ M RA and 50 ng/ml Brain Derived Neurotrophic Factor (BDNF).

The copy number of (A) *NTrkB*, (B) *TG2* and (C) *Bcl-2* mRNA was determined by qRT-PCR and expressed per 1000 copies *GAPDH*. Representative Western blots of total cell extracts from proliferating cells, RA and RA/BDNF differentiated cells probed with (D) anti-*TG2* (cub, 1:1000) and (E) anti-*Bcl-2* (1:1000) accompanied by plots summarising the results of densitometric analysis of Western blots for each protein. Error bars represent standard deviation (n = 3). There was a significant increase in *NTrkB* mRNA copy number and the levels of *TG2* mRNA and protein (One-way ANOVA; *p < 0.05, **p < 0.005) with differentiation. There was a significant decrease in *Bcl-2* protein following 5 d (two-tailed T-Test, p < 0.05; n = 3) and 8 d (one-tailed T-Test; p < 0.05, n = 3) RA treatment.

Probing Western blots with specific antibodies provided discrete binding profiles for *TG2* (Figure 4.5 D) and *Bcl-2* (Figure 4.5 F) but the signals for *NTrkB* were smeared (results not shown). All treatments resulted in an increase in *TG2* protein levels but *Bcl-2* protein levels were decreased with RA treatment and unchanged (compared to proliferating cells) in RA/BDNF treated cells.

4.2.1.2.3. Effect of RA/BDNF-induced differentiation on the expression of Cytoskeletal Proteins

All differentiation treatments reduced the copy number of *NF-H* mRNA but only RA treatment reduced *NF-M* and *NF-L* mRNA levels (Figure 4.6 A, C, E). In contrast protein levels of NF-H (Figure 4.6 B), NF-M (Figure 4.6 D) and NF-L (Figure 4.6 F) were generally unaffected by differentiation, other than an increase in NF-H levels with 8 d RA treatment and a decrease in NF-M levels with 5d RA/3d BDNF treatment.

The effect of the two differentiation protocols on the levels of phosphorylated NF-H and NF-M was investigated by immunoprobng Western blots with phosphorylation-specific antibodies; RT97 which recognises hyper-phosphorylated NF-H (Figure 4.7 A), associated with a more mature phenotype (Shea et al, 1997), smi31 which recognises both pNF-H and pNF-M (Figure 4.7 B) and RNF403 which recognises pNF-M (Figure 4.7 C). In general, the levels of phosphorylated NF-H and NF-M were reduced following differentiation, albeit not significantly.

Although the copy number of *α 1-tubulin* mRNA (Figure 4.8 A) was generally reduced with differentiation (but not significantly, with the exception of 8 d RA treatment), the levels of α -tubulin protein (Figure 4.8 B) were unaffected by RA treatment and increased with RA/BDNF treatment. However, the levels of vimentin (Figure 4.8 C) and β -actin (Figure 4.8 D) protein were unaffected by RA and RA/BDNF treatment.

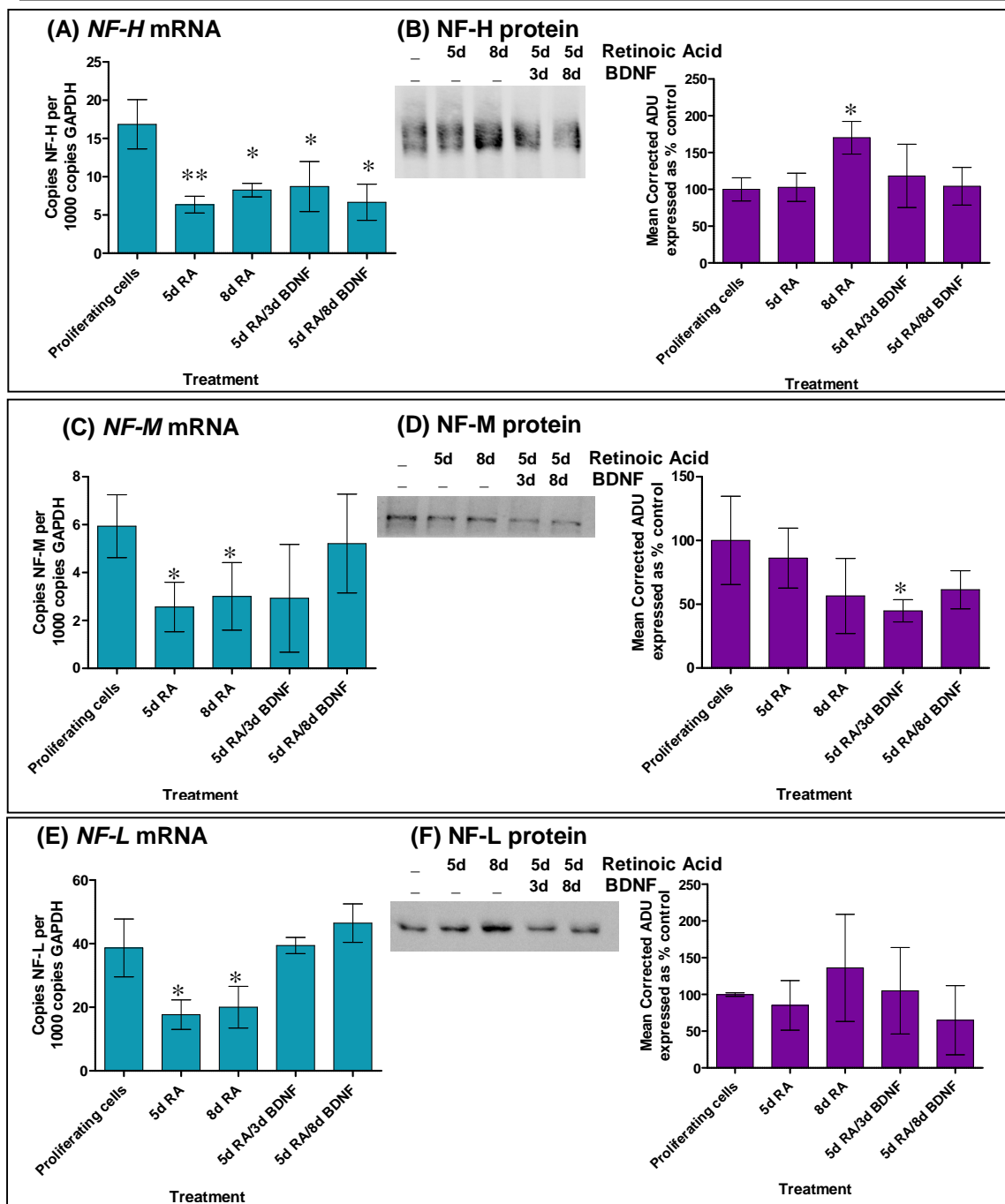


Figure 4.6 The expression of the neurofilament (NF) subunits in SH-SY5Y cells following differentiation with 10 μ M Retinoic Acid (RA) or 10 μ M RA and 50 ng/ml Brain Derived Neurotrophic Factor (BDNF).

The mRNA copy number for (A) *NF-H*, (C) *NF-M* and (E) *NF-L* was determined by qRT-PCR and expressed per 1000 copies *GAPDH*. Representative Western blots of total cell extracts probed with (B) anti-NF-H (n52, 1:2000), (D) anti-NF-M (RMO270, 1:500) and (E) anti-NF-L (DA2, 1:1000) accompanied by plots summarising the results of densitometric analysis. There was significant reduction in the mRNA copy number of *NF-H* (two-tailed T-Test; * $p < 0.05$, ** $p < 0.005$) following RA and RA/BDNF induced differentiation. *NF-M* and *NF-L* copy number was reduced after 5 d (two-tailed T-Test; * $p < 0.05$) and 8 d (one-tailed T-Test; * $p < 0.05$) RA treatment but was unaffected by RA/BDNF treatment. The levels of NF-H protein increased significantly after 8 d RA treatment compared to levels in proliferating cells. The levels of NF-M protein decreased significantly after 5 d RA/3d BDNF induced differentiation (Two-tailed T-Test; $p < 0.05$). Error bars represent standard deviation ($n = 3$).

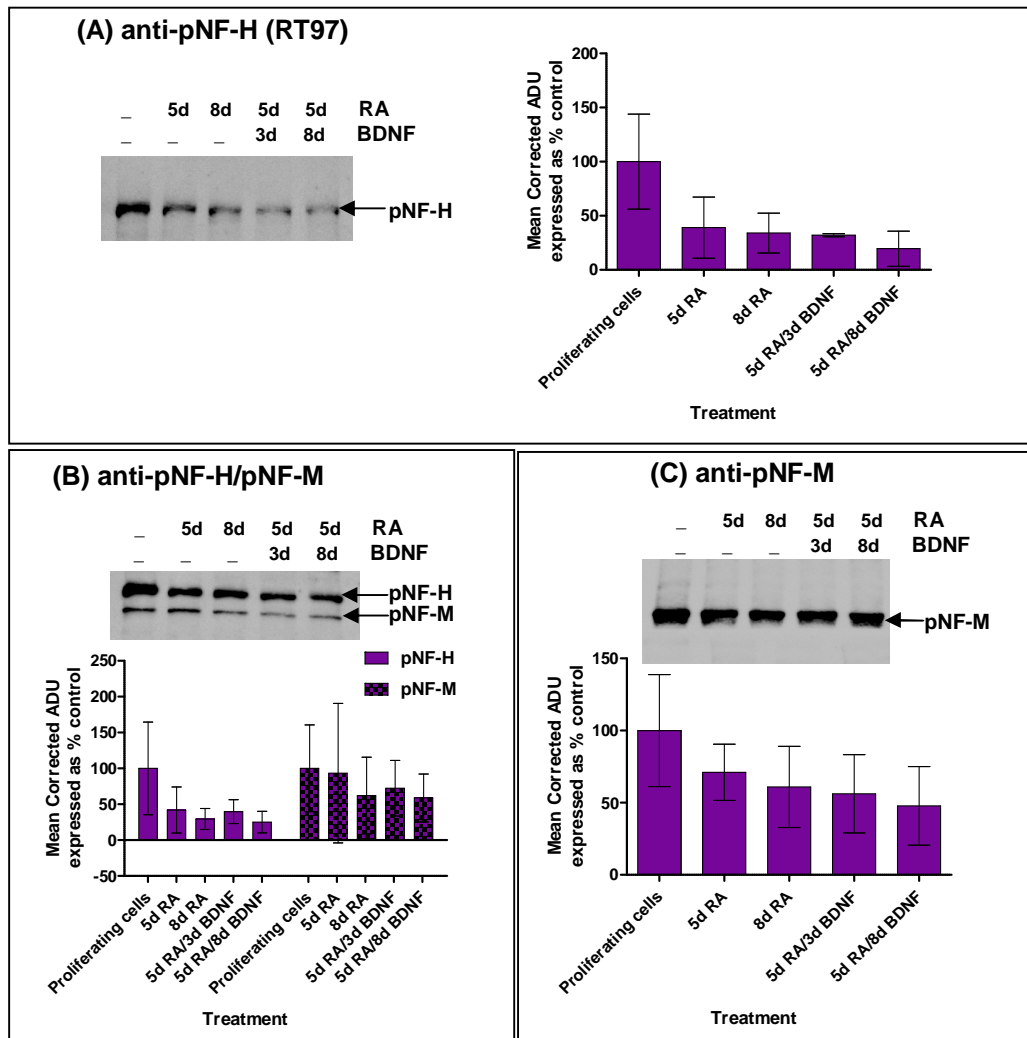


Figure 4.7 Assessment of the effect of differentiation with 10 μ M retinoic acid (RA) or 10 μ M RA and 50 ng/ml Brain Derived Neurotrophic Factor (BDNF) on the phosphorylation of neurofilament (NF) heavy (H) and medium (M) subunits.

Representative Western blots of total cell extracts were probed with (A) anti-hyper phosphorylated NF-H (RT97, 1:50). Error bars represent range (n = 2), (B) smi31 (1:1000) recognising phosphorylated NF-H and NF-M and (C) RNF403 (1:500) recognising phosphorylated NF-M. Each Western blot is accompanied by a plot summarising the results of densitometric analyses of Western blots using AIDA software. Error bars represent standard deviation (n = 3).

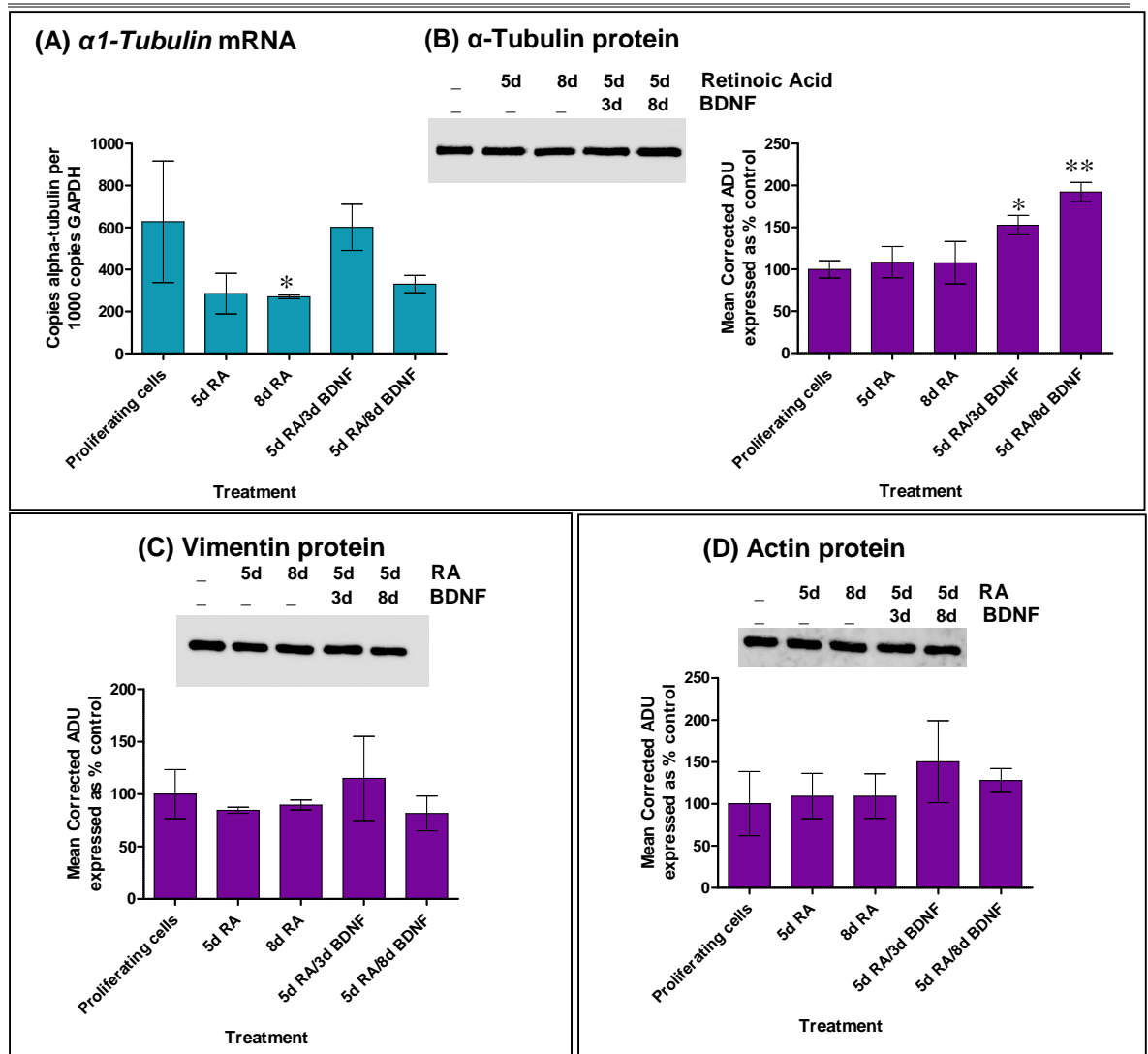


Figure 4.8 The expression of α -tubulin, vimentin and actin in SH-SY5Y neuroblastoma cells differentiated with 10 μ M retinoic acid (RA) or 10 μ M RA and 50 ng/ml Brain Derived Neurotrophic Factor (BDNF).

(A) The Copy number of α 1-tubulin mRNA expressed per 1000 copies *GAPDH* was determined by quantitative Real-Time PCR. There is a significant decrease in the copy number of α 1-tubulin mRNA following 8 days RA treatment (One-tailed T-Test; * $p < 0.05$). Representative Western blots of total cell extracts immunoprobed with (B) anti- α -tubulin (b512, 1:2000), (C) anti-vimentin (RV202, 1:5000) or (D) anti-actin (1:1000) accompanied with plots summarising the results of densitometric analysis of Western blots. There is a significant increase in the levels of α -tubulin protein following RA/BDNF induced differentiation (One-way ANOVA, Bonferonni's posttest, * $p < 0.05$, ** $p < 0.005$) but no significant change in the levels of vimentin or actin protein following RA and RA/BDNF induced differentiation. Error bars represent standard deviation ($n = 3$).

4.2.1.2.4. Effect of RA/BDNF-induced differentiation on Kinesin 5C, Dynein Light Intermediate Chain and the Proteasome ATPase PSMC1

Although the copy number of *kinesin 5C* (*KIF5C*) mRNA (Figure 4.9 A) was unaffected by RA and RA/BDNF treatment, the levels of kinesin 5C protein (Figure 4.9 B) were increased following RA/BDNF treatment. A similar increase in protein levels (seen in two independent experiments) was observed for kinesin 5 A (Figure 4.9 C) - a possible NF motor (Xia et al, 2003). Despite an increase in the mRNA copy number of *Dynein Light Intermediate Chain* (Figure 4.9 D) in cells treated with RA or BDNF for 8 d, the levels of dynein light intermediate chain protein were unaffected by differentiation (Figure 4.9 E).

Due to the importance of efficient protein clearance systems in terminally differentiated cells (Ardley et al, 2003, reviewed in Robinson, 2008) and the establishment of a PD mouse model resulting from *PSMC1* knockdown (Bedford et al, 2008), the effect of RA and RA/BDNF induced differentiation on *PSMC1* expression was investigated. The copy number of *PSMC1* mRNA (Figure 4.10 A) and protein (Figure 4.10 B) was generally unaffected by differentiation, with the exception of increased mRNA levels in cells treated with BDNF for 8 d.

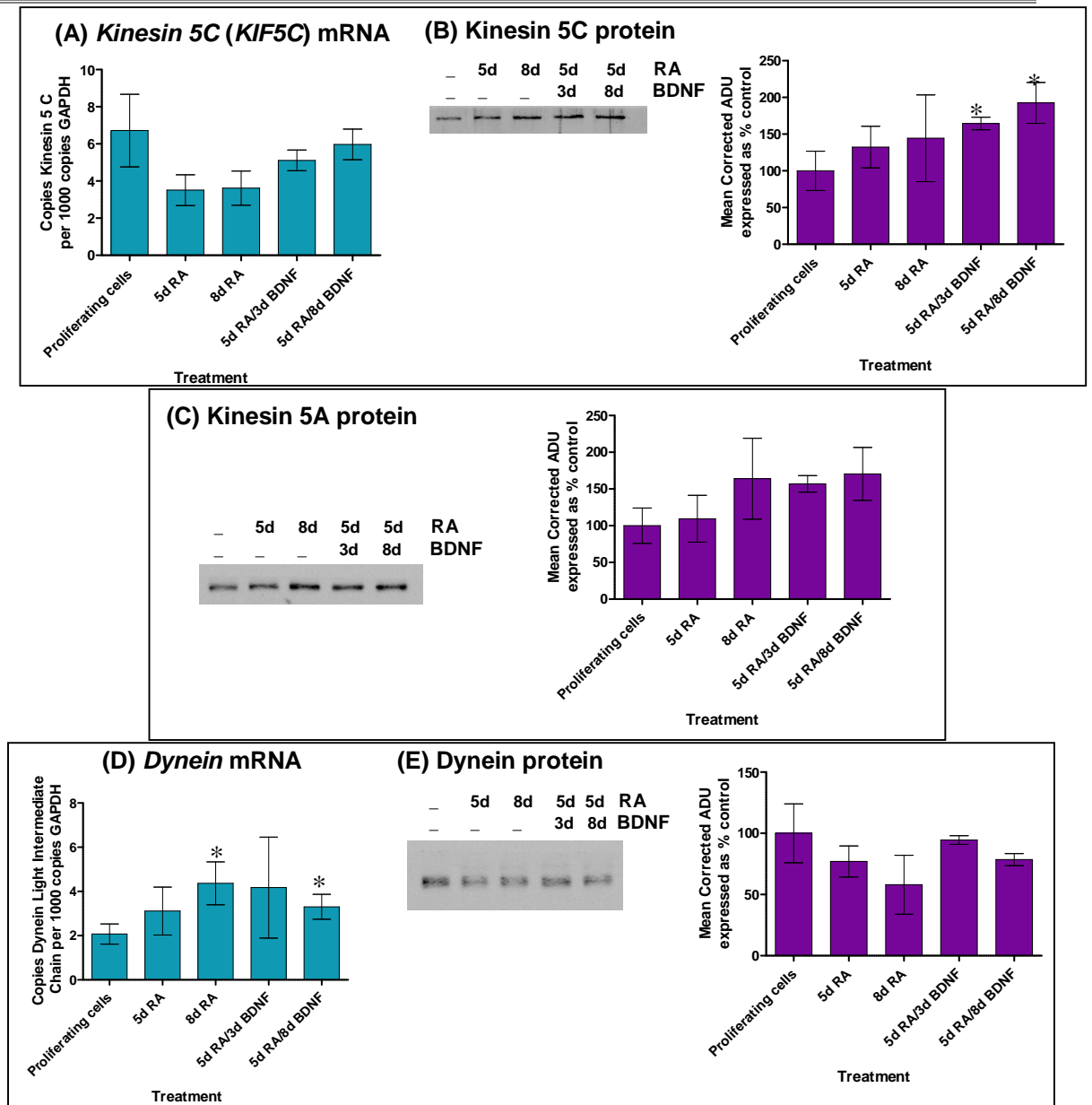


Figure 4.9 The expression of Kinesin 5C, Kinesin 5A and Dynein Light Intermediate Chain in SH-SY5Y cells differentiated with 10 μ M retinoic acid (RA) or 10 μ M RA and 50 ng/ml BDNF.

Plots summarising the results of qRT-PCR of (A) *Kinesin 5C* mRNA and (D) *Dynein Light Intermediate Chain* mRNA expressed per 1000 copies of *GAPDH*. Representative Western blots of total cell extracts probed with (B) anti-Kinesin 5C (1:1000), (C) anti-Kinesin 5A (1:1000) and (E) anti-dynein intermediate chain (Dyn70.1, 1:1000) and plots summarising the results of densitometric analysis of Western blots. There was no significant change in mRNA copy number of Kinesin 5C but for dynein light intermediate chain there was a significant increase in copy number following 8 d RA treatment and 5d RA/8d BDNF treatment (T-Test, $p < 0.05$; $n = 3$). There was a significant increase in Kinesin 5C protein (T-Test, $p < 0.05$; $n = 3$) and an increasing trend in kinesin 5A protein ($n = 2$) following RA/BDNF induced differentiation compared to proliferating cells. There appeared to be no effect of RA and RA/BDNF induced differentiation on levels of dynein intermediate chain in total cell extracts ($n = 2$). Error bars represent SEM ($n = 3$) or range ($n = 2$).

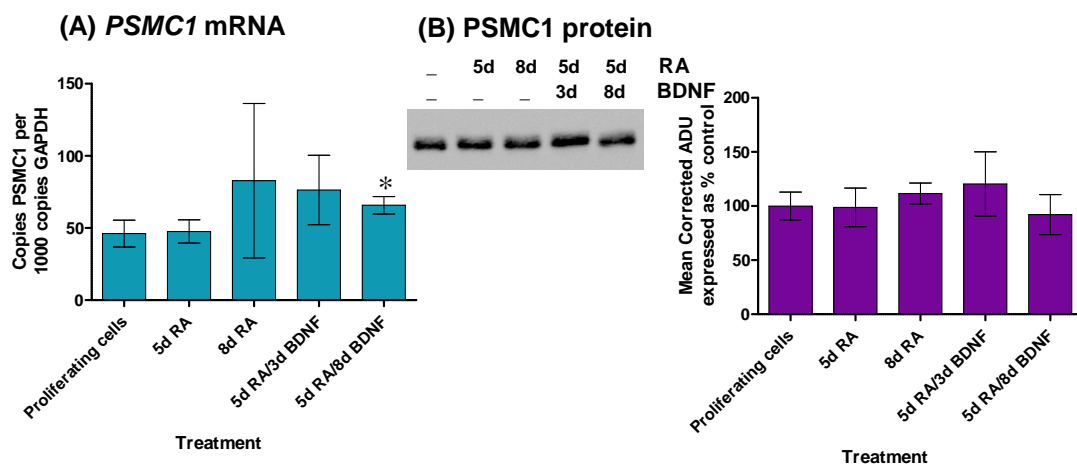


Figure 4.10 The expression of the Proteasome ATPase subunit, PSMC1, in SH-SY5Y cells following differentiation with 10 μ M retinoic acid (RA) or 10 μ M RA and 50 ng/ml Brain Derived Neurotrophic Factor (BDNF).

(A) Plot summarising the results of qRT-PCR of *PSMC1* expressed per 1000 copies of *GAPDH* revealed a significant increase in the mRNA copy number in cells treated with BDNF for 8 days (* $p < 0.05$, T-Test). (B) Representative Western blot of total cell extracts probed with anti-PSMC1 (Sigma, 1:1000) and plot summarising the results of densitometric analyses of Western blots which revealed no significant change in the levels of PSMC1 protein with RA and RA/BDNF induced differentiation. Error bars represent standard deviation ($n = 3$).

4.2.2. Inhibition of Complex I and the Proteasome in RA/BDNF differentiated SH-SY5Y cells

4.2.2.1. Effect of complex I inhibition on the viability of RA/BDNF differentiated SH-SY5Y cells

The effect of a range of MPP⁺ concentrations on the viability of RA/BDNF differentiated SH-SY5Y neuroblastoma cells was assessed morphologically and by MTT reduction after 24, 48 and 72 hours of treatment. Phase contrast images following 72 h treatment (Figure 4.11 A) revealed that 500 μ M MPP⁺ resulted in a marked reduction in the number of viable cells seen in a field of view. Similarly the results of the MTT reduction assay (Figure 4.11 B) suggested a significant concentration and time dependent reduction in cell viability (*Two-way ANOVA, $p > 0.0001$; $n = 4$), with the greatest reduction in viability occurring at the higher concentrations (1 and 2 mM) of MPP⁺ at all times and 500 μ M MPP⁺ resulting in reduced MTT reduction (58.5 ± 13.8 % of control) by 72 h.

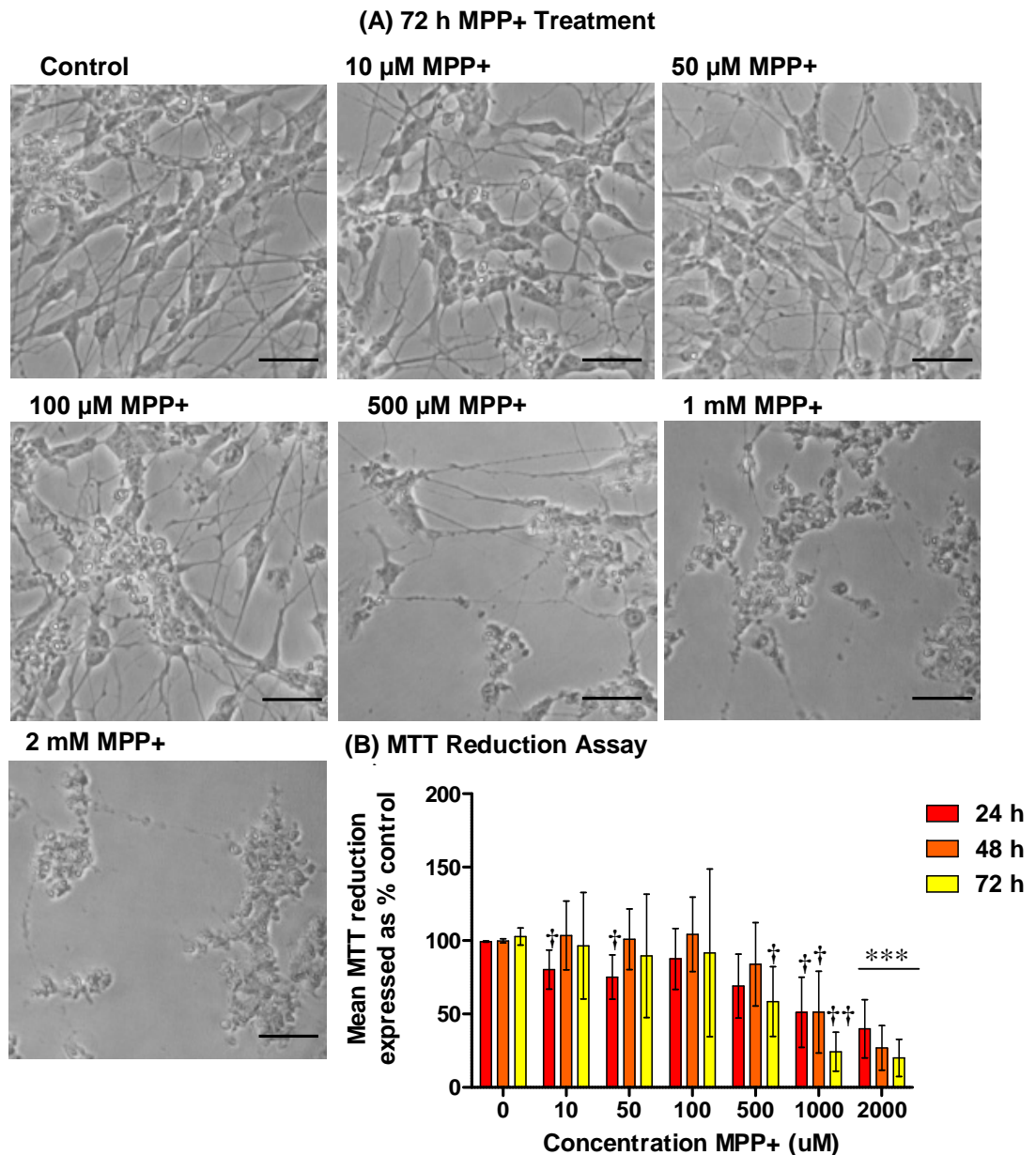


Figure 4.11 The effect of a range of MPP+ concentrations on the viability of cells differentiated with 10 μ M Retinoic Acid (RA) and 50 ng/ml Brain Derived Neurotrophic Factor (BDNF) assessed by MTT reduction assay.

(A) Phase contrast images of RA/BDNF differentiated cells treated with a range of MPP+ concentrations for 72 h. Images were taken at 100 x magnification and the scale bar represents 40 μ m. (B) Plot summarising the results of the MTT reduction assay. Mean corrected absorbance at 570 nm was expressed as a percentage of absorbance of control (untreated RA/BDNF differentiated cells). *A significant decrease in MTT reduction was observed with increasing MPP+ concentration and time (2-way ANOVA, *** $p < 0.0001$). † MTT reduction in treated cells compared to MTT reduction in control cells using Two-tailed T-Test († $p < 0.05$, †† $p < 0.005$). Error bars represent SEM (n = 4).

4.2.2.2. Effect of Complex I Inhibition and Inhibition of Proteasome on Protein Expression

The effect of complex I inhibition and the inhibition of the proteasome in RA/BDNF differentiated SH-SY5Y cells was investigated by treating cells with 500 μ M MPP+ or 10 nM epoxomicin for 24 h. In addition the importance of the proteasome during complex I inhibition was investigated by combining epoxomicin and MPP+ treatments. The effect of these treatments on the expression of a number of proteins including the cytoskeletal proteins, motor proteins, TG2, PSMC1, Bcl-2 and α -synuclein was investigated.

The copy number of *NF-L* mRNA was unaffected by MPP+ and epoxomicin treatment but was reduced following MPP+/epoxo treatment, whereas NF-L protein levels were unaffected by treatment (Figure 4.12 A and B). None of the treatments had an effect on the expression of *NF-H* mRNA and protein (Figure 4.12 C and D) whereas NF-M protein was elevated following epoxomicin and MPP+/epoxomicin treatment although mRNA expression was unaffected (Figure 4.12 E and F). Other than a slight increase in the levels of phosphorylated NF-M with MPP+ treatment seen with smi31, the levels of phosphorylated NF-M and NF-H were largely unaffected by treatment (Figure 4.13).

Treatment did not have a significant effect on the mRNA copy number of *α 1-tubulin* but α -tubulin protein levels were reduced following MPP+/epoxo treatment (Figure 4.14 A and B). Actin protein and *β -actin* mRNA levels were reduced with MPP+ treatment but unaffected by epoxo and MPP+/epoxo treatment (Figure 4.14 C and D). Similarly, the levels of γ -tubulin protein were reduced with MPP+ treatment but unaffected by epoxomicin and MPP+/epoxomicin treatment (Figure 4.14 E). The levels of vimentin protein were reduced with all treatments (Figure 4.14 F).

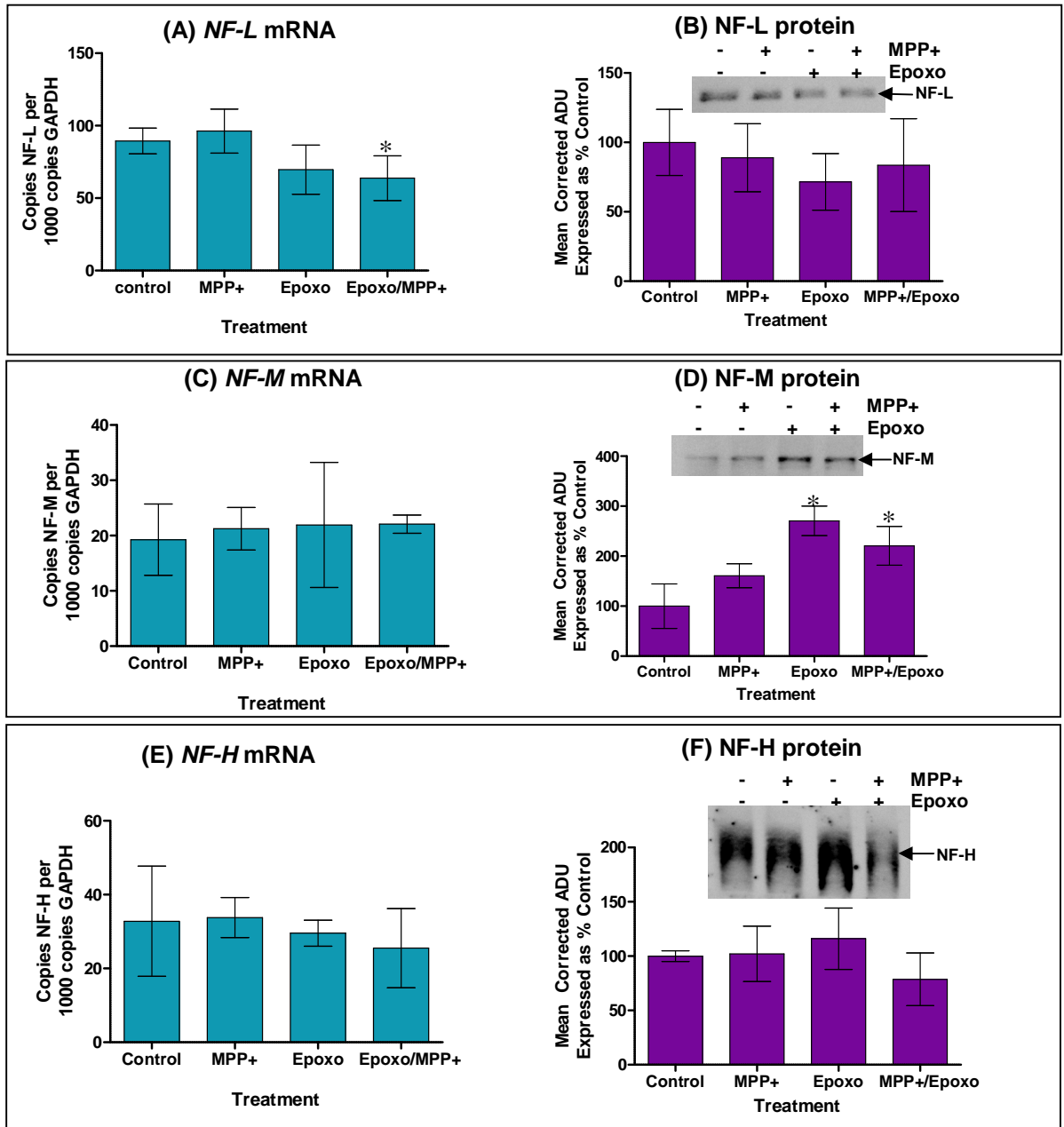


Figure 4.12 Effect of 24 h treatment with 500 μ M MPP+, 10 nM epoxomicin (epoxo) or 500 μ M MPP+ and 10 nM epoxo on the expression of the three neurofilament subunits in RA/BDNF differentiated SH-SY5Y neuroblastoma cells.

Plots summarising the results of qRT-PCR of (A) *NF-L*, (C) *NF-M* and (E) *NF-H* mRNA expressed per 1000 copies *GAPDH*. In general, treatment had no effect on the mRNA expression of the three NF subunits with the exception of a reduction in *NF-L* mRNA with MPP+/Epoxo treatment (One-tailed T-Test, * $p < 0.05$; $n = 3$). Error bars represent standard deviation. Representative Western blots of total cell extracts probed with (B) anti-NF-L (DA2, 1:1000), (D) anti-NF-M (RMO270, 1:500) and (F) anti-NF-H (n52, 1:2000) accompanied by plots summarising the results of densitometric analyses of Western blots. Treatments had no effect on the expression of NF-H ($n = 4$) and NF-L ($n = 5$) protein but an increase in NF-M protein levels was observed with epoxomicin treatment (Two-tailed T-Test, * $p < 0.05$; $n = 5$) and MPP+/epoxo treatment (One-tailed T-Test, * $p < 0.05$; $n = 5$). Error bars represent SEM.

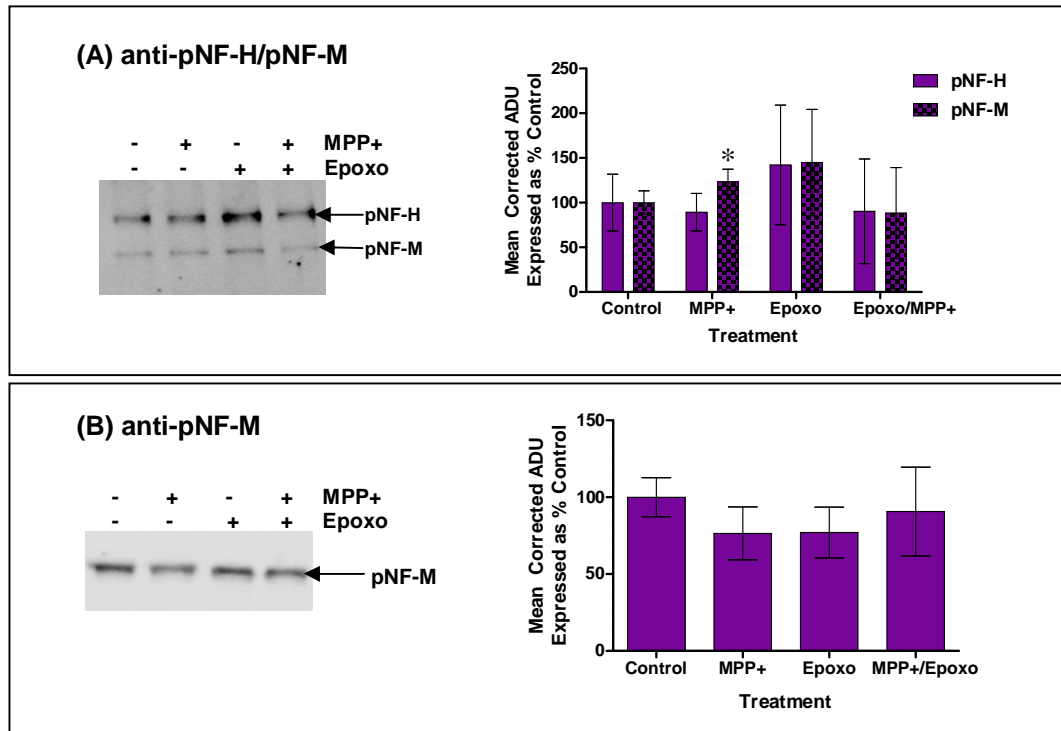


Figure 4.13 Effect of treatment of RA/BDNF differentiated SH-SY5Y neuroblastoma cells with 500 μ M MPP+, 10 nM epoxomicin (epoxo) or 500 μ M MPP+/10 nM epoxo for 24 h on the phosphorylation status of NF-H and NF-M.

Each panel contains a representative Western blot and a plot summarising the results of densitometric analyses of Western blots. (A) Densitometric analyses of Western blots probed with smi31 (1:1000) revealed that generally there was no effect of treatment on the levels of pNF-M and pNF-H except for a slight increase in levels of pNF-M with MPP+ treatment (One-tailed T-Test, $p < 0.05$; $n = 4$). Error bars represent standard deviation. (B) However, densitometric analyses of Western blots probed with RNF403 (1:1000) revealed no significant change in the levels of pNF-M in total cell extracts with treatment compared to control. Error bars represent SEM ($n = 5$).

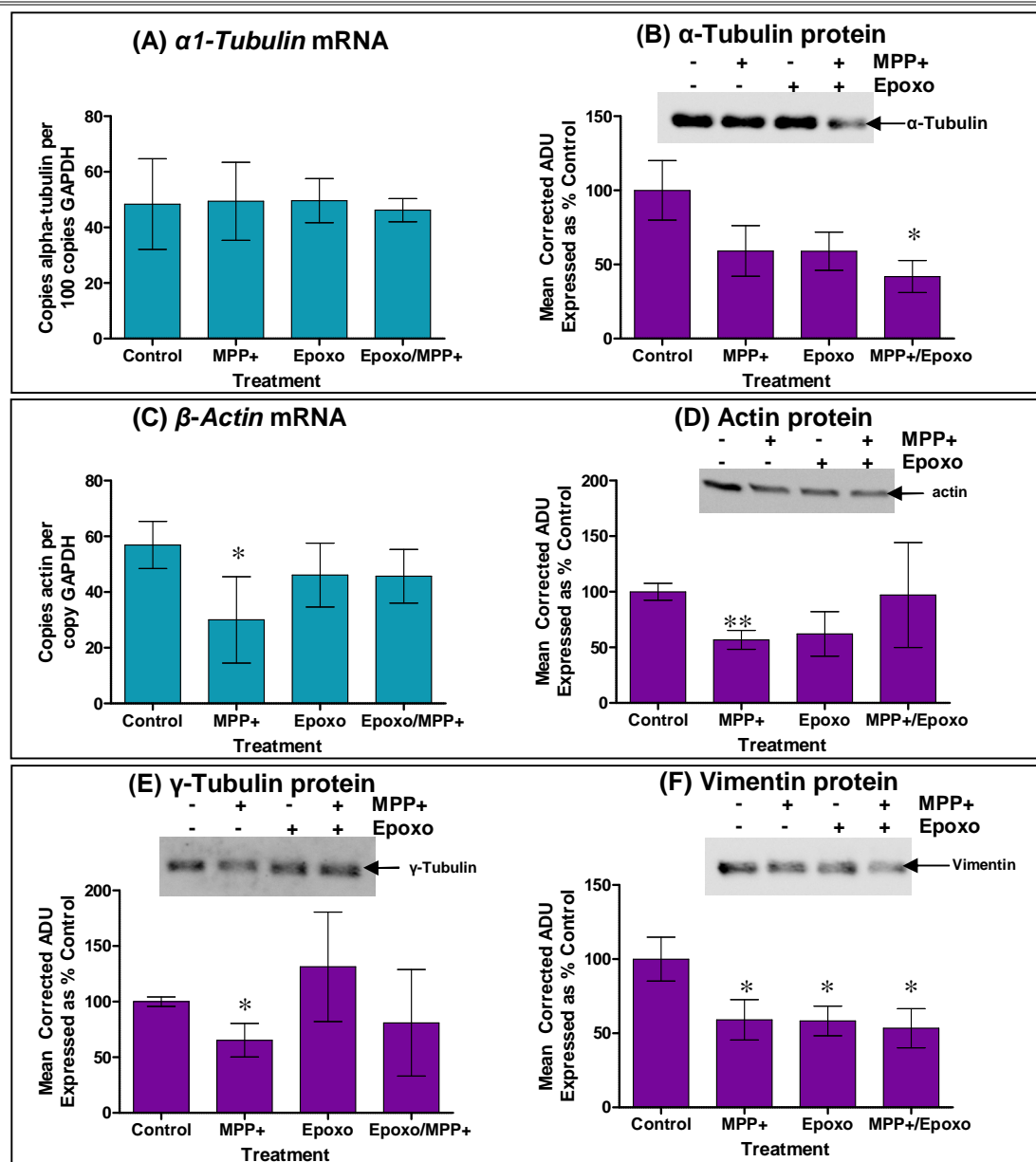


Figure 4.14 Assessment of the expression of α -tubulin, actin, vimentin and γ -tubulin following treatment of RA/BDNF differentiated SH-SY5Y cells with 500 μ M MPP+, 10 nM epoxomicin (epoxo) or 500 μ M MPP+/10 nM Epoxo for 24 h.

The mRNA copy number of (A) α 1-tubulin and (C) β -actin assessed by qRT-PCR expressed per 100 copies or per copy of GAPDH respectively. β -Actin and α 1-tubulin mRNA expression was generally unaffected by treatment except for a decrease in β -actin mRNA with MPP+ treatment (One-tailed T-Test, * p < 0.05; n = 3). Representative Western blots of total cell extracts immunoprobed with (B) anti- α -tubulin (b512, 1:2000), (C) anti-actin (1:1000), (D) anti- γ -tubulin (1:1000) and (E) anti-vimentin (RV202, 1:5000) accompanied by plots summarising the results of densitometric analyses of Western blots. A reduction in α -tubulin protein was observed following MPP+/epoxo treatment (Two-tailed T-Test, * p < 0.05, n = 5) but actin levels were largely unaffected (n = 5). The levels of γ -tubulin protein were reduced following MPP+ treatment (Two-tailed T-Test, * p < 0.05; n = 3) and vimentin levels were reduced with MPP+, MPP+/epoxo (Two-tailed T-Test, * p < 0.05; n = 5) and epoxo (One-tailed T-Test, * p < 0.05; n = 5) treatment. Error bars represent SEM when n = 5 and standard deviation when n = 3.

Kinesin 5C mRNA (Figure 4.15 A) expression was unaffected by treatment as were protein levels (Figure 4.15 B, monitored in two independent experiments), in addition *kinesin 5A* protein levels were also unchanged (Figure 4.15 C, n = 5). However the levels of dynein intermediate chain protein were reduced with all treatments (Figure 4.15 E), although mRNA copy number with treatment remained unchanged (Figure 4.15 D).

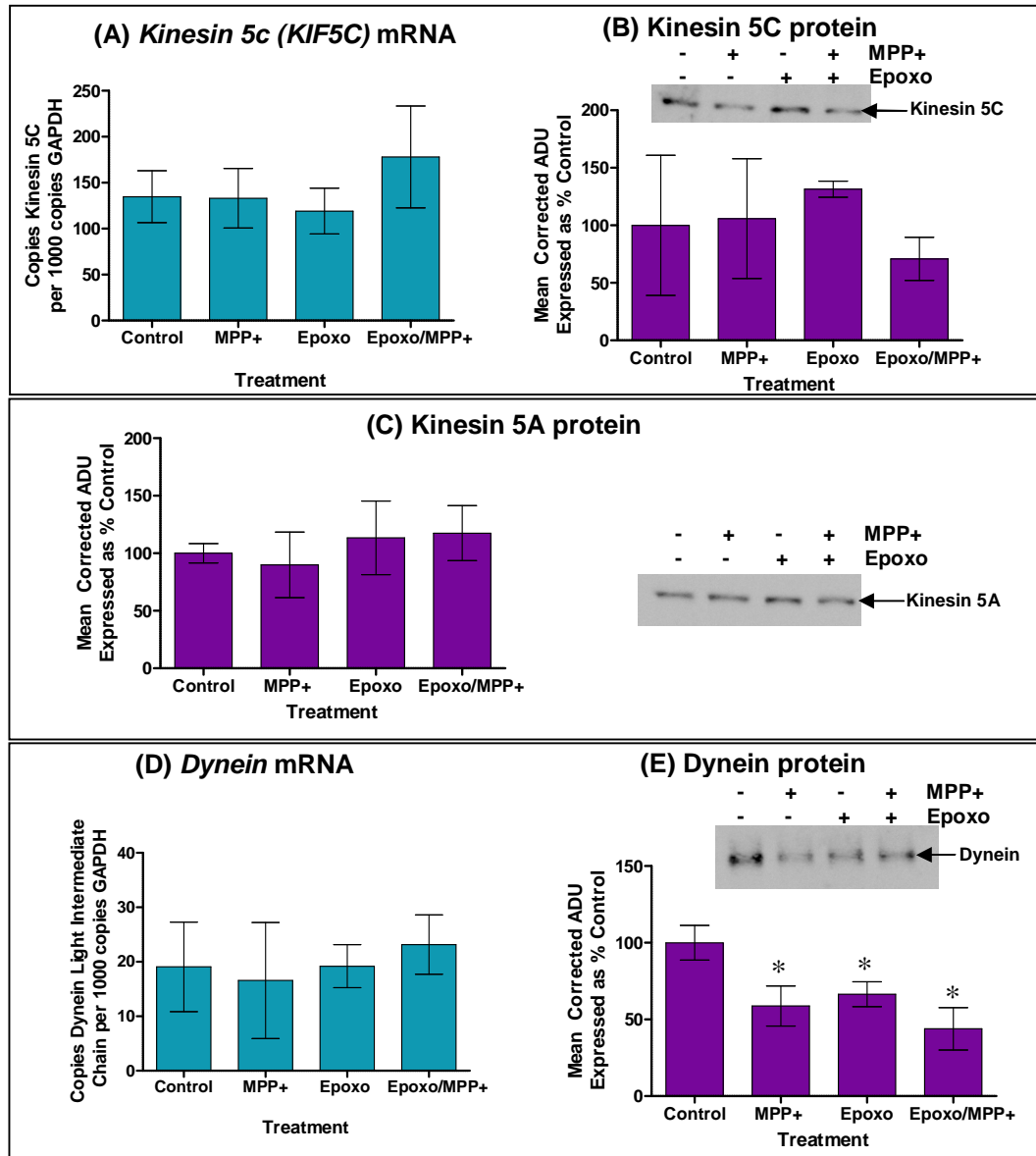


Figure 4.15 Assessment of the expression of *kinesin 5C* and *5A* *dynein light intermediate chain* in RA/BDNF differentiated SH-SY5Y cells treated with 500 μ M MPP+, 10 nM epoxomicin (epoxo) or 500 μ M MPP+/10 nM epoxo for 24 h.

The mRNA copy number of (A) *kinesin 5C* and (D) *dynein light intermediate chain* assessed by qRT-PCR and expressed per 1000 copies *GAPDH* revealed no effect of treatment on mRNA expression. Error bars represent standard deviation (n = 3). Representative Western blots of total cell extracts probed with (B) anti-*Kinesin 5C* (1:1000), (C) anti-*Kinesin 5A* (1:1000) and (E) anti-*dynein intermediate chain* (Dyn 70.1, 1:1000) and plots summarising the results of densitometric analyses of Western blots. The protein levels of *kinesin 5C* (n = 2, error bars represent range) and *kinesin 5A* (n = 5, error bars represent SEM) appeared to be unaffected by treatment but *dynein intermediate chain* protein levels were reduced with all treatments (Two-tailed T-Test, *p < 0.05; n = 5, error bars represent SEM).

Protein and mRNA expression of the proteasome ATPase subunit, *PSMC1*, was largely unaffected by treatment with MPP+, epoxo or MPP+/epoxo (Figure 4.16).

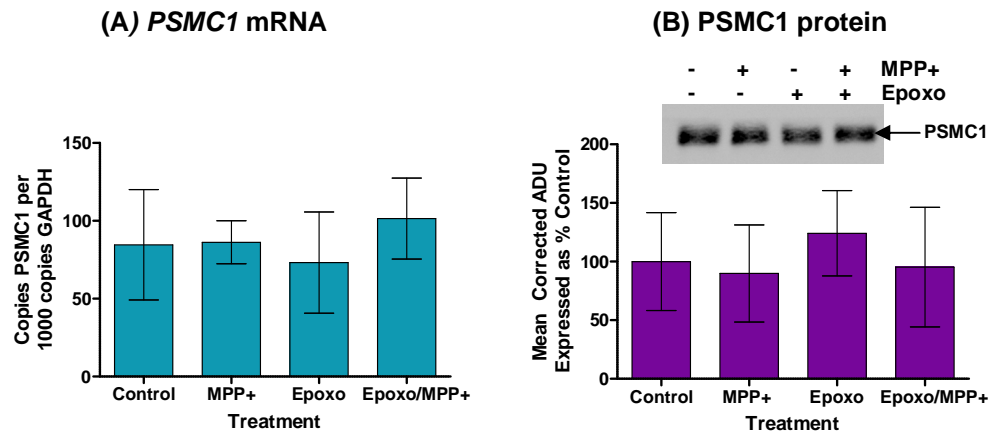


Figure 4.16 Effect of 500 μ M MPP+, 10 nM epoxomicin (epoxo) or 500 μ M MPP+/10 nM epoxo treatment of RA/BDNF differentiated SH-SY5Y neuroblastoma cells on the expression of PSMC1 (A) mRNA copy number assessed by qRT-PCR expressed per 1000 copies *GAPDH* and (B) protein by probing Western blots of total cell extracts with anti-PSMC1 (1:1000) and plot summarising the results of densitometric analyses of Western blots. There was no effect of treatment on the *PSMC1* mRNA or protein levels. Error bars represent standard deviation (n = 3).

MPP+ treatment had no effect on the expression of *TG2* mRNA and protein whereas treatment with epoxomicin reduced mRNA levels while leaving protein levels unchanged and visa versa with MPP+/epoxo treatment (Figure 4.17).

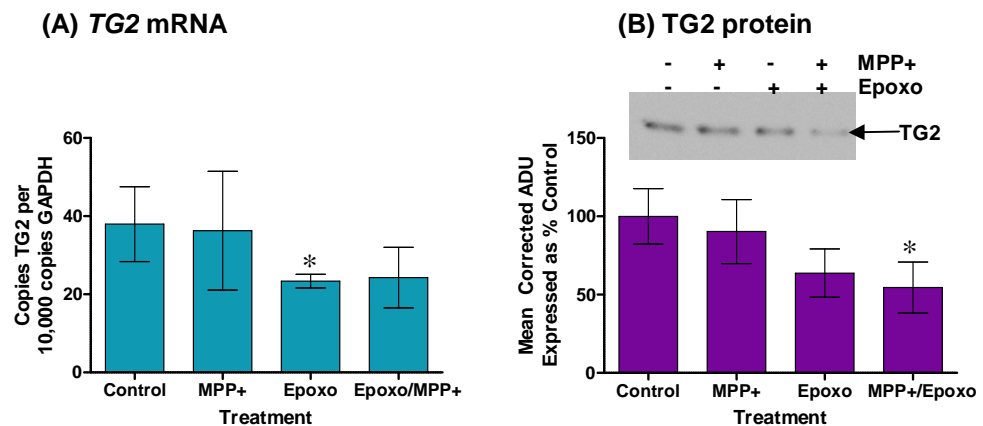


Figure 4.17 Expression of tissue transglutaminase (TG2) in RA/BDNF differentiated cells treated with 500 μ M MPP+, 10 nM epoxomicin (epoxo) or 500 μ M MPP+/10 nM epoxo for 24 h. (A) Plot summarising the results of qRT-PCR which revealed that treatment resulted in a reduction in *TG2* mRNA copy number per 10,000 copies *GAPDH* with epoxomicin treatment (One-tailed T-Test, *p < 0.05; n = 3). Error bars represent standard deviation. (B) Representative Western blot and plot summarising the results of densitometric analyses of Western blots probed with anti-TG2 (cub, 1:1000). A reduction in TG2 protein levels was observed with MPP+/epoxo treatment (One-tailed T-Test, p < 0.05; n = 5). Error bars represent SEM.

Although treatment did not appear to effect *Bcl-2* mRNA expression, the general trend in protein levels from two independent experiments suggested an increase in Bcl-2 levels with epoxomicin and MPP+/epoxo treatment (Figure 4.18).

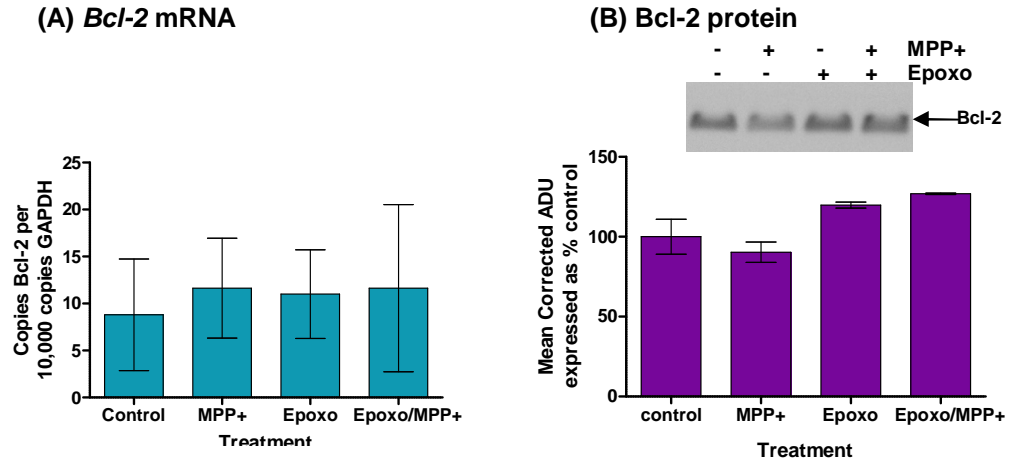


Figure 4.18 Expression of *Bcl-2* in RA/BDNF differentiated SH-SY5Y cells treated with 500 μ M MPP+, 10 nM epoxomicin (epoxo) or 500 μ M MPP+/10 nM epoxo for 24 h.

(A) Plot summarising the results of qRT-PCR which revealed that treatment had no significant effect on *Bcl-2* mRNA copy number per 10,000 copies *GAPDH* ($n = 3$). (B) Representative Western blot and plot summarising the results of densitometric analyses of Western blots probed with anti-*Bcl-2* (1:1000). Error bars represent range ($n = 2$).

Treatment also had no effect on the levels of α -synuclein protein (Figure 4.19).

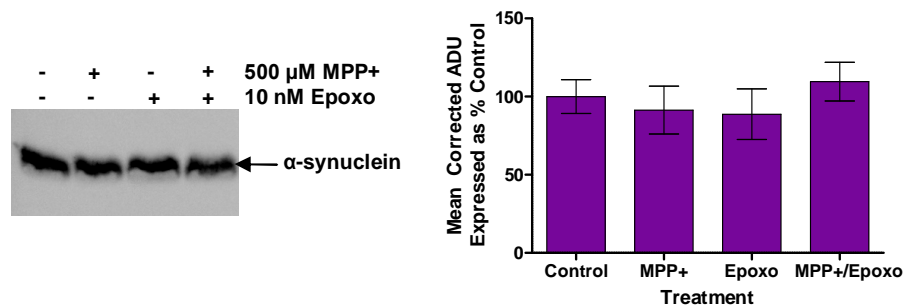


Figure 4.19 Effect of 24 h treatment of RA/BDNF differentiated SH-SY5Y cells with 500 μ M MPP+, 10 nM epoxomicin (epoxo) or 500 μ M MPP+/10 nM epoxo on the expression of α -synuclein.

A representative Western blot and plot summarising the results of densitometric analyses of Western blots probed with anti- α -synuclein (1:1000) revealed that treatment had no effect on α -synuclein levels. Error bars represent SEM ($n = 5$).

4.2.2.3. Effect of Inhibition of Complex I and the Proteasome on the Distribution of Cytoskeletal proteins

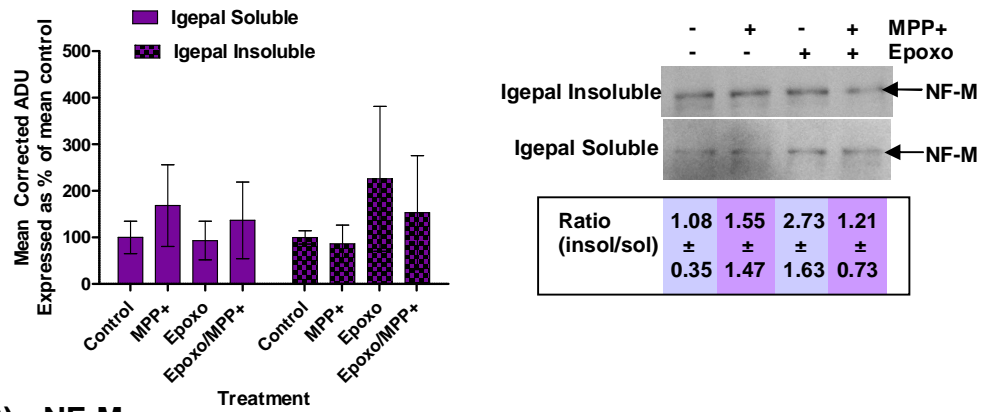
To assess the effect of treatment with MPP⁺, epoxo or MPP⁺/epoxo on the solubility of cytoskeletal proteins; cell lysates were prepared in 50 mM Tris-HCl (pH 8) buffer containing 1 % (v/v) Igepal CA-630 and centrifuged (10 000 x g, 10 min). The resultant cell debris pellet was boiled in 100 µl total extraction buffer [50 mM Tris-HCl pH 6.8, 5 mM EDTA, 1 % (w/v) SDS, 1 mM Sodium orthovanadate, 1 % (v/v) HALT protease and phosphatase inhibitor cocktail]. The Lysate supernatant and the cell debris pellet are hereafter referred to as the Igepal soluble fraction and the Igepal insoluble fraction respectively.

The levels of NF-M in the igepal soluble and insoluble cell fractions were not affected by treatment with MPP⁺, epoxo or MPP⁺/epoxo (Figure 4.20 A). Although the levels of pNF-M in the igepal soluble cell fraction were generally unaffected by treatment, levels in the igepal insoluble fraction were elevated with epoxomicin treatment (Figure 4.20 B). Expressing the insoluble and soluble cell fractions as a ratio (insoluble/soluble) revealed that with treatment the levels of pNF-M were greater in the insoluble fraction than the soluble fraction.

The levels of NF-H in the igepal soluble and insoluble cell fractions were generally unaffected by treatment with the exception of the igepal insoluble fraction from cells treated with epoxomicin in which levels were elevated (Figure 4.21 A). In addition, expressing the signal (as % control) from the igepal soluble and insoluble fractions as a ratio revealed an increase in the insoluble fraction compared to the soluble with MPP⁺ and epoxomicin treatments but not with MPP⁺/epoxo treatment.

Other than a reduction in levels of NF-L in the soluble fraction with MPP⁺ treatment, NF-L levels in the igepal soluble and insoluble cell fractions were generally unchanged with treatment (Figure 4.21 B). Similarly, the insoluble/soluble ratios of fractions from treated cells were similar to the ratio from controls.

(A) NF-M



(B) pNF-M

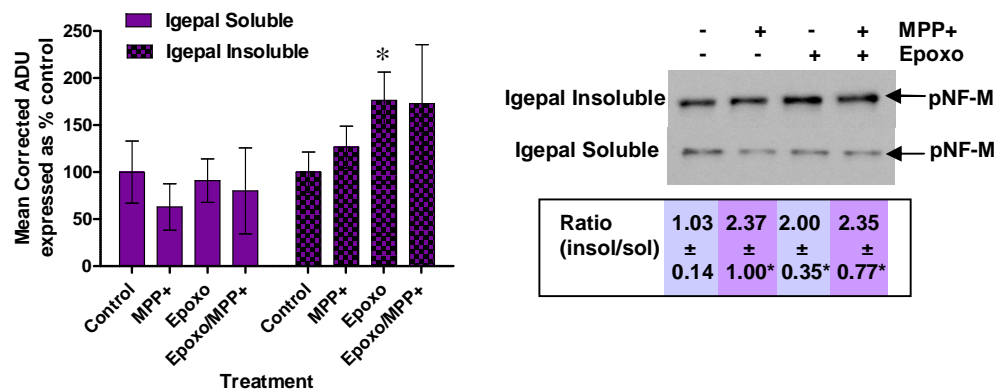


Figure 4.20 The Levels of NF-M and phosphorylated NF-M in IgG soluble and insoluble cell fractions of RA/BDNF differentiated SH-SY5Y cells treated with 500 μ M MPP+, 10 nM epoxomicin (epoxo) or 500 μ M MPP+/10 nM epoxo for 24 h.

Representative Western blots of IgG soluble and insoluble cell fractions probed with (A) anti-NF-M (RMO270, 1:500) or (B) anti-pNF-M (RNF403, 1:1000). Plots summarise the densitometric analyses of Western blots with signal expressed as % of mean control. The levels of NF-M in the igG soluble and insoluble fractions were unaffected by treatment but the levels of pNF-M were greater in the igG insoluble fraction with epoxomicin treatment (T-Test, * $p < 0.05$; $n = 3$). Error bars represent standard deviation. The mean ratio of the signal (as % control) of the igG insoluble versus soluble fraction \pm standard deviation, quoted in the box below the Western blots, was greater for pNF-M with MPP+ (One-tailed T-Test, * $p < 0.05$; $n = 3$), epoxo and MPP+/epoxo treatment (Two-tailed T-Test, * $p < 0.05$; $n = 3$).

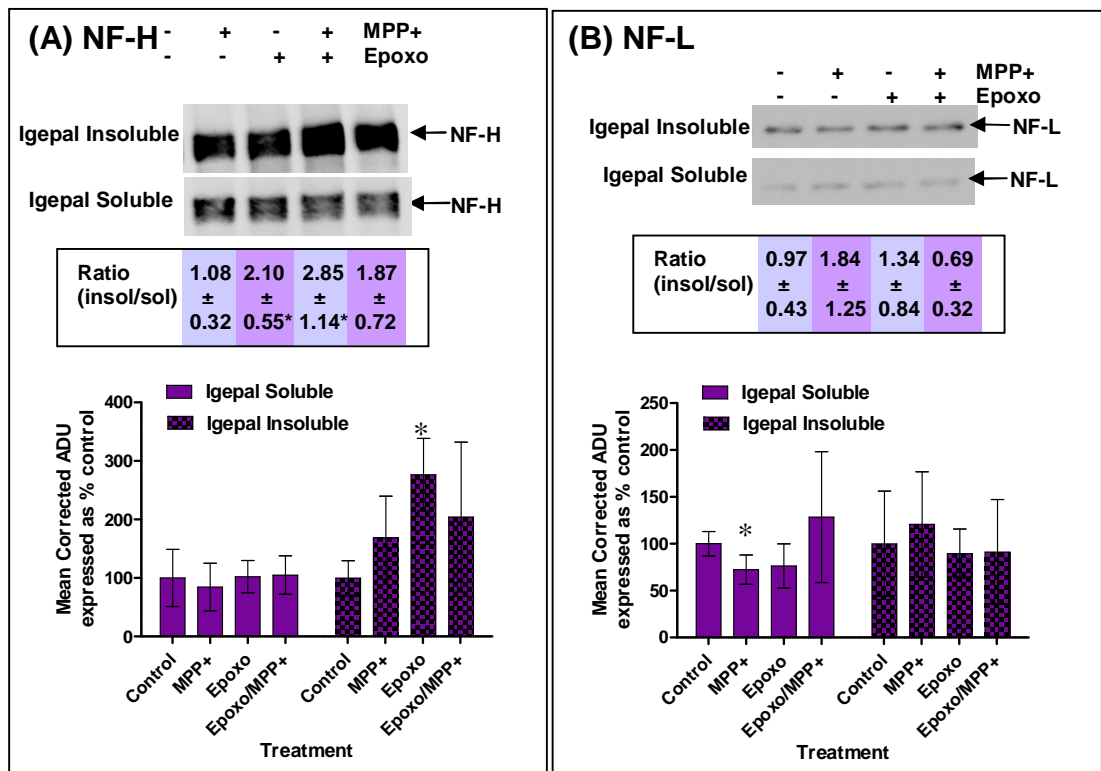


Figure 4.21 Effect of 24 h treatment of RA/BDNF differentiated SH-SY5Y cells with 500 μ M MPP+, 10 nM epoxomicin (epoxo) or 500 μ M MPP+/10 nM epoxo on the levels NF-H and NF-L in igepal soluble and insoluble cell fractions.

Representative Western blots probed with (A) anti-NF-H (n52, 1:2000) and (B) anti-NF-L (DA2, 1:1000) accompanied by plots summarising the results of densitometric analyses of Western blots. The levels of NF-H in the igepal insoluble fraction were increased with epoxomicin treatment (Two-tailed T-Test, * $p < 0.05$; $n = 3$) and the levels of NF-L were reduced in the soluble fraction with MPP+ treatment (One-tailed T-Test, * $p < 0.05$; $n = 3$). The mean ratio of the signal (as % control) of igepal insoluble versus soluble fractions \pm standard deviation is quoted in the box below the Western blots. The ratio of insoluble/soluble for NF-H was greater than controls with MPP+ and epoxo treatment (One-tailed T-Test, * $p < 0.05$; $n = 3$) but not with MPP+/epoxo treatment.

Treatment had no significant effect on the levels α -tubulin in the igepal soluble and insoluble cell fractions compared to control (Figure 4.22 A) but the insoluble/soluble ratio with MPP+ and MPP+/epoxo suggested that levels in the insoluble fraction were increased with respect to levels in the soluble fraction. The levels of vimentin were reduced in the soluble fraction but unchanged in the insoluble fraction with MPP+ treatment; levels were also unchanged in both fractions with epoxomicin and MPP+/epoxo treatment (Figure 4.22 B). Other than a reduction in levels in both fractions with epoxomicin treatment, there was no effect of treatment on the levels of actin in either fraction (Figure 4.22 C).

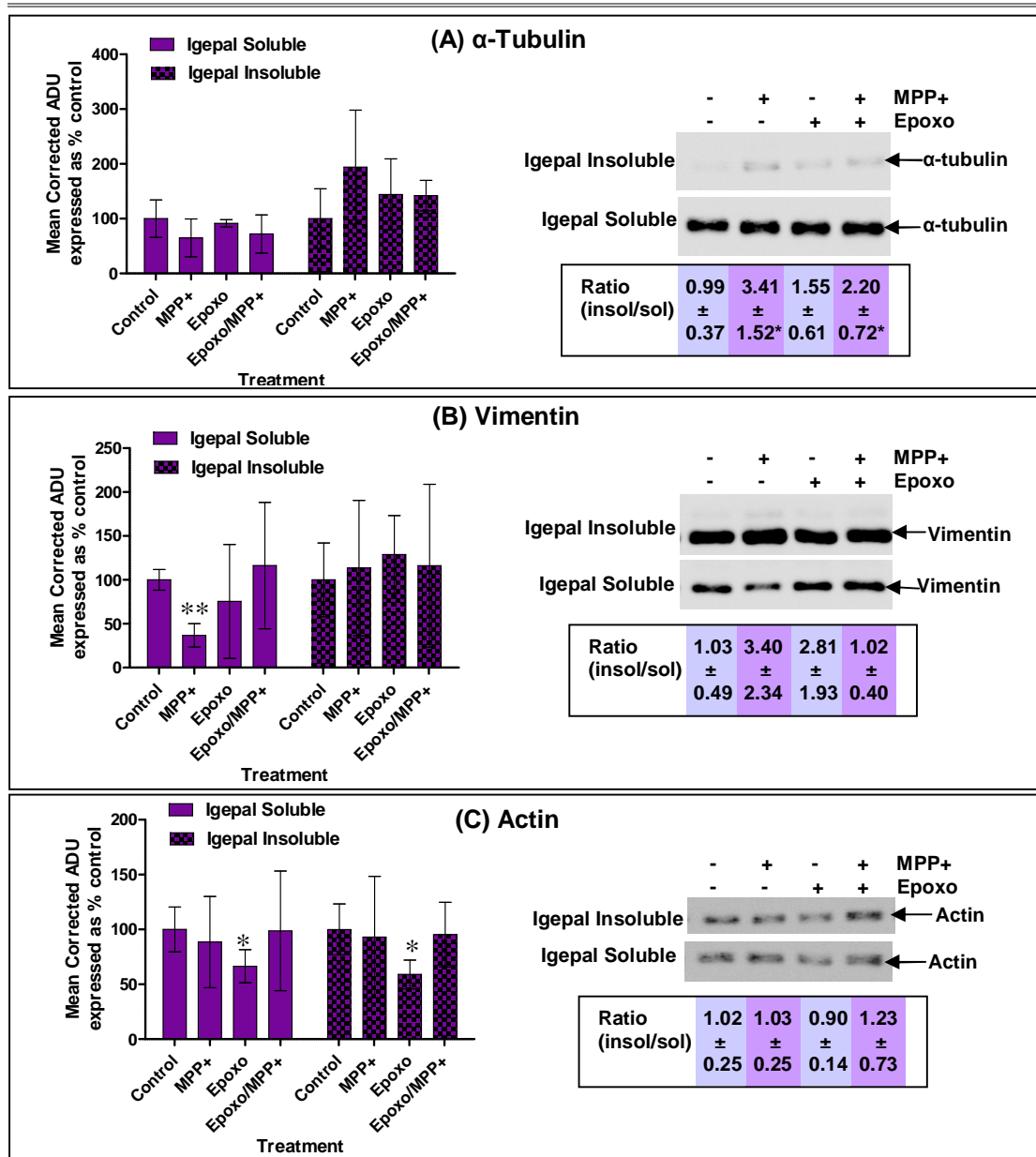


Figure 4.22 Effect of 24 h treatment of RA/BDNF differentiated cells with 500 μ M MPP+, 10 nM epoxomicin (epoxo) or 500 μ M MPP+/10 nM epoxo on the levels of α -tubulin, vimentin and actin in the igepal soluble and igepal insoluble cell fractions.

Representative Western blots probed with (A) anti- α -tubulin (b512, 1:2000), (B) anti-vimentin (RV202, 1:5000) and (C) anti-actin (1:1000). The plots summarise the results of densitometric analyses of Western blots. The levels of vimentin were reduced in the soluble fraction compared to control with MPP+ treatment (Two-tailed T-Test, ** $p < 0.005$; $n = 3$) as were the levels of actin in both fractions with epoxomicin treatment (One-tailed T-Test, * $p < 0.05$; $n = 3$). The mean ratio of the signal (as % control) of igepal insoluble versus soluble fractions \pm standard deviation is quoted in the box below the Western blots. The ratio of insoluble/soluble of α -tubulin is greater with MPP+ and MPP+/epoxo treatment (One-tailed T-Test, $p < 0.05$; $n = 3$). Error bars represent SEM ($n = 3$).

The distribution of neurofilaments following MPP+, epoxomicin and MPP+/epoxo treatment was monitored by immunofluorescence staining of NF-H (Figure 4.23). In MPP+, epoxomicin and MPP+/epoxo treated cells, NF-H staining is concentrated in the cell body and

in some cells areas of intense NF staining are visible (indicated by the arrows). In MPP+ treated cells, regions of intense NF-H staining are also accompanied by some swelling of the axonal processes in that region. These swellings were not observed in epoxomicin treated cells and were not as clearly visible in MPP+/epoxo treated cells.

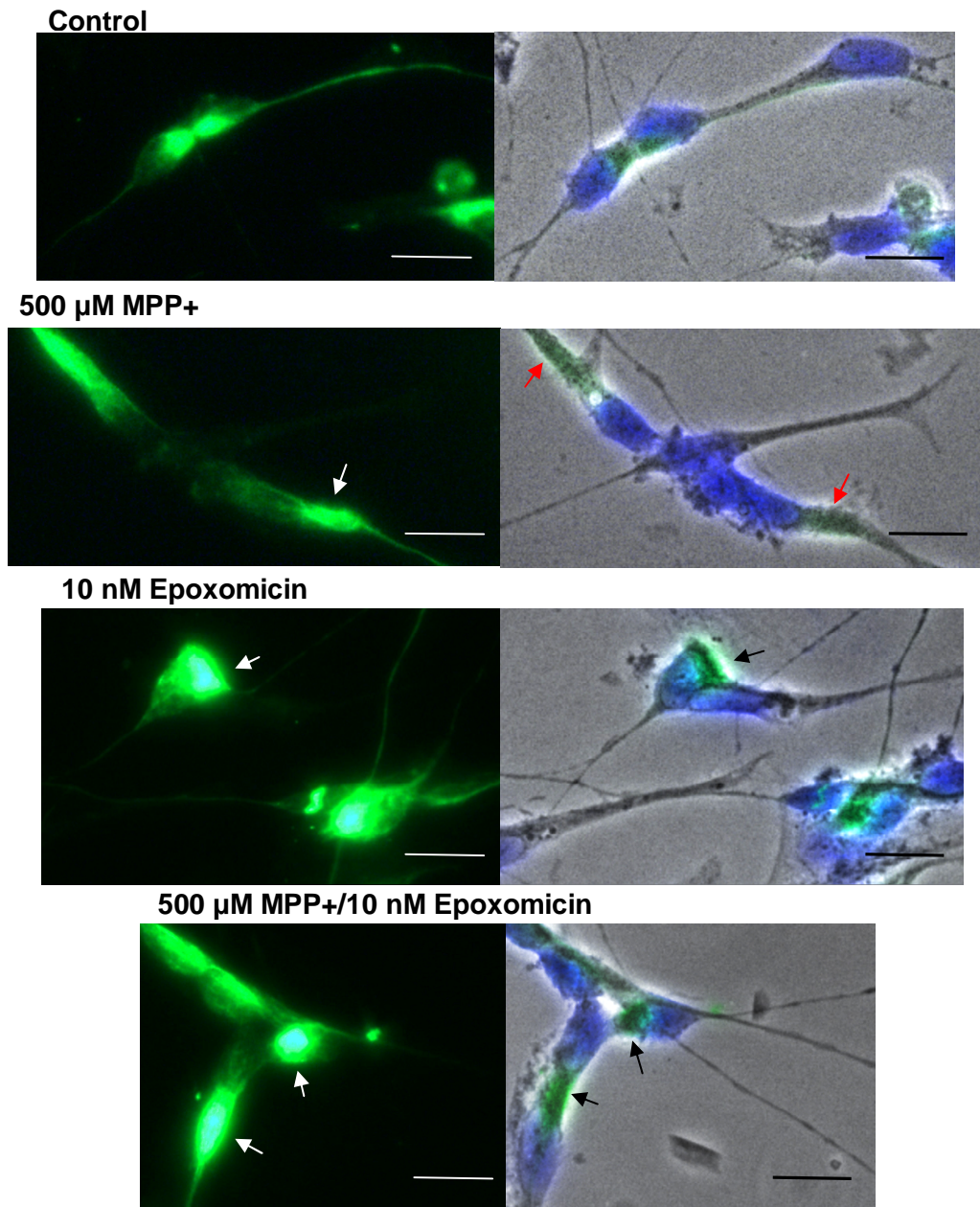


Figure 4.23 The distribution of NF-H in RA/BDNF differentiated SH-SY5Y cells treated with 500 μM MPP+, 10 nM epoxomicin (epoxo) or 500 μM MPP+/10 nM epoxo for 24 h.

Figure shows fluorescence and fluorescence/phase contrast composite images of cells stained with anti-NF-H (green; n52, 1:200), nuclei were counterstained with dapi (blue). Images were taken with a fluorescence microscope using a 40 x objective, scale bars represent 20 μm. Areas of intense NF-H staining in or near the cell body are indicated by arrows. In MPP+ treated cells regions of concentrated NF-H staining are accompanied by axonal swelling as seen in the phase contrast images (red arrow). Regions of axonal swelling were not observed in cells treated with epoxomicin.

Aggresomes are surrounded by a “cage” of intermediate filaments of which vimentin has previously been shown to be a component (Johnston et al, 1998). With this in mind, the effect of treatment on the distribution of vimentin was investigated by immunofluorescence staining (Figure 4.24).

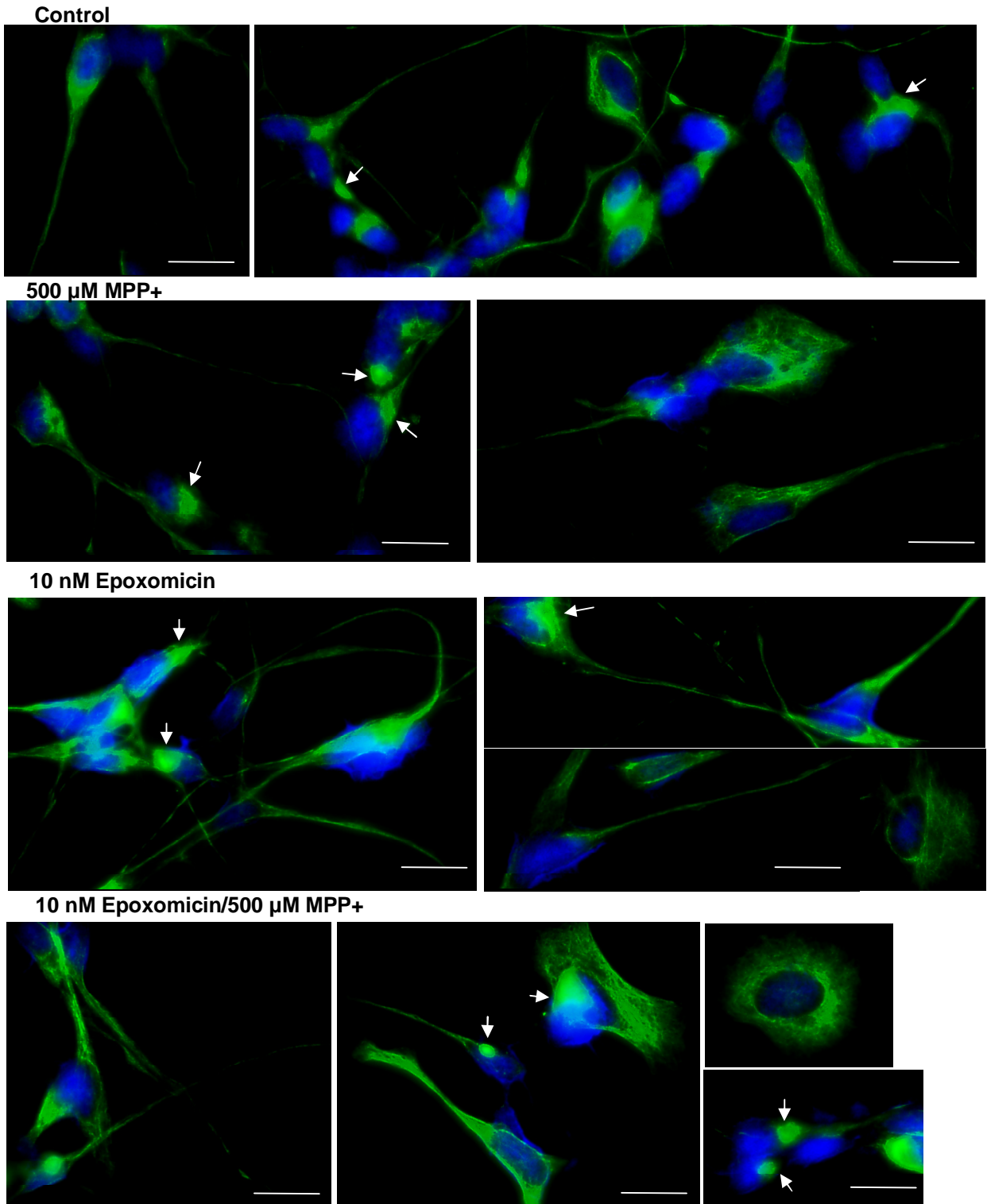


Figure 4.24 The distribution of vimentin in RA/BDNF differentiated SH-SY5Y cells treated with 500 μM MPP+, 10 nM epoxomicin (epoxo) or 500 μM MPP+/10 nM epoxo for 24 h,

Figure shows immunofluorescence images of cells stained with anti-vimentin (green; RV202, 1:500) taken with a fluorescence microscope using a 40 x objective (scale bar represents 20 μm). Nuclei were counterstained with dapi (blue). Areas of intense vimentin staining in the cell body (indicated by arrows) are visible in control and treated cells.

In control cells, strong vimentin staining was evident in both the cell body and the axonal processes. The axonal processes in cells treated with MPP+ were not as strongly stained as in control cells, with most of the staining concentrated in the cell body. Cells treated with epoxomicin or MPP+/epoxo stained strongly in both the cell body and the axonal processes. Regions of intense vimentin staining in the cell body are visible in both control and treated cells making it difficult to see a concentration of vimentin in the perinuclear region which may indicate aggresome formation.

4.2.2.4. Effect of Inhibition of Complex I and the Proteasome on Macroautophagy

The effect of MPP+, epoxo and MPP+/epoxo treatment on macroautophagy was investigated by monitoring the levels of LC3-II in treated cells compared to the levels in controls and in the presence of Bafilomycin A1 (BafA1, inhibitor of macroautophagy). Preliminary results (from two independent experiments) revealed that the levels of LC3-II with MPP+, epoxo and MPP+/epoxo treated cells were barely detectable and similar to the control whereas with BafA1, MPP+/BafA1 or MPP+/epoxo/BafA1 treatment, levels were 20-fold, 10-fold and 5-fold higher than in the control respectively (Figure 5.25).

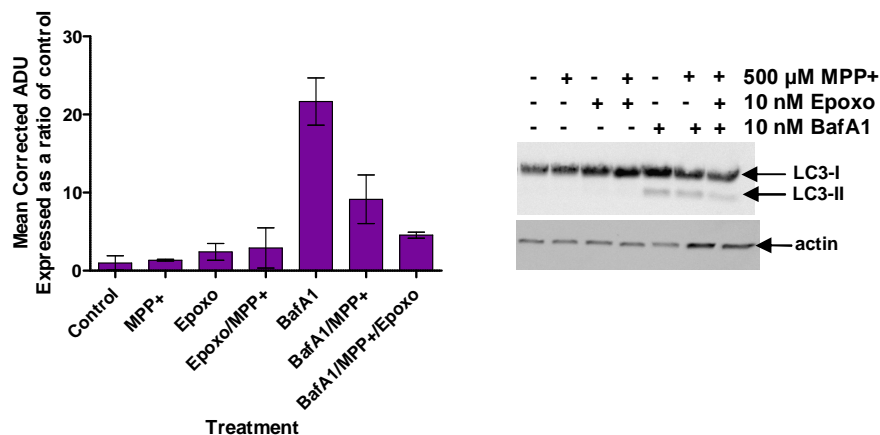


Figure 4.25 Indirect measurement of macroautophagy by monitoring the levels of the autophagic vesicle marker, LC3-II, in RA/BDNF differentiated SH-SY5Y cells treated for 24 h with 500 μM MPP+, 10 nM epoxomicin (epoxo) or 500 μM MPP+/10 nM epoxo with or without 10 nM Bafilomycin A1 (BafA1)

Representative Western blot probed with anti-LC3B (1:1000) and anti-actin (1:1000). The plot summarises the results of densitometric analysis of the LC3-II band from two independent experiments corrected for protein loading by actin. Levels of LC3-II in control cells and MPP+, epoxo and MPP+/epoxo treated cells were barely detectable but levels of LC3-II in BafA1, MPP+/BafA1 and MPP+/epoxo/BafA1 treated cells were increased 20-, 10- and 5-fold respectively. Error bars represent range (n = 2).

In addition to LC3-II, the effect of MPP+, epoxo and MPP+/epoxo treatment on the levels of p62/SQSTM1 was also determined (Figure 4.26). Preliminary results from two independent experiments suggest that p62 levels in MPP+ and epoxo treated cells treated are similar to control levels whereas levels in MPP+/epoxo treated cells are slightly higher. In BafA1, MPP+/BafA1 and MPP+/epoxo/BafA1 treated cells levels were 10-15 fold higher (n = 2).

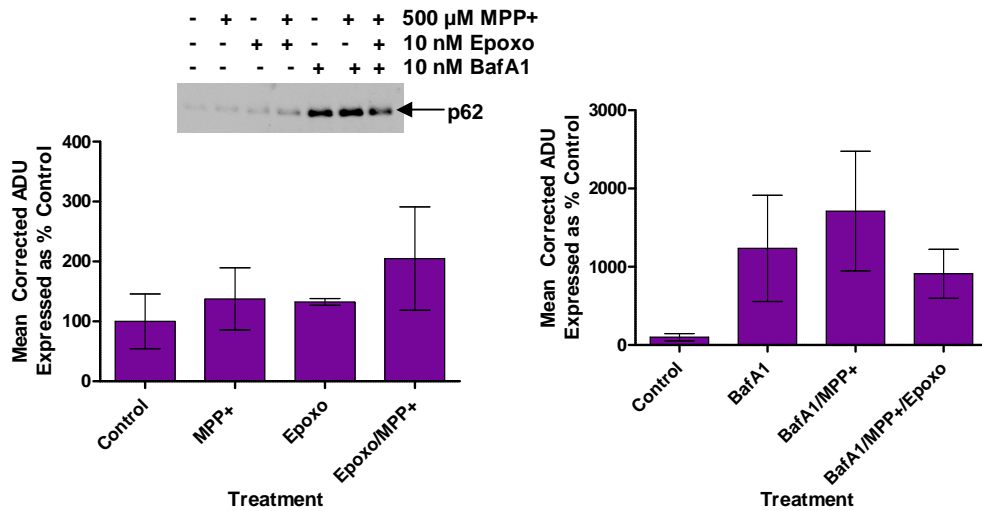


Figure 4.26 The levels of p62 in RA/BDNF differentiated cells treated for 24 h with 500 μM MPP+, 10 nM epoxomicin (epoxo) or 500 μM MPP+/10 nM epoxo with or without Bafilomycin A1 (BafA1). Representative Western blot probed with anti-p62 (1:1000) and plot summarising the results of densitometric analysis of Western blots from two independent experiments. The levels of 62 in MPP+ and epoxo treated cells were similar to control levels while levels with MPP+/epoxo treatment seemed to be slightly higher. Levels of p62 with BafA1, MPP+/BafA1 or MPP+/BafA1/epoxo treatment were increased 10- to 15-fold of levels in the control. Error bars represent range (n = 2).

p62 is often associated with inclusions and protein aggregates, an association that is thought to be indicative of the attempted removal of aggregated proteins by macroautophagy (Pankiv et al, 2007). As such, the effect treatment with MPP+, epoxo and MPP+/epoxo on the solubility in of p62 was assessed by immunoprobng Western blots of igepal soluble and insoluble cell fractions (Figure 4.27). With the exception of MPP+/epoxo treatment in which levels were increased, the levels of p62 in the igepal soluble fraction following MPP+ and epoxo treatments were unchanged. In the igepal insoluble fraction, p62 levels were increased with epoxo and MPP+/epoxo treatment. Following MPP+ treatment, no significant change in p62 levels in the igepal insoluble fraction was observed. An increase in the ratio of insoluble:soluble protein was observed with epoxo treatment but not with MPP+ or MPP+/epoxo.

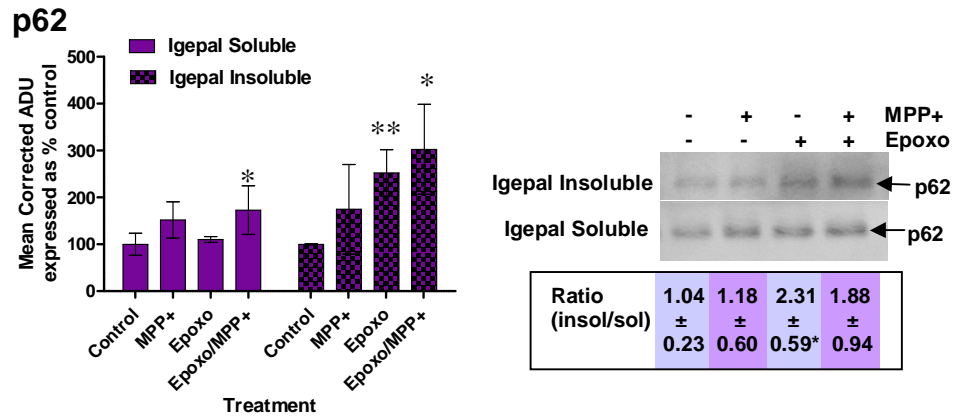


Figure 4.27 Effect of 24 h treatment of RA/BDNF differentiated cells treated with 500 μ M MPP+, 10 nM epoxomicin (epoxo) or 500 μ M MPP+/10 nM epoxo on the solubility of p62/SQSTM1 in igepal-containing cell lysis buffer.

Representative Western blots of igepal soluble and insoluble cell fractions probed with anti-p62 (1:1000). Plot summarising the results of densitometric analyses of Western blots that revealed an increase in the levels of p62 in the igepal soluble fraction with MPP+/epoxo treatment (One-tailed T-Test, * $p < 0.05$; $n = 3$) and in the igepal insoluble cell fraction with epoxo and MPP+/epoxo treatment (Two-tailed T-Test, * $p < 0.05$, ** $p < 0.005$; $n = 3$). Error bars represent standard deviation ($n = 3$). The mean ratio of the signal (as % control) of igepal insoluble versus soluble fractions \pm standard deviation is quoted in the box below the Western blots and revealed that the level of p62 in the insoluble fraction was greater than in the soluble fraction with MPP+/epoxo treatment (Two-tailed T-Test, * $p < 0.05$; $n = 3$).

Double-immunofluorescence staining of p62 (red) with α -tubulin (green, Figure 4.28) and NF-H (green, Figure 4.30) revealed that p62 did not generally co-localise with α -tubulin but there was some evidence of co-localisation (indicated by the yellow colour of overlapping red and green signals) with NF-H. In control cells a small degree of apparent NF-H and p62 colocalisation is visible but the majority of the staining for NF-H and p62 remains distinctly individual. However, in treated cells (but not that obviously in epoxo treated cells), NF-H staining is mainly localized in the perinuclear region where it often co-localized with p62, resulting in strong yellow staining. In all treated cells an accumulation of either NF-H and/or p62 in the perinuclear region (indicated by arrows) was observed.

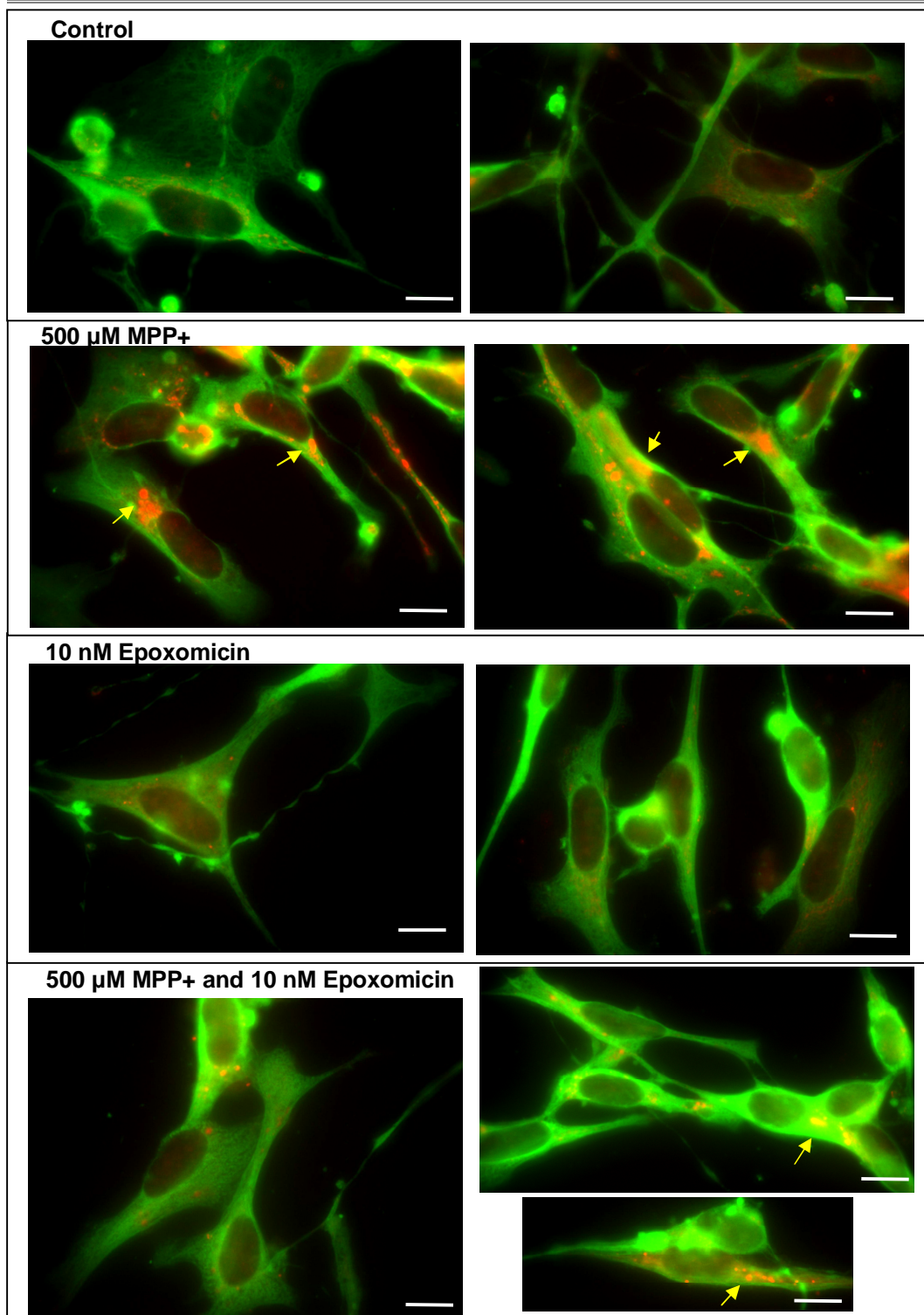


Figure 4.28 Immunofluorescence staining of α -tubulin and p62/SQSTM1 in RA/BDNF differentiated SH-SY5Y cells treated for 24 h with 500 μ M MPP+, 10 nM epoxomicin (epoxo) or 500 μ M MPP+/10 nM epoxo.

Fluorescence microscope images of cells stained with anti- α -tubulin (green; b512, 1:200) and anti-p62 (red; 1:100). p62 bodies appeared more numerous in MPP+ and MPP+/Epoxomicin treated cells (indicated by yellow arrows) than in control cells. Images were taken using a fluorescence microscope with a 100x oil objective, scale bars represent 8 μ m. Two independent fields are shown.

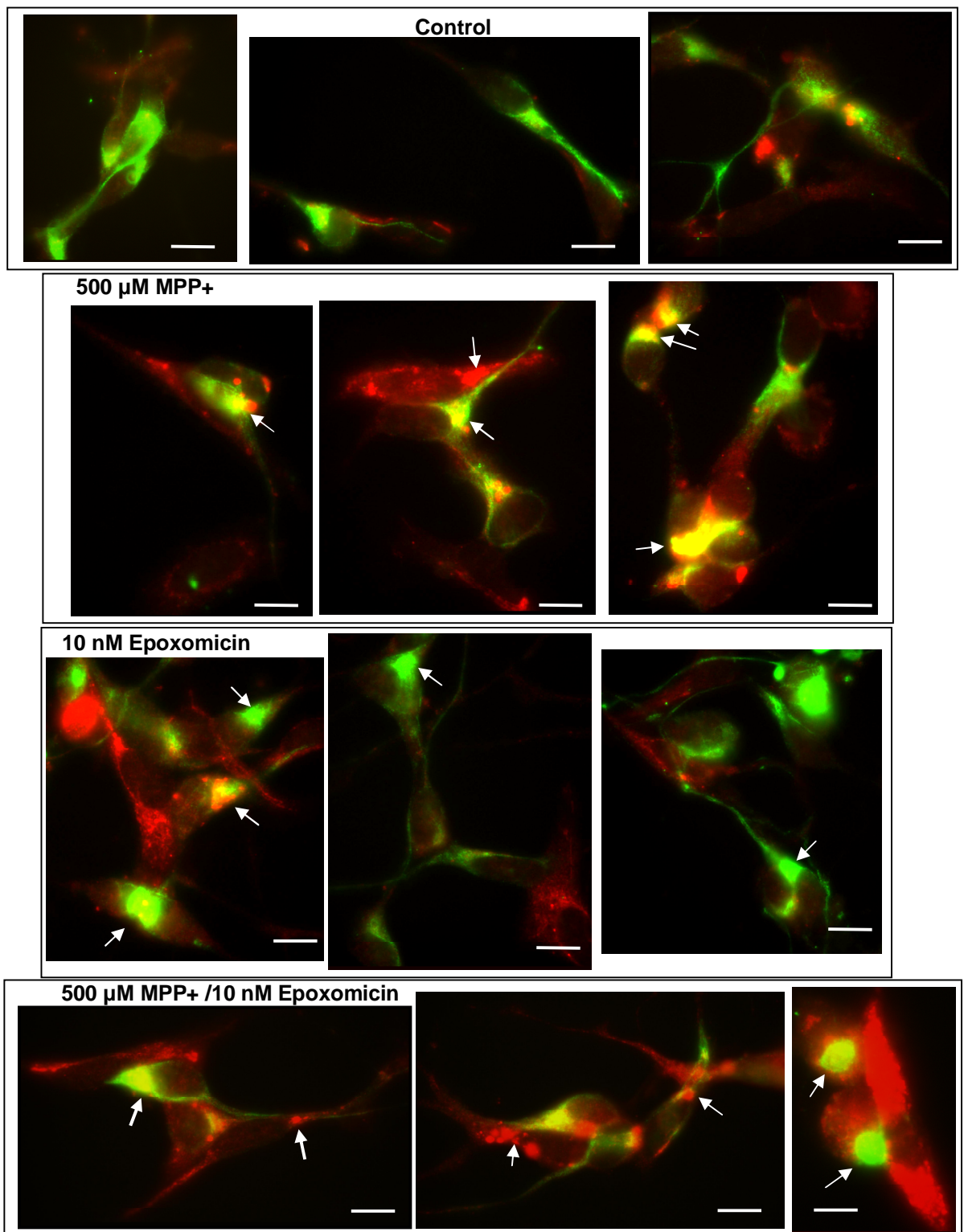


Figure 4.29 Immunofluorescence staining of NF-H and p62/SQSTM1 in RA/BDNF differentiated SH-SY5Y cells either treated for 24 h with 500 μM MPP+, 10 nM epoxomicin (epoxo) or 500 μM MPP+/10 nM epoxo.

Fluorescence microscope images of cells stained with anti-NF-H (green; n52, 1:100) and anti-p62 (red, 1:100). Co-localization of NF-H and p62 (yellow) appeared to be more prevalent in MPP+ and MPP+/Epoxomicin treated cells as did p62 bodies in treated cells. Images were taken using a fluorescence microscope with a 100 x oil objective. Scale bars represent 8 μm. Three independent fields are shown in each case.

As indicated earlier, p62/SQSTM1 has been shown to interact with LC3-II and ubiquitinated proteins and has as such been hypothesized to function in the targeting of aggregated proteins and/or organelles for destruction by macroautophagy. Due to the possible role of macroautophagy in the removal of protein aggregates, treated cells were double immunostained with anti-NF-H and anti-LC3B which recognises LC3-I and LC3-II (Figure 4.30). The majority of LC3 and NF-H appeared to co-localize in control and treated cells (yellow). LC3 staining was distributed between the cell body and the axonal processes in control and MPP+ treated cells. In epoxo and MPP+/epoxo treated cells LC3 was mainly concentrated in a localized region of intense staining within the cell body. Similarly, regions of intense NF-H staining (which co-localized with LC3) were visible in the cell body of MPP+, epoxo and MPP+/epoxo treated cells.

In addition the effect of treatment on cathepsin D levels and activity was determined by immunoprobng Western blots of total cell extracts with anti-cathepsin D (CTD19) which recognises the 52 kD pro-form of cathepsin D and the 34 kD cleaved form (Figure 4.31). Preliminary results from two independent experiments revealed a marked increase in the levels of the 34 kD cleaved form of with epoxomicin treatment and a decrease with MPP+ treatment. Combining treatments with BafA1 resulted in a 4-5 fold increase in the cleaved cathepsin D.

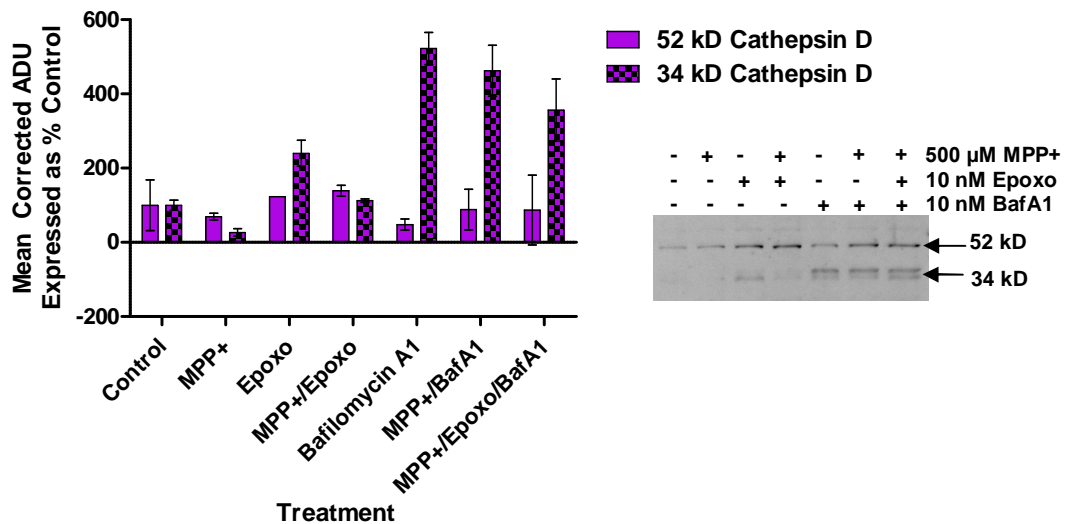


Figure 4.30 Effect of 24 h treatment of RA/BDNF differentiated SH-SY5Y cells with 500 μ M MPP+, 10 nM epoxomicin (epoxo) or 500 μ M MPP+/10 nM epoxo with or without 10 nM Bafilomycin A1 (BafA1) on the levels and activity of Cathepsin D.

Representative Western blot of total cell extracts probed with anti-cathepsin D (CTD19, 1:1000). Plot summarising the results of densitometric analyses of the 52 kD pro-form and 34 kD cleaved forms of Cathepsin D from two independent experiments. The levels of the 34 kD cleaved form were increased in cells treated with epoxo, BafA1, MPP+/BafA1 and MPP+/epoxo/BafA1 but decreased in cells treated with MPP+. Error bars represent range (n = 2).

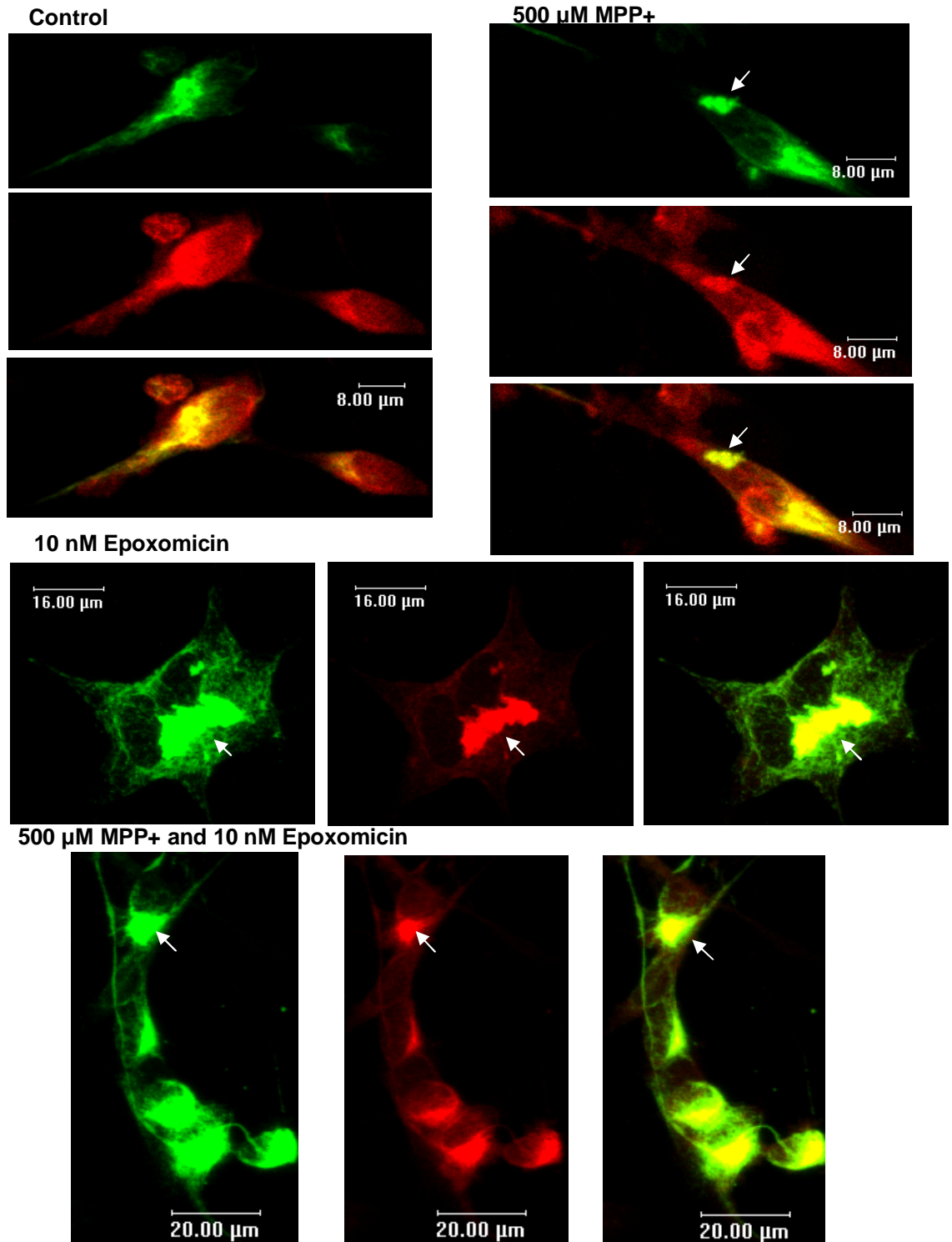


Figure 4.31 Immunofluorescence staining of LC3 and NF-H in RA/BDNF differentiated SH-SY5Y cells treated with MPP+, epoxomicin (epoxo) or MPP+/epoxo.

Immunofluorescence images of RA/BDNF differentiated SH-SY5Y neuroblastoma cells either untreated or treated with 500 μM MPP+, 10 nM Epoxomicin or 500 μM MPP+/10 nM Epoxomicin for 24 h imaged by laser confocal microscopy. Cells were stained with anti-NF-H (green; n52, 1:200) and anti-LC3B (red; 1:100). LC3B staining in Epoxomicin and MPP+/Epoxomicin treated cells was mainly concentrated in the cell body where some of it appeared to co-localize with NF-H staining (yellow). Whereas in control and MPP+ treated cells, LC3B staining was found in the axonal processes and cell body where it appeared to co-localize with NF-H staining (yellow). In MPP+, Epoxomicin and MPP+/Epoxomicin treated cells some protein aggregates (indicated by arrows) were found in the perinuclear region.

4.3 Discussion

4.3.1. The Differentiation of SH-SY5Y neuroblastoma cells

4.3.1.1. Morphological Characteristics of RA and RA/BDNF differentiated SH-SY5Y neuroblastoma cells

The morphological features of proliferating, RA and RA/BDNF differentiated SH- cells were compared to assess the efficiency of RA/BDNF induced differentiation. In phase contrast images, the cell bodies with RA/BDNF treatment were smaller and more rounded in appearance than the cell bodies of proliferating and RA-differentiated cells. RA/BDNF differentiation also resulted in a larger percentage of cells with long axon-like processes that formed an interconnecting network of fibres. These results are similar to those reported by Encinas et al (2000) in their comparison of RA and RA/BDNF induced differentiation of SH-SY5Y cells. Therefore, morphologically RA/BDNF treatment yielded a population of cells with a differentiated phenotype that was more homogeneous than obtained with RA-induced differentiation.

4.3.1.2. The Effect of RA and RA/BDNF induced differentiation of SH-SY5Y neuroblastoma cells on mRNA and protein expression

Comparing the mRNA copy number of GAPDH and two other house-keeping genes (β -actin and the ribosomal subunit L32) in proliferating, RA or RA/BDNF treated cells revealed that all 3 mRNAs showed the same trend but that GAPDH mRNA copy number was more similar across the treatments than β -actin and L32 mRNAs, thus validating the use of GAPDH as a loading control in this work.

The expression of NTrkB mRNA was induced with RA and RA/BDNF treatment (Table 4.2) which agrees with published reports of the induction of NTrkB mRNA and protein expression by RA (Encinas et al, 1999, 2000; Hasegawa et al, 2004).

The expression of TG2 mRNA and protein increased following RA and RA/BDNF induced differentiation (Table 4.2). Again, increased TG2 protein expression following RA-induced differentiation has already been documented (Singh et al, 2003, Tucholski et al, 2001, Zhang et al, 1998). Therefore sequential treatment with BDNF following RA pre-treatment maintains the high level of TG2 expression induced by RA.

There was no evidence of RA and RA/BDNF induced expression of Bcl-2; in fact the level of Bcl-2 protein was lower in RA differentiated cells than in proliferating cells (Table 4.2). This effect was unexpected since differentiation is usually associated with increased levels of Bcl-2 protein to promote cell survival (Zhang et al, 1996) and increased expression of Bcl-2 in SH-SY5Y cells differentiated with RA (Feng & Porter, 1999, Itano et al, 1996, López-Carballo et al, 2002) and TPA (Feng & Porter, 1999, Hanada et al, 1993) has previously been reported. However it has been reported that a decrease in Bcl-2 levels following RA-induced differentiation occurs in the clone used in the present work (Beck, PhD thesis; 2004).

Another marker of neuronal differentiation is the expression of neurofilament proteins (Hoffman et al, 1987, reviewed by Perrot et al, 2008). In PC12 cells induced to differentiate with nerve growth factor (NGF) the expression of NF-L and NF-M was increased (Lindenbaum et al, 1987, Zentrich et al, 2002), a similar finding was also previously reported in SH-SY5Y cells treated with insulin (Wang et al, 1992). However, in the present work instead of an increase in mRNA expression, decreased expression was observed for all three NF subunits with RA treatment and for NF-H with RA/BDNF treatment (Table 4.2).

The overall pattern of NF-L and NF-M mRNA expression is similar which is not unexpected since during neuronal development and differentiation the expression of the neurofilament subunits is coordinated, with NF-M and NF-L expression occurring first, followed by NF-H expression at the latter stages of development. This differential expression pattern suggests that the element controlling the expression of NF-L and NF-M differs from that controlling NF-H expression (Carden et al, 1987, Paterno et al, 1997). Indeed in humans, the NF-M and NF-L genes are closely linked on chromosome 8 while the NF-H gene is on chromosome 22 (reviewed by Perrot et al, 2008).

Table 4.2 Effect of differentiation of SH-SY5Y cells with 10 μ M retinoic acid (RA) or 10 μ M RA and 50 ng/ml Brain Derived Neurotrophic Factor (BDNF) on protein and mRNA expression.

The mRNA copy number (determined by qRT-PCR) is expressed per 1000 copies GAPDH and protein levels (determined from immunoprobed Western blots of total cell extracts) are expressed as a mean percentage of control (level in proliferating cells). For all experiments values are quoted \pm standard deviation (n = 3)¹. Increasing expression is highlighted in yellow (light yellow refers to a trend - from 2 independent experiments) and decreasing expression is highlighted in green. RA and RA/BDNF treatments were compared to proliferating cells and statistical analyses were performed using two-tailed and one-tailed T-Tests, *p > 0.05 and **p < 0.005.

Target Protein	Proliferating Cells		5 d RA		8 d RA		5 d RA/3 d BDNF		5d RA/8 d BDNF	
	mRNA	Protein	mRNA	Protein	mRNA	Protein	mRNA	Protein	mRNA	Protein
<i>NTrkB</i>	0.08 \pm 0.04	-	2.9 \pm 0.5*	-	3.7 \pm 0.7*	-	6.3 \pm 3.1*	-	3.1 \pm 1.7*	-
<i>TG2</i>	0.7 \pm 0.3	98.6 \pm 26.4	9.2 \pm 3.8**	2563 \pm 1416*	10.1 \pm 3.3**	6604 \pm 4319*	11.1 \pm 1.8**	5283 \pm 2350*	5.0 \pm 3.6	3606 \pm 2787*
<i>Bcl-2</i>	2.0 \pm 0.5	100.0 \pm 19.1	1.9 \pm 0.4	64.3 \pm 5.0*	2.4 \pm 0.9	56.0 \pm 21.3*	2.1 \pm 0.4	88.7 \pm 11.9	2.6 \pm 1.1	100.7 \pm 5.0
<i>NF-L</i>	38.7 \pm 6.4	99.8 \pm 2.3	17.7 \pm 4.7*	85.1 \pm 33.8	20.0 \pm 6.5*	136.2 \pm 73.0	39.4 \pm 2.6	104.9 \pm 58.9	46.5 \pm 6.0	64.9 \pm 47.1
<i>NF-M</i>	5.9 \pm 1.3	100.0 \pm 34.6	2.6 \pm 1.0*	86.2 \pm 23.5	3.0 \pm 1.4*	56.53 \pm 29.4	2.9 \pm 2.2	44.8 \pm 8.7*	5.2 \pm 1.2	61.4 \pm 15.0
<i>NF-H</i>	16.9 \pm 3.2	100.0 \pm 15.8	6.4 \pm 1.1**	102.8 \pm 19.1	8.3 \pm 0.9*	170.2 \pm 22.1*	8.7 \pm 3.3*	118.3 \pm 43.0	6.7 \pm 2.4*	104.3 \pm 25.6
<i>Vimentin</i>	-	100 \pm 23.4	-	84.7 \pm 2.9	-	89.7 \pm 4.7	-	115.0 \pm 40.0	-	81.7 \pm 16.5
<i>α-Tubulin</i>	627.6 \pm 289.6	100.0 \pm 10.4	285.5 \pm 96.6	108.5 \pm 18.7	270.1 \pm 9.0*	107.8 \pm 25.3	601.1 \pm 110.0	152.7 \pm 11.5*	330.8 \pm 41.1	192.3 \pm 11.4**
<i>Actin</i>	-	100.3 \pm 38.2	-	109.3 \pm 27.0	-	109.3 \pm 26.6	-	150.3 \pm 48.8	-	128.0 \pm 14.2
<i>Kinesin 5C</i>	6.7 \pm 3.4	100.0 \pm 26.8	3.5 \pm 1.4	132.5 \pm 28.3	3.6 \pm 1.6	144.4 \pm 59.0	5.1 \pm 0.8	164.4 \pm 8.6*	6.0 \pm 1.4	192.5 \pm 27.7*
<i>Kinesin 5A</i>	-	100.0 \pm 24.0	-	109.5 \pm 31.8	-	164.0 \pm 55.2	-	157.0 \pm 11.3	-	170.5 \pm 36.1
<i>Dynein Light Intermediate Chain</i>	2.1 \pm 0.5	100.0 \pm 24.0	3.1 \pm 1.1	77.0 \pm 12.7	4.4 \pm 1.0*	58.0 \pm 24.0	4.2 \pm 2.3	94.5 \pm 3.5	3.3 \pm 0.6*	78.5 \pm 5.0
<i>PSMC1</i>	46.1 \pm 9.3	100.0 \pm 12.9	47.6 \pm 8.1	98.7 \pm 17.9	82.8 \pm 53.5	111.6 \pm 9.7	76.4 \pm 24.1	120.4 \pm 29.8	65.8 \pm 6.1*	92.1 \pm 18.5

¹ Dynein Intermediate Chain and Kinesin 5A protein are the result of two independent experiments, so % ADU of proliferating cells for protein is expressed \pm range

In general no change in the protein levels of the three NF subunits was observed with RA and RA/BDNF treatment, other than an increase in NF-H levels after 8 d RA treatment and a decrease in NF-M levels after 3 d in BDNF (Table 4.2). Truckenmiller et al (2001) reported an increase in NF-M and NF-L protein levels in SH-SY5Y cells after just 6 h RA treatment but a recent study found no significant effect of RA on the levels and distribution of NF-H (Cheung et al, 2009). The decrease in NF-M expression following RA/BDNF induced differentiation supports the work of Encinas et al (2000) in which RA/BDNF-induced differentiation of SH-SY5Y cells resulted in a decrease in NF-M and NF-L protein levels.

Phosphorylation is thought to stabilize the neurofilament network since phosphorylated neurofilaments are more resistant to degradation by proteases (Greenwood et al, 1993). During postnatal brain development NF-M phosphorylation is preceded by its incorporation into the triton-insoluble NF network (Shea et al, 1997) and the differentiation of PC12 cells with NGF has previously been shown to lead to increased NF-M and NF-H phosphorylation (Lindenbaum et al, 1987). However in the present work no evidence of increased NF phosphorylation was observed following RA or RA/BDNF treatment.

Vimentin is the intermediate filament found in cells of mesenchymal origin and is widely expressed in embryos (reviewed by Kim & Coulombe, 2007) and in human foetal brain (Levin et al, 2009). Vimentin expression is associated with an immature phenotype and in neuronal cells is usually superseded by the expression of neurofilament proteins as the cell matures (reviewed by Grant & Pant, 2000, Yabe et al, 2003) although extensive vimentin expression has been reported in Alzheimer's disease brain and in adult mouse brain neurons in response to injury (Levin et al, 2009). RA and RA/BDNF induced differentiation had no effect on the levels of vimentin protein (Table 4.2) and immunofluorescence staining revealed an extensive network of vimentin filaments in differentiated SH-SY5Y cells.

The expression of the human α 1-tubulin gene is limited to cells of neurological origin (Hall & Cowan, 1985) and is associated with neuronal growth and response to axonal injury (Gloster et al, 1994). Following birth the expression of α 1-tubulin initially increases but then decreases during the latter stages of development to the levels observed in adult brain (Moskowitz & Oblinger, 1995). In PC12 cells differentiated with NGF, an increase in α -tubulin expression was observed (Miller et al, 1987), and a transient increase in α -tubulin expression has been reported in SH-SY5Y cells treated with insulin (Wang et al, 1992). In the present work RA induced differentiation reduced α -tubulin mRNA expression but had no effect on α -tubulin protein levels, whilst RA/BDNF treatment resulted in increased α -tubulin protein levels,

which may be involved in the establishment of the extensive network of long axonal processes seen in RA/BDNF differentiated cells.

Axonal transport of proteins and organelles such as mitochondria in cells with long axonal processes is essential for the maintenance of cell health and function. An increase in the expression of kinesin 2 and dynein light chain mRNA has been observed after 6 h RA treatment (Truckenmiller et al, 2001). Although kinesin mRNA levels were largely unaffected by RA and RA/BDNF treatment, an increase in kinesin 5A and 5C protein was observed following RA/BDNF treatment suggesting either an increased rate of protein translation or protein stability. The increase in kinesin 5A and 5C protein levels may be linked to the extension of axonal processes which is dependent on axonal transport. In the case of dynein intermediate chain and PSMC1, protein levels were unaffected by RA or RA/BDNF induced differentiation but after 8 d RA treatment, dynein mRNA levels were increased, and after 8 d BDNF treatment both dynein and PSMC1 mRNA levels were increased. The lack of an increase in protein despite increased transcription suggests that after treatment, either the mRNA is unstable or the protein is more prone to degradation. An increase in the mRNA expression of a proteasome subunit during the first 6 h of RA treatment has previously been reported (Truckenmiller et al, 2001).

It is clear that RA and RA/BDNF induced differentiation did not always affect protein and mRNA expression in a similar manner, suggesting that during differentiation protein expression is also controlled at the post-transcriptional or translational level or that protein stability is altered. This is similar to results obtained in mice with targeted disruption of the NF-L gene in which loss of NF-L resulted in decreased NF-M and NF-H protein levels but no apparent change in mRNA levels (Zhu et al, 1997).

5.3.1.3. Conclusion

An overview of the effect of RA and RA/BDNF induced differentiation on protein expression in the present work is shown in Figure 4.32. Morphologically RA/BDNF differentiated SH-SY5Y cells exhibited a neuronal phenotype with numerous long axonal processes that formed an intricate interconnecting network of fibres. In agreement with other published work, RA and RA/BDNF induced differentiation increased the expression of TG2 and NTrkB. RA/BDNF induced differentiation did result in increased expression of α -tubulin and Kinesin 5A and 5C which may be involved in establishment and maintenance of axonal processes.

However, no increase in the expression of Bcl-2 was observed, instead with RA treatment Bcl-2 protein levels were reduced.

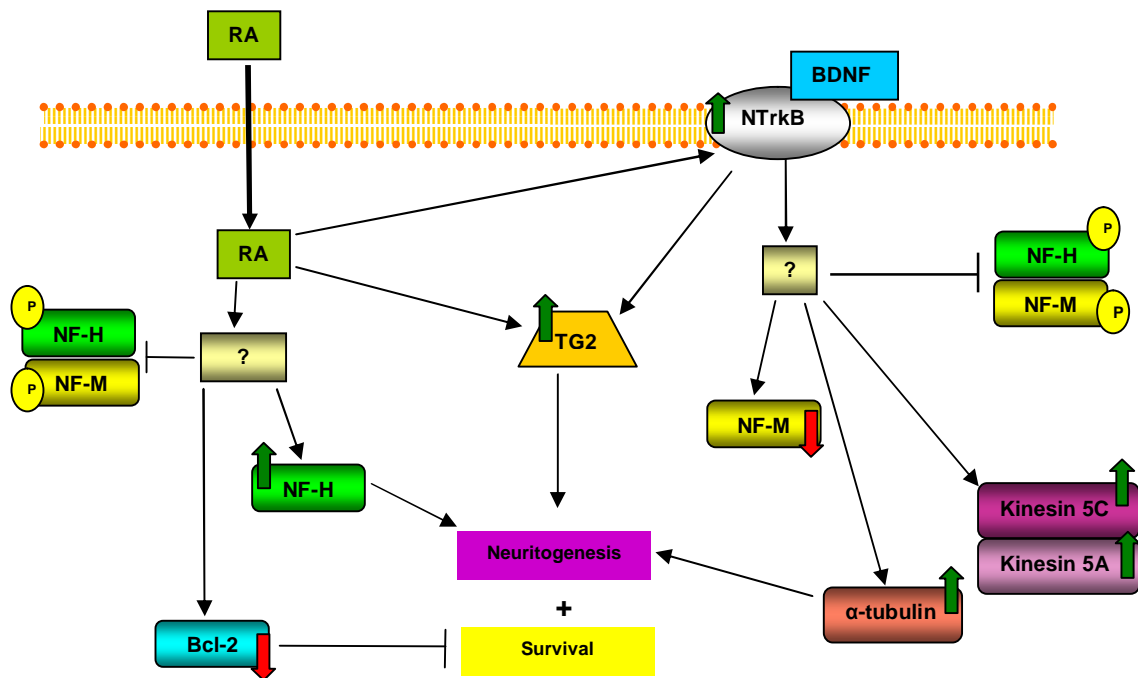


Figure 4.32 Diagrammatic representation summarising of the effect of RA and RA/BDNF induced differentiation on protein expression in SH-SY5Y neuroblastoma cells.

RA treatment induces the expression of Neurotrophic Tyrosine Kinase Receptor B (NTrkB, which allows cells to become responsive to BDNF). RA treatment also induces the expression of Tissue Transglutaminase (TG2) previously shown to be essential for neuritogenesis and cell survival. TG2 expression was maintained at the high level induced by RA during BDNF treatment. Bcl-2 levels were reduced following RA treatment which may have serious implications on the maintenance of cell survival. Bcl-2 levels returned to levels observed in proliferating cells with BDNF treatment. An increase in NF-H levels which may be essential for neuritogenesis was observed with RA treatment. With BDNF treatment NF-H levels were maintained at the levels in proliferating cells but NF-M levels remained lower. The increase in α -tubulin levels with BDNF treatment may be important in the establishment of long axonal processes. BDNF treatment also resulted in increased levels of kinesin 5A and 5C which are essential for transport of proteins and organelles into the axonal processes.

In general, no change in the protein expression and phosphorylation of neurofilament subunits was observed with RA or RA/BDNF induced differentiation, other than an increase in NF-H levels after 8 d RA treatment and a decrease in NF-M levels after 3 d BDNF treatment.

4.3.2. Effect of Inhibition of Complex I and the Proteasome

4.3.2.1. Effects on proteins

The effects of 24 h treatment with MPP⁺ and/or Epoxomicin on mRNA and protein levels and protein distribution is summarised in Table 4.3. Statistically significant increased and decreased levels are highlighted in yellow and green respectively. Trends are also indicated on the table however these observations are not statistically significant and are the result of two independent experiments.

Despite changes in certain proteins, mRNA levels were mostly unaffected by treatment, possibly due to the short time course. The only changes in mRNA expression observed were decreases in NF-L mRNA with MPP⁺/epoxo treatment, actin mRNA with MPP⁺ treatment and TG2 mRNA with epoxo treatment. Therefore it would be interesting to investigate the effects of longer treatment periods on mRNA expression.

With epoxo and MPP⁺/epoxo treatment, NF-M protein levels increased (Table 4.3). In proliferating SH-SY5Y cells, treatment with epoxo did not result in an accumulation of NF-M (refer to Chapter 3) even in the absence of cycloheximide (results not shown). This suggests that the proteasome has a more important role in neurofilament degradation in differentiated cells than in proliferating cells. In addition, all three treatments resulted in an increase in the ratio of pNF-M in igepal insoluble/soluble fractions which suggests a redistribution of pNF-M into the igepal insoluble fraction with treatment. The increase in the igepal insoluble/soluble ratio of NF-H observed with MPP⁺ or epoxo treatment (in the absence of any effect on NF-H in total protein) also suggests a redistribution of NF-H into the insoluble fraction (Table 4.3). Rideout et al (2001) previously reported the production of α -synuclein-positive inclusions that was not accompanied by an overall increase in α -synuclein levels. An increase in the levels of NF-M but not NF-H has previously been reported in a rat model of α -synucleinopathy before the loss of dopaminergic neurons (Chung et al, 2009).

Table 4.3 Table summarising the effects of 24 h treatment of RA/BDNF differentiated SH-SY5Y cells with 500 μ M MPP+, 10 nM epoxomicin (epoxo) or MPP+/epoxo on protein and mRNA expression and the distribution of protein

Increased levels are highlighted in yellow, decreased levels in green and trends are also indicated (result of two independent experiments). Changes in mRNA copy number determined by qRT-PCR, protein expression in total cell extracts, distribution of protein between Igepal-CA630 soluble and insoluble fractions. Statistical analyses were performed using one- and two-tailed T-Tests. n/a = not applicable. Values quoted as fold change \pm standard deviation.

Protein	mRNA			Total Protein			Ratio of Igepal Insoluble/Soluble Protein		
	MPP+	Epoxo	MPP+/Epoxo	MPP+	Epoxo	MPP+/Epoxo	MPP+	Epoxo	MPP+/Epoxo
NF-L	NC	NC	1.4 \pm 0.2* fold \downarrow	NC	NC	NC	NC	NC	NC
NF-M	NC	NC	NC	NC	2.7 \pm 0.6* fold \uparrow	2.2 \pm 0.8* fold \uparrow	NC	NC	NC
pNF-M	n/a	n/a	n/a	NC	NC	NC	2.3 \pm 1.0* fold \uparrow	2.0 \pm 0.4* fold \uparrow	2.4 \pm 0.8*fold \uparrow
NF-H	NC	NC	NC	NC	NC	NC	2.1 \pm 0.6* fold \uparrow	2.9 \pm 1.1* fold \uparrow	NC
pNF-H	n/a	n/a	n/a	NC	NC	NC	-	-	-
α -tubulin	NC	NC	NC	NC	NC	2.4 \pm 0.2* fold \downarrow	3.4 \pm 1.5* fold \uparrow	NC	2.2 \pm 0.7*fold \uparrow
γ -tubulin	-	-	-	1.5 \pm 0.2* fold \downarrow	NC	NC	-	-	-
Actin	1.9 \pm 0.3*fold \downarrow	NC	NC	1.8 \pm 0.2** fold \downarrow	NC	NC	NC	NC	NC
Vimentin	-	-	-	1.7 \pm 0.3* fold \downarrow	1.7 \pm 0.2* fold \downarrow	1.9 \pm 0.3* fold \downarrow	NC	NC	NC
KIF5C	NC	NC	NC	NC	NC	NC	-	-	-
KIF5A	-	-	-	NC	NC	NC	-	-	-
Dynein	NC	NC	NC	1.7 \pm 0.3* fold \downarrow	1.5 \pm 0.2* fold \downarrow	2.3 \pm 0.3* fold \downarrow	-	-	-
TG2	NC	1.6 \pm 0.05* fold \downarrow	NC	NC	NC	1.8 \pm 0.4* fold \downarrow	-	-	-
PSMC1	NC	NC	NC	NC	NC	NC	-	-	-
Bcl-2	NC	NC	NC	NC	\uparrow Trend (ns)	\uparrow Trend (ns)	-	-	-
α -synuclein	-	-	-	NC	NC	NC	-	-	-
p62	-	-	-	NC	NC	\uparrow Trend (ns)	NC	2.3 \pm 0.6* fold \uparrow	NC

The enrichment of NF-H and pNF-M in the insoluble fraction may be indicative of protein aggregation. Indeed immunofluorescence staining of NF-H showed some accumulation of NF-H immunofluorescence in the perinuclear region of cell body following MPP⁺, epoxo and MPP⁺/epoxo treatment. In MPP⁺ treated cells accumulations of NF-H staining were accompanied by some swelling of the axonal process in that region, this swelling was not observed in epoxo treated cells and not as clearly visible in MPP⁺/epoxo treated cells. Neurofilaments have previously been found in inclusion bodies in differentiated and undifferentiated SH-SY5Y cells treated with acrylamide and 2,5-hexanedione (Hartley et al, 1997). Proteasome inhibition with lactacystin has previously been shown to result in increased levels of phosphorylated NF-M and NF-H in PC12 cells resulting from JNK activation (Masaki et al, 2000). Numerous experimental models resulting in the formation of inclusions or aggresomes have employed proteasome inhibition to induce protein aggregation (Bedford et al, 2008, Bolhuis & Richter-Landsberg, 2010, Miwa et al, 2006, Rideout et al, 2001, Rideout & Stefanis, 2002).

Vimentin staining was also investigated because accumulation of vimentin in the perinuclear region has been described in many experimental models of inclusion or aggresome formation (Fu et al, 2005, Kawaguchi et al, 2003, Muqit et al, 2006, Zaarur et al, 2008). Since vimentin staining was extensive in the axonal processes and the cell body following RA/BDNF induced differentiation, it was not possible to detect vimentin accumulation in the perinuclear region.

Actin and γ -tubulin levels were reduced following MPP⁺ treatment and α -tubulin levels were reduced following MPP⁺/epoxo treatment. An enrichment of α -tubulin in the insoluble pool which may be indicative of protein aggregation following MPP⁺ and MPP⁺/epoxo treatment is suggested by the observed increase in the insoluble/soluble ratio (Table 4.3).

A reduction in the levels of dynein intermediate chain was observed with all three treatments but the levels of kinesin 5C and 5A were unaffected (Table 4.3). Previous studies such as the MPP⁺ treatment of PC12 cells reported a decrease in dynein protein expression (Cai et al, 2009) accompanied by a decrease in the co-localisation of dynein and LAMP1 (Cai et al, 2009). In a rat model of α -synucleinopathy an initial decrease in dynein protein expression was followed by an increase in expression. In this model there was no effect at the timepoints investigated on the expression of kinesin 5 protein, although there was a decrease in expression of most of the other kinesin motors at the latter timepoint (Chung et al, 2009).

The importance of efficient axonal transport in neuronal health is highlighted by the implication of defects in axonal transport in neurodegenerative conditions (Ebbing et al, 2008). In a mouse model of frontotemporal dementia progressive loss of dopaminergic neurons of the substantia nigra was preceded by defects in anterograde vesicular and mitochondrial transport (Ittner et al, 2008). MPP⁺ treatment has also previously been reported to result in defects in axonal transport of membranous organelles (Morfini et al, 2007). Inhibition of dynein has also been shown to result in the accumulation of GFP tagged NF-M in the cell body and in the proximal axons (Motil et al, 2007) and GFP tagged NF-H in the distal axons (He et al, 2005). Dynein has also been shown to co-localize with perinuclear inclusions formed in FeCl₂ treated RA/BDNF differentiated cells over-expressing α -synuclein (Hasegawa et al, 2004).

As the retrograde transport motor, dynein is involved in the transport of autophagosomes to lysosomes which are located around the perinuclear region (reviewed by Cai et al, 2009, and Rubinsztein et al, 2009). The importance of the role of dynein in macroautophagy was highlighted by the decrease in both macroautophagy and the clearance of aggregate-prone proteins in PC12 cells expressing mutated dynein or in which dynein activity was chemically impaired (Ravikumar et al, 2005).

Other than a reduction in TG2 levels with MPP⁺/epoxo treatment, no change in the levels of α -synuclein, PSMC1 or TG2 in total protein was observed with treatment. Preliminary results suggest a possible increase in the levels of Bcl-2 with epoxo and MPP⁺/epoxo treatment suggesting a possible adaptive mechanism for survival that needs to be explored (Table 4.3).

Preliminary results from two independent experiments suggest a possible increase in p62 levels following MPP⁺/epoxo treatment. The igepal insoluble/soluble ratio for p62 was increased with epoxo treatment, suggesting an enrichment of p62 into the insoluble pool. No increase was observed in the insoluble/soluble ratio with MPP⁺/epoxo treatment but in this case, an increase in p62 was observed in both the soluble and the insoluble fractions. The increase in p62 in the igepal insoluble fraction may be the result of p62 associating with insoluble aggregated proteins thus targeting them for degradation by macroautophagy via its ability to interact with both ubiquitin and LC3-II (Bjorkoy et al, 2005, Pankiv et al, 2007). The levels of p62 in cell treated with the autophagy inhibitor, Bafilomycin A1 (BafA1), either on its own or with MPP⁺ or MPP⁺/epoxo were 10-15 fold greater than in control cells. Inhibition of macroautophagy with BafA1 has previously been shown to result in increased levels of p62 determined by Western blotting (Bjorkoy et al, 2005).

Immunofluorescence staining revealed that α -tubulin and p62 did not co-localise. However immunofluorescence staining revealed regions of NF-H and p62 co-localization that coincided with the intense regions of concentrated NF-H staining in or near the cell body, suggesting an association of p62 with aggregated NF-H that would be interesting to investigate further. In addition double immunofluorescence of NF-H and LC3 also revealed NF-H and LC3 co-localisation especially in the regions of intense NF-H staining that are suggestive of aggregates.

Defects in the ubiquitin proteasome system and lysosomal pathway have been implicated in the pathogenesis of neurodegenerative conditions characterised by the accumulation of aggregated proteins (reviewed by Keller et al, 2004, and Martinez-Vicente & Cuervo, 2007, Rubinsztein, 2006). In a mouse model producing Lewy body-like inclusions with chronic MPTP treatment, inclusions contained large amounts of lipofuscin which are the products of lipid peroxidation and accumulate in secondary lysosomes; accumulation of which is indicative of lysosomal malfunction (Meredith et al, 2002). Aggregates formed during rotenone treatment of COS-7 cells were eliminated after rotenone was washed out of the system and mitochondrial ATP production was recovered. The removal of the aggregates was partially blocked by proteasome inhibition (Lee et al, 2002). Rideout et al (2004) also reported the elimination of neuronal inclusions formed by proteasome inhibition in rat cortical neurons via the induction of macroautophagy.

Preliminary work investigating the effect of MPP⁺, epoxo and MPP⁺/epoxo treatment on macroautophagy was performed by monitoring LC3-II levels. There was no obvious effect of the treatment on the levels of LC3-II. Inhibiting macroautophagy with BafA1 revealed that MPP⁺/BafA1 and MPP⁺/epoxo/BafA1 treatment for 24 h lead to a smaller increase in LC3-II levels than BafA1 alone which may suggest that MPP⁺ and MPP⁺/epoxo treatments resulted in decreased autophagosome synthesis (Rubinsztein et al, 2009). This is contrary to previous reports in which MPP⁺ treatment of SH-SY5Y cells (Zhu et al, 2007) and proteasome inhibition in rat cortical neurons (Rideout et al, 2004) resulted in increased autophagosome synthesis.

Preliminary results using Western blotting revealed that MPP⁺ treatment decreased the levels of active cathepsin D (a lysosomal protease). This is similar to results in chapter 3, in which MPP⁺ treatment was also shown to result in a decrease in cathepsin D activity using a fluorogenic cathepsin D activity assay. With epoxo treatment however increased levels of active cathepsin D were observed, suggesting increased cathepsin D activity. Proteasome inhibition has previously been shown to result in an increase in cathepsin D

immunofluorescence staining (Rideout et al, 2004). The increase in active cathepsin D observed with treatments that included BafA1 may be a result of an accumulation of lysosomes following impaired fusion of autophagosomes and lysosomes.

4.3.2.2. Conclusion

The effect of 24 hour treatment with MPP+, epoxo and MPP+/epoxo on the levels and distribution of neurofilaments, vimentin, dynein intermediate chain, p62 and LC3 is summarised in Figure 4.33. All three treatments resulted in a reduction in the levels of dynein intermediate chain and vimentin. The reduction in dynein intermediate chain levels may have serious implication for the axonal transport system, defects which have been associated with protein aggregation as mentioned earlier. Enrichment of pNF-M, NF-H, p62 and α -tubulin in the igepal insoluble were also observed, suggestive of protein aggregation.

Treatment of RA/BDNF differentiated cells with MPP+, epoxo and MPP+/epoxo may be promising inclusion-producing models since NF-H with p62 and LC3 co-localizes and accumulates in the perinuclear region. Further work could involve extended treatment regimes since in COS-7 cells expressing human α -synuclein, longer treatments with rotenone resulted in increased inclusion formation that became more resistant to clearance (Lee et al, 2004). Confirmation of inclusion formation and characterisation of inclusions could be accomplished with immunofluorescence staining for other markers of aggresomes and scanning electron microscopy.

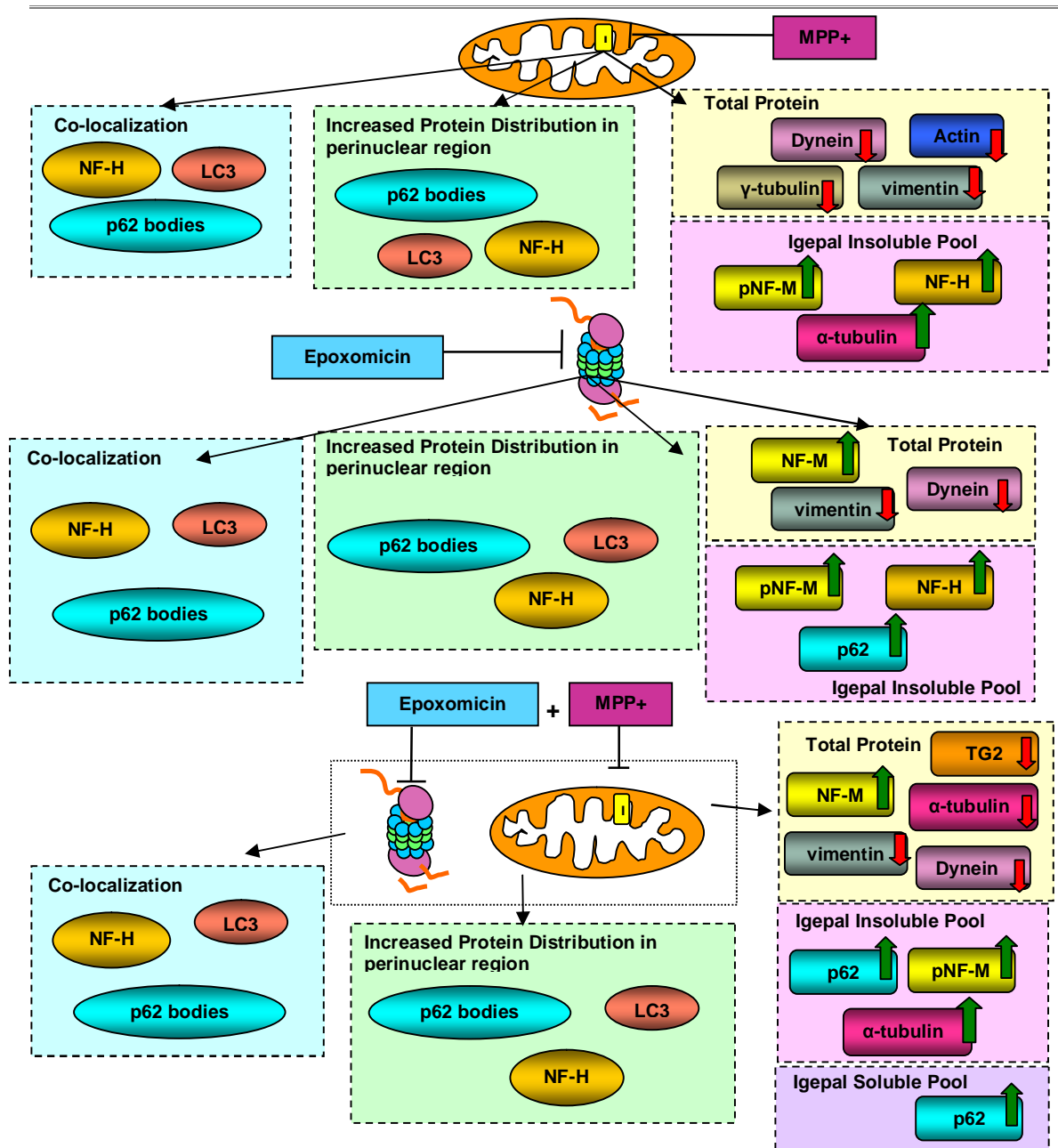


Figure 4.33 Diagrammatic representation of the effects of 24 h treatment of RA/BDNF differentiated SH-SY5Y neuroblastoma cells with 500 μ M MPP+, 10 nM epoxomicin (epoxo) and 500 μ M MPP+/10 nM epoxo on protein levels and distribution.

All three treatments resulted in a reduction (red arrows) in the levels of dynein intermediate chain and vimentin in total cell extracts, an increase (green arrows) in pNF-M and p62 in the igeal insoluble pool and an accumulation of NF-H, p62 and LC3B immunofluorescence in the perinuclear region. Co-localisation of NF-H with p62 and LC3B in the perinuclear region was also observed. MPP+ treatment also resulted in a decrease in actin and γ -tubulin in total protein and an increase in NF-H and α -tubulin in the igeal insoluble pool. Epoxo treatment resulted in an increase in NF-M in total protein and NF-H in the igeal insoluble pool. With MPP+/epoxo treatment a decrease in α -tubulin and TG2 total protein and an increase in NF-M in total protein, α -tubulin in the igeal insoluble pool and p62 in the igeal soluble pool was observed.

CHAPTER 5

***DEVELOPMENT AND CHARACTERISATION
OF GFP TAGGED NEUROFILAMENTS***

5.1. Introduction

5.1.1. Green Fluorescent Protein

Green Fluorescent Protein (GFP) exhibits bright green fluorescence when exposed to blue light. It is composed of 11 β -pleated sheets arranged as a β -barrel with the chromophore located in the centre of the barrel structure (Figure 5.1 A). The chromophore is formed by the amino acid triplet *Ser-Tyr-Gly* at positions 65-66-67 (Figure 5.1 B); the amide nitrogen of Gly67 and the carbonyl of Ser65 react to form a cyclic ring structure and the tyrosine side chain is then oxidized and its hydroxyl group is deprotonated (Heim et al, 1994). The position of the chromophore in the β -barrel protects it from solvent quenching effects and explains why attempts to truncate GFP to decrease its size have not been successful. Since GFP has no cofactor requirement for fluorescence it can be used to track gene expression and protein dynamics by fusing GFP to a protein of interest (reviewed by Miyawaki et al, 2003, Straight, 2007, and Tsien, 1998).

GFP and GFP-like proteins are quite large (25-30 kD) and as such fusion of GFP to a protein may alter its structure and function. To be confident that the GFP fusion protein can be used to study a protein of interest it is necessary to determine whether its presence alters the localization or behaviour of the protein. There are three categories that GFP fusion proteins should ideally fulfil (Straight 2007):

1. The distribution of the GFP fusion protein should be similar to the distribution of the endogenous protein. This can be accomplished with antibody staining
2. If the protein has some kind of enzymatic activity, the GFP fusion protein should retain the same activity and kinetics of the endogenous enzyme.
3. The fusion protein should be produced at levels comparable to the endogenous protein and have a similar half-life.

5.1.2. GFP-tagged Neurofilaments

The tagging of intermediate filaments (IFs) with GFP has revolutionized the study of IF behaviour. In a review of fluorescence-based methods used to study IFs, Flitney and Goldman (2004) suggest that although GFP can be attached to either the N- or C-termini of IF proteins, targeting to the N-terminus best retains IF function. The vast majority of studies employing GFP tagged NFs tend to have the NF proteins tagged with GFP on their N-terminus, of which a few are discussed below.

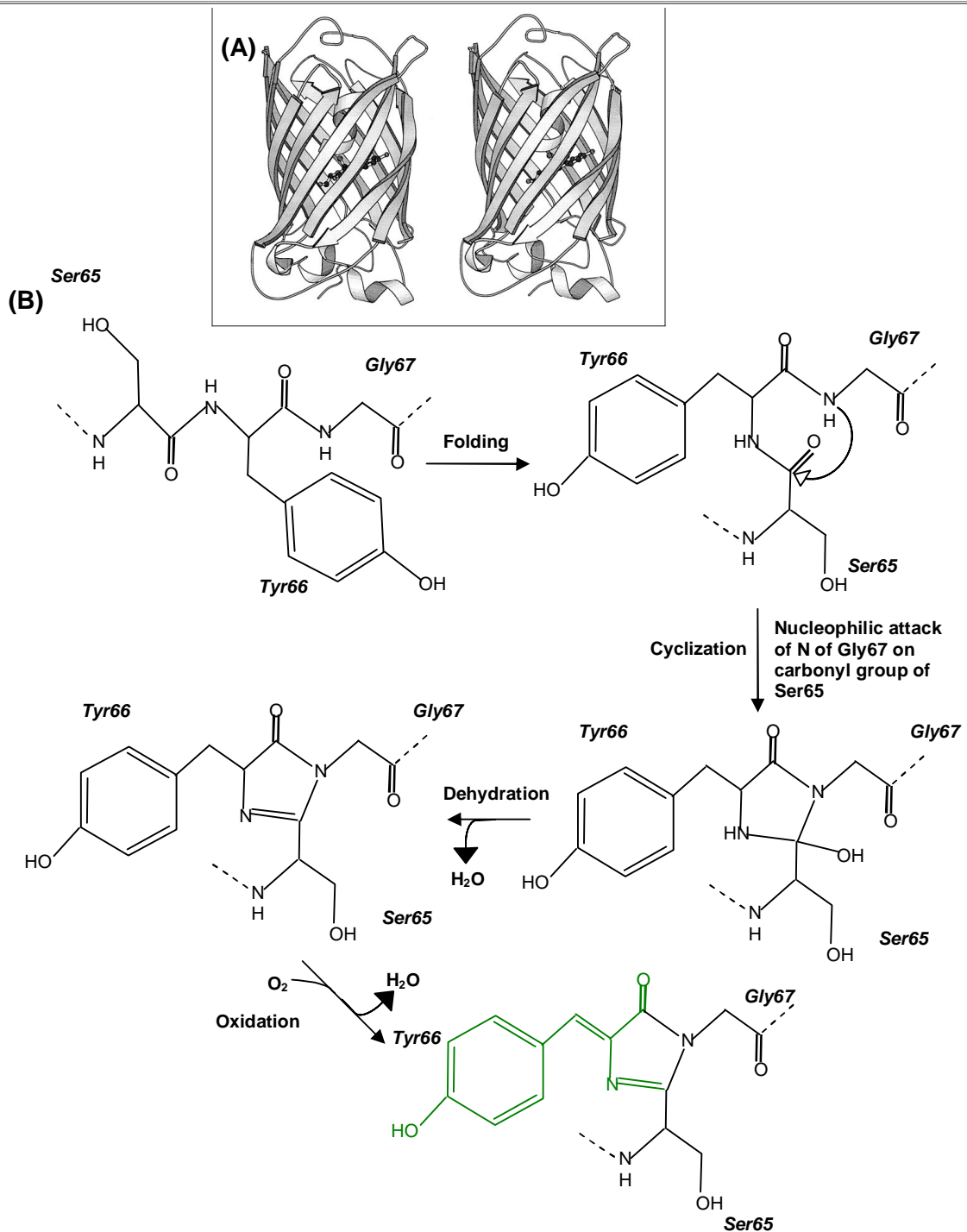


Figure 5.1 The structure of GFP and its chromophore.

(A) The barrel shaped structure of Green fluorescent protein formed by the 11 β -pleated sheets with the chromophore situated in the centre of the barrel (Figure from Tsien 1998). (B) The chromophore is produced by the cyclization of Ser65, Tyr66 and Gly67 and the oxidation of the tyrosine side-chain. The initial step in chromophore formation is folding of the GFP protein, then cyclization is achieved by nucleophilic attack of the carbonyl group of Ser65 by the amide N of Gly67, then dehydration followed by oxidation. The chromophore is shown in green (reviewed by Miyawaki et al, 2003, Straight, 2007, and Tsien, 1998).

The use of GFP tagged NFs has advanced our understanding of NF proteins, due to the opportunity to investigate their behaviour using time-lapse imaging on live cells. The use of GFP/NF-H provided evidence that NFs are transported rapidly but also intermittently, so that

their transport is interrupted by long periods in which NFs are stationary, resulting in an overall slow transport rate (Roy et al, 2000). The rapid and intermittent transport of NFs was confirmed with GFP/NF-M using Fluorescence Recovery After Photobleaching (FRAP) and time-lapse imaging (Wang & Brown, 2001). NFs were also shown to be transported as polymers that contain NF-M, NF-L and two other neuronal IF proteins called α -internexin and peripherin in cultured sympathetic neurons using GFP/NF-M and GFP/NF-L (Yan et al, 2007, Yan & Brown, 2005). Work with GFP/NF-M has also led to the discovery that when neurofilaments enter the growth cone in the distal axon, they quickly reverse direction; resulting in a high proportion of NFs undergoing retrograde transport in the distal axon (Uchida & Brown, 2004).

GFP/NF-M has also been used to investigate the role of the motor proteins, kinesin and dynein in the anterograde and retrograde transport of NFs (Motil et al, 2006, Theiss et al, 2005). The importance of phosphorylation of NF-H and NF-M tail domains by Cdk5 in the regulation of neurofilament transport was investigated using GFP/NF-H (Ackerley et al, 2003) and GFP/NF-M (Moran et al, 2005).

In studies of neurodegeneration, NF-M tagged with GFP on its N-terminus has been used to study the effect of glutamate (Ackerley et al, 2000), arsenic (DeFuria & Shea, 2007), the overexpression of peripherin (Millecamps et al, 2006) and the expression of Charcot-Marie-Tooth disease (CMT) associated NF-L mutations (Brownlee et al, 2002) on neurofilament transport and distribution.

5.1.3. Aims

This chapter describes the development and characterization of GFP tagged NF proteins transiently transfected into SH-SY5Y cells. In addition, the use of GFP tagged NFs was assessed as (a) bait to identify NF-associating proteins by co-immunoprecipitation of GFP and (b) to track changes in NF distribution in real-time following MPP⁺ treatment.

5.2. Results

5.2.1. Development and characterisation of GFP-tagged neurofilament medium chain

5.2.1.1. Cloning of human *NF-M* into *pEGFP-C3*

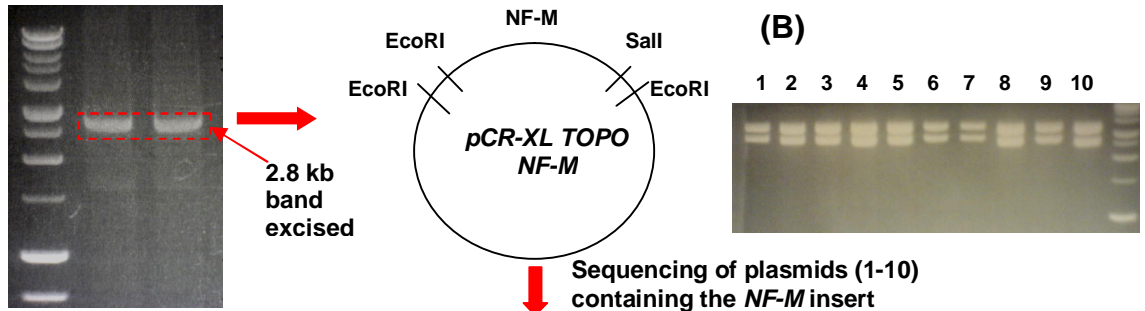
NF-M was amplified from an SH-SY5Y cDNA preparation. Figure 5.2 is a schematic representation describing the cloning of *GFP/NF-M*. To ensure that the DNA insert is always inserted into the GFP plasmid in the correct orientation, the forward and reverse primers (given below) used to amplify *NF-M* were designed with *EcoRI* (highlighted in yellow) and *Sall* (highlighted in teal) restriction endonuclease recognition sequences on their 5' ends respectively. The sequence complementary to the sequence of human *NF-M* is underlined below, the transcription start site is highlighted in green and the transcription stop site is highlighted in red.

Fwd: 5'-GAATTCAGATGAGCTACACGTTGGACTC-3'

Rev: 5'-GTCGACTTAGTCACTCTGGGTGACTTCCTTT-3'

The PCR product was analysed by agarose gel electrophoresis (Figure 5.2 A) and determined to be the expected 2.8 kb for *NF-M*. The 2.8 kb band was excised from the gel, purified and cloned into pCR-XL TOPO for sequencing. Sequence analysis of the cloned DNA and comparison with the database entry for human *NF-M* (NM_005382) confirmed that it was *NF-M*, but also that it contained a PCR derived point mutation resulting in a G→A substitution (Figure 5.2 C). This mutation resulted in a glutamate to lysine amino acid substitution and was reversed by site directed mutagenesis which is described in more detail in section 2.2.12.8. The GFP expression vector used was kindly donated by Carl Miller (Kings College London) and contained a rat *NF-M* insert (*pEGFP-C3 rNF-M*). To clone human *NF-M* into the GFP expression vector (*pEGFP-C3*), *pEGFP-C3 rNF-M* and *pCR-XL TOPO hNF-M* were digested by quantitative double digest (described in section 2.2.12.7.2) with the restriction endonucleases *Sall* and *EcoRI*. The digests were analysed by agarose gel electrophoresis (Figure 5.2 D) and the bands corresponding to *pEGFP-C3* and *hNF-M* were excised, purified from the gel and ligated by T4 DNA ligase. *pEGFP-C3 hNF-M* (GFP/*NF-M*) clones were analysed by restriction endonuclease digestion with *Sall* and *EcoRI* and agarose gel electrophoresis. Clone 3 was selected and sequenced to confirm the sequence was that of *NF-M* and that *GFP* and *NF-M* were in-frame.

(A) PCR amplification of *NF-M* from SH-SY5Y cDNA. *NF-M* PCR product containing *EcoRI* and *Sall* restriction sites cloned into *pCR-XL TOPO* and analysed by restriction endonuclease digest with *EcoRI*

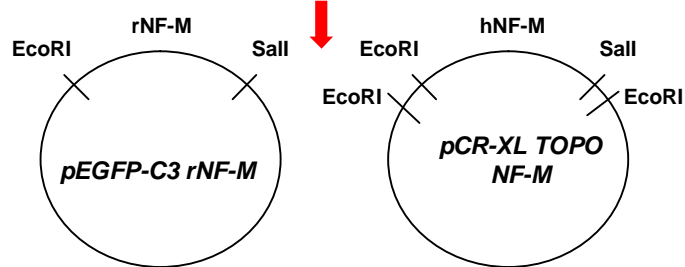


(C) Sequencing of plasmids (1-10) containing the *NF-M* insert

GGTGC ACTACCTG **Glu → Lys** AGCAGCAG Clone 2
 GGTGC ACTACCTGGAGCAGCAG *NF-M* (NM_005382)

Site-directed mutagenesis

GGTGC ACTACCTG **G** AGCAGCAG Clone 2 after mutagenesis
 GGTGC ACTACCTGGAGCAGCAG *NF-M* (NM_005382)

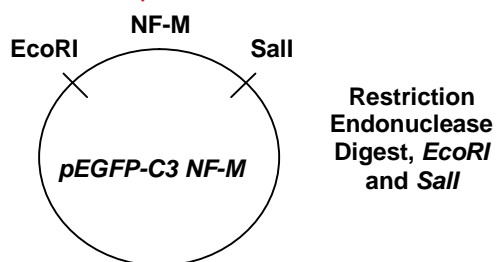


(D) Quantitative Endonuclease Digest, *EcoRI* and *Sall*

4.7 kb *pEGFP-C3* and 2.8 kb *NF-M* bands were excised



Ligation with T4 DNA Ligase



(E) 4.7 kb *pEGFP-C3* and 2.8 kb *NF-M* bands

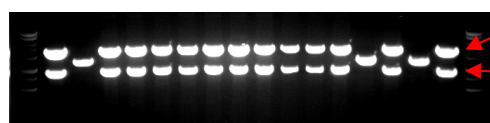


Figure 5.2 A schematic of the cloning procedure used to clone *NF-M* into *pEGFP-C3*.

NF-M was amplified by PCR from a preparation of SH-SY5Y cDNA using forward and reverse primers containing the *EcoRI* and *Sall* recognition sequences respectively. (A) The PCR product was excised and purified from the gel and cloned into the cloning vector *pCR-XL-TOPO*. From a restriction endonuclease digest with *EcoRI* (B) plasmids containing the *NF-M* insert were selected and sent for sequencing. (C) The clone selected for cloning into *pEGFP-C3* (clone 2) had a point mutation (highlighted in red) at position 427 bp which results in a Glutamic acid (*Glu*) to Lysine (*Lys*) amino acid substitution which was removed by site-directed mutagenesis (shown in teal). *NF-M* was isolated from *pCR-XL-TOPO* by restriction endonuclease digestion with *EcoRI* and *Sall* and the *rNF-M* insert in the *pEGFP-C3* vector was removed by restriction endonuclease digestion of *pEGFP-C3 rNF-M* with *EcoRI* and *Sall*. (D) The bands corresponding to *pEGFP-C3* (4.7 kb) and *NF-M* (2.8 kb) were excised (indicated in red) and purified from the gel. *NF-M* and *pEGFP-C3* were ligated by T4 DNA ligase and plasmid preparations were analysed by restriction endonuclease digests with *EcoRI* and *Sall* (E).

5.2.1.2. Characterisation of GFP/NF-M expression in SH-SY5Y cells

Western blots of total cell extracts from GFP/NF-M expressing cells probed with anti-GFP, anti-NF-M and anti-pNF-M can be found in Figure 5.3 A. On blots probed with anti-GFP (Figure 5.3 A i), a 30 kD band corresponding to GFP was found in extracts from GFP expressing cells, and a 180 kD band corresponding to the predicted molecular weight of 180 kD for GFP/NF-M was found in extracts from GFP/NF-M expressing cells. The apparent molecular weights of GFP/NF-M and GFP were determined using their Rf values to compare their electrophoretic mobility to that of molecular weight standards run on the same gel (Appendix II). On blots probed with anti-NF-M (Fig 5.3 A ii) and anti-pNF-M (Fig 5.3 A iii), GFP expressing cells contained endogenous NF-M (150 kD) whilst GFP/NF-M expressing cells contained both endogenous NF-M (150 kD) and GFP/NF-M (180 kD). Again, the apparent molecular weights of endogenous NF-M and GFP/NF-M were confirmed using Rf values (Appendix II).

Laser confocal microscopy confirmed that the pattern of GFP/NF-M expression in GFP/NF-M expressing cells (Figure 5.3 B ii) was similar to NF-M expression in wild-type cells visualised by immunofluorescence staining of NF-M with anti-NF-M (RMO270, Figure 5.3 B i).

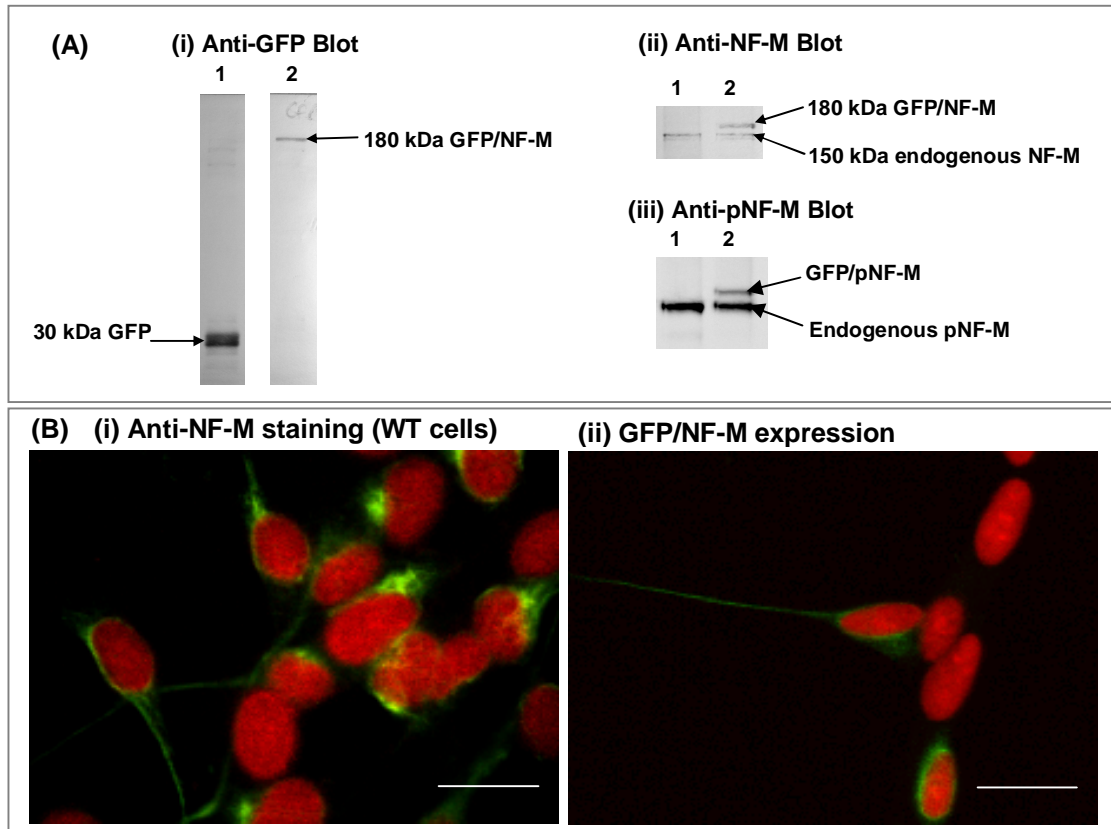


Figure 5.3 The Characterisation of GFP/NF-M expression in SH-SY5Y cells.

(A) Western blots of total cell extracts of SH-SY5Y neuroblastoma cells transfected with (1) GFP and (2) GFP-tagged NF-M probed with anti-GFP and anti-NF-M antibodies.; (i) the anti-GFP blot shows a 180 kDa band corresponding to the GFP/NF-M fusion protein and (ii) the anti-NF-M and (iii) anti-pNF-M blots both have a band corresponding with the endogenous NF-M and a band corresponding to the GFP/NF-M fusion protein. (B) Confocal microscope images of (i) wild-type SH-SY5Y cells stained with anti-NF-M (green) and (ii) GFP/NF-M expressing cells showing GFP/NF-M expression (green). Nuclei were counterstained with propidium iodide. Cells were viewed using the 63 x objective. Scale bar represents 20 μ m.

To further characterize GFP/NF-M expression, its co-localization with the other NF subunits was investigated by laser confocal microscopy and immunofluorescence staining with anti-NF antibodies (Figure 5.4). Immunofluorescence staining with anti-NF-H (n52, Figure 5.4 A), anti-pNF-M/pNF-H (smi31, Figure 5.4 B) and anti-NF-L (DA2, Figure 5.4 C) and anti-NF-M (RMO270, Figure 5.4 D) revealed that GFP/NF-M colocalised with all three NF subunits.

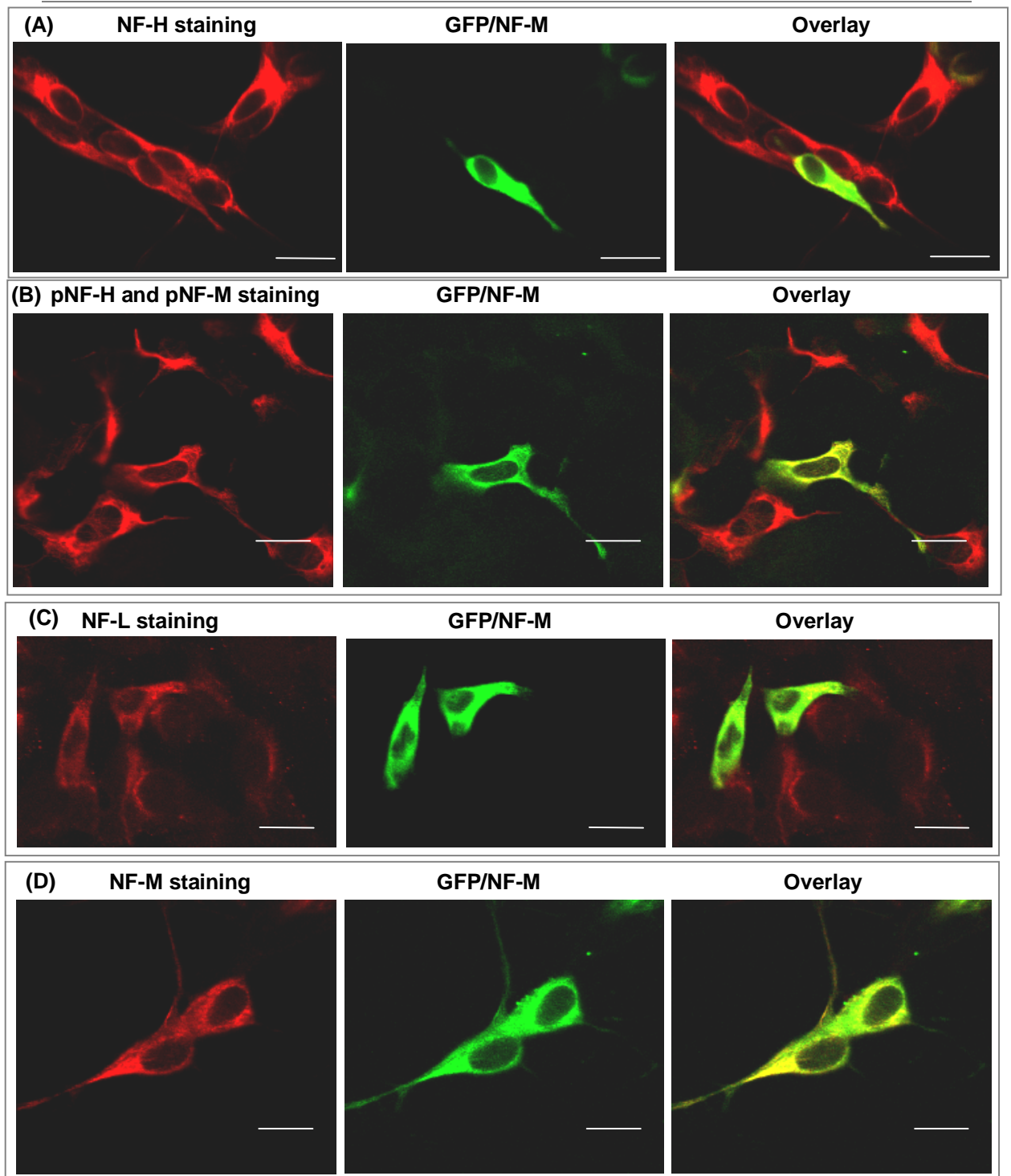


Figure 5.4 Assessment of GFP/NF-M co-localisation with endogenous neurofilaments (NFs).

Confocal microscope images of SH-SY5Y neuroblastoma cells expressing GFP/NF-M showing the co-localization of GFP/NF-M with each of the NF subunits. GFP/NF-M expressing cells were stained with (A) anti-NF-H (n52, 1:200), (B) anti-phosphoryated NF-H and NF-M (smi31, 1:100), (C) anti-NF-L (DA2, 1:100) and (D) anti-NF-M (RMO270, 1:50). The antibody staining - detected using a goat anti-mouse alexafluor 568 conjugated secondary antibodies - is shown in red on the left hand side of each panel and GFP fluorescence of the GFP-tagged NF-M is shown in green in the centre of each panel. As the red and green images are overlaid as seen on the right of each panel, areas of co-localization are highlighted yellow. Cells were viewed with a 63 x oil objective, scale bar represents 20 μm .

The transfection efficiency of the LipofectAMINE™2000 transfection with GFP/NF-M was estimated from the mean number of propidium iodide stained nuclei and the mean number of cells with GFP fluorescence in laser confocal microscope images from 5 different experiments (the number of images analysed per experiment are indicated in brackets in Table 5.1). The mean percentage of GFP/NF-M expressing cells was 19.2 ± 2.0 % of the total number of cells.

Table 5.1 The transfection efficiency of GFP/NF-M in Human SH-SY5Y neuroblastoma cells using LipofectAMINE™2000.

The mean numbers of cells expressing GFP/NF-M fluorescence were expressed as a percentage of the mean number of total cells (determined from the number of propidium iodide stained nuclei). The numbers of cells were counted in laser confocal microscope images from 5 different experiments, the number of images of different fields of view that were analysed are indicated in the brackets.

<i>Experiment</i>	<i>Mean number of Propidium iodide stained nuclei</i>	<i>Mean number of cells with GFP fluorescence</i>	<i>Transfected cells (%)</i>
<i>1 (3)</i>	48.3	8.3	17.2
<i>2 (6)</i>	14.7	3.8	26.1
<i>3 (7)</i>	20.3	3.9	19.0
<i>4 (4)</i>	12.3	2.0	16.3
<i>5 (3)</i>	19.3	3.3	17.2
<i>mean ± SEM</i>	23.0 ± 7.3	4.3 ± 1.2	19.2 ± 2.0

To assess whether attachment of GFP altered the degradation of GFP/NF-M, the half-life of GFP/NF-M was determined by treating GFP/NF-M expressing cells with CHX over a 72 hour time course and immunoprobng Western blots of total cell extracts with anti-GFP or anti-NF-M. The half-lives of GFP/NF-M calculated from the anti-GFP (Figure 5.5 B) and anti-NF-M blots (Figure 5.5 C) were similar at 13.8 ± 2.2 h and 17.4 ± 0.8 h respectively. When looking at the lower band on the anti-NF-M blot thought to correspond with endogenous NF-M (figure 5.5 A and D), the signal peaks at 24 hours and then decreases again after 48 hours. Figure 5.5 E was produced from the sum of both bands of the anti-NF-M Western blot. The half-life calculated from the ‘line of best fit’ in this case was 20.2 ± 1.4 h, which is slightly longer than that calculated from the anti-GFP Western blot.

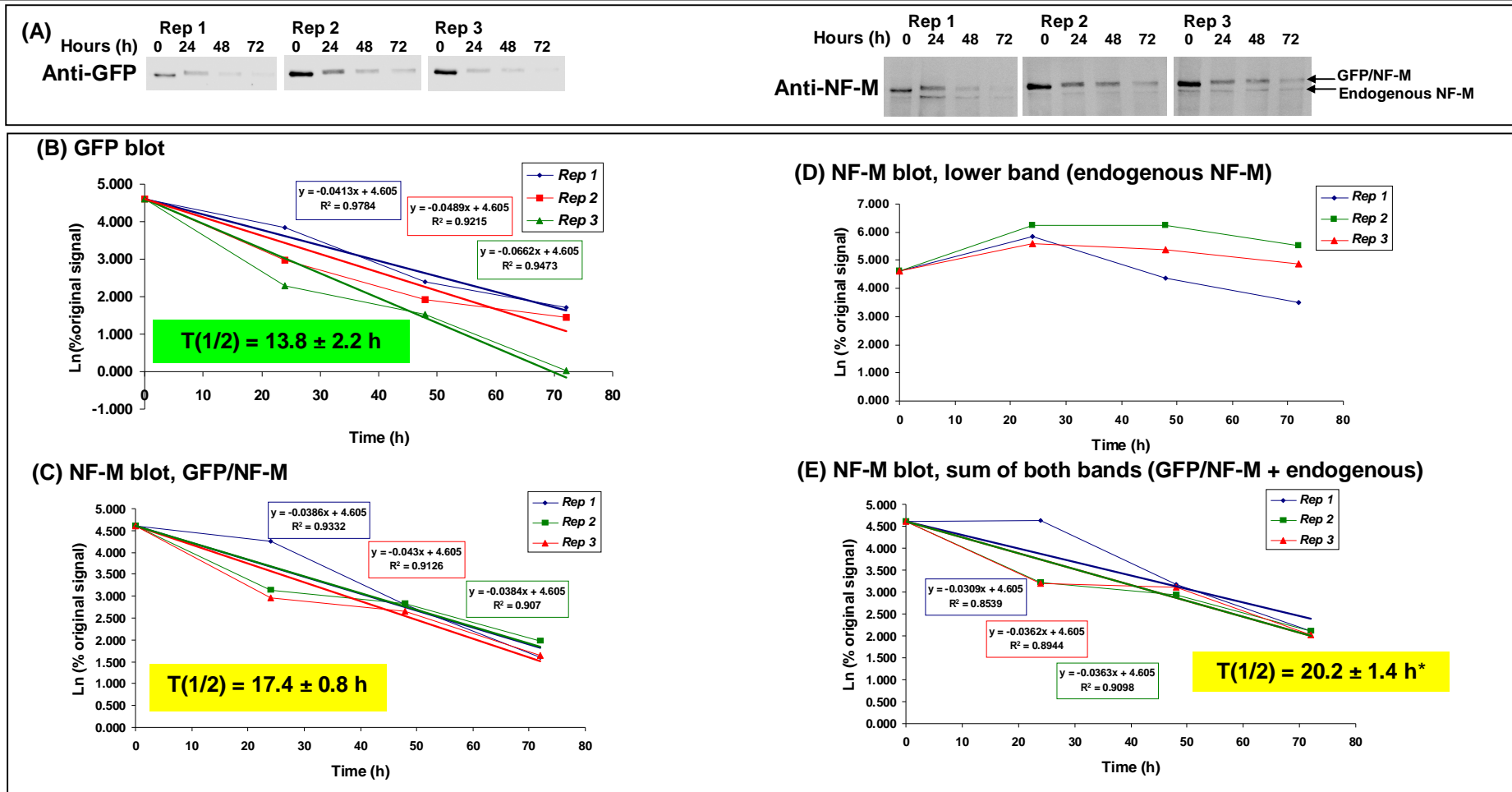


Figure 5.5 Assessment of the half-life of GFP/NF-M using Western blots of total cell extracts from SH-SY5Y neuroblastoma cells expressing GFP/NF-M and treated with 10 µg/ml cycloheximide over a 72 hour time-course. (A) Western blots were probed with anti-GFP antibody (1:5000; abcam) or anti-NF-M (1:500; RMO270, Zymed). (B) and (C) Half-life of GFP/NF-M from three experiments was calculated from the slope of the ‘line of best fit’ obtained when plotting the natural logarithm of the percentage original signal for each experiment (ie signal at 0 h) against time (h). (D) Plot of the natural logarithm of percentage original signal for the lower band on the anti-NF-M blot which corresponds with endogenous NF-M shows an peak in the signal at 24 h. (E) Half-life of NF-M calculated using both bands on the anti-NF-M blot was significantly greater than half-life calculated from the anti-GFP blot (* T-Test, $p < 0.05$; $n = 3$). Half-lives quoted are mean half-lives from 3 independent experiments ± SEM.

5.2.2. Development and characterisation of GFP-tagged neurofilament light chain

5.2.2.1. Cloning of human *NF-L* into *pEGFP-C3*

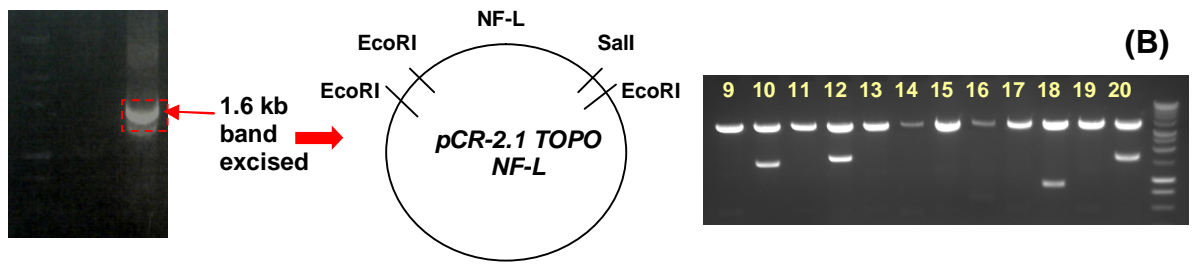
Again, to ensure that *NF-L* (amplified from SH-SY5Y cDNA) was inserted into the GFP expression vector in the correct orientation, the forward and reverse primers (given below) were designed with *EcoRI* (highlighted in yellow) and *Sall* (highlighted in teal) restriction endonuclease recognition sequences on their 5' ends respectively. The start codon is highlighted in green, the stop codon is highlighted in red and the part of the primer sequence homologous to human *NF-L* is underlined:

Fwd: 5'-GAATTC^{CC}ATGAGTTCCTTCAGCTACGAG-3'
 Rev: 5'-GTCGACGGGGGT^{TCA}ATCTTTCTTCTTAGC-3'

The PCR product was analysed by agarose gel electrophoresis (Figure 5.6 A) and determined to be the expected 1.6 kb for *NF-L*. This band was excised from the gel, purified and cloned into *pCR-2.1 TOPO* for sequencing. Sequence analysis of the cloned DNA with the database entry for human *NF-L* (NM_006158) confirmed that it was *NF-L*, but also that it contained a PCR derived point mutation resulting in an A→G substitution (Figure 5.6 C). This mutation which results in an arginine to lysine amino acid substitution was reversed by site directed mutagenesis (described in more detail in section 2.2.12.8.).

Human *NF-L* was cloned into the GFP expression vector (*pEGFP-C3*) by preparing quantitative double digests (described in section 2.2.12.7.2) of *pEGFP-C3 rNF-M* and *pCR-2.1 hNF-L* with the restriction endonucleases *Sall* and *EcoRI*. The digests were analysed by agarose gel electrophoresis (figure 5.6 D) and the bands corresponding to *pEGFP-C3* and *hNF-L* were excised, purified from the gel and ligated by T4 DNA ligase. *pEGFP-C3 hNF-L* clones were analysed by restriction endonuclease digestion with *Sall* and *EcoRI* and agarose gel electrophoresis (figure 5.6 E). Clone 11 was selected and sequenced to confirm *hNF-L* identity and that *GFP* and *NF-L* were in-frame.

(A) PCR amplification of *NF-L* from SH-SY5Y cDNA *NF-L* PCR product containing *EcoRI* and *Sall* restriction sites cloned into *pCR-2.1 TOPO* and analysed by restriction endonuclease digest with *EcoRI*

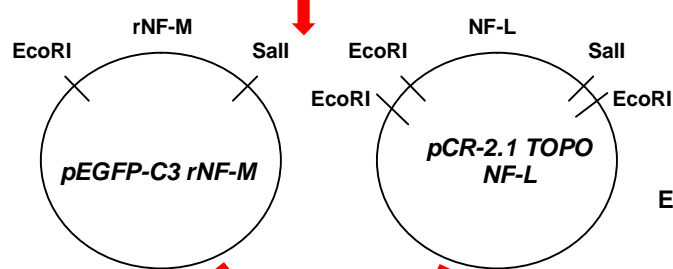


Sequencing of plasmids (10, 12 and 20) containing the *NF-L* insert

(C)
 GAAGAAGCAAAA **Arg → Lys** AAGAAGAAG Clone 12
 GAAGAAGCAAAAAGAAGAAGAAG *NF-L* (NM_006158)

Site-directed mutagenesis

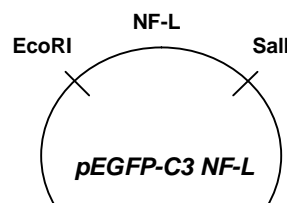
GAAGAAGCAAAA **G**AGAAGAAG Clone 12 after mutagenesis
 GAAGAAGCAAAAAGAAGAAGAAG *NF-L* (NM_006158)



Quantitative Endonuclease Digest, *EcoRI* and *Sall*



Ligation with T4 DNA Ligase



Restriction Endonuclease Digest, *EcoRI* and *Sall*

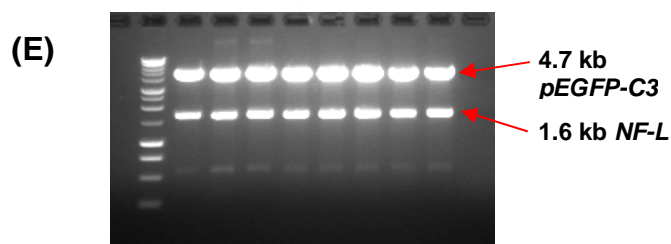


Figure 5.6 A schematic of the cloning procedure used to clone *NF-L* into *pEGFP-C3*.

NF-L was amplified by PCR from a preparation of SH-SY5Y cDNA using forward and reverse primers containing the *EcoRI* and *Sall* recognition sequences respectively (A) and cloned into the cloning vector *pCR-2.1-TOPO*. From a restriction endonuclease digest with *EcoRI* (B) plasmids containing the *NF-L* insert were selected and sent for sequencing. (C) The clone selected for cloning into *pEGFP-C3* (clone 12) had a point mutation (highlighted in red) at position 1616 bp which results in an Arginine (Arg) to Lysine (Lys) amino acid substitution which was removed by site-directed mutagenesis (shown in blue). *NF-L* was isolated from *pCR-2.1-TOPO* by digestion with *EcoRI* and *Sall* and the *rNF-M* insert in the *pEGFP-C3* vector was removed by restriction endonuclease digestion of *pEGFP-C3 rNF-M* with *EcoRI* and *Sall*. (D). The bands corresponding to *pEGFP-C3* (4.7 kb) and *NF-L* (1.6 kb) were excised (indicated in red) and purified from the gel. *NF-L* and *pEGFP-C3* were ligated by T4 DNA ligase and plasmid preparations were analysed by restriction endonuclease digests with *EcoRI* and *Sall* (E).

5.2.2.2. Characterisation of GFP/NF-L expression in SH-SY5Y cells

Western blots of total cell extracts of GFP and GFP/NF-L expressing cells probed with anti-GFP (Figure 5.7 A i) confirmed the presence of a 30 kDa band corresponding to GFP in extracts from GFP expressing cells and a 100 kDa band in extracts from GFP/NF-L expressing cells. In blots probed with anti-NFL (Figure 5.7 A ii), a 70 kDa band corresponding to endogenous NF-L was found in extracts of GFP expressing and GFP/NF-L expressing cells as well as an additional band of 100 kDa corresponding to the predicted apparent molecular weight of GFP/NF-L. The apparent molecular weights of GFP, GFP/NF-L and NF-L were all determined by using Rf values to compare their electrophoretic mobility to those of molecular weight standards run on the same gel (Appendix II).

The expression of GFP/NF-L was compared to NF-L expression in wild-type cells by immunofluorescence staining of NF-L (Figure 5.7 B). In GFP/NF-L expressing cells, clumps or aggregates of GFP fluorescence were found in the perinuclear region (Figure 5.7 B ii). Transfection of GFP/NF-L into SH-SY5Y cells produced a mixed population (Figure 5.8) with some cells exhibiting normal NF-L expression pattern (compared to wild-type – Figure 5.7 B i) and others in which aggregations of GFP/NF-L were found.

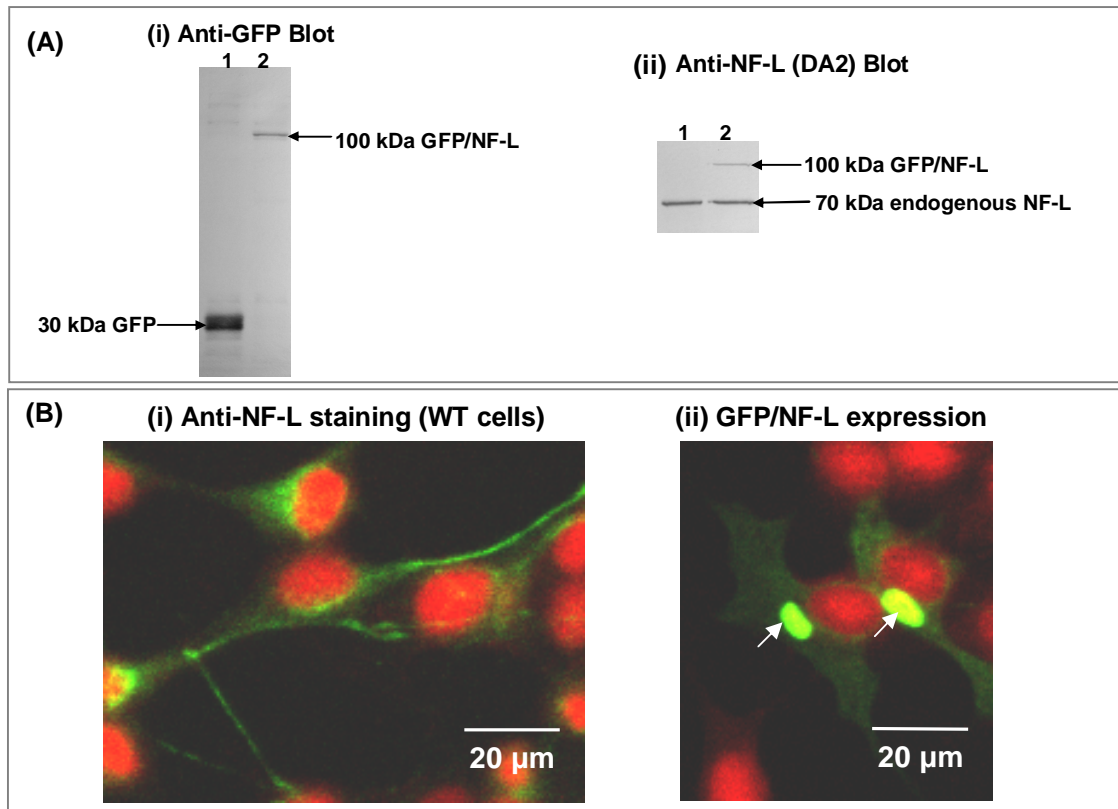


Figure 5.7 Characterisation of GFP/NF-L expression in SH-SY5Y neuroblastoma cells.

(A) Western blots of total cell extracts of SH-SY5Y neuroblastoma cells transfected with (1) GFP and (2) GFP-tagged NF-L probed with anti-GFP and anti-NF-L (DA2). For cell extracts of GFP/NF-L expressing cells, (i) the anti-GFP blot shows a 100 kDa band corresponding to the GFP/NF-L fusion protein and (ii) the anti-NF-L blot shows a 70 kDa band for endogenous NF-L and a 100 kDa band corresponding to the GFP/NF-L fusion protein. (B) Confocal microscope images of (i) wild-type SH-SY5Y stained with anti-NF-L (green) and (ii) GFP/NF-L expressing cells showing GFP/NF-L expression (green) results in a clump of GFP fluorescence in the perinuclear region. Nuclei were counterstained with propidium iodide (red) and cells were viewed using the 63 x objective. Scale bar represents 20 µm.

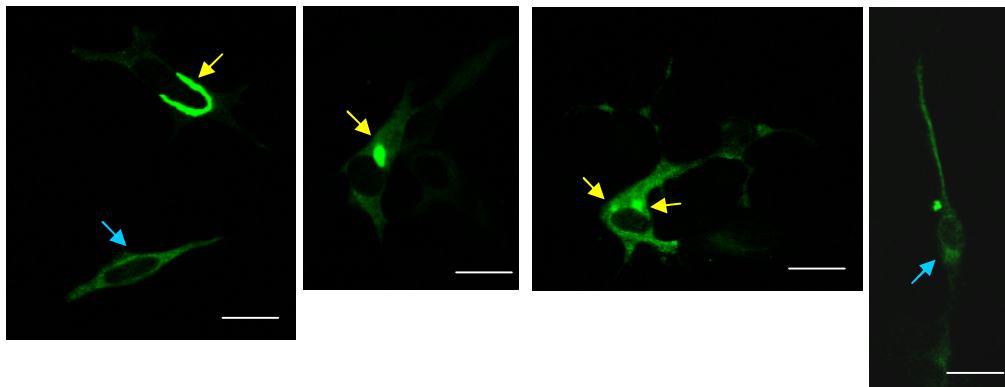


Figure 5.8 GFP/NF-L aggregates were found in SH-SY5Y cells with high GFP/NF-L expression.

Confocal microscope images of GFP/NF-L revealed that most GFP/NF-L expressing cells contain regions of accumulated GFP/NF-L in the perinuclear region (indicated by yellow arrows) but some cells with lower levels of GFP/NF-L expression do not show GFP/NF-L accumulation (indicated by blue arrows). Cells were viewed with the 63 x objective, scale bar represents 20 µm.

5.2.3. Development and characterisation of GFP-tagged neurofilament heavy chain

5.2.3.1. Cloning of human *NF-H* into *pEGFP-C3*

Initial attempts to amplify the entire sequence of *NF-H* did not yield a full-length *NF-H* cDNA sequence (results not shown) which may be due to the high GC content of the first 1000 bp of the *NF-H* sequence (as can be seen in the CpG plot in Figure 5.9 A). The GC-rich region would be prone to the formation of secondary structures which could interfere with primer elongation. As a result of this region of high GC content, a different strategy which involved cloning *NF-H* in two separate parts (the so-called N-terminal part containing this GC-rich region and the C-terminal part) was adopted. A unique *XmnI* endonuclease recognition sequence located within the first 1000 bp of wild-type *NF-H* cDNA was selected as the region of overlap between the N- and C-terminal parts of *NF-H*. To accomplish this, the reverse primer of the N-terminal part and the forward primer of the C-terminal part were complementary to each other and contained the *XmnI* endonuclease recognition sequence (Figure 5.9 B).

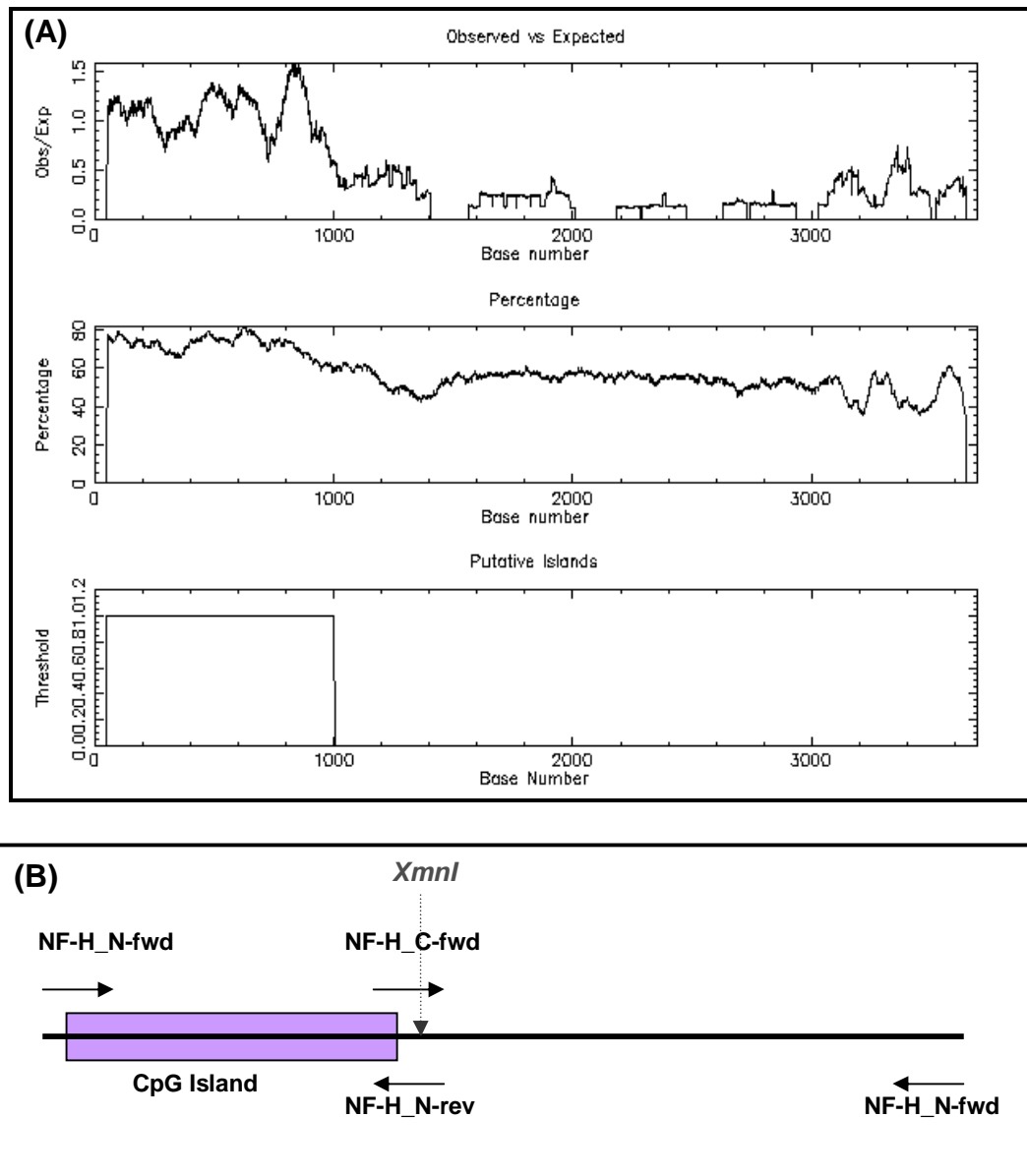


Figure 5.9 CpG plot showing GC content of *NF-H* cDNA and scheme depicting the cloning strategy adopted to clone the GC-rich N-terminus and the C-terminus of *NF-H* separately.

(A) The GC content of *NF-H* cDNA (NM_021076) as determined by CpG plot using EMBOSS/CpG plot tool on EMBL-EBI. The CpG plot shows a high GC content in the first 1000 bp of the *NF-H* sequence which may result in the formation of secondary structures which interfere with the PCR reaction by not allowing the primers to bind. (B) In order to clone *NF-H* in two parts, primers were designed around a unique *XmnI* restriction endonuclease recognition sequence in the *NF-H* sequence that divides the *NF-H* cDNA into roughly two halves. The primers were designed so that the N- and C-terminal parts overlapped at this point. PCR amplification of the two parts will result in an 1110 bp N-terminal part and a 1984 bp C-terminal part.

The cloning procedure of the N-terminal part of *NF-H* into *pCR-2.1-TOPO* is depicted in the top panel of Figure 5.10. The N-terminal part of *NF-H* was amplified using a genomic PCR kit optimized for amplifying GC rich sequences and the forward and reverse primers listed

below (translational start codon highlighted in green, sequence homologous to NF-H is underlined, XmnI recognition sequence highlighted in pink):

Fwd: 5'-TGCTCAGGCCATGATGAGCTTCG-3'

Rev: 5'-TGGTCCTTCGGTAAGTCGTCGAC-3'

The genomic PCR kit contains a GC melt solution (5 M) which melts any secondary stem-loop structures in GC rich regions, allowing primer elongation. The best results were obtained when using 5 µl of GC melt solution in the PCR mix. The lack of a PCR product in the PCR reaction containing no GC melt is noteworthy since it supports the hypothesis that secondary structures formed in the GC rich region prevented primer elongation.

Plasmids containing the 1110 bp insert were sequenced and clones that best matched the data-base sequence for *NF-H* (NM_021076) were selected. The selected clone had one PCR derived C→T mutation at position 164 introducing a *Ser*→*Phe* amino-acid substitution which was removed by site-directed mutagenesis described in more detail in section 2.2.12.8 (Figure 5.10 C). The transformation of the mutagenesis reaction yielded a single *NF-H* clone which was sequenced and confirmed to be correct.

The primers designed for the amplification of the C-terminal part of *NF-H* from a SH-SY5Y cDNA preparation are listed below (translational stop codon is highlighted in red, the sequence homologous to *NF-H* is underlined and the *XmnI* recognition sequence is highlighted in pink):

Fwd: 5'-ACCAGGAAGCCATTCAGCAGCTG-3'

Rev: 5'-TGTTCCGGCGGTTCCCCTTCATT-3'

The C-terminal part of *NF-H* was amplified using five different PCR reactions with different polymerases and buffers (Figure 5.10 D). Of the five reactions, three yielded PCR products of the expected 1.98 kb for the C-terminal part of *NF-H*. The 1.98 kb bands for the Platinum Taq DNA polymerase and the Platinum PCR SuperMix reactions were excised and purified from the gel and cloned into pCR-XL-TOPO. The results of *EcoRI* restriction endonuclease digests of plasmid DNA are shown in Figure 5.10 E. Two clones, originally from the Platinum Taq DNA polymerase reaction and three from the Platinum PCR SuperMix reaction were selected for sequencing. Clone 4 of the Platinum PCR SuperMix was selected because its sequence matched the database entry for *NF-H* (NM_021076).

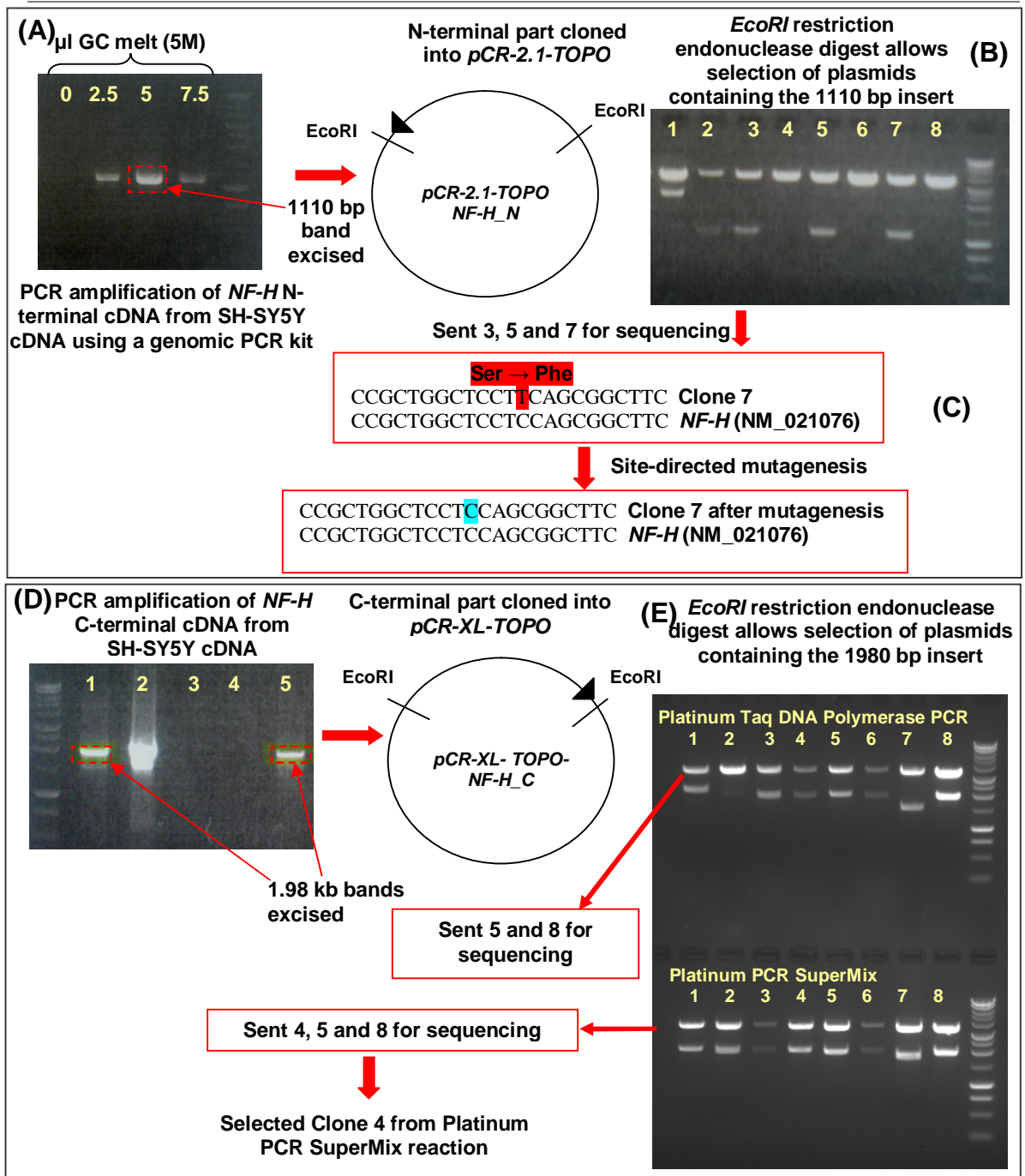


Figure 5.10 A schematic of the cloning procedure used to clone *NF-H* in two parts.

The N-terminal of *NF-H* was amplified by PCR from SH-SY5Y cDNA (A) and cloned into *pCR-2.1-TOPO*. From a restriction endonuclease digest with *EcoRI* (B) plasmids containing the 1110 bp insert were selected and sent for sequencing. (C) The clone selected for cloning into *pEGFP-C3* (clone 7) had a point mutation (highlighted in red) at position 164 bp which results in a Serine (Ser) to Phenylalanine (Phe) amino acid substitution which was removed by site-directed mutagenesis (shown in blue). The C-terminal part of *NF-H* was amplified using five different PCR reactions (1, Platinum Taq DNA polymerase; 2, Platinum Taq DNA polymerase High Fidelity; 3, AccuPrime DNA polymerase using polymerase buffer I; 4, AccuPrime DNA polymerase using polymerase buffer II and 5, Platinum PCR SuperMix) and run a 1% (w/v) agarose gel at 80 mA (D). 1.98 kb bands from reaction 1 and 5 were excised (shown in red), purified from the gel and cloned into *pCR-XL-TOPO*. (E) An *EcoRI* restriction endonuclease digest allowed the selection of plasmids containing the 1.98 kb insert for sequencing.

The separately cloned N- and C-terminal parts of *NF-H* were isolated from their respective cloning vectors by *EcoRI* and *XmnI* double digests and agarose gel electrophoresis (Figure 5.11 A). The N- and C-termini were ligated into *pCR-XL TOPO* by T4 DNA Ligase. The insertion of the full length *NF-H* into *pCR-XL TOPO* was confirmed by restriction endonuclease digestion with *EcoRI* followed by agarose gel electrophoresis (Figure 5.11 B). Four plasmids containing an insert were sequenced, three of which were found to contain an *NF-H* insert, the sequence of which matched the data-base entry for *NF-H* (NM_021076).

Attempts to add the *Sall* and *EcoRI* restriction endonuclease recognition sequences to the *NF-H* insert to ensure correct orientation when cloning it into *pEGFP-C3* were unsuccessful. Therefore *NF-H* was sub-cloned directly into *pEGFP-C3* using the *EcoRI* recognition site. To ensure that when *NF-H* was cloned into *pEGFP-C3* in frame with *GFP* it was necessary to clone a short piece of linker DNA containing a new *EcoRI* recognition sequence flanked by two *BglII* recognition sequences into *pEGFP-C3*.

Figure 5.12 describes the addition of the short piece of linker DNA into the GFP expression vector, the presence of which was confirmed by sequence analysis. *pEGFP-C3 rNF-M* was linearised with *BglII* and ligated with the oligonucleotide linker. To insert *NF-H* into the GFP vector, *pEGFP-C3 rNF-M* (now containing the *EcoRI* linker) and *pCR-XL TOPO-hNF-H* were digested with *EcoRI*. The *pEGFP-C3* vector and *NF-H* were isolated by agarose gel electrophoreses and ligated by T4 DNA Ligase (Figure 5.12 and 5.13).

The presence of the *NF-H* insert was confirmed by restriction endonuclease digestion with *EcoRI* and agarose gel electrophoresis (Figure 5.13 B). To determine which plasmid contained the insert in the correct orientation, plasmids containing the inserts were analysed by restriction endonuclease digestion using either *XhoI* or *SacI* followed by agarose gel electrophoresis (Figure 5.13 C). Of all the plasmids, 4 and 12 were found to be in the incorrect orientation. The plasmid from clone 6 was selected for sequencing and GFP and NF-H were confirmed to be in-frame.

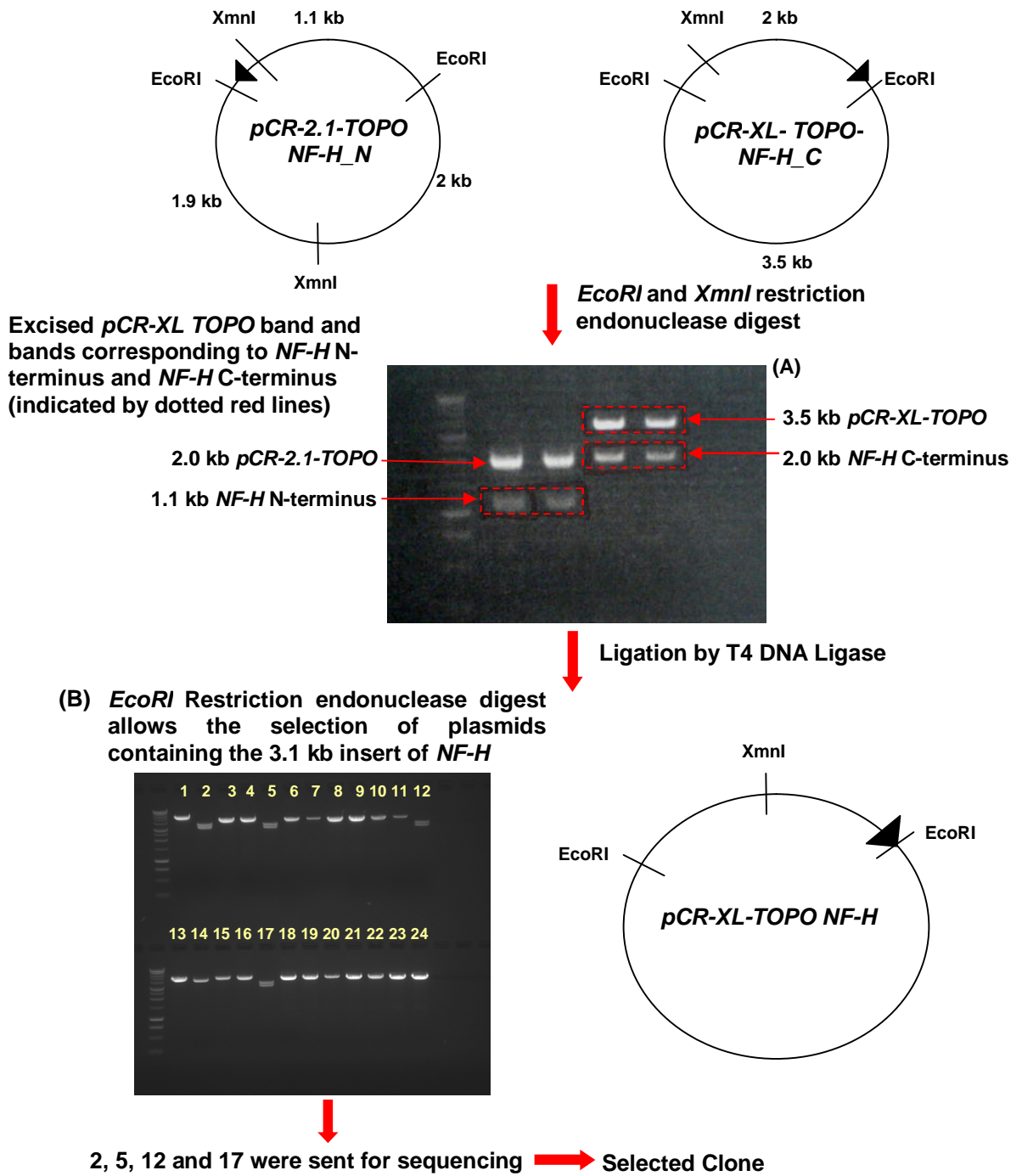


Figure 5.11 A Schematic describing the process by which N- and C-terminal parts of *NF-H* were ligated into the cloning vector (*pCR-XL-TOPO*).

The N- and C-terminal parts of *NF-H* were isolated from their cloning vectors, *pCR-2.1-TOPO NF-H_N* and *pCR-XL-TOPO NF-H_C* respectively by quantitative restriction endonuclease digest with *XmnI* and *EcoRI*. (A) The products of the digests run on a 1% agarose gel, the bands corresponding to the N- and C-terminal parts of *NF-H* and the cloning vector *pCR-XL-TOPO* were excised (indicated in red) and purified from the gel before being ligated together by T4 DNA ligase. (B) Restriction endonuclease digests with *EcoRI* were used to confirm the insertion of the 3.1 kb full-length *NF-H* into *pCR-XL-TOPO*. Plasmids containing the insert were sequenced and a clone was selected for subcloning into *pEGFP-C3*.

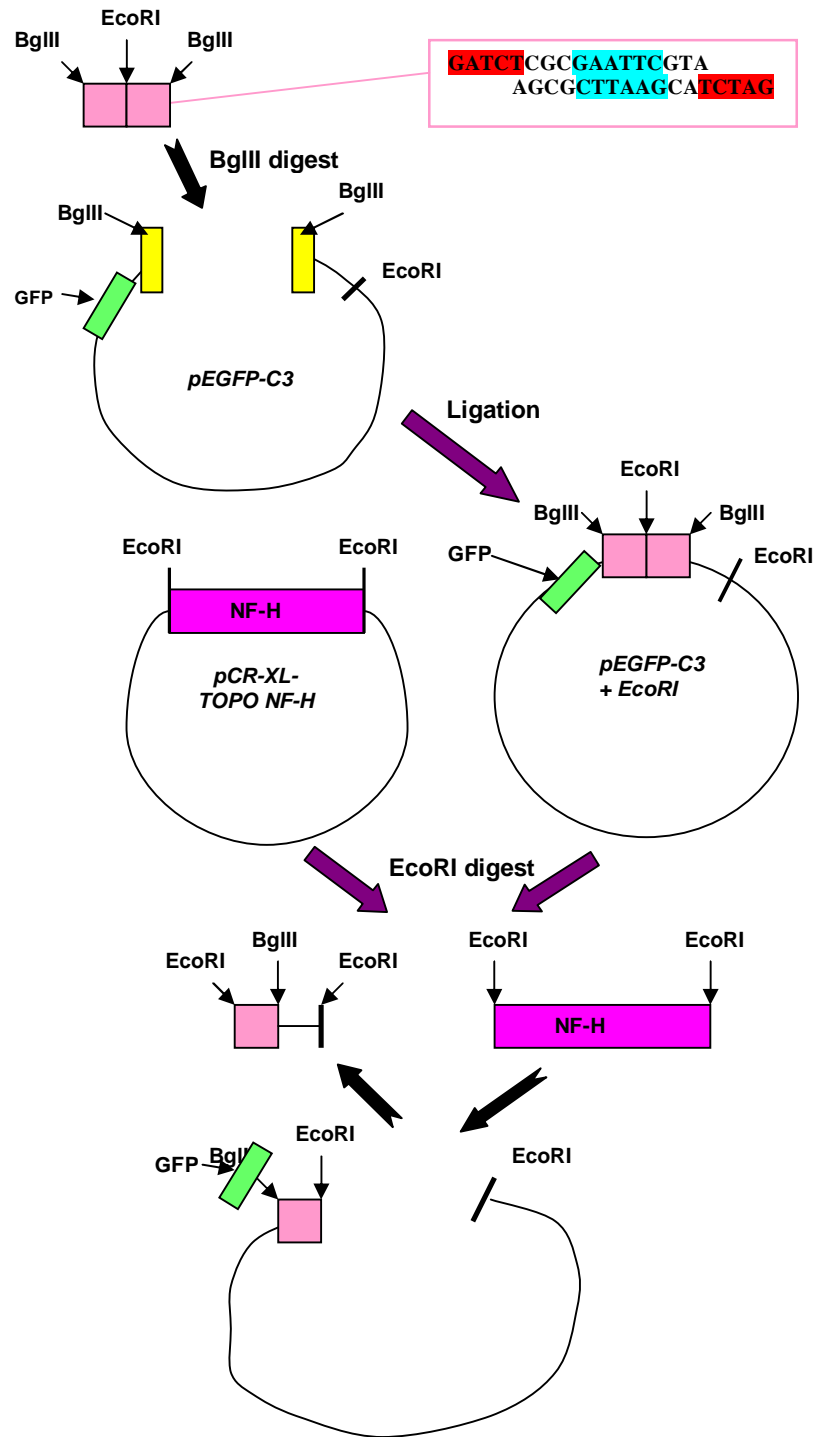


Figure 5.12 The cloning strategy adopted to clone *NF-H* into the *pEGFP-C3* expression vector using an *EcoRI* recognition sequence cloned into *pEGFP-C3*.

The new *EcoRI* recognition sequence was cloned into the vector using a small double-stranded oligonucleotide linker so that the *GFP* sequence and the *NF-H* sequence once cloned into the *EcoRI* site are in frame. The sequence of the double stranded oligonucleotide is in the pink box, the *BglIII* recognition sequence is highlighted in red and the *EcoRI* recognition sequence is highlighted in blue.

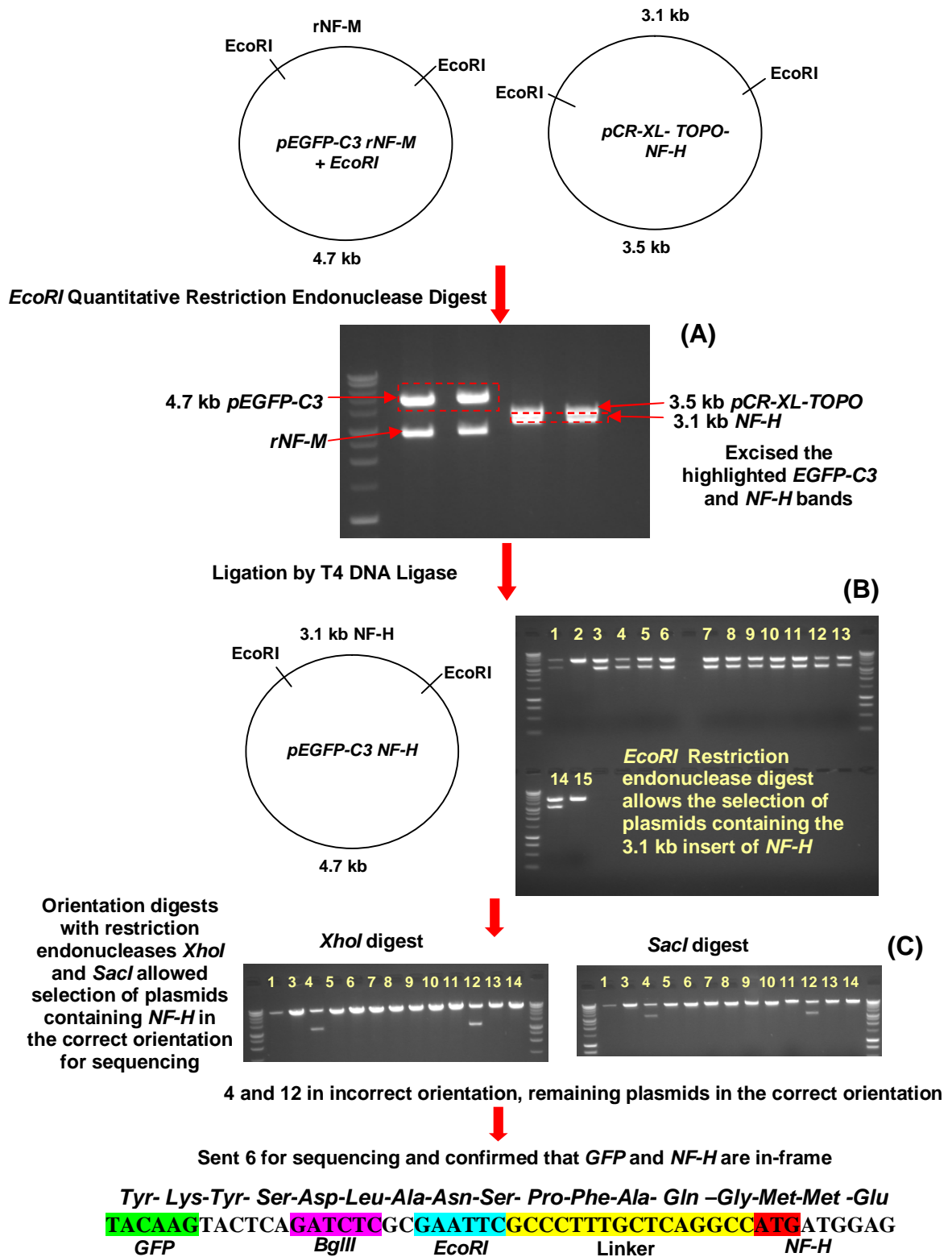


Figure 5.13 A schematic describing the subcloning of *NF-H* into *pEGFP-C3*.

pCR-XL-TOPO hNF-H and *pEGFP-C3 rNF-M* containing the *EcoRI* linker (*pEGFP* + *EcoRI*) were digested with the restriction endonuclease *EcoRI* and run on agarose gels (A), bands corresponding to *NF-H* and *pEGFP-C3* + *EcoRI* bands were excised (indicated in red). *NF-H* was subcloned into the *EcoRI* recognition site of *pEGFP-C3*. Plasmid mini-preps of *pEGFP-C3 NF-H* were analysed by restriction endonuclease digestion with *EcoRI* and (B) agarose gel electrophoresis to confirm the presence of the *NF-H* insert. The orientation of inserts was confirmed with *XhoI* and *SacI* restriction endonuclease digestion (C), selected clone was sent for sequencing. Further sequencing confirmed that *GFP* and *NF-H* was in-frame.

Western blots of total cell extracts probed with anti-GFP revealed that GFP/NF-H was expressed as a truncated protein of approximately 70 kDa (Figure 5.14 A i). This protein also did not react with anti-NF-H (Figure 5.14 A ii) which is raised to the C-terminal tail of NF-H suggesting only the N-terminal part of GFP/NF-H was expressed. The pattern of GFP/NF-H expression was investigated by laser confocal microscopy (Figure 5.14 B ii) and revealed abnormal, speckled GFP/NF-H expression along the axonal processes.

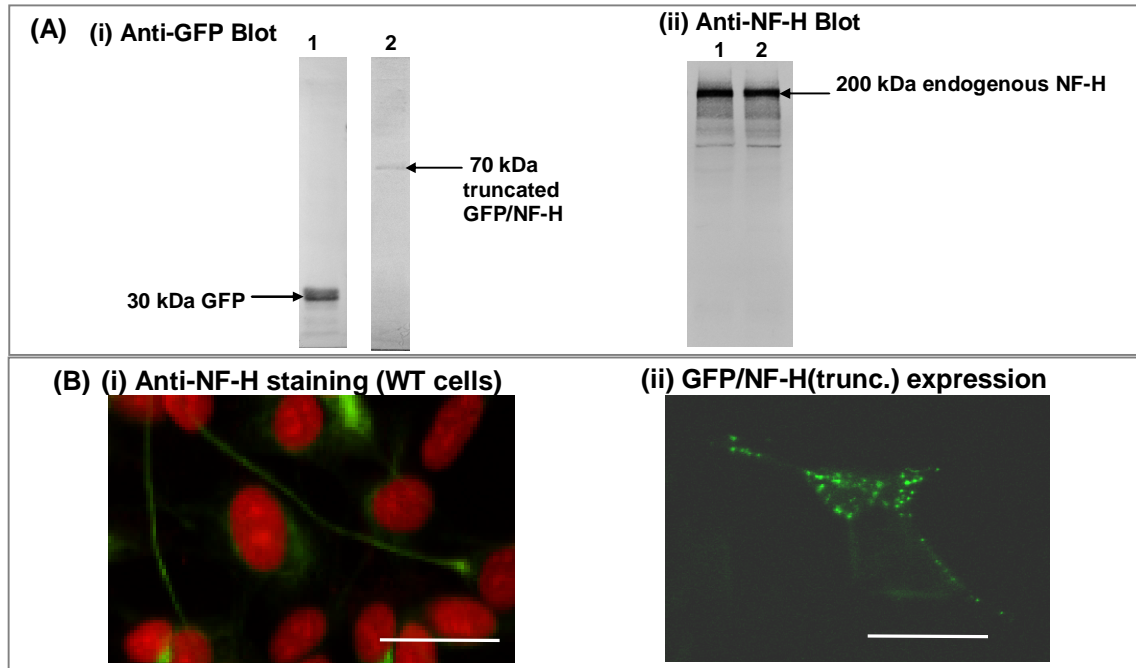


Figure 5.14 Characterisation of truncated GFP/NF-H in SH-SY5Y neuroblastoma cells.

(A) Western blots of total cell extracts of cells transfected with (1) GFP and (2) GFP-tagged NF-H (trunc.) probed with anti-GFP (1:500) and anti-NF-H (n52, 1:200) revealed that the GFP/NF-H is expressed as a 70 kDa truncated protein that did not react with n52. (B) Confocal microscope images of (i) wild-type SH-SY5Y cells stained with anti-NF-H (green). Nuclei were counterstained with propidium iodide, (ii) GFP/NF-H(trunc.) expressing cells showing GFP/NF-H expression (green). For (i) and (ii) Cells were viewed using the 40 x objective and the scale bar represents 40 μm .

The expression of a 70 kDa truncated GFP/NF-H suggested interrupted translation, possibly in the region of the *XmnI* recognition sequence. As such, sequence analysis of the GFP/NF-H plasmid revealed that the region around the *XmnI* recognition sequence (Figure 5.15) contained a single base deletion which results in a premature stop codon. The resultant protein most likely terminates within the rod domain of NF-H.

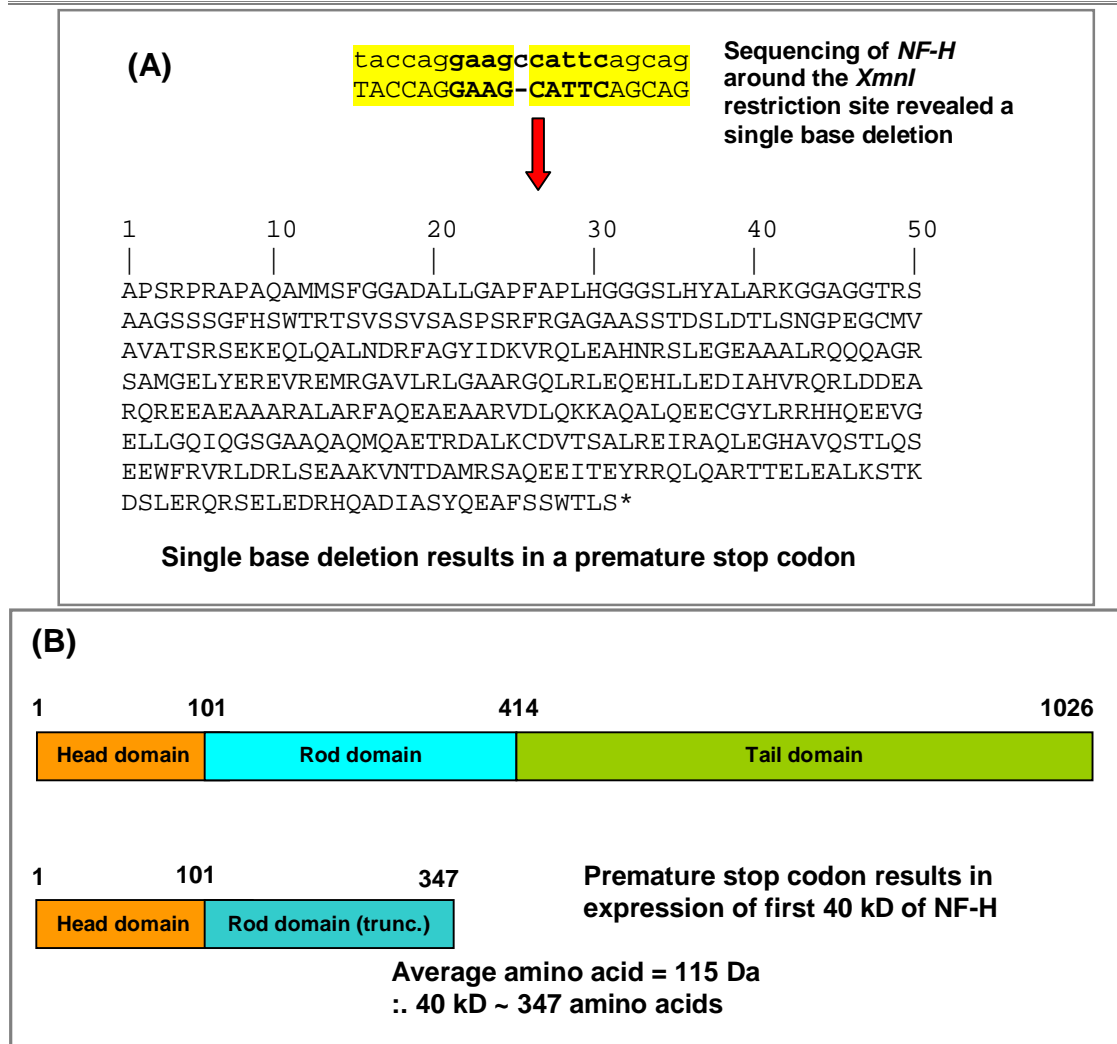


Figure 5.15 Sequence analysis of GFP/*NF-H* plasmid DNA revealed a single base deletion that resulted in a premature stop codon.

(A) Sequence analysis of *GFP/NF-H* DNA in the area including the *XmnI* restriction endonuclease recognition sequence (in bold) revealed a single base deletion resulting in a premature stop codon. (B) Schematic illustrating the structure of human *NF-H* (reviewed by Perrot et al, 2008) and a proposed structure for the truncated *NF-H* resulting from the premature stop codon introduced by the single base deletion in the *XmnI* restriction endonuclease recognition sequence in human *NF-H*. The number of amino acids was calculated from the average molecular weight of amino acids in Daltons.

To correct the single base deletion the missing base was inserted by site-directed mutagenesis, which is described in more detail in section 2.2.12.8. As depicted in Figure 5.16 a primer set containing the missing base was designed around the region of the single-base deletion. Agarose gel electrophoresis of *pEGFP-C3* and the mutagenesis plasmid *pEGFP-C3 hNF-H* confirmed the presence of the 3.1 kb *hNF-H* insert in the mutagenesis plasmid.

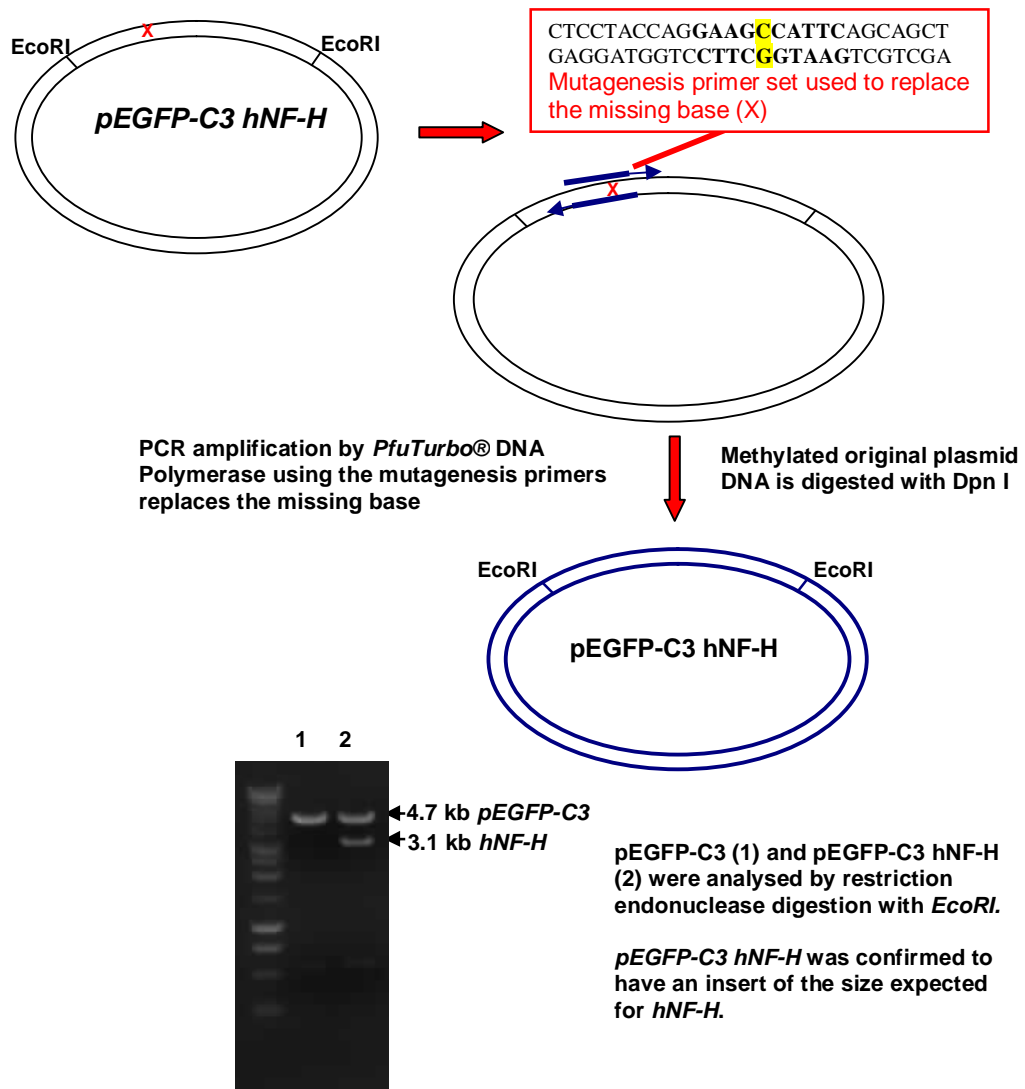


Figure 5.16 A Schematic describing the insertion of the base missing from the *XmnI* recognition sequence.

A Schematic representation of the strategy used to replace the deleted base in the *XmnI* recognition sequence of *GFP/NF-H*, the resultant mutagenesis plasmid was analysed by agarose gel electrophoresis. The base that was inserted is highlighted in yellow in the mutagenesis primers and the *XmnI* recognition sequence is in bold.

5.2.3.2. Characterisation of GFP/NF-H expression in SH-SY5Y cells

Western blots of total cell extracts probed with anti-GFP (Figure 5.17 A i) confirmed the presence of a 30 kDa band consistent with the molecular weight of GFP in GFP expressing cells and a band of approximately 230 kDa consistent with the predicted molecular weight of GFP/NF-H in GFP/NF-H expressing cells. Probing Western blots with anti-NF-H (Figure 5.17 A ii) and anti-pNF-H/pNF-M (Figure 5.17 A iii) revealed that extracts from GFP/NF-H expressing cells contained bands corresponding to endogenous untagged NF-H and the GFP tagged NF-H. The apparent molecular weights of GFP and GFP/NF-H were determined from

their Rf values by comparing their electrophoretic mobility to that of molecular weight standards (Appendix II). GFP/NF-H expression was similar to that of NF-H in wild-type cells (Figure 5.17 B).

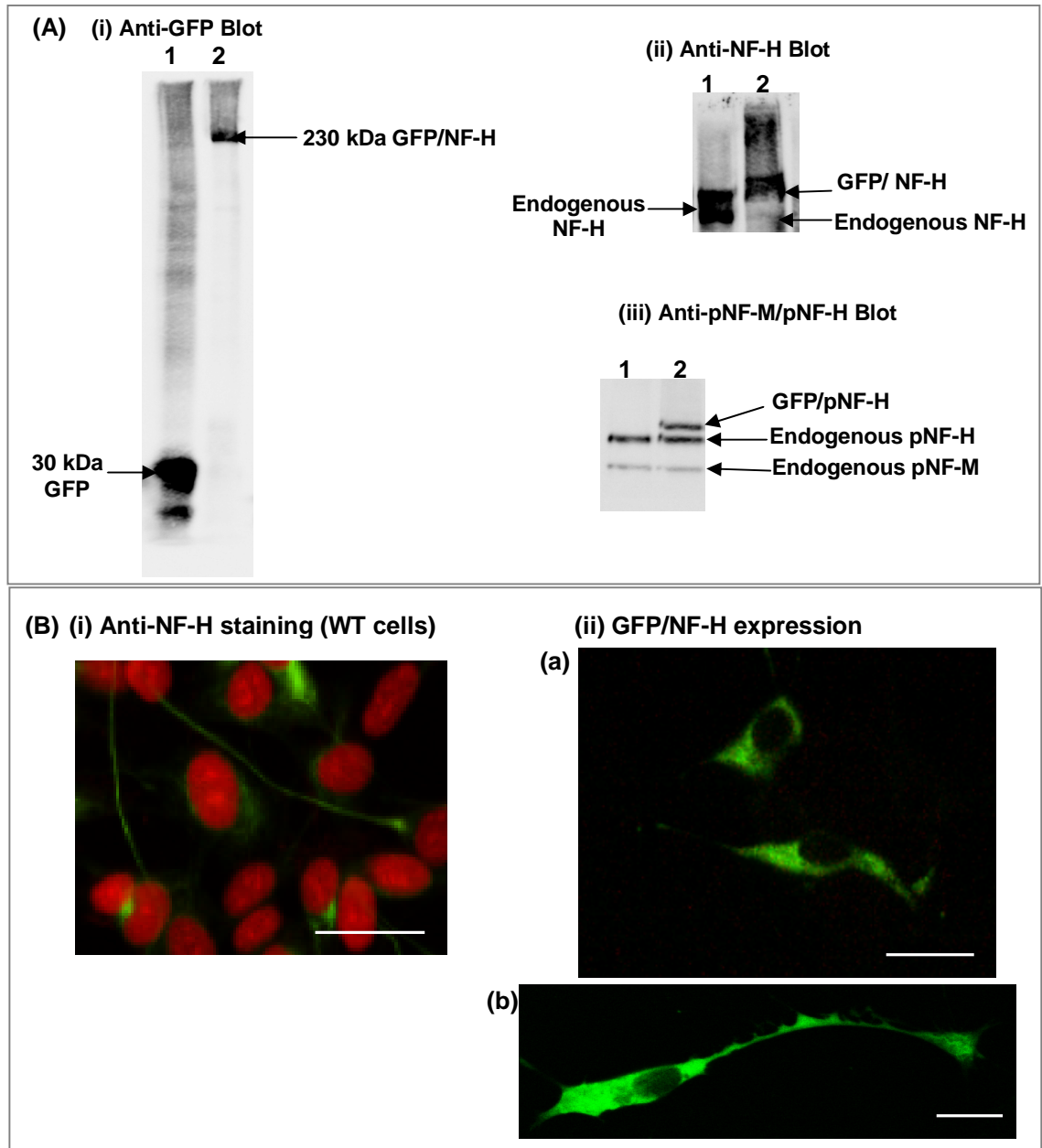


Figure 5.17 Characterisation of GFP/NF-H expression in SH-SY5Y neuroblastoma cells.

(A) Western blots of total cell extracts of SH-SY5Y neuroblastoma cells transfected with (1) GFP and (2) GFP-tagged NF-H probed with anti-GFP and anti-NF-H antibodies; (i) the anti-GFP blot shows a 230 kDa band corresponding to the GFP/NF-H fusion protein. The (ii) anti-NF-H and the (iii) anti-pNF-M/pNF-H both have a band corresponding with the endogenous NF-H band and a band corresponding with the GFP/NF-H fusion protein. (B) Confocal microscope images of (i) wild-type SH-SY5Y cells stained with anti-NF-H (green), nuclei were counterstained with propidium iodide and cells are viewed using the 40 x objective and the scale bar represents 40 μ m. (ii) Cells expressing GFP/NF-H (green) after insertion of the base lost from the XmnI recognition site during the ligation of the N and C termini. Cells were viewed using the 63x oil objective and the scale bar represents 20 μ m. (a) Fixed cells and (b) live cells.

Co-localization studies of GFP/NF-H expressing cells with the other NF subunits (Figure 5.18) revealed a clear co-localization of GFP/NF-H with NF-H, NF-M, and pNF-M/pNF-H.

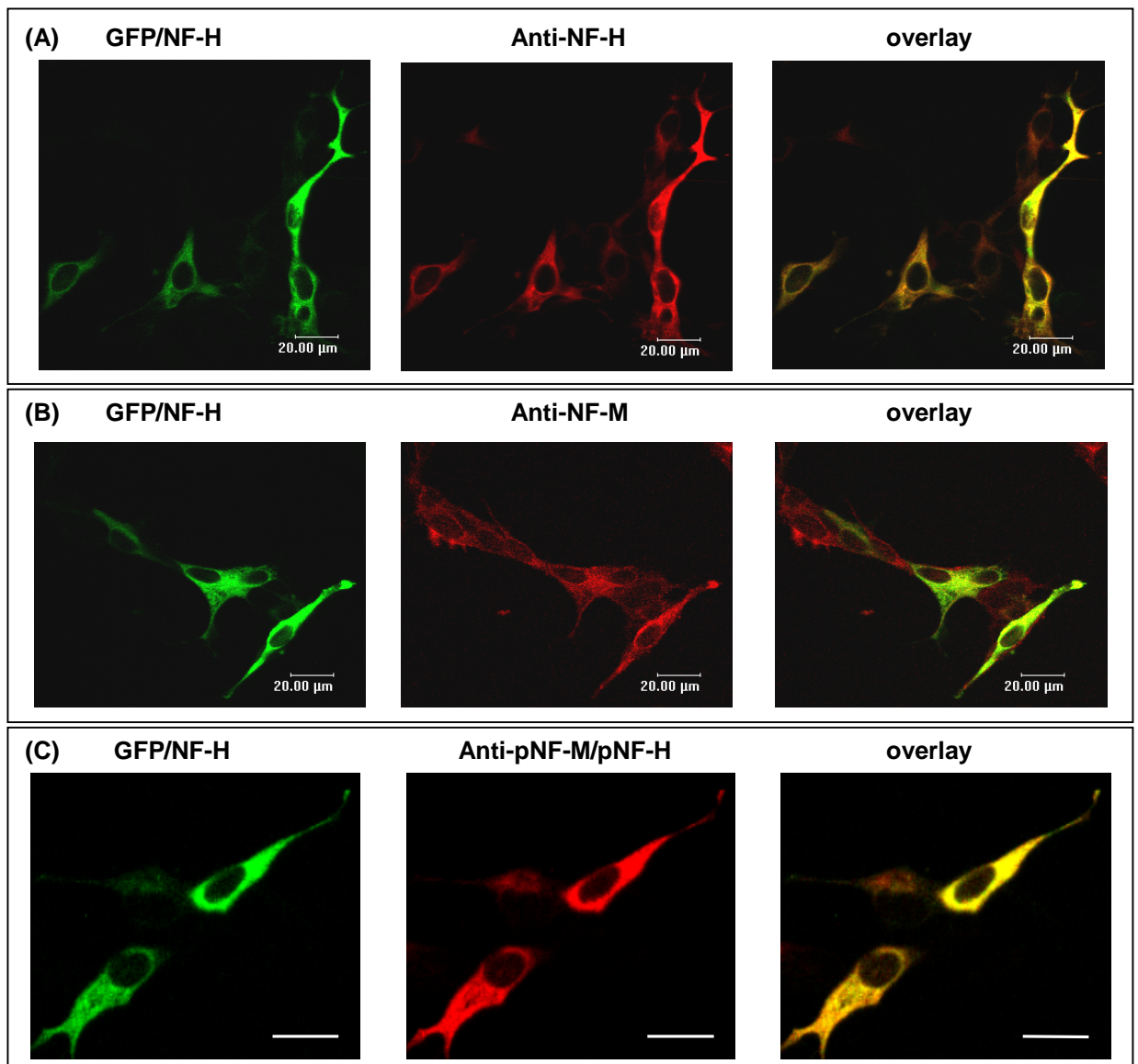


Figure 5.18 Co-localisation of GFP/NF-H with NF-M, NF-H and phosphorylated NF-M and NF-H in SH-SY5Y neuroblastoma cells.

The co-localization of GFP/NF-H with each of the NF subunits. GFP/NF-H expressing cells were stained with (A) anti-NF-H (n52), (B) anti-NF-M (RMO270) and (C) anti-phosphorylated NF-H and NF-M (smi31). The antibody staining - detected using a goat anti-mouse alexafluor 568 conjugated secondary antibodies - is shown in red on the left hand side of each panel and GFP fluorescence of the GFP-tagged NF-M is shown in green in the centre of each panel. As the red and green images are overlaid as seen on the right of each panel, areas of co-localization are highlighted yellow. Cells were viewed with a 63 x oil objective, scale bar represents 20 µm.

The efficiency of transfection of GFP/NF-H with LipofectAMINE™2000 was estimated to be 17.9 ± 6.3 % (Table 5.2).

Table 5.2 The transfection efficiency of GFP/NF-H in Human SH-SY5Y neuroblastoma cells using LipofectAMINE™2000.

The mean numbers of cells expressing GFP/NF-H fluorescence in experiments 1 and 2 were expressed as a percentage of the mean number of total cells (determined from the number of propidium iodide stained nuclei for experiments 1 and 2). The individual number of fields of view analysed for each experiment are given in brackets. For experiment 3 the number of GFP/NF-H expressing cells in live cultures was determined by counting the number of cells with GFP/NF-H fluorescence and the total number of cells visible in bright field images taken concurrently with fluorescence images. The number of individual dishes examined are indicated in brackets.

<i>Experiment</i>	<i>Mean number of Total cells in each field of view</i>	<i>Mean number of cells with GFP fluorescence</i>	<i>Transfected cells (%)</i>
<i>1 (3)</i>	24.3	6.3	26.0
<i>2 (1)</i>	12	1	8.3
<i>3 (5)</i>	21.6	4.2	19.4
<i>mean ± SEM</i>	19.3 ± 4.6	3.8 ± 1.9	17.9 ± 6.3

The half-life of GFP/NF-H (Figure 5.19) estimated from the anti-GFP blot was 13.1 ± 1.6 h whereas the half-life estimated from the anti-NF-H blot was longer at 25.5 ± 1.6 h.

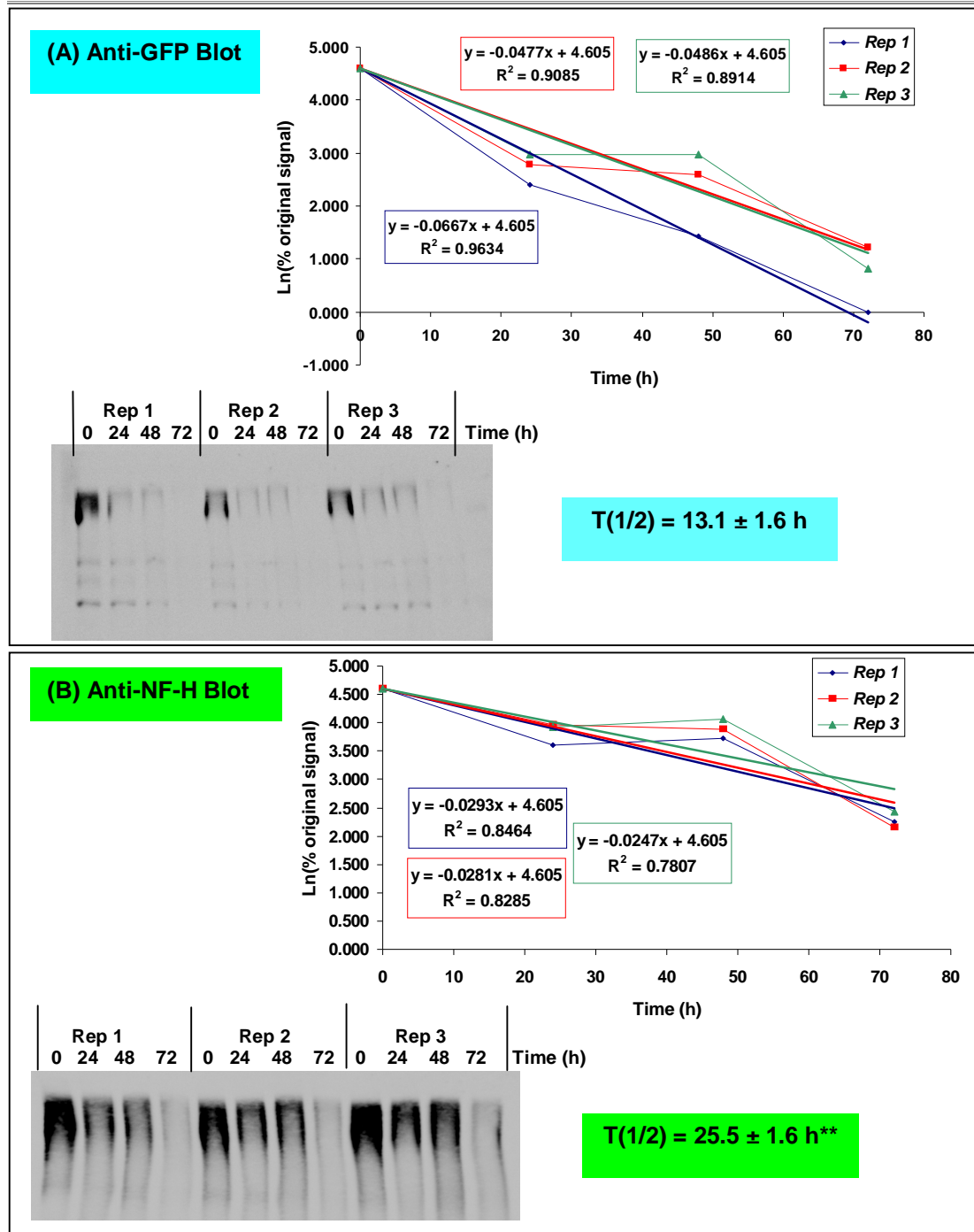


Figure 5.19 Determination of the half-life of GFP/NF-H.

Western blots probed with (A) anti-GFP (1:10000) and (B) anti-NF-H (n52, 1:2000). Plot of the natural logarithm of the percentage of original signal (obtained from densitometric analysis of Western blots) against time (h), from which half-life [T(1/2)] was calculated using the decay rate constant (k) from the equation of the line best of fit. T(1/2) quoted is the mean T(1/2) from 3 independent experiments ± SEM. T(1/2) obtained from the anti-GFP blot is significantly shorter than the T(1/2) obtained from the anti-NF-H blot (**T-Test, $p < 0.005$; $n = 3$).

5.2.4. Immunoprecipitation of GFP tagged neurofilaments

5.2.4.1. Assessment of the solubility of GFP tagged neurofilaments in the immunoprecipitation lysis buffer

The immunoprecipitation procedure using the anti-GFP isolation kit from Miltenyi Biotec (described in more detail in sections 2.2.2.4 and 2.2.5) is outlined in Figure 5.20. The Lysate Supernatant (LS) was obtained from the cell lysate following centrifugation at 10,000 x g for 10 minutes at 4 °C; the resultant cell debris pellet (P), was solubilised in 1 ml of total extraction buffer containing 1 % SDS, followed by heating at 100 °C for 5 minutes. The GFP tagged NFs were isolated from LS using anti-GFP μ beads. The excluded supernatant (ES) refers to the flow-through from the μ -column after application of LS labelled with anti-GFP μ beads to the column.

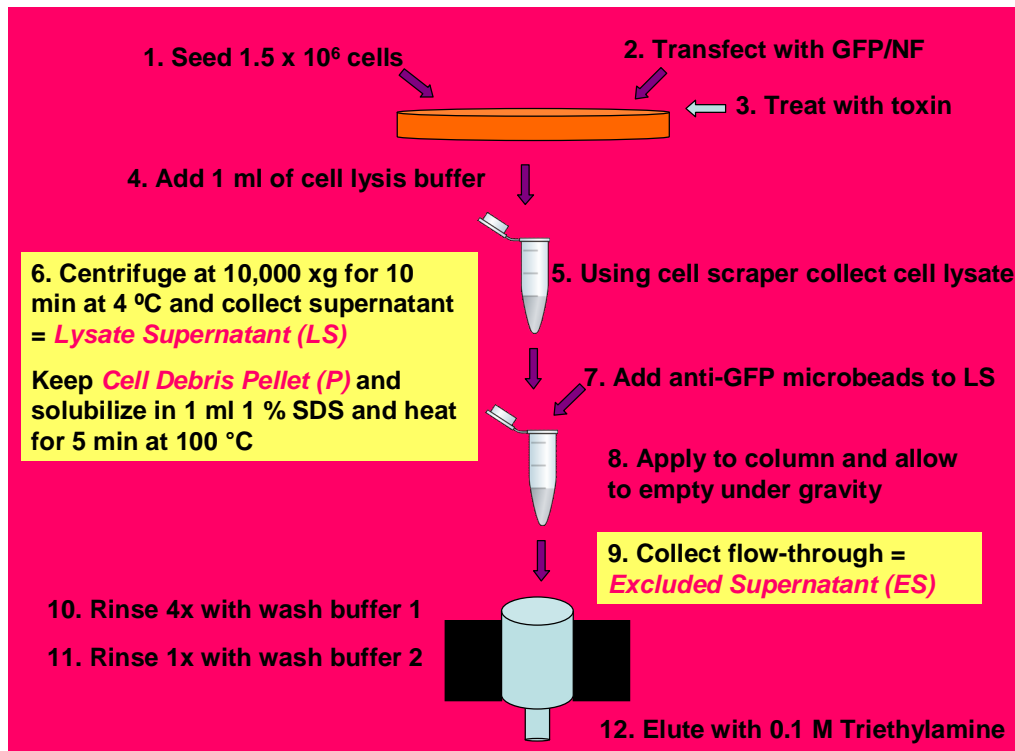


Figure 5.20 An illustration of the protocol used for the immunoprecipitation of GFP-tagged neurofilaments from cell lysates of SH-SY5Y cells.

The provenance of the Lysate Supernatant (LS), the cell debris pellet (P) and the excluded supernatant (ES) is also indicated in points 6 and 9 (yellow boxes).

In the work presented below, a comparison of four transfections was made: mock, GFP, GFP/NF-M and GFP/NF-H:

The solubility of proteins in the igepal-containing lysis buffer was initially assessed by copper-staining Western blots of gels to which equal volumes of LS, ES and P for all four transfections were applied (Figure 5.21). Irrespective of transfection, the majority of the total protein was soluble in the igepal-containing lysis buffer and a small amount was left in P for all four samples.

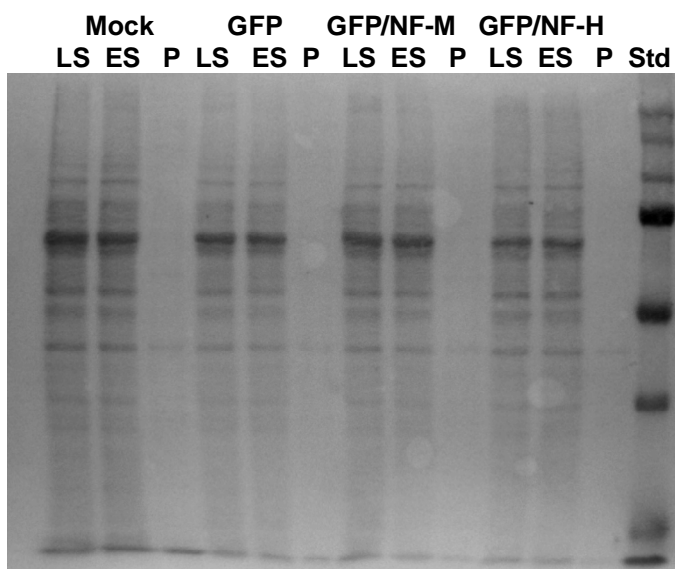


Figure 5.21 Copperstained Western blot of Lysate supernatant (LS), excluded supernatant (ES) and cell debris pellet (P).

Copperstained Western blot of the Lysate Supernatant (LS), excluded supernatant (ES) and cell debris pellet (P) resulting from a 10 000 x g centrifugation of the cell lysate of GFP, GFP-NF-M and GFP/NF-H expressing cells that were harvested in 1 ml of the low salt lysis buffer. The cell debris pellet was solubilised in 1 ml 8 M urea. 20 µl of each sample was loaded per well.

To establish (a) whether GFP and GFP/NFs are solubilised by the lysis buffer, and (b) whether GFP and GFP/NFs are retained in the column, Western blots of the LS, ES and P were probed with anti-GFP (Figure 5.22). Firstly, no reaction with anti-GFP was observed in any of the fractions from mock transfected cells. Secondly, in fractions from GFP and GFP/NF expressing cells, the majority of GFP and GFP/NFs were located in LS with very little in P, indicating that GFP and GFP/NFs are soluble in the igepal lysis buffer used. Comparison of LS and ES from GFP and GFP/NF transfectants revealed that the majority of the GFP and GFP/NF is depleted from ES confirming that GFP and GFP/NFs are retained in the column.

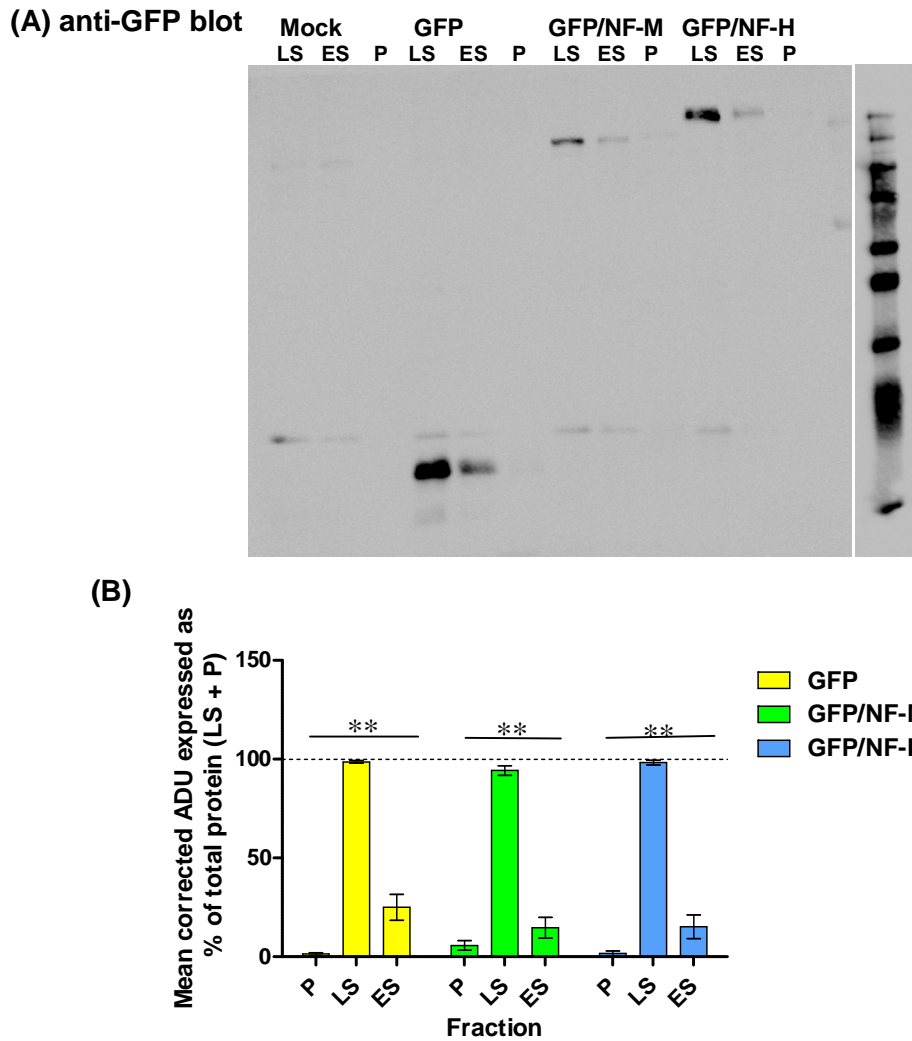


Figure 5.22 Analysis of the levels of GFP or GFP/NF in the lysate supernatant (LS), excluded supernatant (ES) and cell debris pellet (P) from untransfected cells (mock) or cells expressing either GFP, GFP/NF-M or GFP/NF-H.

(A) Representative Western blot of equal volumes of the LS, ES and P probed with anti-GFP (1:7500). (B) Plot comparing the mean corrected ADU expressed as a percentage of total protein (ES + LS) obtained following densitometric analysis of the anti-GFP immunoreactive bands on Western blots for LS, ES and P fractions from GFP, GFP/NF-M and GFP/NF-H expressing cells. Error bars represent standard deviation (n = 3). The different fractions for each transfection were compared by one-way ANOVA (** p < 0.001). The majority of the GFP and GFP/NF-M /H were found in LS with very little in P. GFP and GFP/NF is depleted in ES indicating that it is retained in the column. (n = 3)

Next Western blots of LS, ES and P were probed with antibodies to NFs, vimentin, α -tubulin and actin to establish whether NFs and other cytoskeletal proteins (a) are soluble in the igepal lysis buffer, (b) differ with respect to their distribution in LS, ES and P depending on the transfection and (c) are retained in the column by association with the anti-GFP μ beads.

For all the cytoskeletal proteins, levels were greater in the LS than in P (Figure 5.23 and 5.24). The most soluble protein was α -tubulin (with around 99 % of total protein in the igepal soluble pool), followed by actin (with 85-90 % of total protein in the igepal soluble pool). The intermediate filaments (NFs and vimentin) were less soluble but in general the solubility ranged between 70 – 90 % of total protein. NF-L in mock transfected and GFP expressing cells was least soluble (50 – 60 % of total protein in the soluble pool).

Based on the ES content, there was no indication of depletion of NFs, α -tubulin, vimentin and actin from LS of mock and GFP transfected cells, indicating no binding to the column (Figure 5.23 and 5.24). When extracts from GFP/NF-M and GFP/NF-H expressing cells are fractionated on the anti-GFP column, there is evidence of a depletion of NF-M and NF-H from LS (Figure 5.23 A and B), indicative of the retention of GFP/NFs in the column. For extracts from GFP/NF-M expressing cells, NF-H (Figure 5.23 A) and NF-L (Figure 5.23 C) levels in ES were lower than in LS, suggesting retention of these subunits in the column together with GFP/NF-M. Depletion of NF-M (Figure 5.23 B) and NF-L (Figure 5.23 C) from LS is not as evident in GFP/NF-H extracts as is depletion of NF-L and NF-H from GFP/NF-M extracts, suggesting that a proportion of GFP/NF-H is not assembled into hetero-oligomers with NF-M and NF-L.

There was no evidence of depletion of α -tubulin (Figure 5.24 B) or actin (Figure 5.24 C) from LS of either GFP/NF-M or GFP/NF-H expressing cells following passage through the anti-GFP beads indicating that neither of these proteins is retained in the column together with GFP/NF-M and GFP/NF-H. There is evidence of depletion of vimentin (Figure 5.24 A) from LS of GFP/NF-M and from LS of GFP/NF-H (although to a lesser degree) expressing cells, indicating retention of vimentin in the column together with GFP/NF-M and GFP/NF-H.

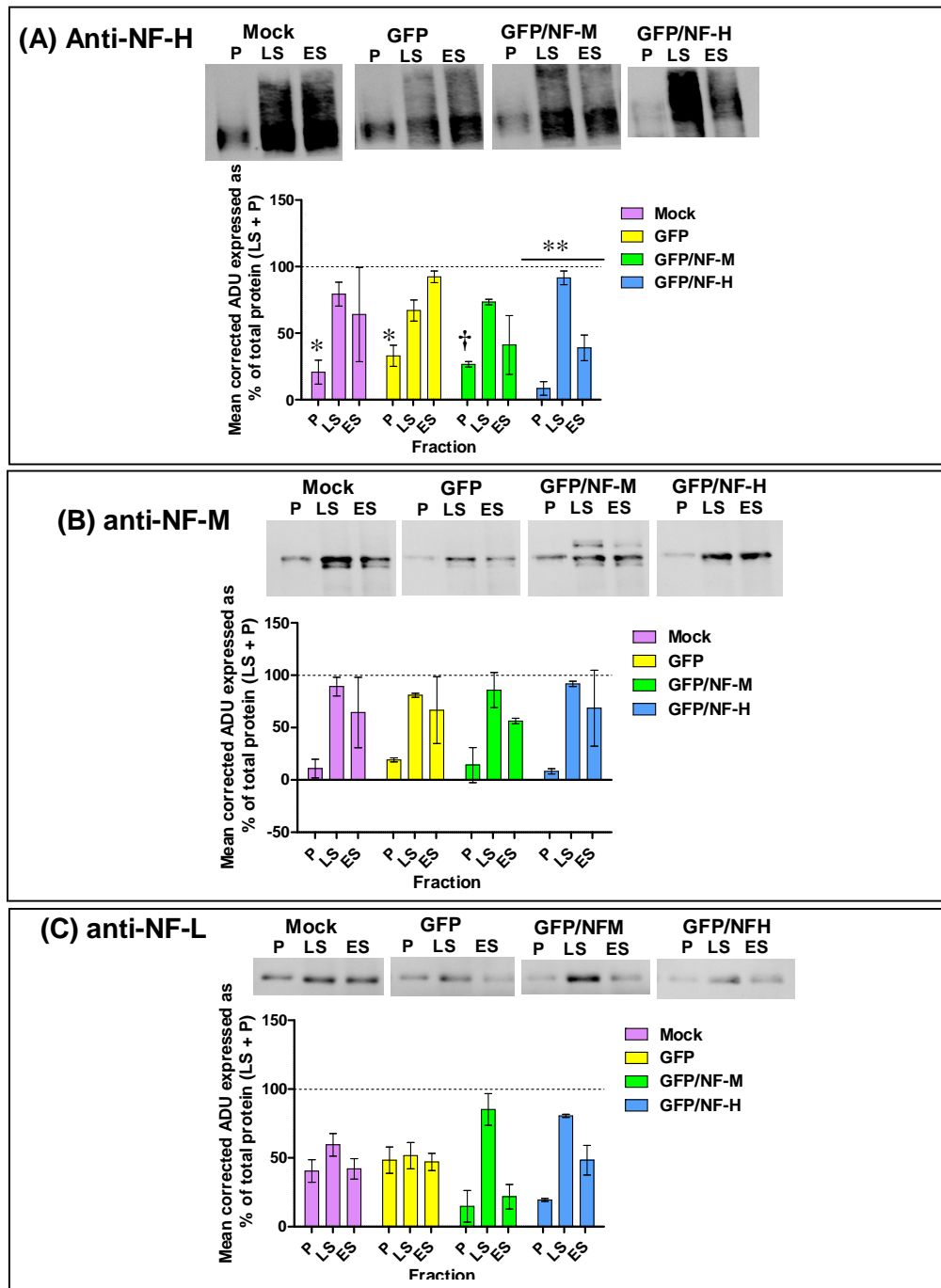


Figure 5.23 The distribution of neurofilaments (NFs) in the lysate supernatant (LS), excluded supernatant (ES) and cell debris pellet (P) from SH-SY5Y neuroblastoma cells.

Analysis of the levels of (A) NF-H, (B) NF-M and (C) NF-L in the cell debris pellet (P), lysate supernatant (LS or Lys Sup) and excluded supernatant (ES or Excl Sup) from mock transfected or GFP, GFP/NF-M or GFP/NF-H expressing cells. Representative Western blots of equal volumes of the LS, ES and P were probed with anti-NF-H (n52, 1:2000), anti-NF-M (RMO270, 1:500) and anti-NF-L (DA2, 1:1000). Plots of mean corrected ADU (arbitrary densitometry units) expressed as percentage of total protein (LS + P) obtained from densitometric analyses of Western blots. There was a significant difference in the levels of NF-H in LS, ES and P in extracts from GFP/NF-H expressing cells (one-way ANOVA; $p < 0.005$). The levels of NF-H in LS were greater than in P in extracts from mock transfected and GFP expressing cells (one-way ANOVA, * $p < 0.05$) and in extracts from GFP/NF-M expressing cells (two-tailed T-test, † $p < 0.05$). There was some indication of a decrease in levels of NF-H, NF-M and NF-L in ES compared to LS in GFP/NF-M and GFP/NF-H expressing cells. In extracts from mock and GFP expressing cells there was no indication of a decrease in the levels of NF-H, NF-M and NF-L in ES compared to LS. Error bars represent standard deviation for NF-H ($n = 3$) and range for NF-M ($n = 2$) and NF-L ($n = 2$).

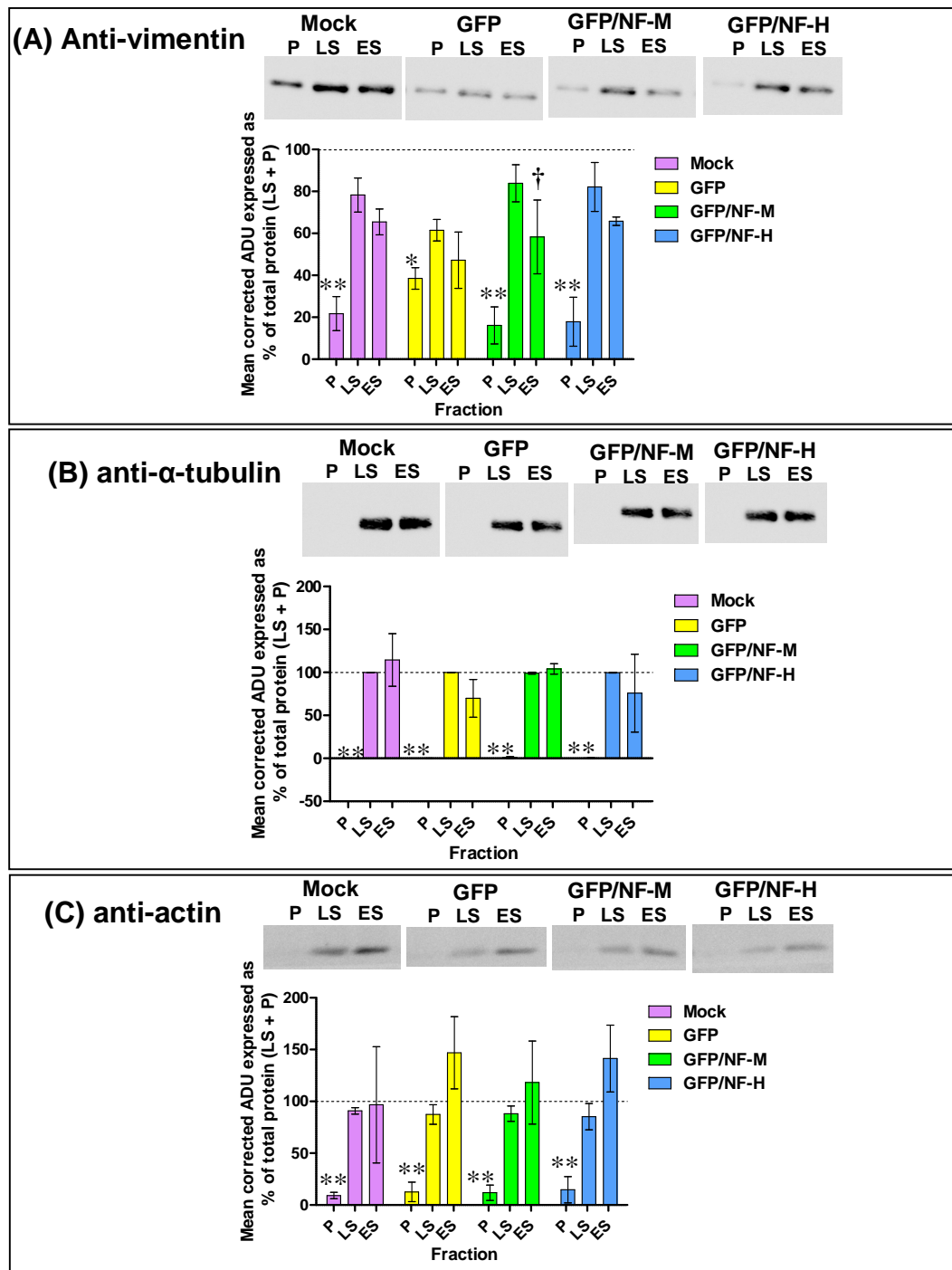


Figure 5.24 The Distribution of vimentin, α -tubulin and actin in the lysate supernatant (LS), excluded supernatant (ES) and pellet (P) from SH-SY5Y neuroblastoma cells.

Representative Western blots of equal volumes of the LS, ES and P probed with (A) anti-vimentin (RV202, 1:5000), (B) anti- α -tubulin (b512, 1:2000) and (C) anti-actin (1:1000) in the P, LS and ES from untransfected cells (mock) or cells transfected with GFP, GFP/NF-M or GFP/NF-H. Plots summarise the results of densitometric analyses of Western blots; mean corrected ADU (arbitrary densitometry units) was expressed as a percentage of ADU of total protein (LS + P). The levels of vimentin, α -tubulin and actin were greater in LS than P in extracts from mock transfected and GFP, GFP/NF-M and GFP/NF-H expressing cells (** $p < 0.005$; One-way ANOVA, Bonferroni post-hoc tests). There was no evidence of a decrease in the levels of α -tubulin or actin in the ES compared LS for all four transfection, or vimentin in the ES of mock transfected and GFP expressing cells. The levels of vimentin in ES were lower than the levels in LS in extracts from GFP/NF-M expressing cells ($\dagger p < 0.05$; One-tailed T-Test) and to some degree in GFP/NF-H expressing cells. Error bars represent standard deviation ($n = 3$).

5.2.4.2. Identification of neurofilament-associating proteins by co-immunoprecipitation with GFP tagged neurofilaments

Two approaches were used to identify neurofilament associating proteins which were co-immunoprecipitated with GFP-tagged neurofilaments; a general proteomic approach using 1D/2D-PAGE/peptide mass fingerprinting (PMF) and a more targeted approach using Western blotting combined with immunoprobings.

5.2.4.2.1. Determination of associated proteins by electrophoresis plus PMF

Immunoprecipitated eluates from mock transfected and GFP, GFP/NF-M and GFP/NF-H expressing cells were separated by one-dimensional SDS-PAGE and the protein profiles of the different immunoprecipitates were compared by silver-staining (Figure 5.25). Bands were excised from the gel (indicated by blue and green boxes) and subjected to in-gel trypsin digestion followed by MS analysis. No identification was made for bands 3 and 6, which are represented by green boxes in Figure 5.25. GFP was identified in the immunoprecipitate from GFP expressing cells, while in immunoprecipitates from GFP/NF-M and GFP/NF-H expressing cells, GFP/NF-M and GFP/NF-H were identified, respectively, together with vimentin. The spectra from which identifications were made can be found in Appendix III.

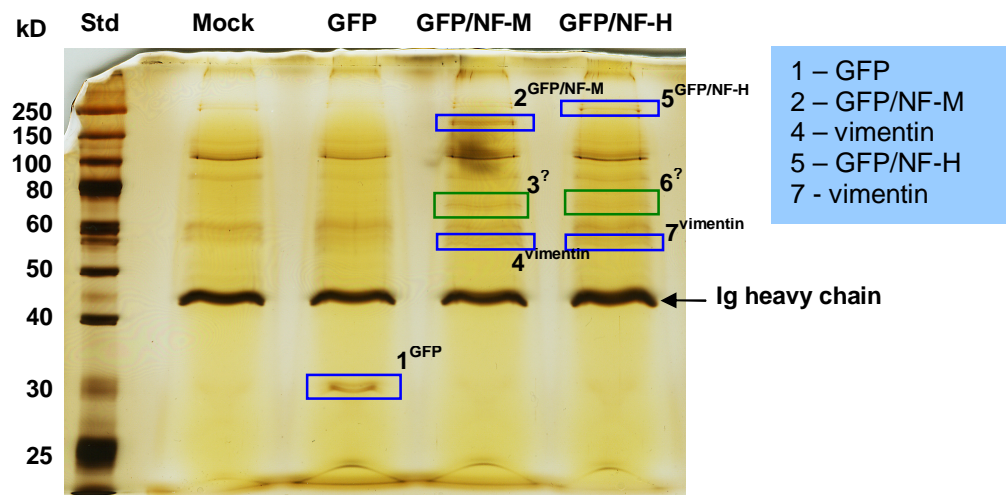


Figure 5.25 SDS-PAGE and silver-staining of immunoprecipitated eluates from cell lysates of mock transfected cells and cells expressing GFP, GFP/NF-M or GFP/NF-H.

In-gel trypsin digestion and mass spectrometry of excised bands (indicated by the blue and green boxes) resulted in the identification of GFP in GFP immunoprecipitate, GFP/NF-M and vimentin in the GFP/NF-M immunoprecipitate and GFP/NF-H and vimentin in the GFP/NF-H immunoprecipitate. The green boxes represent bands for which no identification could be made.

Silver-stained two-dimensional SDS-PAGs of immunoprecipitates from GFP and GFP/NF-M expressing cells can be found in Figure 5.26. The protein profiles of each of the immunoprecipitates were compared using SameSpot software. The spots that were excised are indicated by the green and blue rings which were then subjected to in-gel trypsin digestion. Trypsin digests were analysed by MS (Peptide mass fingerprints are in Appendix III). GFP was identified in the immunoprecipitate from GFP expressing cells. In the immunoprecipitate from GFP/NF-M expressing cells, GFP/NF-M, NF-L, vimentin and Hsc70 (identification confirmed by MSMS) were identified.

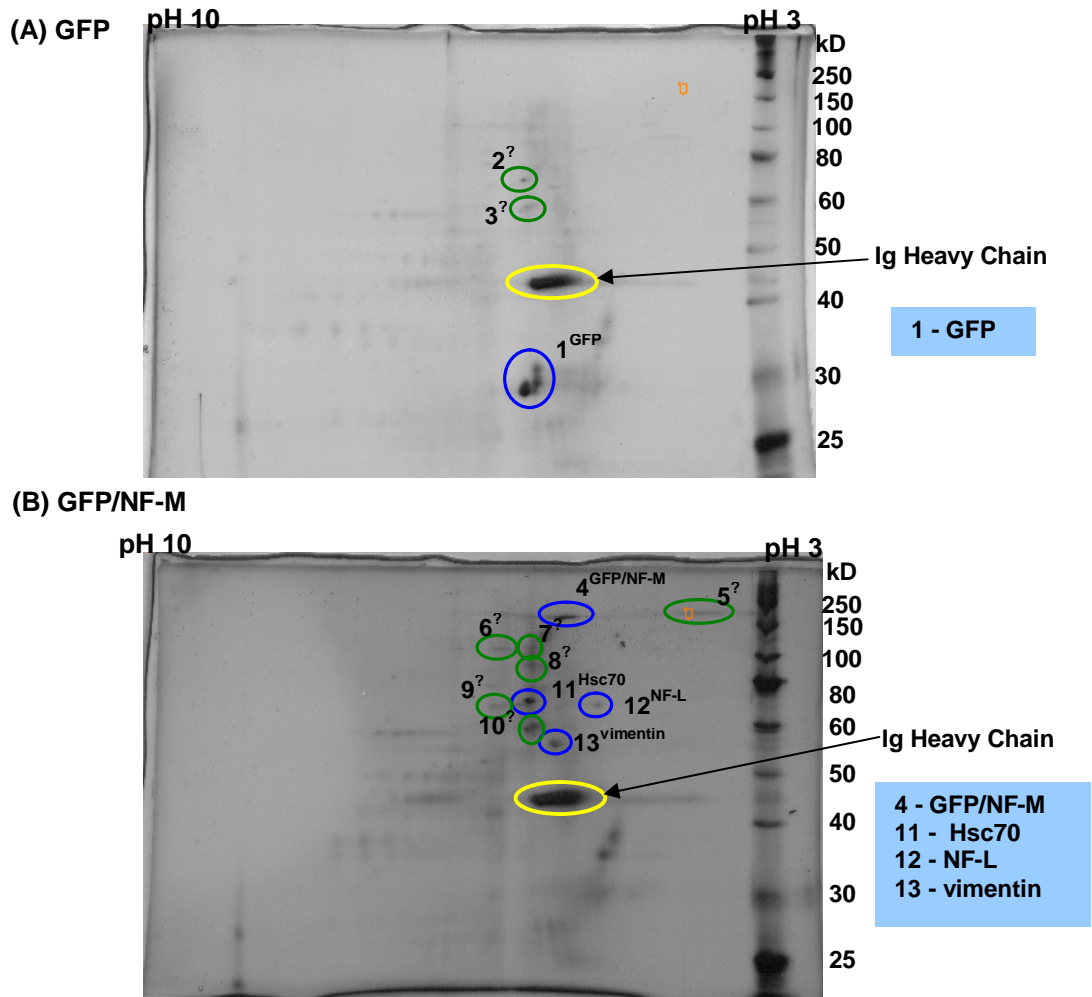


Figure 5.26 Two-dimensional SDS-PAGE of immunoprecipitates from cells expressing GFP or GFP/NF-M.

Gels were silver-stained and protein profiles were compared using SameSpot software. Spots indicated by the green and blue rings were picked and identified by mass spectrometry. Spots for which no identification could be made are indicated by the green rings whereas positive identifications are indicated by the blue rings. Positive identifications are listed in the coloured boxes next to the gels.

5.2.4.2.2. Determination of associated proteins using a targeted approach

Western blots of immunoprecipitates from mock transfected cells or from cells expressing GFP, GFP/NF-M or GFP/NF-H were probed with antibodies to NFs and phosphorylated NFs. Blots revealed that all three NF subunits and pNF-M/pNF-H are co-immunoprecipitated with GFP/NF-M and GFP/NF-H (Figure 5.27 A and B). In addition blots probed with anti-vimentin antibody revealed that vimentin co-immunoprecipitated with GFP/NF-M and GFP/NF-H (Figure 5.27 C). Western blots of immunoprecipitates were probed with anti-Hsc70 antibody to confirm the association of neurofilaments with Hsc70 which was identified by MSMS with GFP/NF-M (Figure 5.27 C); however the reaction of anti-Hsc70 with immunoprecipitates from GFP/NF-M and GFP/NF-H expressing cells was very weak and some reaction was also observed with the immunoprecipitates from mock transfected and GFP expressing cells.

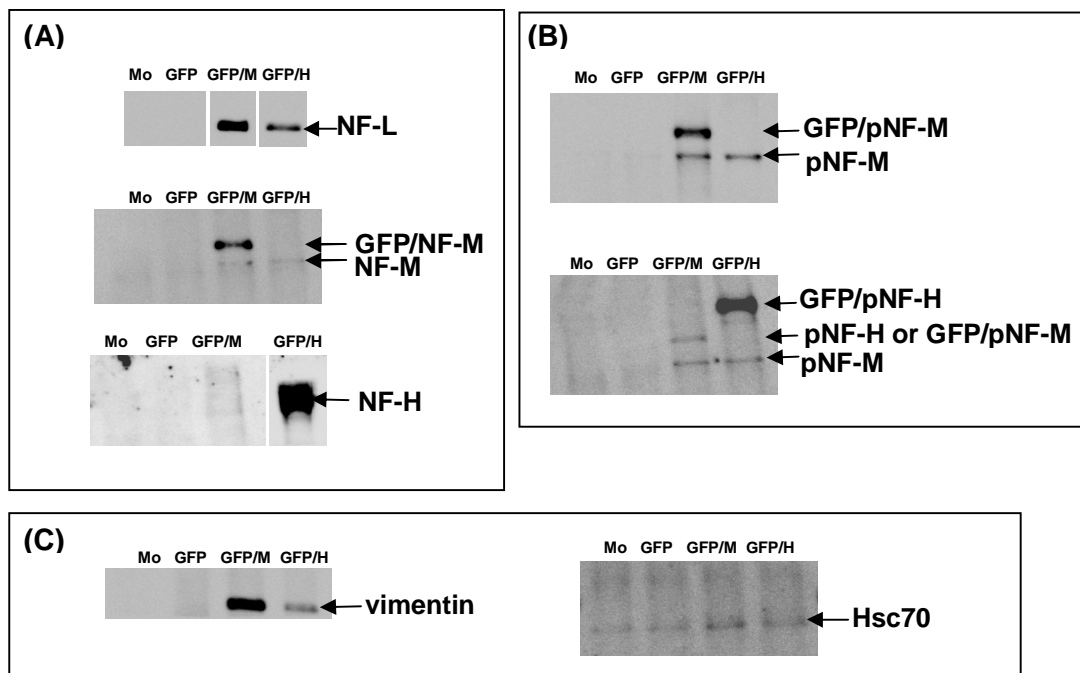


Figure 5.27 Co-immunoprecipitation of GFP/NF-M and GFP/NF-H with all three neurofilament subunits, phosphorylated NF-M and NF-H and vimentin.

Representative Western blots of immunoprecipitates (E1) from SH-SY5Y cells that were either mock transfected (Mo, ie. no plasmid) or transfected with GFP, GFP/NF-M or GFP/NF-H ($n = 3$). (A) Western blots were probed with either anti-NF-L (DA2, 1:1000, top), anti-NF-M (RMO270, 1:500, middle) or anti-NF-H (n52, 1:2000, bottom). (B) Western blots were probed with antibodies to phosphorylated neurofilaments; anti-pNF-M (RNF403, 1:1000, top) and anti-pNF-H/pNF-M (smi31, 1:1000, bottom). (C) Western blots probed with either anti-vimentin (RV202, 1:5000, left) or anti-Hsc70 (1:5000, right).

To identify other possible neurofilament associating proteins, Western blots of GFP/NF-M or GFP/NF-H were probed with antibodies to a number of candidate proteins. The motor proteins Dynein, Kinesin 5A and Kinesin 5C were not detected on Western blots of immunoprecipitates (Figure 5.28 A). Western blots were also probed with antibodies to other cytoskeletal proteins; α -tubulin, actin and α II-spectrin (Figure 5.28 B) which were detected in all immunoprecipitates and therefore were not specifically co-immunoprecipitated with GFP/NF-M and GFP/NF-H. Cdk5 (kinase), PSMC1 (proteasomal subunit) and Tissue Transglutaminase (TG2) were not detected on Western blots of immunoprecipitates (Figure 5.28 C.)

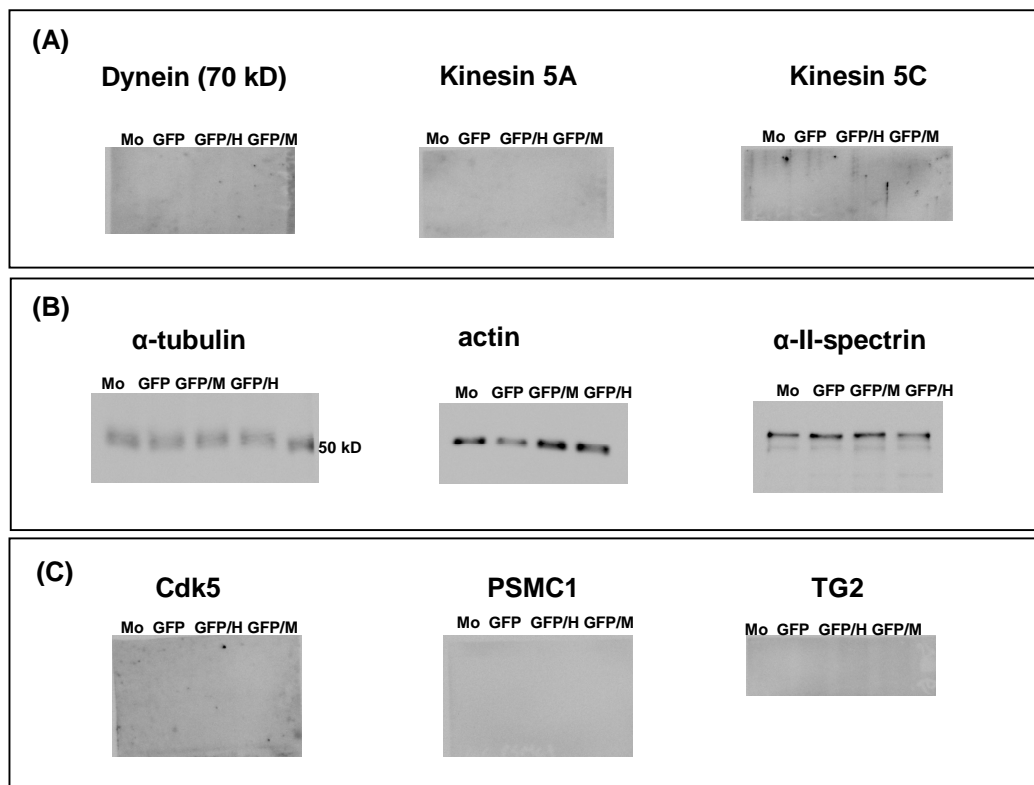


Figure 5.28 Assessment of the presence/absence of a number of target proteins in immunoprecipitates from GFP/NF-M and GFP/NF-H expressing cells.

Western blots of immunoprecipitates from SH-SY5Y neuroblastoma cells that were either mock transfected or transfected with GFP, GFP/NF-M or GFP/NF-H probed with antibodies to a number of candidate proteins. (A) Western blots probed with anti-Dynein (Dyn 70.1, 1:1000), anti-kinesin 5A (1:1000) and anti-kinesin 5C (1:1000). (B) Western blots probed with anti- α -tubulin (b512, 1:2000), anti-actin (1:1000) and anti- α II-spectrin (1:5000). (C) Western blots probed with anti-Cdk5 (1:100), anti-PSMC1 (1:1000) and anti-TG2 (CUB, 1:1000).

5.2.5. The effect of an acute dose of MPP+ treatment on neurofilament dynamics in SH-SY5Y cells

Time-lapse fluorescence and bright field images of SH-SY5Y neuroblastoma cells expressing GFP/NF-M or GFP/NF-H either untreated or treated with 5 mM MPP+ were taken every 5 minutes. Cells were maintained at 37 °C in media containing NaHCO₃ during the duration of the imaging experiment. To minimise the risk of photobleaching and the production of free radicals the shutters were closed in the intermittent periods during which images were not being taken.

The effect of 5 mM MPP+ treatment on the length of axonal processes in GFP/NF-M (Figure 5.29) and GFP/NF-H (Figure 5.30) expressing cells was assessed by comparing the length of axonal processes (measured using ImageJ software) at the start of the time-lapse experiment (t = 0 min) to the length of the axonal processes in the same cells at each time-point during the course of the experiment. For each experiment a mean change in length was determined by measuring process length for all the cells in a field of view. Changes in the length of processes were then expressed as a ratio of the length at the start of the experiment.

There was a significant effect of time on the length of axonal processes in GFP/NF-M and GFP/NF-H expressing cells in both treated and untreated cells (Figure 5.29 A and 5.30 A). To estimate the rate at which axonal processes retract in treated cells compared to controls a linear regression analysis was performed (Figures 5.29 B and 5.30 B). Using Bonferroni post-hoc tests to compare the changes in axonal process length at each time-point, axonal processes were significantly reduced in length after 40 minutes in GFP/NF-H expressing cells and after 20 minutes of exposure in GFP/NF-M expressing cells. In GFP/NF-M and GFP/NF-H expressing control cells, axonal processes retracted at a rate of 0.3 % per minute; in MPP+ treated cells the rate of retraction was respectively 0.9 % and 0.7 % per minute. Time-lapse movies can be found in the CD included with this work.

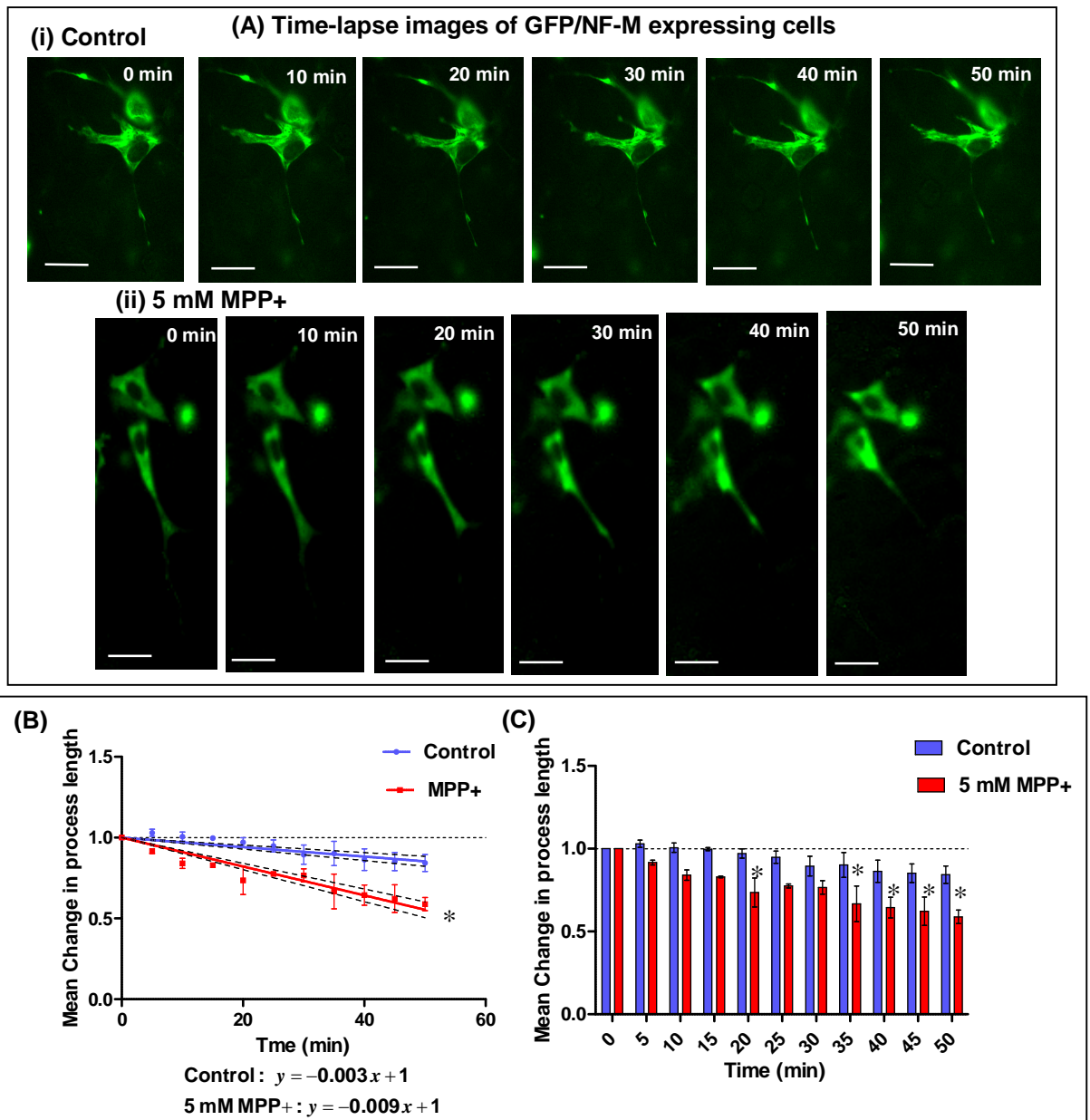


Figure 5.29 Analysis of the mean change in the length of axonal processes in GFP/NF-M expressing cells over time.

Cells were either untreated or treated with 5 mM MPP+ and imaged every 5 minutes over a period of 50 minutes. Scale bar represents 20 μm . (A) Representative images of GFP/NF-M expressing cells showing reduction in axonal process length in 5 mM MPP+ treated cells. (B) Plot displaying the rate of change in axonal process length in treated and untreated (control) cells determined by linear regression analysis. The dotted lines refer to the 95 % confidence interval for the linear regression. The rate of the reduction in axonal process length is greater in treated cells than in controls. (C) Plot summarising the mean change in axonal process length in treated and untreated cells at each time-point. The reduction in axonal process length is significantly greater in treated cells than in control cells as early as 20 minutes into the time-course (* $p > 0.05$; Two-Way ANOVA and Bonferroni posttest). Error bars represent SEM ($n = 3$).

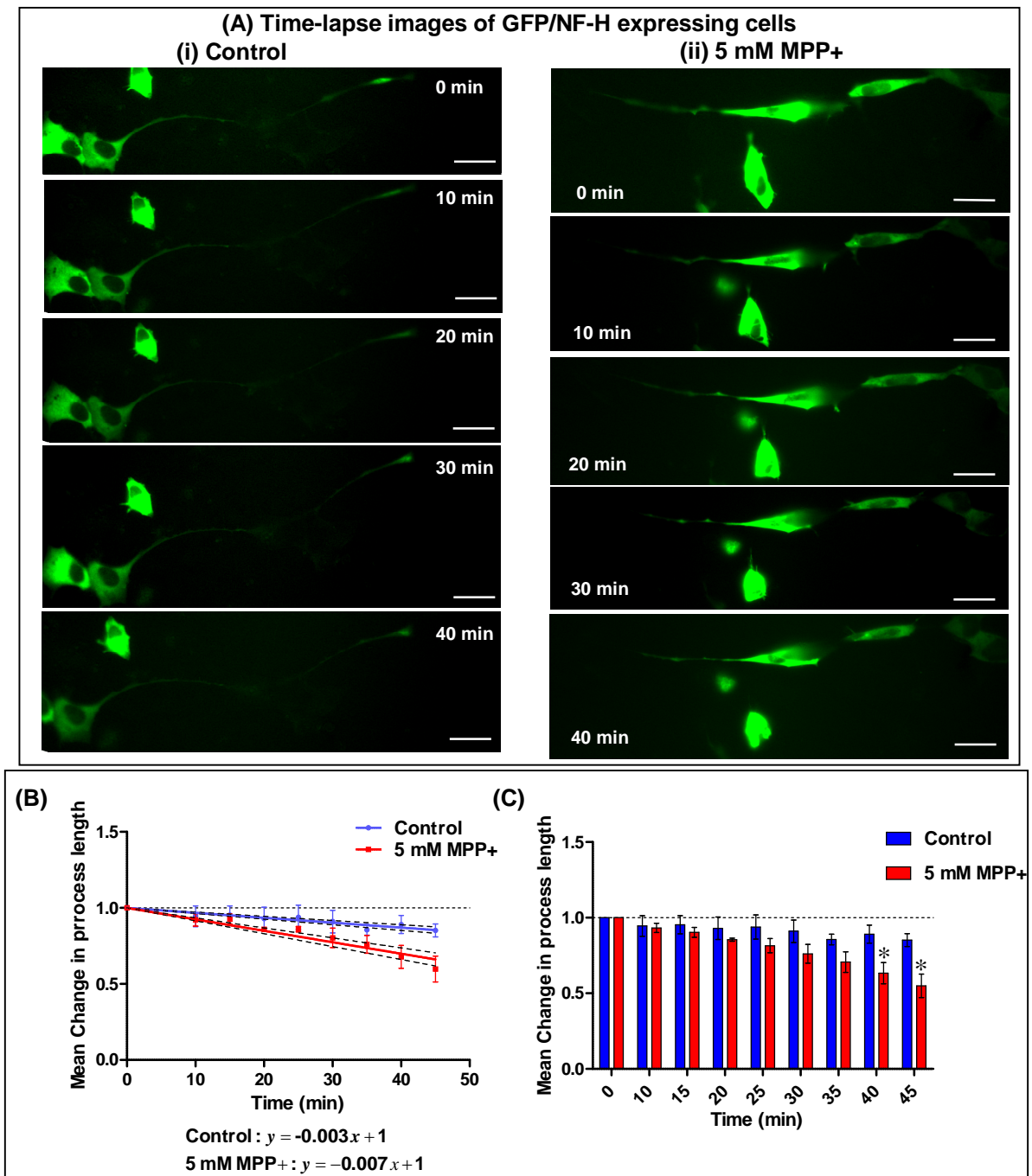


Figure 5.30 Mean change in the length of axonal processes of GFP/NF-H expressing cells during the first 45 minutes treatment with 5 mM MPP+.

Cells were either untreated (control) or treated with 5 mM MPP+ and imaged every 5 minutes. Scale bar represents 20 μm . (B) Plot displaying the rate of change in axonal process length in untreated and treated cells determined by linear regression analysis. The dotted lines indicate the 95 % confidence interval for the linear regression analysis. The rate of reduction in axonal process length is greater in treated cells than in controls. (C) Plot summarising the change in axonal process length in treated and untreated cells at each time-point. The lengths of axonal processes in treated cells were significantly reduced after 40 and 45 minutes of treatment compared to the axonal processes of controls at the same time-point (* $p > 0.05$; Two-Way ANOVA and Bonferroni posttest). Error bars represent SEM ($n = 3$).

To establish whether NFs retract at the same rate as the axonal process, GFP/NF-M fluorescence and bright field (BF) images of cells treated with 5 mM MPP+ were compared over the time-course in one experiment (Figure 5.31 A). Linear regression analysis (Figure 5.31 B) revealed that in this particular experiment the mean rate of GFP/NF-M retraction was 0.7 % of original length per minute while the rate of retraction of the axonal process obtained from the bright field image was 0.6 % of the original length per minute.

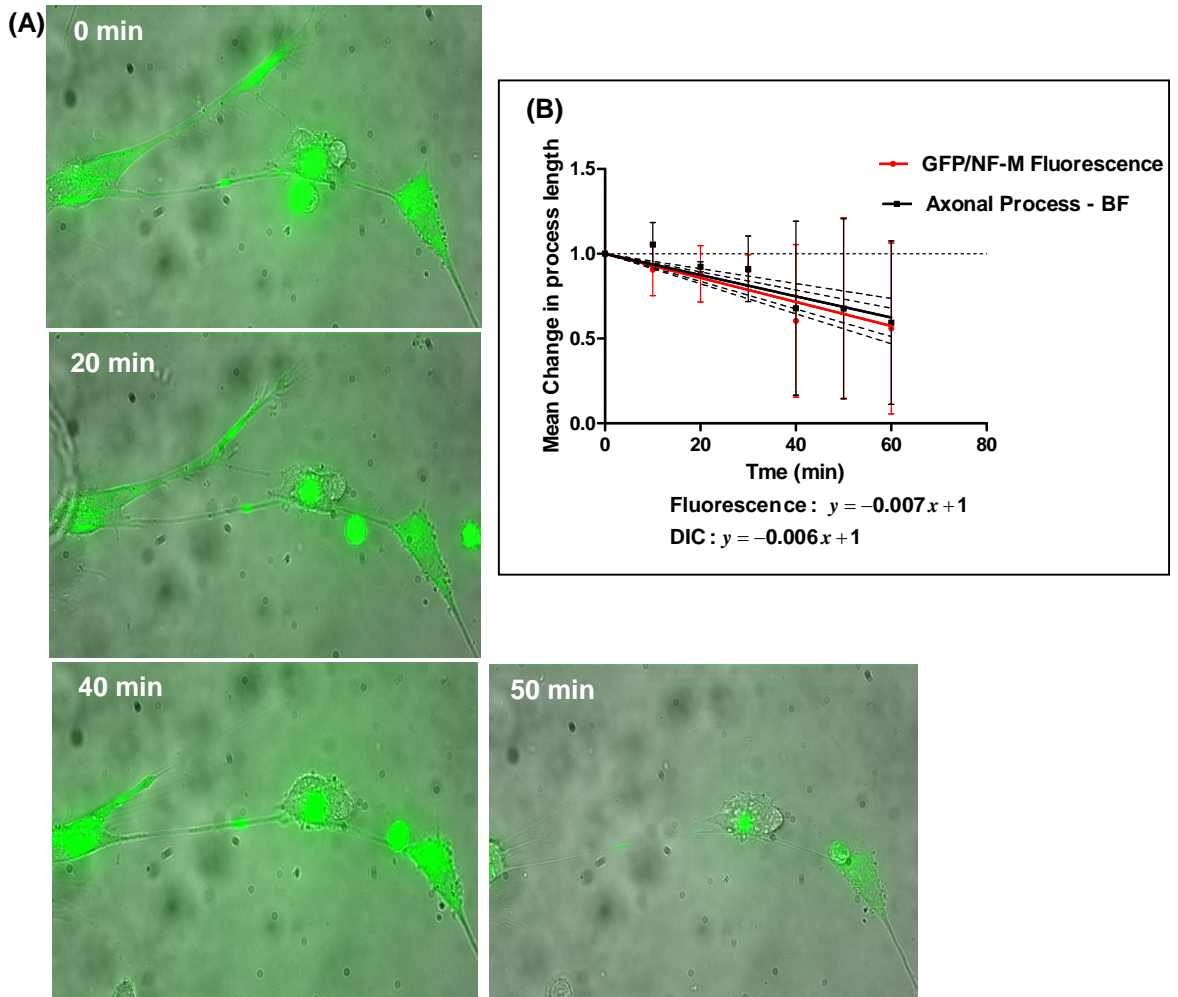


Figure 5.31 Assessment of whether neurofilaments retract at a faster rate than the rest of the axonal process in GFP/NF-M expressing cells treated with 5 mM MPP+ for a period of 1 h.

Time-lapse fluorescence and bright field images were taken every 5 minutes during the course of the experiment. (A) Composite fluorescence and bright field images of GFP/NF-M expressing cells treated with 5 mM MPP+ produced in ImageJ. Scale bar represents 20 μ m. (B) Linear regression analysis of change in axonal length over time revealed no significant difference in the rate of retraction of GFP/NF-M fluorescence and the axonal structure.

5.3. Discussion

5.3.1 GFP tagged neurofilaments

5.3.1.1. Development and characterisation of GFP/NF-M

Western blotting of total cell extracts from GFP/NF-M expressing cells confirmed the expression of a 180 kDa protein consistent with the molecular weight predicted for the GFP/NF-M fusion protein that reacted with both anti-GFP and anti-NF-M. The detection of the phospho-epitopes revealed that GFP/NF-M is also phosphorylated.

GFP/NF-M appeared to be incorporated into the NF network based on the expression pattern (which was similar to NF-M in wild-type cells) and its co-localization with with NF-M, NF-L, pNF-M and pNF-H. It is noteworthy that in the case of NF-H staining, some GFP/NF-M expressing cells did not seem to stain very strongly for NF-H. Additional evidence for the association of GFP/NF-M with endogenous NF-M, NF-L and NF-H resulted from their co-immunoprecipitation with GFP/NF-M.

Studies with mice lacking either NF-H or NF-M have provided evidence that there is some redundancy in the functioning of these two subunits, such that if one subunit is missing, the expression of the other subunit is increased (Nakagawa et al, 1995, Rao et al, 2002).

Half-life determinations of GFP/NF-M revealed that the half-life of GFP/NF-M (13.8 ± 2.2 h to 20.2 ± 1.4 h) is shorter than that of NF-M which was previously calculated to be 53.5 ± 3.6 h (Table 3.2-2), suggesting that GFP/NF-M is more labile than the endogenous NF-M. The peak in 150 kD NF-M levels after 24h was unexpected and suggests that the levels of NF-M have increased after 24 hours; an explanation of this phenomenon may be that the GFP portion of the GFP/NF-M fusion protein is preferentially cleaved off leaving the NF-M portion of the fusion protein free to join the pool of endogenous NF-M.

5.3.1.2. Development and characterisation of GFP/NF-L

Western blotting of total cell extracts from GFP/NF-L expressing cells confirmed the presence of a 100 kDa protein that reacted with both antibodies to both NF-L and GFP consistent with the predicted apparent molecular weight of GFP/NF-L. However, confocal microscopy revealed aggregates of GFP fluorescence in the cell body, suggesting that GFP/NF-L failed to be incorporated into the NF network.

Since the head and rod domains of NF-L are critical for NF-L self-assembly into homopolymers *in vitro* (Kim et al, 2007); the position of the GFP tag on the N-terminus of GFP/NF-L may be preventing its incorporation into the NF network. However NF-L tagged N-terminally with GFP has been used successfully in other studies without aberrant aggregation (Kim et al, 2007, Lin et al, 2004, Yan et al, 2007, Yuan et al, 2009).

Alternatively, the aggregation of GFP/NF-L may be caused by the disruption in the stoichiometry of NF-L to NF-M/H which is important during neuronal development (reviewed by Julien, 1999, Kong et al, 1998). Support for this explanation comes from the presence of a small minority of GFP/NF-L expressing cells that have an expression pattern that resembles the typical NF staining, suggesting that in these cells the expression of GFP/NF-L was low enough not to disrupt NF subunit stoichiometry. A similar observation in which the expression of GFP/NF-L resulted in aggregates was reported by Yuan et al (2009) who also attributed aggregation to be the result of a disruption in subunit stoichiometry since co-expression with NF-M or NF-H prevented aggregation.

5.3.1.3. Development and characterisation of GF/NF-H

Initially the expression of GFP-tagged NF-H did not yield a GFP/NF-H fusion protein of the expected molecular weight of 230 kDa, but instead resulted in a 70 kDa truncated protein that was detectable by anti-GFP but was not detectable by the anti-NF-H antibody used. The anti-NF-H antibody used (n52) is specific for the C-terminal domain KSP motifs of NF-H (Harris, Ayyub & Shaw, 1991), suggesting that the C-terminal domain is missing from the GFP fusion protein. Reanalysis of the GFP/NF-H nucleotide sequence revealed a single base deletion in the *XmnI* restriction endonuclease recognition sequence that resulted in a premature stop codon which interrupted translation giving rise to a truncated GFP/NF-H protein. This GFP/NF-H plasmid was renamed GFP/NF-H(trunc).

Confocal microscopy also revealed that the truncated GFP/NF-H did not exhibit the typical staining pattern observed for NF, suggesting that it is not incorporated into the NF network. The truncated GFP/NF-H is in itself interesting since it appears to have a punctate staining pattern all along axonal processes suggesting that the truncated protein is transported into the axon but is unable to incorporate into the NF network.

The single base deletion was corrected by re-inserting the missing base by site-directed mutagenesis. Analysis of total cell extracts from cells expressing the corrected GFP/NF-H by

Western blotting revealed expression of a 230 kDa protein (consistent with the predicted apparent molecular weight for the GFP/NF-H fusion protein) that was not only detected by anti-GFP and anti-NF-H but also by smi31 which recognises pNF-H, indicating that GFP/NF-H can also be phosphorylated.

GFP/NF-H expression exhibited a similar pattern to NF-H expression in wild-type cells albeit at a greater level than seen in wild-type cells. GFP/NF-H was colocalised with all three NF subunits suggesting that it is incorporated into the NF network. In addition, co-immunoprecipitation of GFP/NF-H with all three NF subunits reaffirmed its association with endogenous NFs.

Half-life determinations of GFP/NF-H (13.1 ± 1.6 h to 25.5 ± 1.6 h) estimated using Western blots probed with anti-GFP and anti-NF-H revealed that the half-life of GFP/NF-H is shorter than that of NF-H which was previously calculated to be 48.6 ± 4.4 h (Table 3.2-2). Therefore, as with NF-M, GFP labelling of NF-H has made the protein more labile.

5.3.1.4. Conclusion

The selection of GFP tagged neurofilaments for this work was dependent on their ability to exhibit a phenotype that closely resembles that of the endogenous neurofilaments. Since GFP/NF-L expression resulted in the aggregation of GFP fluorescence in the perinuclear region, its use as a tool to study neurofilament dynamics was discounted. Both GFP/NF-M and GFP/NF-H exhibited an expression pattern that closely resembles that of endogenous neurofilaments. They were also shown to associate with the neurofilament subunits suggesting that they are incorporated into the neurofilament structure. As such, both GFP/NF-M and GFP/NF-H were selected for use as tools to study the effects of mitochondrial dysfunction (resulting from treatment with MPP+) on neurofilament distribution and their association with other proteins. A limitation of both GFP/NF-M and GFP/NF-H is their shorter half-lives which suggest that tagging NFs with GFP increases their rate of degradation, perhaps by targeting them for degradation by pathways that may not ordinarily be involved in their turnover.

5.3.2. Neurofilament associating proteins identified by co-immunoprecipitation

Analysis of the composition of the lysate supernatant and the pellet confirmed that α -tubulin and actin were highly soluble in the lysis buffer and that in general around 80 % of IF protein was also soluble. Reduced levels of GFP and GFP tagged NFs in the excluded supernatants confirmed that they were retained in the μ -column, binding to the anti-GFP μ -beads. In addition, reduced levels of non-labelled NF subunits and vimentin in the excluded supernatant suggested that they were also retained in the μ -column via their interaction with the GFP tagged NFs. There was no loss of actin and α -tubulin which suggests that they do not interact with NFs directly.

Mass spectrometry and Western blotting of immunoprecipitates of GFP/NF-M and GFP/NF-H expressing cells has identified vimentin as a neurofilament-associating protein in SH-SY5Y neuroblastoma cells. The association of vimentin with neurofilaments has previously been described in radially orientated filaments of early bipolar neuroblasts during development (Cochard & Paulin, 1984), early differentiating neurons in rat embryos (Bignami et al, 1982) and by double immuno-fluorescence and immuno-electron microscopy of vimentin and NFs in differentiated PC12 cells which revealed that vimentin and NFs did co-localise in some filaments (Yabe et al, 2003). Immunofluorescence and immunoprecipitation studies confirmed that vimentin is preferentially associated with the more motile hypophosphorylated population of NFs. In fact, using pulse chase metabolic labelling of NF-H and live cell imaging of GFP/NF-M Yabe et al (2003) were able to show that newly synthesized NF-M and NF-H are transiently associated with vimentin.

A combination of mass spectrometry and Western blotting confirmed that GFP tagged NFs were also associated with all three NF subunits (NF-H, NF-M and NF-L). In addition immunoprobng with antibodies to phospho-epitopes of NF-M and NF-H confirmed not only the presence of endogenous phosphorylated NF-M and NF-H but also phosphorylated forms of the GFP tagged NFs in immunoprecipitates. Although phosphorylated NFs are usually associated with the more insoluble stationary NF network, their presence in the more motile fraction from which the immunoprecipitates were prepared is not entirely unexpected. Shea et al (1997) reported the presence of phosphorylated NF-H in triton-soluble fraction of developing brains from mice which only declined 120 days after birth. Table 5.3 summarises the results of mass spectrometry and Western blotting of immunoprecipitates SH-SY5Y expressing either GFP/NF-M or GFP/NF-H.

Table 5.3 Summary of the results of immunoprobbed Western blots of GFP/NF-M and GFP/NF-H immunoprecipitates used to identify NF-associating proteins.

Western blots of immunoprecipitates from Human SH-SY5Y neuroblastoma cells that were either mock transfected or transfected with GFP, GFP/NF-M or GFP/NF-H, immunoprobbed with antibodies to a number of candidate proteins to identify proteins that may co-immunoprecipitate with GFP/NF-M or GFP/NF-H.

<i>Protein</i>	<i>Type</i>	<i>Result of Western blot</i>
<i>Dynein</i>	Motor protein	Not detected
<i>Kinesin 5C</i>	Motor protein	Not detected
<i>Kinesin 5A</i>	Motor protein	Not detected
<i>α-tubulin</i>	Cytoskeletal, MTs	Not specific to GFP/NF-M and GFP/NF-H
<i>actin</i>	Cytoskeletal, MFs	Not specific to GFP/NF-M and GFP/NF-H
<i>NF-L</i>	Cytoskeletal, IF	Associates with GFP/NF-M and GFP/NF-H
<i>NF-M and pNF-M</i>	Cytoskeletal, IF	Associates with GFP/NF-M and GFP/NF-H
<i>NF-H and pNF-H</i>	Cytoskeletal, IF	Associates with GFP/NF-M and GFP/NF-H
<i>vimentin</i>	Cytoskeletal, IF	Associates with GFP/NF-M and GFP/NF-H
<i>α-II-spectrin</i>	Cytoskeletal	Not specific to GFP/NF-M and GFP/NF-H
<i>Cdk5</i>	Kinase	Not detected
<i>PSMC1</i>	Proteasome subunit	Not detected
<i>TG2</i>	Cross-linking enzyme	Not detected
<i>Hsc70</i>	Chaperone	Not specific to GFP/NF-M and GFP/NF-H

5.3.2. Acute MPP+ treatment results in axonal retraction

Some retraction of axonal processes occurred in control cells with time during the time-lapse experiment which may suggest that exposure to fluorescent light is having some effect on cellular health. However, in general the structure of control cells was more static than that of cells treated with 5 mM MPP+ in which extensive reorganisation of the cytoskeleton was evident in most cells. Indeed in some MPP+ treated cells axonal processes projecting one way retracted completely and extended in the opposite direction, suggesting that cells were trying to search out a more suitable environment. In general, the rate of retraction of processes in GFP/NF-M and GFP/NF-H expressing cells treated with MPP+ was greater than that of control cells. A comparison of the rate of retraction of GFP fluorescence in the axonal process and the axonal process itself seen with in bright field suggested that the retraction of NFs following treatment occurred simultaneously with the rest of the axonal structure.

5.3.4. Conclusion

GFP tagged neurofilaments are associated with all three NF subunits as well as vimentin. The lack of identification of NF associated proteins other than NF subunits and vimentin is most likely due to limitations in detection. Future work involving the immunoprecipitation of GFP/NFs would concentrate on increasing the yield of GFP/NF immunoprecipitate. This could be achieved by improving the transfection efficiency of the GFP/NF transfection, using more cells or pooling samples.

Time-lapse imaging of 5 mM MPP⁺ treated cells revealed that an acute dose of MPP⁺ treatment results in a general retraction of axonal processes with neurofilaments and the rest of the axonal structural elements moving simultaneously. Future work involving time-lapse and live cell imaging could involve longer treatment regimes with lower doses of MPP⁺. In addition, organelle stains such as mitotracker and lysotracker could be used to monitor changes in their distribution with treatment and how these changes relate to changes in neurofilament distribution.

-

CHAPTER 6

CONCLUSIONS AND FUTURE DIRECTIONS

6.1. Degradative pathways involved in the turnover of cytoskeletal proteins

6.1.1. The half-lives and degradative pathways involved in the turnover of cytoskeletal proteins in SH-SY5Y cells

The half-lives of NF-L, α -tubulin and vimentin estimated in this work were all similar to the half-life of α -tubulin estimated by Ren et al (2003) in HEK293 cells. The half-lives of NF-M and NF-H were longer than that of NF-L which may be due to their increased phosphorylation status which increases their resistance to proteolysis (Greenwood et al, 1993). *In vivo* the half-lives of cytoskeletal proteins are usually quoted in days (Millecamps et al, 2007, Nixon & Logvinenko, 1986, Safaei & Fischer, 1990) and often exhibit biphasic decay rates with the soluble pool being degraded at a faster rate than the insoluble pool (Nixon & Logvinenko, 1986, Safaei & Fischer, 1990). The shorter half-life estimated in this work may be due to the use of proliferating cultured cells in which (due to their quick doubling time) proteins may be turned over more quickly than *in vivo*. Also, no evidence for biphasic decay rates was observed in this work. Whether this would also be true in differentiated cells is not known and could form the basis of future work.

Use of specific protease inhibitors in the presence of CHX established that α -synuclein is degraded by the UPS, macroautophagy and calpain. The role of cysteine cathepsins could not be ruled out since CHX resulted in a huge reduction in cysteine cathepsin activity; suggesting very rapid turnover of this protease. The same approach failed to establish the degradative pathways for any of the other cytoskeletal proteins, except NF-H which appeared to be degraded by macroautophagy and the lysosomal protease cathepsin D. A role for cathepsin D in NF turnover has previously been suggested (Nixon & Marotta, 1984, Suzuki et al, 1988), but in these studies cathepsin D was also shown to degrade NF-L and NF-M *in vitro* (although there was some discrepancy over which NF subunit was most susceptible to cathepsin D proteolysis). One is therefore uncertain as to why a pathway can not be ascribed to NF-L, α -tubulin and vimentin, given that they have a similar half-life to α -synuclein and that there is little evidence of the compensatory activation of other proteolytic pathways in the presence of specific inhibitors. It is possible that the cysteine cathepsins may be involved and in future attempts could be made to test this by monitoring protein levels in the absence of CHX.

6.1.2. Effects of complex I inhibition on cytoskeletal protein turnover

Following complex I inhibition with MPP⁺, the half-lives of all the cytoskeletal proteins were shorter (although not significantly) than the half-lives in CHX-treated controls. In the absence of CHX, MPP⁺ reduced the activity of the proteasome and cathepsin D; this reduction was not evident in the presence of CHX, probably because CHX itself resulted in a reduction in proteasome and cathepsin D activity. MPP⁺ has previously been reported to reduce proteasome activity in SH-SY5Y cells and to directly reduce the activity of purified 20S proteasome (Caneda-Ferron et al, 2008). Whilst MPTP treatment in marmosets results in reduced expression of the α -subunits and components of the regulatory caps (Zeng et al, 2006).

The activity of the cysteine cathepsins was elevated in MPP⁺ and MPP⁺/CHX treated cells; this increase can not solely be attributed to increased expression since increased cysteine cathepsin activity was also observed in the absence of new protein synthesis. Increased cysteine cathepsin levels have also been observed in mitochondrial DNA depleted osteosarcoma cells with impaired mitochondrial respiration (Hamer et al, 2009) and cathepsin L mRNA expression was elevated in MPP⁺ treated PC12 cells (Xu et al, 2005). The increase in cysteine cathepsin activity may account for the lack of decreased cytoskeletal protein turnover in MPP⁺ treated cells, suggesting a role for the cysteine cathepsins in the degradation of cytoskeletal proteins.

Of particular interest in this work is the apparent protective effect of cysteine cathepsins in MPP⁺ treated cells as cysteine cathepsin inhibition resulted in increased cell death. Cysteine cathepsins appear to have contradictory roles in cell survival and cell death since their activation is ordinarily associated with apoptotic and necrotic cell death (Droga-Mazovec et al, 2008, Stoka et al, 2001, Turk & Stoka, 2007, Vasiljeva & Turk, 2008, Wang et al, 2006) whilst in cancer cells increased cysteine cathepsin activity promotes cell survival (Colella et al, 2010, Gocheva et al, 2006, Zhu & Uckun, 2000). In addition, cathepsin L and B double deficient mutant mice die soon after birth and exhibit features of early onset neurodegeneration (Stahl et al, 2007), a condition which can be rescued with the expression of human cathepsin L (Sevenich et al, 2006). So, a fuller understanding of why mitochondrial dysfunction is resulting in increased cysteine cathepsin activity in SH-SY5Y cells is required.

MPP⁺ treatment in the presence of CHX also resulted in an increase in LC3-II levels, indicative of the number of autophagic vesicles. In this work, comparison of LC3-II levels in

MPP⁺, BafA1 and MPP⁺/BafA1 treated cells suggested a reduction of autophagic degradation with MPP⁺ treatment. This result contradicts Zhu et al (2007) who observed that MPP⁺ induces macroautophagy in SH-SY5Y cells (but in the absence of a protein synthesis inhibitor) but is supported by another study in which MPP⁺ reduced dynein function and impaired clearance of α -synuclein by macroautophagy (Cai et al, 2009). A recent report has suggested that MPP⁺ inhibits LC3-II phosphorylation and as such induces autophagosome vesicle synthesis (Cherra et al 2010). However induction of autophagosome synthesis does not preclude an inhibition of macroautophagy since for macroautophagy to proceed to completion, autophagosomes and lysosomes need to fuse. It is this fusion of autophagosome and lysosome that may be inhibited by MPP⁺.

Figure 6.1 summarises the findings in the present work and proposed consequences of these observations.

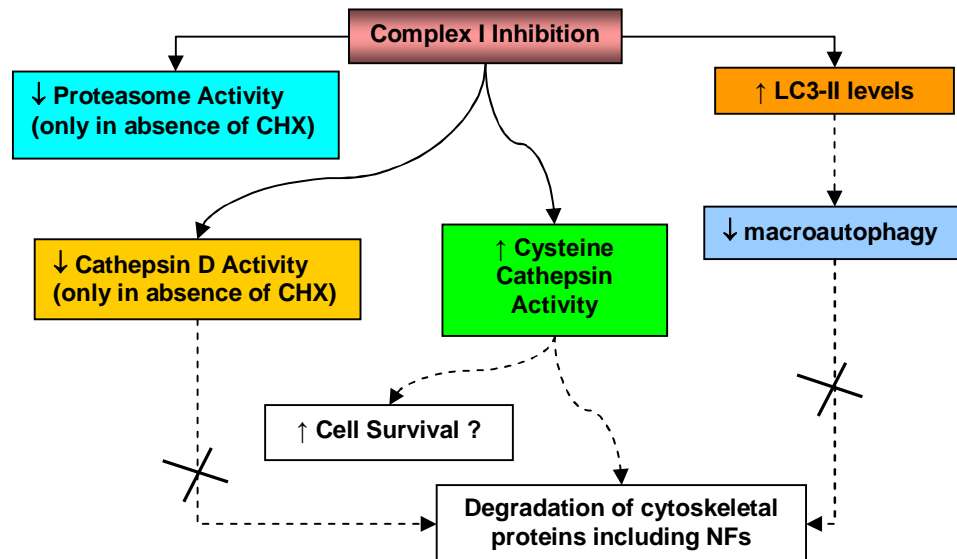


Figure 6.1 Flow diagram illustrating the effects of complex I inhibition on the activity of proteolytic pathways.

Treatment of SH-SY5Y neuroblastoma cells with MPP⁺ (2 mM) for 48 h in the presence or absence of 10 μ g/ml cycloheximide (CHX). MPP⁺ treatment resulted in a reduction in proteasome and cathepsin D activity. No effect on proteasome and cathepsin D activity was observed in MPP⁺/CHX treated cells compared to CHX treated controls. MPP⁺ treatment also resulted in an increase in cysteine cathepsin activity and the levels of LC3-II which suggests the inhibition of macroautophagy. Due to the inhibition of cathepsin D and macroautophagy and the increase in cysteine cathepsin activity, it may be cysteine cathepsins that are involved in the turnover of cytoskeletal proteins in MPP⁺ treated proliferating SH-SY5Y cells. Clear boxes and dotted lines represent proposed consequences/significance of observations.

6.1.3. DA-mediated oxidative stress and cytoskeletal protein turnover

In cells treated with 100 μ M DA, estimations of the half-lives of cytoskeletal proteins were problematic due to a large degree of experimental variation but in general half-life appeared to be increased. Treatment with 100 μ M DA resulted in a reduction in proteasome activity but only in the presence of CHX. As mentioned before, the effects of 100 and 500 μ M DA on the proteasome was established to be the result of DA mediated oxidative damage (Caneda-Ferron et al, 2008). In the present work the reduction in proteasome activity with 100 μ M DA in the presence of CHX may be due to oxidative damage of proteasome subunits which can not be replaced due to the inhibition of protein synthesis. 100 μ M DA also resulted in an increase in LC3-II levels which when comparing LC3-II levels of cells treated with DA, BafA1 or DA/BafA1 suggested an inhibition of macroautophagy may be responsible for increased LC3-II levels. Interestingly, by monitoring α II-spectrin cleavage, an increase in the appearance of the calpain specific cleavage product was observed with 100 μ M DA treatment, suggesting an activation of calpain. Calpain activation has previously been shown to induce Cdk5 activity by p35 cleavage (Tamada et al, 2005) which in turn is known to phosphorylate NFs (Pant et al, 1997, Sun et al, 1996) increasing their resistance to proteolysis (Greenwood et al, 1993).

Treatment with 500 μ M DA resulted in extensive cell death, a reduction in the half-lives of cytoskeletal proteins and the apparent activation of caspase 3, suggested by the production of the 120 kD caspase 3-specific cleavage product of α II-spectrin (reviewed in Wang, 2000). Proteasome activity was virtually abolished with 500 μ M DA and LC3-II levels could not be elevated by BafA1 co-treatment. Due to the extensive degree of cell death observed in cultures treated with 500 μ M, these effects are most likely due to the activation of cell death proteases.

Figure 6.2 summarizes the findings of the present work and the proposed consequences of these observations.

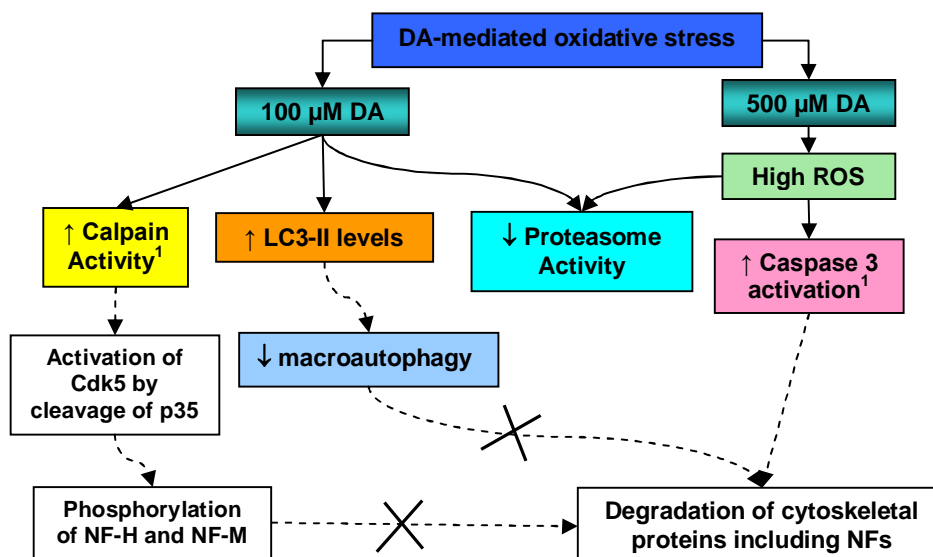


Figure 6.2 Flow diagram illustrating the effects of dopamine (DA)-mediated oxidative stress on the activity of proteolytic pathways.

Treatment of SH-SY5Y neuroblastoma cells with 100 μM DA in the presence of 10 $\mu\text{g/ml}$ cycloheximide (CHX) resulted in an increase in LC3-II levels which suggested an inhibition of macroautophagy. 100 μM DA treatment also resulted in reduced proteasome activity (monitored by measuring chymotrypsin-like activity, CLA) and an apparent activation of calpain¹. Treatment of SH-SY5Y with 500 μM DA/CHX virtually abolished proteasome activity (monitored by measuring CLA) and resulted in an apparent activation of caspase 3¹.

¹The effect on calpain and caspase 3 activation was determined indirectly by monitoring the levels of αII -spectrin calpain-specific and caspase 3-specific cleavage products on Western blots probed with anti- αII -spectrin (Sigma).

6.2. Assessment of protein aggregation in RA/BDNF differentiated SH-SY5Y cells following mitochondrial dysfunction and proteasome inhibition

6.2.1. Effects of mitochondrial dysfunction

MPP⁺ treatment resulted in an accumulation of NF-H in the cell body that was accompanied by a local swelling of the axonal structure in that region. Enrichment of NF-H, pNF-M and α -tubulin in the insoluble fraction and the co-localization of NF-H in the perinuclear region with p62 and LC3 is suggestive of aggregate formation and the attempted clearance of aggregates by macroautophagy (Bjorkoy et al, 2005, Pankiv et al, 2007).

The decrease in the levels of dynein intermediate chain observed with MPP⁺ treatment may interfere with dynein function and subsequently impair macroautophagy (Cai et al, 2009) since dynein function is required for autophagosome and lysosome fusion (Ravikumar et al, 2005). Impaired dynein function also inhibits the entry of NFs from the cell body to axonal

processes (Motil et al, 2006) which could also result in a local accumulation of NFs in the cell body.

Preliminary results also suggested a decrease in the levels of active cathepsin D which may impair cathepsin D-dependent lysosomal degradation. Work with proliferating cells suggested an increase in cysteine cathepsin activity with MPP⁺ treatment (section 3.2.4.2.4) and since cathepsin L is able to degrade cathepsin D (Zheng et al, 2008), the decrease in active cathepsin D observed in this work may be the result of cleavage by cathepsin L. A schematic summarising the effects of MPP⁺ treatment is given below in Figure 6.3, together with some proposed mechanisms.

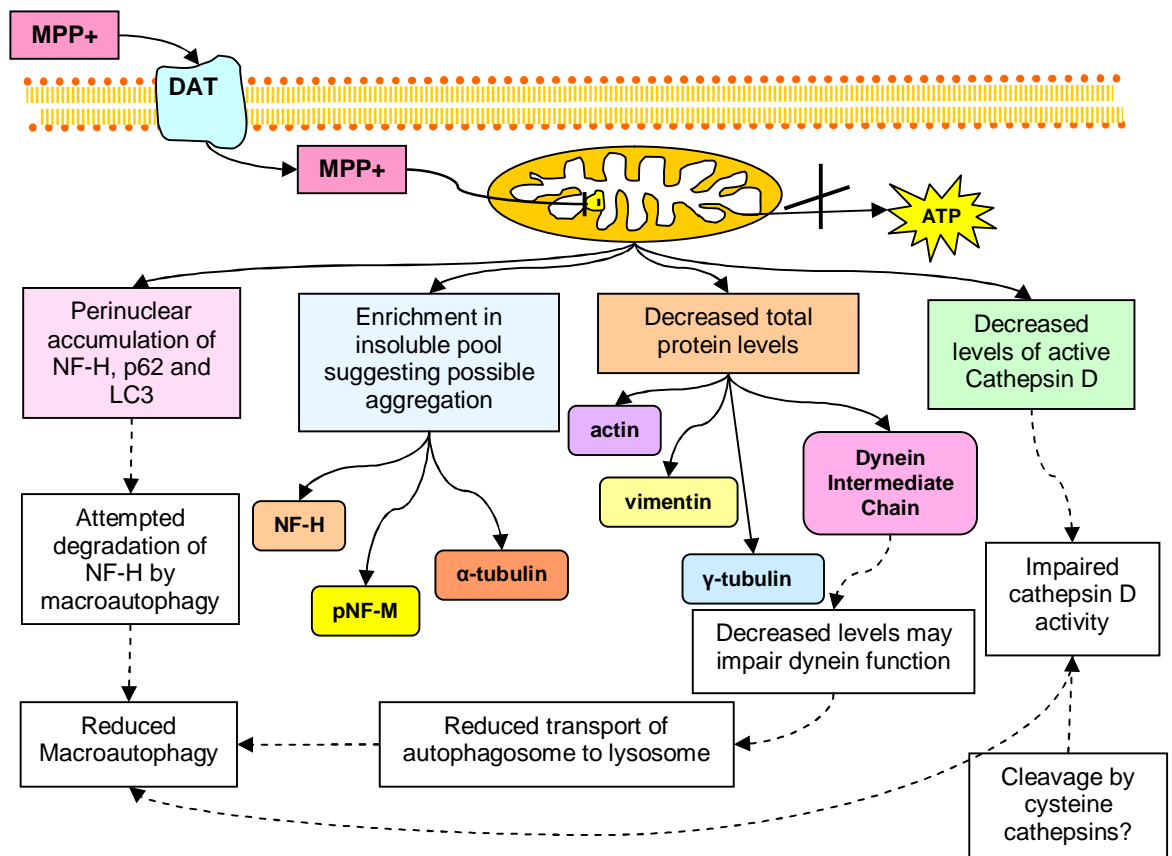


Figure 6.3 Scheme representing the effects of 24 h treatment of RA/BDNF differentiated SH-SY5Y neuroblastoma cells with 500 μM MPP⁺.

Treatment with 500 μM MPP⁺ resulted in an increased distribution of NF-H in the cell body that concentrated in the perinuclear region accompanied with a swelling of the processes in these regions. These accumulations of NF-H also colocalized with p62 and LC3 suggesting the attempted degradation of NF-H accumulations by macroautophagy. Increased levels of pNF-M, NF-H, α-tubulin and p62 in the insoluble cell fraction with MPP⁺ treatment suggests aggregate formation. The increased presence of p62 in the insoluble fraction may be indicative of its function to target aggregated proteins for degradation by macroautophagy. Decreased levels of actin, vimentin, γ-tubulin and dynein light intermediate chain were observed with MPP⁺ treatment. Decreased levels of dynein may impair dynein function resulting in impaired macroautophagy which may prevent the clearance of aggregated proteins. Preliminary results also suggested decreased levels of active cathepsin D which may result in decreased cathepsin D-dependent lysosomal degradation. Proposed consequences/significance of observations are given in clear boxes.

6.2.2. Effects of proteasome inhibition

Treatment of RA/BDNF differentiated cells with epoxomicin also resulted in a local accumulation of NF-H in the cell body but in this case NF-H accumulation did not coincide with regions of axonal swelling as seen in MPP+ treated cells. These regions of NF-H accumulation also co-localized with p62 and LC3. The increased appearance of p62, pNF-M and NF-H in the igepal insoluble cell fraction with epoxo treatment suggests a decrease in their solubility which is suggestive of aggregation. The presence of p62 and the co-localization of LC3 is suggestive of the attempted degradation of protein aggregates by macroautophagy (Bjorkoy et al, 2005, Pankiv et al, 2007).

Epoxo treatment also resulted in increased levels of NF-M protein which may be the result of decreased turnover and aggregation in the insoluble pool. Decreased levels of vimentin and dynein intermediate chain protein were also observed. As mentioned earlier decreased levels of dynein may interfere with dynein function which could impair macroautophagy (Cai et al, 2009, Ravikumar et al, 2005) and/or the delivery of NFs from the cell body into the axonal processes (Motil et al, 2006). The levels of active cathepsin D were increased with epoxo treatment, a compensatory activation of cathepsin D has previously been reported with proteasome inhibition (Rideout et al, 2004).

A schematic summarizing the effects of epoxo treatment is given below in Figure 6.4, together with some proposed mechanisms.

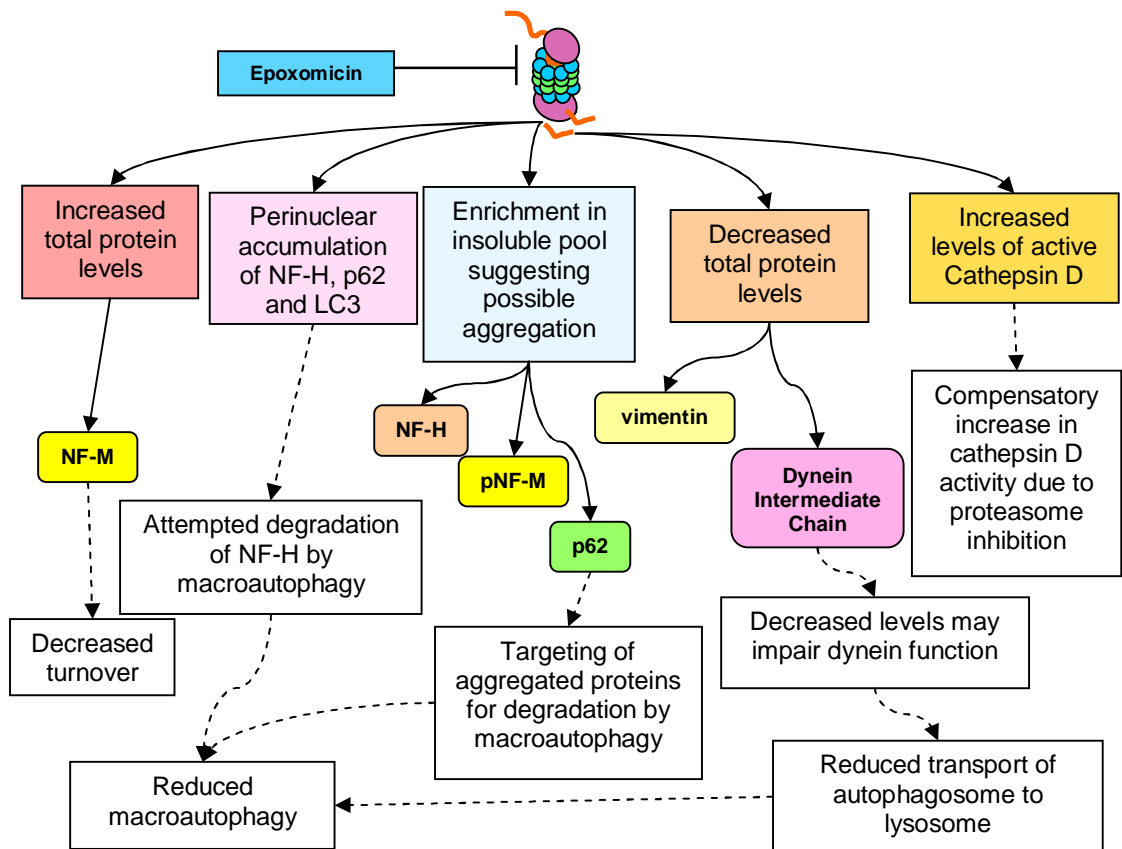


Figure 6.4 Scheme representing the effects of 24 h treatment of RA/BDNF differentiated SH-SY5Y neuroblastoma cells with 10 nM Epoxomicin (epoxo).

Treatment with epoxo resulted in an increased distribution of NF-H in the cell body that concentrated in the perinuclear region. These accumulations of NF-H also co-localized with p62 and LC3 suggesting the attempted degradation of NF-H accumulations by macroautophagy. Increased levels of pNF-M, NF-H and p62 in the insoluble cell fraction are suggestive of aggregate formation. The increased presence of p62 in the insoluble fraction may be indicative of its function to target aggregated proteins for degradation by macroautophagy. Decreased levels of vimentin and dynein light intermediate chain and increased levels of NF-M were observed in total cell extracts. Increased levels of NF-M may be the result of decreased turnover. Decreased levels of dynein may impair dynein function resulting in impaired macroautophagy which may prevent the clearance of aggregated proteins. Preliminary results also suggested an increase in the levels of active cathepsin D which suggests a compensatory activation of cathepsin D. Proposed consequences/significance of observations are indicated by the clear boxes and dotted lines.

6.2.3. Effects of a combination of mitochondrial dysfunction and proteasome inhibition

As observed in MPP⁺ and epoxo treated cells, MPP⁺/epoxo treated cells also exhibited local accumulations of NF-H in the cell body that co-localized with p62 and LC3. Again, the enrichment of pNF-M, α -tubulin and p62 in the igepal insoluble fraction suggests protein aggregation and co-localization of p62 and LC3 is suggestive of the induction of macroautophagy to clear aggregated proteins.

Increased levels of NF-M and decreased levels of TG2, vimentin, α -tubulin and dynein intermediate chain were observed following MPP⁺/epoxo treatment. Increased levels of NF-M may be the result of decreased NF-M proteolysis resulting in or from protein aggregation in the insoluble fraction. In RA differentiated SH-SY5Y cells, MPP⁺ treatment resulted in the activation of TG2 induced cross-linking activity (Beck et al, 2006) and TG2 had been shown to be involved in α -synuclein aggregation in COS-7 and HEK293 cells expressing human α -synuclein (Junn et al, 2003). The decreased TG2 levels observed with MPP⁺/epoxo treatment may be an adaptive response to prevent cross-linking of aggregated proteins which may prevent the effective clearance of protein aggregates in these cells. The decreased levels of dynein intermediate chain in total protein may have implications for dynein motor function and macroautophagy (Cai et al, 2009, Ravikumar et al, 2005) and the delivery of NFs into the axonal processes (Motil et al, 2006), ultimately resulting in protein aggregation in the cell body. A schematic summarising the effects of MPP⁺/epoxo treatment is given below in Figure 6.5, together with some proposed mechanisms.

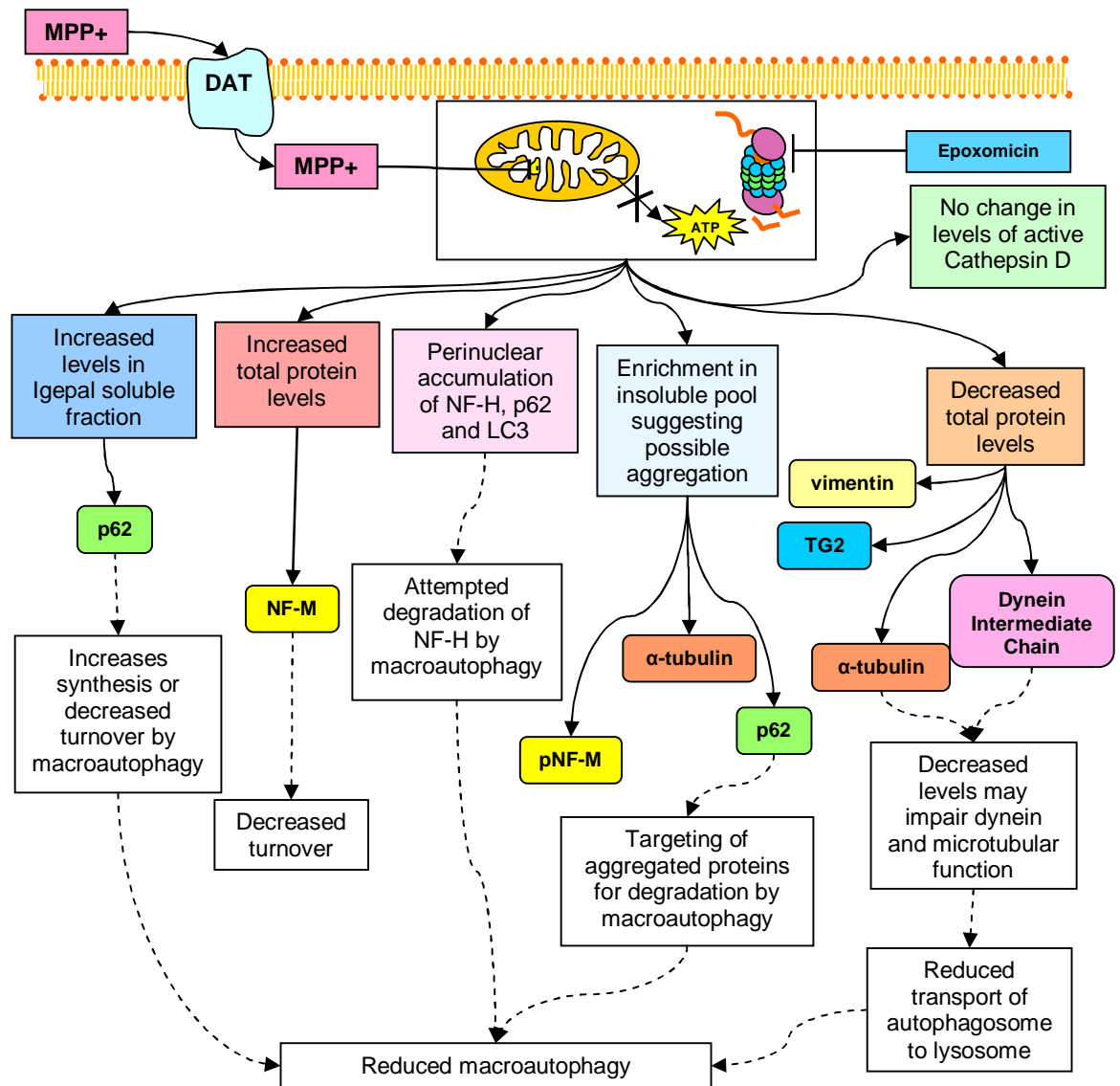


Figure 6.5 Scheme representing the effects of 24 h treatment of RA/BDNF differentiated SH-SY5Y neuroblastoma cells with 500 μM MPP⁺ and 10 nM Epoxomicin.

Treatment with MPP⁺/epoxo resulted in an increased distribution of NF-H in the cell body that concentrated in the perinuclear region. These accumulations of NF-H also co-localized with p62 and LC3 suggesting the attempted degradation of NF-H accumulations by macroautophagy. Increased levels of pNF-M, α -tubulin and p62 in the insoluble cell fraction are suggestive of aggregate formation. The increased presence of p62 in the insoluble fraction may be indicative of its function to target aggregated proteins for degradation by macroautophagy. Increased levels of p62 were also observed in the IgG-soluble cell fraction. Decreased levels of TG2, vimentin, α -tubulin and dynein light intermediate chain and increased levels of NF-M were observed in total cell extracts. Increased levels of NF-M may be the result of decreased turnover. Decreased levels of dynein may impair dynein function resulting in impaired macroautophagy which may prevent the clearance of aggregated proteins. Preliminary results also suggested no change in the levels of active cathepsin D. Proposed consequences/significance of observations are indicated by the clear boxes and the dotted lines.

6.3. Future directions

Further validation of the effects of 100 μ M DA on the activation calpain is required. Although most of the synthetic peptides to assay calpain activity are not very specific (reviewed in Goll et al, 2003), the inclusion of the endogenous calpain inhibitor (calpastatin) may provide additional evidence for the role of calpain. In addition, methods to monitor intracellular calcium levels following DA treatment may provide further information.

Future work could concentrate on investigating the effects of MPP⁺ treatment on protein degradative pathways by monitoring its effects on protein and mRNA expression of the proteins involved in degradative pathways. The effects of MPP⁺ on protein degradative pathways in proliferating and RA/BDNF differentiated cells could also be compared. To clarify the effect of MPP⁺ on macroautophagy additional methods that can be used to measure macroautophagy are required. Methods which monitor autophagosome content such as electron microscopy, fluorescence labelling of autophagosomes and Western blot detection of LC3-II levels measure the induction of macroautophagy but do not establish whether these autophagosomes fuse with lysosomes (Klionsky et al, 2008). The measurement of autophagic flux by monitoring the turnover of autophagic protein substrates such as p62 would enable one to establish whether macroautophagy proceeds to completion (Klionsky et al, 2008).

Further investigation of the apparent protective effects of the cysteine cathepsins in MPP⁺ toxicity is required. To establish whether the effect is limited to proliferating neuroblastoma cells and a characteristic of the original neuroblastoma or whether it may be of relevance to neurodegeneration, the role of cysteine cathepsins in MPP⁺ toxicity in RA/BDNF differentiated cells should be investigated. Although Mantle et al (1995) did not show a significant increase in the activity of cathepsin L in grey and white matter of the frontal cortex from post-mortem PD brain, the mean activity values suggested a slight increase in activity but due to a large degree of deviation, no statistical significance was found. They also concentrated on the frontal cortex and did not look at cathepsin activity in the substantia nigra which may have been more relevant for PD. It would therefore be interesting to compare cathepsin activities and expression (in particular that of cysteine cathepsins such as cathepsin L and B) in human PD substantia nigra and in the substantia nigra of PD animal models.

In this work RA/BDNF differentiated cells were treated for 24 h with MPP⁺, epoxo or MPP⁺/epoxo; future work could concentrate on characterising the effects of treatment over longer treatment periods and to establish what other proteins co-localize with the NF-H, p62

and LC3 accumulated in the cell body. It would also be interesting to establish whether in these cells aggregated proteins are cleared either at a later time-point in treatment or when the treatment is removed. The clearance of aggregates after removal of treatment has been described for COS-7 cells treated with rotenone (Lee et al, 2002), but in COS-7 cells overexpressing parkin, inclusions induced by proteasome inhibition were not cleared following removal of the proteasome inhibitor (Ackerley et al, 2003).

All three treatment regimes resulted in decreased dynein intermediate chain levels which may have implications for dynein function and as such the delivery of NFs into the axonal processes from the cell body, the retrograde transport of NFs and organelles in axonal processes and macroautophagy (Cai et al, 2009, He et al, 2005, Hirokawa et al, 1998, Motil et al, 2006, Motil et al, 2007, Ravikumar et al, 2005, Theiss et al, 2005, Webb et al, 2004). It would therefore be beneficial to investigate the effects of all three treatments on the functioning of motor proteins and the consequences thereof.

According to Encinas et al (2000) RA/BDNF differentiated cells are stable for at least 3 weeks as long as they have access to BDNF, it would therefore be possible to produce chronic models investigating the effects of mitochondrial dysfunction and proteasome inhibition on NFs and other proteins.

Further work using siRNA technology to knockdown the expression of the NF subunits may provide additional information regarding the role of NFs in inclusion formation following complex I and/or proteasome inhibition of differentiated cells. Due the changes in the distribution of p62 following complex I and/or proteasome inhibition presented in this work, future work could concentrate on clarifying the role of p62 in inclusion formation and whether p62 interacts with NFs directly or whether NFs are ubiquitinated before p62 association. Recently p62 and parkin have been implicated in the regulation of mitophagy (Geisler et al 2010a); it may therefore be interesting to evaluate whether NFs are involved in this process due to their reported association with active mitochondria (Wagner, 2003).

6.4. The use of GFP tagged NFs to monitor NF dynamics

6.4.1. Development and characterisation of GFP/NFs

All three neurofilament subunits (NF-H, NF-M and NF-L) were amplified from cDNA preparations of SH-SY5Y cells and cloned into the GFP expression vector (pEGFP-C3). Characterisation of the expression of all three GF/NF subunits in SH-SY5Y cells revealed that all three constructs were of the predicted molecular weight and immunoreactive with antibodies to GFP and antibodies to both phosphorylation dependent and phosphorylation independent epitopes of the respective NF subunits. Immunofluorescence and confocal imaging of GFP/NF-M and GFP/NF-H expressing cells revealed that the distribution pattern of both of these GFP/NF subunits was similar to that of endogenous NFs and that they co-localized with the other NF subunits.

However in most GFP/NF-L expressing cells, GFP fluorescence was confined to a localized region in the cell body that resembled an inclusion, suggesting either that GFP/NF-L is not assembled into the NF network or that the over-expression of NF-L resulting from the GFP/NF-L expression disrupts NF assembly. The importance of NF subunit stoichiometry during neuronal development has previously been suggested (Kong et al, 1998, Xu et al, 1996, Zhu et al, 1997).

The possibility of using GFP/NF-M and GFP/NF-H expressing cells for time-lapse imaging of live cultures treated with MPP⁺ was assessed by treating cells with 5 mM MPP⁺ and imaging cells every 5 minutes over the course of an hour. Time-lapse imaging of MPP⁺ treated cells revealed extensive reorganisation and retraction of the axonal cytoskeleton within the first 30-40 minutes of treatment.

6.4.2. Assessment of GFP/NF co-immunoprecipitation

GFP/NFs were successfully immunoprecipitated using anti-GFP μ beads from Miltenyi Biotec. As mentioned earlier the GFP/NFs immunoprecipitated in this work constituted the more motile soluble pool of NFs rather than the more insoluble less motile component (Yabe et al, 2001). Mass spectrometry and immunoprobings of Western blots identified the presence of all three NF subunits and vimentin in immunoprecipitates. As mentioned earlier vimentin association with NFs has previously been reported in the developing nervous system (Bignami et al, 1982, Cochard & Paulin, 1984) and in PC12 cells, vimentin was shown to associate with the more dispersed population of NF which constitute the more motile soluble

component (Yabe et al, 2003). However due to the low levels of immunoprecipitated proteins it was not possible to identify any other NF associating proteins during the project.

6.4.3. Further recommendations for the use of GFP/NF subunits

Future work with GFP/NF-L could involve the characterisation of the GFP/NF-L 'inclusions' in the cell body. Defective axonal transport and aggregation of NFs in inclusions has been observed in CMT disease resulting from mutations in the head and rod domains of NF-L (Brownlees et al, 2002, Pérez-Ollé et al, 2005, Zhai et al, 2007). It would be interesting to establish whether the other NF subunits are also trapped in the GFP/NF-L aggregations and whether these aggregates have some of the features of aggresomes.

Further work involving time-lapse imaging of live cells expressing GFP/NF-M or GFP/NF-H could concentrate on the effects of lower doses of MPP⁺ on the transport rate of NFs and the distribution of GFP/NFs in relation to other axonally transported proteins and organelles such as mitochondria and lysosomes. Defective axonal transport has been implicated in a number of neurodegenerative conditions (reviewed by De Vos et al, 2008, Ittner et al, 2008, and Roy et al, 2005) and the effects of MPP⁺ treatment on the motor proteins and on the axonal transport of neurofilaments and mitochondria have not been fully explored although there is some evidence that MPP⁺ results in altered axonal transport (Morfini et al, 2007) and affects dynein level and function (Cai et al, 2009).

Due to the low yield of immunoprecipitates from cell lysates of GFP/NF expressing cells, future work using co-immunoprecipitation needs to concentrate on improving yield. The main short coming of the transient GFP/NF transfection has been the low transfection efficiency which would need to be improved either by comparing some of the newer transfection reagents available which claim to be more efficient than the LipofectAMINE transfection reagent used in this work. An alternative approach (which may be more beneficial) could be to produce stably transfected cell lines, the advantage of which would also be a more homogenous population of cells all expressing a similar level of GFP tagged NFs.

6.5. Summary

In conclusion, using a number of different biochemical approaches and methods in **proliferating cells**:

- The half-lives of NF-H and NF-M were determined to be 48-53 h whilst the half-lives of NF-L, α -tubulin, vimentin and α -synuclein were shorter at 31-41 h.
- A role for cathepsin D and macroautophagy in NF-H turnover in unstressed cells was established.
- Some evidence for the activation of cysteine cathepsins with MPP⁺ treatment and their involvement in ensuring cell survival was obtained.
- MPP⁺ treatment led to a reduction in cathepsin D activity, macroautophagy and the proteasomal activity but no reduction in the turnover of cytoskeletal proteins was observed.
- Some evidence for the reduced degradation of all cytoskeletal elements in cells treated with 100 μ M DA, accompanied by calpain activation and the inhibition of the proteasome and macroautophagy. Notably, with 100 μ M DA treatment, no effect on cysteine cathepsins was observed and inhibition of cysteine cathepsins in 100 μ M DA treated cells did not result in increased cell death.

Using RA/BDNF **differentiated** cells a role for mitochondrial dysfunction (induced by MPP⁺) and/or proteasome inhibition (epoxomicin) in the accumulation and aggregation of neurofilaments was suggested due to:

- the enrichment of NFs in the igepal insoluble fraction
- the localized accumulation of NF-H in the cell body

A role for macroautophagy in this experimental model was also suggested due to:

- the enrichment of p62 in the igepal insoluble fraction
- co-localization of NF-H accumulations with both p62 and LC3

Further characterisation of the effects of mitochondrial dysfunction and/or proteasome inhibition on protein aggregation and protein degradative pathways could further our understanding of the pathogenesis of neurodegenerative conditions.

A schematic attempting to integrate the observations made in the present work within the current understanding and hypotheses as reviewed in Chapter 1 can be found in appendix VI.

-
-

CHAPTER 7

REFERENCE LIST

References

- Ackerley S, Grierson AJ, Banner S, Perkinson MS, Brownlees J, Byers HL, Ward M, Thornhill P, Hussain K, Waby JS, Anderton BH, Cooper JD, Dingwall C, Leigh PN, Shaw CE, & Miller CCJ (2004) p38 α stress-activated protein kinase phosphorylates neurofilaments and is associated with neurofilament pathology in amyotrophic lateral sclerosis. *Molecular and Cellular Neuroscience* **26**: 354-364
- Ackerley S, Grierson AJ, Brownlees J, Thornhill P, Anderton BH, Leigh PN, Shaw CE, & Miller CCJ (2000) Glutamate Slows Axonal Transport of Neurofilaments in Transfected Neurons. *The Journal of Cell Biology* **150**: 165-176
- Ackerley S, Thornhill P, Grierson AJ, Brownlees J, Anderton BH, Leigh PN, Shaw CE, & Miller CCJ (2003) Neurofilament heavy chain side arm phosphorylation regulates axonal transport of neurofilaments. *The Journal of Cell Biology* **161**: 489-495
- Ahn K, Kim Y, Kim S, Huh Y, Park C, & Jeong J (2009) Okadaic acid protects human neuroblastoma SH-SY5Y cells from 1-methyl-4-phenylpyridinium ion-induced apoptosis. *Neuroscience Letters* **449**: 93-97
- Alam ZI, Daniel SE, Lees AJ, Marsden DC, Jenner P, & Halliwell B (1997) A generalised increase in protein carbonyls in the brain in Parkinson's but not incidental Lewy body disease. *Journal of Neurochemistry* **69**: 1326-1329
- Alvira D, Ferrer I, Gutierrez-Cuesta J, Garcia-Castro B, Pallas M, & Camins A (2008) Activation of the calpain/cdk5/p25 pathway in the girus cinguli in Parkinson's disease. *Parkinsonism and Related Disorders* **14**: 309-313
- Anderton BH, Breinburg D, Downes MJ, Green PJ, Tomlinson BE, Ulrich J, Wood JN, & Kahn J (1982) Monoclonal antibodies show that neurofibrillary tangles and neurofilaments share antigenic determinants. *Nature* **298**: 84-86
- Ardley HC, Hung CC, & Robinson PA (2005) The aggravating role of the ubiquitin-proteasome system in neurodegeneration. *Febs Letters* **579**: 571-576
- Ardley HC, Scott GB, Rose SA, Tan NGS, Markham AF, & Robinson PA (2003) Inhibition of proteasomal activity causes inclusion formation in neuronal and non-neuronal cells overexpressing Parkin. *Molecular Biology of the Cell* **14**: 4541-4556
- Axe EL, Walker SA, Manifava M, Chandra P, Roderick HL, Habermann A, Griffiths G, & Ktistakis NT (2008) Autophagosome formation from membrane compartments enriched in phosphatidylinositol 3-phosphate and dynamically connected to the endoplasmic reticulum. *The Journal of Cell Biology* **182**: 685-701
- Ballard PA, Tetrad JW, & Langston JW (1985) Permanent human parkinsonism due to 1-methyl-4-phenyl-1,2,3,6-tetrahydropyridine (MPTP): Seven cases. *Neurology* **35**: 949
- Baliga BS, Pronczuk AW, & Munro HN (1969) Mechanism of Cycloheximide Inhibition of Protein Synthesis in a Cell-free System Prepared from Rat Liver. *Journal of Biological Chemistry* **244**: 4480-4489
- Bandhyopadhyay U & Cuervo AM (2007) Chaperone-mediated autophagy in aging and neurodegeneration: Lessons from α -synuclein. *Experimental Gerontology* **42**: 120-128
- Barrachina M, Castaño E, Dalfó E, Maes T, Buesa C, & Ferrer I (2006) Reduced ubiquitin C-terminal hydrolase-1 expression levels in dementia with Lewy bodies. *Neurobiology of Disease* **22**: 265-273
- Barrett AJ, Kembhavi AA, Brown MA, Kirschke H, Knight CG, Tamai M, & Hanada K (1982) L-trans-Epoxysuccinyl-leucylamido(4-guanidino)butane (E-4) and its analogues as inhibitors of cysteine proteinases including cathepsins B, H and L. *Biochemical Journal* **201**: 189-198

- Beck, KE (2004) Changes in the cytoskeleton and signalling pathways in differentiated human neuroblastoma cells following MPP+ exposure. *PhD Thesis Nottingham Trent University*
- Beck KE, De Girolamo LA, Griffin M, & Billett EE (2006) The role of tissue transglutaminase in 1-methyl-4-phenylpyridinium (MPP+)-induced toxicity in differentiated human SH-SY5Y neuroblastoma cells. *Neuroscience Letters* **405**: 46-51
- Bedford L, Hay D, Devoy A, Paine S, Powe DG, Seth R, Gray T, Topham I, Fone K, Rezvani N, Mee M, Soane T, Layfield R, Sheppard PW, Ebendal T, Usoskin D, Lowe J, & Mayer RJ (2008) Depletion of 26S Proteasomes in Mouse Brain Neurons Causes Neurodegeneration and Lewy-Like Inclusions Resembling Human Pale Bodies. *The Journal of Neuroscience* **28**: 8189-8198
- Bedford L, Paine S, Sheppard PW, Mayer RJ, & Roelofs J (2010) Assembly, structure, and function of the 26S proteasome. *Trends Cell Biology* **20**: 391-401
- Bennett MC, Bishop JF, Leng Y, Chock PB, Chase TN, & Mouradian MM (1999) Degradation of alpha -Synuclein by Proteasome. *Journal of Biological Chemistry* **274**: 33855-33858
- Bergeron C, Petrunka C, Weyer L, & Pollanen MS (1996) Altered neurofilament expression does not contribute to Lewy body formation. *American Journal of Pathology* **148**: 267-272
- Betarbet R, Sherer TB, & Greenamyre JT (2005) Ubiquitin-proteasome system and Parkinson's diseases. *Experimental Neurology* **191**: S17-S27
- Betarbet R, Sherer TB, MacKenzie G, Garcia-Osuna M, Panov AV, & Greenamyre JT (2000) Chronic systemic pesticide exposure reproduces features of Parkinson's disease. *Nature Neuroscience* **3**: 1301-1306
- Bezard E, Dovero S, Bioulac B, & Gross C (1997) Effects of Different Schedules of MPTP Administration on Dopaminergic Neurodegeneration in Mice. *Experimental Neurology* **148**: 288-292
- Biedler JL, Helson L, & Spengler BA (1973) Morphology and Growth, Tumorigenicity, and Cytogenetics of Human Neuroblastoma Cells in Continuous Culture. *Cancer Research* **33**: 2643-2652
- Biedler JL, Roffler-Tarlov S, Schachner M, & Freedman LS (1978) Multiple Neurotransmitter Synthesis by Human Neuroblastoma Cell Lines and Clones. *Cancer Research* **38**: 3751-3757
- Bignami A, Raju T, & Dahl D (1982) Localization of vimentin, the nonspecific intermediate filament protein, in embryonal glia and in early differentiating neurons: In vivo and in vitro immunofluorescence study of the rat embryo with vimentin and neurofilament antisera. *Developmental Biology* **91**: 286-295
- Bjorkoy G, Lamark T, Brech A, Outzen H, Perander M, Overvatn A, Stenmark H, & Johansen T (2005) p62/SQSTM1 forms protein aggregates degraded by autophagy and has a protective effect on huntingtin-induced cell death. *Journal of Cell Biology* **171**: 603-614
- Blanchet PJ, Konitsiotis S, Hyland K, Arnold LA, Pettigrew KD, & Chase TN (1998) Chronic Exposure to MPTP as a Primate Model of Progressive Parkinsonism: A Pilot Study with a Free Radical Scavenger. *Experimental Neurology* **153**: 214-222
- Blum D, Torch S, Lambeng N, Nissou MF, Benabid AL, Sadoul R, & Verna JM (2001) Molecular pathways involved in the neurotoxicity of 6-OHDA, dopamine and MPTP: contribution to the apoptotic theory in Parkinson's disease. *Progress in Neurobiology* **65**: 135-172
- Boada J, Cutillas B, Roig T, Bermudez J, & Ambrosio S (2000) MPP+-Induced Mitochondrial Dysfunction Is Potentiated by Dopamine. *Biochemical and Biophysical Research Communications* **268**: 916-920
- Bocquet A, Berges R, Frank R, Robert P, Peterson AC, & Eyer J (2009) Neurofilaments Bind Tubulin and Modulate Its Polymerization. *Journal of Neuroscience* **29**: 11043-11054

- Bolhuis S & Richter-Landsberg C (2010) Effect of proteasome inhibition by MG-132 on HSP27 oligomerization, phosphorylation and aggresome formation in oligodendroglial cells. *Journal of Neurochemistry* **114**: 960-971
- Bonifati V, Rizzu P, van Baren MJ, Schaap O, Breedveld GJ, Krieger E, Dekker MCJ, Squitieri F, Ibanez P, Joosse M, van Dongen JW, Vanacore N, van Swieten JC, Brice A, Meo G, van Duijn CM, Oostra BA, & Heutink P (2003) Mutations in the DJ-1 Gene Associated with Autosomal Recessive Early-Onset Parkinsonism. *Science* **299**: 256-259
- Braak H, Del Tredici K, Rub U, de Vos RAI, Jansen Steur ENH, & Braak E (2003) Staging of brain pathology related to sporadic Parkinson's disease. *Neurobiology of Aging* **24**: 197-211
- Brion J & Couke A (1995) Cortical and Brainstem-Type Lewy Bodies are Immunoreactive for the Cyclin-Dependent Kinase 5. *American Journal of Pathology* **147**: 1465-1476
- Brown A (1998) Contiguous phosphorylated and non-phosphorylated domains along axonal neurofilaments. *Journal of Cell Science* **111**: 455-467
- Brown HG, Troncoso JC, & Hoh JH (1998) Neurofilament-L homopolymers are less mechanically stable than native neurofilaments. *Journal of Microscopy* **191**: 229-237
- Brown A, Wang L, & Jung P (2005) Stochastic Simulation of Neurofilament Transport in Axons: The "Stop-and-Go" Hypothesis. *Molecular Biology of the Cell* **16**: 4243-4255
- Brownlee J, Ackerley S, Grierson AJ, Jacobsen NJO, Shea K, Anderton BH, Leigh PN, Shaw CE, & Miller CCJ (2002) Charcot-Marie-Tooth disease neurofilament mutations disrupt neurofilament assembly and axonal transport. *Human Molecular Genetics* **11**: 2837-2844
- Burbulla LF, Krebichl G, & Krüger R (2010) Balance is the challenge - The impact of mitochondrial dynamics in Parkinson's disease. *European Journal of Clinical Investigation* **40**(8): 1-13
- Burnett BG & Pittman RN (2005) The polyglutamine neurodegenerative protein ataxin 3 regulates aggresome formation. *Proceedings of the National Academy of Sciences* **102**: 4330-4335
- Butterfield DA & Kanski J (2001) Brain protein oxidation in age-related neurodegenerative disorders that are associated with aggregated proteins. *Mechanisms of Ageing Development* **122**: 945-962
- Cai Z, Shi J, Yang Y, Cao B, Wang F, Huang J, Yang F, Zhang P, & Liu C (2009) MPP impairs autophagic clearance of alpha-synuclein by impairing the activity of dynein. *NeuroReport* **20**: 569-573
- Caneda-Ferron B, De Girolamo LA, Costa T, Beck KE, Layfield R, & Billett EE (2008) Assessment of the direct and indirect effects of MPP+ and dopamine on the human proteasome: implications for Parkinson's disease aetiology. *Journal of Neurochemistry* **105**: 225-238
- Carden MJ, Trojanowski JQ, Schlaepfer WW, & Lee VM (1987) Two-stage expression of neurofilament polypeptides during rat neurogenesis with early establishment of adult phosphorylation patterns. *The Journal of Neuroscience* **7**: 3489-3504
- Cassarino DS, Fall CP, Swerdlow RH, Smith TS, Halvorsen EM, Miller SW, Parks JP, Jr. P, & Jr. B (1997) Elevated reactive oxygen species and antioxidant enzyme activities in animal and cellular models of Parkinson's disease. *Biochimica et Biophysica Acta (BBA) - Molecular Basis of Disease* **1362**: 77-86
- Castellani R, Smith MA, Richey GL, & Perry G (1996) Glycooxidation and oxidative stress in Parkinson disease and diffuse Lewy body disease. *Brain Research* **737**: 195-200
- Castino R, Bellio N, Nicotra G, Follo C, Trincheri NF, & Isidoro C (2007) Cathepsin D-Bax death pathway in oxidative stressed neuroblastoma cells. *Free Radical Biology and Medicine* **42**: 1305-1316

- Caudle WM, Colebrooke RE, Emson PC, & Miller GW (2008) Altered vesicular dopamine storage in Parkinson's disease: a premature demise. *Trends in Neurosciences* **31**: 303-308
- Chan WK-, Yabe JT, Pimenta AF, Ortiz D, & Shea TB (2003) Growth cones contain a dynamic population of neurofilament subunits. *Cell Motility and The Cytoskeleton* **54**: 195-207
- Chen J, Nakata T, Zhang Z, & Hirokawa N (2000) The C-terminal tail domain of neurofilament protein-H (NF-H) forms the crossbridges and regulates neurofilament bundle formation. *Journal of Cell Science* **113**: 3861-3869
- Chen L & Feany MB (2005) [alpha]-Synuclein phosphorylation controls neurotoxicity and inclusion formation in a Drosophila model of Parkinson disease. *Nature Neuroscience* **8**: 657-663
- Chen MJ, Yap YW, Choy MS, Koh CHV, Seet SJ, Duan W, Whiteman M, & Cheung NS (2006) Early induction of calpains in rotenone-mediated neuronal apoptosis. *Neuroscience Letters* **397**: 69-73
- Chera B, Schaecher KE, Rocchini A, Imam SZ, Sribnick EA, Ray SK, Ali SF, & Banik NL (2004) Immunofluorescent labeling of increased calpain expression and neuronal death in the spinal cord of 1-methyl-4-phenyl-1,2,3,6-tetrahydropyridine-treated mice. *Brain Research* **1006**: 150-156
- Cherra SJ, Kulich SM, Uechi G, Balasubramani M, Mountzouris J, Day BW, & Chu CT (2010) Regulation of the autophagy protein LC3 by phosphorylation. *The Journal of Cell Biology* **190**: 533-539
- Cheung Y, Lau WK, Yu M, Lai CS, Yeung S, So K, & Chang RC (2009) Effects of all-trans-retinoic acid on human SH-SY5Y neuroblastoma as in vitro model in neurotoxicity research. *NeuroToxicology* **30**: 127-135
- Chou Y & Goldman RD (2000) Intermediate Filaments on the Move. *The Journal of Cell Biology* **150**: 101F-106
- Chu Y, Dodiya H, Aebischer P, Olanow CW, & Kordower JH (2009) Alterations in lysosomal and proteasomal markers in Parkinson's disease: Relationship to alpha-synuclein inclusions. *Neurobiology of Disease* **35**: 385-398
- Chung CY, Koprach JB, Siddiqi H, & Isacson O (2009) Dynamic Changes in Presynaptic and Axonal Transport Proteins Combined with Striatal Neuroinflammation Precede Dopaminergic Neuronal Loss in a Rat Model of AAV alpha-synucleinopathy. *The Journal of Neuroscience* **29**: 3365-3373
- Cochard P & Paulin D (1984) Initial expression of neurofilaments and vimentin in the central and peripheral nervous system of the mouse embryo in vivo. *Journal of Neuroscience* **4**: 2080-2094
- Colella R, Lu G, Glazewski L, Korant B, Matlapudi A, England MR, Craft C, Frantz CN, & Mason RW (2010) Induction of cell death in neuroblastoma by inhibition of cathepsins B and L. *Cancer Letters* **294**: 195-203
- Coleman TR & Lazarides E (1992) Continuous growth of vimentin filaments in mouse fibroblasts. *Journal of Cell Science* **103**: 689-698
- Coux O, Tanaka K, & Goldberg AL (1996) Structure and Functions of the 20S and 26S Proteasomes. *Annual Review of Biochemistry* **65**: 801-847
- Crocker SJ, Smith PD, Jackson-Lewis V, Lamba WR, Hayley SP, Grimm E, Callaghan SM, Slack RS, Melloni E, Przedborski S, Robertson GS, Anisman H, Merali Z, & Park DS (2003) Inhibition of Calpains Prevents Neuronal and Behavioral Deficits in an MPTP Mouse Model of Parkinson's Disease. *Journal of Neuroscience* **23**: 4081-4091
- Cuervo AM & Dice JF (2000) Age-related Decline in Chaperone-mediated Autophagy. *Journal of Biological Chemistry* **275**: 31505-31513
- Cuervo AM, Stefanis L, Fredenburg R, Lansbury PT, & Sulzer D (2004) Impaired Degradation of Mutant {alpha}-Synuclein by Chaperone-Mediated Autophagy. *Science* **305**: 1292-1295

- Dabbeni-Sala F, Di Santo S, Franceschini D, Skaper SD, & Giusti P (2001) Melatonin protects against 6-OHDA-induced neurotoxicity in rats: a role for mitochondrial complex I activity. *FASEB Journal* **15**: 164-170
- Dalfó E & Ferrer I (2008) Early α -synuclein lipoxidation in neocortex in Lewy body diseases. *Neurobiology of Aging* **29**: 408-417
- DeFuria J & Shea TB (2007) Arsenic inhibits neurofilament transport and induces perikaryal accumulation of phosphorylated neurofilaments: Roles of JNK and GSK-3 β . *Brain Research* **1181**: 74-82
- De Girolamo LA & Billett EE (2005) The role of c-Jun NH2-terminal kinase in aberrant neurofilament phosphorylation. *Febs Journal* **272**: 32-32
- De Girolamo LA & Billett EE (2006) Role of extracellular-regulated kinase and c-Jun NH2-terminal kinase in 1-methyl-4-phenyl-1,2,3,6-tetrahydropyridine-induced neurofilament phosphorylation. *Journal of Neuroscience Research* **83**: 680-693
- De Iuliis A, Grigoletto J, Recchia A, Giusti P, & Arslan P (2005) A proteomic approach in the study of an animal model of Parkinson's disease. *Clinica Chimica Acta* **357**: 202-209
- DeFuria J & Shea TB (2007) Arsenic inhibits neurofilament transport and induces perikaryal accumulation of phosphorylated neurofilaments: Roles of JNK and GSK-3 β . *Brain Research* **1181**: 74-82
- Demuth H, Schierhorn A, Bryan P, Höfke R, Kirschke H, & Brömme D (1996) N-peptidyl, O-acyl hydroxamates: comparison of the selective inhibition of serine and cysteine proteinases. *Biochimica et Biophysica Acta (BBA) - Protein Structure and Molecular Enzymology* **1295**: 179-186
- Denton T & Howard BD (1987) A Dopaminergic Cell Line Variant Resistant to the Neurotoxin 1-Methyl-4-Phenyl-1,2,3,6-Tetrahydropyridine. *Journal of Neurochemistry* **49**: 622-630
- De Vos KJ, Grierson AJ, Ackerley S, & Miller CCJ (2008) Role of Axonal Transport in Neurodegenerative Diseases. *Annual Reviews of Neuroscience* **31**: 151-173
- Di Monte DA (2001) The role of environmental agents in Parkinson's disease. *Clinical Neuroscience Research* **1**: 419-426
- Dowjat WK, Wisniewski H, & Wisniewski T (2001) Alzheimer's disease presenilin-1 expression modulates the assembly of neurofilaments. *Neuroscience* **103**: 1-8
- Droga-Mazovec G, Bojič L, Petelin A, Ivanova S, Romih R, Repnik U, Salvesen GS, Stoka V, Turk V, & Turk B (2008) Cysteine Cathepsins Trigger Caspase-dependent Cell Death through Cleavage of Bid and Antiapoptotic Bcl-2 Homologues. *Journal of Biological Chemistry* **283**: 19140-19150
- Dutta S, Chiu YC, Probert AW, & Wang KKW (2002) Selective Release of Calpain Produced α II-Spectrin (α -Fodrin) Breakdown Products by Acute Neuronal Cell Death. *Biological Chemistry* **383**: 785-791
- Ebbing B, Mann K, Starosta A, Jaud J, Schols L, Schule R, & Woehlke G (2008) Effect of spastic paraplegia mutations in KIF5A kinesin on transport activity. *Human Molecular Genetics* **17**: 1245-1252
- Encinas M, Iglesias M, Llecha N, & Comella JX (1999) Extracellular-Regulated Kinases and Phosphatidylinositol 3-Kinase Are Involved in Brain-Derived Neurotrophic Factor-Mediated Survival and neurogenesis of the Neuroblastoma Cell Line SH-SY5Y. *Journal of Neurochemistry* **73**: 1409-1421
- Encinas M, Iglesias M, Liu Y, Wang H, Muhaisen A, Cena V, Gallego C, & Comella JX (2000) Sequential Treatment of SH-SY5Y Cells with Retinoic Acid and Brain-Derived Neurotrophic Factor Gives Rise to Fully Differentiated, Neurotrophic Factor-Dependent, Human Neuron-Like Cells. *Journal of Neurochemistry* **75**: 991-1003

- Fabunmi RP, Wigley WC, Thomas PJ, & DeMartino GN (2000) Activity and Regulation of the Centrosome-associated Proteasome. *Journal of Biological Chemistry* **275**: 409-413
- Fallon J, Matthews RT, Hyman BT, & Beal MF (1997) MPP⁺ Produces Progressive Neuronal Degeneration Which Is Mediated by Oxidative Stress. *Experimental Neurology* **144**: 193-198
- Fasani F, Bocquet A, Robert P, Peterson A, & Eyer J (2004) The amount of neurofilaments aggregated in the cell body is controlled by their increased sensitivity to trypsin-like proteases. *Journal of Cell Science* **117**: 861-869
- Feng Z & Porter AG (1999) NF- κ B/Rel Proteins Are Required for Neuronal Differentiation of SH-SY5Y Neuroblastoma Cells. *Journal of Biological Chemistry* **274**: 30341-30344
- Fernandes ND, Sun Y, & Price BD (2007) Activation of the Kinase Activity of ATM by Retinoic Acid Is Required for CREB-dependent Differentiation of Neuroblastoma Cells. *Journal of Biological Chemistry* **282**: 16577-16584
- Fitzgerald JC, Ufer C, De Girolamo LA, Kuhn H, & Billett EE (2007) Monoamine oxidase-A modulates apoptotic cell death induced by staurosporine in human neuroblastoma cells. *Journal of Neurochemistry* **103**: 2189-2199
- Flitney EW & Goldman RD Fluorescence-based methods for studying IFs. *Methods in Cell Biology* **78**: 297-319
- Fonck C & Baudry M (2001) Toxic effects of MPP⁺ and MPTP in PC12 cells independent of reactive oxygen species formation. *Brain Research* **905**: 199-206
- Fornai F, Lenzi P, Gesi M, Ferrucci M, Lazzeri G, Busceti CL, Ruffoli R, Soldani P, Ruggieri S, Alessandri MG, & Paparelli A (2003) Fine Structure and Biochemical Mechanisms Underlying Nigrostriatal Inclusions and Cell Death after Proteasome Inhibition. *Journal of Neuroscience* **23**: 8955-8966
- Fornai F, Schluter OM, Lenzi P, Gesi M, Ruffoli R, Ferrucci M, Lazzeri G, Busceti CL, Pontarelli F, Battaglia G, Pellegrini A, Nicoletti F, Ruggieri S, Paparelli A, & Sudhof TC (2005) Parkinson-like syndrome induced by continuous MPTP infusion: Convergent roles of the ubiquitin-proteasome system and α -synuclein. *Proceedings of the National Academy of Sciences* **102**: 3413-3418
- Forno LS, Sternberger LA, Sternberger NH, Strefling AM, Swanson K, & Eng LF (1986) Reaction of Lewy Bodies with antibodies to phosphorylated and non-phosphorylated neurofilaments. *Neuroscience Letters* **64**: 253-258; 253
- Fowler JS, Volkow ND, Wang G-, Pappas N, Logan J, MacGregor R, Alexoff D, Shea C, Schlyer D, Wolf AP, Warner D, Zezulkova I, & Cilento R (1996) Inhibition of monoamineoxidase B in the brains of smokers. *Nature* **379**: 733-736
- Fu L, Gao Ys, Tousson A, Shah A, Chen TL, Vertel BM, & Sztul E (2005) Nuclear Aggresomes Form by Fusion of PML-associated Aggregates. *Molecular Biology of the Cell* **16**: 4905-4917
- Gal J, Ström A, Kilty R, Zhang F, & Zhu H (2007) p62 Accumulates and Enhances Aggregate Formation in Model Systems of Familial Amyotrophic Lateral Sclerosis. *Journal of Biological Chemistry* **282**: 11068-11077
- Galloway PG, Grundke I, Iqbal K, & Perry G (1988) Lewy Bodies Contain Epitopes Both Shared and Distinct from Alzheimer Neurofibrillary Tangles. *Journal of Neuropathology and Experimental Neurology* **47**: 654-663
- Galloway PG, Mulvihill P, & Perry G (1992) Filaments of Lewy bodies contain insoluble cytoskeletal elements. *American Journal of Pathology* **140**: 809-822
- Geetha T & Wooten MW (2002) Structure and functional properties of the ubiquitin binding protein p62. *FEBS Letters* **512**: 19-24

- Geisler S, Holmstrom KM, Skujat D, Fiesel FC, Rothfuss OC, Kahle PJ, & Springer W (2010a) PINK1/Parkin-mediated mitophagy is dependent on VDAC1 and p62/SQSTM1. *Nature Cell Biology* **12**: 119-131
- Geisler S, Holmstrom KM, Treis A, Skujat D, Weber SS, Fiesel FC, Kahle PJ, & Springer W (2010b) The PINK1/Parkin-mediated mitophagy is compromised by PD-associated mutations. *Autophagy* **6**: 1-8
- Gessner W, Brossi A, Shen RS, & Abell CW (1985) Further Insight Into the Mode of Action of the Neurotoxin 1-Methyl-4-Phenyl-1,2,3,6-Tetrahydropyridine (MPTP). *Febs Letters* **183**: 345-348
- Glickman MH & Ciechanover A (2002) The Ubiquitin-Proteasome Proteolytic Pathway: Destruction for the Sake of Construction. *Physiological Reviews* **82**: 373-428
- Glinka Y, Tipton KF, & Youdim MBH (1996) Nature of Inhibition of Mitochondrial Respiratory Complex I by 6-Hydroxydopamine. *Journal of Neurochemistry* **66**: 2004-2010
- Gloster A, Wu W, Speelman A, Weiss S, Causing C, Pozniak C, Reynolds B, Chang E, Toma JG, & Miller FD (1994) The T α 1 α -tubulin promoter specifies gene expression as a function of neuronal growth and regeneration in transgenic mice. *Journal of Neuroscience* **14**: 7319-7330
- Glover V, Gibb C, & Sandler M (1986) Monoamine oxidase B (MAO-B) is the major catalyst for 1-methyl-4-phenyl-1,2,3,6-tetrahydropyridine (MPTP) oxidation in human brain and other tissues. *Neuroscience Letters* **64**: 216-220
- Gocheva V, Zeng W, Ke D, Klimstra D, Reinheckel T, Peters C, Hanahan D, & Joyce JA (2006) Distinct roles for cysteine cathepsin genes in multistage tumorigenesis. *Genes and Development* **20**: 543-556
- Goldberg AL (2003) Protein degradation and protection against misfolded or damaged proteins. *Nature* **426**: 895-899
- Goll DE, Thompson VF, Li HQ, Wei W, & Cong JY (2003) The calpain system. *Physiological Reviews* **83**: 731-801
- Gou JP, Eyer J, & Leterrier JF (1995) Progressive Hyperphosphorylation of Neurofilament Heavy Subunits with Aging: Possible Involvement in the Mechanism of Neurofilament Accumulation. *Biochemical and Biophysical Research Communications* **215**: 368-376
- Gour-Salin BJ, Lachance P, Magny MC, Plouffe C, Menard R, & Storer AC (1994) E64 [trans-epoxysuccinyl-L-leucylamido-(4-guanido)butane] analogues as inhibitors of cystine proteinases: investigation of S2 subsite interactions. *Biochemical Journal* **299**: 389-392
- Grant P & Pant HC (2000) Neurofilament protein synthesis and phosphorylation. *Journal of Neurocytology* **29**: 843-872
- Greenwood JA, Troncoso JC, Costello AC, & Johnson GVW (1993) Phosphorylation Modulates Calpain-Mediated Proteolysis and Calmodulin Binding of the 200-kDa and 160-kDa Neurofilament Proteins. *Journal of Neurochemistry* **61**: 191-199
- Groll M, Bajorek M, Kohler A, Moroder L, Rubin DM, Huber R, Glickman MH, & Finley D (2000) A gated channel into the proteasome core particle. *Nature Structural Biology* **7**: 1062-1067
- Groll M, Ditzel L, Lowe J, Stock D, Bochtler M, Bartunik HD, & Huber R (1997) Structure of 20S proteasome from yeast at 2.4 Å resolution. *Nature* **386**: 463-471
- Groll M & Huber R (2004) Inhibitors of the eukaryotic 20S proteasome core particle: a structural approach. *Biochimica et Biophysica Acta (BBA) - Molecular Cell Research* **1695**: 33-44
- Groll M, Kim KB, Kairies N, Huber R, & Crews CM (2000) Crystal Structure of Epoxomicin:20S Proteasome Reveals a Molecular Basis for Selectivity of α' , β' -Epoxyketone Proteasome Inhibitors. *Journal of the American Chemical Society* **122**: 1237-1238

- Gupta M, Gupta BK, Thomas R, Bruemmer V, Sladek Jr. JR, & Felten DL (1986) Aged mice are more sensitive to 1-methyl-4-phenyl-1,2,3,6-tetrahydropyridine treatment than young adults. *Neuroscience Letters* **70**: 326-331
- Gupta RP, Abdel-Rahman A, Jensen KF, & Abou-Donia MB (2000) Altered expression of neurofilament subunits in diisopropyl phosphorofluoridate-treated hen spinal cord and their presence in axonal aggregations. *Brain Research* **878**: 32-47
- Hall JL & Cowan NJ (1985) Structural features and restricted expression of a human {alpha}-tubulin gene. *Nucleic Acids Research* **13**: 207-223
- Hamano T, Gendron TF, Ko L, & Yen S (2009) Concentration-dependent Effects of Proteasomal Inhibition on tau Processing in a Cellular Model of Tauopathy. *International Journal of Clinical Experimental Pathology* **2**: 561-573
- Hamazaki H (1996) Cathepsin D is involved in the clearance of Alzheimer's β -amyloid protein. *FEBS Letters* **396**: 139-142
- Hamer I, Delaive E, Dieu M, Abdel-Sater F, Mercy L, Jadot M, & Arnould T (2009) Up-regulation of cathepsin B expression and enhanced secretion in mitochondrial DNA-depleted osteosarcoma cells. *Biology of the Cell* **101**: 31-41
- Hanada M, Krajewski S, Tanaka S, Cazals-Hatem D, Spengler BA, Ross RA, Biedler JL, & Reed JC (1993) Regulation of Bcl-2 Oncoprotein Levels with Differentiation of Human Neuroblastoma Cells. *Cancer Research* **53**: 4978-4986
- Hara T, Nakamura K, Matsui M, Yamamoto A, Nakahara Y, Suzuki-Migishima R, Yokoyama M, Mishima K, Saito I, & Okano H (2006) Suppression of basal autophagy in neural cells causes neurodegenerative disease in mice. *Nature* **441**: 885-889
- Harris J, Ayyub C, Shaw G (1991) A molecular dissection of the carboxyterminal tails of the major neurofilament subunits NF-M and NF-H. *Journal of Neuroscience Research* **30**: 47-62
- Hartley CL, Anderson VER, Anderson BH, & Robertson J (1997) Acrylamide and 2,5-hexanedione induce collapse of neurofilaments in SH-SY5Y human neuroblastoma cells to form perikaryal inclusion bodies. *Neuropathology and Applied Neurobiology* **23**: 364-372
- Hasegawa M, Fujiwara H, Nonaka T, Wakabayashi K, Takahashi H, Lee VM, Trojanowski JQ, Mann D, & Iwatsubo T (2002) Phosphorylated alpha-synuclein is ubiquitinated in alpha-synucleinopathy lesions. *Journal of Biological Chemistry* **277**: 49071-49076
- Hasegawa T, Matsuzaki M, Takeda A, Kikuchi A, Akita H, Perry G, Smith MA, & Itoyama Y (2004) Accelerated [alpha]-synuclein aggregation after differentiation of SH-SY5Y neuroblastoma cells. *Brain Research* **1013**: 51-59
- Hattori T, Kitagawa K, Uchida C, Oda T, & Kitagawa M (2003) Cks1 is degraded via the ubiquitin-proteasome pathway in a cell cycle-dependent manner. *Genes to Cells* **8**: 889-896
- He Y, Francis F, Myers KA, Yu W, Black MM, & Baas PW (2005) Role of cytoplasmic dynein in the axonal transport of microtubules and neurofilaments. *Journal of Cell Biology* **168**: 697-703
- Heijink E, Scholten SW, Bolhuis PA, & de Wolff FA (2000) Effects of 2,5-hexanedione on calpain-mediated degradation of human neurofilaments in vitro. *Chemico-Biological Interactions* **129**: 231-247
- Heim R, Prasher DC, & Tsien RY (1994) Wavelength mutations and posttranslational autoxidation of green fluorescent protein. *Proceedings of the National Academy of Sciences* **91**: 12501-12504
- Heinemeyer W, Fischer M, Krimmer T, Stachon U, & Wolf DH (1997) The Active Sites of the Eukaryotic 20 S Proteasome and Their Involvement in Subunit Precursor Processing. *Journal of Biological Chemistry* **272**: 25200-25209
- Hernandez D, Paisan Ruiz C, Crawley A, Malkani R, Werner J, Gwinn-Hardy K, Dickson D, Wavrant DeVrieze F, Hardy J, & Singleton A (2005) The dardarin G2019S mutation is a common

- cause of Parkinson's disease but not other neurodegenerative diseases. *Neuroscience Letters* **389**: 137-139
- Hill WD, Lee VM-, Hurtig HI, Murray JM, & Trojanowski JQ (1991) Epitopes Located in Spatially Separate Domains of Each Neurofilament Subunit Are Present in Parkinson's Disease Lewy Bodies. *The Journal of Comparative Neurology* **309**: 150-160
- Hirokawa N, Noda Y, & Okada Y (1998) Kinesin and dynein superfamily proteins in organelle transport and cell division. *Current Opinion in Cell Biology* **10**: 60-73
- Hirokawa N (1982) Cross-linker system between neurofilaments, microtubules and membranous organelles in frog axons revealed by the quick-freeze, deep-etching method. *The Journal of Cell Biology* **94**: 129-142
- Hirrlinger J, Schulz JB, & Dringen R (2002) Effects of dopamine on the glutathione metabolism of cultured astroglial cells: implications for Parkinson's disease. *Journal of Neurochemistry* **82**: 458-467
- Hirsch E, Graybiel AM, & Agid YA (1988) Melanized dopaminergic neurons are differentially susceptible to degeneration in Parkinson's disease. *Nature* **334**: 345-348
- Hoffman PN, Cleveland DW, Griffin JW, Landes PW, Cowan NJ, & Price DL (1987) Neurofilament gene expression: a major determinant of axonal caliber. *Proceedings of the National Academy of Sciences* **84**: 3472-3476
- Hom DG, Jiang D, Hong EJ, Mo JQ, & Andersen JK (1997) Elevated expression of glutathione peroxidase in PC12 cells results in protection against methamphetamine but not MPTP toxicity. *Molecular Brain Research* **46**: 154-160
- Hu Y & Russek SJ (2008) BDNF and the diseased nervous system: a delicate balance between adaptive and pathological processes of gene regulation. *Journal of Neurochemistry* **105**: 1-17
- Hui K (1988) A Novel Dipeptidyl Aminopeptidase in Rat Brain Membranes, Its Isolation, Purification, and Characterization. *The Journal of Biological Chemistry* **263**: 6613-6618
- Ichimura Y, Kominami E, Tanaka K, & Komatsu M (2008) Selective turnover of p62/A170/SQSTM1 by autophagy. *Autophagy* **4**: 1063-1066
- Itakura E, Kishi C, Inoue K, & Mizushima N (2008) Beclin 1 Forms Two Distinct Phosphatidylinositol 3-Kinase Complexes with Mammalian Atg14 and UVRAG. *Molecular Biology of the Cell* **19**: 5360-5372
- Itano Y, Ito A, Uehara T, & Nomura Y (1996) Regulation of Bcl-2 protein expression in human neuroblastoma SH-SY5Y cell: positive and negative effects of protein kinases C and A, respectively. *Journal of Neurochemistry* **67**: 131-137
- Ito H, Kamei K, Iwamoto I, Inaguma Y, Garcia-Mata R, Sztul E, & Kato K (2002) Inhibition of Proteasomes Induces Accumulation, Phosphorylation, and Recruitment of HSP27 and $\alpha\beta$ -Crystallin to Aggresomes. *Journal of Biochemistry* **131**: 593-603
- Ittner LM, Fath T, Ke YD, Bi M, van Eersel J, Li KM, & Gunning P (2008) Parkinsonism and impaired axonal transport in a mouse model of frontotemporal dementia. *Proceedings of the National Academy of Sciences* **105**: 15997-16002
- Iwasaki Y, Yamamoto H, Iizuka H, Yamamoto T, & Konno H (1987) Suppression of neurofilament degradation by protease inhibitors in experimental spinal cord injury. *Brain Research* **406**: 99-104
- Iwatsubo T, Yamaguchi H, Fujimuro M, Yokosawa H, Ihara Y, Trojanowski JQ, & Lee VM- (1996) Lewy Bodies: Purification from Diffuse Lewy Body Disease Brains. *Annals New York Academy of Sciences* **786**: 195-205

- Jäger S, Groll M, Huber R, Wolf DH, & Heinemeyer W (1999) Proteasome β -type subunits: unequal roles of propeptides in core particle maturation and a hierarchy of active site function. *Journal of Molecular Biology* **291**: 997-1013
- Jämsä A, Hasslund K, Cowburn RF, Bäckström A, & Vasänge M (2004) The retinoic acid and brain-derived neurotrophic factor differentiated SH-SY5Y cell line as a model for Alzheimer's disease-like tau phosphorylation. *Biochemical and Biophysical Research Communications* **319**: 993-1000
- Janmey PA, Leterrier J, & Herrmann H (2003) Assembly and structure of neurofilaments. *Current Opinion in Colloid & Interface Science* **8**: 40-47
- Javitch JA, D'Amato RJ, Strittmatter SM, & Snyder SH (1985) Parkinsonism-inducing neurotoxin, *N*-methyl-4-phenyl-1,2,3,6-tetrahydropyridine: Uptake of the metabolite *N*-methyl-4-phenylpyridine by dopamine neurons explains selective toxicity. *Proceedings of the National Academy of Sciences* **82**: 2173-2177
- Jenner P (2001) Parkinson's disease, pesticides and mitochondrial dysfunction. *Trends in Neurosciences* **24**: 245-246
- Johnston JA, Ward CL, & Kopito RR (1998) Aggresomes: A Cellular Response to Misfolded Proteins. *The Journal of Cell Biology* **143**: 1883-1898
- Josephs KA, Holton JL, Rossor MN, Braendgaard H, Ozawa T, Fox NC, Petersen RC, Pearl GS, Ganguly M, Rosa P, Laursen H, Parisi JE, Waldemar G, Quinn NP, Dickson DW, & Revesz T (2003) Neurofilament inclusion body disease: a new proteinopathy? *Brain* **126**: 2291-2303
- Juhász G, Hill JH, Yan Y, Sass M, Baehrecke EH, Backer JM, & Neufeld TP (2008) The class III PI(3)K Vps34 promotes autophagy and endocytosis but not TOR signaling in *Drosophila*. *The Journal of Cell Biology* **181**: 655-666
- Julien JP & Mushynski WE (1982) Multiple phosphorylation sites in mammalian neurofilament polypeptides. *Journal of Biological Chemistry* **257**: 10467-10470
- Julien JP (1999) Neurofilament functions in health and disease. *Current Opinion in Neurobiology* **9**: 554-560
- Jung C, Chylinski TM, Pimenta A, Ortiz D, & Shea TB (2004) Neurofilament Transport Is Dependent on Actin and Myosin. *The Journal of Neuroscience* **24**: 9486-9496
- Jung C, Lee S, Ortiz D, Zhu Q, Julien J, & Shea TB (2005) The high and middle molecular weight neurofilament subunits regulate the association of neurofilaments with kinesin: Inhibition by phosphorylation of the high molecular weight subunit. *Molecular Brain Research* **141**: 151-155
- Junn E, Lee SS, Suhr UT, & Mouradian MM (2002) Parkin Accumulation in Aggresomes Due to Proteasome Impairment. *Journal of Biological Chemistry* **277**: 47870-47877
- Junn E, Ronchetti RD, Quezado MM, Kim SY, & Mouradian MM (2003) Tissue transglutaminase-induced aggregation of alpha -synuclein: Implications for Lewy body formation in Parkinson's disease and dementia with Lewy bodies. *Proceedings of the National Academy of Sciences* **100**: 2047-2052
- Kaplan DR, Matsumoto K, Lucarelli E, & Thielet CJ (1993) Induction of TrkB by retinoic acid mediates biologic responsiveness to BDNF and differentiation of human neuroblastoma cells. *Neuron* **11**: 321-331
- Kaplan DR & Miller FD (1997) Signal transduction by the neutrophin receptors. *Current Opinion in Cell Biology* **9**: 213-221
- Kappahn RJ, Bigelow EJ, & Ferrington DA (2007) Age-dependent inhibition of proteasome chymotrypsin-like activity in the retina. *Experimental Eye Research* **84**: 646-654

- Kamakura K, Ishiura S, Suzuki K, Sugita H, & Toyokura Y (1985) Calcium-Activated neutral protease in the peripheral nerve, which requires μM order Ca^{2+} , and its effect on the neurofilament triplet. *Journal of Neuroscience Research* **13**: 391-403
- Katsuse O, Iseki E, Marui W, & Kosaka K (2003) Developmental stages of cortical Lewy bodies and their relation to axonal transport blockage in brains of patients with dementia with Lewy bodies. *Journal of Neurological Sciences* **211**: 29-35
- Kawaguchi Y, Kovacs JJ, McLaurin A, Vance JM, Ito A, & Yao T (2003) The Deacetylase HDAC6 Regulates Aggresome Formation and Cell Viability in Response to Misfolded Protein Stress. *Cell* **115**: 727-738
- Keeney PM, Xie J, Capaldi RA, & Bennett JP (2006) Parkinson's disease brain mitochondrial complex I has oxidatively damaged subunits and is functionally impaired and misassembled. *Journal of Neuroscience* **26**: 5256-5264
- Keeney PM, Xie J, Capaldi RA, & Bennett Jr JP (2006) Parkinson's Disease Brain Mitochondrial Complex I has Oxidatively Damaged Subunits and Its Functionally Impaired and Misassembled. *Neurobiology of Disease* **26**: 5256-5264
- Keller JN, Huang FF, & Markesbery WR (2000) Decreased levels of proteasome activity and proteasome expression in aging spinal cord. *Neuroscience* **98**: 149-156
- Keller JN, Dimayuga E, Chen Q, Thorpe J, Gee J, & Ding Q (2004) Autophagy, proteasomes, lipofuscin, and oxidative stress in the aging brain. *The International Journal of Biochemistry & Cell Biology* **36**: 2376-2391
- Kiffin R, Kaushik S, Zeng M, Bandyopadhyay U, Zhang C, Massey AC, Martinez-Vicente M, & Cuervo AM (2007) Altered dynamics of the lysosomal receptor for chaperone-mediated autophagy with age. *Journal of Cell Science* **120**: 782-791
- Kim HJ, Lee D, Lee CH, Chung KC, Kim J, & Paik SR (2006) Calpain-resistant fragment(s) of α -synuclein regulates the synuclein-cleaving activity of 20S proteasome. *Archives of Biochemistry and Biophysics* **455**: 40-47
- Kim KB, Myung J, Sin N, & Crews CM (1999) Proteasome inhibition by the natural products epoxomicin and dihydroeponemycin: Insights into specificity and potency. *Bioorganic & Medicinal Chemistry Letters* **9**: 3335-3340
- Kim S, Cho S, Lee I, Lee YH, Kang JH, Choi JH, Suh P, & Chang J (2007) In vitro assay of neurofilament light chain self-assembly using truncated mutants. *Journal of Neuroscience Methods* **161**: 199-204
- Kim S & Coulombe PA (2007) Intermediate filament scaffolds fulfill mechanical, organizational, and signaling functions in the cytoplasm. *Genes & Development* **21**: 1581-1597
- Kim SJ, Sung JY, Um JW, Hattori N, Mizuno Y, Tanaka K, Paik SR, Kim J, & Chung KC (2003) Parkin Cleaves Intracellular α -Synuclein Inclusions via the Activation of Calpain. *Journal of Biological Chemistry* **278**: 41890-41899
- Kimura N, Kumamoto T, Ueyama H, Horinouchi H, & Ohama E (2007) Role of proteasomes in the formation of neurofilamentous inclusions in spinal motor neurons of aluminum-treated rabbits. *Neuropathology* **27**: 522-530
- Kisselev AF, Akopian TN, Woo KM, & Goldberg AL (1999) The Sizes of Peptides Generated from Protein by Mammalian 26 and 20 S Proteasomes. IMPLICATIONS FOR UNDERSTANDING THE DEGRADATIVE MECHANISM AND ANTIGEN PRESENTATION. *Journal of Biological Chemistry* **274**: 3363-3371
- Kisselev AF, Callard A, & Goldberg AL (2006) Importance of the Different Proteolytic Sites of the Proteasome and the Efficacy of Inhibitors Varies with the Protein Substrate. *Journal of Biological Chemistry* **281**: 8582-8590

- Kisselev AF, Songyang Z, & Goldberg AL (2000) Why Does Threonine, and Not Serine, Function as the Active Site Nucleophile in Proteasomes? *Journal of Biological Chemistry* **275**: 14831-14837
- Kitada T, Asakawa S, Hattori N, Matsumine H, Yamamura Y, Minoshima S, Ykochi M, Mizuno Y, & Shimizu N (1998) Mutations in the *parkin* gene cause autosomal recessive juvenile parkinsonism. *Nature* **392**: 605-608
- Klionsky DJ, Abeliovich H, Agostinis P, Agrawal DK, Aliev G, Askew DS, Baba M, Baehrecke EH, Bahr BA, Ballabio A, Bamber BA, Bassham DC, Bergamini E, Bi X, Biard-Piechaczyk M, Blum JS, Bredesen DE, Brodsky JL, Brumell JH, Brunk UT et al (2008) Guidelines for the use and interpretation of assays for monitoring autophagy in higher eukaryotes. *Autophagy* **4**: 151-175
- Kong J, Tung VW-, Aghajanian J, & Xu Z (1998) Antagonistic Roles of Neurofilament Subunits NF-H and NF-M Against NF-L in Shaping Dendritic Arborization in Spinal Motor Neurons. *The Journal of Cell Biology* **140**: 1167-1176
- Kopito RR (2000) Aggresomes, inclusion bodies and protein aggregation. *Trends in Cell Biology* **10**: 524-530
- Korolainen MA, Goldsteins G, Nyman TA, Alafuzoff I, Koistinaho J, & Pirttila T (2006) Oxidative modification of proteins in the frontal cortex of Alzheimer's disease brain. *Neurobiology of Aging* **27**: 42-53
- Korolchuk VI, Mansilla A, Menzies FM, & Rubinsztein DC (2009) Autophagy Inhibition Compromises Degradation of Ubiquitin-Proteasome Pathway Substrates. *Molecular Cell* **33**: 517-527
- Kruger R, Kuhn W, Muller T, Woitalla D, Graeber M, Kosel S, Przuntek H, Epplen JT, Schols L, & Riess O (1998) AlaSOPro mutation in the gene encoding α -synuclein in Parkinson's disease. *Nature Genetics* **18**: 106-108
- Kunz S, Niederberger E, Ehnert C, Coste O, Pfenninger A, Kruij J, Wendrich TM, Schmidtko A, Tegeder I, & Geisslinger G (2004) The calpain inhibitor MDL 28170 prevents inflammation-induced neurofilament light chain breakdown in the spinal cord and reduces thermal hyperalgesia. *Pain* **110**: 409-418
- Langston JW (1985) MPTP neurotoxicity: An overview and characterization of phases of toxicity. *Life Sciences* **36**: 201-206
- Langston JW, Langston EB, & Irwin I (1984) MPTP-induced parkinsonism in human and non-human primates - Clinical and experimental aspects. *Acta Neurologica Scandinavica* **70 (suppl 100)**: 49-54
- Lasek RJ, Paggi P, & Katz MJ (1993) The maximum rate of neurofilament transport in axons: a view of molecular transport mechanisms continuously engaged. *Brain Research* **616**: 58-64
- Lavedan C, Buchholtz S, Nussbaum RL, Albin RL, & Polymeropoulos MH (2002) A mutation in the human neurofilament M gene in Parkinson's disease that suggests a role for the cytoskeleton in neuronal degeneration. *Neuroscience Letters* **322**: 57-61
- Lee HJ, Shin SY, Choi C, Lee YH, & Lee SJ (2002) Formation and removal of α -synuclein aggregates in cells exposed to mitochondrial inhibitors. *Journal of Biological Chemistry* **277**: 5411-5417
- Lee H, Khoshaghideh F, Patel S, & Lee S (2004) Clearance of α -Synuclein Oligomeric Intermediates via the Lysosomal Degradation Pathway. *Journal of Neuroscience* **24**: 1888-1896
- Lee HS, Park CW, & Kim YS (2000) MPP+ Increases the Vulnerability to Oxidative Stress Rather Than Directly Mediating Oxidative Damage in Human Neuroblastoma Cells. *Experimental Neurology* **165**: 164-171
- Leroy E, Boyer R, Auburger G, Leube B, Ulm G, Mezey E, Harta G, Brownstein MJ, Jonnalagada S, Chernova T, Dehejia A, Lavedan C, Gasser T, Steinbach PJ, Wilkinson KD, & Polymeropoulos MH (1998) The ubiquitin pathway in Parkinson's disease. *Nature* **395**: 451-452

- Lev N, Melamed E, & Offen D (2006) Proteasomal inhibition hypersensitizes differentiated neuroblastoma cells to oxidative damage. *Neuroscience Letters* **399**: 27-32
- Levin EC, Acharya NK, Sedeyn JC, Venkataraman V, D'Andrea MR, Wang H, & Nagele RG (2009) Neuronal expression of vimentin in the Alzheimer's disease brain may be part of a generalized dendritic damage-response mechanism. *Brain Research* **1298**: 194-207
- Lewis SB, Velat GJ, Miralia L, Papa L, Aikman JM, Wolper RA, Firment CS, Liu MC, Pineda JA, Wang KKW, & Hayes RL (2007) Alpha-II spectrin breakdown products in aneurysmal subarachnoid hemorrhage: a novel biomarker of proteolytic injury. *Journal of Neurosurgery* **107**: 792-796
- Licker V, Kövari E, Hochstrasser DF, & Burkhard PR (2009) Proteomics in human Parkinson's disease research. *Journal of Proteomics* **73**: 10-29
- Lin H, Zhai J, Canete-Soler R, & Schlaepfer WW (2004) 3' Untranslated Region in a Light Neurofilament (NF-L) mRNA Triggers Aggregation of NF-L and Mutant Superoxide Dismutase 1 Proteins in Neuronal Cells. *Journal of Neuroscience* **24**: 2716-2726
- Lin H, Zhai J, & Schlaepfer WW (2005) RNA-binding protein is involved in aggregation of light neurofilament protein and is implicated in the pathogenesis of motor neuron degeneration. *Human Molecular Genetics* **14**: 3643-3659
- Lindenbaum MH, Carbonetto S, & Mushynski WE (1987) Nerve growth factor enhances the synthesis, phosphorylation, and metabolic stability of neurofilament proteins in PC12 cells. *Journal of Biological Chemistry* **262**: 605-610
- Liu Y, Fallon L, Lashuel HA, Liu Z, & Jr. L (2002) The UCH-L1 Gene Encodes Two Opposing Enzymatic Activities that Affect [alpha]-Synuclein Degradation and Parkinson's Disease Susceptibility. *Cell* **111**: 209-218
- López-Carballo G, Moreno L, Masiá S, Pérez P, & Baretino D (2002) Activation of the Phosphatidylinositol 3-Kinase/Akt Signaling Pathway by Retinoic Acid Is Required for Neural Differentiation of SH-SY5Y Human Neuroblastoma Cells. *Journal of Biological Chemistry* **277**: 25297-25304
- Lotharius J & O'Malley KL (2000) The Parkinsonism-inducing drug 1-methyl-4-phenylpyridinium triggers intracellular dopamine oxidation - A novel mechanism of toxicity. *Journal of Biological Chemistry* **275**: 38581-38588
- Luo Y, Umegaki H, Wang X, Abe R, & Roth GS (1998) Dopamine Induces Apoptosis through an Oxidation-involved SAPK/JNK Activation Pathway. *Journal of Biological Chemistry* **273**: 3756-3764
- Luzio JP, Pryor PR, & Bright NA (2007) Lysosomes: fusion and function. *Nature Reviews Molecular Cell Biology* **8**: 622-632
- Lyras L, Cairns NJ, Jenner A, Jenner P, & Halliwell B (1997) An assessment of oxidative damage to proteins, lipids, and DNA in brain from patients with Alzheimer's disease. *Journal of Neurochemistry* **68**: 2061-2069
- Lyras L, Perry RH, Perry EK, Ince PG, Jenner A, Jenner P, & Halliwell B (1998) Oxidative damage to proteins, lipids, and DNA in cortical brain regions from patients with dementia with Lewy bodies. *Journal of Neurochemistry* **71**: 302-312
- Machiels BM, Henfling MER, Gerards WLH, Broers JLV, Bloemendal H, Ramaekers FCS, & Schutte B (1997) Detailed analysis of cell cycle kinetics upon proteasome inhibition. *Cytometry* **28**: 243-252
- Malik MA, Blusztajn JK, & Greenwood CE (2000) Nutrients as trophic factors in neurons and the central nervous system: Role of retinoic acid. *Journal of Nutritional Biochemistry* **11**: 2-13

- Malkus K, Tsika E, & Ischiropoulos H (2009) Oxidative modifications, mitochondrial dysfunction, and impaired protein degradation in Parkinson's disease: how neurons are lost in the Bermuda triangle. *Molecular Neurodegeneration* **4**: 24
- Manser C, Stevenson A, Banner S, Davies J, Tudor EL, Ono Y, Nigel Leigh P, McLoughlin DM, Shaw CE, & Miller CCJ (2008) Deregulation of PKN1 activity disrupts neurofilament organisation and axonal transport. *FEBS Letters* **582**: 2303-2308
- Mantle D, Falkous G, Ishiura S, Perry RH, & Perry EK (1995) Comparison of cathepsin protease activities in brain tissue from normal cases and cases with Alzheimer's disease, Lewy body dementia, Parkinson's disease and Huntington's disease. *Journal of Neurological Science* **131**: 65-70
- Marciniszyn J, Hartsuck JA, & Tang J (1976) Mode of inhibition of acid proteases by pepstatin. *Journal of Biological Chemistry* **251**: 7088-7094
- Mari M, Griffith J, Rieter E, Krishnappa L, Klionsky DJ, & Reggiori F (2010) An Atg9-containing compartment that functions in the early steps of autophagosome biogenesis. *The Journal of Cell Biology* **190**: 1005-1022
- Martinez-Vicente M & Cuervo AM (2007) Autophagy and neurodegeneration: when the cleaning crew goes on strike. *Lancet Neurology* **6**: 352-361
- Masaki R, Saito T, Yamada K, & Ohtani-Kaneko R (2000) Accumulation of phosphorylated neurofilaments and increase in apoptosis-specific protein and phosphorylated c-Jun induced by proteasome inhibitors. *Journal of Neuroscience Research* **62**: 75-83
- Mata IF, Wedemeyer WJ, Farrer MJ, Taylor JP, & Gallo KA (2006) LRRK2 in Parkinson's disease: protein domains and functional insights. *Trends in Neurosciences* **29**: 286-293
- McNaught KS, Belizaire R, Jenner P, Olanow CW, & Isacson O (2002) Selective loss of 20S proteasome [alpha]-subunits in the substantia nigra pars compacta in Parkinson's disease. *Neuroscience Letters* **326**: 155-158
- McNaught KS & Jenner P (2001) Proteasomal function is impaired in substantia nigra in Parkinson's disease. *Neuroscience Letters* **297**: 191-194
- McNaught KS & Olanow CW (2006) Protein aggregation in the pathogenesis of familial and sporadic Parkinson's disease. *Neurobiology of Aging* **27**: 530-545
- McNaught KS, Shashidharan P, Perl DP, Jenner P, & Olanow CW (2002) Aggresome-related biogenesis of Lewy bodies. *European Journal of Neuroscience* **16**: 2136-2148
- McNaught P, Belizaire R, Isacson O, Jenner P, & Olanow CW (2003) Altered Proteasomal Function in Sporadic Parkinson's Disease. *Experimental Neurology* **179**: 38-46
- Mehdi S (1991) Cell-penetrating inhibitors of calpain. *Trends in Biochemical Sciences* **16**: 150-153
- Meredith GE, Totterdell S, Petroske E, Santa Cruz K, Jr. C, & Lau YS (2002) Lysosomal malfunction accompanies alpha-synuclein aggregation in a progressive mouse model of Parkinson's disease. *Brain Research* **956**: 156-165
- Millecamps S, Gowing G, Corti O, Mallet J, & Julien J (2007) Conditional NF-L Transgene Expression in Mice for In Vivo Analysis of Turnover and Transport Rate of Neurofilaments. *Journal of Neuroscience* **27**: 4947-4956
- Millecamps S, Robertson J, Lariviere R, Mallet J, & Julien JP (2006) Defective axonal transport of neurofilament proteins in neurons overexpressing peripherin. *Journal of Neurochemistry* **98**: 926-938
- Miller FD, Naus CC, Durand M, Bloom FE, & Milner RJ (1987) Isotypes of alpha-tubulin are differentially regulated during neuronal maturation. *The Journal of Cell Biology* **105**: 3065-3073

- Miwa H, Kubo T, Suzuki A, & Kondo T (2006) Intragastric proteasome inhibition induces alpha-synuclein-immunopositive aggregations in neurons in the dorsal motor nucleus of the vagus in rats. *Neuroscience Letters* **401**: 146-149
- Miyawaki A, Nagai T, & Mizuno H (2003) Mechanism of protein fluorophore formation and engineering. *Current Opinion in Chemical Biology* **7**: 557-562
- Mizushima N, Levine B, Cuervo AM, & Klionsky DJ (2008) Autophagy fights disease through cellular self-digestion. *Nature* **451**: 1069-1075
- Moldoveanu T, Hosfield CM, Lim D, Elce JS, Jia Z, & Davies PL (2002) A Ca²⁺ Switch Aligns the Active Site of Calpain. *Cell* **108**: 649-660
- Molina-Porcel L, Llado A, Rey MJ, Molinuevo JL, Martinez-Lage M, Esteve FX, Ferrer I, Tolosa E, & Blesa R (2008) Clinical and Pathological Heterogeneity of Neuronal Intermediate Filament Inclusion Disease. *Archives of Neurology* **65**: 272-275
- Moran CM, Donnelly M, Ortiz D, Pant HC, Mandelkow E, & Shea TB (2005) Cdk5 inhibits anterograde axonal transport of neurofilaments but not that of tau by inhibition of mitogen-activated protein kinase activity. *Molecular Brain Research* **134**: 338-344
- Morfini G, Pigino G, Opalach K, Serulle Y, Moreira JE, Sugimori M, Llinas RR, & Brady ST (2007) 1-Methyl-4-phenylpyridinium affects fast axonal transport by activation of caspase and protein kinase C. *Proceedings of the National Academy of Sciences* **104**: 2442-2447
- Morin JG & Hastings JW (1971) Energy transfer in a bioluminescent system. *Journal of cellular physiology* **77**: 313-318
- Moskowitz PF & Oblinger MM (1995) Transcriptional and post-transcriptional mechanisms regulating neurofilament and tubulin gene expression during normal development of the rat brain. *Molecular Brain Research* **30**: 211-222
- Motil J, Chan WK-, Dubey M, Chaudhury P, Pimenta A, Chylinski TM, Ortiz DT, & Shea TB (2006) Dynein mediates retrograde neurofilament transport within axons and anterograde delivery of NFs from perikarya into axons: Regulation by multiple phosphorylation events. *Cell Motility and The Cytoskeleton* **63**: 266-286
- Motil J, Dubey M, Chan WKH, & Shea TB (2007) Inhibition of dynein but not kinesin induces aberrant focal accumulation of neurofilaments within axonal neurites. *Brain Research* **1164**: 125-131
- Mouatt-Prigent A, Karlsson JO, Agid Y, & Hirsch EC (1996) Increased m-calpain expression in the mesencephalon of patients with parkinson's disease but not in other neurodegenerative disorders involving the mesencephalon: a role in nerve cell death? *Neuroscience* **73**: 979-987
- Mouradian MM (2002) Recent advances in the genetics and pathogenesis of Parkinson disease. *Neurology* **58**: 179-185
- Muqit MMK, bou-Sleiman PM, Saurin AT, Harvey K, Gandhi S, Deas E, Eaton S, Payne Smith MD, Venner K, Matilla A, Healy DG, Gilks WP, Lees AJ, Holton J, Revesz T, Parker PJ, Harvey RJ, Wood NW, & Latchman DS (2006) Altered cleavage and localization of PINK1 to aggresomes in the presence of proteasomal stress. *Journal of Neurochemistry* **98**: 156-169
- Nakagawa T, Chen J, Zhang Z, Kanai Y, & Hirokawa N (1995) Two distinct functions of the carboxyl-terminal tail domain of NF-M upon neurofilament assembly: cross-bridge formation and longitudinal elongation of filaments. *The Journal of Cell Biology* **129**: 411-429
- Nakamura S, Kawamoto Y, Nakano S, Nakano S, Akiguchi I, & Kimura J (1997) p35^{neck5a} and cyclin-dependent kinase 5 colocalize in Lewy bodies of brains with Parkinson's disease. *Acta Neuropathology* **94**: 153-157
- Nakamura M, Yamada M, Ohsawa T, Morisawa H, Nishine T, Nishimura O, & Toda T (2006) Phosphoproteomic profiling of human SH-SY5Y neuroblastoma cells during response to 6-

- hydroxydopamine-induced oxidative stress. *Biochimica et Biophysica Acta (BBA) - Molecular Cell Research* **1763**: 977-989
- Nakaso K, Ito S, & Nakashima K (2008) Caffeine activates the PI3K/Akt pathway and prevents apoptotic cell death in a Parkinson's disease model of SH-SY5Y cells. *Neuroscience Letters* **432**: 146-150
- Nakaso K, Yoshimoto Y, Nakano T, Takeshima T, Fukuhara Y, Yasui K, Araga S, Yanagawa T, Ishii T, & Nakashima K (2004) Transcriptional activation of p62/A170/ZIP during the formation of the aggregates: possible mechanisms and the role in Lewy body formation in Parkinson's disease. *Brain Research* **1012**: 42-51
- Nath R, Raser KJ, Stafford D, Hajimohammadreza I, Posner A, Allen H, Talanian RV, Yuen P, Gilbertsen RB, & Wang KK (1996) Non-erythroid alpha-spectrin breakdown by calpain and interleukin 1 beta-converting-enzyme-like protease(s) in apoptotic cells: contributory roles of both protease families in neuronal apoptosis. *Biochemical Journal* **319**: 683-690
- Navarro A, Lopez-Cepero JM, Bandez MJ, Sanchez-Pino M, Gomez C, Cadenas E, & Boveris A (2008) Hippocampal mitochondrial dysfunction in rat aging. *American Journal of Physiology. Regulatory, Integrative and Comparative Physiology* **294**: R501-509
- Nguyen MD, Lariviere RC, & Julien JP (2001) Dereglulation of Cdk5 in a Mouse Model of ALS: Toxicity Alleviated by Perikaryal Neurofilament Inclusions. *Neuron* **30**: 135-148
- Nikam S, Nikam P, Ahaley SK, & Sontakke AV (2009) Oxidative Stress in Parkinson's Disease. *Indian Journal of Clinical Biochemistry* **24**: 98-101
- Nixon RA & Lewis SE (1987) Phosphorylation and Dephosphorylation of Neurofilament Proteins in Retinal Ganglion Cell Neurons in vivo. *Advances in Experimental Medicine and Biology* **221**: 167-186
- Nixon RA & Lewis SE (1986) Differential turnover of phosphate groups on neurofilament subunits in mammalian neurons in vivo. *Journal of Biological Chemistry* **261**: 16298-16301
- Nixon R, Lewis S, & Marotta C (1987) Posttranslational modification of neurofilament proteins by phosphate during axoplasmic transport in retinal ganglion cell neurons. *Journal in Neuroscience* **7**: 1145-1158
- Nixon RA & Logvinenko KB (1986) Multiple fates of newly synthesized neurofilament proteins: evidence for a stationary neurofilament network distributed nonuniformly along axons of retinal ganglion cell neurons. *Journal of Cell Biology* **102**: 647-659
- Nixon RA & Marotta CA (1984) Degradation of Neurofilament Proteins by Purified Human Brain Cathepsin D. *Journal of Neurochemistry* **43**: 507-516
- Nixon RA (2006) Autophagy in neurodegenerative disease: friend, foe or turncoat? *Trends Neuroscience* **29**: 528-535
- Obata T (2002) Dopamine efflux by MPTP and hydroxyl radical generation. *Journal of Neural Transmission* **109**: 1159-1180
- Olanow CW, Watts RL, & Koller WC (2001) An algorithm (decision tree) for the management of Parkinson's disease (2001): Treatment guidelines. *Neurology* **56**: Suppl 5
- Olanow CW, Perl DP, DeMartino GN, & McNaught KS (2004) Lewy-body formation is an aggresome-related process: a hypothesis. *The Lancet Neurology* **3**: 496-503
- Pahlman S, Ruusala A, Abrahamsson L, Mattsson MEK, & Esscher T (1984) Retinoic acid-induced differentiation of cultured human neuroblastoma cells: a comparison with phorbol ester-induced differentiation. *Cell Differentiation* **14**: 134-144
- Pahlman S, Ruusala A, Abrahamsson L, Odelstad L, & Nilsson K (1983) Kinetics and concentration effects of TPA-induced differentiation of cultured human neuroblastoma cells. *Cell Differentiation* **12**: 165-170

- Pankiv S, Clausen TH, Lamark T, Brech A, Bruun J, Outzen H, Øvervatn A, Bjørkøy G, & Johansen T (2007) p62/SQSTM1 Binds Directly to Atg8/LC3 to Facilitate Degradation of Ubiquitinated Protein Aggregates by Autophagy. *Journal of Biological Chemistry* **282**: 24131-24145
- Panov A, Dikalov S, Shalbuyeva N, Taylor G, Sherer T, & Greenamyre JT (2005) Rotenone Model of Parkinson Disease: MULTIPLE BRAIN MITOCHONDRIA DYSFUNCTIONS AFTER SHORT TERM SYSTEMIC ROTENONE INTOXICATION. *Journal of Biological Chemistry* **280**: 42026-42035
- Pant AC, Veeranna, Pant HC, & Amin N (1997) Phosphorylation of human high molecular weight neurofilament protein (hNF-H) by neuronal cyclin-dependent kinase 5 (cdk5). *Brain Research* **765**: 259-266
- Parker WD, Boyson SJ, & Parks JK (1989) Abnormalities of the Electron-Transport Chain in Idiopathic Parkinsons-Disease. *Annals of Neurology* **26**: 719-723
- Paterno GD, Gillespie LL, Julien J, & Skup D (1997) Regulation of neurofilament L, M and H gene expression during retinoic acid-induced neural differentiation of P19 embryonal carcinoma cells. *Molecular Brain Research* **49**: 247-254
- Pérez-Ollé R, López-Toledano MA, Goryunov D, Cabrera-Poch N, Stefanis L, Brown K, & Liem RKH (2005) Mutations in the neurofilament light gene linked to Charcot-Marie-Tooth disease cause defects in transport. *Journal of Neurochemistry* **93**: 861-874
- Perrot R, Berges R, Bocquet A, & Eyer J (2008) Review of the Multiple Aspects of Neurofilament Functions, and their Possible Contribution to Neurodegeneration. *Molecular Neurobiology* **38**: 27-65
- Petzold A (2005) Neurofilament phosphoforms: Surrogate markers for axonal injury, degeneration and loss. *Journal of the Neurological Sciences* **233**: 183-198
- Pillay CS, Elliott E, & Dennison C (2002) Endolysosomal proteolysis and its regulation. *Biochemical Journal* **363**: 417-429
- Pollanen MS, Bergeron C, & Weyer L (1992) Detergent-Insoluble Cortical Lewy Body Fibrils Share Epitopes with Neurofilament and Tau. *Journal of Neurochemistry* **58**: 1953-1956
- Polymeropoulos MH, Lavedan C, Leroy E, Ide SE, Dehejia A, Dutra A, Pike B, Root H, Rubenstein J, Boyer R, Stenroos ES, Chandrasekharappa S, Athanassiadou A, Papapetropoulos T, Johnson WG, Lazzarini AM, Duvoisin RC, Di Iorio G, Golbe LI, & Nussbaum RL (1997) Mutation in the α -Synuclein Gene Identified in Families with Parkinson's Disease. *Science* **276**: 2045-2047
- Presgraves SP, Ahmed T, Borwege S, & Joyce JN (2004) Terminally Differentiated SH-SY5Y Cells Provide a Model System for Studying Neuroprotective Effects of Dopamine Agonists. *Neurotoxicity Research* **5**: 579-598; 579
- Qiao L, Hamamichi S, Caldwell K, Caldwell G, Yacoubian T, Wilson S, Xie Z, Speake L, Parks R, Crabtree D, Liang Q, Crimmins S, Schneider L, Uchiyama Y, Iwatsubo T, Zhou Y, Peng L, Lu Y, Standaert D, Walls K et al (2008) Lysosomal enzyme cathepsin D protects against alpha-synuclein aggregation and toxicity. *Molecular Brain* **1**: 17
- Rajan RS, Illing ME, Bence NF, & Kopito RR (2001) Specificity in intracellular protein aggregation and inclusion body formation. *Proceedings of the National Academy of Sciences* **98**: 13060-13065
- Ramirez A, Heimbach A, Grundemann J, Stiller B, Hampshire D, Cid LP, Goebel I, Mubaidin AF, Wriekat A, Roeper J, Al-Din A, Hillmer AM, Karsak M, Liss B, Woods CG, Behrens MI, & Kubisch C (2006) Hereditary parkinsonism with dementia is caused by mutations in ATP13A2, encoding a lysosomal type 5 P-type ATPase. *Nature Genetics* **38**: 1184-1191

- Ramsay RR, Salach JI, Dadgar J, & Singer TP (1986) Inhibition of mitochondrial NADH dehydrogenase by pyridine derivatives and its possible relation to experimental and idiopathic parkinsonism. *Biochemical and Biophysical Research Communications* **135**: 269-275
- Ransom BR, Kunis DM, Irwin I, & Langston JW (1987) Astrocytes convert the parkinsonism inducing neurotoxin, MPTP, to its active metabolite, MPP+. *Neuroscience Letters* **75**: 323-328
- Rao MV, Garcia ML, Miyazaki Y, Gotow T, Yuan A, Mattina S, Ward CM, Calcutt NA, Uchiyama Y, Nixon RA, & Cleveland DW (2002) Gene replacement in mice reveals that the heavily phosphorylated tail of neurofilament heavy subunit does not affect axonal caliber or the transit of cargoes in slow axonal transport. *The Journal of Cell Biology* **158**: 681-693
- Rao MV, Houseweart MK, Williamson TL, Crawford TO, Folmer J, & Cleveland DW (1998) Neurofilament-dependent Radial Growth of Motor Axons and Axonal Organization of Neurofilaments Does Not Require the Neurofilament Heavy Subunit (NF-H) or Its Phosphorylation. *The Journal of Cell Biology* **143**: 171-181
- Ravikumar B, Acevedo-Arozena A, Imarisio S, Berger Z, Vacher C, O'Kane CJ, Brown SDM, & Rubinsztein DC (2005) Dynein mutations impair autophagic clearance of aggregate-prone proteins. *Nature Genetics* **37**: 771-776
- Ren Y, Zhao J, & Feng J (2003) Parkin Binds to alpha /beta Tubulin and Increases their Ubiquitination and Degradation. *Journal of Neuroscience* **23**: 3316-3324
- Rideout HJ, Lang-Rollin ICJ, Savalle M, & Stefanis L (2005) Dopaminergic neurons in rat ventral midbrain cultures undergo selective apoptosis and form inclusions, but do not up-regulate iHSP70, following proteasomal inhibition. *Journal of Neurochemistry* **93**: 1304-1313
- Rideout HJ, Lang-Rollin I, & Stefanis L (2004) Involvement of macroautophagy in the dissolution of neuronal inclusions. *The International Journal of Biochemistry & Cell Biology* **36**: 2551-2562
- Rideout HJ, Larsen KE, Sulzer D, & Stefanis L (2001) Proteasomal inhibition leads to formation of ubiquitin/alpha-synuclein-immunoreactive inclusions in PC12 cells. *Journal of Neurochemistry* **78**: 899-908
- Rideout HJ, Lang-Rollin I, & Stefanis L (2004) Involvement of macroautophagy in the dissolution of neuronal inclusions. *The International Journal of Biochemistry & Cell Biology* **36**: 2551-2562
- Rideout HJ & Stefanis L (2002) Proteasomal Inhibition-Induced Inclusion Formation and Death in Cortical Neurons Require Transcription and Ubiquitination. *Molecular and Cellular Neuroscience* **21**: 223-238
- Riederer P, Sofic E, Rausch W-, Schmidt B, Reynolds GP, Jellinger K, & Youdim MBH (1989) Transition Metals, Ferritin, Glutathione, and Ascorbic Acid in Parkinsonian Brains. *Journal of Neurochemistry* **52**: 515-520
- Robinson PA (2008) Protein stability and aggregation in Parkinson's disease. *Biochemical Journal* **413**: 1-13
- Rosengren LE, Karlsson J, Karlsson J, Persson LI, & Wikkelso C (1996) Patients with Amyotrophic Lateral Sclerosis and Other Neurodegenerative Diseases Have Increased Levels of Neurofilament Protein in CSF. *Journal of Neurochemistry* **67**: 2013-2018
- Ross CA & Poirier MA (2004) Protein aggregation and neurodegenerative disease. *Nature Medicine* **10**: S10-S17
- Ross OA, Braithwaite AT, Skipper LM, Kachergus J, Hulihan MM, Middleton FA, Nishioka K, Fuchs J, Gasser T, Maraganore DM, Adler CH, Larvor L, Chartier-Harlin M-, Nilsson C, Langston JW, Gwinn K, Hattori N, & Farrer MJ (2008) Genomic investigation of alpha-synuclein multiplication and parkinsonism. *Annals of Neurology* **63**: 743-750
- Roy S, Coffee P, Smith G, Liem RKH, Brady ST, & Black MM (2000) Neurofilaments Are Transported Rapidly But Intermittently in Axons: Implications for Slow Axonal Transport. *The Journal of Neuroscience* **20**: 6849-6861

- Roy S, Zhang B, Lee VMY, & Trojanowski JQ (2005) Axonal transport defects: a common theme in neurodegenerative diseases. *Acta Neuropathologica* **109**: 5-13
- Rubinsztein DC (2006) The roles of intracellular protein-degradation pathways in neurodegeneration. *Nature* **443**: 780-786
- Rubinsztein DC, Cuervo AM, Ravikumar B, Sarkar S, Korolchuk V, Kaushik S, & Klionsky DJ (2009) In search of an "autophagometer". *Autophagy* **5**: 585-589
- Rubinsztein DC, Gestwicki JE, Murphy LO, & Klionsky DJ (2007) Potential therapeutic applications of autophagy. *Nature Reviews and Drug Discovery* **6**: 304-312
- Ruiz-León Y & Pascual A (2001) Brain-derived neurotrophic factor stimulates beta-amyloid gene promoter activity by a Ras-dependent/AP-1-independent mechanism in SH-SY5Y neuroblastoma cells. *Journal of Neurochemistry* **79**: 278-285
- Ruiz-León Y & Pascual A (2003) Induction of tyrosine kinase receptor b by retinoic acid allows brain-derived neurotrophic factor-induced amyloid precursor protein gene expression in human sh-sy5y neuroblastoma cells. *Neuroscience* **120**: 1019-1026
- Sadée W, Yu VC, Richards ML, Preis PN, Schwab MR, Brodsky FM, & Biedler JL (1987) Expression of Neurotransmitter Receptors and myc Protooncogenes in Subclones of a Human Neuroblastoma Cell Line. *Cancer Research* **47**: 5207-5212
- Safaei R & Fischer I (1990) Turnover of cytoskeletal proteins in vivo. *Brain Research* **533**: 83-90
- Saha AR, Hill J, Utton MA, Asuni AA, Ackerley S, Grierson AJ, Miller CC, Davies AM, Buchman VL, Anderton BH, & Hanger DP (2004) Parkinson's disease {alpha}-synuclein mutations exhibit defective axonal transport in cultured neurons. *Journal of Cell Science* **117**: 1017-1024
- Sanchez I, Hassinger L, Sihag RK, Cleveland DW, Mohan P, & Nixon RA (2000) Local control of neurofilament accumulation during radial growth of myelinating axons in vivo: Selective role of site-specific phosphorylation. *Journal of Cell Biology* **151**: 1013-1024
- Saudou F, Finkbeiner S, Devys D, & Greenberg ME (1998) Huntingtin Acts in the Nucleus to Induce Apoptosis but Death Does Not Correlate with the Formation of Intranuclear Inclusions. *Cell* **95**: 55-66
- Sawada H, Kohno R, Kihara T, Izumi Y, Sakka N, Ibi M, Nakanishi M, Nakamizo T, Yamakawa K, Shibasaki H, Yamamoto N, Akaike A, Inden M, Kitamura Y, Taniguchi T, & Shimohama S (2004) Proteasome Mediates Dopaminergic Neuronal Degeneration, and Its Inhibition Causes {alpha}-Synuclein Inclusions. *The Journal of Biological Chemistry* **279**: 10710-10719
- Schapira AHV (2009) Etiology and Pathogenesis of Parkinson Disease. *Neurologic Clinics* **27**: 583-603
- Schlaepfer WW, Lee C, Lee VM-, & Zimmerman UJP (1985) An immunoblot study of neurofilament degradation in situ and during calcium-activated proteolysis. *Journal of Neurochemistry* **44**: 502-509
- Schlossmacher MG, Frosch MP, Gai WP, Medina M, Sharma N, Forno L, Ochiishi T, Shimura H, Sharon R, Hattori N, Langston JW, Mizuno Y, Hyman BT, Selkoe DJ, & Kosik KS (2002) Parkin Localizes to the Lewy Bodies of Parkinson Disease and Dementia with Lewy Bodies. *American Journal of Pathology* **160**: 1655-1667
- Schmidt ML, Martin JA, Lee VM-, & Trojanowski JQ (1996) Convergence of Lewy bodies and neurofibrillary tangles in amygdala neurons of Alzheimer's disease and Lewy body disorders. *Acta Neuropathology* **91**: 475-481
- Schmidt ML, Murray J, Lee VM, Hill WD, Wertkin A, & Trojanowski JQ (1991) Epitope map of neurofilament protein domains in cortical and peripheral nervous system Lewy bodies. *American Journal of Pathology* **139**: 53-65

- Schneider L & Zhang J (2010) Lysosomal function in macromolecular homeostasis and bioenergetics in Parkinson's disease. *Molecular Neurodegeneration* **5**: 14
- Schneider-Poetsch T, Ju J, Eyler DE, Dang Y, Bhat S, Merrick WC, Green R, Shen B, & Liu JO (2010) Inhibition of eukaryotic translation elongation by cycloheximide and lactimidomycin. *Nature Chemical Biology* **6**: 209-217
- Seglen PO & Gordon PB (1982) 3-Methyladenine: Specific inhibitor of autophagic/lysosomal protein degradation in isolated rat hepatocytes. *Proceedings of the National Academy of Science* **79**: 1889-1892
- Sevenich L, Pennacchio LA, Peters C, & Reinheckel T (2006) Human cathepsin L rescues the neurodegeneration and lethality in cathepsin B/L double-deficient mice. *Biological Chemistry* **387**: 885-891
- Sin N, Kim KB, Elofsson M, Meng L, Auth H, Kwok BHB, & Crews CM (1999) Total synthesis of the potent proteasome inhibitor epoxomicin: a useful tool for understanding proteasome biology. *Bioorganic & Medicinal Chemistry Letters* **9**: 2283-2288
- Sharma A, Kaur P, Kumar B, Prabhakar S, & Gill KK (2008) Plasma lipid peroxidation and antioxidant status of Parkinson's disease patients in the Indian population. *Parkinsonism and Related Disorders* **14**: 52-57
- Shea TB, Dahl DC, Nixon RA, & Fisher I (1997) Triton-Soluble Phosphovariants of the Heavy Neurofilament Subunit in Developing and Mature Mouse Central Nervous System. *Journal of Neuroscience Research* **48**: 515-523
- Shea TB, Jung C, & Pant HC (2003) Does neurofilament phosphorylation regulate axonal transport? *Trends in Neurosciences* **26**: 397-400
- Shea TB, Wheeler E, & Jung C (1997) Aluminium Inhibits Neurofilament Assembly, Cytoskeletal Incorporation, and Axonal Transport. *Molecular and Chemical Neuropathology* **32**: 17-39
- Shea TB, Yabe JT, Ortiz D, Pimenta A, Loomis P, Goldman RD, Amin N, & Pant HC (2004) Cdk5 regulates axonal transport and phosphorylation of neurofilaments in cultured neurons. *Journal of Cell Science* **117**: 933-941
- Sherer TB, Betarbet R, Stout AK, Lund S, Baptista M, Panov AV, Cookson MR, & Greenamyre JT (2002) An in vitro model of Parkinson's disease: Linking mitochondrial impairment to altered alpha-synuclein metabolism and oxidative damage. *Journal of Neuroscience* **22**: 7006-7015
- Shields DC, Leblanc S, & Banik NL (1997) Calcium-mediated neurofilament protein degradation in rat optic nerve in vitro: Activity and autolysis of calpain proenzyme. *Experimental Eye Research* **65**: 15-21
- Shimoji M, Zhang L, Mandir AS, Dawson VL, & Dawson TM (2005) Absence of inclusion body formation in the MPTP mouse model of Parkinson's disease. *Molecular Brain Research* **134**: 103-108
- Shimomura O, Johnson FH, & Saiga Y (1962) Extraction, purification and properties of aequorin, a bioluminescent protein from the luminous hydromedusan Aequoria. *Journal of cellular and comparative physiology* **59**: 223-239
- Shringarpure R, Grune T, Mehlhase J, & Davies KJA (2003) Ubiquitin Conjugation Is Not Required for the Degradation of Oxidized Proteins by Proteasome. *Journal of Biological Chemistry* **278**: 311-318
- Shults CW (2006) Lewy bodies. *Proceedings of the National Academy of Sciences* **103**: 1661-1668
- Sihag RK & Nixon RA (1990) Phosphorylation of the amino-terminal head domain of the middle molecular mass 145-kDa subunit of neurofilaments. Evidence for regulation by second messenger-dependent protein kinases. *Journal of Biological Chemistry* **265**: 4166-4171

- Simonsen A & Tooze SA (2009) Coordination of membrane events during autophagy by multiple class III PI3-kinase complexes. *The Journal of Cell Biology* **186**: 773-782
- Singh US, Pan J, Kao Y, Joshi S, Young KL, & Baker KM (2003) Tissue Transglutaminase Mediates Activation of RhoA and MAP Kinase Pathways during Retinoic Acid-induced Neuronal Differentiation of SH-SY5Y Cells. *Journal of Biological Chemistry* **278**: 391-399
- Singleton AB, Farrer M, Johnson J, Singleton A, Hague S, Kachergus J, Hulihan M, Peuralinna T, Dutra A, Nussbaum R, Lincoln S, Crawley A, Hanson M, Maraganore D, Adler C, Cookson MR, Muenter M, Baptista M, Miller D, Blacato J et al (2003) Alpha-Synuclein Locus Triplication Causes Parkinson's Disease. *Science* **302**: 841
- Sitek B, Apostolov O, Stühler K, Pfeiffer K, Meyer HE, Eggert A, & Schramm A (2005) Identification of Dynamic Proteome Changes Upon Ligand Activation of Trk-Receptors Using Two-dimensional Fluorescence Difference Gel Electrophoresis and Mass Spectrometry. *Molecular & Cellular Proteomics* **4**: 291-299
- Sitte N, Huber M, Grune T, Ladhoff A, Doecke W, Von Zglinicki T, & Davies KJA (2000) Proteasome inhibition by lipofuscin/ceroid during postmitotic aging of fibroblasts. *The FASEB Journal* **14**: 1490-1498
- Smith MA, Sayre LM, Anderson VE, Harris PLR, Beal MF, Kowall N, & Perry G (1998) Cytochemical demonstration of oxidative damage in Alzheimer disease by immunochemical enhancement of the carbonyl reaction with 2,4-dinitrophenylhydrazine. *Journal of Histochemistry & Cytochemistry* **46**: 731-735
- Smith MP & Cass WA (2007) GDNF reduces oxidative stress in a 6-hydroxydopamine model of Parkinson's disease. *Neuroscience Letters* **412**: 259-263
- Snow BJ, Vingerhoets FJG, Langston JW, Tetud JW, Sossi V, & Calne DB (2000) Pattern of dopaminergic loss in the striatum of humans with MPTP induced parkinsonism. *Journal of Neurology, Neurosurgery and Psychiatry with Practical Neurology* **68**: 313-316
- Song X & Ehrich M (1997) MPTP Affects Cholinergic Parameters in SH-SY5Y Human Neuroblastoma Cells. *In vitro Toxicology* **10**: 437-453
- Soussan L, Barzilai A, & Michaelson DM (1994) Distinctly Phosphorylated Neurofilaments in Different Classes of Neurons. *Journal of Neurochemistry* **62**: 770-776
- Sriram SR, Li X, Ko HS, Chung KKK, Wong E, Lim KL, Dawson VL, & Dawson TM (2005) Familial-associated mutations differentially disrupt the solubility, localization, binding and ubiquitination properties of parkin. *Human Molecular Genetics* **14**: 2571-2586
- Stahl S, Reinders Y, Asan E, Mothes W, Conzelmann E, Sickmann A, & Felbor U (2007) Proteomic analysis of cathepsin B and L-deficient mouse brain lysosomes. *Biochimica et Biophysica Acta (BBA) - Proteins & Proteomics* **1774**: 1237-1246
- Stephans SE, Miller GW, Levey AI, & Greenamyre JT (2002) Acute Mitochondrial and Chronic Toxicological Effects of 1-Methyl-4-Phenylpyridinium in Human Neuroblastoma Cells. *NeuroToxicology* **23**: 569-580
- Sternberger NH, Sternberger LA, & Ulrich J (1985) Aberrant Neurofilament Phosphorylation in Alzheimer Disease. *Proceedings of the National Academy of Sciences* **82**: 4274-4276
- Stocklein W & Piepersberg W (1980) Binding of cycloheximide to ribosomes from wild-type and mutant strains of *Saccharomyces cerevisiae*. *Antimicrobial Agents and Chemotherapy* **18**: 863-867
- Stoka V, Turk B, Schendel SL, Kim T, Cirman T, Snipas SJ, Ellerby LM, Bredesen D, Freeze H, Abrahamson M, Brömme D, Krajewski S, Reed JC, Yin X, Turk V, & Salvesen GS (2001) Lysosomal Protease Pathways to Apoptosis. *Journal of Biological Chemistry* **276**: 3149-3157
- Stokes AH, Freeman WM, Mitchell SG, Burnette TA, Hellmann GM, & Vrana KE (2002) Induction of GADD45 and GADD153 in neuroblastoma cells by dopamine-induced toxicity. *Neurotoxicology* **23**: 675-684

- Stokes AH, Lewis DY, Lash LH, Jerome WG, Grant KW, Aschner M, & Vrana KE (2000) Dopamine toxicity in neuroblastoma cells: role of glutathione depletion by -BSO and apoptosis. *Brain Research* **858**: 1-8
- Straight AF (2007) Fluorescent Protein Applications in Microscopy. *Methods in Cell Biology* **81**: 93-113
- Stys PK & Jiang Q (2002) Calpain-dependent neurofilament breakdown in anoxic and ischemic rat central axons. *Neuroscience Letters* **328**: 150-154
- Su JH, Cummings BJ, & Cotman CW (1996) Plaque biogenesis in brain aging and Alzheimer's disease. I. Progressive changes in phosphorylation states of paired helical filaments and neurofilaments. *Brain Research* **739**: 79-87
- Sullivan PG, Dragicevic NB, Deng J, Bai Y, Dimayuga E, Ding Q, Chen Q, Bruce-Keller AJ, & Keller JN (2004) Proteasome Inhibition Alters Neural Mitochondrial Homeostasis and Mitochondria Turnover. *Journal of Biological Chemistry* **279**: 20699-20707
- Sulzer D (2007) Multiple hit hypothesis for dopamine neuron loss in Parkinson's disease. *Trends in Neurosciences* **30**: 244-250
- Sulzer D, Bogulavsky J, Larsen KE, Behr G, Karatekin E, Kleinman MH, Turro N, Krantz D, Edwards RH, Greene LA, & Zecca L (2000) Neuromelanin biosynthesis is driven by excess cytosolic catecholamines not accumulated by synaptic vesicles. *Proceedings of the National Academy of Sciences* **97**: 11869-11874
- Sun B, Zhou Y, Halabisky B, Lo I, Cho S, Mueller-Steiner S, Wang X, Grubb A, & Gan L (2008) Cystatin C-Cathepsin B Axis Regulates Amyloid Beta Levels and Associated Neuronal Deficits in an Animal Model of Alzheimer's Disease. *Neuron* **60**: 247-257
- Sun D, Leung CL, & Liem RKH (1996) Phosphorylation of the High Molecular Weight Neurofilament Protein (NF-H) by Cdk5 and p35. *Journal of Biological Chemistry* **271**: 14245-14251
- Suzuki H, Takeda M, Nakamura Y, Kato Y, Tada K, Hariguchi S, & Nishimura T (1988) Neurofilament degradation by bovine brain cathepsin D. *Neuroscience Letters* **89**: 240-245
- Takahashi M, Iseki E, & Kosaka K (2000) Cyclin-dependent kinase 5 (Cdk5) associated with Lewy bodies in diffuse Lewy body disease. *Brain Research* **862**: 253-256
- Tamada Y, Nakajima E, Nakajima T, Shearer TR, & Azuma M (2005) Proteolysis of neuronal cytoskeletal proteins by calpain contributes to rat retinal cell death induced by hypoxia. *Brain Research* **1050**: 148-155
- Tanaka M, Kim YM, Lee G, Junn E, Iwatsubo T, & Mouradian MM (2004) Aggregates Formed by {alpha}-Synuclein and Synphilin-1 Are Cytoprotective. *Journal of Biological Chemistry* **279**: 4625-4631
- Tetrud JW & Langston JW (1989) Mptp-Induced Parkinsonism As A Model for Parkinsons-Disease. *Acta Neurologica Scandinavica* **80**: 35-40
- Theiss C, Napirei M, & Meller K (2005) Impairment of anterograde and retrograde neurofilament transport after anti-kinesin and anti-dynein antibody microinjection in chicken dorsal root ganglia. *European Journal of Cell Biology* **84**: 29-43
- Tirmenstein MA, Hu CX, Scicchitano MS, Narayanan PK, McFarland DC, Thomas HC, & Schwartz LW (2005) Effects of 6-hydroxydopamine on mitochondrial function and glutathione status in SH-SY5Y human neuroblastoma cells. *Toxicology in Vitro* **19**: 471-479
- Toda T, Nakamura M, Morisawa H, Hirota M, Nishigaki R, & Yoshimi Y (2010) Proteomic approaches to oxidative protein modifications implicated in the mechanism of aging. *Geriatrics & Gerontology International* **10**: S25-S31

- Tofaris GK, Layfield R, & Spillantini MG (2001) [alpha]-Synuclein metabolism and aggregation is linked to ubiquitin-independent degradation by the proteasome. *FEBS Letters* **509**: 22-26
- Tofaris GK, Razaq A, Ghetti B, Lilley KS, & Spillantini MG (2003) Ubiquitination of {alpha}-Synuclein in Lewy Bodies Is a Pathological Event Not Associated with Impairment of Proteasome Function. *Journal of Biological Chemistry* **278**: 44405-44411
- Toshio O, Yasumitsu Y, Toshiya I, Hiroyasu K, & Lars O (2002) *In vivo* generation of hydroxyl radicals and MPTP-induced dopaminergic neurotoxicity in the striatum. *Biogenic Amines* **V17**: 1-14
- Trivedi N, Jung P, & Brown A (2007) Neurofilaments Switch between Distinct Mobile and Stationary States during Their Transport along Axons. *Journal of Neuroscience* **27**: 507-516
- Truckenmiller ME, Marquis PV, Chris C, Mark C, David MD, William JF, & Kevin GB (2001) Gene expression profile in early stage of retinoic acid-induced differentiation of human SH-SY5Y neuroblastoma cells. *Restorative Neurology and Neuroscience* **18**: 67-80
- Tsien RY (1998) The Green Fluorescent Protein. *Annual Reviews Biochemistry* **67**: 509-544
- Tsvetkov LM, Yeh K, Lee S, Sun H, & Zhang H (1999) p27Kip1 ubiquitination and degradation is regulated by the SCFSkp2 complex through phosphorylated Thr187 in p27. *Current Biology* **9**: 661-666
- Tucholski J, Lesort M, & Johnson GVW (2001) Tissue transglutaminase is essential for neurite outgrowth in human neuroblastoma SH-SY5Y cells. *Neuroscience* **102**: 481-491
- Turk B & Stoka V (2007) Protease signalling in cell death: caspases versus cysteine cathepsins. *FEBS Letters* **581**: 2761-2767
- Uchida A & Brown A (2004) Arrival, Reversal, and Departure of Neurofilaments at the Tips of Growing Axons. *Molecular Biology of the Cell* **15**: 4215-4225
- Uchida A, Yorifuji H, Lee VM-, Kishimoto T, & Hisanaga S- (1999) Neurofilaments of aged rats: The strengthened interneurofilament interaction and the reduced amount of NF-M. *Journal of Neuroscience Research* **58**: 337-348
- Valente EM, Abou-Sleiman PM, Caputo V, Muqit MMK, Harvey K, Gispert S, Ali Z, Del Turco D, Bentivoglio AR, Healy DG, Albanese A, Nussbaum R, Gonzalez-Maldonado R, Deller T, Salvi S, Cortelli P, Gilks WP, Latchman DS, Harvey RJ, Dallapiccola B et al (2004) Hereditary Early-Onset Parkinson's Disease Caused by Mutations in PINK1. *Science* **304**: 1158-1160
- van Leyen K, Siddiq A, Ratan RR, & Lo EH (2005) Proteasome inhibition protects HT22 neuronal cells from oxidative glutamate toxicity. *Journal of Neurochemistry* **92**: 824-830
- Vasiljeva O & Turk B (2008) Dual contrasting roles of cysteine cathepsins in cancer progression: Apoptosis versus tumour invasion. *Biochimie* **90**: 380-386
- Veeranna , Amin ND, Ahn NG, Jaffe H, Winters CA, Grant P, & Pant HC (1998) Mitogen-Activated Protein Kinases (Erk1,2) Phosphorylate Lys-Ser-Pro (KSP) Repeats in Neurofilament Proteins NF-H and NF-M. *Journal of Neuroscience* **18**: 4008-4021
- Veeranna , Kaji T, Boland B, Odrlic T, Mohan P, Basavarajappa BS, Peterhoff C, Cataldo A, Rudnicki A, Amin N, Li BS, Pant HC, Hungund BL, Arancio O, & Nixon RA (2004) Calpain Mediates Calcium-Induced Activation of the Erk1,2 MAPK Pathway and Cytoskeletal Phosphorylation in Neurons: Relevance to Alzheimer's Disease. *American Journal of Pathology* **165**: 795-805
- Veeranna, Yang D, Lee J, Vinod KY, Stavrides P, Amin ND, Pant HC, & Nixon RA Declining phosphatases underlie aging-related hyperphosphorylation of neurofilaments. *Neurobiology of Aging* **In Press, Corrected Proof**
- ves-Rodrigues A, Gregori L, & Figueiredo-Pereira ME (1998) Ubiquitin, cellular inclusions and their role in neurodegeneration. *Trends in Neurosciences* **21**: 516-520

- Wagner OI, Lifshitz J, Janmey PA, Linden M, McIntosh TK, & Leterrier J- (2003) Mechanisms of Mitochondria-Neurofilament Interactions. *Journal of Neuroscience* **23**: 9046-9058
- Wagner OI, Ascano J, Tokito M, Leterrier J, Janmey PA, & Holzbaur ELF (2004) The Interaction of Neurofilaments with the Microtubule Motor Cytoplasmic Dynein. *Molecular Biology of the Cell* **15**: 5092-5100
- Wakabayashi K, Mori F, & Takahashi H (2006) Progression patterns of neuronal loss and Lewy body pathology in the substantia nigra in Parkinson's disease. *Parkinsonism & Related Disorders* **12**: S92-S98
- Wang C, Li Y, Wible B, Angelides KJ, & Ishii DN (1992) Effects of insulin and insulin-like growth factors on neurofilament mRNA and tubulin mRNA content in human neuroblastoma SH-SY5Y cells. *Molecular Brain Research* **13**: 289-300
- Wang KKW (2000) Calpain and caspase: can you tell the difference? *Trends in Neurosciences* **23**: 20-26
- Wang KKW, Nath R, Raser KJ, & Hajimohammadreza I (1996) Maitotoxin induces calpain activation in SH-SY5Y neuroblastoma cells and cerebrocortical cultures. *Archives of Biochemistry and Biophysics* **331**: 208-214
- Wang L & Brown A (2001) Rapid Intermittent Movement of Axonal Neurofilaments Observed by Fluorescence Photobleaching. *Molecular Biology of the Cell* **12**: 3257-3267
- Wang Q, Tolstonog GV, Shoeman R, & Traub P (2001) Sites of Nucleic Acid Binding in Type I-IV Intermediate Filament Subunit Proteins. *Biochemistry* **40**: 10342-10349
- Wang Y, Gu Z, Cao Y, Liang Z, Han R, Bennett MC, & Qin Z (2006a) Lysosomal enzyme cathepsin B is involved in kainic acid-induced excitotoxicity in rat striatum. *Brain Research* **1071**: 245-249
- Wang Y, Mou D, Song J, Rao Z, Li D, & Ju G (2006b) Aberrant activation of CDK5 is involved in the pathogenesis of OPIDN. *Journal of Neurochemistry* **99**: 186-197
- Webb JL, Ravikumar B, Atkins J, Skepper JN, & Rubinsztein DC (2003) {alpha}-Synuclein Is Degraded by Both Autophagy and the Proteasome. *Journal of Biological Chemistry* **278**: 25009-25013
- Webb JL, Ravikumar B, & Rubinsztein DC (2004) Microtubule disruption inhibits autophagosome-lysosome fusion: implications for studying the roles of aggresomes in polyglutamine diseases. *The International Journal of Biochemistry & Cell Biology* **36**: 2541-2550
- Wen GY & Wisniewski HM (1984) Substructures of neurofilaments. *Acta Neuropathologica* **64**: 339-343
- Wigley CW, Fabunmi RP, Lee MG, Marino CR, Muallem s, DeMartino GN, & Thomas PJ (1999) Dynamic Association of Proteasomal Machinery with the Centrosome. *The Journal of Cell Biology* **145**: 481-490
- Williamson TL, Bruijn LI, Zhu Q, Anderson KL, Anderson SD, Julien J, & Cleveland DW (1998) Absence of neurofilaments reduces the selective vulnerability of motor neurons and slows disease caused by a familial amyotrophic lateral sclerosis-linked superoxide dismutase 1 mutant. *Proceedings of the National Academy of Sciences* **95**: 9631-9636
- Winslow AR, Chen C, Corrochano S, Acevedo-Arozena A, Gordon DE, Peden AA, Lichtenberg M, Menzies FM, Ravikumar B, Imarisio S, Brown S, O'Kane CJ, & Rubinsztein DC (2010) α -Synuclein impairs macroautophagy: implications for Parkinson's disease. *The Journal of Cell Biology* **190**: 1023-1037
- Wong J, Hutchison SB, & Liem RK (1984) An isoelectric variant of the 150,000-dalton neurofilament polypeptide. Evidence that phosphorylation state affects its association with the filament. *Journal of Biological Chemistry* **259**: 10867-10874

- Xia C, Roberts EA, Her L, Liu X, Williams DS, Cleveland DW, & Goldstein LSB (2003) Abnormal neurofilament transport caused by targeted disruption of neuronal kinesin heavy chain KIF5A. *The Journal of Cell Biology* **161**: 55-66
- Xie H, Hu L, & Li G (2010) SH-SY5Y human neuroblastoma cell line: *in vitro* cell model of dopaminergic neurons in Parkinson's disease. *Chinese Medical Journal* **123**: 1086-1092
- Xie Z & Klionsky DJ (2007) Autophagosome formation: core machinery and adaptations. *Nature Cell Biology* **9**: 1102-1109
- Xu Z, Cawthon D, McCastlain KA, Slikker W, & Ali SF (2005) Selective alterations of gene expression in mice induced by MPTP. *Synapse* **55**: 45-51
- Xu Z, Marszalek JR, Lee MK, Wong PC, Folmer J, Crawford TO, Hsieh ST, Griffin JW, & Cleveland DW (1996) Subunit composition of neurofilaments specifies axonal diameter. *Journal of Cell Biology* **133**: 1061-1069
- Xu Z, Patterson T, Wren J, Han T, Shi L, Duhart H, Ali S, & Slikker W (2005) A microarray study of MPP+-treated PC12 Cells: Mechanisms of toxicity (MOT) analysis using bioinformatics tools. *BMC Bioinformatics* **6**: S8
- Yabe JT, Chan WK-, Wang F, Pimenta A, Ortiz DD, & Shea TB (2003) Regulation of the transition from vimentin to neurofilaments during neuronal differentiation. *Cell Mobility and the Cytoskeleton* **56**: 193-205
- Yabe JT, Chylinski T, Wang F, Pimenta A, Kattar SD, Linsley M, Chan WKH, & Shea TB (2001) Neurofilaments Consist of Distinct Populations That Can Be Distinguished by C-Terminal Phosphorylation, Bundling, and Axonal Transport Rate in Growing Axonal Neurites. *The Journal of Neuroscience* **21**: 2195-2205
- Yabe JT, Jung C, Chan WK-, & Shea TB (2000) Phospho-Dependent Association of Neurofilament Proteins with Kinesin In Situ. *Cell Mobility and the Cytoskeleton* **45**: 249-262
- Yabe JT, Pimenta A, & Shea TB (1999) Kinesin-mediated transport of neurofilament protein oligomers in growing axons. *Journal of Cell Science* **112**: 3799-3814
- Yamada, T., Kawamata, T., Walker, D. G., McGeer, P.L. (1992) Vimentin immunoreactivity in normal and pathological human brain tissue. *Acta Neuropathologica* **84**: 157-162; 157
- Yamamoto A, Tagawa Y, Yoshimori T, Moriyama Y, Masaki R, & Tashiro Y (1998) Bafilomycin A1 Prevents Maturation of Autophagic Vacuoles by Inhibiting Fusion between Autophagosomes and Lysosomes in Rat Hepatoma Cell Line, H-4-II-E Cells. *Cell Structure and Function* **23**: 33-42
- Yan LJ, Levine RL, & Sohal RS (1997) Oxidative damage during aging targets mitochondrial aconitase. *Proceedings of the National Academy of Sciences* **94**: 11168-11172
- Yan Y, Jensen K, & Brown A (2007) The Polypeptide Composition of Moving and Stationary Neurofilaments in Cultured Sympathetic Neurons. *Cell motility and the cytoskeleton* **64**: 299-309
- Yan Y & Brown A (2005) Neurofilament Polymer Transport in Axons. *Journal of Neuroscience* **25**: 7014-7021
- Yang F, Jiang Q, Zhao J, Ren Y, Sutton MD, & Feng J (2005) Parkin Stabilizes Microtubules through Strong Binding Mediated by Three Independent Domains. *Journal of Biological Chemistry* **280**: 17154-17162
- Yao Y, Toth CR, Wonh ML, Dias P, Burlingame AL, Coffino P, & Wang CC (1999) alpha5 subunit in Trypanosoma brucei proteasome can self-assemble to form a cylinder of four stacked heptamer rings. *Biochemical Journal* **344**: 349-358
- Yazdani U, German DC, Liang CL, Manzano L, Sonsalla PK, & Zeevalk GD (2006) Rat model of Parkinson's disease: Chronic central delivery of 1-methyl-4-phenylpyridinium (MPP+). *Experimental Neurology* **200**: 172-183

- Yoshimori T, Yamamoto A, Moriyama Y, Futai M, & Tashiro Y (1991) Bafilomycin A1, a specific inhibitor of vacuolar-type H(+)-ATPase, inhibits acidification and protein degradation in lysosomes of cultured cells. *Journal of Biological Chemistry* **266**: 17707-17712
- Yu WH, Dorado B, Figueroa HY, Wang L, Planel E, Cookson MR, Clark LN, & Duff KE (2009) Metabolic Activity Determines Efficacy of Macroautophagic Clearance of Pathological Oligomeric α -Synuclein. *American Journal of Pathology* **175**: 736-747
- Yuan A, Nixon RA, & Rao MV (2006) Deleting the phosphorylated tail domain of the neurofilament heavy subunit does not alter neurofilament transport rate in vivo. *Neuroscience Letters* **393**: 264-268
- Yuan A, Rao MV, Kumar A, Julien J, & Nixon RA (2003) Neurofilament Transport In Vivo Minimally Requires Hetero-Oligomer Formation. *The Journal of Neuroscience* **23**: 9452-9458
- Yuan A, Rao MV, Sasaki T, Chen Y, Kumar A, Veeranna, Liem RKH, Eyer J, Peterson AC, Julien JP, & Nixon RA (2006) α -Internexin Is Structurally and Functionally Associated with the Neurofilament Triplet Proteins in the Mature CNS. *Journal of Neuroscience* **26**: 10006-10019
- Yuan A, Sasaki T, Rao MV, Kumar A, Kanumuri V, Dunlop DS, Liem RK, & Nixon RA (2009) Neurofilaments Form a Highly Stable Stationary Cytoskeleton after Reaching a Critical Level in Axons. *Journal of Neuroscience* **29**: 11316-11329
- Zaarur N, Meriin AB, Gabai VL, & Sherman MY (2008) Triggering Aggresome Formation, Dissecting aggresome-targeting and aggregation signals in synphilin 1. *The Journal of Biological Chemistry* **283**: 27575-27584
- Zatloukal K, Stumptner C, Fuchsbichler A, Heid H, Schnoelzer M, Kenner L, Kleinert R, Prinz M, Aguzzi A, & Denk H (2002) p62 Is a Common Component of Cytoplasmic Inclusions in Protein Aggregation Diseases. *American Journal of Pathology* **160**: 255-263
- Zeng BY, Iravani MM, Lin ST, Irifune M, Kuoppamäki M, Al-Barghouthy G, Smith L, Jackson MJ, Rose S, Medhurst AD, & Jenner P (2006) MPTP treatment of common marmosets impairs proteasomal enzyme activity and decreases expression of structural and regulatory elements of the 26S proteasome. *European Journal of Neuroscience* **23**: 1766-1774
- Zentrich E, Han S, Pessoa-Brandao L, Butterfield L, & Heasley LE (2002) Collaboration of JNKs and ERKs in Nerve Growth Factor Regulation of the Neurofilament Light Chain Promoter in PC12 Cells. *Journal of Biological Chemistry* **277**: 4110-4118
- Zhai J, Lin H, Julien J, & Schlaepfer WW (2007) Disruption of neurofilament network with aggregation of light neurofilament protein: a common pathway leading to motor neuron degeneration due to Charcot Marie Tooth disease-linked mutations in NFL and HSPB1. *Human Molecular Genetics* **16**: 3103-3116
- Zhang J, Lesort M, Guttman RP, & Johnson GVW (1998) Modulation of the in Situ Activity of Tissue Transglutaminase by Calcium and GTP. *Journal of Biological Chemistry* **273**: 2288-2295
- Zhang KZ, Westberg JA, Hölttä E, & Andersson LC (1996) BCL2 regulates neural differentiation. *Proceedings of the National Academy of Sciences* **93**: 4504-4508
- Zheng X, Chu F, Mirkin BL, Sudha T, Mousa SA, & Rebbaa A (2008) Role of the proteolytic hierarchy between cathepsin L, cathepsin D and caspase-3 in regulation of cellular susceptibility to apoptosis and autophagy. *Biochimica et Biophysica Acta (BBA) - Molecular Cell Research* **1783**: 2294-2300
- Zhou P (2004) Determining Protein Half-Lives. *Methods in molecular biology* **284**: 67-77
- Zhu D & Uckun FM (2000) Z-Phe-Gly-NHO-Bz, an Inhibitor of Cysteine Cathepsins, Induces Apoptosis in Human Cancer Cells. *Clinical Cancer Research* **6**: 2064-2069
- Zhu J, Horbinski C, Guo F, Watkins S, Uchiyama Y, & Chu CT (2007) Regulation of Autophagy by Extracellular Signal-Regulated Protein Kinases During 1-Methyl-4-Phenylpyridinium-Induced Cell Death. *The American Journal of Pathology* **170**: 75-86

- Zhu Q, Couillard-Després S, & Julien J (1997) Delayed Maturation of Regenerating Myelinated Axons in Mice Lacking Neurofilaments. *Experimental Neurology* **148**: 299-316
- Zhu J, Horbinski C, Guo F, Watkins S, Uchiyama Y, & Chu CT (2007) Regulation of Autophagy by Extracellular Signal-Regulated Protein Kinases During 1-Methyl-4-Phenylpyridinium-Induced Cell Death. *The American Journal of Pathology* **170**: 75-86
- Zimprich A, Biskup S, Leitner P, Lichtner P, Farrer M, Lincoln S, Kachergus J, Hulihan M, Uitti RJ, & Calne DB (2004) Mutations in LRRK2 Cause Autosomal-Dominant Parkinsonism with Pleomorphic Pathology. *Neuron* **44**: 601-607

APPENDICES

I. Determination of the molecular weights of α II-spectrin breakdown products (SBDP)

The molecular weights of α II-spectrin breakdown products were confirmed by comparing the Rf values (calculated by dividing the distance travelled by the band with the distance to the bottom of the blot) of molecular weight standards to that of the SBDPs. For standards, Rf values were plotted against the logarithm of the molecular weight and the 'line of best fit' was used to determine the molecular weight SBDPs (Figure i).

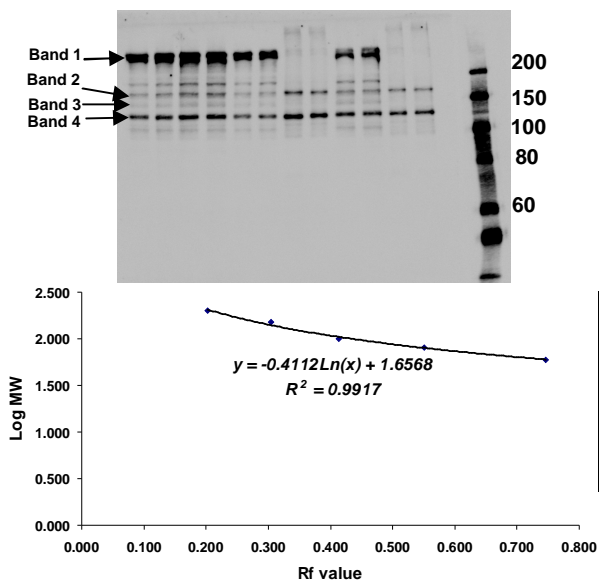
Band 1 is the full-length α II-spectrin and has a molecular weight of 280 kD but the molecular weight calculated is much greater than expected at 387.9 ± 3.78 kDa. When determining molecular weights from Rf values, molecular weight determinations are more accurate in the middle of the blot than at the top where separation is slower therefore the high molecular weight determined for full-length α II-spectrin is most likely an artefact.

Band 2 was proposed as the 150 kD SBDP which is the result of cleavage by both calpain and caspase 3. The molecular weight of this band, estimated from two blots was 160.5 ± 4.96 kD. The molecular weight of this band was slightly greater than expected but since it was a very prominent band in the lane with the prominent 120 kD band (indicating more caspase 3 cleavage); it is most likely the 150 kD caspase 3 SBDP and the higher molecular weight is an artefact.

Band 3 was proposed as the 145 kD calpain specific SBDP. The molecular weight of this band, estimated from two blots was 138.3 ± 4.11 kD.

Band 4 was proposed as the 120 kD caspase 3 specific SBDP. The molecular weight of this band, estimated from two blots was 121.7 ± 3.42 kD.

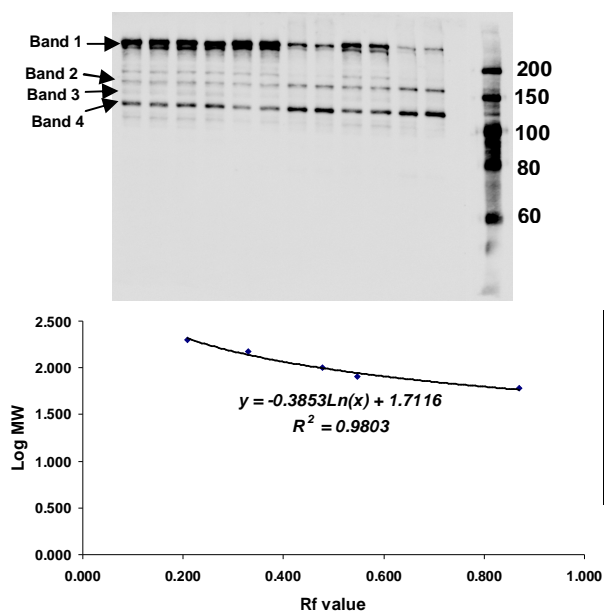
Blot 1 **αII-spectrin blot**



MW	distance (mm)	to dye front (mm)	Rf value	Log MW
200	14	69	0.203	2.301
150	21		0.304	2.176
100	28.5		0.413	2.000
80	38		0.551	1.903
60	51.5		0.746	1.778

	distance (mm)	to dye front (mm)	Rf value	Log(MW)	MW
band 1	7	68	0.103	2.592	390.6
band 2	17.5		0.257	2.215	164.0
band 3	20.5		0.301	2.150	141.2
band 4	23.5		0.346	2.094	124.1

Blot 2



MW	distance (mm)	to dye front (mm)	Rf value	Log MW
200	12	57.5	0.209	2.301
150	19		0.330	2.176
100	27.5		0.478	2.000
80	31.5		0.548	1.903
60	50		0.870	1.778

	distance (mm)	to dye front (mm)	Rf value	Log(MW)	MW
band 1	6	58	0.103	2.586	385.2
band 2	16.5		0.284	2.196	157.0
band 3	19.5		0.336	2.132	135.4
band 4	22.5		0.388	2.076	119.2

	MW (kD)	MW (kD)	mean (kD)	range (kD)
band 1	390.6	385.2	387.9	3.78
band 2	164.0	157.0	160.5	4.96
band 3	141.2	135.4	138.3	4.11
band 4	124.1	119.2	121.7	3.42

Figure i The calculation of the apparent molecular weights of αII-spectrin breakdown products (SBDPs).

II. Optimization of transfection with LipofectAMINE™2000

Previous work in our laboratory has suggested that chemical transfection with LipofectAMINE™ is milder and more efficient than electroporation on SH-SY5Y cells (Dr C Ufer, personal communication). Initial experiments were concerned with the optimization of the parameters for transfection using LipofectAMINE™2000. The transfection efficiency was determined by measuring the level of GFP fluorescence with a fluorometer (FLUOstar OPTIMA, BMG LABTECH) with 485 nm excitation and 520 nm emission filters, cells were also imaged by laser confocal microscopy. Cell viability was monitored by measuring MTT reduction.

To determine the optimum cell density that resulted in high transfection efficiency while minimizing cellular toxicity, cells were seeded at varying cell densities in a 6-well plate and transfecting cells with 1 µg pGFPmax to 3 µl LipofectAMINE™2000. Phase contrast of transfected cells (Figure II.1 A) support MTT reduction data since cells seeded at a cell density > 250 000 cells/well were morphologically similar to untransfected controls. GFP expression in cells seeded at a density of 250 000 cells per well in a 6-well plate is shown in Figure II.1 B. A comparison of the level of GFP fluorescence and MTT reduction at various cell densities (Figure II.1 C) showed a maximum GFP fluorescence and MTT reduction when cells were seeded at a density of 250 000 cells/well.

The optimum ratio of LipofectAMINE™2000 to plasmid DNA with which to transfect cells was determined by seeding cells at a density of 200 000 cells/well in a 6-well plate and transfecting them with 1 µg pGFPmax using 1-6 µl LipofectAMINE. Phase contrast images (Figure II.2 A) revealed that morphologically there were no apparent differences in the appearance of cells transfected using 1-4 µl LipofectAMINE but when using volumes ≥ 5 µl, cells appeared to be in a poorer condition. GFP expression in cells transfected with 1 µl or 4 µl of LipofectAMINE (Figure II.2 B) revealed that more cells exhibit GFP fluorescence when the LipofectAMINE (µl):DNA (µg) ratio was 4:1 rather than 1:1. A comparison of GFP fluorescence and MTT reduction (Figure II.2 C) revealed, the highest levels of GFP fluorescence were observed when the LipofectAMINE:DNA ratios were 2:1, 3:1 or 4:1. MTT reduction revealed that cell viability was similar when using 1-4 µl LipofectAMINE™2000 but this decreased dramatically when using more than 4 µl.

From these experiments the ratio of LipofectAMINE™2000 (μl):DNA (μg) used for the transfection of SH-SY5Y cells was chosen to be 2:1 with an optimum cell density of 250 000 cells/well in a 6-well plate.

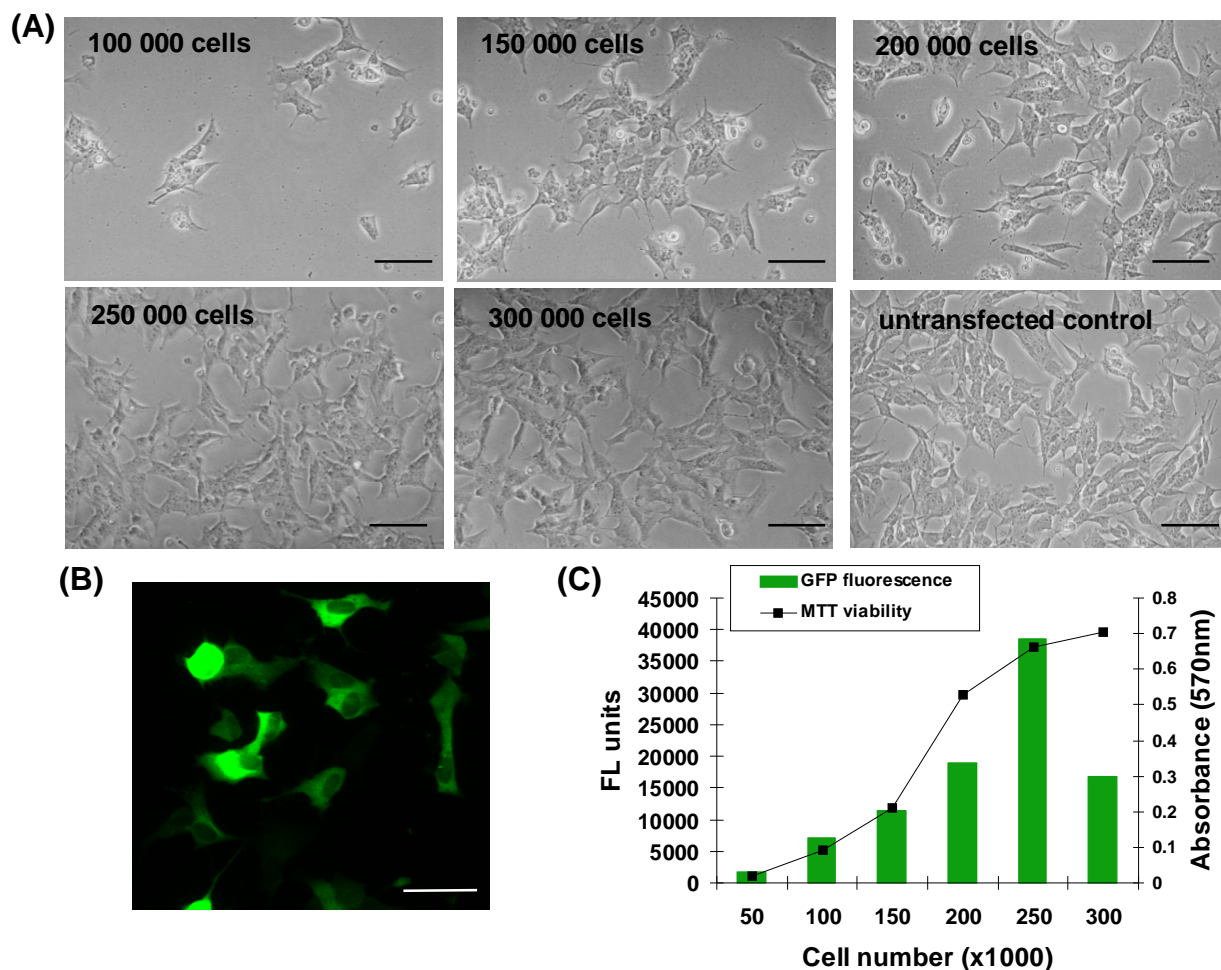


Figure ii Determination of the optimum cell density required for transfection of SH-SY5Y neuroblastoma cells with LipofectAMINE™2000.

Optimum cell density that resulted in the highest transfection efficiency while maintaining cell viability was determined by comparing of the level of GFP fluorescence and MTT reduction. (A) Phase contrast images of cells transfected with 1 μg pGFPmax using 3 μl LipofectAMINE™2000 and seeded at different cell densities in 6-well plates compared to untransfected controls. (B) Laser confocal microscope images of cells transfected with 1 μg pGFPmax using 3 μl LipofectAMINE™2000 seeded a cell density of 250 000 cells/well in 6-well plates. (C) Plot comparing the GFP fluorescence of cells seeded in 6-well plates at different cell densities and transfected with 1 μg pGFPmax using 3 μl LipofectAMINE™2000 with cell viability determined by MTT reduction. Scale bar represents 40 μm .

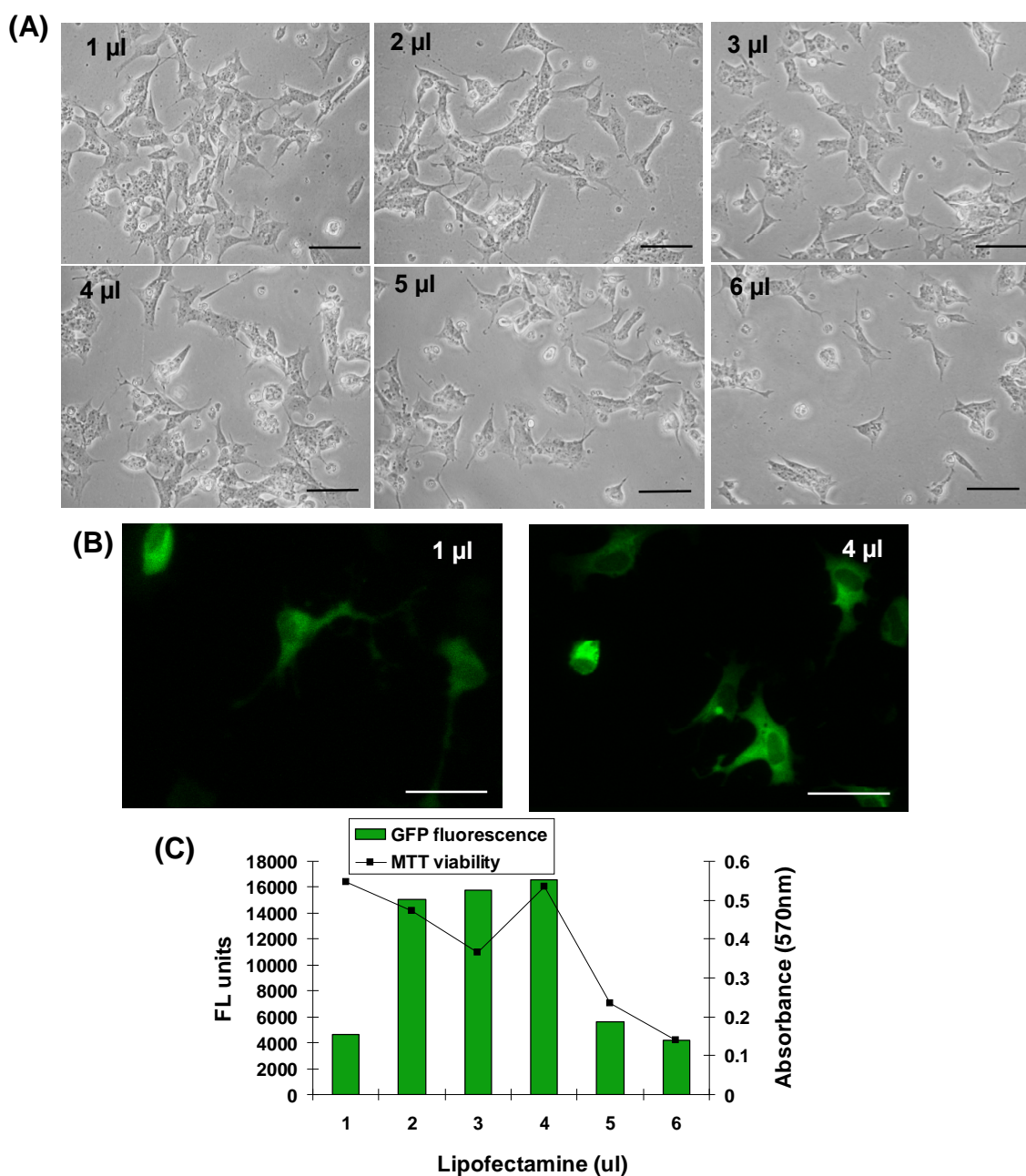


Figure iii Determination of the optimum ratio of LipofectAMINE™2000 to DNA that resulted in the highest transfection efficiency while maintaining cell viability.

The transfection efficiency was assessed by the level of GFP fluorescence and cell viability by MTT reduction. (A) Phase contrast images of cells transfected with 1 µg pGFPmax with different volumes of LipofectAMINE™2000 ranging from 1-6 µl. (B) Laser confocal microscope images of SH-SY5Y neuroblastoma cells transfected with 1 µg pGFPmax with 1 µl or 4 µl of LipofectAMINE™2000. (C) Plot comparing the level of GFP fluorescence of SH-SY5Y neuroblastoma cells transfected with 1 µg pGFPmax with different volumes of LipofectAMINE™2000 ranging from 1 µl to 6 µl with MTT reduction as a measure of cell viability. Scale bar represents 40 µm.

III. Restriction Map and Multiple Cloning Site of pEGFP-C3

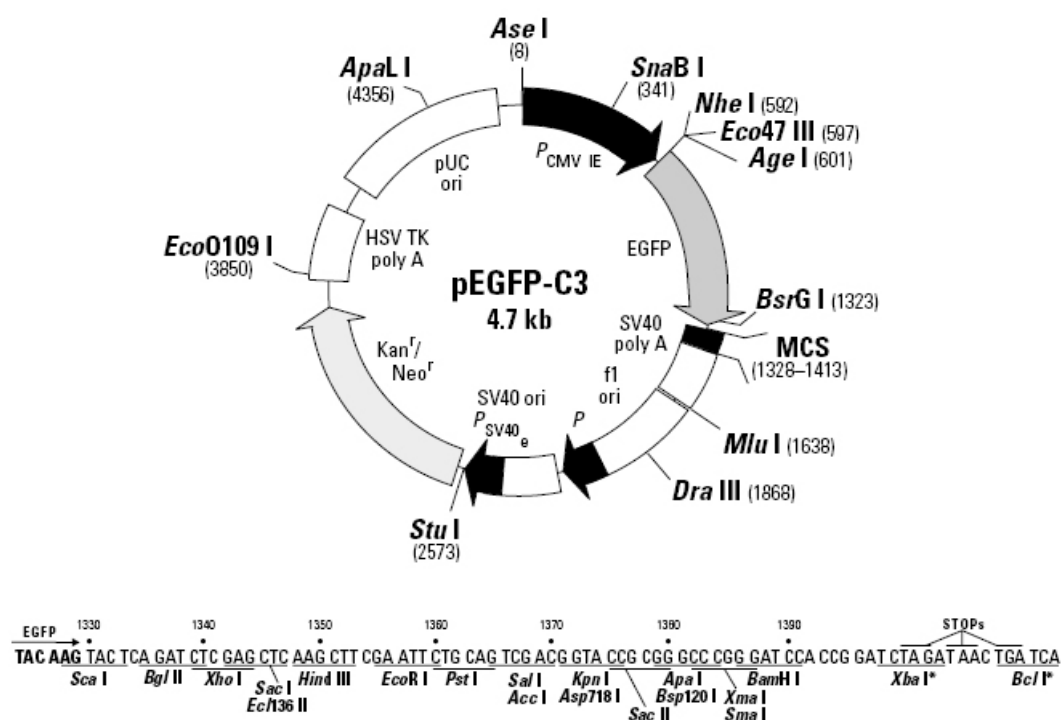
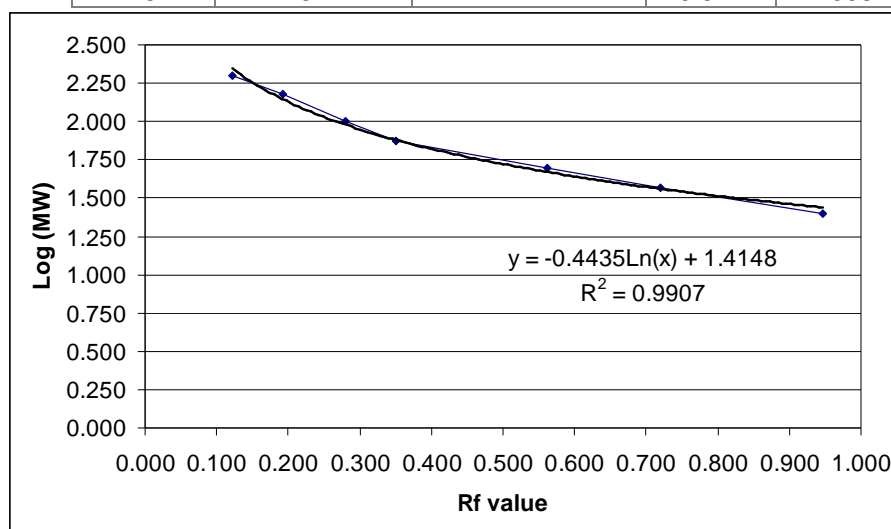


Figure iv Restriction Map and Multiple Cloning Site (MCS) of pEGFP-C3 (Clontech)

IV. Determination of the molecular weight of GFP and GFP-tagged neurofilaments

To confirm the molecular weights of GFP and GFP tagged NFs, total cell extracts were analysed by SDS-PAGE and Western blotting. The Rf values (calculated by dividing the distance travelled by the protein with the distance to the dye front) of molecular weight standards were plotted against the logarithm of molecular weight. The equation of the 'line of best fit' was used to determine the molecular weight of GFP and GFP/NFs from their Rf values (Figures iv-vii).

Anti-GFP Blot	MW (Da)	distance (mm)	to dye front (mm)	Rf value	Log MW
	200	7	57	0.123	2.301
	150	11		0.193	2.176
	100	16		0.281	2.000
	75	20		0.351	1.875
	50	32		0.561	1.699
	37	41		0.719	1.568
	25	54		0.947	1.398



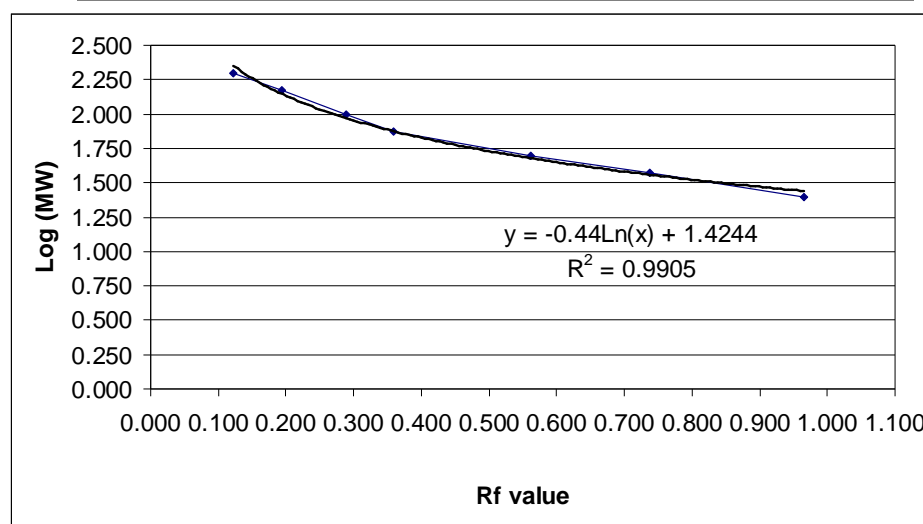
	distance (mm)	to dye front (mm)	Rf value	Log(MW)	MW (Da)
GFP	48.5	56.5	0.858	1.483	30.4
GFP/NFL	16	56.5	0.283	1.974	94.3
GFP/NFH(trunc)	22.5	57.5	0.391	1.831	67.8
GFP/NFM	8.5	57	0.149	2.259	181.5

Figure v Determination of the molecular weights of GFP and GFP tagged neurofilaments of total cell extracts of SH-SY5Y cells expressing GFP, GFP/NF-M, GFP/NF-L or GFP/NF-H (truncated).

Total cell extracts were analysed by SDS-PAGE and Western blotting followed by immunoprobining with anti-GFP (abcam, 1:10 000). A standard curve of the logarithm of the molecular weights of molecular weight standards run on the same gel as the cell extracts versus the Rf values for each molecular weight standard (distance travelled divided by the distance to the dye front) was used to determine the molecular weights of GFP and GFP/NFs from their Rf values.

Anti-NF-M Blot

MW	distance (mm)	to dye front (mm)	Rf value	Log MW
200	7	57	0.123	2.301
150	11		0.193	2.176
100	16.5		0.289	2.000
75	20.5		0.360	1.875
50	32		0.561	1.699
37	42		0.737	1.568
25	55		0.965	1.398



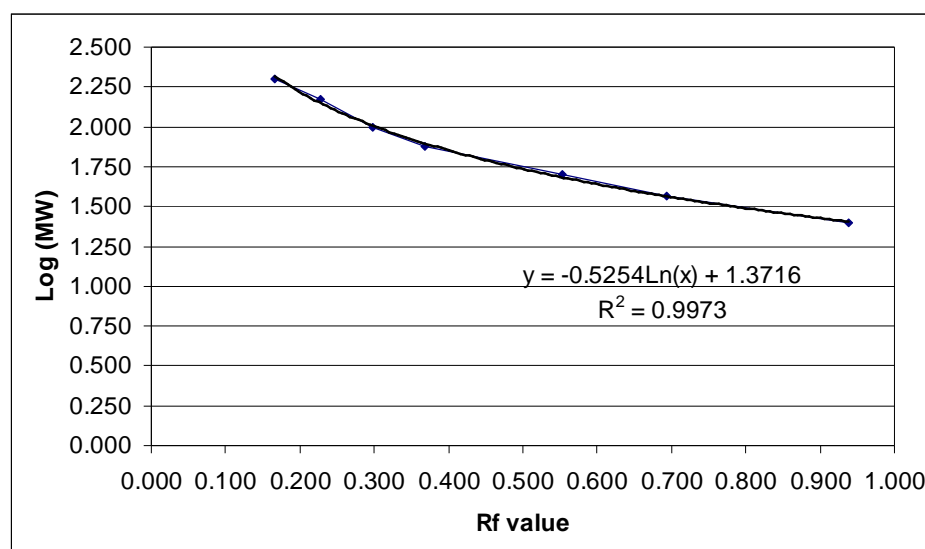
	distance (mm)	to dye front (mm)	Rf value	Log(MW)	MW
GFP/NFM	8.5	56.8	0.150	2.260	182.0
NFM	10.2	56.8	0.180	2.180	151.3

Figure vi Determination of the molecular weight of GFP/NF-M and endogenous NF-M

The apparent molecular weights of GFP/NF-M and NF-M in a total cell extract of cells expressing GFP/NF-M were determined by SDS-PAGE and Western blotting. Western blots were immunoprobed with anti-NF-M (RMO270, 1:500; Invitrogen). A standard curve of the logarithm of the molecular weights of molecular weight standards run on the same gel as the cell extracts versus the Rf values for each molecular weight standard (distance travelled divided by the distance to the dye front), the equation of the line was used to determine the molecular weights of GFP/NF-M and NF-M from their Rf values.

Anti-NF-L Blot

MW	distance (mm)	to dye front (mm)	Rf value	Log MW
200	9.5	57	0.167	2.301
150	13		0.228	2.176
100	17		0.298	2.000
75	21		0.368	1.875
50	31.5		0.553	1.699
37	39.5		0.693	1.568
25	53.5		0.939	1.398



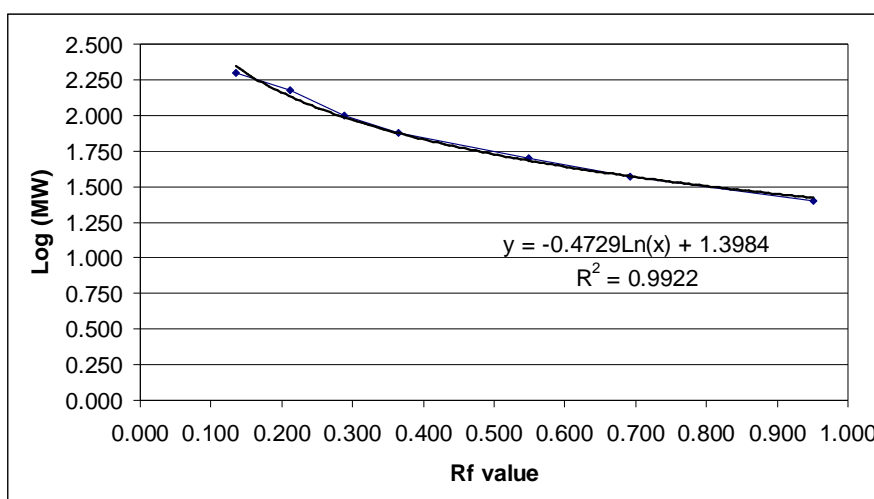
	distance (mm)	to dye front (mm)	Rf value	Log(MW)	MW (Da)
GFP/NFL	17	57	0.298	2.007	101.7
NFL	22.8	57	0.400	1.853	71.3

Figure vii Determination of the molecular weight of GFP/NF-L and endogenous NF-L

The apparent molecular weight of GFP/NF-L and endogenous NF-L in a total cell extract of cells expressing GFP/NF-L was determined by SDS-PAGE and Western blotting. Western blots were immunoprobed with anti-NF-L (DA2, 1:2000; Invitrogen). A standard curve of the logarithm of the molecular weights of molecular weight standards run on the same gel as the cell extracts versus the Rf values for each molecular weight standard (distance travelled divided by the distance to the dye front), the equation of the line was used to determine the molecular weights of GFP/NF-L and NF-L from their Rf values.

Anti-GFP

MW	distance (mm)	to dye front (mm)	Rf value	Log MW
200	7	52	0.135	2.301
150	11		0.212	2.176
100	15		0.288	2.000
75	19		0.365	1.875
50	28.5		0.548	1.699
37	36		0.692	1.568
25	49.5		0.952	1.398



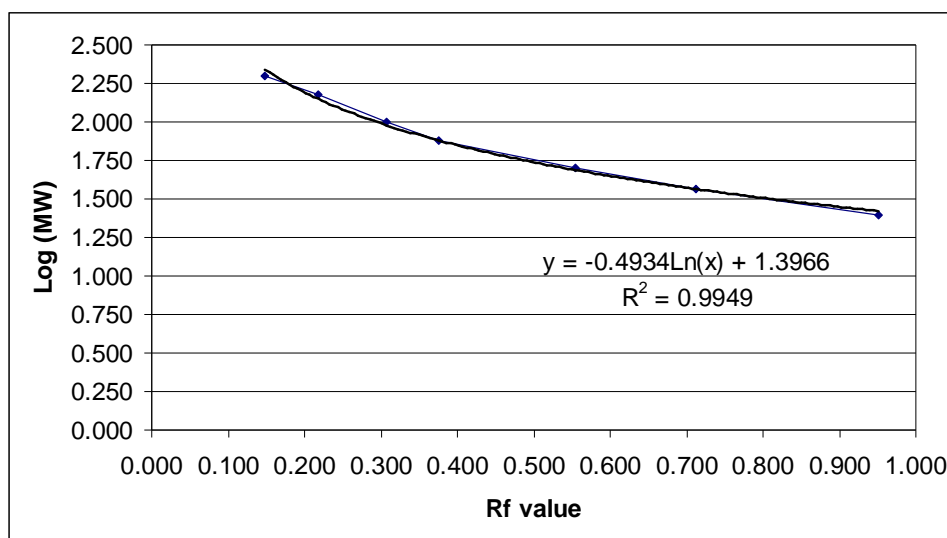
	distance (mm)	to dye front (mm)	Rf value	Log(MW)	MW
GFP	44	52	0.846	1.477	30.0
GFP/NFH	6	52	0.115	2.420	262.8

Figure viii Determination of the molecular weight of GFP and GFP/NF-H

The apparent molecular weights of GFP and GFP/NF-H were determined by SDS-PAGE and Western blotting of total cell extracts of cells expressing GFP or GFP/NF-H. Western blots were immunoprobed with anti-GFP (abcam, 1:10 000) and molecular weights were determined from the Rf values (distance travelled by distance to the dye front) of GFP and GFP/NF-H. A standard curve was produced in which the Rf values of molecular weight standards was plotted against the logarithm of molecular weight. The equation of the line was used to determine the molecular weight.

Anti-NF-H Blot

MW	distance (mm)	to dye front (mm)	Rf value	Log MW
200	7.5	50.5	0.149	2.301
150	11		0.218	2.176
100	15.5		0.307	2.000
75	19		0.376	1.875
50	28		0.554	1.699
37	36		0.713	1.568
25	48		0.950	1.398



	distance (mm)	to dye front (mm)	Rf value	Log(MW)	MW
NF-H	8	50.5	0.158	2.306	202.2
GFP/NFH	7	50.5	0.139	2.372	235.3

Figure ix Determination of the molecular weight of endogenous NF-H and GFP/NF-H

The apparent molecular weight of GFP/NF-H and NF-H from total cell extracts of SH-SY5Y cells expressing GFP/NF-H. Total cell extracts analysed by SDS-PAGE and Western blotting were immunoprobed with anti-NF-H (n52, 1:2000; Sigma). The molecular weights of the proteins were determined from their Rf values (distance travelled divided by the distance to the dye front). A standard curve was produced in which the Rf values of molecular weight standards were plotted against the logarithm of molecular weight. Molecular weight of endogenous NF-H and GFP/NF-H was determined from the equation of the line.

V. Peptide Mass Fingerprints

Green Fluorescent Protein

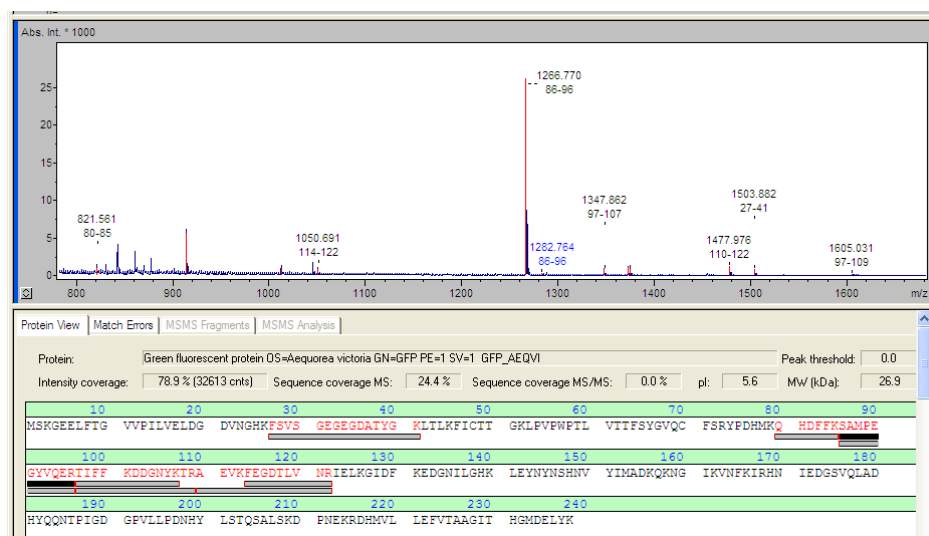


Figure x Identification of GFP by mass spectrometry.

Example of a Peptide mass fingerprint and result of mascot search which identified GFP in immunoprecipitate from GFP expressing cells.

GFP/NF-H

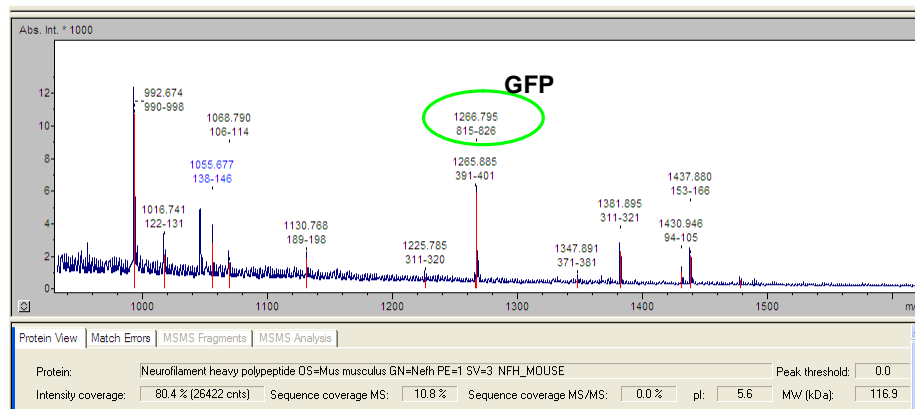
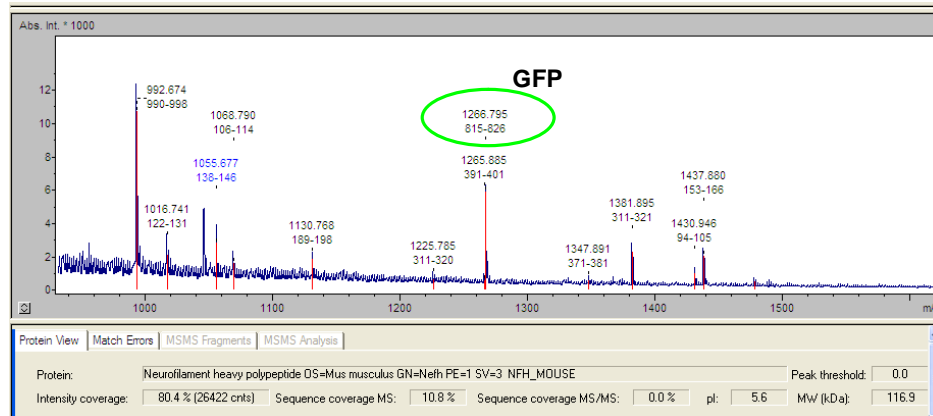


Figure xi Identification of GFP/NF-H by mass spectrometry.

Peptide mass fingerprint and result of mascot search which identified GFP/NF-H in the immunoprecipitate from GFP/NF-H expressing cells from a band excised from a one-dimensional SDS-PAGE gel. The peak circled in green is from GFP.

GFP/NF-M



NF-M

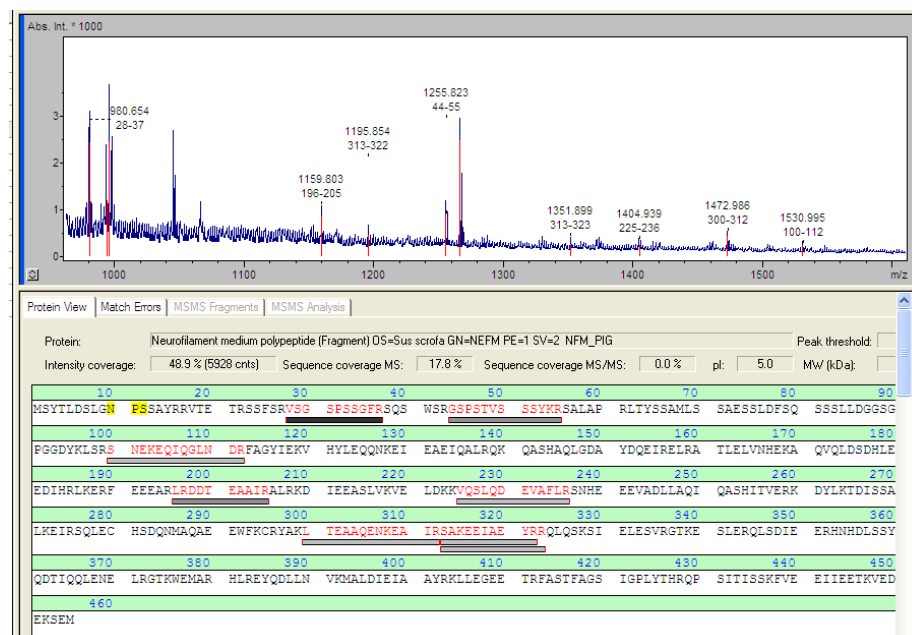


Figure xii Identification of (A) GFP/NF-M and (B) NF-M in by mass spectrometry.

Example of a Peptide mass fingerprint and result of mascot search which identified GFP/NF-M and NF-M in immunoprecipitate from GFP/NF-M expressing cells. The peak circled in green is from GFP.

Vimentin

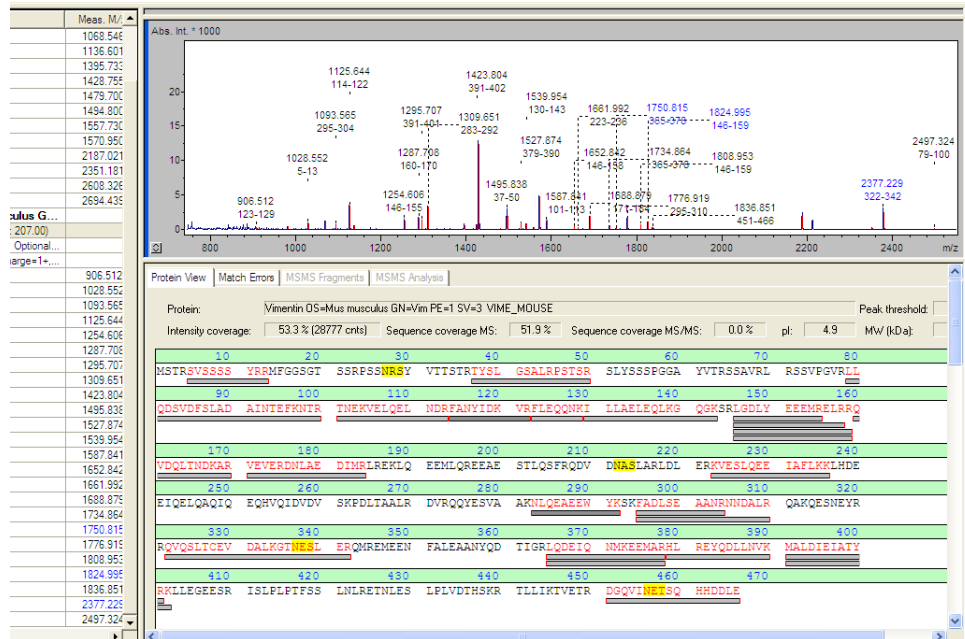
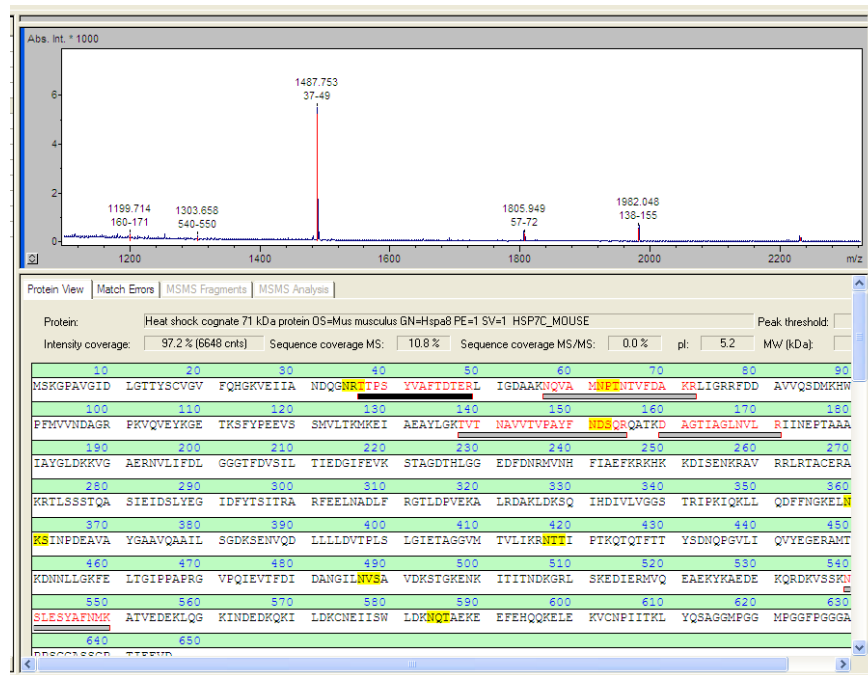


Figure xiii Identification of vimentin by mass spectrometry.

Example of a peptide mass fingerprint and the result of the mascot search which identified vimentin from a spot excised from a two-dimensional SDS-PAGE gel of the immunoprecipitate from GFP/NF-M expressing cells.

Hsc70



MS/MS of peak 1488.577

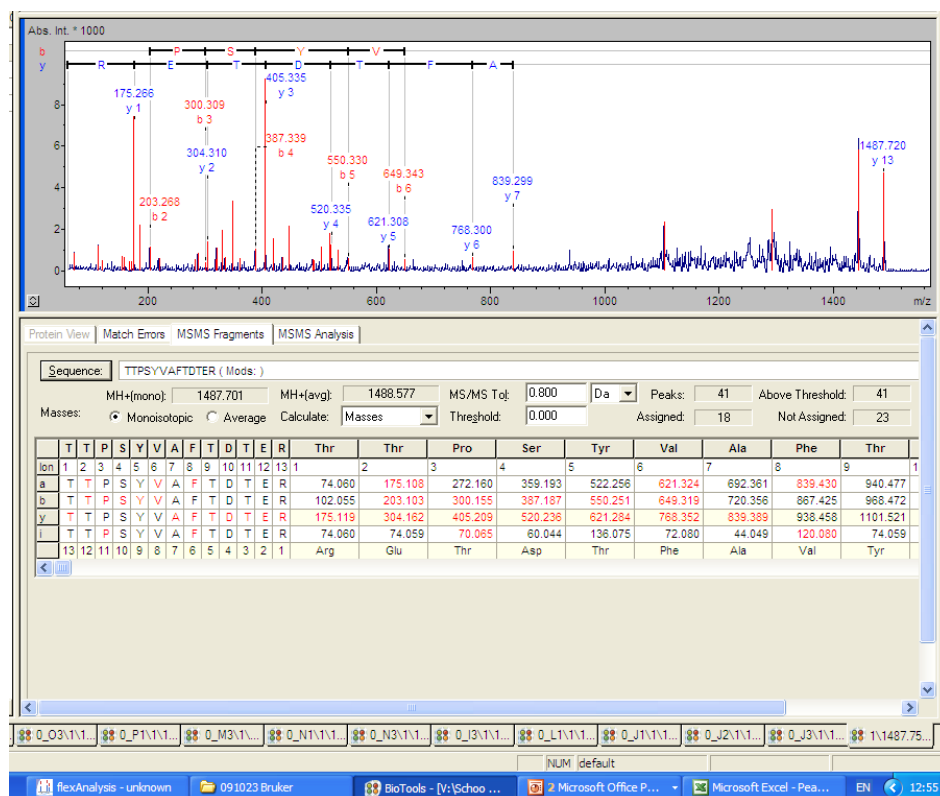


Figure xiv Identification of Hsc70 by mass spectrometry.

Peptide mass fingerprint and the result of the mascot search which identified Hsc70 from a spot excised from a two-dimensional SDS-PAGE gel of the immunoprecipitate from GFP/NF-M expressing cells. Peak 1487.753 (circled in orange) was subjected to MS/MS to confirm the identification of Hsc70.

VI. Proposed effects of complex I inhibition and DA-mediated oxidative stress on degradative pathways and turnover of cytoskeletal proteins

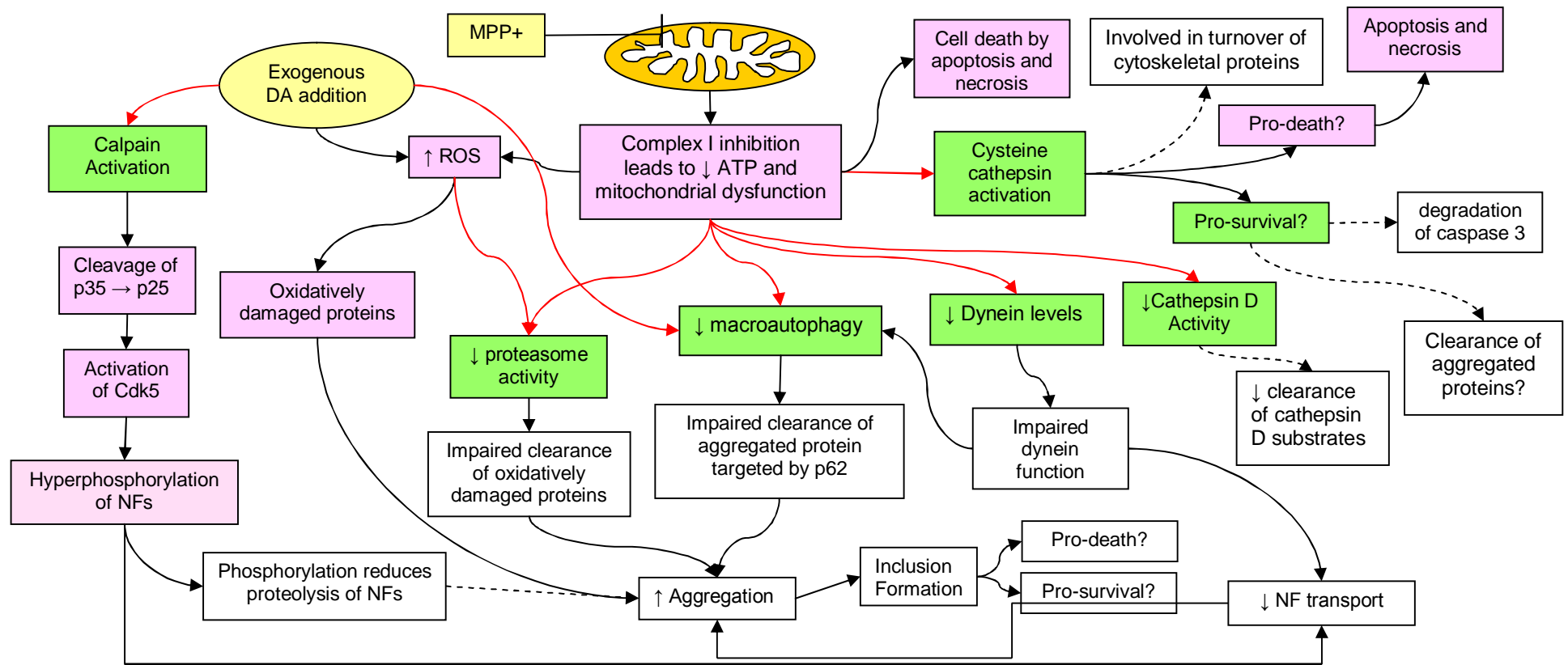


Figure xv Summary of the proposed mechanisms of mitochondrial dysfunction and DA-mediated oxidative stress presented in this thesis integrated with current literature reviewed in chapter 1.

The yellow boxes represent treatments, green boxes and red line represent the findings reported in the present work, the pink boxes and solid black lines represent information from current literature reviewed in chapter 1 of this thesis. The clear boxes and broken lines represent the proposed consequences/significance of the findings in the present work in relation to current literature.

Mitochondrial dysfunction induced by the inhibition of complex I with MPP⁺ results in a reduction in cellular ATP levels and the production of mitochondrial derived oxidative stress. Exogenous addition of DA results in DA-mediated oxidative stress which results in the activation of calpain which activates Cdk5 via the cleavage of p35 to p25. Activation of Cdk5 results in the phosphorylation of NFs, which could lead to the accumulation of hyperphosphorylated NFs. Phosphorylation of NFs increases their resistance to proteolysis resulting in accumulation and reduces their association with motor proteins such as kinesin and dynein, aberrant resulting in impaired NF transport. Both DA and MPP⁺ treatment reduced proteasome activity which has implications for the clearance of oxidatively damaged proteins thus promoting the formation of protein aggregates. A reduction in cathepsin D activity was also observed with MPP⁺ treatment which may result in reduced clearance of cathepsin D protein substrates such as NF-H. Cysteine cathepsins have been implicated in both cell death (apoptotic and necrotic) and cell survival, possibly via the degradation of caspase 3. There was some evidence for the role of cysteine cathepsins in ensuring cell survival in proliferating cells treated with MPP⁺ in the present work but the mechanism is not known. Cysteine cathepsins may also be involved in the turnover of cytoskeletal proteins during complex I inhibition but the significance of this with respect to cell survival is not certain. Perhaps cysteine cathepsin activity is elevated to promote the clearance of aggregated proteins to compensate for reduced cathepsin D activity and macroautophagy which may suggest that the clearance of aggregated proteins is cytoprotective. Dynein levels are reduced with MPP⁺ treatment which has previously been shown to result in impaired dynein function which may reduce NF transport from the cell body to axonal processes resulting in cell body accumulation of NFs and/or transport of NFs in axonal processes resulting in NF accumulation in neurites. Dynein function is also important for the fusion of autophagosome and lysosome in macroautophagy, therefore the observed reduction in macroautophagy with MPP⁺ treatment may be the result of impaired dynein function and/or a direct effect of mitochondrial dysfunction on macroautophagy. Impaired macroautophagy results in impaired clearance of protein aggregates targeted for degradation by p62/SQSTM1 resulting in inclusion formation. Reduced macroautophagy was also observed with the addition of exogenous DA which could reduce the clearance of aggregated proteins.
